Department of Civil Engineering
University of Bristol

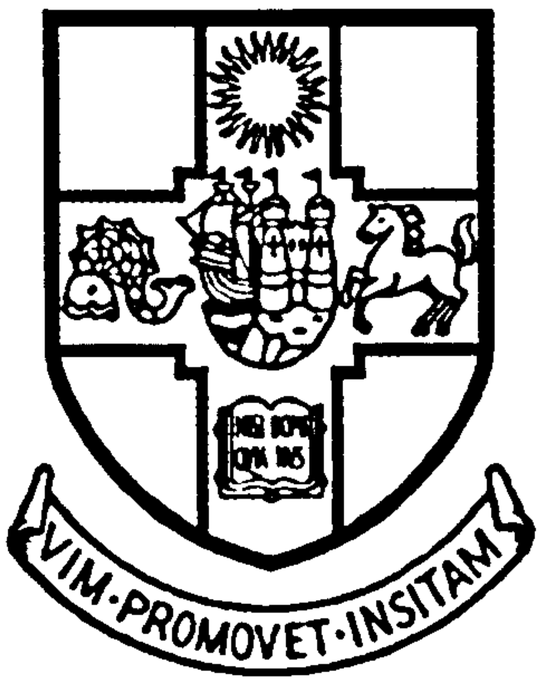

Earthquake Analysis of Concrete Gravity Dam-Foundation Systems

by

Milan Simic

A thesis submitted to the University of Bristol
in accordance with the requirements of the degree of
Doctor of Philosophy in the Faculty of Engineering

December 1994

Abstract

The consequences of the potential failure of concrete gravity dams would be disastrous, and their safety must be evaluated for the most unfavourable loading conditions, usually earthquake. With constantly reducing computational costs, nonlinear numerical analyses emerge as the most cost-effective solution for this exercise. Unfortunately, the nonlinear analyses of combined reservoir-dam-foundation systems are not yet fully developed, partly because of the complicated interaction mechanisms. This work concentrates on numerous aspects of the dam-foundation interaction.

A comprehensive methodology, based on the substructure method in the time domain which uses the near-field seismic input motions, and is able to deal with seismic cracking of concrete gravity dam-foundation systems, is formulated. Since rock formations underneath gravity dams are effectively semi-infinite, a sufficiently accurate time domain approximation of the energy radiation condition is tailored to become compatible with the seismic input scheme. The cracking of dam concrete and foundation rock is described through a continuum mechanics model with strain softening and preservation of fracture energy. The analytical procedure is described through a step by step approach, facilitating the incorporation into a standard nonlinear finite element package. Each step of the procedure is illustrated with numerical examples.

. The main conclusions concern the choice of the viscous transmitting boundary for modelling the radiation damping, the choice of the seismic interface input scheme and its relationship with the transmitting boundary, finite element discretisation, effects of water penetration into open cracks, ultimate modes of failure of concrete gravity dam-foundation systems and the overconservative performance of the rigid foundation model.

Acknowledgements

I would like to express my gratitude to Dr C.A. Taylor for all the stimulating discussions and for having the right suggestions at the right time while supervising this work.

I am also very grateful to Professor R.T. Severn for accepting me to study in the Earthquake Engineering Research Centre of Bristol University, and for providing constant encouragement and support.

The research was funded by a number of institutions. The financial help from all of them (Committee of Vice-Chancellors and Principals, University of Bristol, Mott MacDonald Charitable Trust, British Scholarship Trust for Yugoslavs and the British Council) is gratefully appreciated.

Finally, my special thanks go to my wife, Ana.

Declaration

The research described in this thesis was conducted between October 1991 and November 1994, under the supervision of Dr C.A. Taylor. The work described is entirely due to the author, except where indicated otherwise in the text.

This thesis has not been submitted in support of any other degree or qualification, and the views expressed in it are those of the author and not of the University of Bristol.

The following papers and articles are based on the research described herein:

Studying waves Bristol fashion, feature article in International Water Power & Dam Construction, Volume 45, Number 8, March 1994.

Seismic behaviour of concrete gravity dams, **Daniell, W.E., Mir, R.A., Simic, M. & Taylor, C.A.**, 10th European Conference on Earthquake Engineering, Vienna, Austria, August 28 - September 2, 1994.

The seismic behaviour of gravity dams in areas of low seismicity, **Taylor, C.A., Daniell, W.E., Mir, R.A., Simic, M. & Hinks, J.L.**, Proceedings of the 8th Conference of the British Dam Society, Exeter, UK, September 14-17, 1994.

Concrete gravity dam-foundation discretisation as a function of radiation damping, **Simic, M. & Taylor, C.A.**, Dam Engineering, provisionally accepted for publication.

Limited tension nonlinearities of concrete gravity dam-foundation systems under static loading, **Simic, M. & Taylor, C.A.**, Dam Engineering, provisionally accepted for publication.

Nonlinear cracking analysis of concrete gravity dam-foundation systems under earthquake loading, **Simic, M. & Taylor, C.A.**, Earthquake Engineering and Structural Dynamics, submitted for review and possible publication.

Signed: M. Simic

Date: 7/12/94

Table of Contents

List of Tables

List of Figures

Chapter 7

Chapter 8

Chapter 9

List of Symbols

Chapter 3

$F_1(p)$	complex function of time and coordinates
$F_2(q)$	complex function of time and coordinates
$F_3(p)$	complex function of time and coordinates
$F_4(q)$	complex function of time and coordinates
G	shear modulus (Lamé's elastic constant)
H	depth of the buried point load
$H(t)$	Heaviside function
h	depth of the buried line load
l_i	direction cosines
p	complex function of time and coordinates
q	complex function of time and coordinates
r	radius, vector magnitude, and distance from the buried point load
t	time
u^δ	displacement function due to Dirac delta function load
u_{ij}^δ	displacement function component due to Dirac delta function load
u^F	displacement function due to general excitation load F
u^H	displacement function due to Heaviside function load
v^δ	displacement function due to Dirac delta function load
v^H	displacement function due to Heaviside function load
v_p	velocity of P-waves
v_s	velocity of S-waves
w^δ	displacement function due to Dirac delta function load
x	coordinate axis and epicentral distance from the buried line load
x_j	coordinate axis
$\vec{x}$	position vector

β	ratio between v_p and v_s and Newmark integration method parameter
Δt	time step
δ_{ij}	Kronecker delta symbol
$\delta(t)$	Dirac delta function
γ	ratio between v_s and v_p and Newmark integration method parameter
θ	Wilson integration method parameter
ρ	mass density
σ	half-space normal surface loading
τ	half-space tangential surface loading
ξ	radius of the P-wave at time t
ξ'	radius of the S-wave at time t
ζ	angle defined as $\sin\zeta = x/v_p t$

Chapter 4

A_1	Cohen-Jennings paraxial boundary matrix
A_2	Cohen-Jennings paraxial boundary matrix
A_3	Cohen-Jennings paraxial boundary matrix
A	area
a	dimensionless parameter of the viscous transmitting boundary
B_1	Clayton-Engquist paraxial boundary matrix
b	dimensionless parameter of the viscous transmitting boundary
C_1	Clayton-Engquist paraxial boundary matrix
C_2	Clayton-Engquist paraxial boundary matrix
C_3	Clayton-Engquist paraxial boundary matrix
C_j^N	binomial coefficients
C_{ii}	diagonal terms of the consistent radiation damping matrix
C_{ii}^*	diagonal terms of the lumped radiation damping matrix
C_{ij}	terms of the consistent radiation damping matrix

C_{jk}	terms of the consistent radiation damping matrix
C_r	radiation damping matrix
D	stress-velocity matrix
d	distance between 'information points'
E_{11}	elastic wave equation matrix
E_{12}	elastic wave equation matrix
E_{22}	elastic wave equation matrix
E_i	incident energy
E_r	reflected energy
k	wave number
l	finite element length
N	finite element shape function matrix
N	order of approximation
n	number of element boundary nodes
t	time
$U(x,y,t)$	linear wave field
u	displacement vector
$\dot{u}$	velocity vector
$\dot{u}$	normal velocity
$u_i(\xi_i - vt)$	amplitude function of a plane wave propagating in the ξ_i-direction
$\dot{v}$	tangential velocity
v	plane wave velocity along the ξ-axis
v'	plane wave velocity along the x-axis
v_p	velocities of S-waves
v_r	velocity of Rayleigh waves
v_s	velocities of S-waves
x	coordinate axis
y	coordinate axis
z	depth under free surface

Δt	time step
μ	Poisson's ratio
Θ	incident angle
ρ	mass density
σ	stress matrix
σ	normal stress
τ	shear stress
ω	angular frequency
$\xi_i - vt$	forward characteristic

Chapter 5

add	'addition' of the dam
B	boundary
C	damping matrix
c	damping submatrix
D	dam
d	dynamic displacements
E	embedment
F	far-field excitation
F	foundation
ff	free-field
I	interface
K	stiffness matrix
k	stiffness submatrix
M	mass matrix
m	mass submatrix
N	nonlinear part of the dam-foundation system
ps	pseudostatic displacements
R	force vector, influence coefficient matrix

$\ddot{r}$	total acceleration vector
$\dot{r}$	total velocity vector
r	total displacement vector
rb	rigid body displacements
$\ddot{u}$	added acceleration vector
$\dot{u}$	added velocity vector
u	added displacement vector
$\ddot{v}$	free-field acceleration vector, scattered acceleration vector
$\dot{v}$	free-field velocity vector, scattered velocity vector
v	free-field displacement vector, scattered displacement vector

Chapter 6

C	Rayleigh damping matrix
E_d	modulus of elasticity of the dam
E_f	modulus of elasticity of the foundation
$F(\omega)$	Ricker wavelet Fourier transform
H	height of the dam H
K	stiffness matrix
M	mass matrix
t	time
t_0	Ricker wavelet parameter
t_s	Ricker wavelet parameter
$\ddot{v}$	acceleration record
x	foundation size parameter
α	Rayleigh damping parameter
β	Rayleigh damping parameter, Newmark method parameter
γ	Newmark method parameter
μ_d	Poisson's ratio of the dam
μ_f	Poisson's ratio of the foundation

ρ_d	mass density of the dam
ρ_f	mass density of the foundation
τ	Ricker wavelet parameter

Chapter 7

c	cohesion
d	infinitesimal increment
E	modulus of elasticity
F	yield criterion
G	shear modulus
G_f	fracture energy
I_1^a	cap yield function parameter
I_1	stress invariant
J_2	stress invariant
J_3	stress invariant
K	Drucker-Prager parameter
k	hardening (softening) parameter
l	characteristic finite element length
n	direction normal to the crack
Q	plastic potential function
S_i	principal deviatoric stress
T	tension cut-off limit parameter
t	direction tangential to the crack
α	Drucker-Prager parameter
β	ratio between principal stresses σ_{p2} and σ_{p3}
Δ	incremental value
ε	strain
ε_c	uniaxial compressive strain at σ_c
ε^p	plastic strain

$\dot{\varepsilon}^p$	plastic strain rate
ε_t	uniaxial tensile strain at σ_t
ε_u	uniaxial compressive strain at σ_u
$\dot{\varepsilon}^{vp}$	viscoplastic strain rate
ϕ	angle of friction
η_n	normal stiffness reduction factor
η_s	shear stiffness reduction factor
κ	strain softening parameter
λ	proportionality constant
μ	fluidity (viscosity) parameter
θ_0	stress invariant (Lode's angle)
σ	stress vector
σ	stress
σ_c	uniaxial maximum compressive stress
σ_m	hydrostatic part of the stress tensor
σ_{pi}	principal stress
σ_{pij}	discrete stress values
σ_{pijk}	discrete stress values
σ_t	uniaxial cut-off tensile stress
σ_u	uniaxial ultimate compressive stress
σ_y	yield stress

Chapter 8

c	cohesion
D	parameter of the ADINA improved Drucker-Prager model
E_d	modulus of elasticity of the dam
E_f	modulus of elasticity of the foundation
I_1^a	initial position of the compression cap
K	Drucker-Prager parameter

n	ratio of absolute strength values σ_t/σ_c
T	tension cut-off limit parameter
u	horizontal displacement
u^{wp}	horizontal displacement with water penetration effects
W	parameter of the ADINA improved Drucker-Prager model
α	Drucker-Prager parameter
β	ratio between principal stresses σ_{p2} and σ_{p3}
ε_c	uniaxial compressive strain at σ_c
ε_u	uniaxial compressive strain at σ_u
ϕ	angle of friction
η_n	normal stiffness reduction factor
η_s	shear stiffness reduction factor
μ_d	Poisson's ratio of the dam
μ_f	Poisson's ratio of the foundation
ρ_d	mass density of the dam
ρ_f	mass density of the foundation
σ_c	uniaxial compressive strength
σ_{pij}	discrete stress values
σ_{pijk}	discrete stress values
σ_t	uniaxial tensile strength
σ_u	uniaxial ultimate compressive stress

Chapter 9

a	Ricker wavelet amplitude
E_d	modulus of elasticity of the dam
E_f	modulus of elasticity of the foundation
$\boldsymbol{r}$	total displacement vector
t	time
t_0	Ricker wavelet parameter

t_s	Ricker wavelet parameter
u	added displacement vector
v	free-field displacement vector, scattered displacement vector
β	ratio between principal stresses σ_{p2} and σ_{p3}
ε_c	uniaxial compressive strain at σ_c
ε_u	uniaxial compressive strain at σ_u
μ_d	Poisson's ratio of the dam
μ_f	Poisson's ratio of the foundation
ρ_d	mass density of the dam
ρ_f	mass density of the foundation
σ_c	uniaxial compressive strength
σ_{pij}	discrete stress values
σ_{pijk}	discrete stress values
σ_t	uniaxial tensile strength
σ_u	uniaxial ultimate compressive stress

Introduction

The civil engineering community has long been aware of the fact that the safety record of its deeds is crucial to the well-being and reputation of the whole profession.

In critical conditions (extreme flooding, earthquakes, bombing raids), the safety considerations of important structures become even more significant. If 'important structures' were quantified through a loss of life and property due to potential failure, large dams would certainly be one of the top-ranked categories. However, in all cases, the chain of actions required to attain satisfactory safety confidence is similar. First, the behaviour of the structure and its potential modes of failure must be fully understood. After choosing the appropriate modelling technique, some kind of analysis is carried out.

In this thesis, concrete gravity dams in earthquake conditions will be considered. By placing the emphasis on the improvement of analytical procedures, the first two steps (understanding of the behaviour and choice of the modelling technique) will be constantly kept in mind and referred to.

The need for improvement and validation of earthquake analysis procedures for concrete gravity dams arises from two main concerns. With the emergence of roller compacted concrete (RCC) technology, interest in concrete gravity dams has been revived, with new dams being constructed in seismically active zones. Secondly, there is an immediate need for earthquake safety evaluation of existing dams, many of which have been designed and analysed using old, oversimplified methods.

1.1 Research Objectives

For decades, the Earthquake Engineering Research Centre (EERC) of Bristol University has been conducting research in the area of earthquake behaviour of concrete dams. Currently, a set of three parallel activities deal with concrete gravity dams. Prototype scale dams are monitored (Taylor et al., 1994), shaking table scale model tests are conducted in the laboratory conditions (Mir, 1994; Mir & Taylor, 1994), and analytical tools are developed. After the analytical investigation into dam-reservoir interaction (Greeves, 1991), this work represents another integral part of the last activity by concentrating on dam-foundation interaction.

The research in Bristol has two ultimate aims. The first is to articulate concise guidelines and clear recommendations regarding earthquake response of concrete gravity dams, and to communicate them to practising dam engineers. The second aim is to produce a comprehensive finite element code which would include all the recent research findings.

So far, few concrete gravity dams have suffered serious damage in an earthquake and none has totally collapsed. Therefore, gravity dam designers and analysts have little prototype scale information to advise them on the potential modes of failure. The few available prototype observations must be interpreted carefully and any conclusions must not be automatically extrapolated to other cases. On the other hand, scale model tests can provide valuable information, but are difficult and expensive to conduct. With the current tendency of ever-reducing computational costs, nonlinear numerical analyses are the most cost-effective solution and play an important role in extending our understanding of the behaviour and potential failure of concrete gravity dams. Unfortunately, such analyses are far from being fully developed. This thesis addresses one aspect of this problem; the nonlinear behaviour of dam-foundation interaction.

The dam-foundation zone is often the most critical in a gravity dam-foundation system. All the loads pass through it, yet its properties and strengths are the least well known and understood, presenting the greatest challenge to engineering judgement. The present limitations in nonlinear analytical techniques lead to one of the following two simplifications:

a) Only the body of the dam can be nonlinear. The foundation is treated either as fully rigid or flexible. In the flexible foundation case, the formulation of the viscoelastic half-space in the frequency domain, which takes into account the radiation damping, is probably the most popular.

b) Both the dam and foundation are nonlinear. In this case, the seismic input motions are prescribed in the far-field and no provision is made for the modelling of radiation damping. The seismic energy remains trapped in the system and artificially increases the response.

The main objective of this work is to remove the above limitations. This can be further divided as follows:

1. To formulate the analytical procedure for the nonlinear analysis of concrete gravity dam-foundation systems which takes into account the radiation damping through the effectively semi-infinite foundation rock and uses the near-field seismic input motions.

2. To describe the formulated analytical procedure through a step by step approach, facilitating the incorporation into a standard nonlinear finite element package.

3. To illustrate each step of the procedure with numerous numerical examples.

4. To assess the failure mechanisms of concrete gravity dam-foundation systems.

1.2 Structure of the Thesis

Chapter 2 reviews the current knowledge about earthquake analysis of concrete gravity dams.

Chapter 3 gives further insight into the half-space foundation behaviour by presenting the existing knowledge about the time domain theory of infinite and half-space media. Emphasis is given to the energy radiation problem and other problems with respect to the finite element modelling technique. Other common modelling techniques are also described.

Chapter 4 presents the most popular transmitting boundaries - approximate boundary solutions which have to be used for finite element analyses of unbounded media in the time domain. After identifying the transmitting boundary which seems most promising in the light of the ultimate objective of this work, a number of numerical tests are carried out to confirm its suitability.

Chapter 5 first introduces the structure (concrete gravity dam) and couples it with the foundation. The main aspects of concrete gravity dam-foundation interaction are presented in an attempt to distinguish them from the general theory of soil-structure interaction. The crucial part of the Chapter consists of the mathematical formulations for two different seismic input schemes: boundary and interface.

In Chapter 6, preliminary linear earthquake analyses of concrete gravity dam-foundation systems are carried out. Their goal is to establish the appropriate seismic input scheme for different foundation conditions and to recommend the size and refinement of the foundation finite element mesh as a function of radiation damping. Also, a procedure for combining the viscous transmitting boundary with static loading is devised and tested. The practical significance of the research findings is illustrated on the example of earthquake analysis of a real concrete gravity dam in Wales.

Chapter 7 classifies and describes the nonlinearities most likely to occur in dam-foundation systems. Several possibilities for representing limited tension nonlinearities are examined, emphasising those that will be used in the subsequent Chapters.

In Chapter 8, nonlinear static analyses of concrete gravity dam-foundation systems are carried out. The loading required to induce the nonlinear behaviour is provided by continuously increasing the reservoir water level. The main purpose of this Chapter is to serve as a calibration test for the numerical models presented in Chapter 7 and to identify possible modes of failure.

Chapter 9 incorporates all elements of this research by carrying out nonlinear earthquake analyses for different foundation conditions. These analyses are novel because they do not require a free-field analysis of the site, successfully approximate the energy radiation conditon and allow for limited tension nonlinearities to occur both in the dam and surrounding foundation. The nonlinear analyses are compared with the linear ones; both sets being performed by using a standard, general purpose finite element code, adapted by the author to treat the coupled dam-foundation problems.

The intermediate conclusions are presented in each of the preceding Chapters. Chapter 10 summarises the whole work by drawing attention only to the most important conclusions and by reflecting on possible further work.

Earthquake Analysis of Concrete Gravity Dams: Present Knowledge and Research Strategy

In the first part of this Chapter, the current knowledge about earthquake analysis of concrete gravity dams will be reviewed. A primary objective is to identify areas where further work is needed.

In the second part of this Chapter, the issues in carrying out a practical analysis of a gravity dam will be considered from the practising dam engineer's point of view. The overall research strategy is then formulated through the attempt to resolve some of these issues.

2.1 Present Knowledge

Until the late Sixties, little attention had been given to seismic analyses of concrete gravity dams and their earthquake resistant design. It was only after the December 1967 Koyna earthquake which caused structural damage to Koyna Dam (Saini et al., 1972; Chopra & Chakrabarti, 1972), that the civil engineering community became aware of the dangers and consequences associated with the possible earthquake-induced damage of concrete gravity dams. This awareness resulted in a dramatic increase in the number of publications. Coupled with the simultaneous advances in the Finite Element Method and computation technology, a similar trend, perhaps at somewhat reduced rate, has continued to the present day.

The state-of-the-art earthquake analyses of concrete gravity dams would now be typically carried out by using finite elements. Therefore, only aspects relevant to this analytical procedure are presented in this Section. They are divided into six groups: modelling, discretisation, loading, material models, dam-reservoir interaction and dam-foundation interaction.

2.1.1 Modelling

Before developing a numerical model of the earthquake behaviour of a concrete gravity dam, choices regarding the analysis domain and discretisation technique have to be made. Depending on the choice, all four combinations are possible: pure finite element modelling in the time domain, pure finite element modelling in the frequency domain, coupled boundary and finite element modelling in the time domain and coupled boundary and finite element modelling in the frequency domain.

Furthermore, several simplified procedures have been proposed (Chopra, 1978; Fenves & Chopra, 1985a; Fenves & Chopra, 1985b), but their performances have not been fully tested and they will not be repeated herein.

2.1.1.1 Time Domain or Frequency Domain?

Historically, the assumption of linear behaviour and computational developments in the area of fast Fourier transforms have enabled the first modern earthquake analyses of concrete gravity dams to be carried out in the frequency domain (Chopra, 1968; Chopra, 1970). As the understanding of the problem evolved, it became clear that strong-motion earthquakes induce nonlinear behaviour of the dam and foundation materials. Since true nonlinear analyses of dam-foundation-reservoir systems can be performed only in the time domain, only the knowledge relevant to this domain will be further explored. In the meantime, the computational capabilities have undergone tremendous improvements and they do not pose serious limitations on the time-domain analyses anymore.

2.1.1.2 Boundary Element Method or Finite Element Method?

The state-of-the-art Boundary Element Method offers a theoretical basis for the modelling of processes that are significant to the behaviour of concrete gravity dams under earthquake loading. The method is especially suited to model the unbounded domains because the energy radiation conditions are modelled rigorously. Pekau et al. (1991) have shown how reservoir interaction, foundation interaction and concrete fracture may be treated. However, this approach suffers from two main disadvantages: boundary element remeshing is necessary after each change in the cracking pattern; and second, commercial boundary element computer codes that can deal with the problems of concrete gravity dams are still scarce. Therefore, the pure Boundary Element Method is unlikely to be common tool for earthquake analyses of concrete gravity dams for some time.

On the other hand, the pure Finite Element Method is a reasonably well established computational tool and practising dam engineers are familiar with its meaning and practical applications. Its major drawback is the inability to treat the unbounded

media such as reservoir and foundation under dynamic conditions. A standard finite element discretisation would lead to the spurious wave reflection at the artificial boundaries of the finite element mesh.

In order to take the best of both methods, boundary and finite elements may be coupled. Usually, the dam is discretised by finite elements while the foundation and reservoir are represented by boundary elements (Touhei & Ohmachi, 1993). Thus, the unbounded media are rigorously modelled and the analyst needs to discretise only the finite element part of the coupled system.

2.1.2 Discretisation

In this work, only the pure Finite Element Method will be used. To compensate for the inability to model the unbounded media, the finite element mesh has to be equipped with so-called transmitting boundaries, which are an approximation to the exact solution. This will be further covered in Subsection 2.1.6.

Two other issues that need to be resolved before conducting the actual analysis concern its dimensionality and finite element mesh idealisation.

2.1.2.1 Two-Dimensional or Three-Dimensional Analysis?

Concrete gravity dams with their foundations and reservoirs are clearly three-dimensional (3D) objects and adopting 3D analysis models would certainly be more accurate. Nevertheless, a two-dimensional (2D) approximation considerably reduces the computational effort and can therefore be recommended whenever physical conditions allow this simplification (Clough & Zienkiewicz, 1987).

A 2D analysis may be used for all dams with ungrouted vertical joints (plane stress) and for dams with grouted vertical joints located in wide valleys (plane strain). Following the same principles, the 3D model is unavoidable only for dams with

grouted vertical joints located in narrow valleys. Here, only 2D approximations will be treated.

2.1.2.2 Mesh Idealisation

Having selected a 2D problem, the next step in the finite element analysis is to perform a microidealisation and macroidealisation of the finite element mesh.

Microidealisation of the finite element mesh consists of choosing the type and maximum size of the element. A family of isoparametric elements with variable number of nodes (usually four, eight, or nine, depending on the level of interpolation) is the best current choice (Clough & Zienkiewicz, 1987). The maximum size of finite elements in the reservoir-dam-foundation system is governed by two phenomena: the seismic wave propagation (Achenbach, 1973) and the cracking of dam concrete and foundation rock (Brühwiler & Wittmann, 1990). The first phenomenon becomes important with respect to the problem of wave reflection at the artifical boundaries (as mentioned in the previous Subsection), while the latter is only encountered in nonlinear analyses and concerns the velocity of crack propagation. It is not yet clear which of the two phenomena is more stringent. This will be further explored in the following Chapters. If the mesh is not fine enough, it can restrict the propagation of frequencies in a certain range.

Macroidealisation of the finite element mesh deals with the boundaries of the finite element mesh. The dam, being a finite medium, can be fully modelled by finite elements. The foundation and the reservoir are infinite media and artificial boundaries have to be placed at some distance from the dam. Even if the mesh is equipped with transmitting boundaries, this distance is not known in advance (Zienkiewicz et al., 1986). This problem will be investigated in the subsequent Chapters with the aim of producing clear recommendations.

2.1.3 Loading

When an earthquake strikes the reservoir-dam-foundation system, the existing static loads are already present and the system is in static equilibrium. The main static loads typically considered for the analyses of concrete gravity dams are dead weight and hydrostatic pressure. Apart from a number of other relatively minor loads (USBR, 1976), the uplift force effects deserve to be mentioned. They have been debated since the end of the last century but the landmark of the modern approach was created after the publication of the series of articles by Leliavsky (1959/60).

As for the seismic loading, the source of an earthquake is usually far away and at the significant depth from the dam site. These dimensions cannot be compared to the size of the dam and even if all the details about the source mechanism and travel path of the seismic waves were available, it would be still meaningless to analyse earthquake problems together with their sources (Wolf, 1985). Therefore, only the area confined to the vicinity of the dam will be treated.

Despite a number of stochastic analyses already conducted in this area, it will be assumed that the earthquake input can be given as a single event for which a deterministic solution is sought.

The ICOLD Committee on Seismic Aspects of Dam Design (Lane, 1983) recommended the earthquake analyses of dams subjected to the Design Basis Earthquake (DBE) and Maximum Credible Earthquake (MCE). According to the abovementioned deterministic approach, for either type a single event is assumed. The current practice in the earthquake resistant design of concrete gravity dams uses linear analysis techniques for determining the response to both the DBE and MCE. Occasionally, nonlinear analysis techniques are used for determining the response to the MCE.

For both the DBE and MCE, two different approaches can be used to specify the seismic input. The first possibility is to apply the motions at the boundaries of the

foundation block. The second is to use the free-field or scattered motions as input, in which case the standard equations of motion need to be modified. These issues will be discussed in greater length in later Chapters.

The earthquake loading can be prescribed through a response spectrum or time history approach. The former is based on the number of past earthquakes and takes account of the regional geological conditions. Usually, it can be obtained from national codes or recommendations (e.g. Principia Mechanica Ltd, 1981). The main disadvantage of the response spectrum approach is that it is valid only for linear analyses. For nonlinear analyses, the time-history approach has to be used. It consists of specifying the time histories of earthquake acceleration, and sometimes, of earthquake velocity and displacement, at, or in the ground where the structure is to be founded. These records can be obtained by making seismological predictions or by generating time-histories compatible with the local response spectra. Here, only the time-history approach will be considered as it enables the analysis of both linear and nonlinear systems and their comparison.

2.1.4 Material Models

The inability of dam concrete and foundation rock to withstand high tensile stresses is one of their most important features. Under strong earthquake loading, the expected development of cracks requires suitable nonlinear material modelling. The main currently available numerical procedures for describing cracking mechanisms in mass, unreinforced concrete and foundation rock are:

a) Smeared crack approach (Vargas-Loli & Fenves, 1989; El-Aidi & Hall, 1989; Bhattacharjee & Léger, 1993). Cracking is distributed throughout the elements and is mainly confined to the stress-strain relationship. Computational procedures applied in elasto-plastic analyses can also be adopted with some adjustments.

b) Discrete crack approach (Skrikerud & Bachmann, 1986; Ayari & Saouma, 1990). Elements are physically separated when a criterion for the initiation or extension of the crack at the interelement boundary is met. Hence, the crack geometry can be easily determined.

c) Fracture mechanics approach (Broek, 1978; Bazant, 1990; Gioia et al., 1992). The concepts of fracture mechanics are introduced and stress intensity factors are employed in stage by stage procedures. Many ideas that have originated in fracture mechanics are currently being successfully combined with the smeared and discrete crack approaches (Ayari & Saouma, 1990; Bhattacharjee & Léger, 1993).

2.1.5 Dam-Reservoir Interaction

It has long been recognised that the interaction between the reservoir and the dam is a significant factor in the earthquake response analysis of concrete gravity dams (Westergaard, 1933). More recently, this subject was investigated in the frequency domain in the series of papers by Chopra and his co-workers (Chopra, 1967; Chakrabarti & Chopra, 1973; Chopra & Chakrabarti, 1981; Hall & Chopra, 1982; Hall, 1986). If the reservoir is to be discretised, this is typically done either by boundary elements (Humar & Jablonski, 1988) or by finite elements. If the time domain is used in the latter case, the two techniques for the analysis of interaction effects are (Greeves, 1991):

a) Pressure method. The unknowns in the reservoir mesh are pressures. If the effects of water compressibility are to be taken into account, special procedures have to be applied. Also, the necessity for interface elements arises because the unknowns in the other two domains (dam and foundation) are displacements.

b) Displacement method. The unknowns in the reservoir mesh are displacements. Thus, a water element automatically represents a compressible fluid, which

means that compressibility is implicitly assumed and that cavitation can be modelled as a material nonlinearity.

However, it was shown (Greeves, 1991) that in many cases the Westergaard (1933) added mass approach achieves satisfactory results. If this approach is used, it is not necessary to discretise the reservoir.

2.1.6 Dam-Foundation Interaction

A massive and stiff structure like a concrete gravity dam has significant influence on the foundation and vice versa.

In reality, the rock foundations for concrete gravity dams are neither idealised half-spaces nor single or multi-layered soil deposits above the bedrock; they are discontinuous media whose behaviour is predominantly influenced by the state of their faults, joints and fissures. A substructure method (Gutierrez & Chopra, 1978; Lysmer, 1978) has emerged as an effective technique which facilitates the representation of coupled problems, such as reservoir-dam-foundation systems. This method takes into account the particular requirements imposed by each of the individual subsystems while still treating the system as a whole.

Within the substructure method, each subsystem can be linear or nonlinear. For the linear foundation and frequency domain, Fenves & Chopra (1984) used the viscoelastic half-space described by Dasgupta & Chopra (1979), while Lotfi et al. (1987) used the layered foundation. If nonlinearities in the foundation are expected, it is difficult to predict their exact nature and to evaluate their relative importance. The finite element techniques for jointed rock have been extensively studied and used with great success in static analyses (Pande et al., 1990). Joint opening and closing mechanisms have been of particular interest. Unfortunately, experience in this field is still limited when dynamic analysis is concerned. Another group of nonlinearities typical for earthquake concrete gravity dam-foundation analyses are the so-called

contact nonlinearities: separation and sliding along construction joints, and separation, uplifting and sliding of the dam along the contact surface with the foundation (Léger & Katsouli, 1989; Ibrahimbegovic & Wilson, 1990).

In static gravity dam-foundation analyses, zero displacements are usually prescribed in the foundation at a certain distance from the dam. On the other hand, in dynamic (earthquake) gravity dam-foundation analyses, a similar procedure would be possible only if the boundaries were placed sufficiently far from the dam, i.e. at the distance from which seismic waves could not be reflected back to the area near the dam for the whole duration of the analysis. Having in mind the average velocity of seismic waves in rock, it becomes clear that a foundation of this size cannot be rationally treated. The foundation finite element mesh has to be truncated by placing artificial boundaries closer to the dam. To eliminate the spurious reflections of radiated waves and to prevent an energy buildup which would eventually lead to the increase of dam response, special boundary conditions have to be implemented. They all lead to boundary approximations that are local both in space and time, and have therefore been named local transmitting boundaries. If the analysis is to be carried out in the time domain, the boundary should also possess the property of frequency independence and the ability of handling approximately all types of waves, without imposing any restrictions on the foundation geometry. The development and implementation of various transmitting boundaries (also called non-reflecting, quiet, silent, absorbing, radiating, anechoic) will be discussed in detail in the following Chapters.

2.2 Practical Issues in Dam Analysis

In this Section, it is assumed that a practising dam engineer is confronted with the task of carrying out the earthquake analysis of a concrete gravity dam. Although he

or she may have access to all the currently available knowledge and computer facilities, some doubts will remain and several questions will be asked. The most important dilemmas will be highlighted here and the attempt to shed some light on them will be in the core of the following Chapters and this work as a whole.

2.2.1 Response Spectrum or Time History Analysis?

When planning a seismic analysis, probably the first dilemma is whether to use a response spectrum or time-history record as a representation of the DBE or MCE earthquake.

In the response spectrum approach, there is a number of inherent difficulties. Even if the mechanical properties of the foundation are fully known, it is not clear what size of the foundation should be taken for the numerical model. For existing dams, this problem can be circumvented by field testing. Natural frequencies are measured on site (Taylor et al., 1994), facilitating the calibration of the unknown foundation size (BEELAB, 1993/94). For dams in the design process, natural frequencies cannot be determined and have to be evaluated numerically, which introduces yet another uncertainty into the analysis. Finally, it must be emphasised again that the response spectrum approach is valid only for linear analyses, which may only be appropriate for the DBE earthquake.

Under higher earthquake loading (e.g. MCE), it is plausible that nonlinearities would occur. This practically eliminates the response spectrum and requires the time history approach, giving rise to a new set of dilemmas. What nonlinearities may occur? Where do they occur? How to model them?

2.2.2 Energy Radiation

In a reservoir-dam-foundation coupled system, the dam is the only subsystem of a finite size. As earthquake energy is introduced into the system, and after causing the

latter's vibration and activation of multiple interaction mechanisms, a part of the energy is radiated towards the infinity of the foundation and reservoir. This phenomenon is known as energy radiation (or radiation damping). Being frequency dependent, it can be modelled accurately only by a frequency domain analysis. In a time domain analysis, approximate solutions, the so-called transmitting boundaries, have to be used.

All the previous facts are known to our practising engineer. What is not known is which of the many already devised transmitting boundaries is best suited for earthquake analysis of concrete gravity dams. Where to place it? How to incorporate it within the model as a whole?

2.2.3 Spatial and Temporal Discretisation

Spatial discretisation of the finite element reservoir-dam-foundation model consists of determining the minimum acceptable overall size of the unbounded media (i.e. reservoir and foundation), and at the local level, determining the finite element size. The global, overall size is governed by the interaction mechanisms and energy radiation conditions. The element size is governed by the velocity of propagation of possible nonlinearites and the velocity of seismic wave propagation with respect to the energy radiation condition.

Temporal discretisation of the dynamic finite element equations of motion consists of determining the appropriate time step for the direct time integration.

Consequently, the questions with which the practising dam engineer is now confronted can be formulated as: What is the minimum size of the foundation and reservoir that requires finite element modelling and how to determine it? What is the minimum, maximum and optimal size of finite elements? What time-step should be used?

2.2.4 Seismic Input

In the best-case scenario, a dam engineer conducting the earthquake analysis of a concrete gravity dam can expect to obtain the free-field earthquake records from a seismologist. These are ground surface records at the location of the future dam site. However, a concrete gravity dam is a massive structure and will certainly change these records, at least locally. In other words, a special mathematical procedure has to be devised which would take account of this aspect of dam-foundation interaction. Standard structural dynamics procedures where the motion is applied at the rigid base of the structure are no longer valid.

The questions for the dam engineer are: What is the appropriate mathematical procedure and how to recognise it? How to apply it within existing computer codes?

2.3 Concluding Remarks

As a conclusion to Chapter 2, the research strategy used in this thesis is highlighted.

After briefly reviewing the current knowledge about earthquake analysis of concrete gravity dams, probable dilemmas and questions that a practising dam engineer might ask were identified. The subsequent Chapters will follow the path formed by these questions and will attempt to find suitable answers by formulating practical recommendations and concise guidelines. In other words, the final aim of this work is to offer a coherent methodology for carrying out nonlinear earthquake analyses of concrete gravity dams with the appropriate modelling of energy radiation and seismic input.

Infinite and Half-Space Media in Time Domain: Theory

Sharp geological discontinuities at reasonable depths below the surface of concrete dam sites are seldom found and the medium under consideration is practically semi-infinite. An obvious possibility is to adopt the half-space foundation, which can be coupled with the concrete dam. The problems arising from such dam-foundation coupling will be presented in Chapter 5.

Most of the published work on half-space idealisation was done in the frequency domain because it enables rigorous modelling of the unbounded domains by taking energy radiation conditions into account. The main drawback of the frequency domain is that nonlinear behaviour cannot be properly accommodated. In order to include nonlinearities (Chapters 7, 8 and 9), the time domain is chosen and only time-domain results will be presented in this Chapter. This choice implies that the semi-infinity of the half-space and related energy radiation (radiation damping) must be approximated with spatially and temporally local, frequency independent transmitting boundaries. They will be treated in Chapter 4 (foundation only) and Chapter 6 (dam-foundation system) in more detail.

The aim of this Chapter is to give further insight into the half-space foundation behaviour by presenting the underlying theory of infinite and half-space media. Three modelling techniques will be described, with the particular emphasis on the Finite Element Method as the chosen method for all subsequent analyses.

3.1 Fundamentals

Continuum mechanics is a discipline which analyses the motion and deformation of continuous media subjected to external or internal excitations. Elastodynamics is its subdiscipline covering the case in which the medium under consideration is an elastic solid and in which the excitation is of a dynamic nature. The elastodynamic disturbances are transmitted from one point to another in the form of energy-carrying elastic waves, and the phenomenon on the whole is therefore often called wave propagation. In an infinite homogeneous and isotropic solid, for example, only body waves (primary-P and secondary-S waves) propagate, while in the case of a half-space, additional surface Rayleigh waves are generated. Many excellent textbooks were written on the subject of elastodynamics and wave propagation (Ewing et al., 1957; Achenbach, 1973; Graff, 1975; Eringen & Suhubi, 1975; Miklowitz, 1978).

If the medium under consideration is the Earth, the science which analyses its mechanical disturbances is known as seismology. These disturbances may be caused naturally (earthquakes, winds, volcanic eruptions), or artificially by human activity (explosions, induced earthquakes). The waves which develop are called seismic waves. Once the fundamental equations of elastodynamics are defined and seismic waves identified, the purpose of seismology is to give mathematical descriptions of seismic sources and to couple them with the equations of motion.

On a smaller scale, the equations of elastodynamics can also be used as a basis for numerical modelling of foundations and soil-structure interaction phenomena.

3.1.1 Green's Functions

Fundamental equations of elastodynamics are typically formulated as partial differential equations in space and time, with the appropriate boundary and initial conditions. Provided that certain requirements are met (Green, 1969), it is possible

to transform the governing differential equations of the problem into integral equations. Such a procedure reduces the number of spatial dimensions by one.

The kernel functions of the derived integral equations are called Green's functions and they form the essential link between the differential and integral formulation. Both in seismological and soil-structure interaction problems, the physical meaning of the time domain Green's function is that it represents a formula for some dynamic property of the system (e.g. displacement, stress, force) in terms of the quantities that originated the disturbance. These quantities can be either body forces or tractions and/or displacements prescribed on the surface of the elastic medium under consideration. The energy radiation conditions at infinity are implicitly included in Green's functions, which makes them ideally suited as a theoretical basis for the modelling of infinite and semi-infinite domains.

Unfortunately, it is very difficult to construct a time-domain Green's function in an explicit form for more complicated media. For example, it is not possible to determine the Green's functions directly in the time domain for a layered half-space, and it is necessary to perform the calculations in the frequency domain (Wolf, 1988).

3.1.1.1 Application of Green's Functions in Seismology

In seismology, it is fundamentally important to interpret the recorded motions (seismograms) and to give them a convenient mathematical description. Somehow, these motions need to be correlated with the sources of disturbance. If the source is external to the Earth (strong winds and ocean waves, shallow volcanic eruptions, surface and atmospheric explosions), it can be analysed as a traction time history applied to the Earth's surface. If the source is internal (earthquakes, underground explosions, deep volcanic eruptions), it is more difficult to develop its analytical representation. From the dimensionality point of view, internal sources can be divided into two categories: faulting and volume (Aki & Richards, 1980).

In the case of earthquake faulting, the source is confined to a finite fault plane and involves motions of varying directions and magnitudes. However, for many purposes, a unidirectional body force in an infinite medium is the adequate source model for the seismic motions observed from an earthquake. Alternative formulations are also possible: the spherical cavity (Wolf, 1988) and double couple (Aki & Richards, 1980) in an infinite space.

Regardless of which of the above source models is chosen, the motions it causes can be described by Green's functions.

3.1.1.2 Application of Green's Functions in Soil-Structure Interaction

In soil-structure interaction, the unbounded soil contributes to the equations of motion through the history of the force-displacement relationship at the interface between the structure and the soil. In other words, the only 'soil unknowns' are located on its boundary because the dynamic behaviour of the interior of the soil is fully described by Green's functions, satisfying the radiation conditions.

The Green's functions can also be applied for the performance evaluation of various transmitting boundaries. Since the radiation conditions (radiation damping) are already implicitly incorporated into these functions, they provide an exact solution for the particular elastodynamic problem. On the other hand, the implementation of frequency independent, local transmitting boundaries is only an approximate solution to the same problem. By trying to match the exact solution achived by the Green's function, the performance of different transmitting boundaries can be assessed and compared.

3.1.2 Convolution

The time dependence of the quantities that originated the disturbance described by the Green's functions has not been considered so far. Although this dependence may be

quite general, the usual practice is to find the dynamic response of the system to an input which varies in time as a Dirac delta function - $\delta(t)$. Once the response to such an impulse is known, the problem is regarded as solved because the response to an arbitrary input can be obtained by convolution.

Without going into mathematical details about convolution (Miklowitz, 1978), the case of the displacement function u^F for general variation of the excitation F in time t, can be expressed as

$$u^F(t) = \int_0^t F(t-\tau)\, u^\delta(\tau)\, d\tau \tag{3.1}$$

where u^δ is the displacement of the system due to a Dirac impulse (i.e. displacement Green's function). The integral in Equation (3.1) is called the convolution integral, and its properties allow for alternative formulations, such as:

$$\int_0^t F(t-\tau)\, u^\delta(\tau)\, d\tau = \int_0^t u^\delta(t-\tau)\, F(\tau)\, d\tau \tag{3.2}$$

It is also very useful to find the dynamic response of the system to an input which vary in time as a Heaviside step function - $H(t)$. Firstly, for large t, this dynamic solution should converge to the static solution. Secondly, the excitation in the form of a rectangular pulse can be defined as the difference between two Heaviside step functions (Figure 3.1), enabling yet another analytical solution.

3.2 Infinite Space

The Green's functions for the concentrated body force acting within a homogeneous, isotropic, unbounded elastic medium can sometimes be used in seismology to model the seismic motions observed from an earthquake. In general soil-structure interaction analyses, this means that they can model the free-field motions.

The solution to this problem was first given by Stokes in 1849 and is therefore known as the Stokes' problem. The results of the derivation for the general time-varying force (Eringen & Suhubi, 1975) are the second-order tensor for the displacements and the third-order tensor for the stresses. When the force varies in time as $\delta(t)$, the displacement tensor becomes a displacement Green's function and the stress tensor becomes a stress Green's function. Very often, they are called fundamental solutions.

The force in the unbounded medium under consideration can act either as a concentrated, point load; or as a uniform, line load. The first case (Figure 3.2a) is clearly a three-dimensional one, while the second (Figure 3.2b) may be treated as a two-dimensional, plane strain problem.

3.2.1 Three-Dimensional Problem

The fundamental solutions for the three-dimensional problem can be expressed explicitly, and many equivalent forms are possible (Eringen & Suhubi, 1975; Aki & Richards, 1980; Wolf, 1988). Herein, the formulation by Wolf (1988) will be used:

The Dirac delta load function is applied in the x_j-direction at the origin of the coordinate system at time zero. The displacements are observed at the point specified by the position vector $\vec{x}$, with the direction cosines l_i (i=1,2,3) and magnitude r. The displacement component u_{ij}^{δ} in the x_i-direction at time t is

$$u_{ij}^{\delta} = \frac{1}{4\pi\rho}(3l_il_j-\delta_{ij})\frac{t}{r^3}\left[H\left(t-\frac{r}{v_p}\right)-H\left(t-\frac{r}{v_s}\right)\right]+\frac{1}{4\pi\rho v_p^2}l_il_j\frac{1}{r}\delta\left(t-\frac{r}{v_p}\right)+$$

$$+\frac{1}{4\pi\rho v_s^2}(\delta_{ij}-l_il_j)\frac{1}{r}\delta\left(t-\frac{r}{v_s}\right) \qquad (3.3)$$

where ρ is the mass density; H and δ are the Heaviside and Dirac function, respectively; δ_{ij} is the Kronecker delta; and v_p and v_s are the velocities of P-waves

and S-waves, respectively. The corresponding stress components are given by Eringen & Suhubi (1975).

The main properties of the three-dimensional displacement Green's function (3.3) were discussed by Aki & Richards (1980). The first term is called a near-field term because it dominates when $r \rightarrow 0$. The second term is a far-field P-wave (P-wave propagation with corresponding velocity v_p), and the third term is called a far-field S-wave (S-wave propagation with corresponding velocity v_s). They both dominate when $r \rightarrow \infty$. Although the majority of seismic data is collected in the far-field, occasionally, in earthquake engineering, the data are collected in the near-field.

3.2.2 Two-Dimensional Problem

The fundamental solutions (Green's functions) for the two-dimensional problem can be derived in two ways. The first derivation is a special case of the three-dimensional counterpart (Eringen & Suhubi, 1975), where it becomes clear that the displacement components are uncoupled into the plane and antiplane parts, in which case only the plane part matters. The second way of deriving the two-dimensional Green's functions is an independent one (Eason et al., 1955/56; Achenbach, 1973). Again, only the final formulation by Wolf (1988) will be used:

The Dirac delta load function is applied in the x_j-direction at the origin of the coordinate system at time zero. The displacements are observed at the point specified by the position vector $\vec{x}$, with the direction cosines l_i (i=1,2) and magnitude r. The displacement component u_{ij}^{δ} in the x_i-direction at time t is:

$$u_{ij}^{\delta} = \frac{1}{2r^2\pi\rho}\left(\frac{2t^2 - \frac{r^2}{v_p^2}}{\sqrt{t^2 - \frac{r^2}{v_p^2}}} l_i l_j - \sqrt{t^2 - \frac{r^2}{v_p^2}}\,\delta_{ij}\right) H\left(t - \frac{r}{v_p}\right) -$$

$$-\frac{1}{2r^2\pi\rho}\left[\frac{2t^2-\frac{r^2}{v_s^2}}{\sqrt{t^2-\frac{r^2}{v_s^2}}}l_i l_j-\left(\frac{r^2}{v_s^2\sqrt{t^2-\frac{r^2}{v_s^2}}}+\sqrt{t^2-\frac{r^2}{v_s^2}}\right)\delta_{ij}\right]H\left(t-\frac{r}{v_s}\right) \qquad (3.4)$$

Similarly to the three-dimensional case, the first term on the righthand side of Equation (3.4) describes the propagation of P-waves (corresponding velocity v_p), while the second term describes the propagation of S-waves (corresponding velocity v_s).

Since the direction of the load is arbitrary, it is always possible to choose the coordinate system so that one of the axes coincides with the direction of the load. This approach was adopted by Eason et al. (1955/56), with the line force being applied in the x-direction, as shown in Figure 3.3. On that occasion, the Green's functions for both the displacements and stresses were presented. The results were later confirmed by Achenbach (1973), although with a different coordinate system and by using different methods.

If the line load F in an infinite two-dimensional elastic solid (Figure 3.3) varies with time as a Heaviside step function, the displacements u^H (x-direction) and v^H (y-direction) can be obtained either by convolution of Equation (3.4) or by integral transforms. Eason et al. (1955/56) used the latter approach to demonstrate that the displacements and stresses produced by such a force are as given by Equations (3.5) - (3.9). By looking at Equation (3.4), it is clear that the solutions are singular at the P-wave ($v_p t$) and S-wave ($v_s t$) front. Therefore, Equations (3.5) - (3.9) are presented for intervals ($r>v_p t$), ($v_s t<r<v_p t$) and ($r<v_s t$), unless otherwise indicated.

$$\frac{2G\pi\beta^2 r^4}{Fxy\xi}v^H=\begin{cases}0\\ \sqrt{\xi^2-r^2}\\ \sqrt{\xi^2-r^2}-\beta\sqrt{\xi^2-r^2}\end{cases} \qquad (3.5)$$

$$\frac{4G\pi\beta^2 r^2}{F}u^H = \begin{cases} 0 \\ \left(1-\frac{2y^2}{r^2}\right)\xi\sqrt{\xi^2-r^2}+r^2\ln\left(\frac{\xi}{r}+\sqrt{\frac{\xi^2}{r^2}-1}\right) \\ \left(1-\frac{2y^2}{r^2}\right)\xi\left(\sqrt{\xi^2-r^2}-\beta\sqrt{\xi^2-r^2}\right)+ \\ +r^2\left[\ln\left(\frac{\xi}{r}+\sqrt{\frac{\xi^2}{r^2}-1}\right)+\beta^2\ln\left(\frac{\xi}{r}+\sqrt{\frac{\xi^2}{r^2}-1}\right)\right] \end{cases} \tag{3.6}$$

$$\frac{\pi\beta^2 r^2}{Fx\xi}(\sigma_y-\sigma_x)^H = \begin{cases} 0 \\ \left(1-\frac{2y^2}{r^2}\right)\frac{1}{\sqrt{\xi^2-r^2}}+\frac{2}{r^2}\sqrt{\xi^2-r^2} \\ \frac{1}{\sqrt{\xi^2-r^2}}-\frac{2y^2}{r^2}\left(\frac{1}{\sqrt{\xi^2-r^2}}-\beta\frac{1}{\sqrt{\xi^2-r^2}}\right)+ \\ +\frac{2}{r^2}\left(1-\frac{4y^2}{r^2}\right)\left(\sqrt{\xi^2-r^2}-\beta\sqrt{\xi^2-r^2}\right) \end{cases} \tag{3.7}$$

$$-\frac{2\pi\beta^2 r^2}{Fy\xi}\tau_{xy}{}^H = \begin{cases} 0 \\ \frac{2x^2}{r^2}\frac{1}{\sqrt{\xi^2-r^2}}-\frac{2}{r^2}\left(1-\frac{4x^2}{r^2}\right)\sqrt{\xi^2-r^2} \\ \beta\frac{1}{\sqrt{\xi^2-r^2}}-\frac{2x^2}{r^2}\left(\beta\frac{1}{\sqrt{\xi^2-r^2}}-\frac{1}{\sqrt{\xi^2-r^2}}\right)+ \\ +\frac{2}{r^2}\left(1-\frac{4x^2}{r^2}\right)\left(\beta\sqrt{\xi^2-r^2}-\sqrt{\xi^2-r^2}\right) \end{cases} \tag{3.8}$$

$$\frac{\pi\beta^2 r^2}{Fx(\beta^2-1)\xi}(\sigma_y+\sigma_x)^H=\begin{cases}0 & (r>\xi)\\ -\dfrac{1}{\sqrt{\xi^2-r^2}} & (r<\xi)\end{cases} \tag{3.9}$$

In Equations (3.5) - (3.9), r is the radial distance from the origin; G is the shear modulus (Lamé's elastic constant); $\xi=v_p t$ and $\xi'=v_s t$ are the radii of the corresponding P-wave and S-wave fronts; and $\beta=v_p/v_s$.

It should be noted that the stress results converge towards the static values for $t\rightarrow\infty$. Also, while comparing the original equations given by Eason et al. (1955/56) with the finite element solutions in Chapter 4, a mistake in the original solution (probably due to typing) was found. The corrections were made and Equations (3.5) - (3.9) are correctly presented here.

3.2.3 Comparison Between Two and Three-Dimensional Fundamental Solutions

There is a significant difference between the three-dimensional and two-dimensional fundamental solutions for displacements (Equations (3.3) and (3.4), respectively).

In the first case, the wave fronts are spherical. The motions of the points on the surface of a sphere of the radius r exist only for

$$\frac{r}{v_p}\le t\le\frac{r}{v_s}$$

where the instants r/v_p and r/v_s represent the arrival times of P-waves and S-waves, respectively. No motions exist before the arrival of the P-wave and after the arrival of the S-wave.

In the two-dimensional case, the wave fronts are cylindrical. The motions of the points on the surface of a cylinder of the radius r exist for

$$\frac{r}{v_p} \leq t$$

where the instant r/v_p represents the arrival time of the P-wave. Contrary to the three-dimensional case, the displacements continue to exist until $t \rightarrow \infty$. This two-dimensional wave propagation phenomenon is sometimes called diffusion (Eringen & Suhubi, 1975) and is attributable to the fact that the line load signals emitted from points along the *z*-axis (Figure 3.3) continuously arrive at the observation point.

3.3 Half-Space

In 1887, Lord Rayleigh discovered a seismic wave which travels parallel to the surface of an elastic half-space with a velocity slightly less than that of the S-wave. This surface wave decays exponentially into the interior of the half-space and it was later called the Rayleigh wave.

Lamb (1904) investigated four different, but essentially related problems of the propagation of pulses in elastic half-spaces. He treated three-dimensional (point load) and two-dimensional (line load) cases of surface and buried sources. Probably the most important conclusion for the surface source problem was that the largest, nondispersive disturbance at the surface of the far-field is due to the Rayleigh surface wave. Because of the lasting significance of his work, the term 'Lamb's problem' is now used for all elastic half-space problems in which the main interest is in the exact time domain calculations of disturbances emanating from impulsive sources.

Solution techniques for problems of wave propagation in an elastic half-space have changed drastically since the days of Lord Rayleigh and Lamb. Modern integral transform methods (Achenbach, 1973; Miklowitz, 1978) and the appropriate numerical methods are now regarded as standard tools for solving transient

elastodynamic problems. However, in this Section, no reference will be made to the solution techniques and only the results will be discussed.

3.3.1 Buried Source

In Section 3.1, the sources causing seismic waves were divided into external (strong winds and waves, surface and atmospheric explosions, vibrating machine footings) and internal (earthquakes, underground explosions), with respect to the Earth's surface.

If the source is internal to the Earth, its analytical model can be either a concentrated body force acting in an infinite elastic space (Section 3.2), or a P-wave source 'buried' in a half-space. The choice depends on the ratio between the distance of the observation point (from the epicentre) and the depth of the source. Both models are suitable for small distances and large depths, because the disturbances are mostly due to body waves (P- and S-waves). On the other hand, for larger distances and smaller depths, the influence of Rayleigh waves becomes dominant and therefore only the second model is appropriate.

Once the solution for the source buried in a half-space is known, it is usually possible to find the solution for the surface source as a special, limiting case with zero depth (Pekeris, 1955a; Pekeris, 1955b; Miklowitz, 1978). Alternatively, the solution for the surface source problem can be found independently (Sauter, 1950; Lang, 1961).

If the buried source is considered, the load can act as a point load or as a line load. The first case (Figure 3.4a) is a three-dimensional one, while the latter (Figure 3.4b) may be treated as a two-dimensional, plane strain problem.

After Lamb, the two-dimensional problem (Figure 3.4b) with the load in the form of a Heaviside function, was first studied by Lapwood (1949/50) and then by Garvin (1956), who presented closed form solutions for the surface displacements. His plots are reproduced here in Figure 3.5, from where it becomes clear that for $x/h>20$ the

Rayleigh disturbance takes its shape forever and that it does not decay in space and time.

The three-dimensional problem (Figure 3.4a) with the load varying in time as a Heaviside step function, was most thoroughly studied by Pekeris (1955b). The numerical evaluation of his results was summarised by Miklowitz (1978), whose plots for vertical and horizontal surface displacements are reproduced here in Figures 3.6a and 3.6b, respectively. These plots illustrate the following facts:

a) The P-wave wavefront experiences a step discontinuity.

b) For $r/H<1/\sqrt{2}$, the S-wave wavefront experiences a step discontinuity and the Rayleigh wave does not exist.

c) For $r/H>5$, the Rayleigh wave is present with the ever increasing importance as $r/H\rightarrow\infty$.

d) For $H=0$ (the surface source problem), the Rayleigh wave is singular. This case will be examined in detail in the following Subsection.

In one of the first finite element models of wave propagation phenomena (Shipley et al., 1968), the case $r/H=5$, presented in Figures 3.6a and 3.6b, was compared with the numerical results. Further details about the comparison between analytical and numerical solutions will be given in Section 3.4.

Finally, Johnson (1974) collected in one place all Green's functions for the three-dimensional Lamb's problem caused by a buried source. The distinction was made between the contributions from different types of waves.

3.3.2 Surface Source

If the source causing seismic waves is external to the Earth's surface, only one analytical model is possible. Analogies with the infinite space cannot be made because the largest disturbance in the surface far-field is always due to Rayleigh waves.

It will be shown in Chapter 5 that if an interface input scheme is used for earthquake dam-foundation interaction, the seismic excitation (normally considered as an internal source) can be expressed in the form of time-varying forces, external to the foundation medium. Therefore, the solutions of the surface source problems (various Green's functions) are of great importance in the area of time domain soil-structure earthquake interaction.

Again, the load can act as a point or line force. The first case (Figure 3.7a) is three-dimensional and will be discussed first, while the latter (Figure 3.7b) is a two-dimensional, plane strain problem, which will be treated later.

3.3.2.1 Three-Dimensional Problem

Although this Chapter is primarily concerned with transient vibrations, the solution of the problem of wave propagation in a three-dimensional half-space, harmonically excited by a vertically oscillating circular footing (Figure 3.8) was presented in such an informative way by Woods (1968), that it can be used as a reference for much of the following considerations.

Both body and surface Rayleigh waves propagate radially outward from the source (Figure 3.8), but body waves have hemispherical wave fronts. All the waves encounter an ever increasing volume of the material, which decreases the wave energy and eventually reduces the displacements. This phenomenon is better known as radiation damping (or geometrical damping). The amplitude of the body waves decreases in proportion to the ratio of r^{-1} in the interior of the half-space and in proportion to r^{-2} along the surface of the half-space, where r is the radial distance from the source. The Rayleigh wave can be described by two components, vertical and horizontal, each of which decreases as $r^{-0.5}$ along the surface, but considerably more with depth and according to different distributions.

The solutions for the horizontal (radial) and vertical surface displacements of a half-space due to a vertical point impulse converging to the Dirac delta function (Figure 3.7a) were first presented by Lamb (1904), whose results were later repeated by many (Ewing et al., 1957; Graff, 1975; Prakash, 1981). The plots of these results are here reproduced in Figure 3.9. The inital form of both displacement components depends on the shape of the impulse and is due to the P-wave. The displacements associated with the arrivals of the P- and S-wave are directed away from the source and above the surface of the half-space. The final displacements are due to the Rayleigh wave, which, at large distances from the source, may be the only clearly distinguishable wave. They are directed away and down from the source, and attenuate as $r^{-0.5}$, where r is the radial distance from the source.

In an independent procedure, Wolf (1988) has concluded that it is not possible to determine directly the time domain Green's functions for a layered half-space, and that the calculations must be performed in the frequency domain, before returning to the time domain. For the special case of a homogeneous half-space, he derived the surface Green's functions due to vertical and horizontal surface point loads (Figure 3.7a), which vary with time as a Gaussian distribution. This load has a convenient Fourier transform and can be made convergent to the Dirac delta function. The results obtained by Wolf (1988) agree well with those shown in Figure 3.9. However, if the load were precisely in the form of a Dirac impulse, the displacement associated with the arrival of the Rayleigh wave would be infinite.

The solutions for the horizontal (radial) and vertical displacements of a half-space due to a vertical point load varying with time as a Heaviside step function were obtained by Pekeris (1955a). He derived the closed-form solutions for the surface displacements in the case for which the Poisson's ratio is 0.25. These results were later quoted by many and finally used for comparison with the boundary element modelling technique (Manolis & Beskos, 1988). Pekeris' results (Figures 3.6a and 3.6b, case H=0) suggest that the displacements are infinite at the arrival of the

Rayleigh wave and that the disturbance is one-sided (no change of sign). Later, Lang (1961) published integral expressions for the displacements throughout the whole half-space, identifying contributions from different types of waves. Miklowitz (1978) confirmed that the influence of the Rayleigh wave is considerable only very close to the surface and that some of the discontinuities and singularities disappear for a ramp load.

The solutions for the horizontal (radial and tangential) and vertical surface displacements of a half-space due to a tangential point load (Figure 3.7a), varying with time as a Heaviside step function, were obtained and plotted by Chao (1960). He also presented the expressions and plots for the interior of the half-space, but only along the line which is perpendicular to the surface and which contains the point of the applied load.

3.3.2.2 Two-Dimensional Problem

The general displacement field of the half-space in the state of plane strain due to the horizontal and vertical line load in the form of a Dirac delta function (Figure 3.10) was presented by Eringen & Suhubi (1975). It proved difficult to separate the real and imaginary parts for the whole interior of the half-space, but the final solutions for the surface are relatively simple. The expressions given by Sauter (1950) are by far the most compact of all, and are therefore the preferred option here:

For the coordinate system and loading as in Figure 3.10, and for $\gamma = v_s/v_p$ and $\sin\zeta = x/v_p t$, the horizontal displacement u^δ and vertical displacement w^δ on the surface of the half-space are either

$$\begin{Bmatrix} u^\delta \\ w^\delta \end{Bmatrix} = \frac{\gamma \sin^2\zeta \cos\zeta}{v_p v_s t \pi \rho} \begin{Bmatrix} -2\gamma\sqrt{\sin^2\zeta - \gamma^2} \\ \sin^2\zeta - 2\gamma^2 \end{Bmatrix} \frac{\left(\sin^2\zeta - 2\gamma^2\right)\sigma + 2\gamma\sqrt{\sin^2\zeta - \gamma^2}\,\tau}{\left(\sin^2\zeta - 2\gamma^2\right)^4 + 16\gamma^6 \cos^2\zeta\left(\sin^2\zeta - \gamma^2\right)} \quad (3.10)$$

if $v_s t < x < v_p t$, or

$$\begin{Bmatrix} u^{\delta} \\ w^{\delta} \end{Bmatrix} = \frac{\sin^2\zeta}{v_p v_s t \pi \rho} \begin{Bmatrix} \sqrt{\gamma^2 - \sin^2\zeta}\,\tau \\ \gamma\cos\zeta\,\sigma \end{Bmatrix} \frac{1}{\left(\sin^2\zeta - 2\gamma^2\right)^2 - 4\gamma^3\cos\zeta\sqrt{\gamma^2 - \sin^2\zeta}} \tag{3.11}$$

if $0<x<v_s t$.

The solutions for the horizontal and vertical surface displacements due only to a vertical line load converging to the Dirac delta function (Figure 3.7b) were first presented by Lamb (1904). His results were later confirmed for the proper Dirac delta function in the paper by Sauter (Equations (3.10) and (3.11) for τ=0). The general displacement field (in the whole interior and on the surface) was described in the closed form by Forrestal et al. (1966). Eringen & Suhubi (1975) also showed that the general stress field exibits the same singularities as the displacement field. Miklowitz (1978) presented an alternative formulation for the displacements at the surface and at the plane of symmetry (y-axis in Figure 3.7b or z-axis in Figure 3.10). All these authors have used different methods and obtained different formulations, but the results achieved were the same.

Herein, the solution by Forrestal et al. (1966) will be stated because the numerical aspects of the problem have been treated with greatest care. The general displacement field of the half-space due to a vertical line Dirac delta function load (Figure 3.7b) is

$$u^{\delta} = \frac{-\gamma^2}{G\pi}\mathrm{Im}\left(F_1(p)\frac{dp}{dt} - 2\gamma F_2(q)\frac{dq}{dt}\right) \tag{3.12a}$$

$$v^{\delta} = \frac{\gamma^2}{G\pi}\mathrm{Re}\left(F_3(p)\frac{dp}{dt} - 2\gamma^2 F_4(q)\frac{dq}{dt}\right) \tag{3.12b}$$

where p, q, $F_1(p)$, $F_2(q)$, $F_3(p)$ and $F_4(q)$ are complex functions of time and coordinates (Cartesian or polar).

Equations (3.12) can further be used in the convolution integral of Equation (3.1) for obtaining the response to an arbitrary time variation of the excitation. The integration is straightforward except near the various wave fronts, i.e. when singularities of the

Green's functions are encountered, for which Forrestal et al. (1966) have found useful numerical cures.

As already mentioned, Equations (3.12) greatly simplify at the surface and at the plane of symmetry. The former will be analysed in detail in Chapter 4 through the comparison with the finite element model equipped with transmitting boundaries. At this stage, it suffices to say that the horizontal surface displacement vanishes after the arrival of the S-wave, except for a delta function propagating with the velocity of Rayleigh waves. The vertical displacement does not vanish with time but does show an infinite two-sided discontinuity propagating with the velocity of Rayleigh waves. Any continuous load instead of the Dirac pulse would induce the continuous displacement field in the interior and at the surface of the half-space, except for the horizontal surface displacement at the Rayleigh wave front. This disturbance is nondecaying in space and time; and does not change its shape as it propagates, no matter what the time variation of the loading is. In other words, the nature of the Rayleigh disturbance is attributable to the two-dimensional behaviour of the system under consideration, not to the nature of the loading. As in the three-dimensional case, the Rayleigh wave causes dominant displacements in the surface far-field.

Further information about the response of the half-space subjected to the vertical surface line load of the Dirac delta function time behaviour can be obtained by examining the generated waves which establish the character of the motion. The pattern of waves and corresponding wavefronts for fixed time are shown in Figure 3.11. The circular cylindrical P- and S-wave propagate with velocities v_p and v_s, respectively; and cover the regions A and B, respectively. The singular Rayleigh wave propagates along the surface of the half-space with its own speed. The fourth wave occupies the region C and is called the head wave or von Schmidt wave (Achenbach, 1973). The P-wave propagating at the surface (the so-called grazing incidence) generates shear waves with centres at the surface. The envelope of these waves represents the head wave front.

3.3.2.3 Comparison Between Two and Three-Dimensional Surface Source Problems

As in the case of the infinite space (Subsection 3.2.3), there is an important difference between the three and two-dimensional solutions for the surface source half-space problem. The similarities and differences will be demonstrated by comparing the vertical surface displacements due to the vertical Dirac pulse.

For both solutions, the first displacements occur after the arrival of the P-wave. They are opposite to the direction of the load and fairly small until the arrival of the S-wave. Then, they both increase until the occurence of a two-sided singularity (change of sign through infinity) at the arrival of the Rayleigh wave. The displacements are now in the direction of the load. However, the three-dimensional solution converges to zero (Figure 3.9), while the two-dimensional only decreases, exhibiting a tail. This phenomenon was also observed in the case of the infinite space and is attributable to the fact that the signals emitted from all points of the line load continuously arrive to the observation point.

3.4 Numerical Modelling

Sections 3.2 and 3.3 have demonstrated that it is very difficult to obtain the explicit, closed form solutions for even the simplest elastodynamic problems. If the material and geometry of the problem under consideration are more complicated, various numerical methods are often the only alternative. The existing analytical solutions of the simple problems can then be regarded as special cases and can serve as reference examples.

Two main approaches exist in the numerical modelling of elastodynamic phenomena. In the first, the emphasis is on modelling of the governing equations to the extent which facilitates numerical treatment (finite difference method, integral equation method, etc.). The emphasis in the second approach is on the physical discretisation

of either the medium itself or its boundary (Finite Element or Boundary Element Method, respectively). In this Section, the three most popular numerical techniques which can be used for the modelling of infinite and semi-infinite media will be briefly overviewed. As the Finite Element Method is the chosen method for all subsequent analyses, the problems regarding its application will be covered in more detail.

3.4.1 Finite Difference Method

In the finite difference method, it is required that the particular elastodynamic problem is represented in the form of differential equations (ordinary or partial). The domain under consideration is covered by a grid and all the derivatives in the equation are replaced by their central difference approximations, enabling the computation of the displacement vector throughout the points of the grid at time $t+\Delta t$ whenever the displacement vectors are known at time $t-\Delta t$ and t.

The finite difference method for the half-space wave propagation problems was treated by Aboudi (1971), who concentrated on the numerical simulation of sources of different order in the case of a three-dimensional, homogeneous isotropic elastic half-space. The finite difference formulation of the equations of motion was presented, together with the stability requirements. The work was later extended to a nonlinear elastic material, but only for the two-dimensional problem. The reliability of the numerical procedure was examined by comparison with the corresponding linear elastic analytical solutions. The vertical and horizontal displacements due to vertical and horizontal surface loads (Aboudi & Benveniste, 1975); and stresses and displacements due to a vertical surface load (Aboudi, 1976) were presented.

3.4.2 Boundary Element Method

It was mentioned in Section 3.1 that the governing differential equations of elastodynamics with their initial and boundary conditions may be transformed into

integral equations. Such a procedure offers two advantages: the number of spatial dimensions is reduced by one and there is no need to consider the boundary conditions since they are already satisfied by the kernels of the integral equations (Green's functions). For the soil-structure interaction, this means that the relevant equations are mathematically brought to the boundary between the two media, e.g. to the surface of the soil in the case where the embedment is negligible (Sandi, 1960).

Regardless of the problem under consideration, the presence of the boundary of any kind introduces the term 'boundary integral equations'. The numerical procedure which deals with the discretisation of this boundary into elements in order to solve the problem is called the Boundary Element Method. Its underlying theory and many applications were presented in a textbook by Manolis & Beskos (1988). The coupling of boundary and finite elements in the time domain for soil-structure and wave propagation problems was elaborated by Von Estorff & Kausel (1989) and Von Estorff & Prabucki (1990). Papers by Antes (1985) and Von Estorff et al. (1990) concentrated on the transient wave propagation in a two-dimensional half-space. In all these analyses, the typically used Green's functions were those for the infinite space (Equations (3.3) and (3.4)). This means that the problems involving the half-space have to be modelled with a larger number of elements in order to simulate the traction-free surface. The alternative approach is computationally very attractive and consists of using the half-space Green's functions (Section 3.3). Unfortunately, their numerical implementation in a Boundary Element Method computer code has been reported only recently (Triantafyllidis, 1991).

3.4.3 Finite Element Method

In the finite element method, the medium is discretised into finite elements. If the equations of motion are formulated in the time domain, the unbounded nature of the problem (infinite space or semi-infinite half-space) requires the use of extremely large models or special boundary conditions (Hadjian et al., 1974). These boundary

conditions are called transmitting boundaries (or nonreflecting, absorbing, quiet, silent, radiating, anechoic). The best-known spatially and temporally local, frequency independent transmitting boundaries will be presented in Chapter 4.

The implementation of such boundary conditions into finite element systems causes additional computational problems when solving the equations of motion. Some of the transmitting boundaries require explicit time integration procedures and some introduce nonproportional damping. In the latter case, the direct time integration of the equations of motion is, if not the most efficient, certainly the most straightforward way to deal with this problem.

3.4.3.1 Algorithms for Direct Time Integration

There are two general classes of algorithms for direct time integration of equations of motion: explicit and implicit. Both of them predict the response at time $t+\Delta t$, but based on the equilibrium at different instants. Explicit algorithms enforce the equilibrium in time t, and implicit algorithms in time $t+\Delta t$. The best known explicit time integration technique is probably the central difference method, while the Houbolt, Newmark and Wilson-θ methods are the most popular implicit time integration techniques. Both explicit and implicit algorithms have advantages and disadvantages (Goudreau & Taylor, 1972; Belytschko et al., 1975; Hilber et al., 1977; Hulbert, 1991), but in some practical situations (Hughes & Liu, 1978b) neither of them is optimally suited by itself. For such problems, Hughes & Liu (1978a) have presented a new family of implicit-explicit algorithms, for which the finite element mesh simply needs to be divided into the implicit and explicit groups.

Another way to classify time integration algorithms is according to the number of steps. It is sometimes desirable that the solution at time $t+\Delta t$ depends only on the values at time t - these algorithms are called one-step methods. On the other hand, the solution of multistep methods depends on more than one previous time step. The

representatives of one-step methods are the Newmark, Wilson-θ and Hilber-Hughes-Taylor (Hilber et al., 1977) methods. The central difference method is a two-step one, while the Houbolt method is a three-step method.

3.4.3.2 Wave Propagation or Structural Dynamics ?

The direct time integration procedure used for the finite element analysis is closely related to the phenomenon under study. Usually, the dynamic problems are divided into wave propagation and structural dynamics category (Belytschko et al., 1975).

Wave propagation problems are those in which the behaviour at the wave front and its accurate prediction are of the engineering importance. Problems that fall into this category are the shock response due to impact or explosion, and problems in which wave effects such as reflection and diffraction are important. These problems are rich in frequency content, i.e. they have a broad frequency range.

Structural dynamics (or vibration, or inertial) problems are those in which the low frequencies dominate the response. If it were not for the unproportional damping due to the implementation of transmitting boundaries, these problems would be easily solved by the modal superposition technique. A typical problem of this category is the seismic response.

The ratio between the rising time and duration of the load on one side and the time required for a wave to travel across the body of interest on the other side, can serve as a preliminary criterion for categorising the particular problem. If this ratio is greater than three, the problem is often of the inertial type (Belytschko et al. 1977). However, further judgement is needed if a final decision is to be made on whether wave propagation effects are important or not. For example, the overall deformations may be governed by the whole time-history of the loading and only by few lower frequencies, while cracking may depend on the maximum tensile stress at the wave front.

The problems described in Sections 3.2 and 3.3 clearly belong to the wave propagation category. First, the input is in the form of a pulse (Dirac delta or Heaviside step), which implies a broad frequency range. Second, the finite element modelling of infinite and semi-infinite media should be able to deal with the reflection phenomena, namely with the reduction of reflections from artificial boundaries. On the other hand, the overall earthquake response of concrete dams (which is the main subject of this thesis) belongs to the structural dynamics category. In the case of earthquake dam-foundation interaction problems (where the foundation is modelled as a half-space), the distinction between the two categories is not so clear. Numerical studies intended to solve this dilemma will be presented in Chapter 6. Nevertheless, it is always the more stringent category (usually wave propagation) which dictates the time integration procedure. Therefore, the aspects and consequences of the application of direct time integration techniques to wave propagation problems should be described in more detail.

3.4.3.3 Some Aspects of Directly Integrated Wave Propagation Solutions

The troubling aspects of directly integrated wave propagation solutions will be described for a loading with sharp wave front (Heaviside step function load, various pulses), because they are more pronounced in this case than in the case of smooth loading.

Although the real examples will be given in Chapter 4, at this stage it suffices to look at the typical comparison between the finite element wave propagation solution and analytical solution of the same problem (Figure 3.12). The following characteristics of the finite element solution are obvious:

a) The analytical step discontinuity in time is approximated by a finite time rise.

b) The magnitude of the response at the end of that time rise is greater than the analytical step response - the so-called overshooting (Belytschko et al., 1975).

c) The finite element solution oscillates about the analytical solution with a decreasing amplitude at a constant frequency - the so-called spurious oscillation.

It is important to notice that the stated characteristics are not a result of the particular time integration algorithm, as they will be present in the exact solution of any semi-discretised system (Shipley et al., 1968). Furthermore, it is difficult to imagine that any realistic physical system may respond in such an idealised way, as that presented by the 'analytical solution' in Figure 3.12. Unfortunately, by considering problems on purely mathematical grounds, it is not possible to predict which part of the oscillation is 'spurious' and which part is the result of the system's properties. Therefore, all oscillations present in the response of the system have to be treated as unwanted.

There are many wave propagation problems for which analytical solutions do not exist, and it is necessary to establish a correct interpretation procedure of overshot and spuriously oscillated finite element results. Typically, envelopes of the oscillation peaks and valleys are drawn, and a single curve is drawn midway between them (Shipley et al., 1968). This procedure is shown in Figure 3.12. Obviously, overshooting and spurious oscillations are not desirable properties. Several methods are available for their reduction, among which the most commonly used (Belytschko et al., 1975) are the use of dissipative time integration procedures, i.e. the introduction of numerical (algorithmic) damping; the postprocessing of solutions by digital filters; and the preprocessing of input loadings by digital filters.

The introduction of algorithmic damping (numerical dissipation) is the easiest way to control the spurious high-frequency oscillations and to smooth the overall finite element solution. Numerous time integration algorithms possess this property, and the best known are:

a) The Newmark family of methods with parameter values of $\gamma>0.5$ and $\beta>(\gamma+0.5)^2/4$. $\gamma=0.5$ is a nondissipative case, and the dissipation of the algorithm increases with γ (Hilber et al., 1977).

b) Wilson-θ method. Even for the usual θ=1.4, the method is thought to be highly dissipative.

c) Houbolt method.

d) Hilber-Hughes-Taylor method. A three parameter family of algorithms which contains the Newmark family and introduces a new form of dissipation, the so-called negative α-dissipation.

Ideally, an algorithm should eliminate spurious high-frequency oscillations after only one time step and this property is called asymptotic annihilation. Hulbert (1991) has proved that the only unconditionally stable, second-order accurate, three-step method possessing asymptotic annihilation is Houbolt's method. Unfortunately, Houbolt's method excessively damps the lower frequencies and does not permit parametric control over the amount of dissipation. The Newmark and Wilson methods damp the lower frequencies to a lesser extent and permit parametric control over the amount of dissipation.

It was already mentioned that low frequencies are dominant in the structural dynamics problems. Since the finite element mesh can reproduce these frequencies easily, the accuracy of the chosen direct time integration method depends almost solely on the temporal discretisation, i.e. on the time step. In wave propagation problems, the accuracy of the chosen direct time integration method depends not only on the temporal discretisation, but also on the spatial discretisation. The current state-of-the-art finite element wave propagation analysis recommends only uniform meshes of low-order elements (Laturelle, 1989; Wang et al., 1992). If nonuniform (irregular) meshes are used, the elements of different stiffness act as material interfaces while the coarser part of the mesh eliminates the frequencies beyond its own resolution. Laturelle (1989) has demonstrated that the time step should be neither too big nor too small, and that the Newmark integration method is more efficient than the central difference method, which is contrary to the common belief that the explicit algorithms perform better in wave propagation problems. This will be investigated further in

Chapter 4. Finally, for the Newmark average acceleration method, Wang et al. (1992) proposed a new criterion for spatial and temporal discretisation based on the minimisation of the combined error due to amplitude dissipation and velocity dispersion. When compared to the standard one, this criterion not only improves the accuracy - it is also computationally more efficient.

3.5 Concluding Remarks

Very often, in earthquake response analyses of concrete dam-foundation systems, geological conditions at real concrete dam sites require the foundation modelled as a semi-infinite medium. Prior to any further, more complicated interaction analyses (Chapters 6, 8 and 9), simple computational models of the foundation alone need to be verified through the comparison with the available theoretical solutions (Chapter 4). Therefore, the theory of homogeneous, isotropic and elastic infinite and half-spaces has been extracted out of the broader environment of elastodynamics by presenting the relevant Green's functions. Half-space solutions for surface sources are particularly important. Priority was given to two-dimensional solutions, which are more appropriate for concrete gravity dams. Alternatively, three-dimensional solutions would have to be used for arch dams.

The finite difference, finite element and boundary element methods of numerical modelling have been briefly described. Although all of them are able to represent the foundation alone, only the last two can be used for interaction problems. While the boundary element method is confined to the linearly elastic media, the finite element method can be used in the case of nonlinear foundations, which is a considerable advantage. However, the extent of the finite element mesh (in the otherwise infinite medium) has to be determined first for the linear case. Also, in order to model the

energy radiation conditions, the foundation boundary should be equipped with transmitting boundaries.

Once the finite element method has been chosen for the modelling of earthquake dam-foundation interaction, the only remaining problem is to solve the dynamic equation. The most straightforward way to do this is by direct time integration. If the loading has a sharp wave front and/or the boundary reflection conditions are severe, the problem falls into the wave propagation category. This implies that the construction of spurious oscillation envelopes and introduction of algorithmic damping are needed for the correct interpretation of finite element results. The new criterion by Wang et al. (1992) can be used for spatial and temporal discretisation. The smoother the loading is, the problem is more likely to fall into the structural dynamics category. This implies that the requirements for spatial and temporal discretisation are less stringent.

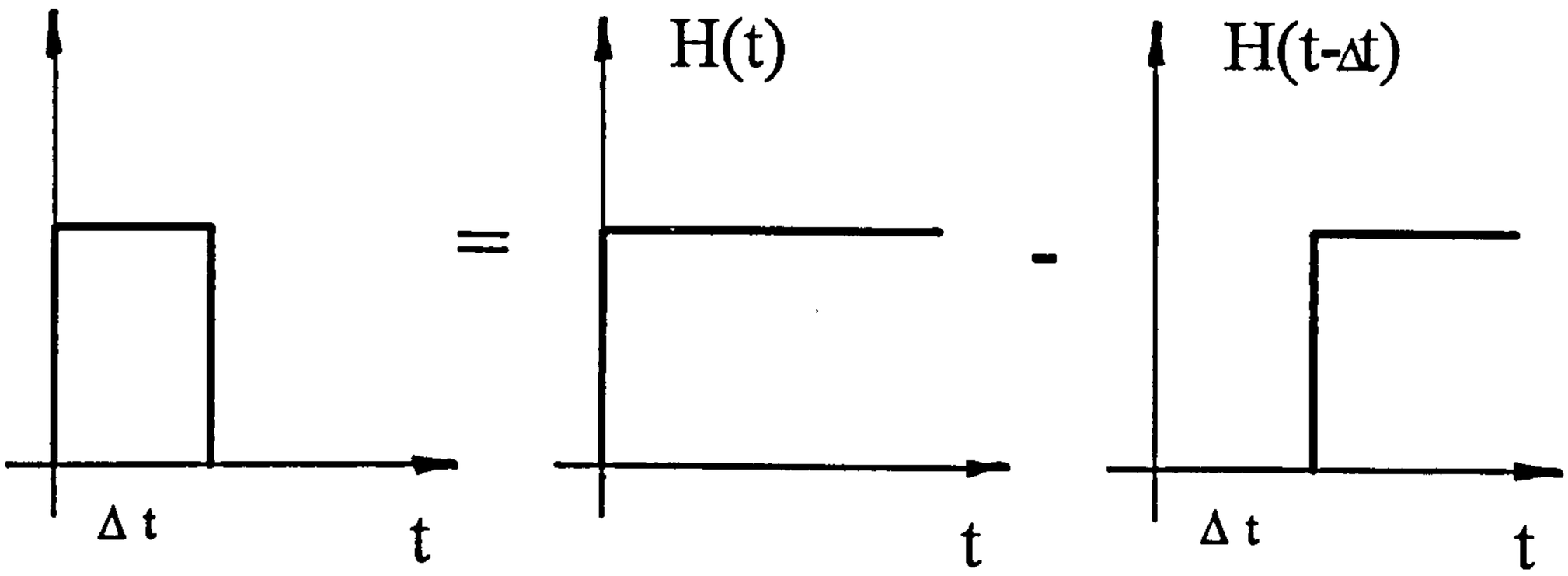

Figure 3.1 - Rectangular pulse as the difference between two Heaviside functions

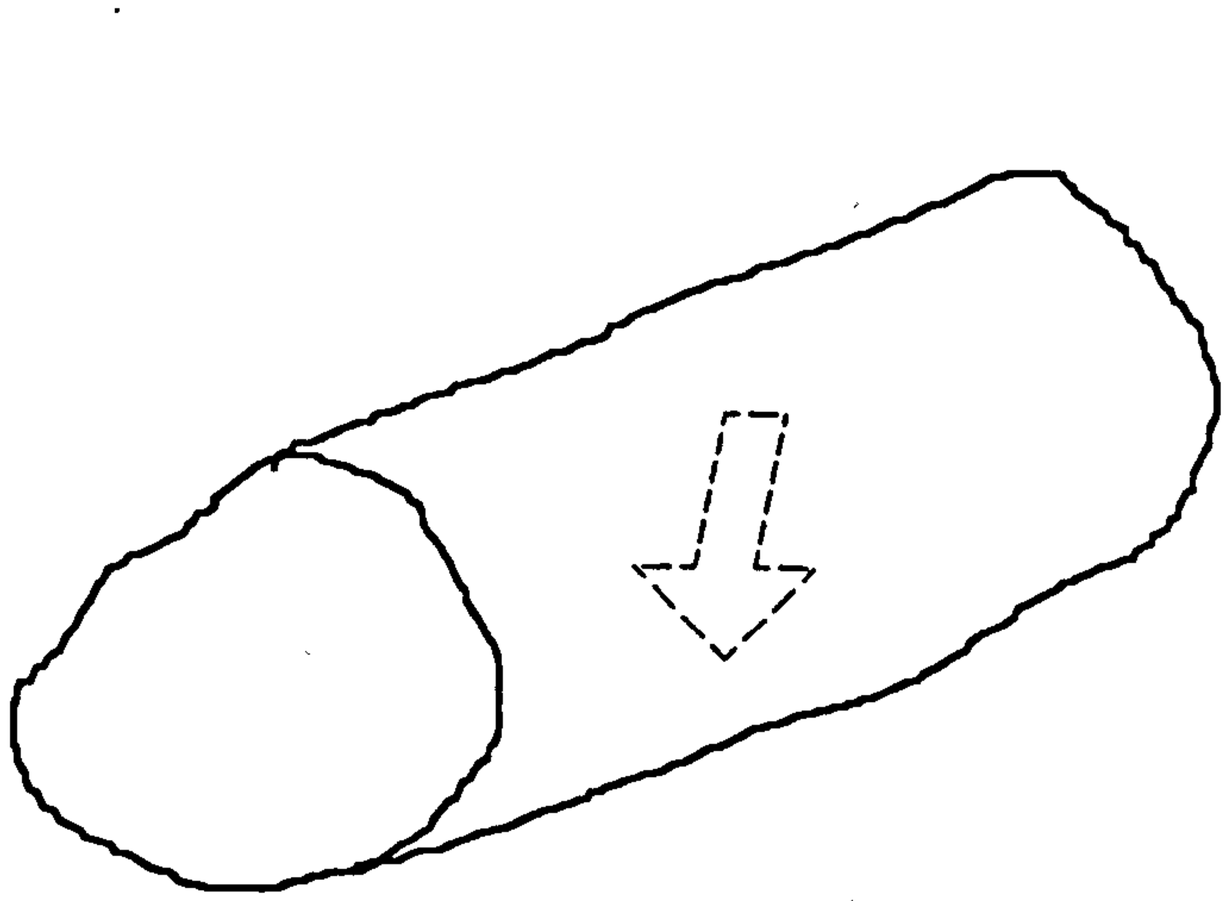

Figure 3.2a - Three-dimensional infinite space (point load)

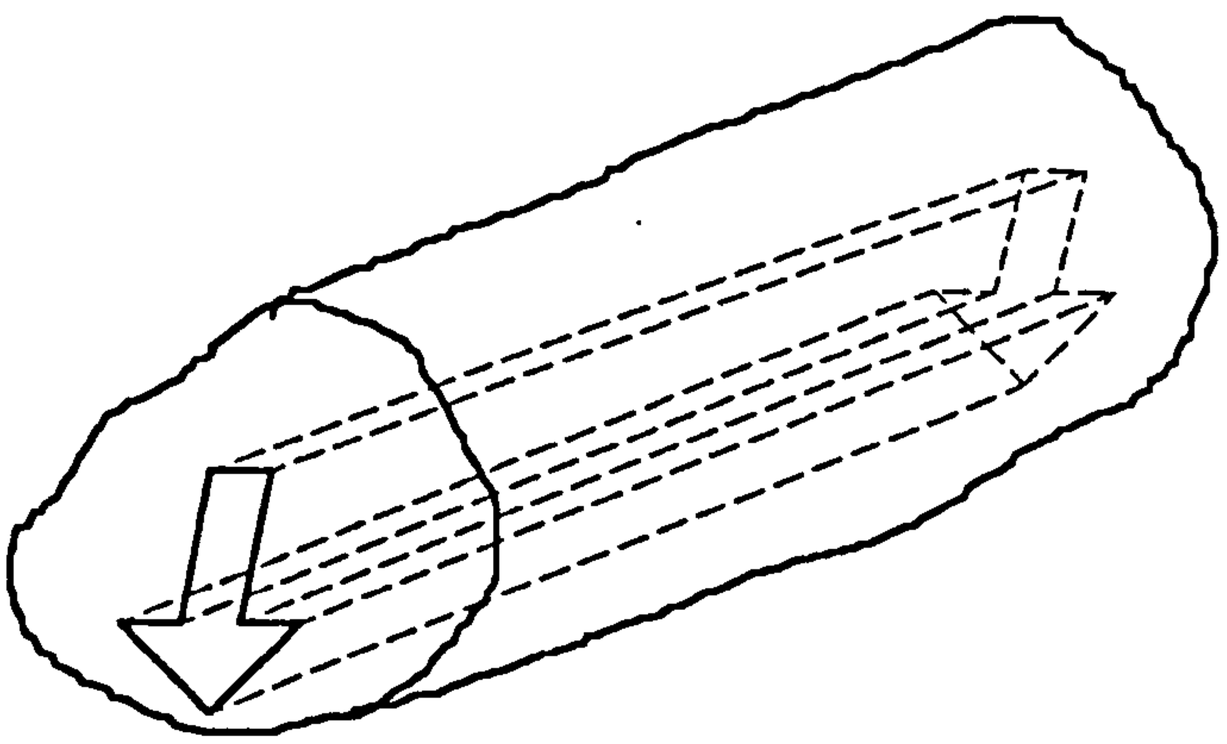

Figure 3.2b - Two-dimensional infinite space (line load)

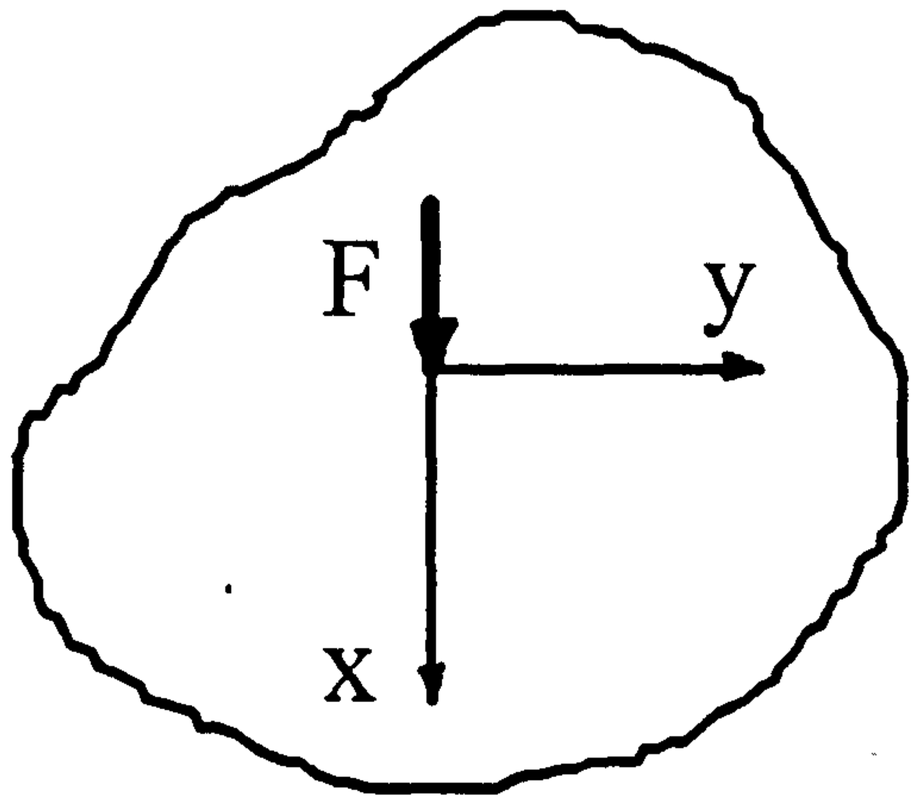

Figure 3.3 - Line force in the *x*-direction

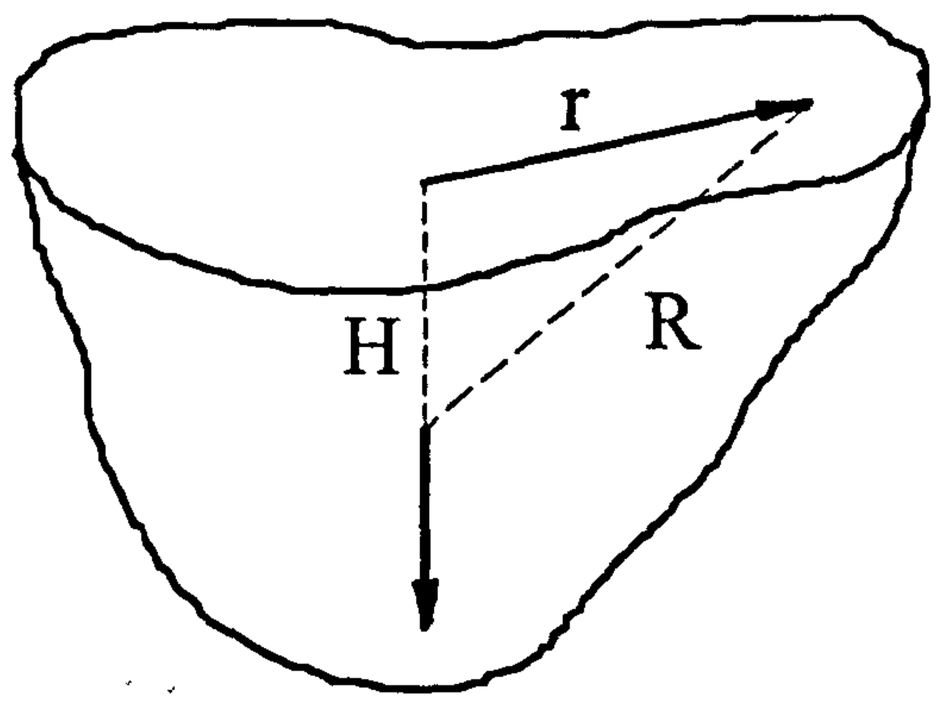

Figure 3.4a - Three-dimensional half-space (buried point load)

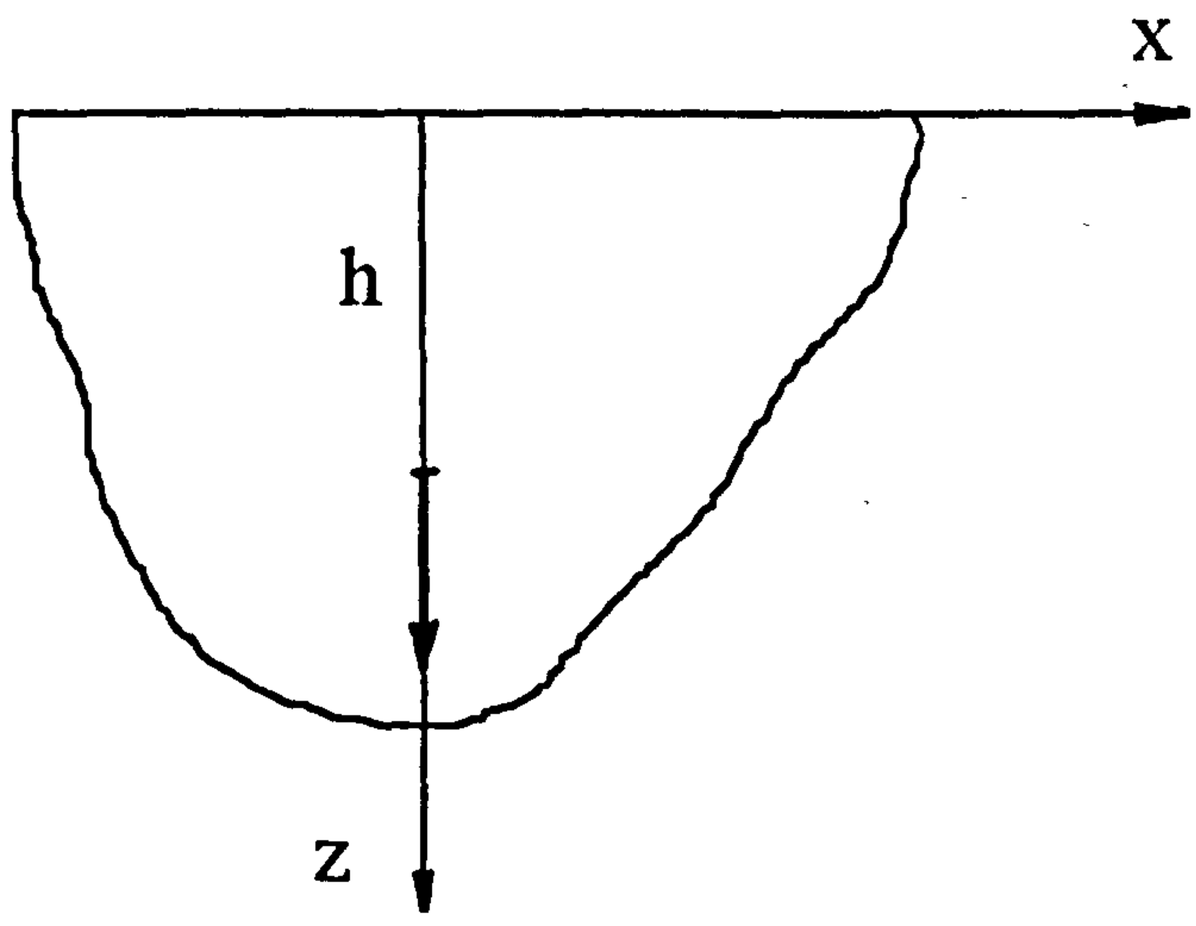

Figure 3.4b - Two-dimensional half-space (buried line load)

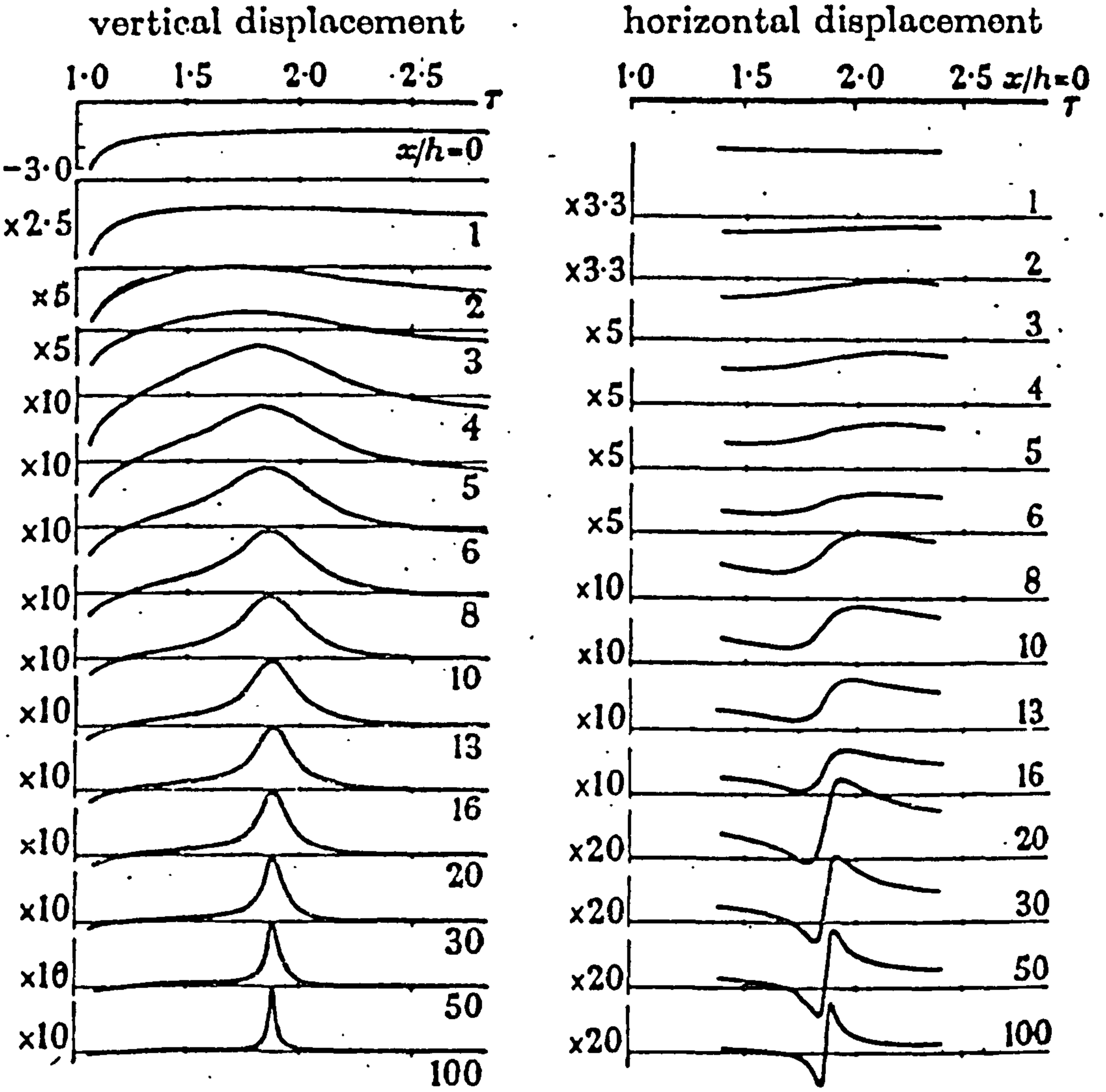

Figure 3.5 - 2-D vertical and horizontal surface displacements for different *x/h*

(Garvin, 1956)

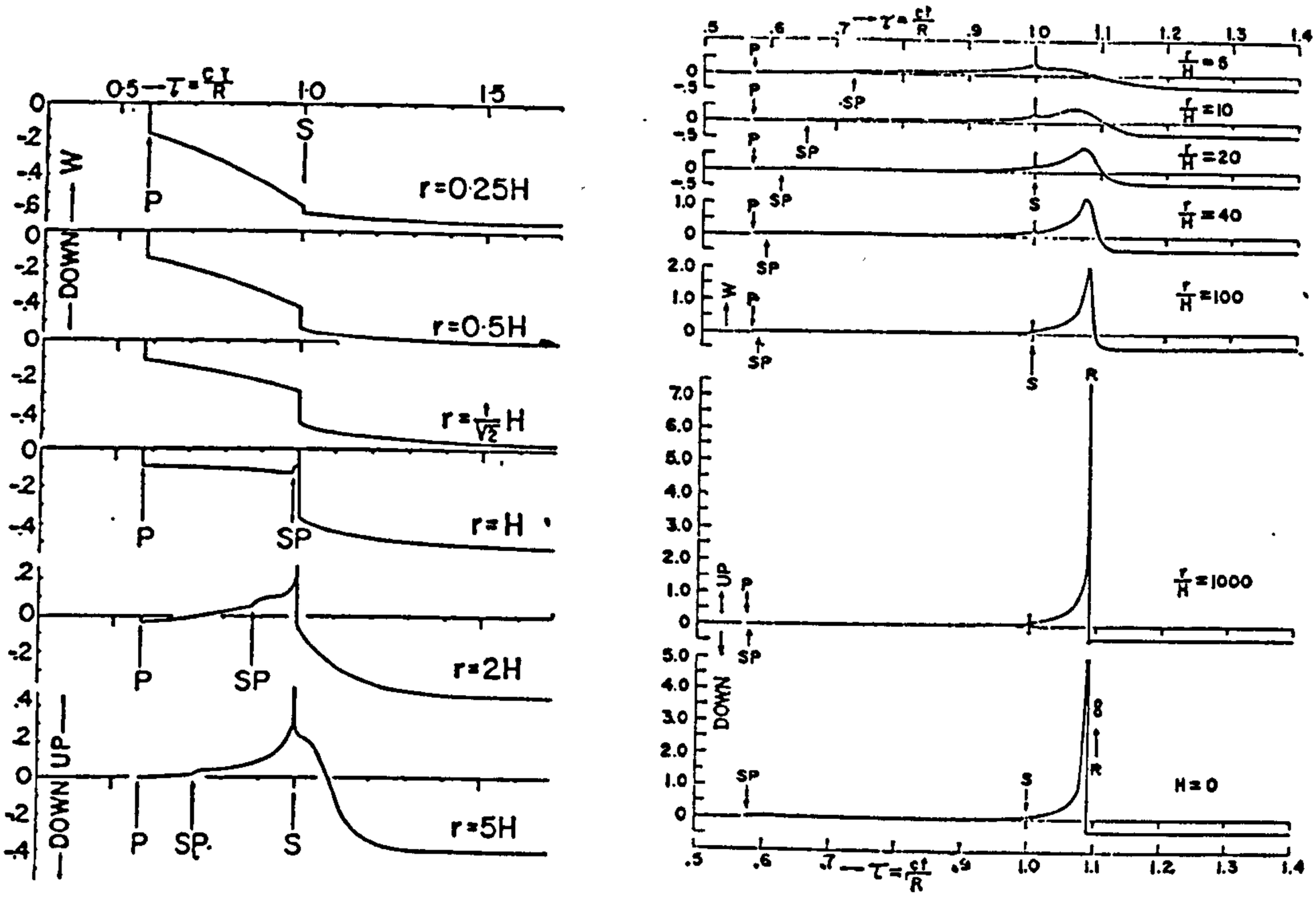

Figure 3.6a - 3-D vertical surface displacements for different *r/H*

(Miklowitz, 1978)

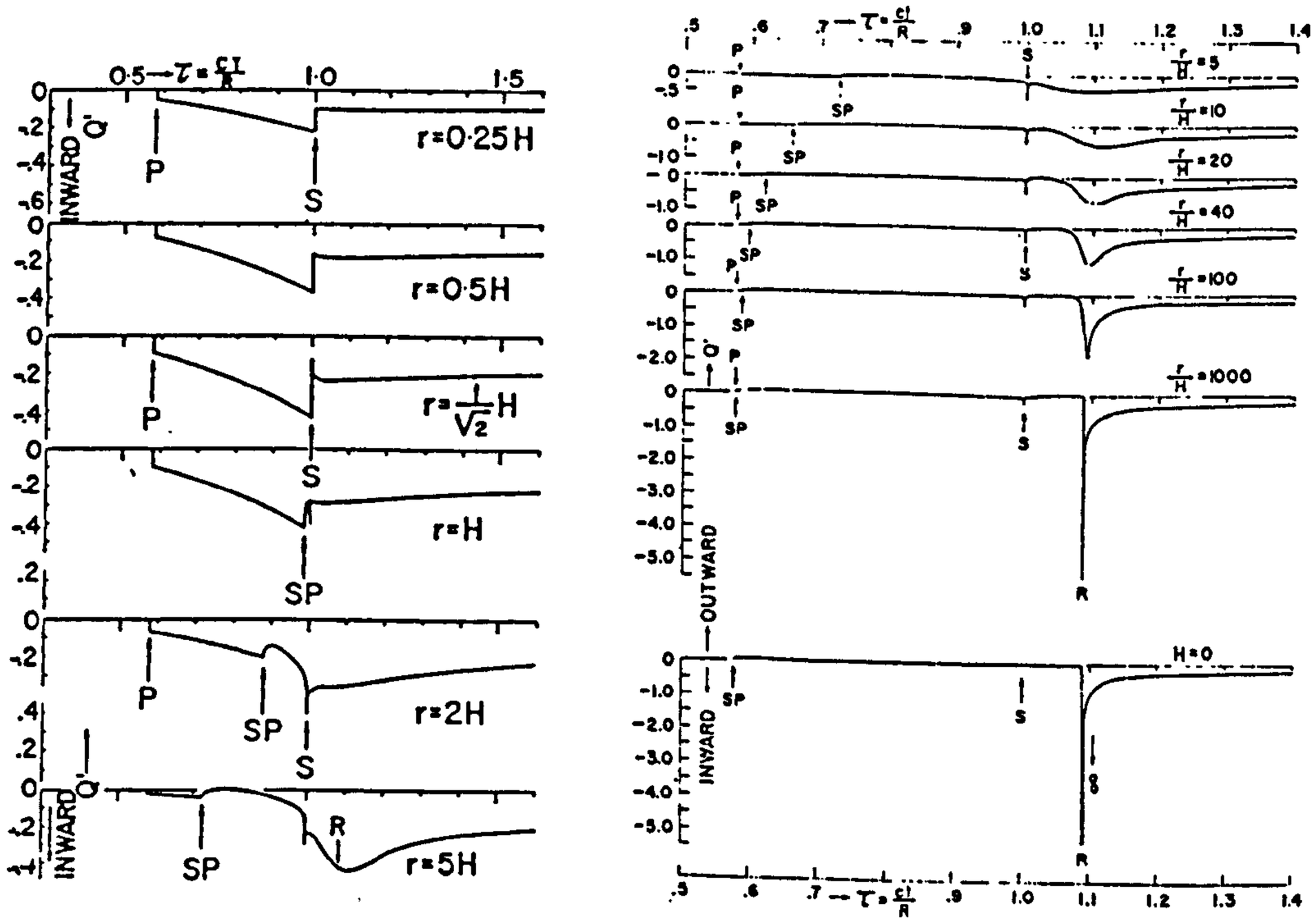

Figure 3.6b - 3-D horizontal surface displacements for different *r/H*

(Miklowitz, 1978)

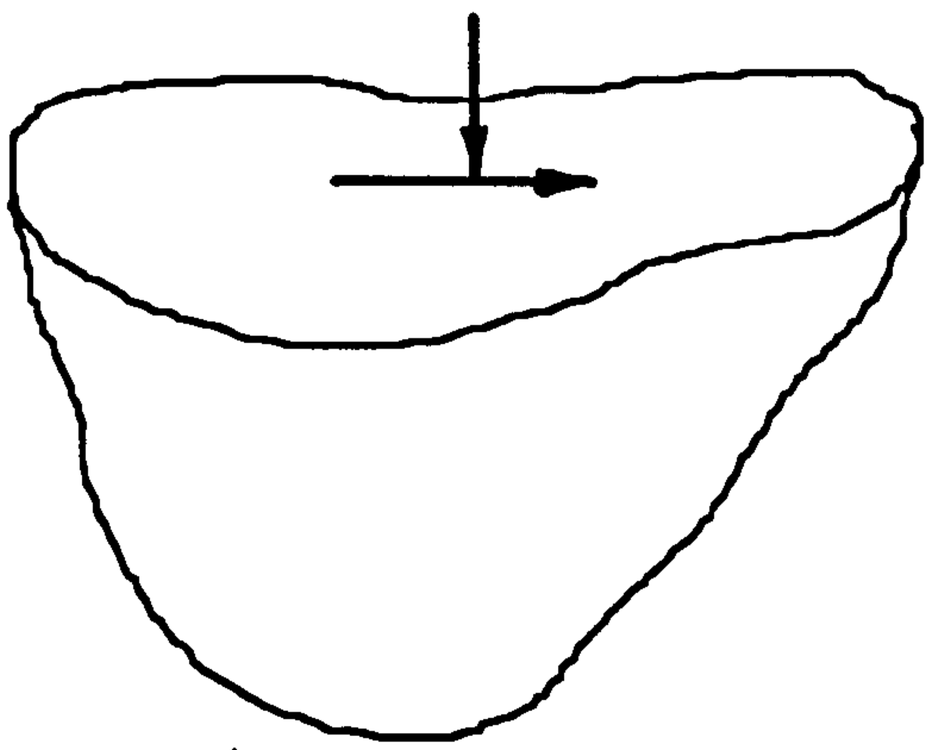

Figure 3.7a - Three-dimensional half-space (surface point load)

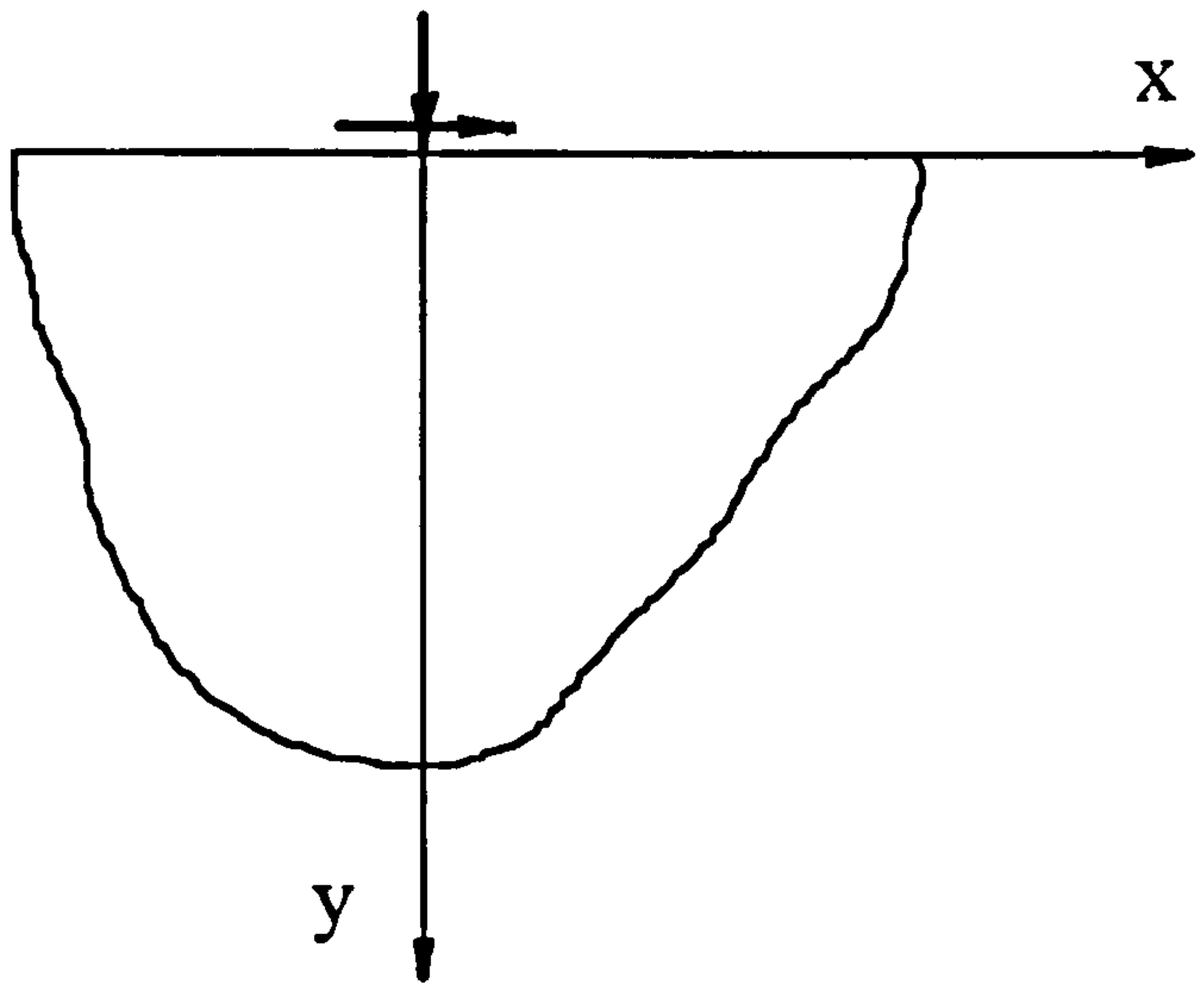

Figure 3.7b - Two-dimensional half-space (surface line load)

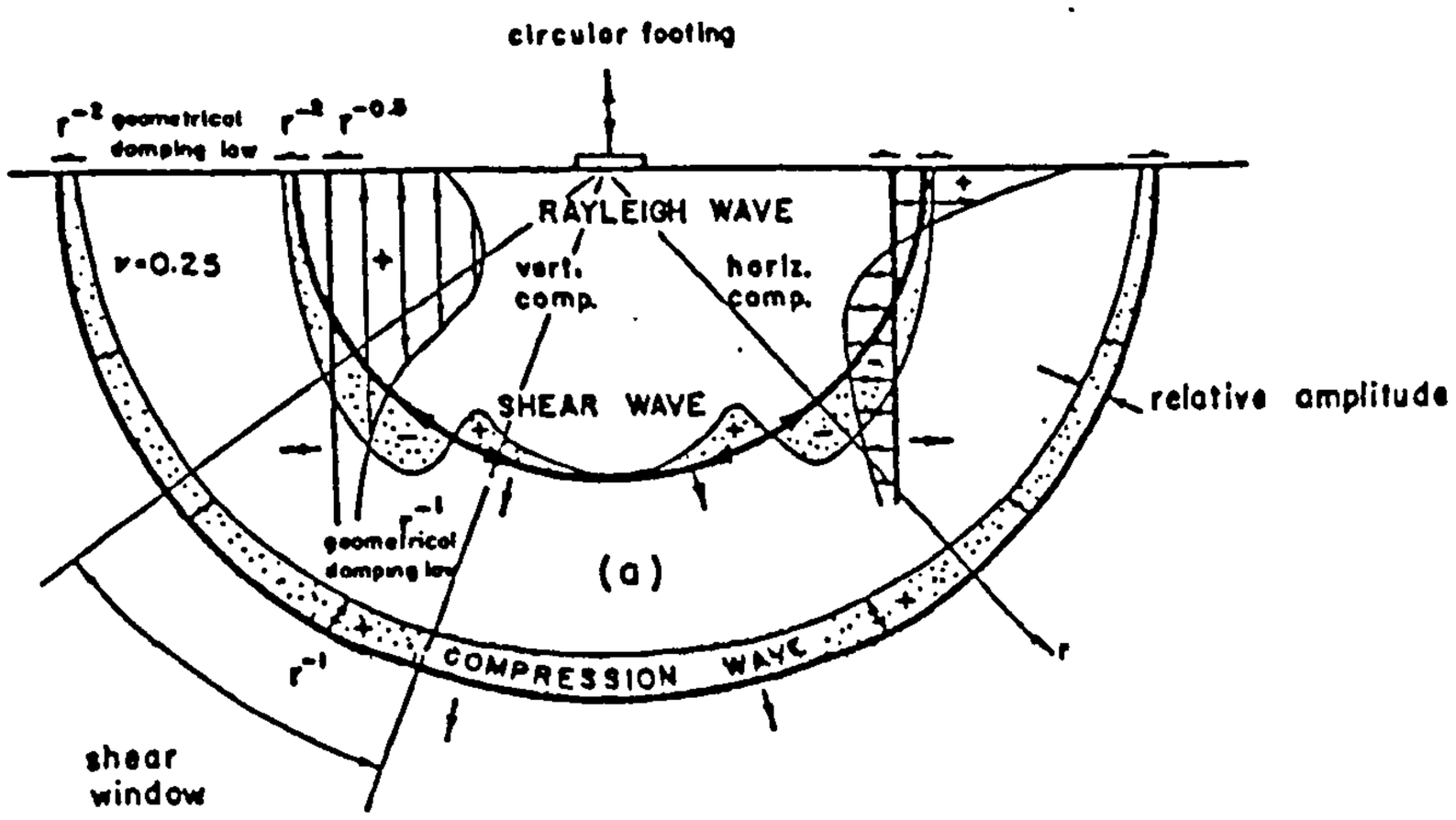

Figure 3.8 - Displacement waves in a 3-D half-space (vertical point load)

(Woods, 1968)

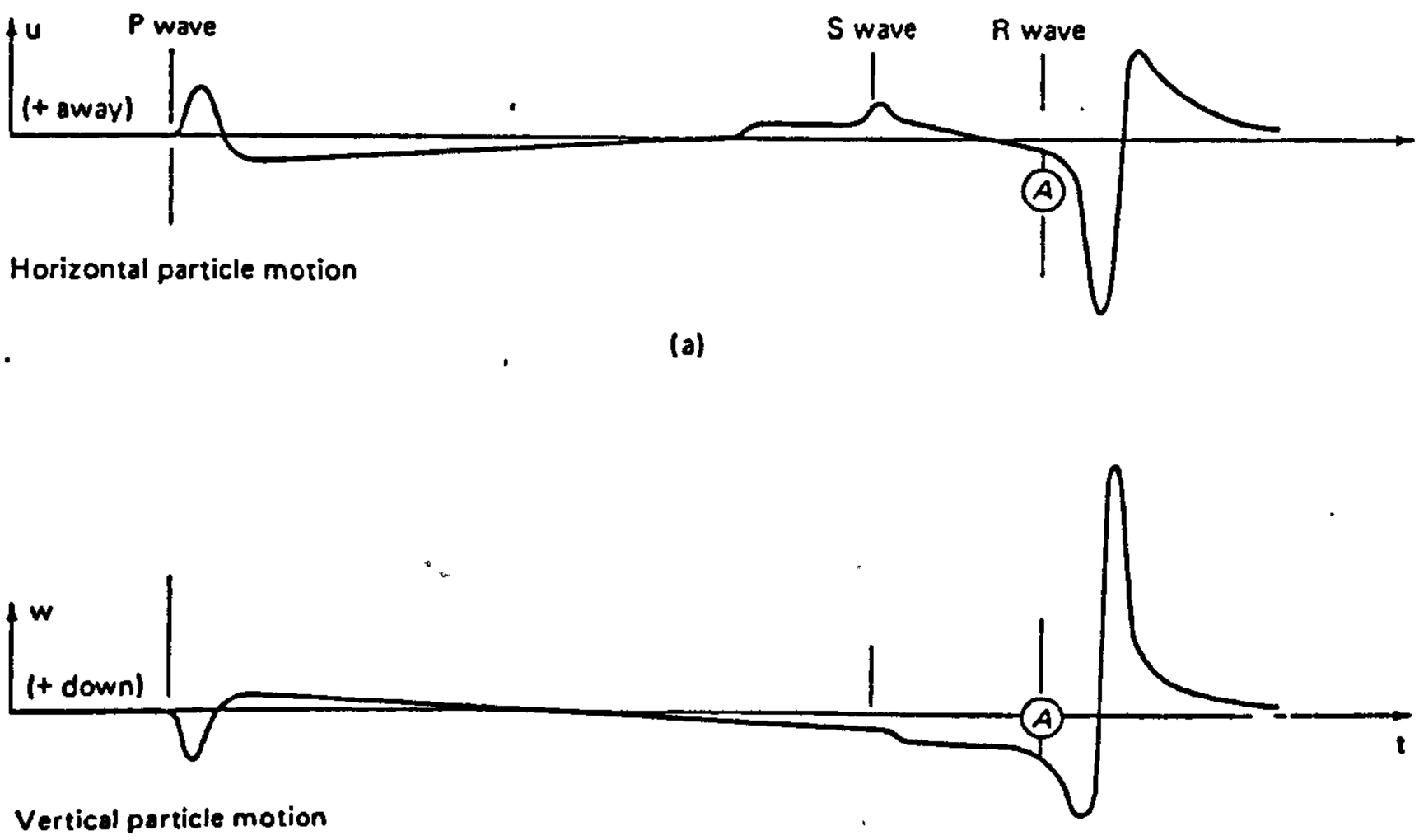

Figure 3.9 - 3-D horizontal and vertical surface displacements (vertical point load)

(Prakash, 1981)

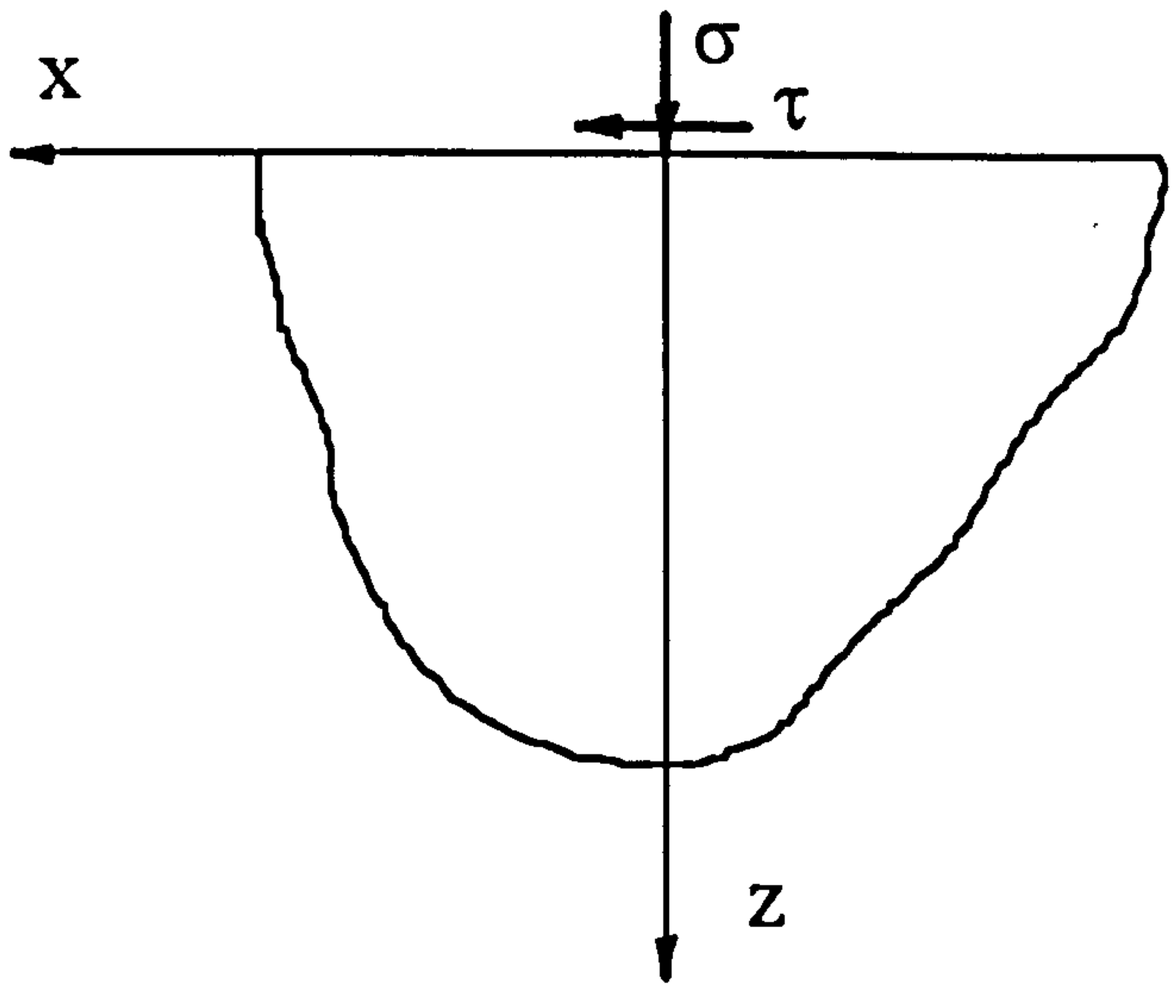

Figure 3.10 - 2-D half-space coordinates and loading for the Sauter's solution

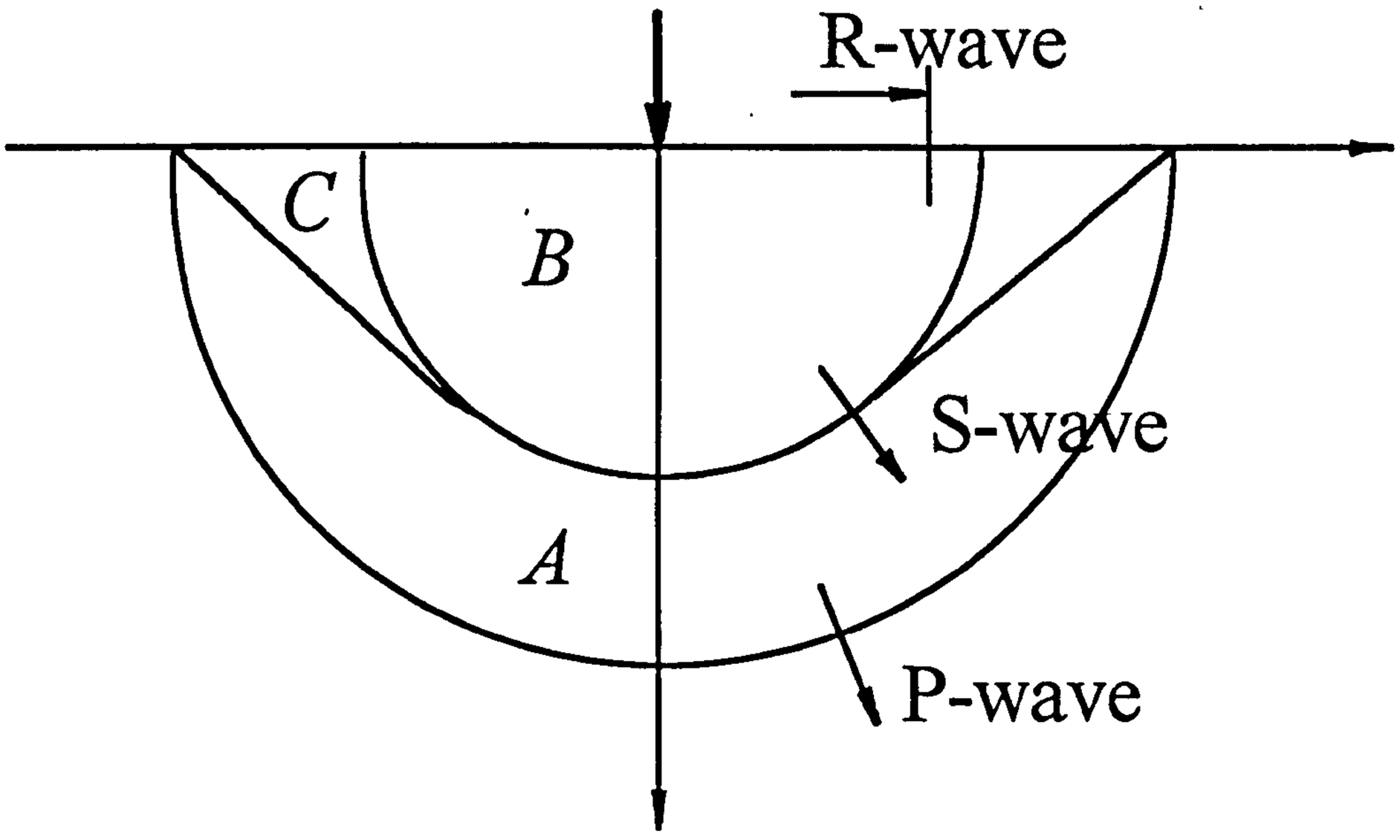

Figure 3.11 - Wavefronts in a 2-D half-space (vertical line load)

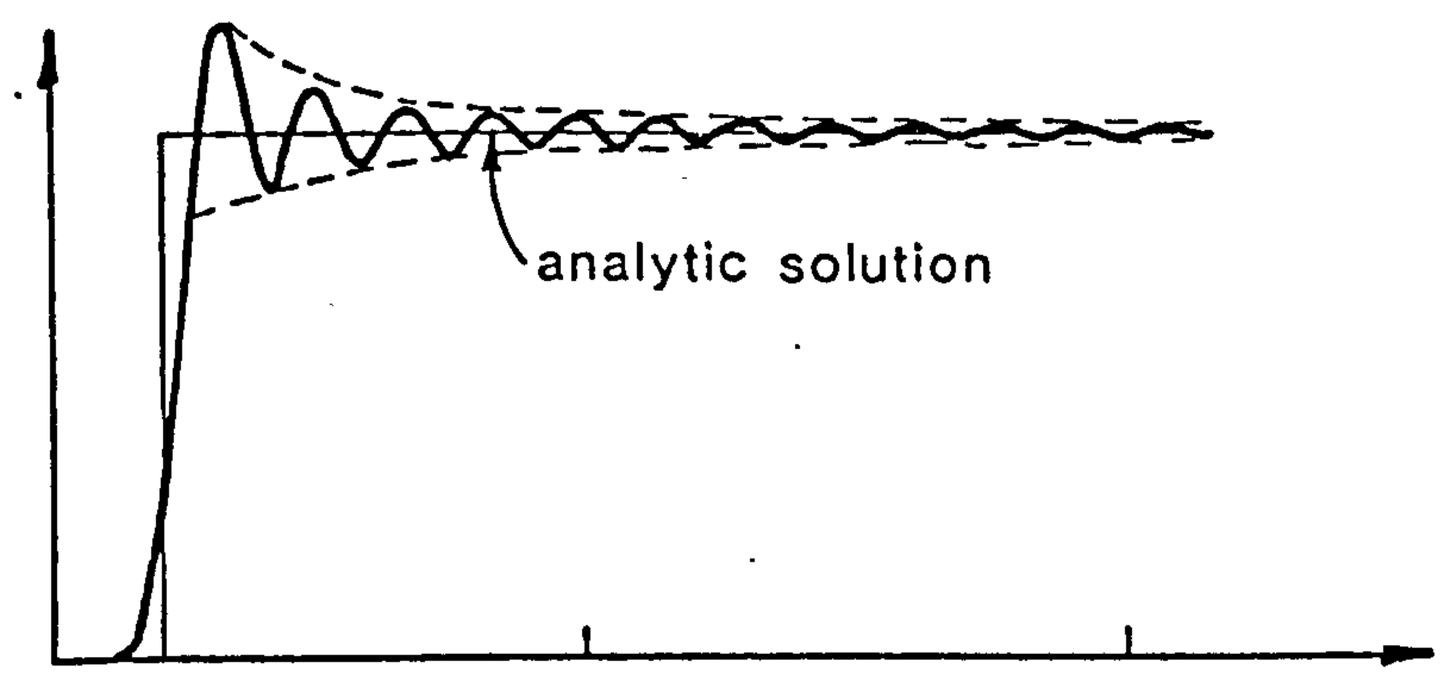

Figure 3.12 - Finite element and analytical wave propagation solutions

Transmitting Boundaries and their Applications to Linear Analyses of Infinite and Half-Space Foundations

The theory of infinite and half-space media was presented in Chapter 3. The possibilities and problems of numerical modelling were also identified. If it is intended to use the Finite Element Method in the time domain (as it is, for all the analyses in the subsequent Chapters), the unbounded nature of the problem requires the introduction of special boundary conditions. These boundary conditions are best known as transmitting boundaries.

In this Chapter, after examining their role in the light of the ultimate aim of this work (nonlinear dam-foundation interaction), some of the transmitting boundaries will be presented. The numerical examples from the literature will be then reviewed in order to identify which transmitting boundary seems most promising for modelling half-space foundations. The chosen transmitting boundary will be subjected to a number of numerical tests whose objectives are to confirm its suitability and to determine its parameters more closely.

Once the concrete dam is introduced and coupled with the foundation (Chapter 5), the seismic input mechanisms for the analysis of the interaction system will become available. This will enable another scrutiny of the chosen transmitting boundary in Chapter 6, now as part of the whole dam-foundation system.

4.1 Transmitting Boundaries and Concrete Dam-Foundation Interaction

Concrete dams are huge structures and their influence on the supporting medium cannot be neglected. In a proper analysis, the foundation must be included in the computational model. For finite element analyses, this means that it is necessary to model and discretise a significant amount of foundation.

In static problems, the foundation material simply introduces the flexibility of the support medium. Although there are many ways to truncate the foundation finite element mesh (a very simple and extremely effective method has recently been presented by Sharan (1992)), the standard procedure is to prescribe zero displacements at a certain distance from the dam.

In dynamic (earthquake) analyses of concrete dam-foundation systems, such a procedure is possible only if the truncation is made very far from the dam. The energy radiated away from the dam is carried by the outgoing seismic waves which must not reach the artificially created boundary during the analysis. For realistic materials and velocities of seismic waves, it becomes clear that the size of the foundation for such an analysis would have to be enormous and definitely not feasible within the current state-of-the-art finite element computations. The only remaining option is to truncate the foundation much closer to the dam, knowing that the outgoing seismic waves would impinge and reflect from the artifically created boundary (this would happen even if the boundary is free of any prescribed displacements or stresses). The fact that the seismic waves have been reflected instead of being transmitted through the boundary has serious consequences to the energy balance of the dam-foundation system. Practically the whole earthquake energy remains trapped in the system causing the increase of its response.

Obviously, for a valid dam-foundation analysis, a mechanism for the elimination of spurious reflections has to be found and implemented into finite element

computational procedures. In other words, the radiation conditions and radiation damping (explained in Chapter 3) have to be simulated, if not satisfied. In time domain analyses, the practical choice is limited to the following two approaches:

a) The internal material damping of the foundation is artificially increased in order to reduce the wave amplitudes before and after the reflection at the boundaries (Toki & Miura, 1983; Hall, 1986). This approach may achieve satisfactory results in some cases, but highly unsatisfactory results in other cases (Wolf, 1988). Therefore, it cannot be generally recommended for all dynamic problems. Its performance will be studied in the numerical tests later in this Chapter.

b) The development of various transmitting (or non-reflecting, quiet, silent, absorbing, radiating, anechoic) boundaries. They are usually placed at the edges of the foundation finite element mesh in the attempt to simulate the transmission of the outgoing seismic waves. Generally, they can be divided into two groups: consistent and local boundaries.

If the boundaries are able to absorb perfectly all types of waves they are called consistent boundaries. Unfortunately, the force-displacement relationship on such a boundary is frequency dependent which means that it can be properly formulated only in the frequency domain. Moreover, the frequency dependent consistent boundaries are global in space, i.e. they couple all the boundary nodes (Lysmer & Waas, 1972). Wolf (1988) has demonstrated that the reformulation of consistent boundaries in the time domain causes time coupling in addition to space coupling. This means that the information from all the nodes on the boundary and from all the previous time steps are required in order to advance just one step in a transient analysis, which amounts to the boundary element formulation, mentioned in Chapter 3.

Several procedures have been developed to overcome the above deficiencies. They all lead to boundary approximations that are local both in space and time, and have therefore been named local transmitting boundaries. Their main properties are

frequency independence and the use of information only from neighbouring nodes and from a few recent time steps. Ideally, local transmitting boundaries should be able to handle approximately all types of waves. Because of their approximate nature, the choice of their location (i.e. the place where the foundation finite element mesh may be truncated) is not arbitrary. It depends on the frequency content and duration of the excitation, and the amount of internal foundation damping. Although some general recommendations are available (Wolf, 1988), the best practice is to determine the location of the boundary independently for every particular case. For earthquake concrete dam-foundation interaction this will be established in Chapter 6. Some of the best known local transmitting boundaries will be presented in the following sections.

The problems of energy radiating away from the dam are not confined only to the foundation; they exist in the reservoir, although not on the same scale. After Weber et al. (1990) discovered that local transmitting boundaries typically used for energy absorption in solids (foundations) are not appropriate for fluids (reservoirs), computationally expensive solutions dominated until Yang et al. (1993) suggested an explicit time-domain transmitting boundary specially designed for dam-reservoir interaction.

4.2 Viscous Boundary

The viscous boundary formulation was first proposed for two dimensional elastic wave problems by Lysmer and Kuhlemeyer (1969) and is therefore often called Lysmer-Kuhlemeyer standard viscous boundary. After its huge success, White et al. (1977) suggested a way to improve its performance. Their boundary was named the 'unified viscous boundary'. Both standard and unified viscous boundaries may be

implemented in existing finite element computer codes in two ways - using either consistent or lumped viscous damping matrices.

4.2.1 Standard Viscous Boundary

The fact that a viscous damper is the exact boundary solution for one dimensional propagation of longitudinal waves in a semi-infinite prismatic rod prompted Lysmer and Kuhlemeyer (1969) to extend this principle to a two dimensional, homogeneous, isotropic and linear elastic foundation. They assumed that the stress boundary conditions may be expressed as

$$\begin{Bmatrix} \sigma \\ \tau \end{Bmatrix} = \begin{bmatrix} \rho a v_p & 0 \\ 0 & \rho b v_s \end{bmatrix} \begin{Bmatrix} \dot{u} \\ \dot{v} \end{Bmatrix} \qquad \text{or} \qquad \boldsymbol{\sigma} = \mathbf{D}\,\dot{\mathbf{u}} \tag{4.1}$$

in which σ and τ are the normal and shear stress respectively; $\dot{u}$ and $\dot{v}$ are the normal and tangential velocities respectively; ρ is the mass density; v_p and v_s are the velocities of P-waves and S-waves respectively; and a and b are dimensionless parameters.

As the first step in the analysis of the boundary, geometric wave propagation properties of the incident P- and S-waves were considered. In the second step, a criterion for the ability of the viscous boundary to absorb impinging elastic body waves was established - the ratio between the energy of the reflected waves (E_r) and the energy of the incident waves (E_i). For given parameters a and b, the energy ratio E_r/E_i depends on the incident angle Θ ($\Theta=0^0$ coincides with the boundary while $\Theta=90^0$ is normal to the boundary) and Poisson's ratio μ. For $\mu=0.25$ and incident P- and S-waves, the variation of the energy ratio with Θ is shown in Figure 4.1. It is obvious that the free boundary ($a=b=0$) and practically fixed (rigid) boundary ($a=b=100$) reflect almost all the energy. The same Figure shows that nearly perfect absorption is obtained for angles $\Theta>30^0$ and for $a=b=1$. For $\Theta=90^0$ the boundary is perfect.

Lysmer and Kuhlemeyer (1969) also tested the performance of the viscous boundary for the absorption of Rayleigh waves. If perfect absorption is to be achieved (the so-called Rayleigh viscous boundary), a and b need to be functions of the angular frequency ω, depth under the free surface z, and Poisson's ratio μ. Figure 4.2 shows this dependence for μ=0.25, where k is the wave number ($k=\omega/v_r$, v_r being the velocity of Rayleigh waves). Clearly, the Rayleigh viscous boundary can be designed with variable a and b for one frequency only, which makes it suitable for steady-state analyses. In transient time-domain analyses, the frequency ω has to be substituted somehow. This problem will be examined in detail in Chapter 6. On the other hand, if constant values for a and b are used throughout the depth of the foundation (e.g. $a=b=1$), it was thought that insufficient absorption of Rayleigh waves would occur.

4.2.2 Unified Viscous Boundary

White et al. (1977) have developed the so-called unified viscous boundary applicable to anisotropic foundations and introduced some improvements with respect to the standard viscous boundary. For the sake of comparison with other boundaries, only the results for isotropic media under plane strain conditions are presented.

Starting from the initial estimates, a numerical search is made for the optimal values of a and b, i.e. the values which maximise the efficiency of the boundary and minimise the amplitudes of the reflected waves. White et al. (1977) adopted a somewhat different measure of the boundary absorption ability than Lysmer and Kuhlemeyer. The values of a and b which satisfy the above requirements depend on Poisson's ratio and are as follows:

μ	0.05	0.01	0.15	0.20	0.25	0.30	0.35	0.40	0.45
a	0.967	0.975	0.982	0.986	0.986	0.986	0.992	1.007	1.011
b	0.761	0.756	0.751	0.747	0.744	0.742	0.740	0.746	0.773

4.2.3 Consistent and Lumped Approach to Viscous Boundary

The presence of the viscous transmitting boundary at the edges of the foundation finite element mesh gives rise to the radiation damping matrix $\mathbf{C}_r$. It can be added to the internal damping matrix or treated as the only cause of damping in the foundation. According to the analogy with consistent and lumped mass matrices in the finite element method formulation, similar procedures may be applied to damping matrices. The consistent radiation damping matrix (not to be confused with consistent transmitting boundary) can be calculated from

$$\mathbf{C}_r = \int_A \mathbf{N}^T \mathbf{D} \mathbf{N} \, dA \tag{4.2}$$

where **N** is the element shape function matrix for elements over the area A (hence the name consistent), and where **D** is the nodal stress-velocity matrix from Equation (4.1). Equation (4.2) for the 4-noded finite square element of length l at the foundation boundary (Figure 4.3) becomes:

$$\mathbf{C}_r = \frac{\rho l}{6} \begin{bmatrix} 0 & 0 & 0 & 0 & 0 & 0 & 0 & 0 \\ 0 & 0 & 0 & 0 & 0 & 0 & 0 & 0 \\ 0 & 0 & 0 & 0 & 0 & 0 & 0 & 0 \\ 0 & 0 & 0 & 0 & 0 & 0 & 0 & 0 \\ 0 & 0 & 0 & 0 & 2av_p & 0 & av_p & 0 \\ 0 & 0 & 0 & 0 & 0 & 2bv_s & 0 & bv_s \\ 0 & 0 & 0 & 0 & av_p & 0 & 2av_p & 0 \\ 0 & 0 & 0 & 0 & 0 & bv_s & 0 & 2bv_s \end{bmatrix} \tag{4.3}$$

There are several simple lumping procedures which can be used to diagonalise the consistent radiation damping matrix (Chow, 1985). The effect of all of them can be visualised as attaching a pair of dampers in each boundary node, with given coefficients of viscosity in the normal and tangential direction.

The first procedure consists of distributing the viscous damping force at the boundary nodes according to the associated boundary length on both sides of the particular node. The second procedure scales the diagonal terms of the consistent damping matrix so that the correct viscous force is preserved. The diagonal terms C_{ii}^{*} of the new lumped radiation damping matrix may be computed from

$$C_{ii}^{*} = \frac{C_{ii}}{\sum_{j=1}^{n} C_{ij}} \tag{4.4}$$

where C_{ii} are the diagonal terms of the consistent radiation damping matrix, and n is the number of element boundary nodes. The third procedure scales the sum of each row of the consistent damping matrix so that the correct viscous force is preserved. The diagonal terms C_{ii}^{*} of the new lumped radiation damping matrix are:

$$C_{ii}^{*} = \frac{\sum_{j=1}^{n} C_{ij}}{\sum_{j=1}^{n}\sum_{k=1}^{n} C_{jk}} \tag{4.5}$$

For the element depicted in Figure 4.3, all three lumping procedures lead to the same result (which is not the case for 8-noded elements (Simic, 1993a)):

$$\mathbf{C}_r = \frac{\rho l}{2}\begin{bmatrix} 0 & 0 & 0 & 0 & 0 & 0 & 0 & 0 \\ 0 & 0 & 0 & 0 & 0 & 0 & 0 & 0 \\ 0 & 0 & 0 & 0 & 0 & 0 & 0 & 0 \\ 0 & 0 & 0 & 0 & 0 & 0 & 0 & 0 \\ 0 & 0 & 0 & 0 & av_p & 0 & 0 & 0 \\ 0 & 0 & 0 & 0 & 0 & bv_s & 0 & 0 \\ 0 & 0 & 0 & 0 & 0 & 0 & av_p & 0 \\ 0 & 0 & 0 & 0 & 0 & 0 & 0 & bv_s \end{bmatrix} \tag{4.6}$$

4.3 Superposition Boundary

Smith (1974) initiated the original idea about the superposition boundary. He proposed a procedure for cancelling boundary reflections by superimposing two dynamic solutions with different boundary conditions: one with fixed boundaries and the other with free boundaries. In the case of a homogeneous medium with a single plane boundary, Smith's method completely eliminates the reflections of all types of waves. However, in the presence of more than one artificial boundary, it requires a large number of dynamic solutions. In order to overcome these deficiencies, Smith's ideas were refined (Kunar & Rodriguez-Ovejero, 1980) by introducing constant velocity and constant stress boundaries and by defining a boundary neighbourhood where solutions are averaged. Thus, the reflections are 'cancelled as they occur' and not allowed to propagate outside the boundary zone.

4.3.1 Smith Superposition Boundary

In the original formulation by Smith (1974), the problem of reflection at the boundaries was uncoupled into two problems: one solution for the out-of-plane SH-waves and the other for the in-plane P- and SV-waves. Since the emphasis here is given to two dimensional problems, only the in-plane solution will be presented.

Starting from a single artificial boundary, Smith defined two boundary value problems: a) The displacements normal to the boundary and the stresses tangential to the boundary are set to zero; b) The displacements tangential to the boundary and the stresses normal to the boundary are set to zero. First, the incident P-wave was considered. As a result of the first boundary value problem, a reflection of the P-wave in phase with the incident wave occured, without any SV reflection. As a result of the second boundary value problem, a reflection of the P-wave out of phase with the incident wave occured, without any SV reflection. Second, the incident SV-

wave was considered. Similarly, there was no reflected P-wave in either solution and the two reflected SV-waves were of opposite signs in the two boundary value problems. Consequently, the superposition of the two solutions would completely eliminate the reflections of body waves, and a name 'superposition boundary' was attributed to this kind of transmitting boundary. Smith also indicated that the Rayleigh-wave reflections might be cancelled by using the same method.

The advantages of the formulation are the applicability for all types of waves and the independence of frequency and angle of incidence. However, its serious drawbacks are the inability to prevent multiple reflections of a given wave at the same boundary, difficulties when oblique and curved boundaries are imposed, and the exponential growth of the number of dynamic analyses required in the case of more than one artificial boundary. If n is the number of surfaces on which the reflections are to be eliminated, 2^n complete dynamic solutions need to be obtained.

4.3.2 Refined Superposition Boundary

In order to overcome the aforementioned difficulties, a numerical procedure was proposed (Kunar & Rodriguez-Ovejero, 1980). It is performed only once, except in a narrow band of elements adjacent to the boundary where the necessity of two solutions arise. Because of the nature of the method, an explicit time integration scheme has to be used, enabling the cancellation of reflected waves 'as they occur'. The refined superposition boundary also replaces fixed and free boundary conditions with constant velocity and constant stress boundary conditions.

In the implementation of the refined superposition boundary, two narrow boundary zones have to be independently connected to the main finite element mesh (Figure 4.4). The two zones are assigned the same spatial coordinates but each of them has half of the total stiffness and mass. The boundary conditions of the zones are complementary - one has the prescribed velocity in the direction normal to the

boundary and prescribed force (stress) in the tangential direction. The inverse case stands for the other zone. When the first wave propagating from the main finite element mesh arrives at the border with two boundary zones, the prescribed boundary conditions are zero. Usually, the 'slave' nodes are assigned the same velocities as the 'master' nodes in order to transmit the wave motion to the boundary zones. All the variables are then computed for the present time step in the main mesh and in both boundary zones. After the reflection at the boundaries, the amplitudes of the waves in the two zones will have the same magnitudes but different signs. If the two solutions are averaged in the boundary zones before the reflected waves can reach the main mesh, the reflections would be cancelled as they occur. In an explicit direct time integration procedure, the calculation time step is usually short enough so that information cannot propagate physically from one node to another. In other words, averaging all the variables every three time steps in a three element wide boundary zone would eliminate completely the reflections before they can propagate back into the main mesh. The resulting velocities and forces on the boundaries of the two zones are updated and they now serve as new, prescribed boundary conditions until the next averaging. The problem of multiple reflections encountered in the Smith superposition boundary was overcome and the computational effort is considerably reduced because the calculations for each time step are performed only once in the main mesh and twice in the narrow boundary zones.

4.4 Paraxial Boundary

The paraxial boundary is based on a technique in which the standard equations of wave propagation in a zone beside the boundary are replaced by the so-called paraxial wave equations. These equations are only approximate but they allow wave propagation in one direction (and hence the name 'para-axial') and restrict it in the opposite direction. Engquist & Majda (1977) proposed a paraxial boundary for the

scalar (out-of-plane) wave equation. Clayton and Engquist (1977) revised their work in order to establish the analogies which enabled them to derive a paraxial boundary for the elastic (in-plane) wave equation. Unfortunately, it was possible to implement their formulation only into finite difference numerical models. Finally, Cohen and Jennings (1983) considerably improved the applicability of the paraxial boundary by incorporating it into finite element procedures.

4.4.1 Clayton-Engquist Approach to Paraxial Boundary

Clayton and Engquist (1977) expanded some earlier ideas and devised the so-called paraxial equations which approximate the full wave propagation equations. The starting point in their consideration was the two-dimensional (coordinates x and z) elastic wave equation for a homogeneous, isotropic medium

$$\mathbf{u}_{tt} - \mathbf{E}_{11}\mathbf{u}_{xx} - \mathbf{E}_{12}\mathbf{u}_{xz} - \mathbf{E}_{22}\mathbf{u}_{zz} = \mathbf{0} \tag{4.7}$$

where the subscripts denote partial spatial and temporal derivatives; and where $\mathbf{u}$ is the displacement vector, and $\mathbf{E}$ matrices as follows:

$$\mathbf{u} = \begin{Bmatrix} u \\ w \end{Bmatrix} \qquad \mathbf{E}_{11} = \begin{bmatrix} v_p^2 & 0 \\ 0 & v_s^2 \end{bmatrix} \qquad \mathbf{E}_{12} = \left(v_p^2 - v_s^2\right)\begin{bmatrix} 0 & 1 \\ 1 & 0 \end{bmatrix} \qquad \mathbf{E}_{22} = \begin{bmatrix} v_s^2 & 0 \\ 0 & v_p^2 \end{bmatrix} \tag{4.8}$$

in which v_p and v_s are the velocities of P- and S-waves, respectively. Based on their experience from the scalar wave equation, Clayton and Engquist assumed that the paraxial approximation to the full wave propagation equation (4.7) can be expressed in the following two forms:

$$\mathbf{u}_z + \mathbf{B}_1\mathbf{u}_t = \mathbf{0} \tag{4.9}$$

$$\mathbf{u}_{tz} + \mathbf{C}_1\mathbf{u}_{tt} + \mathbf{C}_2\mathbf{u}_{tx} + \mathbf{C}_3\mathbf{u}_{xx} = \mathbf{0} \tag{4.10}$$

After taking triple (two spatial and one temporal) Fourier transforms of Equations (4.7), (4.9) and (4.10), the coefficient matrices $\mathbf{B}_1$, $\mathbf{C}_1$, $\mathbf{C}_2$ and $\mathbf{C}_3$ can be determined by matching the appropriate terms in the transformed equations. The results are:

$$\mathbf{B}_1 = \mathbf{C}_1 = \begin{bmatrix} 1/v_s & 0 \\ 0 & 1/v_p \end{bmatrix} \mathbf{C}_2 = (v_s - v_p)\begin{bmatrix} 0 & 1/v_s \\ 1/v_p & 0 \end{bmatrix} \mathbf{C}_3 = \frac{1}{2}\begin{bmatrix} v_s - 2v_p & 0 \\ 0 & v_p - 2v_s \end{bmatrix} \quad (4.11)$$

By using Equation (4.9) or (4.10) instead of (4.7) on the boundary of the computational model, only the outgoing wave field is modelled because the propagation in the opposite direction (reflected wave field) is mathematically impossible. The approximations stated so far modelled only waves moving in the positive *z*-direction, and a similar derivation can be applied for the negative *z*-direction. If paraxial boundaries for the *x*-direction are needed, partial derivatives *x* and *z* should be interchanged in the above equations.

The presented procedure is well suited and can easily be implemented into a finite difference model. All the interior points are first solved by using the finite difference formulae of the full wave equation (4.7). Then, the values in the boundary points are calculated by using the finite difference formulae of the paraxial approximations. Since both Equations (4.9) and (4.10) are spatially the first-order extrapolations, only the nearest set of interior points is needed for each boundary.

4.4.2 Cohen-Jennings Approach to Paraxial Boundary

A straightforward application of the Clayton-Engquist paraxial boundary to finite element procedures is not possible. Two zones (not lines of points as in the finite difference method) would be needed: one internal where the standard wave equations are applicable, and one external where the paraxial equations hold. Smooth transmission of the waves between the two zones cannot be achieved. Even the waves which do get through and arrive in the paraxial zone do not propagate correctly and a significant part of the energy is reflected back into the internal zone. Wolf (1988) reported 'catastrophic results' when he tried to implement the Clayton-Engquist boundary directly in an one-dimensional finite element example.

Cohen and Jennings (1983) adopted a somewhat different approach to the basic paraxial ideas which enabled them to improve the boundary's performance. Starting from the same elastic wave Equation (4.7) and by assuming the wave propagation in the positive *x*-direction, they derived the paraxial equation

$$\mathbf{u}_{tt} + \mathbf{A}_1\mathbf{u}_{tx} + \mathbf{A}_2\mathbf{u}_{tz} + \mathbf{A}_3\mathbf{u}_{zz} = \mathbf{0} \tag{4.12}$$

where

$$\mathbf{A}_1 = \begin{bmatrix} v_p & 0 \\ 0 & v_s \end{bmatrix} \quad \mathbf{A}_2 = (v_p - v_s)\begin{bmatrix} 0 & 1 \\ 1 & 0 \end{bmatrix} \quad \mathbf{A}_3 = -\begin{bmatrix} v_p(v_s - v_p/2) & 0 \\ 0 & v_s(v_p - v_s/2) \end{bmatrix} \tag{4.13}.$$

There are practically no important differencies between the Clayton-Engquist approximation given by Equation (4.10) and the Cohen-Jennings approximation given by Equation (4.12), provided that one of them is rewritten so that both apply for the same direction (either *x* or *z*). When premultiplied with the mass density ρ, Equation (4.12) may be expressed in the form suitable for finite element discretisation:

$$\rho\ddot{\mathbf{u}}\int_A \mathbf{N}^T\mathbf{N}\,dA + \rho\mathbf{A}_1\dot{\mathbf{u}}\int_A \mathbf{N}^T\mathbf{N}_x\,dA + \rho\mathbf{A}_2\dot{\mathbf{u}}\int_A \mathbf{N}^T\mathbf{N}_z\,dA + \rho\mathbf{A}_3\mathbf{u}\int_A \mathbf{N}^T\mathbf{N}_{zz}\,dA = 0 \tag{4.14}$$

Equation (4.14) looks like the standard dynamic finite element equation where the first term correspond to the inertial force, the second and third term correspond to the damping force, and the last term resembles the stiffness force. Cohen & Jennings (1983) recognised that these terms have a different order of importance and therefore differently influence the accuracy of the paraxial boundary. If the first two terms are taken, the paraxial boundary is of the zeroth-order; if the first three terms are taken, the boundary is of the first-order, and so on. By further introducing higher order terms, it is expected that the paraxial boundary could become more and more efficient. For a successful implementation of the paraxial boundary into finite element procedures, three interventions are needed (Cohen & Jeenings, 1983):

By observing the last term of Equation (4.14), i.e. matrix $\mathbf{A}_3$, it was shown that the paraxial approximation is numerically always stable for Poisson's ratios less than 1/3.

If Poisson's ratio is larger than 1/3, the easiest way of achieving numerical stability is to equalise the upper diagonal element of the matrix $\mathbf{A}_3$ to zero. Since the last term of Equation (4.14) is the least important, its partial discarding negligibly affects the overall accuracy.

Second, the so-called 'upwinding technique' (Cohen & Jennings, 1983) enables the appropriate finite element treatment of the second term in Equation (4.14) and corrects the tendency of the finite element mesh to produce spurious oscillations. In effect, the technique requires the application of a nonsymmetric quadrature rule when calculating the contribution of this term. Standard Gaussian quadrature may be used for the integration of other terms.

Finally, in order to allow the smooth wave transmission, an interface element was introduced between the internal and paraxial zone. It contributes partially to the standard wave equation terms and partially to the paraxial boundary terms.

4.5 Extrapolation Boundary

The extrapolation boundary procedure was proposed by Liao and Wong (1984). The displacements of the nodes on the artificial boundary are extrapolated from information at earlier time steps along the line perpendicular to the boundary. Since this is a 'one-way' procedure, the outward wave propagation has to be considered on its own.

The starting point in the Liao-Wong derivation was a representation of the linear wave field by plane wave expansion. In the two dimensional space, with Cartesian coordinates x and y, and time t, this can be written as

$$U(x,y,t) = \sum_i u_i(\xi_i - vt) \tag{4.15}$$

where $u_i(\xi_i - vt)$ is the plane wave propagating in the positive ξ_i-direction with the velocity v. The sum in Equation (4.15) represents a collection of plane waves, while the argument, $\xi_i - vt$, is often called the forward characteristic. One particular inclined wave (from now on, the subscript i will be omitted) approaching the artificial boundary from the ξ-direction is shown in Figure 4.5. The x-axis is normal to the boundary and B is the boundary node under consideration. The wave propagates with the velocity v, so both P- and S-waves can be treated. Taking advantage of the one-dimensional wave propagation in direction ξ, the displacement for the time step $t+\Delta t$ at the boundary point B can be easily predicted in the form of

$$u[\xi_B - v(t+\Delta t)] = u[(\xi_B - v\Delta t) - vt] = u[(\xi_B - 2v\Delta t) - v(t-\Delta t)] = \ldots$$

$$= \ldots = \ldots = u\{(\xi_B - mv\Delta t) - v[t-(m-1)\Delta t)]\} \qquad (4.16)$$

where u is the wave amplitude function. Equation (4.16) clearly shows that the prediction can be made by using displacements at one of the points backward along the ξ-axis (E_1, E_2, ..., E_m in Figure 4.5) from the previous time steps (t, $t-\Delta t$, ..., $t-(m-1)\Delta t$). The extrapolations can be equally well performed regardless which of the points is used, as long as the time step is appropriate. This is due to the fact that the plane wave travels along the distance $v\Delta t$ during one time step.

The problem with Equation (4.16) is that the directions ξ_i of wave propagation are not available in the numerical procedure. Therefore, the information points must be introduced on the x-axis instead of ξ-axis. The plane wave along the x-axis propagates with the velocity $v'=v/\cos\Theta$, where Θ is the angle of incidence shown in Figure 4.5. Since each plane wave has its own Θ, it is impossible to prescribe the points A_1, A_2, ..., A_m in advance. The so-called information points must be introduced at the distances in multiples of d from the point B. Obviously, the numerical extrapolation procedure becomes more accurate as d approaches $v'\Delta t$. In the actual algorithm with a number of waves (each of them having its own v'), some kind of overall representative estimate has to be established for v', which also affects the value of d. The simplest practical rule is to adopt the value of d smaller than the

finite element size Δx (Figure 4.6). For the arrangement shown in this Figure, it is necessary to interpolate somehow the values at the information nodes from the mesh nodes. The alternative method is to interpolate between time steps at the mesh nodes.

Although Equation (4.16) was derived for one plane wave, it is applicable to the total wave by means of the summation procedure indicated in Equation (4.15). After some mathematical transformations, Liao & Wong (1984) have obtained two types of extrapolation series. The more compact version is

$$U(x_B, y_B, t+\Delta t) = \sum_{j=1}^{N} (-1)^{j+1} C_j^N \, U[x_B - jd, y_B, t-(j-1)\Delta t] \tag{4.17}$$

where N is the order of approximation and C_j^N are the binomial coefficients which may be represented as:

$$C_j^N = \frac{N!}{(N-j)!\,j!} \tag{4.18}$$

According to Equations (4.17) and (4.18), approximations of various order are available. Most commonly used are the first, second and third-order approximations which can be respectively written as:

$$U(x_B, y_B, t+\Delta t) = U(x_B - d, y_B, t)$$

$$U(x_B, y_B, t+\Delta t) = 2U(x_B - d, y_B, t) - U(x_B - 2d, y_B, t-\Delta t) \tag{4.19}$$

$$U(x_B, y_B, t+\Delta t) = 3U(x_B - d, y_B, t) - 3U(x_B - 2d, y_B, t-\Delta t) + U(x_B - 3d, y_B, t-2\Delta t)$$

4.6 Overview of Numerical Examples in the Literature

Apart from the four transmitting boundaries presented in the previous four Sections, there are many others (Robinson, 1977; Al-Hunaidi et al., 1990; Madabhushi, 1993, to name just a few) which were not covered in this review. The main criterion for the inclusion of a particular boundary was its popularity among researchers and advanced

practising engineers in the field of soil-structure interaction. Although this approach may not be the most correct from the scientific point of view, it enables almost immediate application of the findings of this research into everyday engineering practice.

Technical literature abounds in examples about the implementation of transmitting boundaries, but only some of them are relevant to the present study. For instance, the examples on transmitting boundaries for one-dimensional problems (rods, out of plane motion due to SH waves) are not so important despite the fact that they have been extrapolated to two-dimensional problems (Kausel, 1988).

A preliminary choice of the transmitting boundary which will be used in the subsequent work can be based on a good overview of the published results. Once this choice is made, the boundary can be tested to confirm its suitability and determine its parameters in detail. After establishing the necessary dam-foundation equations in Chapter 5, the chosen boundary (if proved successful in the first set of tests) can be further scrutinised within the whole interaction system. This approach is preferred to the other option - to test all the boundaries and then reach a conclusion about the preliminary choice.

4.6.1 Footing on a Half-Space

This is one of the most thoroughly examined models, partly because the analytical solutions are available for both the plane strain and axisymmetrical conditions. A weightless, perfectly rigid, vertically and harmonically excited, frictionless footing resting on a homogeneous elastic half space is considered. The steady-state nature of the problem renders a complex response solution possible. Lysmer & Kuhlemeyer (1969) have tested the axisymmetrical case with the standard viscous boundary. White et al. (1977) have used the plane strain case with the unified viscous boundary. Chow (1985) has examined both cases by paying special attention to the lumping

procedures. Simons & Randolph (1986) have tested the axisymmetrical case through the comparison between standard viscous, unified viscous and refined superposition boundary.

The main conclusions of these studies were:

a) The solutions achieved with both unified and standard viscous boundaries are close to the analytical solution. In this particular case, the unified viscous boundary performed slightly better.

b) The differences in results obtained with the consistent and various lumped viscous boundary radiation damping matrices were insignificant.

c) In spite of the considerably increased computational effort, the refined superposition boundary formulation did not offer any improvement over the viscous boundary formulation.

4.6.2 Pulse Loading on a Half-Space

This is a very simple transient model consisting of a vertical or horizontal pulse load acting at the surface of a half-space. Smith (1974) has examined the performance of the original superposition boundary by applying the explicit Runge-Kutta integration algorithm. Cohen & Jennings (1983) have used horizontal and vertical pulse loadings in conjunction with paraxial and viscous (standard and unified) boundaries. An explicit time integration method was employed in the extended-paraxial domain, while viscous boundaries were always treated implicitly (Newmark method with parameters which provided some numerical damping). Al-Hunaidi et al. (1990) compared their newly developed energy deletion boundary with the standard viscous and paraxial boundaries.

The following conclusions were drawn:

a) The viscous boundaries caused a permanent, residual, rigid body movement of the finite element mesh.

b) It was necessary to employ some numerical (algorithmic) damping in order to reduce the numerical noise, i.e. high frequency oscillations.

c) The standard and unified viscous boundaries performed almost identically in all ways. In other words, the behaviour of the viscous boundary was relatively insensitive to changes in parameters *a* and *b*.

d) The paraxial boundary was slightly superior over the viscous boundary in the example calculations, but certainly not as much as expected from analytical wave reflection considerations.

4.6.3 Rayleigh Wave in a Half-Space

The Rayleigh wave field can be prescribed in an elastic half-space by generating horizontal and vertical displacements at one side of the foundation finite element mesh. Cremonini et al. (1988) have tested the efficiency of various transmitting boundaries (Smith superposition, standard viscous, unified viscous and extrapolation). The explicit direct time integration method was used for solving the equations of motion. Cohen & Jennings (1983) have examined the standard viscous and paraxial boundaries. The equations of motion were solved by using the explicit method with a negligible amount of numerical damping. Al-Hunaidi et al. (1990) compared the energy deletion boundary with the standard viscous and paraxial boundary. The explicit predictor-corrector algorithm was used.

The main findings of these studies were:

a) Despite a common belief that the viscous boundary is ineffective when dealing with Rayleigh waves, it was shown that it functions at least as well as for body waves.

b) In the joint study of all the four presented boundaries, the unified viscous boundary performed best, slightly better than the standard viscous boundary. The Smith superposition boundary followed, while the extrapolation boundary gave the worst results.

4.6.4 Other Examples

Liao & Wong (1984) have compared the reflection coefficients of an inclined plane wave impinging upon a flat boundary for the paraxial and extrapolation boundary. Also, a comparison between the same boundaries was produced for the transmission of a spherical harmonic wave (with coupled P- and S-waves) through a plane boundary. The explicit central difference scheme was the chosen method for solving the equations of motion. It was found that the extrapolation boundary outperformed the paraxial boundary.

Simons & Randolph (1986) have studied the step loading (loading with a non-vanishing time average) in conjunction with the viscous and refined superposition boundary. Explicit time integration was used. It was concluded that none of the boundaries can support a static load component and that loadings with non-vanishing time average should be treated with caution.

For the structure-foundation interaction, Kunar & Rodriguez-Ovejero (1980) have implemented the viscous boundary at the base of the foundation and the refined superposition boundary at the vertical faces of the foundation. In order to specify the proper seismic input, an alternative input model was proposed in the form of force time history, computed at the base of the system by modifying the standard deconvolution procedure. Explicit time integration was used.

4.7 Concluding Remarks and the Preliminary Choice of the Transmitting Boundary

In this Section, concluding remarks on the four transmitting boundaries presented in Sections 4.2 - 4.5 will be given. Based on these remarks and the overview from the previous Section, a preliminary choice of the transmitting boundary will be made.

4.7.1 Concluding Remarks on the Viscous Transmitting Boundary

The main advantage of the viscous boundary is the simplicity of its implementation in standard finite element computer codes. This fact becomes even more obvious if the lumping procedures are applied.

It was thought (Lysmer & Kuhlemeyer, 1969; White et al., 1977) that the major drawbacks of the viscous transmitting boundary are the poor absorption of body waves with incident angles $\Theta<30^0$ (Figure 4.1) and the unsatisfactory absorption of Rayleigh waves. The first problem is not so serious as the efficiency of the boundary can be increased by enlarging the foundation mesh, i.e. by reducing the importance of outgoing waves with small angles of incidence. The second problem is more serious because of its consequences to the structure-foundation interaction systems. It was widely believed that around 2/3 of radiated energy in these systems is due to Rayleigh waves (Miller & Pursey, 1955). However, numerical studies (Cohen & Jennings, 1983; Simons & Randolph, 1986; Cremonini et al., 1988) have indicated that the viscous transmitting boundary performs quite well even in cases with a high contribution of Rayleigh wave energy. More importantly, Meek & Wolf (1993) have recently proved that the contribution of P- and S-wave energy dramatically increases with the increase of the structure-foundation contact length, which is very important for the structures with long bases, like concrete gravity dams.

In some cases (Chow, 1985; Cremonini et al., 1988), the unified viscous boundary performed slightly better than the standard viscous boundary, but the general conclusion is that the behaviour of the viscous transmitting boundary is relatively insensitive to changes in parameters a and b (Cohen & Jennings, 1983; Simic, 1993b).

The numerical stability of the viscous boundary depends on the type of the integration procedure. For an implicit scheme, the boundary itself is unconditionally stable if the rest of the algorithmic requirements are met. For an explicit scheme, the parameters have to be evaluated for each specific case (Cohen & Jennings, 1983).

The viscous transmitting boundary causes a permanent, residual, rigid body movement of the finite element mesh. The system behaves like a 'float' in the viscous medium created by the dampers; it is successively pushed and pulled as it follows the pattern of the dynamic excitation. Fortunately, these residual displacements are relatively insignificant when compared to the overall displacements (Cohen & Jennings, 1983), particularly in the area of main interest (the structure and neighbouring foundation in structure-foundation interaction problems).

The viscous transmitting boundary cannot support a static load. Since the simultaneous action of static and earthquake loading is a prerequisite for successful structure-foundation interaction analyses, the solution to this problem has to be found if this boundary is to be used for subsequent nonlinear dam-foundation analyses.

Although the accuracy of lumping procedures is problem dependent, it was found (White et al., 1977; Simons & Randolph, 1986) that the differences in results obtained from the consistent and lumped radiation damping matrices are insignificant. Chow (1985) discovered that the lumping procedure expressed by Equation (4.5) is the most promising, but further studies are needed to establish the accuracy criteria for every particular problem.

4.7.2 Concluding Remarks on the Superposition Transmitting Boundary

Theoretically, the superposition boundary should work for all types of waves which are of interest in in-plane elastodynamic problems (P and S body waves and surface Rayleigh waves). It is independent of frequency and angle of incidence, but the nature of its computational procedure requires only explicit direct integration in the time domain.

The number of elements in the boundary zones should be optimal. For one-dimensional problems (Simons & Randolph, 1986), it was shown that a two element boundary zone represents a considerable improvement over one-element boundary zone. It was also shown that further increase of the number of elements in the boundary zone does not offer any improvement worthy of extra computational effort. This conclusion was later applied and confirmed in a two dimensional analysis.

When using the superposition boundary, i.e. an explicit time integration procedure, the time step should be chosen carefully. A general recommendation is that averaging in the boundary zones should be performed at a time interval shorter than the time required by the fastest wave to propagate through the whole zone. The type of the chosen element also has the influence on this problem (Kunar & Rodriguez-Ovejero, 1980).

Applications of the superposition boundary have indicated that its performance is either equivalent (Simons & Randolph, 1986) or worse (Cremonini et al., 1988) to that of the viscous transmitting boundary.

4.7.3 Concluding Remarks on the Paraxial Transmitting Boundary

In finite element applications of the paraxial boundary, the radiation damping matrix (similar to that of the viscous boundary) arises. The total damping matrix becomes nonproportional and, although implicit algorithms may be used, the explicit direct integration of equations of motion is particularly well suited. The stability analysis

conducted by Cohen & Jennings (1983) confirmed that the necessary interface and paraxial elements under the explicit time integration scheme share the stability properties of the main domain.

Finite element modelling of wave propagation phenomena is always accompanied with high-frequency oscillations (see Chapter 3). Transmitting boundaries are not able to remove these oscillations, but it was found that the paraxial boundary makes them even worse (Cohen & Jennings, 1983). One of the possible solutions to the problem is to introduce numerical damping in the computational scheme, as detailed in Chapter 3.

A drastic superiority of the paraxial boundary over the viscous boundary, foreseen in the theoretical wave reflection analyses, was not confirmed in example calculations reported in the previous Section, where only a slight advantage was observed.

The paraxial boundary, although with a negligible stiffness term (the last term on the lefthand side of Equation (4.14)) is not able to withstand a static load. When treating the nonlinear dam-foundation interface as a contact nonlinearity, Ibrahimbegovic & Wilson (1990) encountered this problem, but failed to explain how the static load was combined with the paraxial boundary.

4.7.4 Concluding Remarks on the Extrapolation Transmitting Boundary

The nature of the extrapolation boundary requires explicit time integration. The main advantages of the boundary are the relative ease of implementation into standard finite element codes and a possibility of controlled accuracy.

It was already mentioned that the choice of d in Equations (4.19) affects the accuracy of the extrapolation procedure, regardless of the order of approximation. The closer the value of d is to $v'\Delta t$, the more accurate is the whole procedure. Unfortunately, the velocity v' can be used only to describe one plane wave. For a group of plane waves with different angles of incidence and different physical velocities, some kind

of estimate has to be used. Liao & Wong (1984) have suggested the use of v_s for out-of-plane SH-wave problems and v_p for in-plane problems. They also reported that 'good results' were obtained when using λ/d=10 (λ is the dominant wavelength) and 'excellent' when using λ/d=20. Clearly, these ratios can be used as guidelines when choosing the initial value for d in the extrapolation boundary procedure.

There are two ways of increasing the accuracy of the extrapolation transmitting boundary: increasing the order of extrapolation approximation (N) and decreasing the time step Δt; but Kausel (1988) warned that higher-order boundaries may lead to dynamic instabilities for high frequency excitations.

Conclusions regaring the performance of the extrapolation boundary are not unanimous. Despite the four examples discussed by Liao & Wong (1984) and the conclusion by Wolf (1988) that it is able to deal successfully with surface waves, Cremonini et al. (1988) claimed that the extrapolation boundary performed worse than all other boundaries in absorbing the Rayleigh-waves.

4.7.5 Preliminary Choice of the Transmitting Boundary

At this stage, the crucial point is the preliminary choice of the transmitting boundary which will be tested on infinite and half-space foundations in the remainder of this Chapter. If the boundary proves successful in these tests, it will be further examined in Chapter 6, within the time-domain finite element analysis of concrete gravity dam-foundation systems.

This preliminary choice is based on the extensive overview of numerical examples in the literature (Section 4.6) and the above remarks on all the presented boundaries. It can be concluded that the viscous transmitting boundary performs well enough to be recommended for subsequent applications. The boundary is by far the easiest to implement into finite element codes; and although not designed for the absorption of surface waves, various tests have demonstrated that it can handle the Rayleigh waves

with a reasonable accuracy. As explained in Subsection 4.7.1, the only pratical disadvantage of the viscous boundary is that it cannot support the static load. This problem will be tackled in Chapter 6, where the boundary will be applied within the concrete gravity dam-foundation system.

4.8 Viscous Transmitting Boundary for Infinite and Half-Space Media

Since the viscous transmitting boundary has been preliminary chosen as suitable for modelling infinite and half-space media, this presumption should be confirmed by performing relevant tests and by determining the boundary's parameters.

In this Section, the boundary is tested first on infinite and then on half-space media. For both cases, uniform finite element meshes of 4-noded elements are used, as typically recommended for wave propagation problems (Laturelle, 1989; Wang et al., 1992). It was explained in Subsection 3.4.3 that due to the discretised nature of finite element systems, the obtained numerical solutions oscillate and wave fronts are smoothed. Different element stiffnesses of nonuniform meshes and high-order elements would only amplify these unwanted side-effects (Laturelle, 1989; Simic, 1993b). On the other hand, because the viscous transmitting boundary was found relatively insensitive to changes in parameters a and b (Cohen & Jennings, 1983; Simic, 1993b), only the standard viscous boundary is used in this Section.

4.8.1 Infinite Space

Due to double symmetry of the two-dimensional infinite space (Figure 3.3), only one quarter is discretised by finite elements. The mesh with boundary conditions, relevant node numbers and location of the quartered force is shown in Figure 4.7. The displacements and stresses in two directions (force direction and lateral direction, i.e. direction perpendicular to the force direction) are observed at node 221.

4.8.1.1 Heaviside Line Load

The finite element solutions due to the Heaviside line load (righthand side of Figure 3.1) are compared with the analytical solution obtained through the computer program HEAVI (Simic, 1993e) which is based on Equations (3.5) - (3.9).

First, the importance of finite element boundaries is investigated by prescribing fixed, free and viscous transmitting boundary conditions. For the two specified displacements (displacement in the force direction and lateral displacement), the comparison shown in Figures 4.8a and 4.8b clearly indicates that the only acceptable solution is the one with the viscous transmitting boundary. Even in this case, the disagreement from the analytical solution is still considerable and can be attributed to the fact that for $t \rightarrow \infty$, the Heaviside load has all the properties of the static load.

Second, the influence of the direct integration method on the displacements and stresses is shown in Figures 4.9a-4.9d. Three direct integration methods, as described in Subsection 3.4.3, are used: central difference (explicit method with no algorithmic damping, denoted CD), Newmark (implicit method with parameters $\gamma = 0.55$ and $\beta = 0.276$, i.e. with algorithmic damping) and Wilson (implicit method with parameter $\theta = 1.4$, i.e. with algorithmic damping). As the differences between the Newmark and Wilson schemes were negligible, the results of the latter are not shown. All four plots, but particularly the stress plots in Figures 4.9c and 4.9d, clarify the effects of spurious high-frequency oscillations. These effects are unwanted and may be reduced by applying the direct integration method with algorithmic damping (e.g. Newmark method).

4.8.1.2 Rectangular Pulse Line Load

The finite element solutions due to the rectangular pulse line load are compared with the analytical solution obtained through the computer program RECPUL (Simic,

1993e) which is based on Equations (3.5) - (3.9) and Figure 3.1. The duration of the pulse was chosen to be Δt=0.006s.

As in the previous Paragraph, the importance of finite element boundaries was first investigated by prescribing fixed, free and viscous transmitting boundary conditions. The comparison for the specified two displacements (Figures 4.10a and 4.10b) confirms the previous conclusion that the only acceptable solution is the one with the viscous transmitting boundary. Again, the discrepancy between the analytical and transmitting boundary finite element solution can be noted for the displacement in the force direction (Figure 4.10a), which can be attributed to the existence of the tail in the analytical solution. If the solution converges to zero (like the displacement perpendicular to the force direction, shown in Figure 4.10b), the discrepancy for $t \rightarrow \infty$ is not observed. In other words, the dynamic excitation should have a vanishing time average if the viscous transmitting boundary is to be used successfully.

Second, the influence of the direct integration method on the displacements and stresses was once again investigated and shown in Figures 4.11a-4.11d, confirming the earlier conclusions: the unwanted spurious high-frequency oscillations may be reduced by applying the direct integration method with algorithmic damping (e.g. Newmark method) and the analytical stresses (which converge to zero) are well matched with the finite element solution. The results produced by the Wilson integration method were not shown because the difference from the Newmark method was negligible.

Third, an attempt was made to simulate the energy radiation on the finite element mesh with the fixed boundary. Internal, viscous, mass-proportional Rayleigh damping was used throughout the mesh, instead of the radiation damping. Both solutions are compared with the analytical solution for the two displacements in Figures 4.12a and 4.12b. Clearly, Rayleigh damping is able to reproduce correctly neither the general pattern of the oscillation nor the peak values. Therefore, it cannot be used as the model for the radiation damping.

4.8.2 Half-Space

Due to symmetry of the two-dimensional half-space (Figure 3.10), only one half is discretised by finite elements. The mesh with boundary conditions, relevant node numbers and location of the halved force is shown in Figure 4.13. The displacements in the force direction and perpendicular to the force direction (i.e. lateral displacement) are observed at node 221.

The finite element solutions due to the Dirac-delta line load are compared with the analytical solutions obtained through the computer program FRITZ (Simic, 1993e) based on Equations (3.10) and (3.11). However, the time discretisation of finite element models does not allow for the exact representation of Dirac-delta functions and a pulse whose duration was Δt=0.001s had to be used.

As in the previous Subsection, the fixed, free and viscous transmitting boundary conditions were investigated first. A comparison of the displacement results is shown in Figures 4.14a and 4.14b. At about t=0.013s, the results produced by the fixed and free mesh begin to lose the convergence towards the analytical solution. The mesh equipped with the viscous transmitting boundary is the only one whose convergence remains around the analytical solution. Even in this case, the disagreement is still significant and can be attributed to the fact that both the discontinuous waves and infinitely short load cannot be accommodated within the finite element method formulation.

The influence of the direct integration method on the displacement results is shown in Figures 4.15a and 4.15b. Again, the difference between the Newmark and Wilson method is not visible and they both prove to be superior to the explicit, central difference method.

4.8.3 Concluding Remarks on the Analyses of Infinite and Half-Space Media

All the analyses performed in this Section on infinite and half-space media have confirmed that the viscous transmitting boundary is suitable for modelling radiation damping. However, in some situations, special care should be taken. The performance of the viscous transmitting boundary is not so efficient when the loading has a non-vanishing time average (e.g. like a Heaviside or static load) or when the expected response has the 'tail' (e.g. like the displacement in the force direction for a rectangular pulse load in an infinite space). Since the ultimate purpose of this investigation is to confirm the boundary's suitability for the earthquake loading, which has a vanishing time average and exhibits no tail, it can be concluded that the viscous transmitting boundary will have no drawbacks in that respect.

The performance of the Newmark direct integration scheme was better than the performance of the central difference scheme, mainly because it was possible to control the algorithmic damping and reduce high-frequency oscillations. Also, it was shown that the internal Rayleigh damping cannot be used as a substitute for the radiation damping.

In this Section, the viscous transmitting boundary was examined on standard wave propagation problems with sharp and dicontinuous wave fronts which has tested the limits of the finite element discretisation. It is reasonable to expect that the boundary will perform even better for smoother, earthquake-type loading. This will be attempted in Chapter 6. Furthermore, only uniform meshes have been used so far. For the dam-foundation systems under earthquake loading, the nonuniform foundation meshes in conjunction with viscous transmitting boundaries will be tested in Chapter 6.

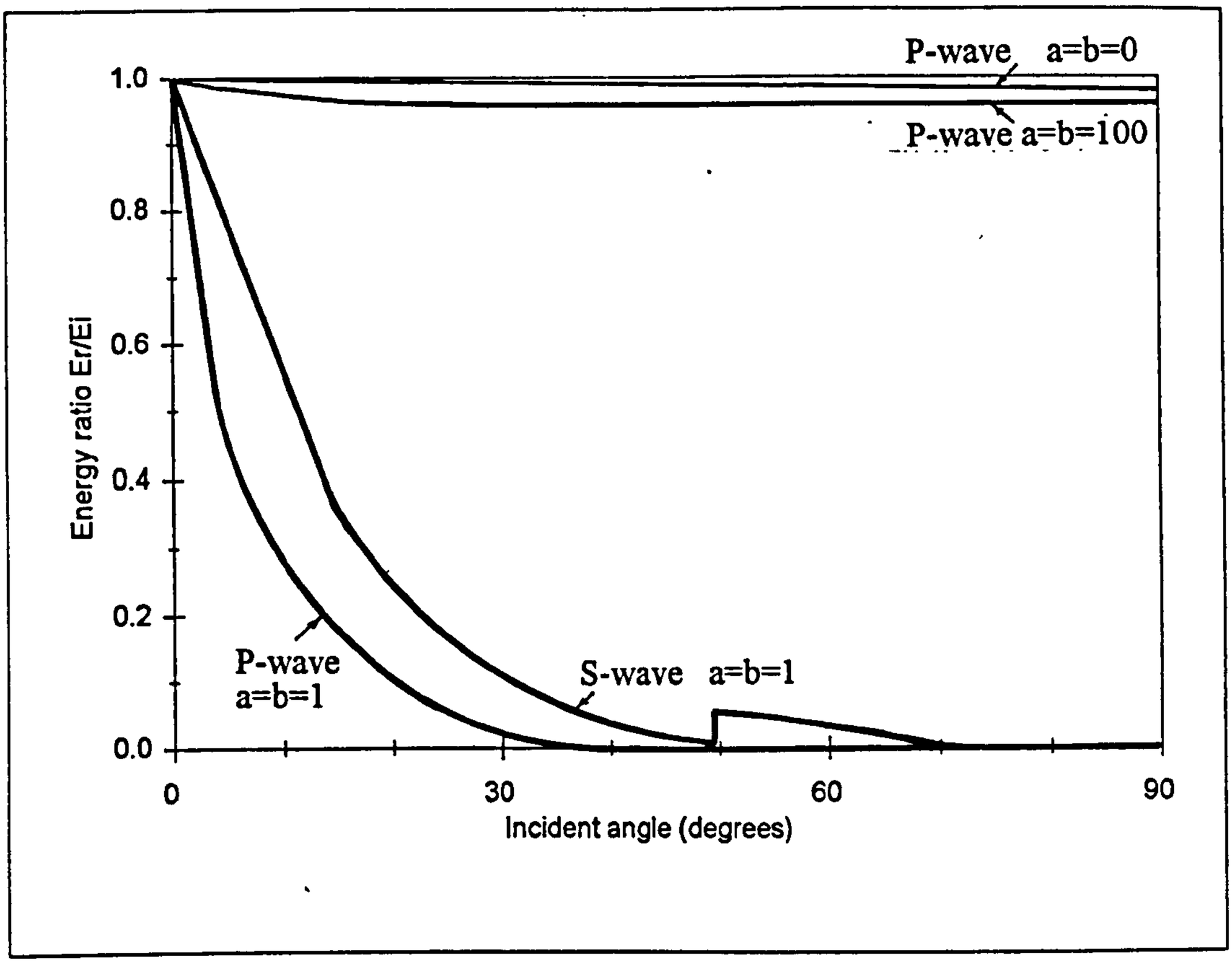

Figure 4.1 - Absorption of body wave energy by the standard viscous boundary

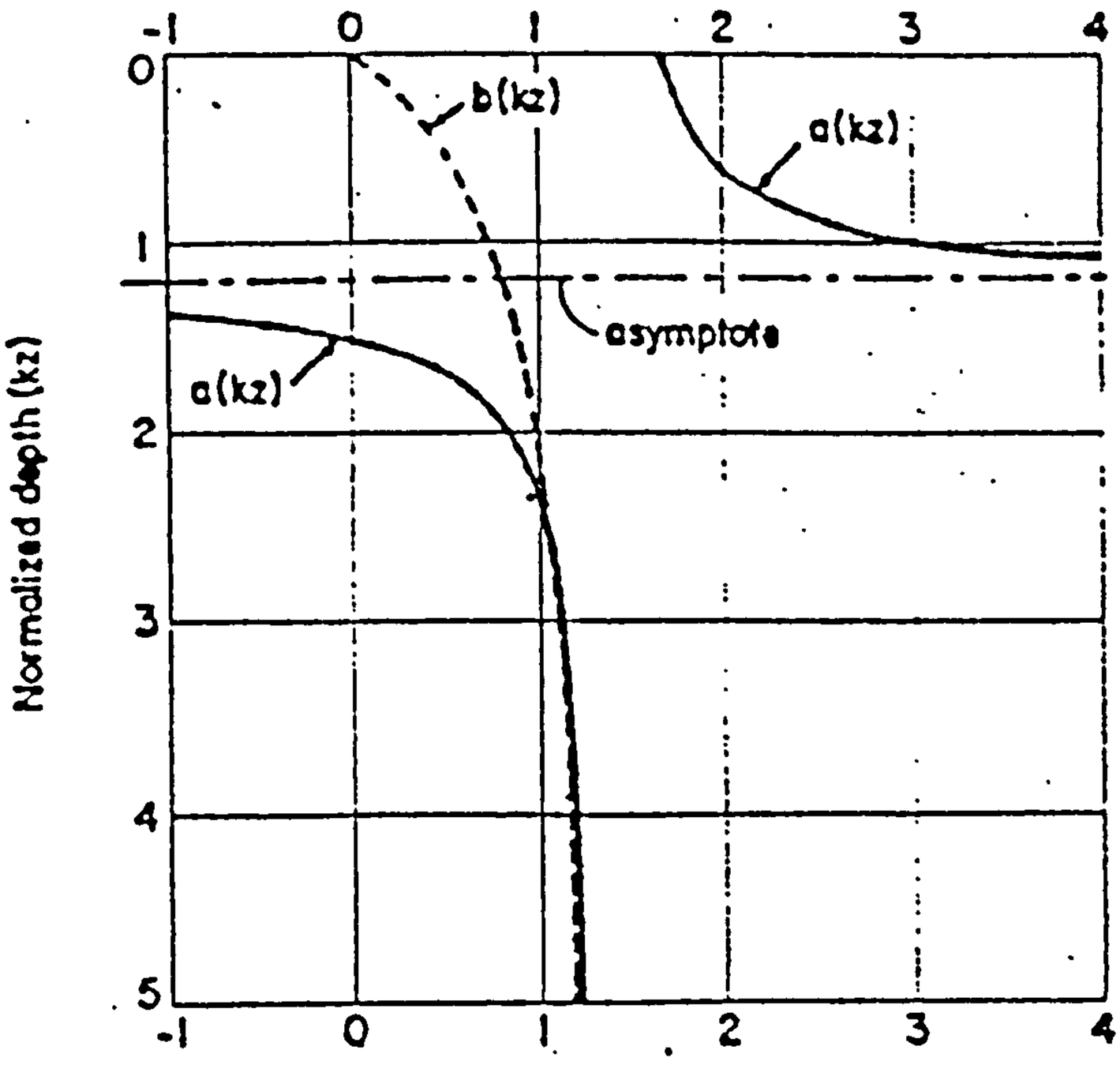

Figure 4.2 - Functions *a* and *b* for the Rayleigh viscous boundary

(Lysmer & Kuhlemeyer, 1969)

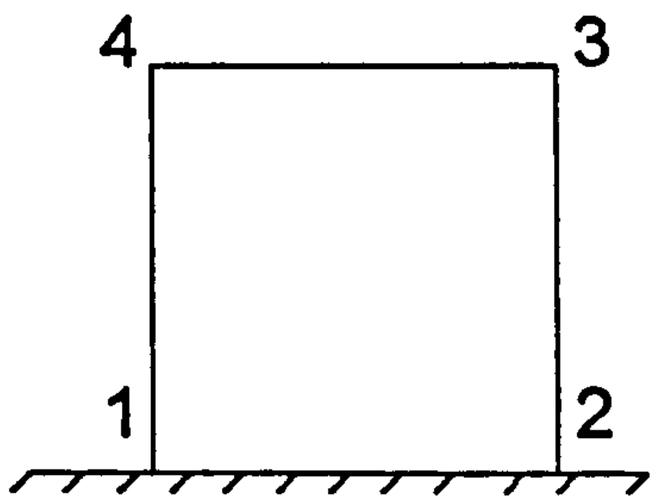

Figure 4.3 - Four-noded finite element for the definition of the viscous boundary

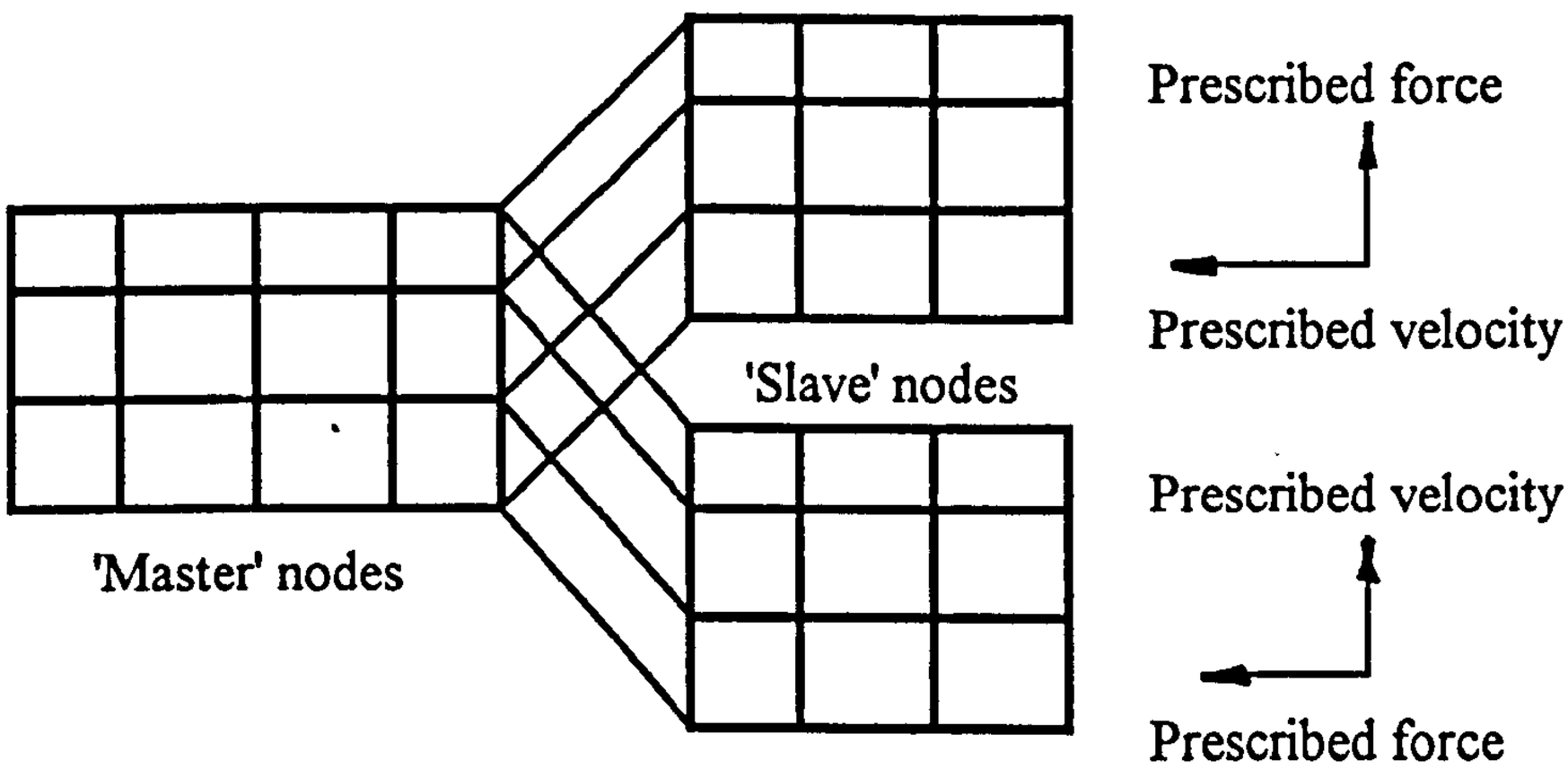

Figure 4.4 - Two independent boundary zones connected to the main mesh

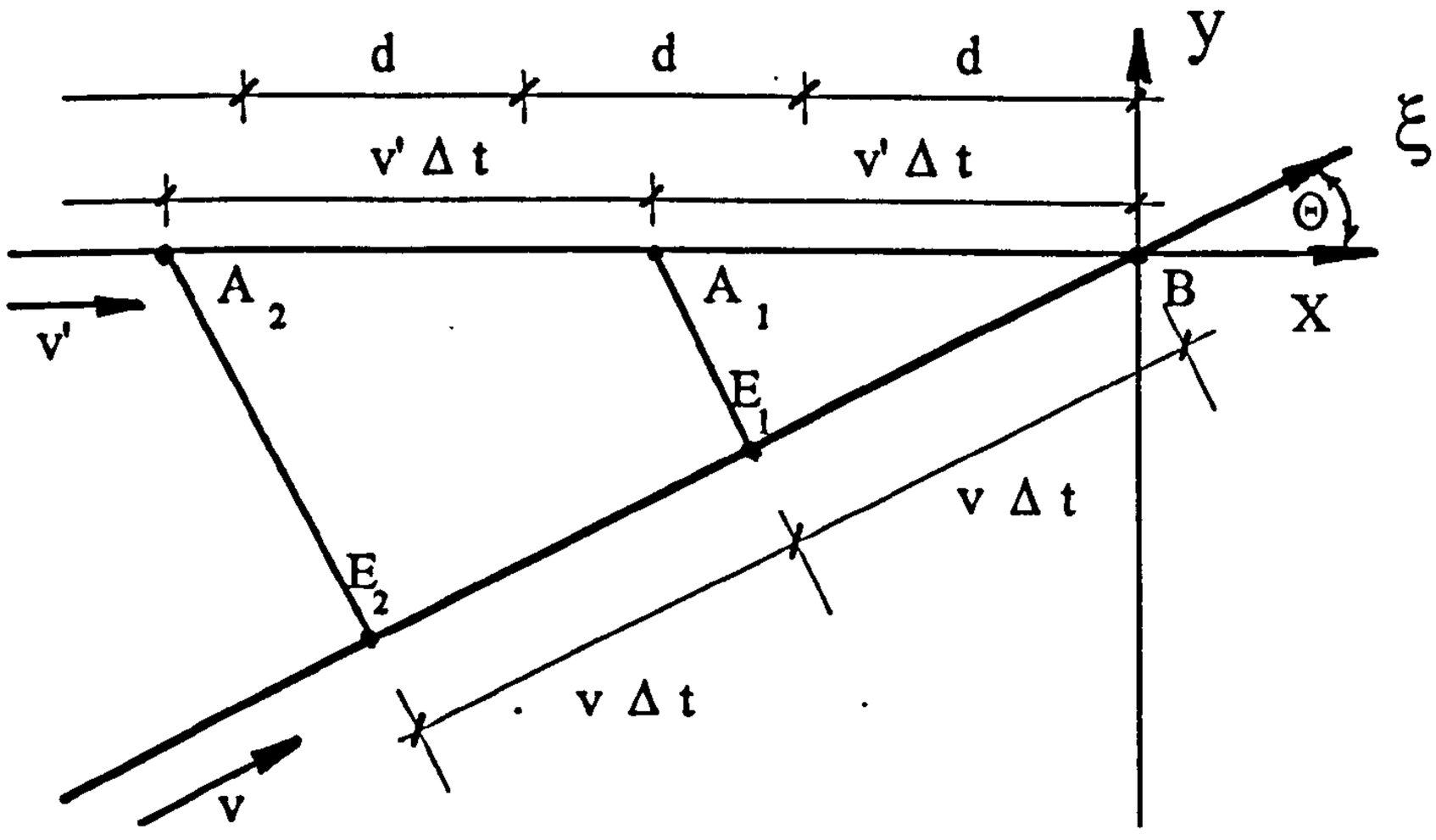

Figure 4.5 - Plane wave propagation in the direction ξ

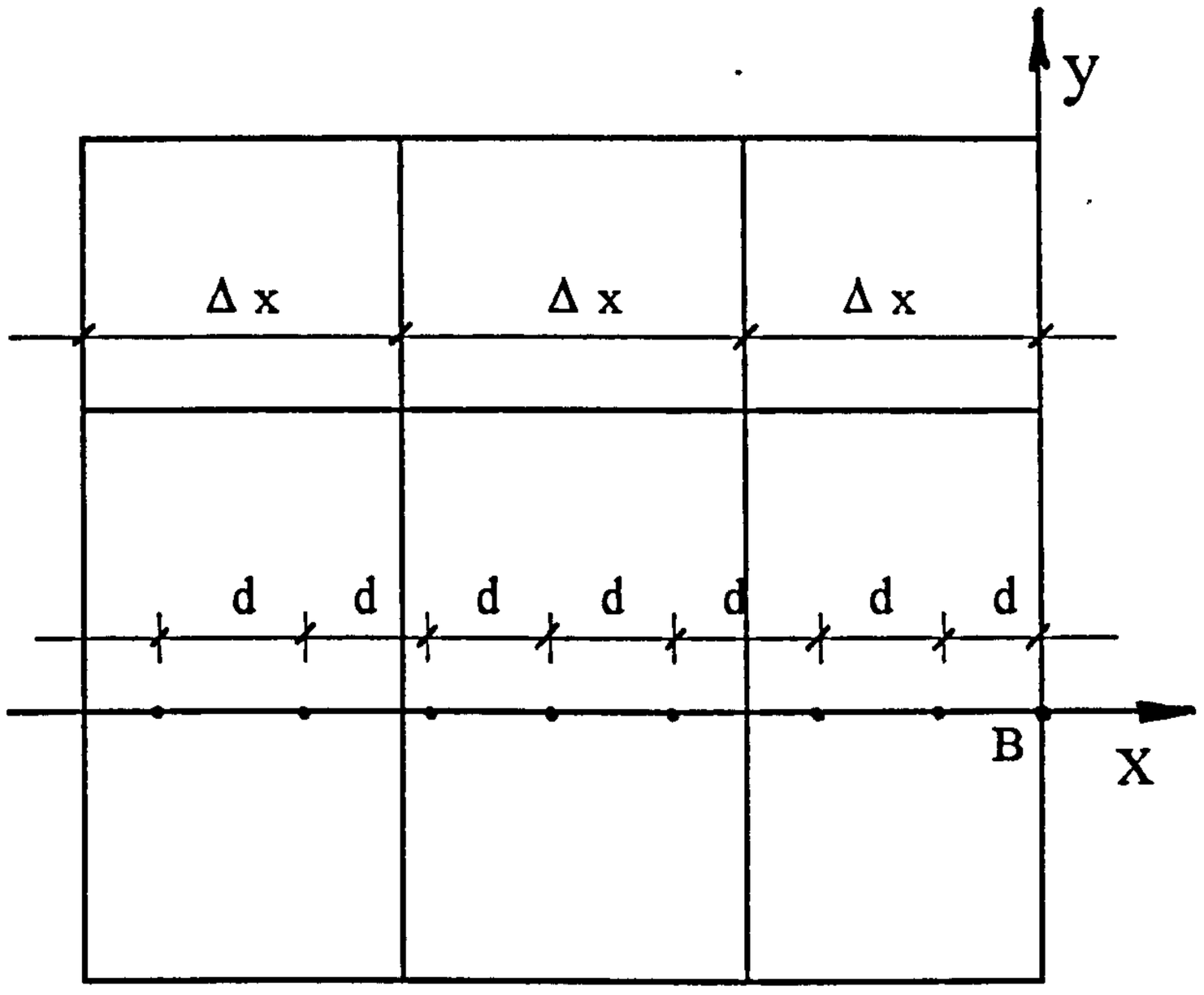

Figure 4.6 - Typical arrangement of information nodes and mesh nodes

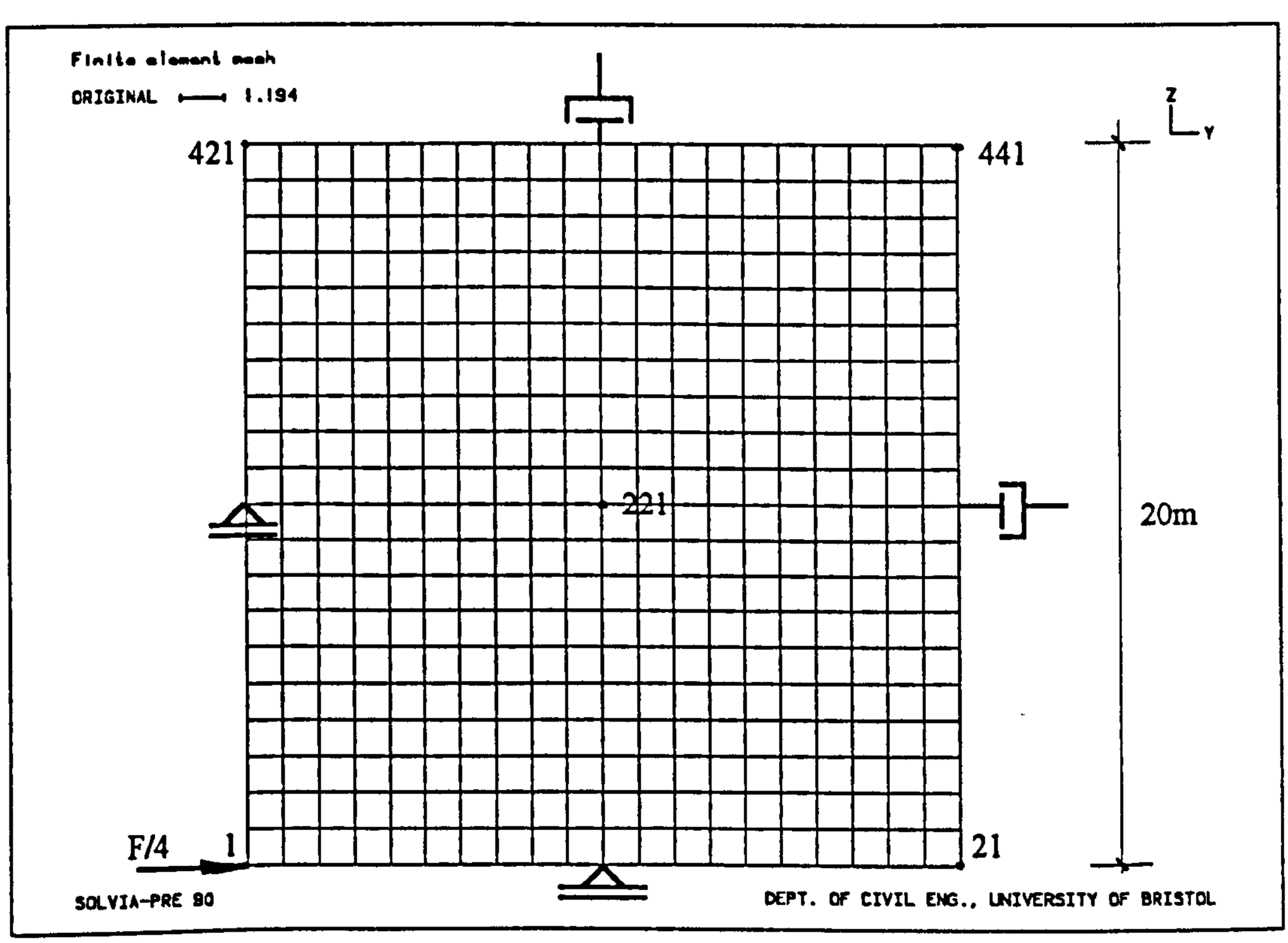

Figure 4.7 - Finite element mesh of one quarter of the infinite space

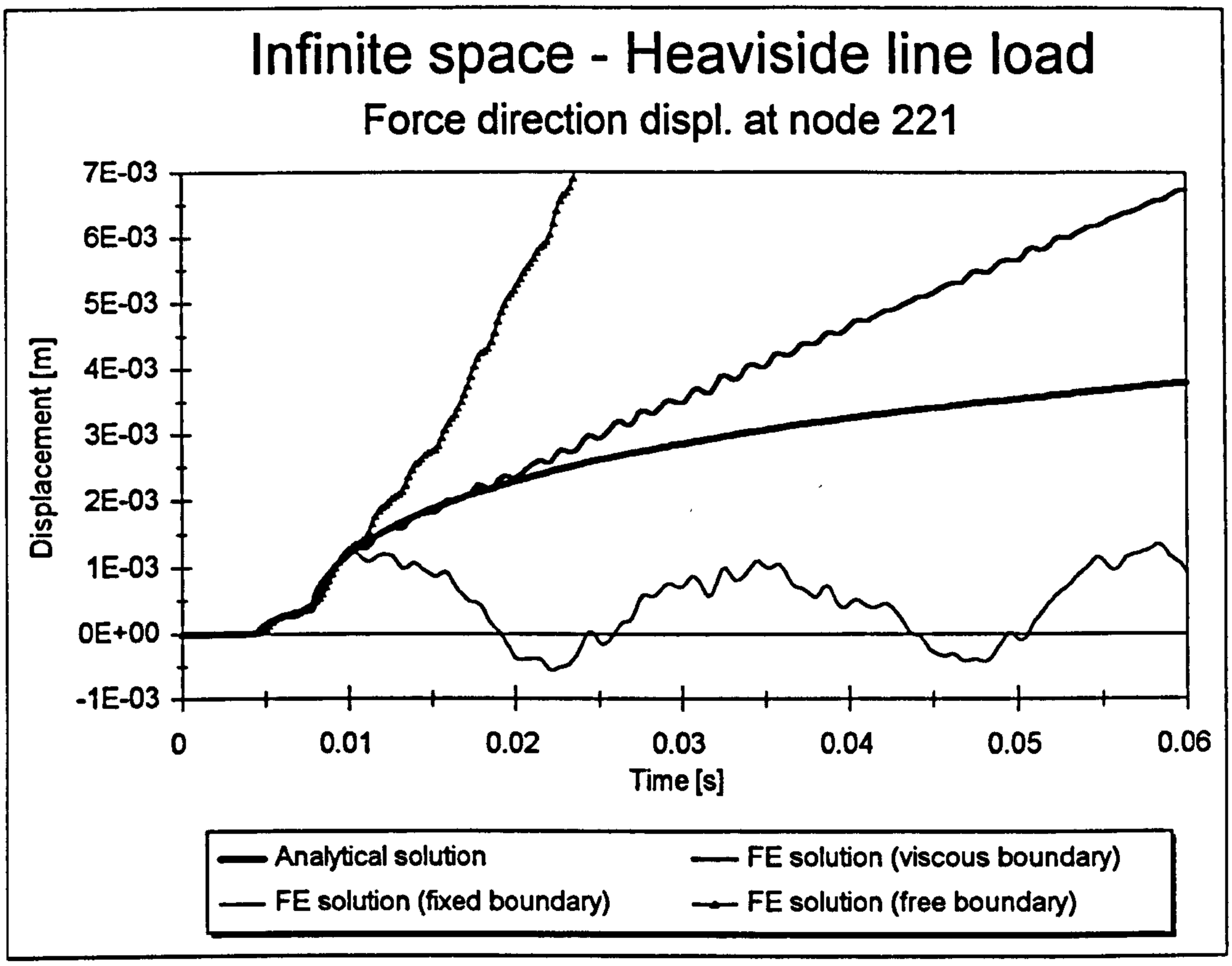

Figure 4.8a - Influence of boundary conditions (displacement in the force direction)

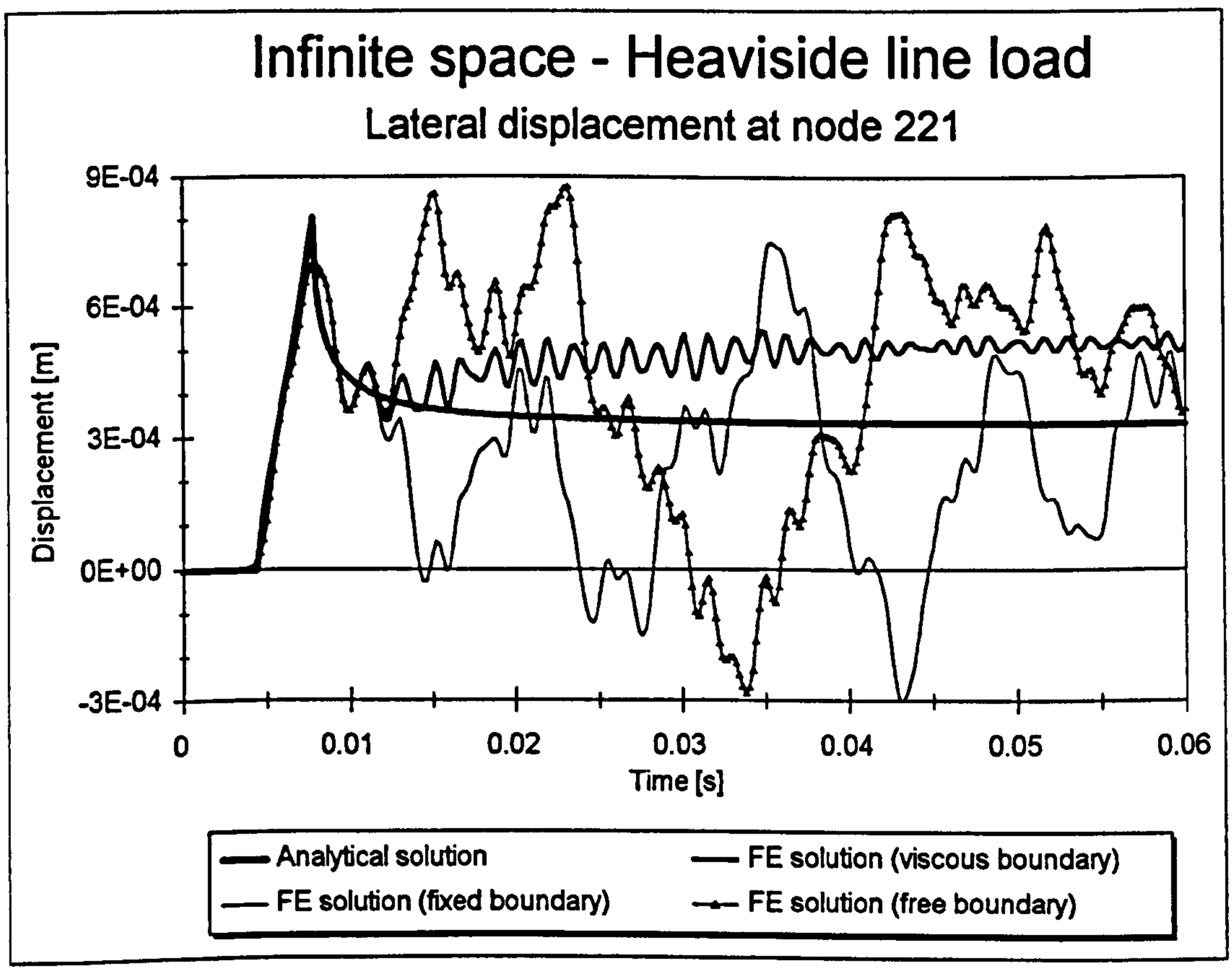

Figure 4.8b - Influence of boundary conditions (lateral displacement)

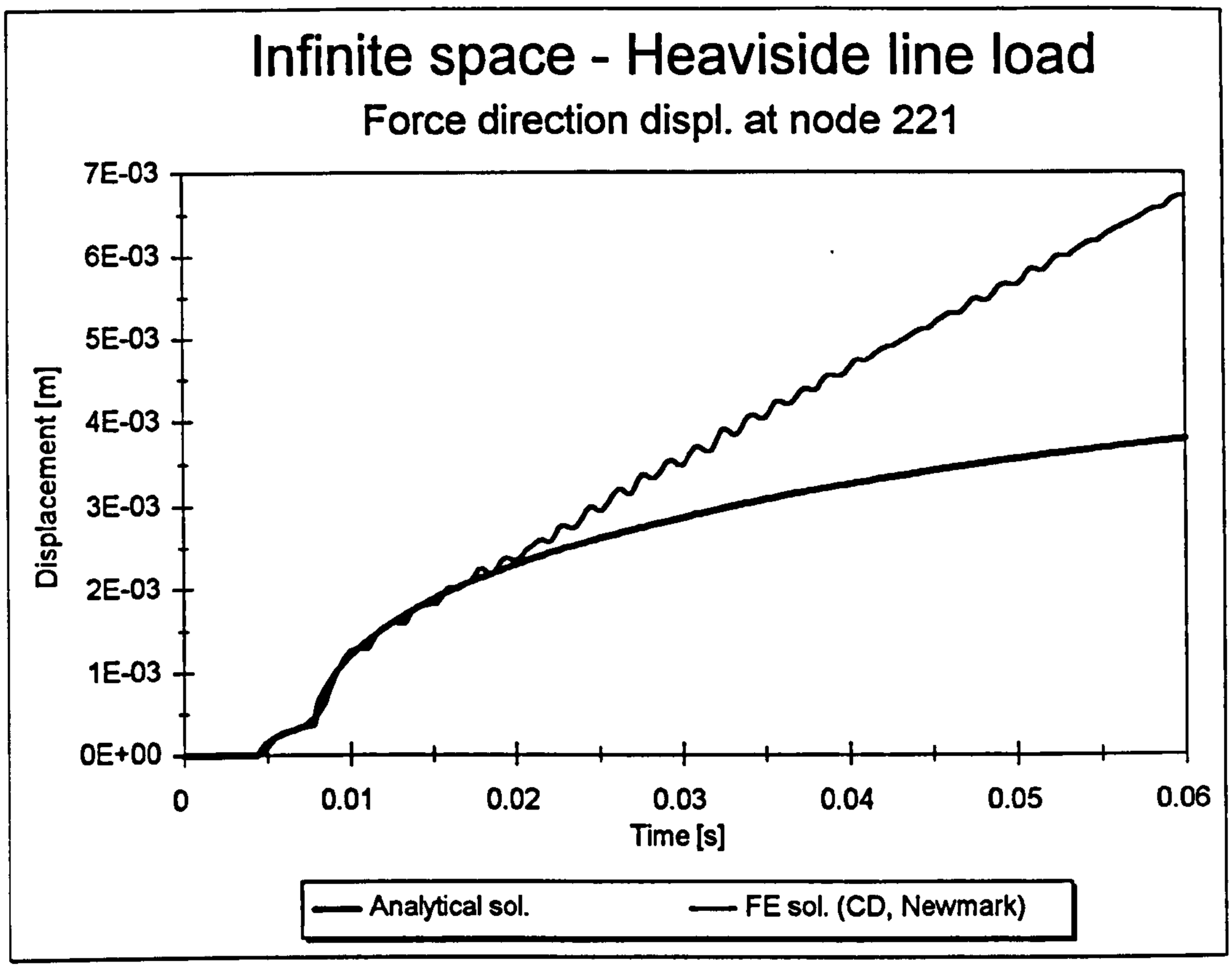

Figure 4.9a - Influence of integration method (displacement in the force direction)

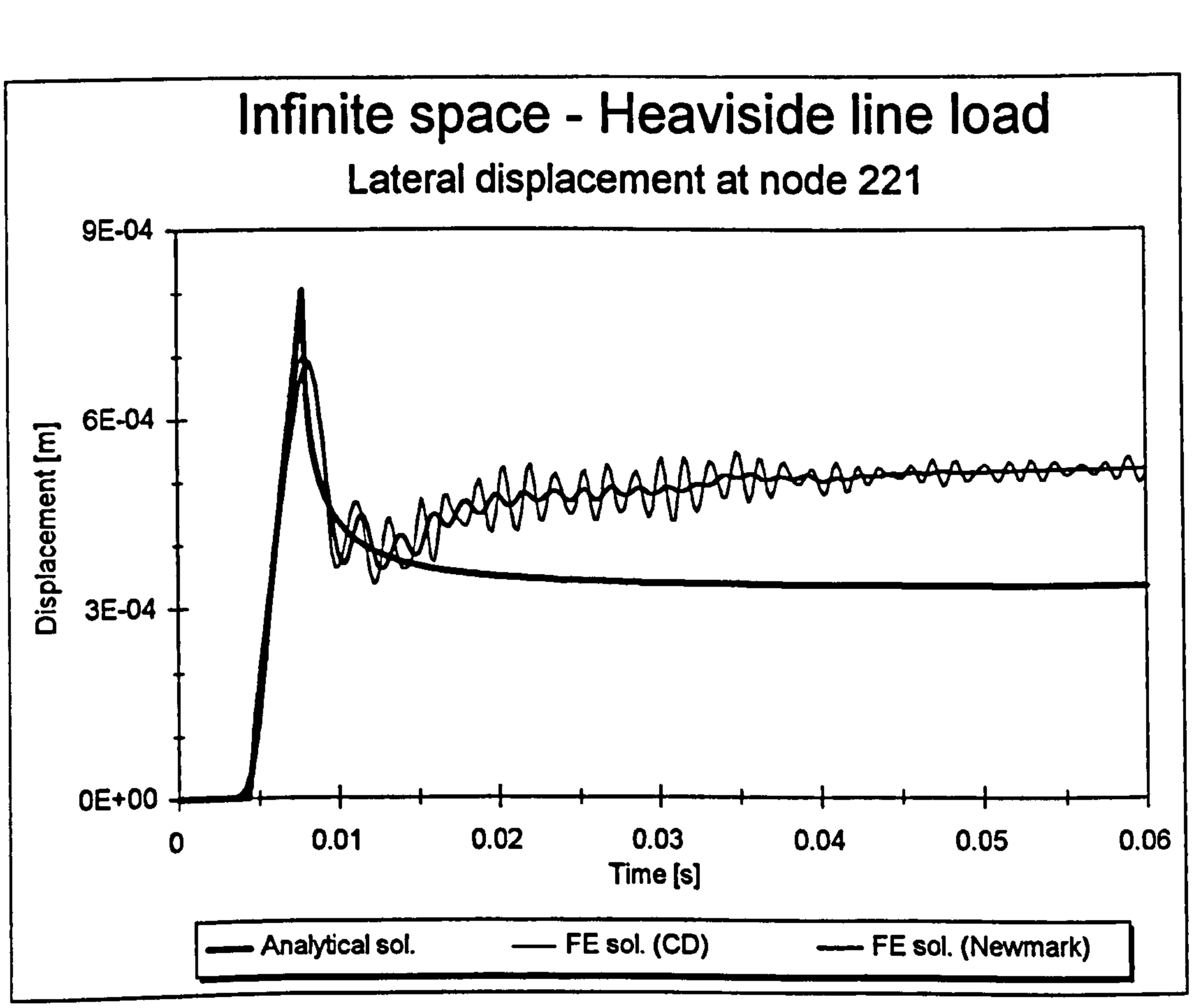

Figure 4.9b - Influence of integration method (lateral displacement)

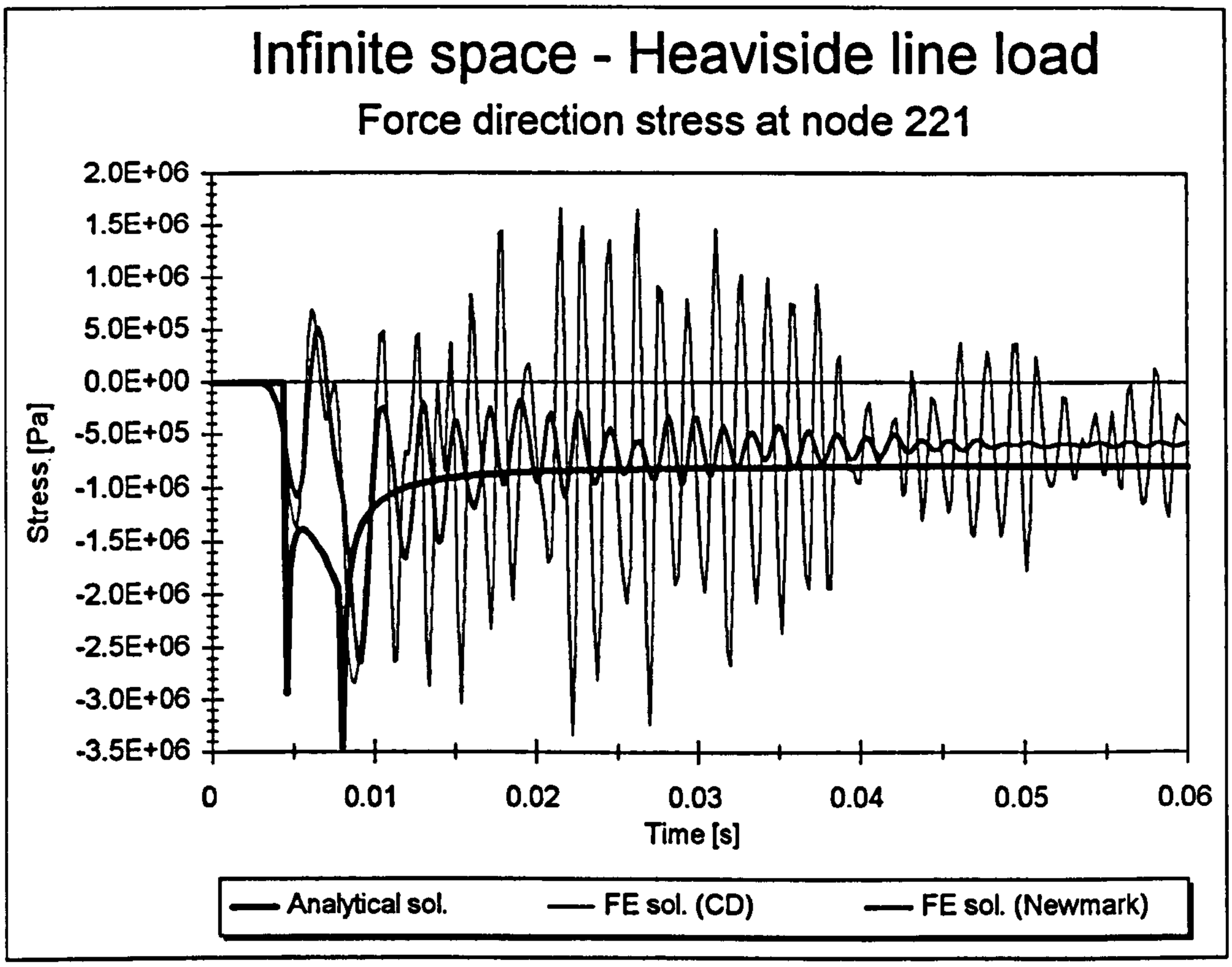

Figure 4.9c - Influence of integration method (stress in the force direction)

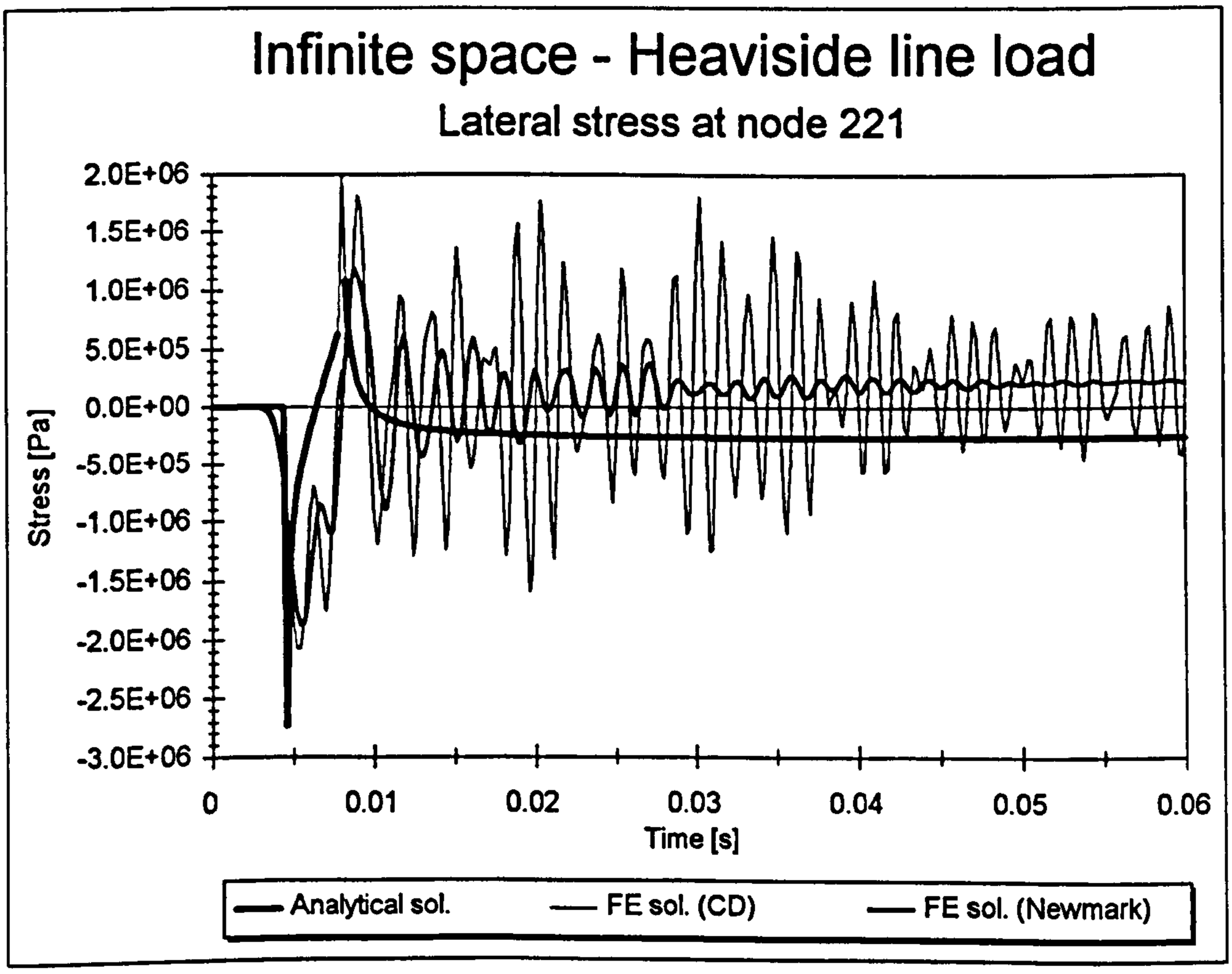

Figure 4.9d - Influence of integration method (lateral stress)

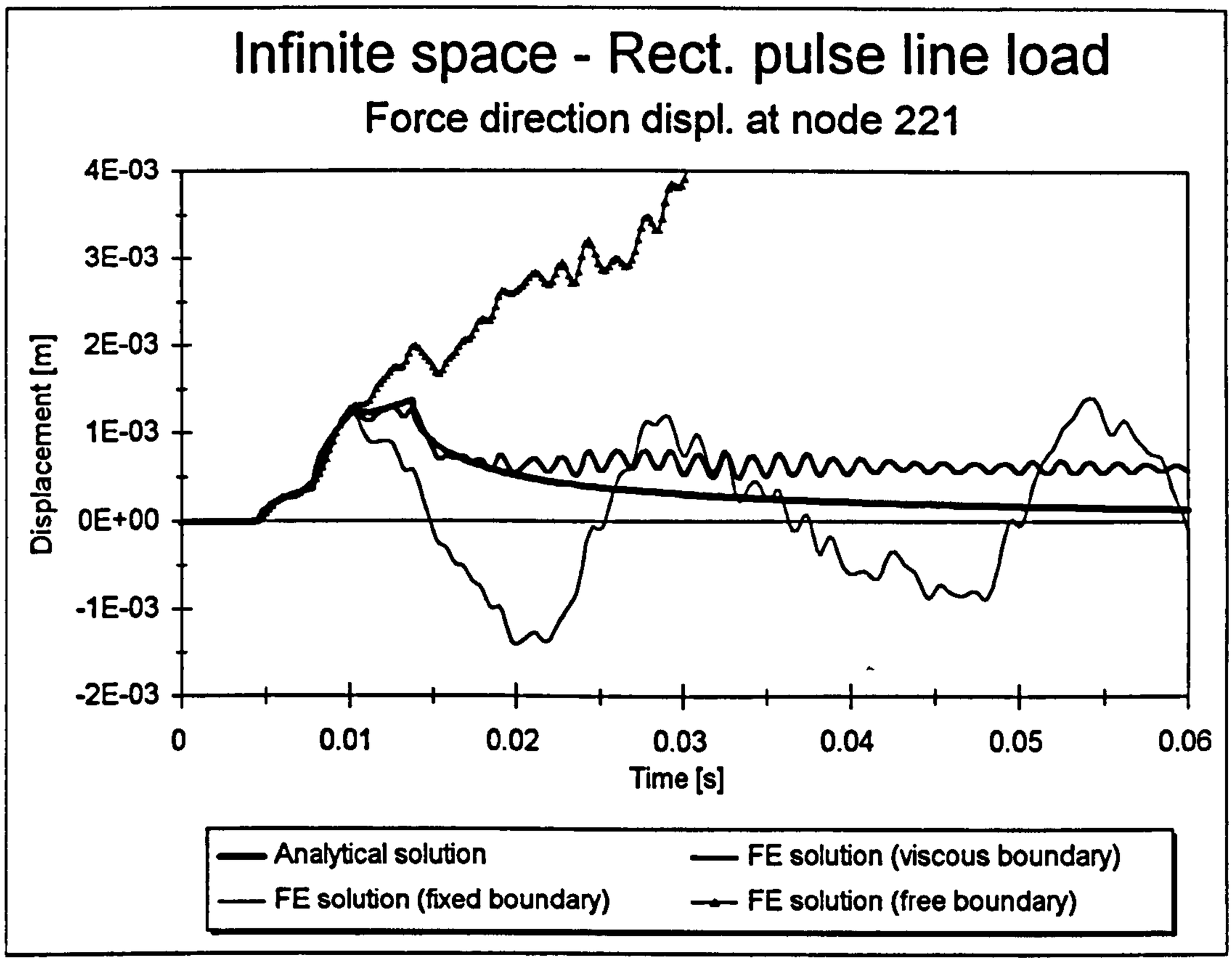

Figure 4.10a - Influence of boundary conditions (displacement in the force direction)

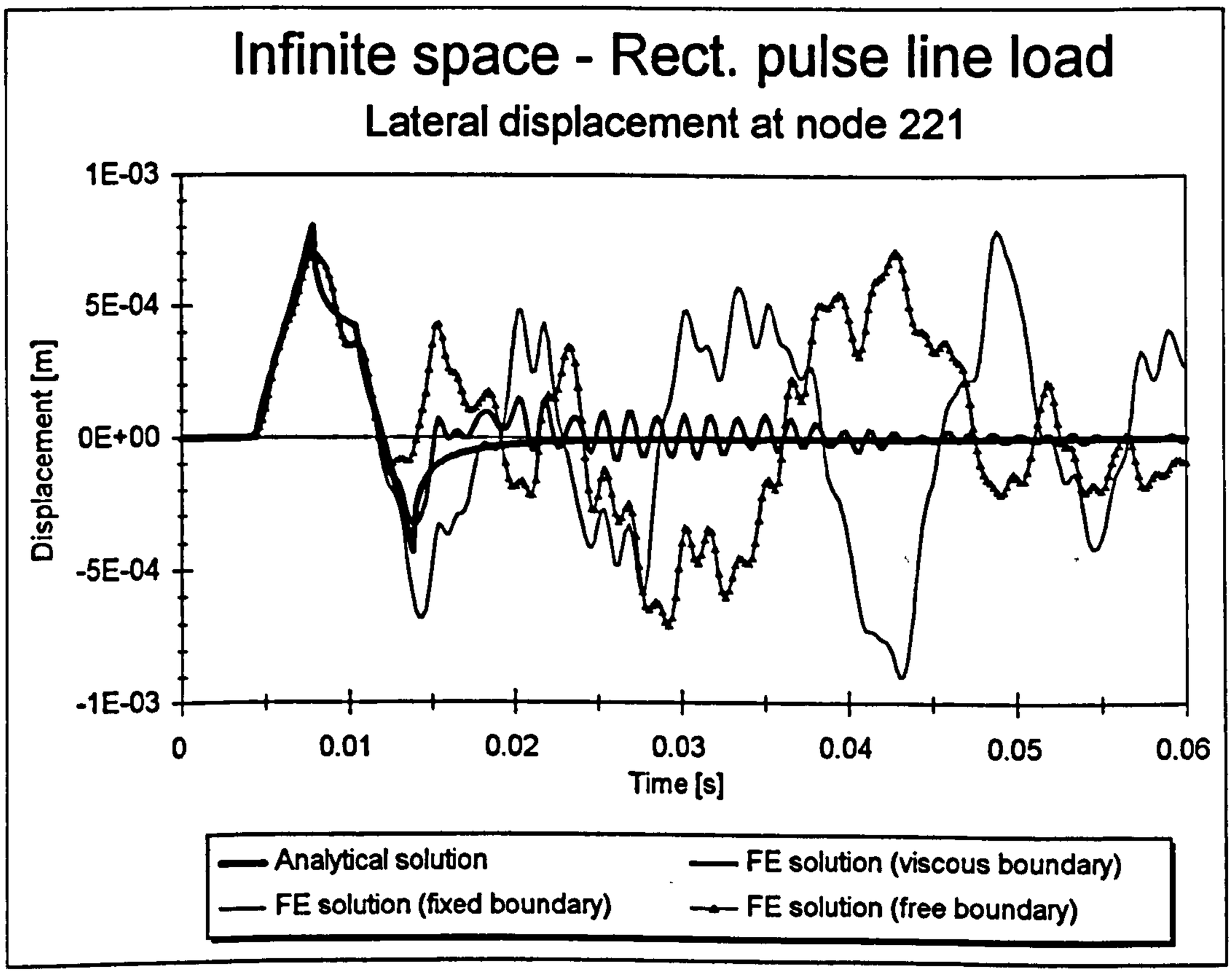

Figure 4.10b - Influence of boundary conditions (lateral displacement)

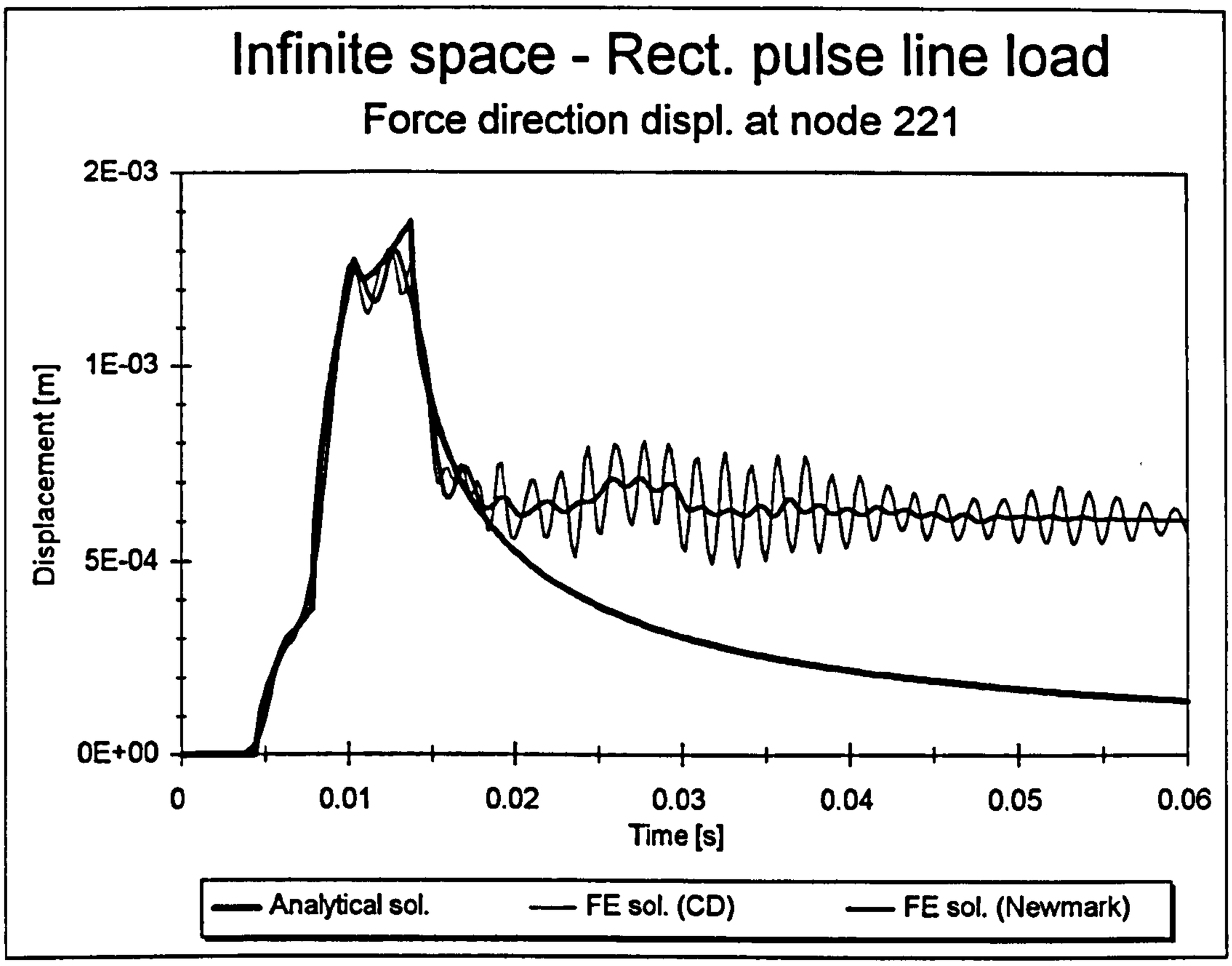

Figure 4.11a - Influence of integration method (displacement in the force direction)

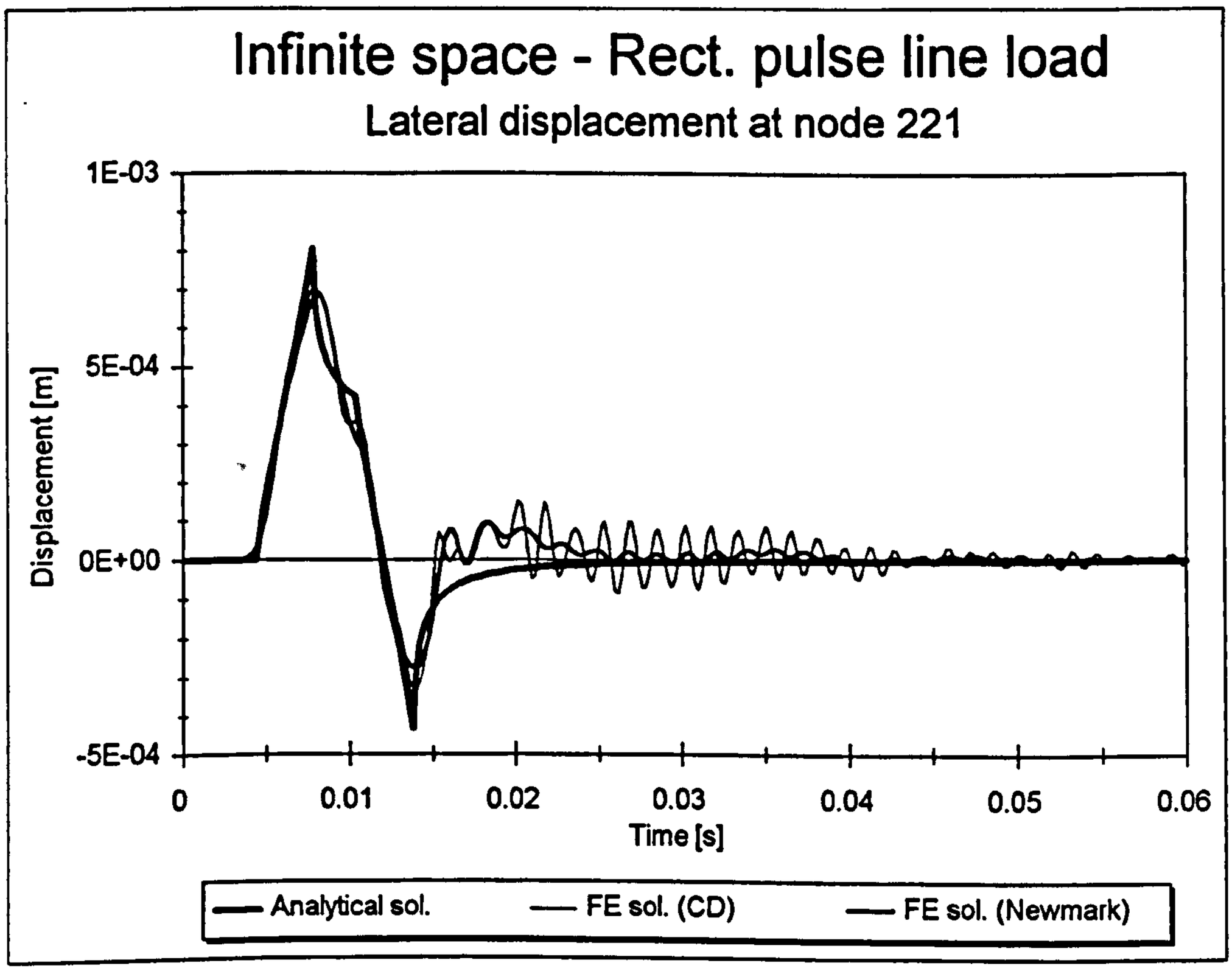

Figure 4.11b - Influence of integration method (lateral displacement)

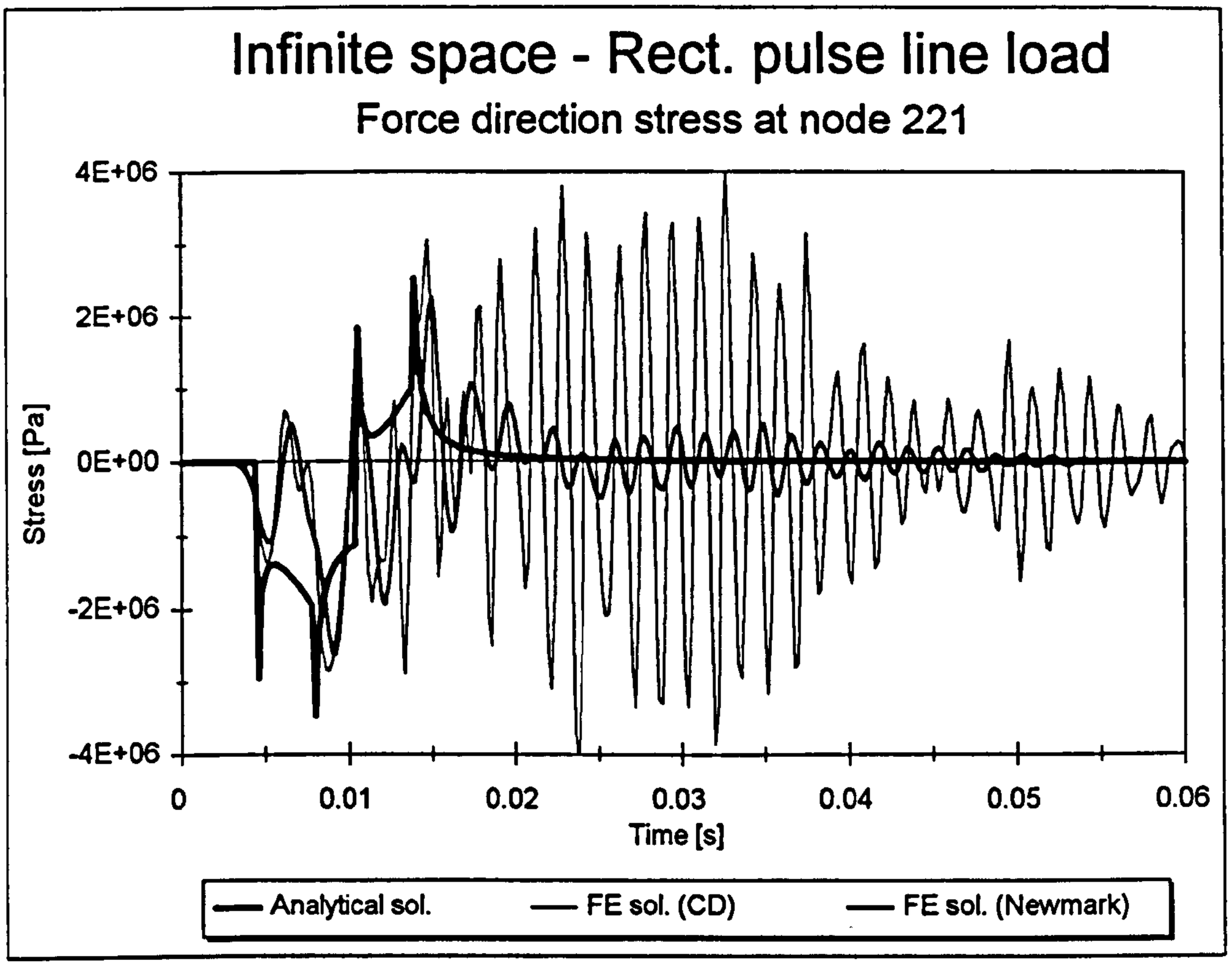

Figure 4.11c - Influence of integration method (stress in the force direction)

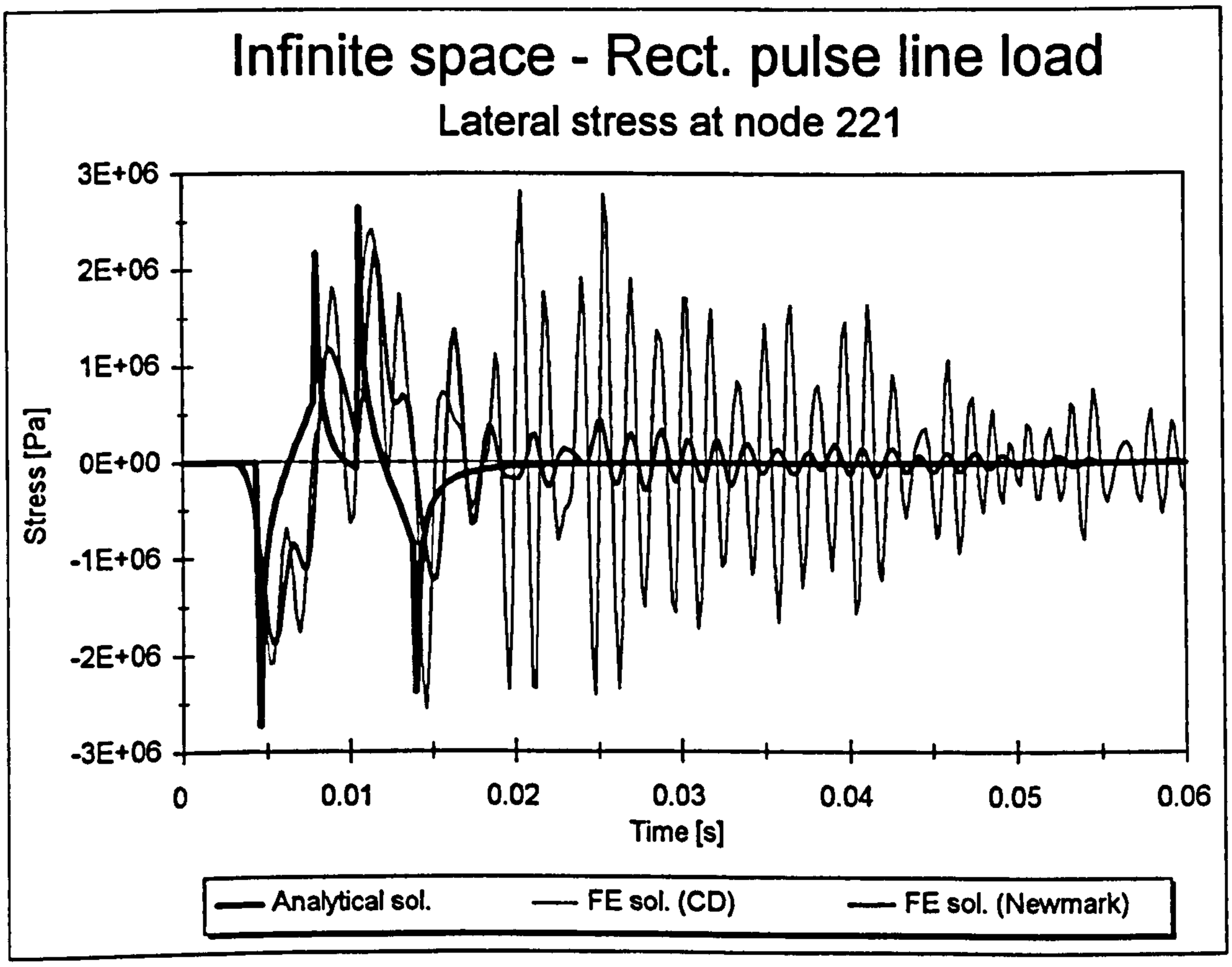

Figure 4.11d - Influence of integration method (lateral stress)

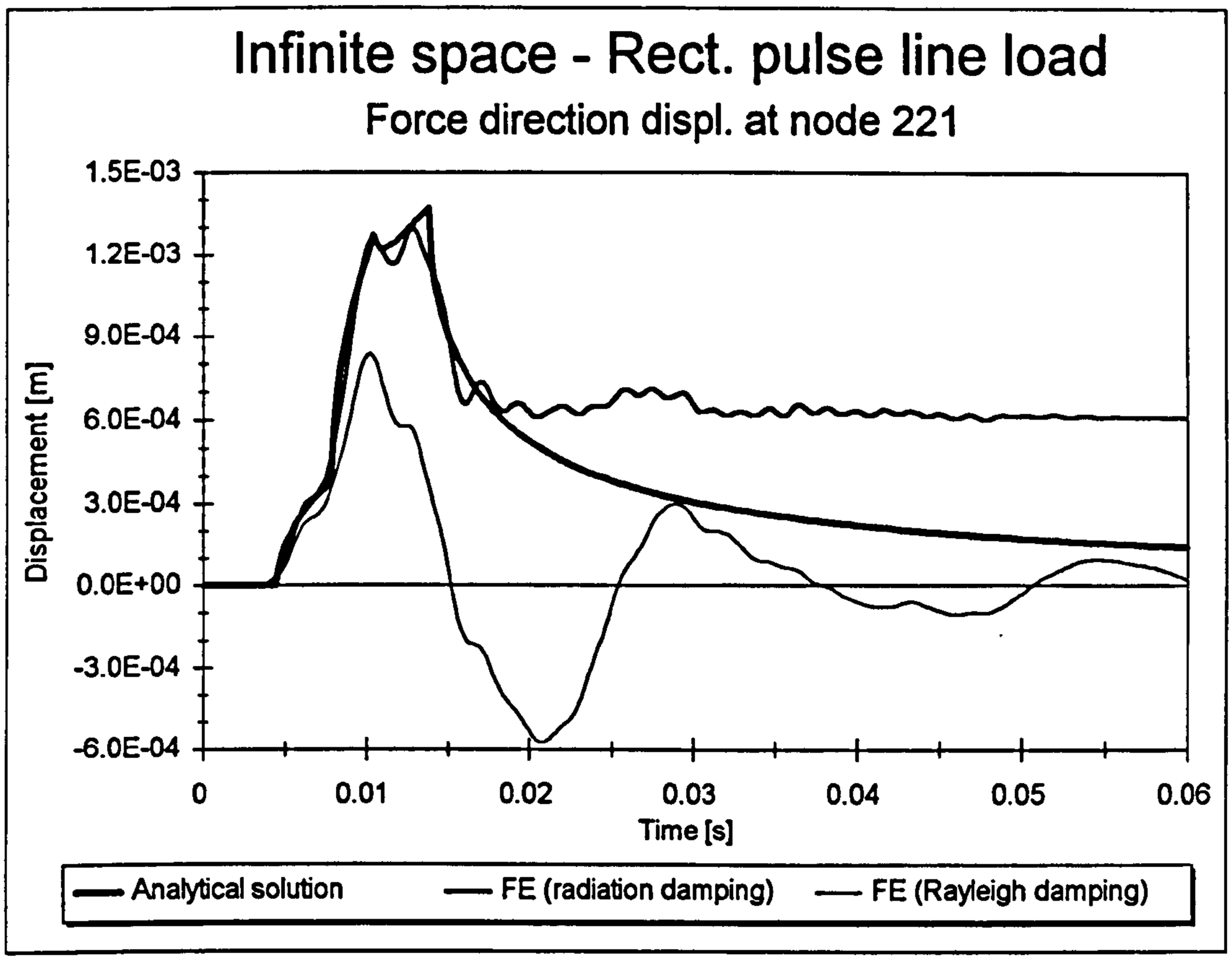

Figure 4.12a - Damping comparison (displacement in the force direction)

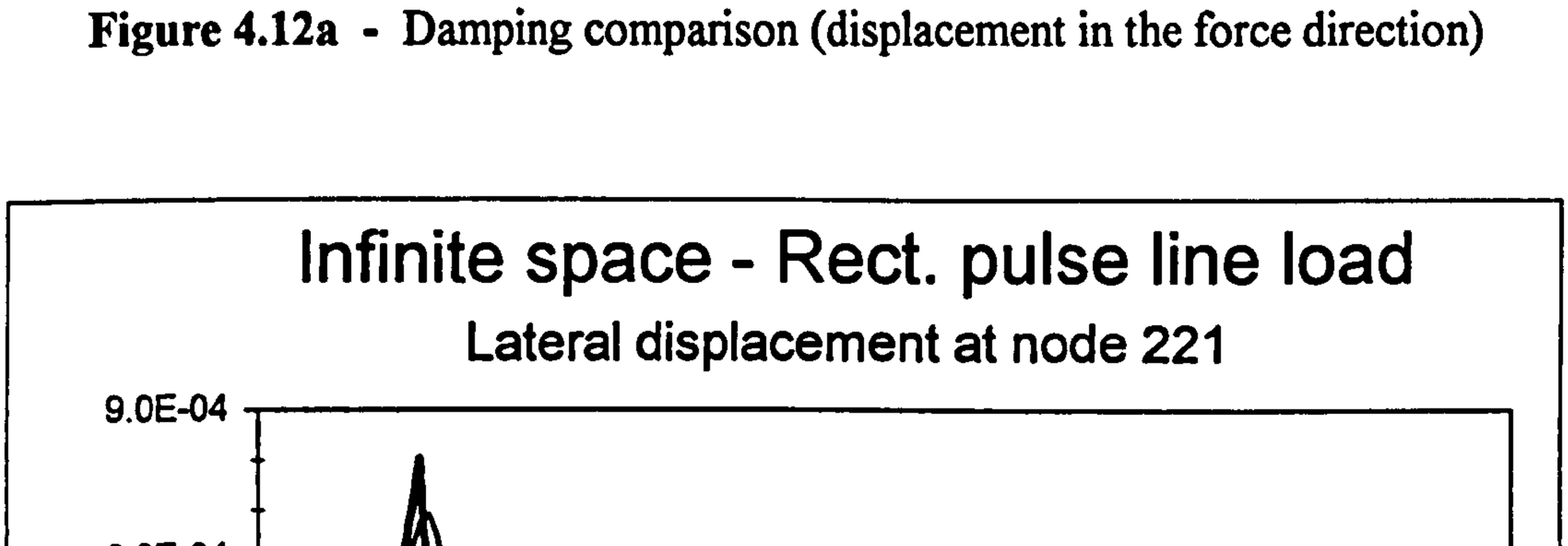

Figure 4.12b - Damping comparison (lateral displacement)

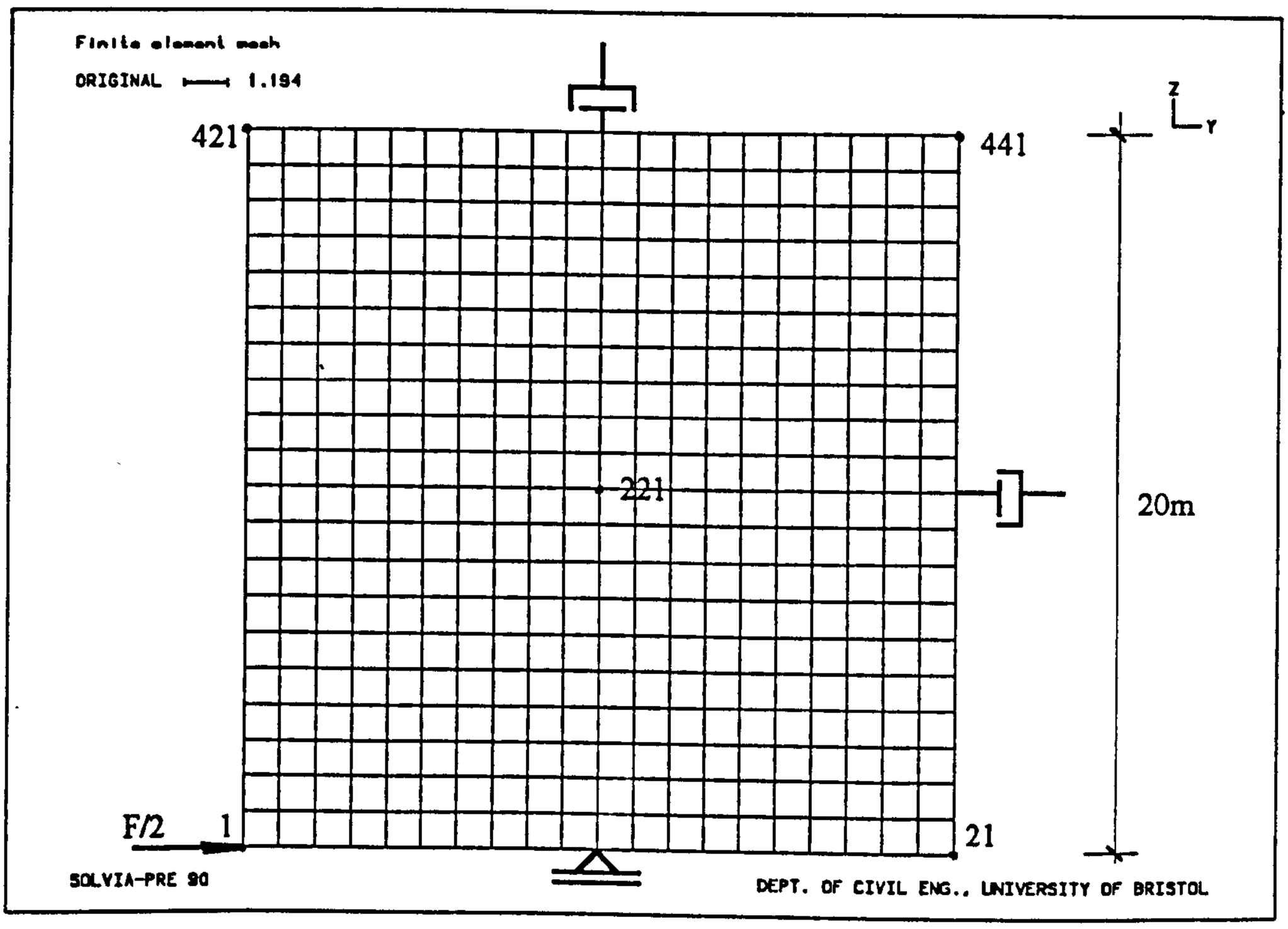

Figure 4.13 - Finite element mesh of one half of the half-space

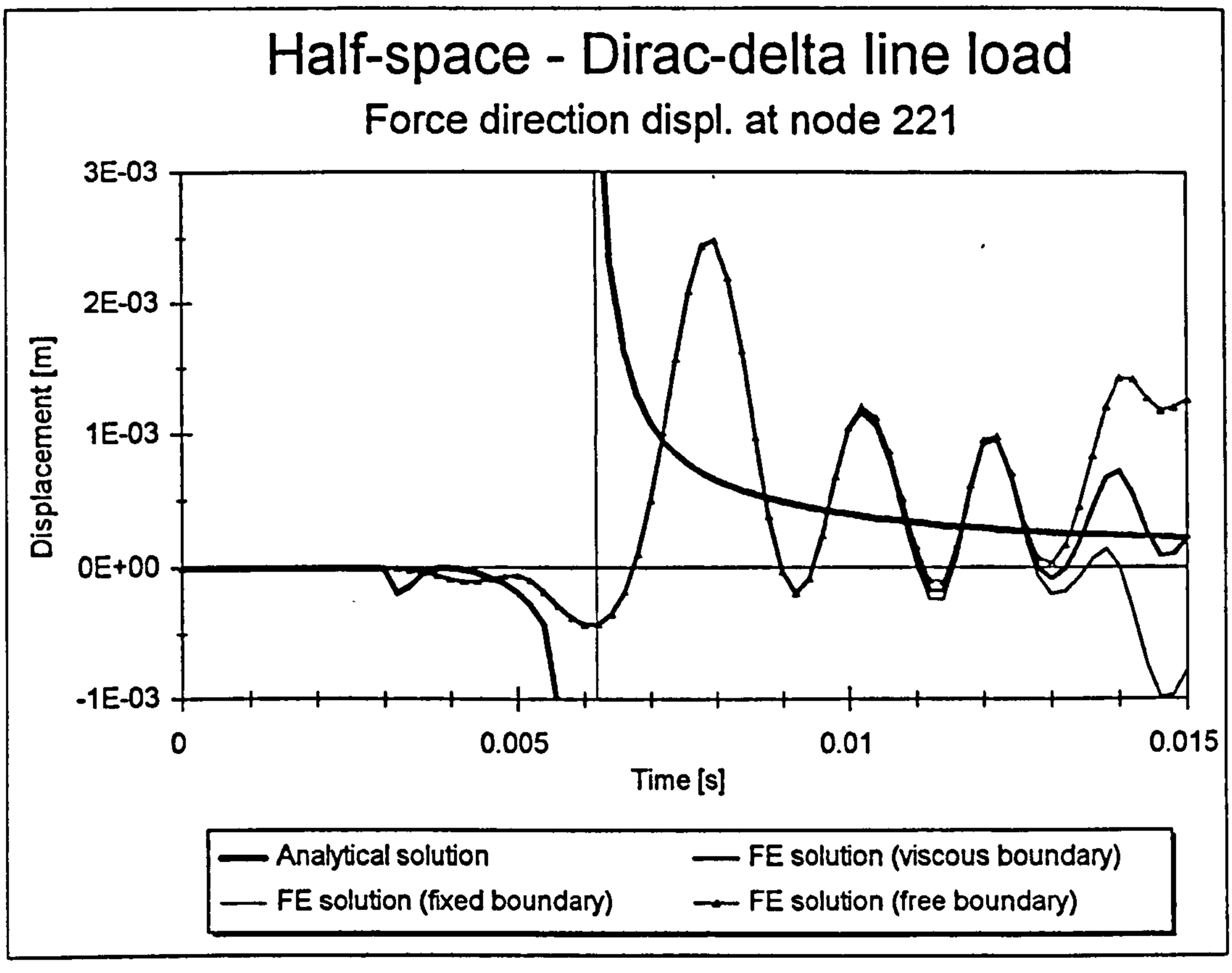

Figure 4.14a - Influence of boundary conditions (displacement in the force direction)

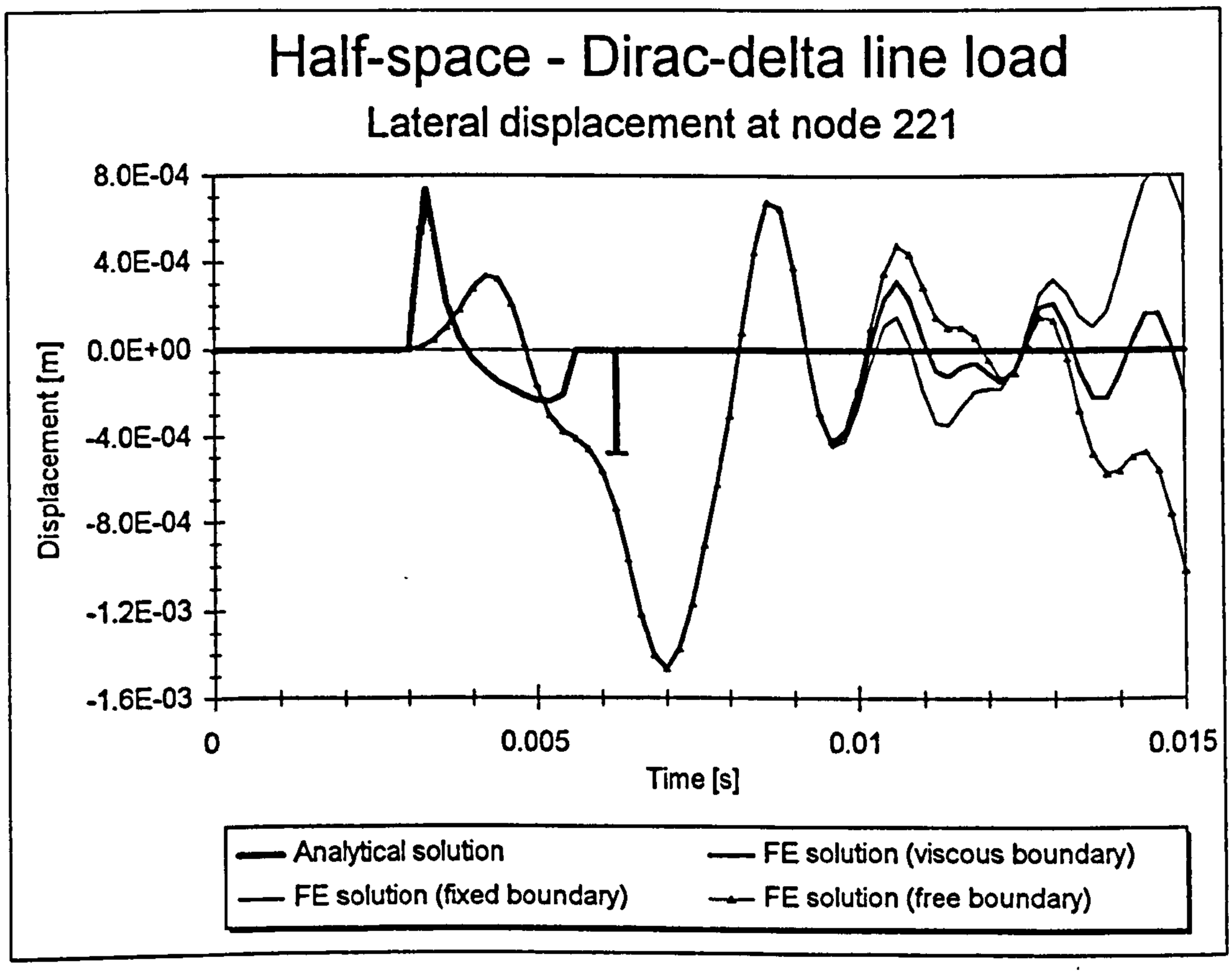

Figure 4.14b - Influence of boundary conditions (lateral displacement)

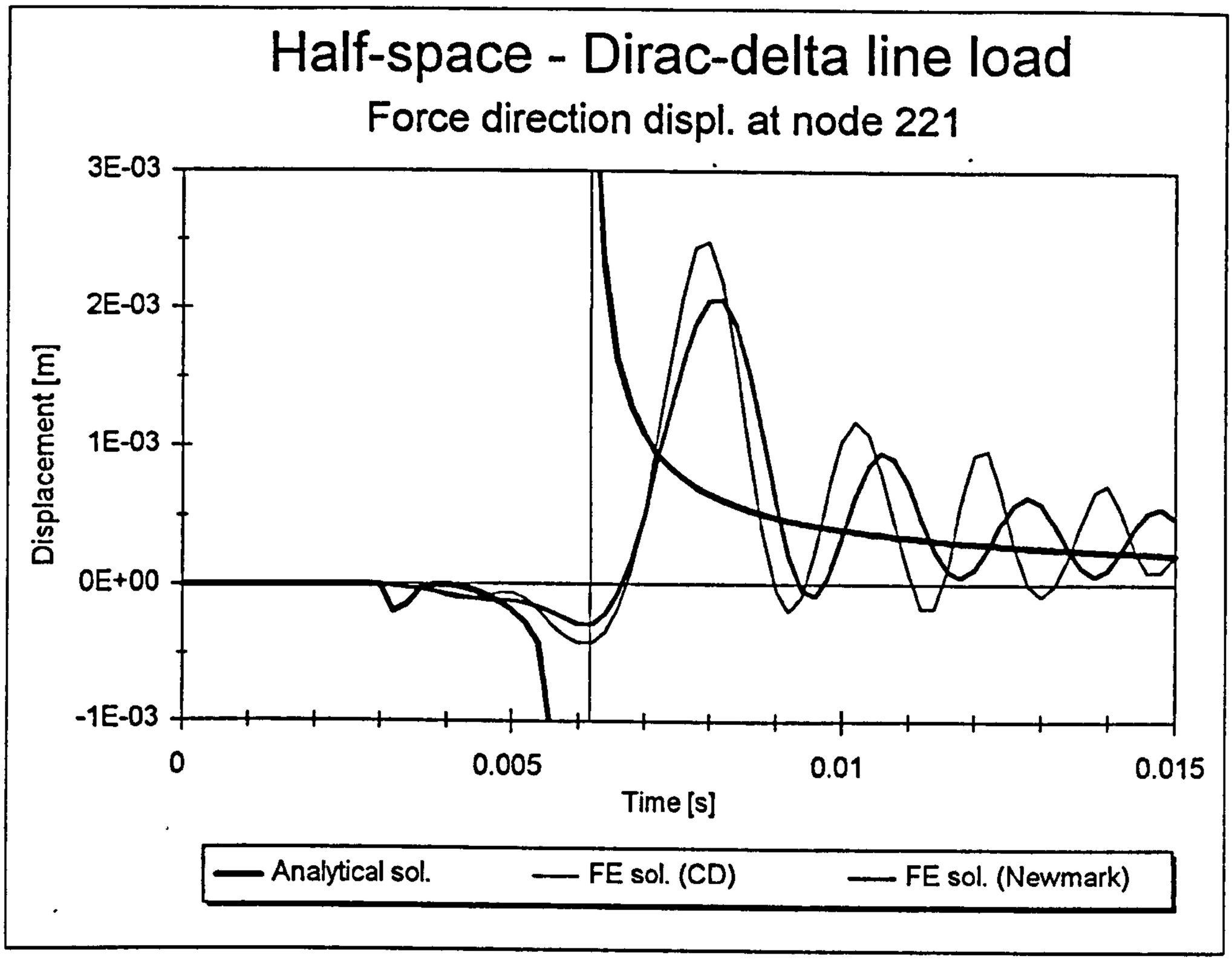

Figure 4.15a - Influence of integration method (displacement in the force direction)

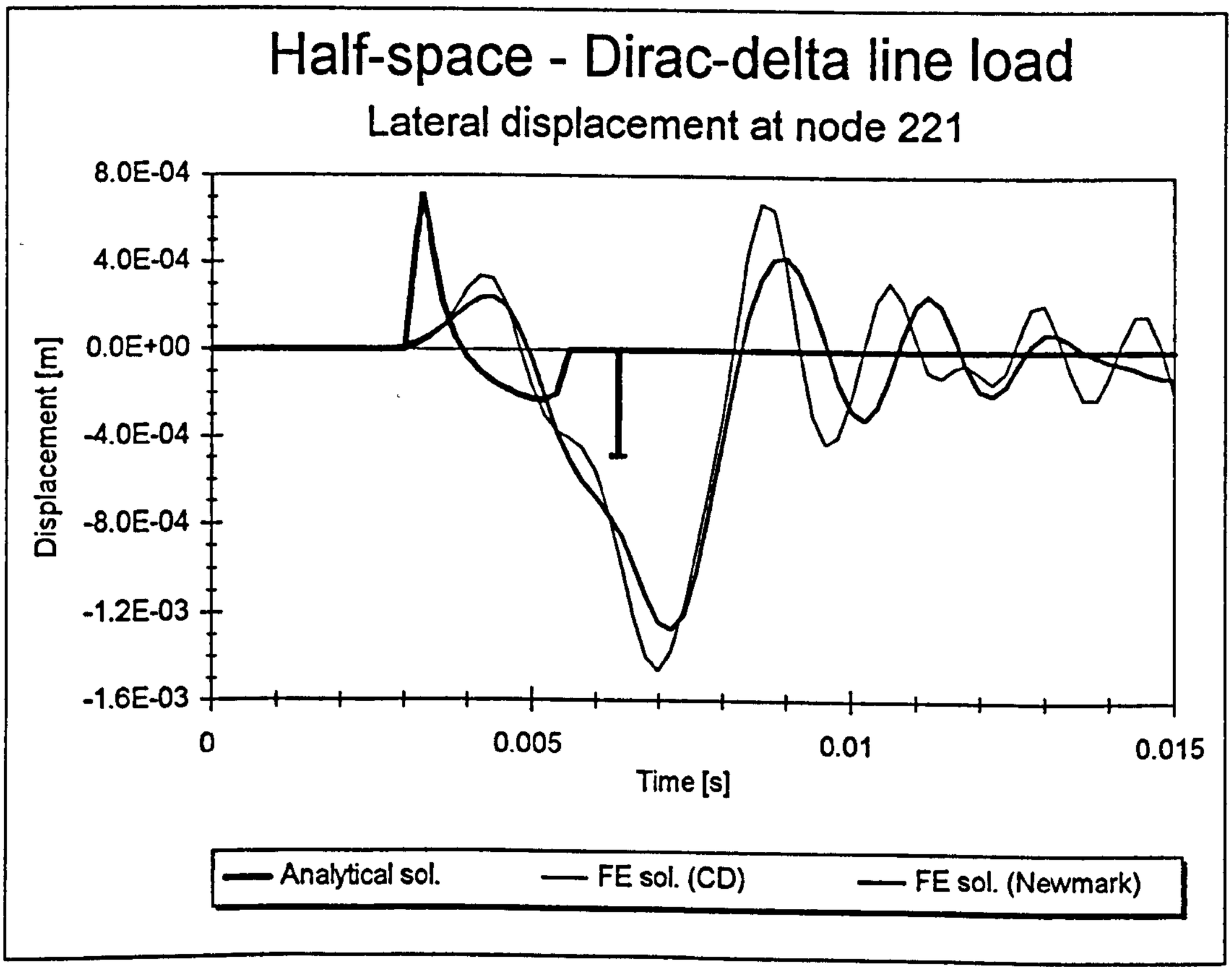

Figure 4.15b - Influence of integration method (lateral displacement)

Seismic Input Mechanisms for Concrete Gravity Dam-Foundation Systems: Theory

Building on the theoretical overview in Chapter 3, Chapter 4 has shown that infinite and semi-infinite media can be modelled by using the Finite Element Method in the time domain. In most cases, the foundations for concrete gravity dams are also semi-infinite. Despite various physical and material discontinuities which will be considered in Chapter 7, the global, half-space effect of the enormous rock mass below these dams cannot be easily altered.

In this Chapter, the structure (concrete gravity dam) is introduced for the first time in the thesis and coupled with its foundation. Under earthquake loading, the seismic input for such a coupled system is not easy to define. In order to shed some light on the arising problems, the main aspects of concrete gravity dam-foundation interaction will be presented by trying to distinguish them from the general theory of soil-structure interaction. In what follows, mathematical formulations for two different seismic input methods will be reviewed. The complete method is associated with the so-called boundary input scheme, while the substructure method is related to the interface input scheme.

To enable the extension towards nonlinear problems (Chapters 7, 8 and 9), all equations will be formulated for the pure Finite Element Method in the time domain. Beforehand, they will be used for initial, linear studies in Chapter 6.

5.1 Concrete Gravity Dam-Foundation Interaction

For a proper analysis of any concrete gravity dam, a significant amount of foundation should be included in any analytical model as soon as its basic properties (at least) are known.

Under earthquake conditions, the standard structural dynamics approach cannot be applied because it is based on the presumption that the excitation is known at the base of the structure. In this case, the 'structure' is the whole dam-foundation system with no clearly identifiable 'base'. The only alternative is to use the rigorous interaction approach, i.e. the theory of soil-structure interaction.

Advances in the nuclear industry and the necessity to ensure the safety of nuclear reactor buildings in the late Sixties and Seventies have put various soil-structure phenomena in the forefront of civil engineering research (Seed et al., 1977; Wolf, 1985; Wolf, 1988). From the first considerations with emphasis on the frequency domain (Lysmer, 1978), attention began to shift towards the time domain (Bayo & Wilson, 1983) once the importance of nonlinear material behaviour due to strong earthquake motions has been recognised. Although the nonlinear soil-structure interaction equations in the time domain were presented on a number of occasions (Bayo & Wilson, 1983; Bayo & Wilson, 1984; Ibrahimbegovic, 1989), they were never extended and applied to nonlinear, cracking problems of concrete dam-foundation systems. To do so, it is very important to acknowledge and accommodate the differences between the general soil-structure interaction problem on one side and the concrete gravity dam-foundation interaction problem on the other. The former, although its name does not necessarily imply so, encompasses a wide range of foundation conditions, beginning with very soft soil and ending with hard rock foundation conditions. On the other hand, most concrete gravity dams require foundation conditions which can be met only by rock formations. This means that the latter case, having to treat the rock foundation only, is less general. Furthermore,

the former case, at least theoretically, covers all types of structures, whereas the latter only deals with excessively massive and rigid structures such as concrete gravity dams. However, the apparent loss of physical generality in the second case is beneficial from the mathematical point of view, as the equations can be simplified and solved more easily. The relevant simplifications will be identified through the derivation of equations in this Chapter and while carrying out actual nonlinear earthquake analyses of dam-foundation systems in Chapter 9.

Earthquake motions which can be observed at the site prior to the construction of the dam are called free-field motions. They will be considered in more detail in the following Subsection. Excavating the foundation and building the structure causes changes in the dynamic system, particularly in the so-called near-field. The near-field motions of the interaction system (provided that the same far-field earthquake excitation is applied) differ from the free-field motions.

The first numerical treatment of soil-structure interaction solely within the framework of finite element analysis began some twenty years ago. Although the computational cost of nonlinear analyses was prohibitive at that time, two important distinctions were made: the first between the kinematic and inertial interaction mechanism (Seed at al., 1977); and the second between the complete and substructure methods of analysis (Lysmer, 1978). They will be considered in more detail in Subsections 5.1.2 and 5.1.3.

5.1.1 Free-Field Response of the Site

The basic assumption of all earthquake interaction problems is that the seismograms of the particular earthquake are known. The earthquake under consideration is treated as deterministic, and it can be either a DBE (Design Basis Earthquake) or MCE (Maximum Credible Earthquake) event (Lane, 1983). The seismograms are usually given at one point on the ground surface of the future dam site.

Unfortunately, this assumption is not often met in reality but saves a great deal of seismological speculation.

The first step in many soil-structure interaction problems is to solve the free-field response of the site, before the excavation and construction take place. Typically starting just from the one, already mentioned point on the ground surface, spatial and temporal variations of motion throughout the site (or at least in the part which will be used in the computational model) should be determined.

As far as the seismic input is concerned, this means that the far-field motion at the distant boundary should be obtained for the complete interaction method of analysis (boundary input scheme). Alternatively, the near-field motion, close to the surface, should be obtained for the substructure method of analysis (interface input scheme). Although the term 'free-field input scheme' is often used for the latter (Zienkiewicz et al., 1986), in the opinion of this author, this is not quite proper since scattered motions (and not free-field) are used in some cases, as will be elaborated in Section 5.3. 'Interface input scheme' would be better suited because motions are always prescribed at some kind of interface. Moreover, the word 'interface' points out at the particular location, which is consistent with the alternative, 'boundary' input scheme.

. The task of determining the free-field response of the site is extremely difficult because of the need to decompose the recorded surface time histories into different types of waves. In the two dimensional case, i.e. for the in-plane problem, the ground surface motion can arise from P, SV and surface Rayleigh-waves. Since the identification of the wave pattern is not a straightforward procedure, restrictive assumptions have to be made. One of the most popular and widely used is the assumption that the motions of the free-field result from the vertical propagation of shear (SV) waves. The problem becomes one dimensional and may be solved in the frequency domain (the so-called deconvolution analysis by the inverse application of the equations of SV-wave propagation in a layered foundation). Only horizontal motions exist and all points at the same depth have the same motion.

In order to obtain more rigorous conclusions on the determination of in-plane free-field response of the sites, Wolf (1983, 1985) performed a parametric study, varying the nature of the wave pattern on a soft soil and rock site. Since concrete gravity dams cannot be built on soft soils, only the conclusions from the rock site are repeated here:

a) If only one component of the known surface motion (e.g. the horizontal) needs to be matched, it can be associated either with a body wave or with a surface wave.

b) If both components of the surface motion (horizontal and vertical) need to be matched, they can arise from a combination of P and SV-waves. Surface waves alone cannot be used to match both components and a body wave has to be included (preferably a P-wave).

c) If the horizontal surface motion is associated with Rayleigh-waves, stronger reduction of the motion with depth throughout the frequency range is observed than for vertically propagating SV-waves.

For some soil-structure interaction analyses (as will be shown in Section 5.3), it is not enough to determine the free-field response of the site. Instead, the so-called scattering problem has to be solved. In the theory of elastic waves (Ewing et al., 1957; Graff, 1975; Miklowitz, 1978), scattering problems arise when waves propagating through a half-space encounter discontinuities or boundaries of complex shape such as cavities, inclusions or excavations. For the purpose of earthquake analysis of concrete gravity dam-foundation systems, this problem is limited to the excavation for the dam. A free-field problem is shown in Figure 5.1a; the scattering one in Figure 5.1b. The task required for some of the substructure methods (Section 5.3) consists of determining motions along an interface in the foundation (either the excavation line - the future dam-foundation interface, or a deeper, foundation-foundation interface). Unfortunately, if it proves difficult to solve the general free-field problem, it is even more difficult to solve the scattering problem. Therefore, it

is desirable to replace the scattered motions with free-field motions, whenever possible.

5.1.2 Interaction Mechanisms

After the excavation and construction of the structure on a former free-field site, the whole dynamic system is completed. The arising interaction mechanism in earthquake conditions is very complex. Incident seismic waves propagate through the foundation, finally reaching the structure. A load causing displacements is almost immediately accompanied by the generation of outgoing waves and a relief of the dynamic loading.

Despite the relatively complicated coupling mechanism, it has long been attempted to use analytical models for soil-structure interaction and to keep them updated with the advances in computational techniques. In one of the first attempts (Seed et al., 1977), a complete interaction analysis was carried out in two steps and a clear distinction between the two interaction parts, kinematic and inertial, was established. It was assumed that the excitation was known in the form of far-field, basement rock input. In the first step, the structure had no mass. The computed motions, relative to the basement rock motion, differed from the free-field motions due to the stiffness and damping of the structure. This part of the interaction was called kinematic because the structure acted as a kinematic constraint in the response. In the second step, the excitation consisted of forces applied to the structure. These forces were the product of the mass of the structure and the acceleration determined by adding the acceleration obtained in the first step to the basement rock acceleration. The computed motions again differed from the free-field motions. This part of the interaction was called inertial because the inertial properties of the structure changed the response. When added, the two steps form a complete analysis. However, it is obvious that the described partition principle does not simplify the calculation of the overall response. Its main contribution was a further insight into the interaction

phenomena by means of establishing whether and in what cases it is possible to neglect the first step and carry out the inertial interaction analysis only, thus greatly simplifying the whole problem. The following conclusions on ignoring the kinematic interaction analysis were reached (Seed et al., 1977):

a) Such a procedure is perfectly justified in the case of surface structures.

b) For embedded structures, the assumption that only an inertial interaction analysis can provide accurate results is equivalent to assuming that for the kinematic interaction analysis, the foundation above the base of the structure is rigid.

When these conclusions are applied to concrete gravity dams it becomes obvious that in most cases, the inertial interaction can provide sufficiently accurate results because the embedment is not considerable (approximately one tenth of the height of the dam) and because the surrounding rock foundation is fairly rigid. Further details on this matter will be given in Section 5.3.

Regardless of the type of the adopted interaction model, transmitting boundaries have to be implemented as described in Chapter 4. The foundation is of the rock half-space type and the radiation damping effects are significant. Wolf (1988) stated some basic recommendations on where to place the transmitting boundaries:

a) For body waves, the farther away from the vibrating source the boundary is placed, the more accurate it is.

b) For surface waves, placing the viscous, paraxial and extrapolation boundaries farther away from the vibrating source does not improve the accuracy.

It is obvious that these recommendations were made for the case of an external load which is applied directly on the foundation. However, in earthquake conditions, when the load is introduced through the foundation, it is essential to ensure that the transmitting boundaries refer not to the total motion, but only to the total minus free-field (or scattered) motion. This fact is very important as far as seismic input is

concerned - it disables the use of the boundary input scheme with transmitting boundaries, unless special procedures are implemented.

5.1.3 Methods of Interaction Analysis

The two methods of interaction analysis, complete and substructure, were already mentioned and they will be briefly overviewed here. The rigorous mathematical formulations of their respective seismic input schemes (boundary and interface) will be presented in Sections 5.2 and 5.3, respectively.

The complete method requires knowledge either of the source or far-field excitations. Clearly, in the case of earthquake excitation, where the source might be tens or hundreds of kilometres away, a complete source analysis would not be feasible. Moreover, for the knowledge of the far-field excitation, a full free-field analysis of the site would have to be undertaken, with all necessary restrictive assumptions characterising the current state-of-the-art (Wolf, 1985). In other words, a complete method is a two-step method, comprising of the free-field and complete interaction analysis. Further difficulties with this approach are associated with the performance of transmitting boundaries, and this will be addressed in Section 5.4.

The substructure method was initially devised out of the desire to break the soil-structure system into its two constituent parts. Probably its most important feature is that it requires only knowledge of the near-field excitation, usually in the form of free-field ground motions. Therefore, no free-field analysis of the site is necessary, which means that the substructure method is a one-step method, comprising only of the interaction analysis. Historically, the substructure method gained its popularity in the frequency domain, where both the structure and soil had their respective equations defined and then combined to obtain the frequency domain equations of the whole system (Fenves & Chopra, 1984). Obviously, only linear elastic materials could have been treated. The logical way forward was to allow for the rise of

nonlinearities, which necessitated the introduction of the time-domain. The intermediate solution was to allow nonlinearities in the structure only (leaving the soil to be defined by the equations of the continuum, in the frequency domain). The more general case, the one that will be treated in Section 5.3, is to allow the nonlinear behaviour both in the structure and soil.

5.1.4 Location of Nonlinearities

The nonlinearities which might develop in concrete gravity dam-foundation systems will be treated in detail in Chapter 7. At this stage and for the purpose of derivation of equations in the following Sections, it suffices to divide them with respect to the location of their occurence.

The first possibility is that the nonlinear behaviour is encountered in the whole system. This situation is shown in Figure 5.2a, where the letter *N* is used to point out to the nonlinearities. The boundary input scheme would have to be used, with the response of the whole system being expressed in terms of total displacements.

The other possibility is that the nonlinear behaviour is confined to the dam and to a relatively small part of the foundation close to the dam. This situation is often called 'local nonlinearity' and is shown in Figure 5.2b. It is based on common sense and includes most practical cases except contact nonlinearities (joints and faults) deeper in the foundation . In this case, both the boundary and interface input schemes can be used. The only limiting assumption is that the excavation and superposition of the dam must not affect the global seismic input, i.e. the earthquake in the far-field (Aydinoglu, 1980).

The special case of the 'local nonlinearity model' is shown in Figure 5.2c, where nonlinearities are confined to the dam and interface. In this particular case, the interface is flat and superficial (not embedded).

5.2 Boundary Input Scheme

The concrete gravity dam-foundation system shown in Figure 5.3 is considered. The nodes along the dam-foundation interface are denoted by I while the remaining nodes of the dam and foundation are denoted by D and F, respectively. B is used to represent the boundary and together with the others will appear in the form of subscripts for submatrices **m**, **c** and **k**, of the mass, damping and stiffness matrix (**M**, **C** and **K**, respectively).

The time domain equation of motion of the total system for earthquake excitation can be formulated after assembling the property matrices

$$\begin{bmatrix} \mathbf{m}_{DD} & \mathbf{m}_{DI} & \mathbf{0} & \mathbf{0} \\ \mathbf{m}_{ID} & \mathbf{m}_{II} & \mathbf{m}_{IF} & \mathbf{0} \\ \mathbf{0} & \mathbf{m}_{FI} & \mathbf{m}_{FF} & \mathbf{m}_{FB} \\ \mathbf{0} & \mathbf{0} & \mathbf{m}_{BF} & \mathbf{m}_{BB} \end{bmatrix} \begin{Bmatrix} \ddot{\mathbf{r}}_D \\ \ddot{\mathbf{r}}_I \\ \ddot{\mathbf{r}}_F \\ \ddot{\mathbf{r}}_B \end{Bmatrix} + \begin{bmatrix} \mathbf{c}_{DD} & \mathbf{c}_{DI} & \mathbf{0} & \mathbf{0} \\ \mathbf{c}_{ID} & \mathbf{c}_{II} & \mathbf{c}_{IF} & \mathbf{0} \\ \mathbf{0} & \mathbf{c}_{FI} & \mathbf{c}_{FF} & \mathbf{c}_{FB} \\ \mathbf{0} & \mathbf{0} & \mathbf{c}_{BF} & \mathbf{c}_{BB} \end{bmatrix} \begin{Bmatrix} \dot{\mathbf{r}}_D \\ \dot{\mathbf{r}}_I \\ \dot{\mathbf{r}}_F \\ \dot{\mathbf{r}}_B \end{Bmatrix} +$$

$$+ \begin{bmatrix} \mathbf{k}_{DD} & \mathbf{k}_{DI} & \mathbf{0} & \mathbf{0} \\ \mathbf{k}_{ID} & \mathbf{k}_{II} & \mathbf{k}_{IF} & \mathbf{0} \\ \mathbf{0} & \mathbf{k}_{FI} & \mathbf{k}_{FF} & \mathbf{k}_{FB} \\ \mathbf{0} & \mathbf{0} & \mathbf{m}_{BF} & \mathbf{m}_{BB} \end{bmatrix} \begin{Bmatrix} \mathbf{r}_D \\ \mathbf{r}_I \\ \mathbf{r}_F \\ \mathbf{r}_B \end{Bmatrix} = \begin{Bmatrix} \mathbf{0} \\ \mathbf{0} \\ \mathbf{0} \\ \mathbf{R}_B \end{Bmatrix} \tag{5.1}$$

where $\ddot{\mathbf{r}}$, $\dot{\mathbf{r}}$ and $\mathbf{r}$ are the subvectors (according to the appropriate subscripts) of the total acceleration, velocity and displacement vectors, respectively. $\mathbf{R}_B$ denotes the vector of the reaction forces at the boundary.

If the artificial boundaries of the foundation model (in the case of an existing basement rock only the lateral boundaries are artificial) are placed so far away from the dam that its influence on the dynamic response is not felt, the motion of the boundaries $\mathbf{r}_B$ coincides with its free-field motion, i.e. with the far field motion. Since the equilibrium subequation for the boundary nodes is used only to obtain the

reaction forces $\mathbf{R}_B$, it may be omitted. The final time domain equation of motion of the total system, in the case of the boundary input scheme, can be obtained after rearranging the previous matrix equation:

$$\begin{bmatrix} \mathbf{m}_{DD} & \mathbf{m}_{DI} & \mathbf{0} \\ \mathbf{m}_{ID} & \mathbf{m}_{II} & \mathbf{m}_{IF} \\ \mathbf{0} & \mathbf{m}_{FI} & \mathbf{m}_{FF} \end{bmatrix} \begin{Bmatrix} \ddot{\mathbf{r}}_D \\ \ddot{\mathbf{r}}_I \\ \ddot{\mathbf{r}}_F \end{Bmatrix} + \begin{bmatrix} \mathbf{c}_{DD} & \mathbf{c}_{DI} & \mathbf{0} \\ \mathbf{c}_{ID} & \mathbf{c}_{II} & \mathbf{c}_{IF} \\ \mathbf{0} & \mathbf{c}_{FI} & \mathbf{c}_{FF} \end{bmatrix} \begin{Bmatrix} \dot{\mathbf{r}}_D \\ \dot{\mathbf{r}}_I \\ \dot{\mathbf{r}}_F \end{Bmatrix} + \begin{bmatrix} \mathbf{k}_{DD} & \mathbf{k}_{DI} & \mathbf{0} \\ \mathbf{k}_{ID} & \mathbf{k}_{II} & \mathbf{k}_{IF} \\ \mathbf{0} & \mathbf{k}_{FI} & \mathbf{k}_{FF} \end{bmatrix} \begin{Bmatrix} \mathbf{r}_D \\ \mathbf{r}_I \\ \mathbf{r}_F \end{Bmatrix} =$$

$$= - \begin{Bmatrix} \mathbf{0} \\ \mathbf{0} \\ \mathbf{m}_{FB}\ddot{\mathbf{r}}_B + \mathbf{c}_{FB}\dot{\mathbf{r}}_B + \mathbf{k}_{FB}\mathbf{r}_B \end{Bmatrix} \tag{5.2}$$

The seismic input on the righthand side of Equation (5.2) is prescribed as an effective load for which the knowledge of the boundary acceleration $\ddot{\mathbf{r}}_B$, velocity $\dot{\mathbf{r}}_B$ and displacement $\mathbf{r}_B$ is necessary. Unfortunately, it is extremely difficult to know the earthquake excitation in the far-field. For the the current state-of-the-art analyses, stringent assumptions, elaborated in Subsections 5.1.1 and 5.1.3, are needed. However, this approach has two advantages. The first is the absence of any limitation on the type of motion that may be imposed at boundary nodes. A different history of motion may be specified for each boundary node, meaning that the earthquake waves travelling through the foundation can be represented with both spatial and temporal variation (Zienkiewicz et al., 1986). The second advantage arises from the fact that the response is expressed in terms of total motion, making the formulation valid for the case of full nonlinear behaviour of the dam and foundation. Unfortunately, the computer code which would be able to deal with both problems simultaneously has not yet been reported, although some initial steps were made by Hallquist (1991).

5.2.1 Linear Analysis

Equation (5.2) can be used for linear earthquake response analysis without any amendments. Different motion histories may be specified for each boundary node more easily than in the nonlinear analysis. By doing so, priority is given to the travelling wave effects, rather than nonlinear effects.

In a linear analysis, the superposition principle is valid and the total displacement **r** may be partitioned

$$\mathbf{r} = \mathbf{r}^{ps} + \mathbf{r}^{d} \tag{5.3}$$

where $\mathbf{r}^{ps}$ is the vector of pseudostatic displacements due to nonuniform boundary displacements and $\mathbf{r}^{d}$ is the vector of displacements relative to the boundary, which induce linear dynamic behaviour. The analogous meaning applies for velocities and accelerations:

$$\dot{\mathbf{r}} = \dot{\mathbf{r}}^{ps} + \dot{\mathbf{r}}^{d} \qquad\qquad \ddot{\mathbf{r}} = \ddot{\mathbf{r}}^{ps} + \ddot{\mathbf{r}}^{d} \tag{5.4}$$

According to Equations (5.3) and (5.4), and making use of the abbreviated symbols **M**, **C** and **K** for the matrices on the lefthand side of Equation (5.2), the latter may be rewritten in the following form:

$$\mathbf{M}\ddot{\mathbf{r}}^{d} + \mathbf{C}\dot{\mathbf{r}}^{d} + \mathbf{K}\mathbf{r}^{d} = -\begin{Bmatrix} \mathbf{0} \\ \mathbf{0} \\ \mathbf{m}_{FB}\ddot{\mathbf{r}}_{B} + \mathbf{c}_{FB}\dot{\mathbf{r}}_{B} + \mathbf{k}_{FB}\mathbf{r}_{B} \end{Bmatrix} - \mathbf{M}\ddot{\mathbf{r}}^{ps} - \mathbf{C}\dot{\mathbf{r}}^{ps} - \mathbf{K}\mathbf{r}^{ps} \tag{5.5}$$

The pseudostatic displacements $\mathbf{r}^{ps}$ can be determined from the static equilibrium equation which may be obtained by deleting the dynamic terms in Equation (5.2)

$$\mathbf{K}\mathbf{r}^{ps} = -\begin{bmatrix} \mathbf{0} \\ \mathbf{0} \\ \mathbf{k}_{FB} \end{bmatrix}\mathbf{r}_{B} \quad \Rightarrow \quad \mathbf{r}^{ps} = -\mathbf{K}^{-1}\begin{bmatrix} \mathbf{0} \\ \mathbf{0} \\ \mathbf{k}_{FB} \end{bmatrix}\mathbf{r}_{B} = \mathbf{R}^{ps}\mathbf{r}_{B} \tag{5.6}$$

where $\mathbf{R}^{ps}$ is the influence coefficient matrix which links the $\mathbf{r}^{ps}$ vector with the $\mathbf{r}_{B}$ vector, expressing displacements of the system due to nonuniform unit boundary

displacements. Since matrix $\mathbf{R}^{ps}$ is not time dependent, the pseudostatic velocities and accelerations are:

$$\dot{\mathbf{r}}^{ps} = \mathbf{R}^{ps}\dot{\mathbf{r}}_B \qquad \ddot{\mathbf{r}}^{ps} = \mathbf{R}^{ps}\ddot{\mathbf{r}}_B \tag{5.7}$$

If Equations (5.6) and (5.7) are applied to (5.5), it becomes:

$$\mathbf{M}\ddot{\mathbf{r}}^{d} + \mathbf{C}\dot{\mathbf{r}}^{d} + \mathbf{K}\mathbf{r}^{d} =$$

$$= -\left(\begin{bmatrix} \mathbf{0} \\ \mathbf{0} \\ \mathbf{m}_{FB} \end{bmatrix} + \mathbf{M}\mathbf{R}^{ps} \right)\ddot{\mathbf{r}}_B - \left(\begin{bmatrix} \mathbf{0} \\ \mathbf{0} \\ \mathbf{c}_{FB} \end{bmatrix} + \mathbf{C}\mathbf{R}^{ps} \right)\dot{\mathbf{r}}_B - \left(\begin{bmatrix} \mathbf{0} \\ \mathbf{0} \\ \mathbf{k}_{FB} \end{bmatrix} + \mathbf{K}\mathbf{R}^{ps} \right)\mathbf{r}_B$$

However, the third term on the righthand side of the previous equation vanishes because of the definition of matrix $\mathbf{R}^{ps}$ in Equation (5.6). The same applies for the second term in case of stiffness proportional damping. Even if this is not the case, it was found (Zienkiewicz et al., 1986) that this term has a negligible effect for any practical type of damping. Therefore, the final equation for the dynamic component of motion may be written as:

$$\mathbf{M}\ddot{\mathbf{r}}^{d} + \mathbf{C}\dot{\mathbf{r}}^{d} + \mathbf{K}\mathbf{r}^{d} = -\left(\begin{bmatrix} \mathbf{0} \\ \mathbf{0} \\ \mathbf{m}_{FB} \end{bmatrix} + \mathbf{M}\mathbf{R}^{ps} \right)\ddot{\mathbf{r}}_B \tag{5.8}$$

Equation (5.8) is convenient because the seismic input requires only the knowledge of the acceleration history of the far-field, boundary nodes, which itself is still a considerable task. Corresponding velocities and displacements need not be calculated. After solving Equation (5.8) for the dynamic motion component, the pseudostatic component should be added in order to obtain the total motion. The deformation of the system depends on both components of the motion ($\mathbf{r}^{d}$ and $\mathbf{r}^{ps}$).

A special case of the boundary input scheme arises when a basement rock exists at some depth in the foundation. Then, it can be argued that the motion (acceleration)

of the boundary B is uniform. Matrix $\mathbf{R}^{ps}$ becomes matrix $\mathbf{R}^{rb}$ which ensures that the pseudostatic motions of the dam-foundation system, $\mathbf{r}^{ps}$, turn into rigid body motions, $\mathbf{r}^{rb}$. The expression inside the parentheses on the righthand side of Equation (5.8) then becomes just a directional mass of the whole system. The deformation of the system depends only on the dynamic motion component ($\mathbf{r}^{d}$), relative to the motion of the basement rock. The solution of the now simplified version of Equation (5.8) can be obtained by using standard structural dynamics finite element packages and procedures for linear problems, the classical modal superposition method included. The analogy between dam-foundation interaction and standard structural dynamics is now complete: the 'structure' is the whole dam-foundation system, the 'base' is the basement rock, and the earthquake excitation is known at the 'base' of the 'structure'. However, the straightforward application of the known surface free-field motions at the basement rock yields unacceptable results due to site amplification effects (Léger & Boughoufalah, 1989). Clough (1980) has suggested an approximation which assumes that the foundation is massless. Although this assumption allows the use of standard structural dynamics finite element packages and applies surface free-field acceleration at the basement rock, only the dam response results are meaningful. The significance of its approximation will be investigated in detail in Chapter 6.

5.2.2 Nonlinear Analysis

For a nonlinear analysis, the superposition principle is not valid and the partition in the form of Equations (5.3) and (5.4) is not possible. Still, the full nonlinear behaviour of the whole dam-foundation system remains an attractive option if the seismic motion is uniform along the boundary, i.e. when rigid body motions occur. By following the earlier reasoning, priority is given to the nonlinear effects, rather than travelling wave effects.

In this case, the total displacements **r** may be defined as the sum of the rigid body displacements, $\mathbf{r}^{rb}$, and displacements relative to the boundary, which induce nonlinear dynamic behaviour, $\mathbf{r}^{d}$:

$$\mathbf{r} = \mathbf{r}^{rb} + \mathbf{r}^{d} \tag{5.9}$$

The same applies to the velocities and accelerations in all parts of the system:

$$\dot{\mathbf{r}} = \dot{\mathbf{r}}^{rb} + \dot{\mathbf{r}}^{d} \qquad \ddot{\mathbf{r}} = \ddot{\mathbf{r}}^{rb} + \ddot{\mathbf{r}}^{d} \tag{5.10}$$

According to the partitions in Equations (5.9) and (5.10), Equation (5.2) may be expressed only in terms of $\mathbf{r}^{d}$ because the rigid body motions have no effect on the nonlinear mechanism. The derivation sequence is similar to the one presented in the linear case and will not be repeated. Again, it is important to note that eventually, on the righthand (excitation) side, only rigid body, inertia force terms remain. Thus, the seismic input depends only on rigid body accelerations and the corresponding velocities and displacements need not be calculated.

5.3 Interface Input Scheme

Before proceeding to the derivation of equations for this input scheme, it is useful to summarise the important points about the scheme and the associated substructure method of interaction analysis.

The substructure method in the time domain is used. The whole system is divided into two substructures and both are spatially discretised by finite elements only. The structure under consideration is a concrete gravity dam, a massive and stiff structure, which implies that the dam-foundation interaction effects are expected to be significant. The foundation under consideration is a rock half-space, which implies that the radiation damping effects are expected to be important.

In the substructure method of analysis, the interface seismic input scheme is used for earthquake response analysis. It is not necessary to determine the earthquake motions along the boundaries of the foundation and it suffices to know either the free-field or scattered motions along an interface close to the surface. Unfortunately, if this seismic input concept is applied, only local nonlinearities (Subsection 5.1.4) can be treated.

The interface input scheme will be presented first for the surface supported structures (Clough & Penzien, 1975). Relying on the contributions from other researchers (Bayo & Wilson, 1983), the more complicated case of embedded structures will be formulated in a way which is particularly well suited to allow for the extension towards nonlinear analyses. Moreover, it will be shown how to incorporate possible nonuniform earthquake motions, i.e. the effects of travelling seismic waves. Similar equations were used by Kojic & Trifunac (1991) when investigating nonuniform excitation of a linear elastic arch dam.

Bielak and Christiano (1984) proposed a somewhat different approach to the substructure method, obtaining a slightly modified seismic input scheme which was later applied by Cremonini et al. (1988). For the sake of completeness, their approach will also be presented.

5.3.1 Surface Supported Structures: Ground Level Interface

The concrete gravity dam-foundation system in Figure 5.4 is considered. The letter D is used to represent the dam, F stands for the foundation and I depicts the surface interface between the two. All these letters will appear in the form of subscripts for submatrices $\mathbf{m}$, $\mathbf{c}$ and $\mathbf{k}$, of the mass, damping and stiffness matrices ($\mathbf{M}$, $\mathbf{C}$ and $\mathbf{K}$, respectively). The starting point in this substructure approach is the division of the vector of total displacements $\mathbf{r}$ into the free-field motion component $\mathbf{v}$ and added motion component $\mathbf{u}$:

$$\begin{Bmatrix} \mathbf{r}_D \\ \mathbf{r}_I \\ \mathbf{r}_F \end{Bmatrix} = \begin{Bmatrix} \mathbf{0} \\ \mathbf{v}_I \\ \mathbf{v}_F \end{Bmatrix} + \begin{Bmatrix} \mathbf{u}_D \\ \mathbf{u}_I \\ \mathbf{u}_F \end{Bmatrix} \qquad \text{or} \qquad \mathbf{r} = \mathbf{v} + \mathbf{u} \tag{5.11}$$

Correspondingly, all property matrices can be divided in the same manner, as shown here for the mass matrix

$$\begin{bmatrix} \mathbf{m}_{DD} & \mathbf{m}_{DI} & \mathbf{0} \\ \mathbf{m}_{ID} & \mathbf{m}_{II} & \mathbf{m}_{IF} \\ \mathbf{0} & \mathbf{m}_{FI} & \mathbf{m}_{FF} \end{bmatrix} = \begin{bmatrix} \mathbf{0} & \mathbf{0} & \mathbf{0} \\ \mathbf{0} & \mathbf{m}_{II}^{F} & \mathbf{m}_{IF} \\ \mathbf{0} & \mathbf{m}_{FI} & \mathbf{m}_{FF} \end{bmatrix} + \begin{bmatrix} \mathbf{m}_{DD} & \mathbf{m}_{DI} & \mathbf{0} \\ \mathbf{m}_{ID} & \mathbf{m}_{II}^{D} & \mathbf{0} \\ \mathbf{0} & \mathbf{0} & \mathbf{0} \end{bmatrix}$$

or $$\mathbf{M} = \mathbf{M}_{ff} + \mathbf{M}_{add} \tag{5.12}$$

where $\mathbf{M}_{ff}$ is the free-field mass matrix (of the original site prior to the construction of the dam) and $\mathbf{M}_{add}$ is the mass matix due to the 'addition' of the dam.

The free-field motion $\mathbf{v}$ may be determined by considering the foundation alone

$$\mathbf{M}_{ff}\,\ddot{\mathbf{v}} + \mathbf{C}_{ff}\,\dot{\mathbf{v}} + \mathbf{K}_{ff}\,\mathbf{v} = \mathbf{F} \tag{5.13}$$

where $\mathbf{F}$ is the far-field excitation.

After the construction of the dam, it is assumed that the far-field excitation does not change, i.e. that the complete system is now subjected to the same earthquake as the free-field was. Therefore, the equation of total motion for the complete dam-foundation system may be written as

$$\mathbf{M}\ddot{\mathbf{r}} + \mathbf{C}\dot{\mathbf{r}} + \mathbf{K}\mathbf{r} = \mathbf{F} \tag{5.14}$$

or in the partitioned form according to Equations (5.11) and (5.12):

$$(\mathbf{M}_{ff} + \mathbf{M}_{add})(\ddot{\mathbf{v}} + \ddot{\mathbf{u}}) + (\mathbf{C}_{ff} + \mathbf{C}_{add})(\dot{\mathbf{v}} + \dot{\mathbf{u}}) + (\mathbf{K}_{ff} + \mathbf{K}_{add})(\mathbf{v} + \mathbf{u}) = \mathbf{F} \tag{5.15}$$

If the righthand side of Equation (5.15) is replaced by Equation (5.13), the equation of added motion for the complete system is obtained in the form:

$$\mathbf{M}\ddot{\mathbf{u}} + \mathbf{C}\dot{\mathbf{u}} + \mathbf{K}\mathbf{u} = -\begin{bmatrix} \mathbf{m}_{DI} \\ \mathbf{m}_{II}^{D} \\ \mathbf{0} \end{bmatrix} \ddot{\mathbf{v}}_{\mathrm{I}} - \begin{bmatrix} \mathbf{c}_{DI} \\ \mathbf{c}_{II}^{D} \\ \mathbf{0} \end{bmatrix} \dot{\mathbf{v}}_{\mathrm{I}} - \begin{bmatrix} \mathbf{k}_{DI} \\ \mathbf{k}_{II}^{D} \\ \mathbf{0} \end{bmatrix} \mathbf{v}_{\mathrm{I}} \tag{5.16}$$

To the best of author's knowledge, an equation analogous to Equation (5.16) first appeared in a classic textbook (Clough & Penzien, 1975), and its importance was reiterated in a state-of-the-art report (Lysmer, 1978). However, the ability of Equation (5.16) to deal with soil-structure interaction problems of limited nonlinearity was not emphasised in those early works and was noted only recently (Ibrahimbegovic, 1989; Ibrahimbegovic & Wilson, 1990). The nonlinear behaviour is confined to the dam because the nonlinearities have to be formulated in terms of total displacements and, as Equation (5.11) clearly shows, added displacements **u** are equal to the total displacements **r** only in the case of the dam.

Furthermore, the righthand, excitation side of Equation (5.16) embodies the main feature of substructure methods - that apart from standard property matrices only the knowledge of interface free-field motions (accelerations, velocities and displacements) is required. In this case, the interface is superficial, i.e. at the ground level.

For linear elastic interaction systems, the superposition principle is valid and Equation (5.16) can be further simplified by dividing the vector of added displacements **u** into the pseudostatic and dynamic component (Clough & Penzien, 1975)

$$\mathbf{u} = \mathbf{u}^{ps} + \mathbf{u}^{d} \tag{5.17}$$

where $\mathbf{u}^{ps}$ is the vector of pseudostatic displacements due to possible nonuniform interface displacements and $\mathbf{u}^{d}$ is the vector of dynamic displacements. The same applies for the velocities and accelerations:

$$\dot{\mathbf{u}} = \dot{\mathbf{u}}^{ps} + \dot{\mathbf{u}}^{d} \qquad \ddot{\mathbf{u}} = \ddot{\mathbf{u}}^{ps} + \ddot{\mathbf{u}}^{d} \tag{5.18}$$

The pseudostatic displacements $\mathbf{u}^{ps}$ can be determined from the static equilibrium equation which may be obtained by deleting the dynamic terms in Equation (5.16)

$$\mathbf{K}\mathbf{u}^{ps} = -\begin{bmatrix} \mathbf{k}_{DI} \\ \mathbf{k}_{II}^{D} \\ \mathbf{0} \end{bmatrix}\mathbf{v}_I \qquad \Rightarrow \qquad \mathbf{u}^{ps} = -\mathbf{K}^{-1}\begin{bmatrix} \mathbf{k}_{DI} \\ \mathbf{k}_{II}^{D} \\ \mathbf{0} \end{bmatrix}\mathbf{v}_I = \mathbf{R}^{ps}\mathbf{v}_I \tag{5.19}$$

where $\mathbf{R}^{ps}$ is the influence coefficient matrix which links the $\mathbf{u}^{ps}$ vector with the $\mathbf{v}_I$ vector, expressing displacements of the system due to nonuniform unit interface displacements. Since matrix $\mathbf{R}^{ps}$ is not time dependent, the pseudostatic velocities and accelerations are:

$$\dot{\mathbf{u}}^{ps} = \mathbf{R}^{ps}\dot{\mathbf{v}}_I \qquad \ddot{\mathbf{u}}^{ps} = \mathbf{R}^{ps}\ddot{\mathbf{v}}_I \tag{5.20}$$

Now, with Equations (5.19) and (5.20), Equation (5.16) can be easily written in terms of dynamic motions only:

$$\mathbf{M}\ddot{\mathbf{u}}^{d} + \mathbf{C}\dot{\mathbf{u}}^{d} + \mathbf{K}\mathbf{u}^{d} =$$

$$= -\left(\begin{bmatrix} \mathbf{m}_{DI} \\ \mathbf{m}_{II}^{D} \\ \mathbf{0} \end{bmatrix} + \mathbf{M}\mathbf{R}^{ps} \right)\ddot{\mathbf{v}}_I - \left(\begin{bmatrix} \mathbf{c}_{DI} \\ \mathbf{c}_{II}^{D} \\ \mathbf{0} \end{bmatrix} + \mathbf{C}\mathbf{R}^{ps} \right)\dot{\mathbf{v}}_I - \left(\begin{bmatrix} \mathbf{k}_{DI} \\ \mathbf{k}_{II}^{D} \\ \mathbf{0} \end{bmatrix} + \mathbf{K}\mathbf{R}^{ps} \right)\mathbf{v}_I$$

However, the third term on the righthand side of the previous equation vanishes because of the definition of matrix $\mathbf{R}^{ps}$ in Equation (5.19). The same applies for the second term in the case of stiffness proportional damping. Even if this is not the case, it was found (Zienkiewicz et al., 1986) that this term has a negligible effect for any practical type of damping. Therefore, the final equation for the dynamic component of motion may be written as:

$$\mathbf{M}\ddot{\mathbf{u}}^{d} + \mathbf{C}\dot{\mathbf{u}}^{d} + \mathbf{K}\mathbf{u}^{d} = -\left(\begin{bmatrix} \mathbf{m}_{DI} \\ \mathbf{m}_{II}^{D} \\ \mathbf{0} \end{bmatrix} + \mathbf{M}\mathbf{R}^{ps} \right) \ddot{\mathbf{v}}_{I} \qquad (5.21)$$

In Equation (5.21), the seismic input depends only on the free-field accelerations at the ground level (future interface). The solution of Equation (5.21) yields $\mathbf{u}^{d}$, to which both the pseudostatic $\mathbf{u}^{ps}$ and free-field motion $\mathbf{v}$ need to be added in order to obtain the total motion $\mathbf{r}$.

A special case of the interface input scheme arises when the motion (acceleration) of the interface ($\ddot{\mathbf{v}}_{I}$) is uniform. Matrix $\mathbf{R}^{ps}$ becomes matrix $\mathbf{R}^{rb}$ which ensures that the pseudostatic motions of the dam, $\mathbf{u}_{D}^{ps}$, turn into rigid body motions. The expression inside the parentheses on the righthand side of Equation (5.21) then becomes just a directional mass of the dam. The deformation (change of strain and stress) of the dam depends only on the dynamic motion component ($\mathbf{u}_{D}^{d}$), relative to the motion of the interface.

5.3.2 Embedded Structures: Deep Interface

As noted earlier, the dam-foundation interface of the interaction system which was depicted in Figure 5.4 and analysed through Equations (5.11) - (5.21) is flat and superficial. Although the size of the embedment of concrete gravity dams (approximately 1/10th of the height of the dam) suggests that its role in the interaction mechanism is not as decisively important as in some other cases (e.g. nuclear reactor buildings), the mathematical formulation for embedded structures should be mentioned. Lysmer (1978) has presented the substructure methods in a form convenient for treatment in the frequency domain. A distinction was made between rigid and flexible embedments. Substructure methods for the flexible embedment were further subdivided into 'flexible boundary' and 'flexible volume' methods. The

former requires the solution of the scattering problem, i.e. knowledge of the scattered motions along the embedded structure-foundation interface. The term 'boundary' refers to this interface and is therefore somewhat misleading; it would be better to use 'flexible embedment interface' instead. The latter method avoids the solution of the scattering problem by considering interaction at all embedded nodes. In order to maintain consistency with the previous terminological suggestion; 'flexible embedment volume' can be used. An important step forward was made when both flexible embedment methods (interface and volume) were proposed entirely in the time domain (Bayo & Wilson, 1983; Bayo & Wilson, 1984). The flexible embedment interface method paved the way for nonlinear analyses, while the flexible embedment volume method enabled the solution of linear elastic interaction problems without solving the scattering problem. In what follows, it will be shown that this may be achieved by formulating the properties of the embedded part as the difference between the properties of the structure and foundation.

5.3.2.1 Flexible Embedment Volume Method for Linear Interaction Problems

The dam-foundation system shown in Figure 5.5 is considered. The nodes along the dam-foundation interface are denoted by I while the remaining nodes of the foundation are denoted by F. Letters D and E are used to represent the dam - D is for the part above the ground surface and E is for the embedded part. All these letters will appear in the form of subscripts for submatrices $\mathbf{m}$, $\mathbf{c}$ and $\mathbf{k}$, of the mass, damping and stiffness matrices ($\mathbf{M}$, $\mathbf{C}$ and $\mathbf{K}$, respectively). The starting point in the derivation is again the division of the vector of total displacements $\mathbf{r}$ into the free-field component $\mathbf{v}$ and added motion component $\mathbf{u}$:

$$\begin{Bmatrix} \mathbf{r}_D \\ \mathbf{r}_E \\ \mathbf{r}_I \\ \mathbf{r}_F \end{Bmatrix} = \begin{Bmatrix} \mathbf{0} \\ \mathbf{v}_E \\ \mathbf{v}_I \\ \mathbf{v}_F \end{Bmatrix} + \begin{Bmatrix} \mathbf{u}_D \\ \mathbf{u}_E \\ \mathbf{u}_I \\ \mathbf{u}_F \end{Bmatrix} \qquad \text{or} \qquad \mathbf{r} = \mathbf{v} + \mathbf{u} \qquad (5.22)$$

Correspondingly, all property matrices can be divided in the same manner, as shown here for the mass matrix

$$\begin{bmatrix} \mathbf{m}_{DD} & \mathbf{m}_{DE} & \mathbf{m}_{DI} & \mathbf{0} \\ \mathbf{m}_{ED} & \mathbf{m}_{EE} & \mathbf{m}_{EI} & \mathbf{0} \\ \mathbf{m}_{ID} & \mathbf{m}_{IE} & \mathbf{m}_{II} & \mathbf{m}_{IF} \\ \mathbf{0} & \mathbf{0} & \mathbf{m}_{FI} & \mathbf{m}_{FF} \end{bmatrix} =$$

$$= \begin{bmatrix} \mathbf{0} & \mathbf{0} & \mathbf{0} & \mathbf{0} \\ \mathbf{0} & \overline{\mathbf{m}}_{EE} & \overline{\mathbf{m}}_{EI} & \mathbf{0} \\ \mathbf{0} & \overline{\mathbf{m}}_{IE} & \overline{\mathbf{m}}_{II} & \overline{\mathbf{m}}_{IF} \\ \mathbf{0} & \mathbf{0} & \overline{\mathbf{m}}_{FI} & \overline{\mathbf{m}}_{FF} \end{bmatrix} + \begin{bmatrix} \mathbf{m}_{DD} & \mathbf{m}_{DE} & \mathbf{m}_{DI} & \mathbf{0} \\ \mathbf{m}_{ED} & \mathbf{m}_{EE} - \overline{\mathbf{m}}_{EE} & \mathbf{m}_{EI} - \overline{\mathbf{m}}_{EI} & \mathbf{0} \\ \mathbf{m}_{ID} & \mathbf{m}_{IE} - \overline{\mathbf{m}}_{IE} & \mathbf{m}_{II} - \overline{\mathbf{m}}_{II} & \mathbf{0} \\ \mathbf{0} & \mathbf{0} & \mathbf{0} & \mathbf{0} \end{bmatrix}$$

or $$\mathbf{M} = \mathbf{M}_{ff} + \mathbf{M}_{add} \qquad (5.23)$$

where $\mathbf{M}_{ff}$ is the free-field mass matrix (of the original site prior to the construction of dam) and $\mathbf{M}_{add}$ is the mass matrix due to the addition of the dam. '$\overline{\mathbf{m}}$' in $\mathbf{M}_{ff}$ denotes the free-field and it is obvious that the free-field properties for the foundation (*F* nodes) are the total properties (e.g. $\mathbf{m}_{FF} = \overline{\mathbf{m}}_{FF}$). Similarly, the added properties for the dam above the surface (*D* nodes) are the total properties (e.g. $\mathbf{m}_{DD}$).

The derivation of dynamic equations follows the same principles as in the case of surface supported structures (Equations (5.13) - (5.15)); and the final equation of added motion for the whole interaction systems can be written as:

$$\mathbf{M}\ddot{\mathbf{u}} + \mathbf{C}\dot{\mathbf{u}} + \mathbf{K}\mathbf{u} =$$

$$= -\begin{bmatrix} \mathbf{m}_{DE} & \mathbf{m}_{DI} \\ \mathbf{m}_{EE} - \bar{\mathbf{m}}_{EE} & \mathbf{m}_{EI} - \bar{\mathbf{m}}_{EI} \\ \mathbf{m}_{IE} - \bar{\mathbf{m}}_{IE} & \mathbf{m}_{II} - \bar{\mathbf{m}}_{II} \\ \mathbf{0} & \mathbf{0} \end{bmatrix} \begin{Bmatrix} \ddot{\mathbf{v}}_E \\ \ddot{\mathbf{v}}_I \end{Bmatrix} - \begin{bmatrix} \mathbf{c}_{DE} & \mathbf{c}_{DI} \\ \mathbf{c}_{EE} - \bar{\mathbf{c}}_{EE} & \mathbf{c}_{EI} - \bar{\mathbf{c}}_{EI} \\ \mathbf{c}_{IE} - \bar{\mathbf{c}}_{IE} & \mathbf{c}_{II} - \bar{\mathbf{c}}_{II} \\ \mathbf{0} & \mathbf{0} \end{bmatrix} \begin{Bmatrix} \dot{\mathbf{v}}_E \\ \dot{\mathbf{v}}_I \end{Bmatrix} -$$

$$- \begin{bmatrix} \mathbf{k}_{DE} & \mathbf{k}_{DI} \\ \mathbf{k}_{EE} - \bar{\mathbf{k}}_{EE} & \mathbf{k}_{EI} - \bar{\mathbf{k}}_{EI} \\ \mathbf{k}_{IE} - \bar{\mathbf{k}}_{IE} & \mathbf{k}_{II} - \bar{\mathbf{k}}_{II} \\ \mathbf{0} & \mathbf{0} \end{bmatrix} \begin{Bmatrix} \mathbf{v}_E \\ \mathbf{v}_I \end{Bmatrix} \tag{5.24}$$

The righthand side of Equation (5.24) is the seismic excitation in the form of effective forces which depend on the free-field accelerations, velocities and displacements in parts E and I of the original site. The scattering problem need not be solved. Since only linear interaction problems are considered, Equation (5.24) can be further simplified by dividing the added motions into the pseudostatic and dynamic component. The derivation is completely analogous to the derivation for surface supported structures (Equations (5.17) - (5.21)), and will not be repeated here.

5.3.2.2 Extension of the Flexible Embedment Interface Method to Nonlinear Interaction Problems

If the flexible embedment volume method is applied to linear soil-structure interaction, the solution of the scattering problem need not be found. The free-field motion will suffice, provided that the properties of the embedded part are formulated as in Equation (5.24). On the other hand, for the flexible embedment interface method, the scattering problem must be solved by determining scattered motions (accelerations, velocities and displacements) along the interface between the embedment of the structure and foundation.

The main idea of the flexible embedment interface method may be extended to the formulation of locally nonlinear soil-structure interaction problems in the time domain. The formulation is particularly well suited for dam-foundation interaction, where nonlinearities are indeed confined to a small area which can be predicted from linear elastic analyses. The system under consideration is shown in Figure 5.6. The letter *N* is used to represent the nonlinear part of the system (the whole dam with its embedment and the part of the foundation close to the dam); *F* stands for the linear part of the foundation, and *I* depicts the interface between the two. The vector of total displacements **r** is now divided into the scattered motion component **v** and added motion component **u**:

$$\begin{Bmatrix} \mathbf{r}_N \\ \mathbf{r}_I \\ \mathbf{r}_F \end{Bmatrix} = \begin{Bmatrix} \mathbf{0} \\ \mathbf{v}_I \\ \mathbf{v}_F \end{Bmatrix} + \begin{Bmatrix} \mathbf{u}_N \\ \mathbf{u}_I \\ \mathbf{u}_F \end{Bmatrix} \qquad \text{or} \qquad \mathbf{r} = \mathbf{v} + \mathbf{u} \tag{5.25}$$

A similar partition applies for the property matrices. Otherwise, the derivation of equations follows precisely the same pattern as for surface supported structures (Equations (5.13) - (5.15)); the only difference being the use of scattered motions instead of free-field ones. Even the final equation for the added motion component is analogous to Equation (5.16):

$$\mathbf{M}\ddot{\mathbf{u}} + \mathbf{C}\dot{\mathbf{u}} + \mathbf{K}\mathbf{u} = -\begin{bmatrix} \mathbf{m}_{NI} \\ \mathbf{m}_{II}^{N} \\ \mathbf{0} \end{bmatrix} \ddot{\mathbf{v}}_I - \begin{bmatrix} \mathbf{c}_{NI} \\ \mathbf{c}_{II}^{N} \\ \mathbf{0} \end{bmatrix} \dot{\mathbf{v}}_I - \begin{bmatrix} \mathbf{k}_{NI} \\ \mathbf{k}_{II}^{N} \\ \mathbf{0} \end{bmatrix} \mathbf{v}_I \tag{5.26}$$

Since Equation (5.26) is nonlinear, only the mass matrix of the whole system, **M**, and the mass submatrix on the righthand side are constant. Both the damping and stiffness matrix of the whole system, **C** and **K** respectively, are dependent on the nonlinearities and hence variable. In the general case, the damping and stiffness submatrices on the righthand side are variable. However, if there are no

nonlinearities immediately close to the interface *I*, it can be argued that the whole excitation, righthand side of Equation (5.26), is constant. It is also important to note the difference between the linear and nonlinear interaction problem for embedded structures; in the former case, the 'interface' describes the interface between the structure and the foundation; in the latter case, it is the interface between the nonlinear and linear part of the system. Therefore, if the partition of the system is performed as in Figure 5.6, there are no limitations on the size and shape of the dam embedment, and the whole system can be treated with Equation (5.26). In the case of surface supported structures (Figure 5.4), the interface *I* is both the boundary between the structure and foundation, and the boundary between the linear and nonlinear parts of the system.

Although equations analogous to Equation (5.26) have been published (Bayo & Wilson, 1983; Bayo & Wilson, 1984), actual nonlinear analyses were not carried out on these occasions. Later, Ibrahimbegovic & Wilson (1990) applied equations related to Equation (5.26) when investigating nonlinear interface behaviour of concrete gravity dams (dam uplifting). In that case, there was no need to solve the scattering problem because the dam was surface supported and the nonlinearity was confined to the surface interface. All this indicates that the reason why Equation (5.26) did not gain more popularity lies in the fact that its solution is achieved in two phases. The first phase is the solution of the scattering problem in order to obtain the vectors $\ddot{\mathbf{v}}_I$, $\dot{\mathbf{v}}_I$ and $\mathbf{v}_I$. The second phase consists of calculating the nonlinear response, i.e. determining the added displacements according to Equation (5.16). As already mentioned in Subsection 5.1.1, the first phase is much more difficult. However, in this case, the foundation is of the rock half-space type and this problem is not so serious. First, site amplification effects (typical for the layered foundations) practically do not exist. Second, possible interfaces are at a smaller foundation depth and the motions along their width may be assumed as uniform. This applies even for

the relatively deeper interfaces, like those between the nonlinear and linear parts of the system).

5.3.3 Bielak - Christiano's Approach

Bielak & Christiano (1984) introduced a somewhat different approach to seismic input for nonlinear interaction problems. They realised that the boundary input scheme is not appropriate if transmitting boundaries are to be used and that it is necessary to prescribe the seismic excitation in the form of effective generalised forces within the domain of computation. Although these requirements are met in the standard substructure formulation presented in Subsection 5.3.2, the need to solve the scattering problem for Equation (5.26) still remains; which the two authors tried to avoid.

When applied to the dam-foundation case, a soil-structure interaction system examined by Bielak & Christiano (1984) and later by Cremonini et al. (1988), looks like the one in Figure 5.7. It is divided into two completely separate substructures, of which the first can exhibit nonlinear behaviour and consists of the dam and surrounding foundation. The second substructure is the linear part of the foundation. The letters N, I and F have the same meaning as before, and superscripts are used to indicate the substructure from which the contribution to property matrices is made.

The equation of motion for the first substructure, after the usual partition, can be written in matrix form as

$$\begin{bmatrix} \mathbf{m}_{NN} & \mathbf{m}_{NI} \\ \mathbf{m}_{IN} & \mathbf{m}_{II}^{N} \end{bmatrix} \begin{Bmatrix} \ddot{\mathbf{r}}_N \\ \ddot{\mathbf{r}}_I \end{Bmatrix} + \begin{bmatrix} \mathbf{c}_{NN} & \mathbf{c}_{NI} \\ \mathbf{c}_{IN} & \mathbf{c}_{II}^{N} \end{bmatrix} \begin{Bmatrix} \dot{\mathbf{r}}_N \\ \dot{\mathbf{r}}_I \end{Bmatrix} + \begin{bmatrix} \mathbf{k}_{NN} & \mathbf{k}_{NI} \\ \mathbf{k}_{IN} & \mathbf{k}_{II}^{N} \end{bmatrix} \begin{Bmatrix} \mathbf{r}_N \\ \mathbf{r}_I \end{Bmatrix} = \begin{Bmatrix} \mathbf{0} \\ \mathbf{R}_I^{N} \end{Bmatrix} \tag{5.27}$$

where $\mathbf{r}_N$ and $\mathbf{r}_I$ are the total displacement vectors of the parts N and I, respectively. The same applies for total velocities and accelerations. $\mathbf{R}_I^N$ is the vector of nodal interaction forces from the nonlinear part of the system, acting on the interface I.

The equation of motion for the second substructure is

$$\begin{bmatrix} \mathbf{m}_{II}^{F} & \mathbf{m}_{IF} \\ \mathbf{m}_{FI} & \mathbf{m}_{FF} \end{bmatrix} \begin{Bmatrix} \ddot{\mathbf{u}}_I \\ \ddot{\mathbf{u}}_F \end{Bmatrix} + \begin{bmatrix} \mathbf{c}_{II}^{F} & \mathbf{c}_{IF} \\ \mathbf{c}_{FI} & \mathbf{c}_{FF} \end{bmatrix} \begin{Bmatrix} \dot{\mathbf{u}}_I \\ \dot{\mathbf{u}}_F \end{Bmatrix} + \begin{bmatrix} \mathbf{k}_{II}^{F} & \mathbf{k}_{IF} \\ \mathbf{k}_{FI} & \mathbf{k}_{FF} \end{bmatrix} \begin{Bmatrix} \mathbf{u}_I \\ \mathbf{u}_F \end{Bmatrix} = \begin{Bmatrix} \mathbf{R}_I^{F} \\ \mathbf{0} \end{Bmatrix} \tag{5.28}$$

where $\mathbf{u}_I$ and $\mathbf{u}_F$ are the displacement vectors of the parts I and F, relative to the free-field displacements. The same applies for the velocities and accelerations. $\mathbf{R}_I^F$ is the vector of nodal interaction forces from the linear part of the system, acting on the interface I, where the following conditions of continuity can be prescribed

$$\mathbf{r}_I = \mathbf{u}_I + \mathbf{v}_I \qquad\qquad -\mathbf{R}_I^N - \mathbf{R}_I^F = \mathbf{R}_I \tag{5.29}$$

in which $\mathbf{v}_I$ is the free-field displacement of the interface I and $\mathbf{R}_I$ is the vector of resulting interface forces.

Equations (5.27) and (5.28) can be added after eliminating $\mathbf{R}_I^N$, $\mathbf{R}_I^F$ and $\mathbf{u}_I$ with the aid from Equation (5.29). Thus, the governing equation of motion for a complete nonlinear interaction system becomes

$$\mathbf{M}\begin{Bmatrix} \ddot{\mathbf{r}}_N \\ \ddot{\mathbf{r}}_I \\ \ddot{\mathbf{u}}_F \end{Bmatrix} + \mathbf{C}\begin{Bmatrix} \dot{\mathbf{r}}_N \\ \dot{\mathbf{r}}_I \\ \dot{\mathbf{u}}_F \end{Bmatrix} + \mathbf{K}\begin{Bmatrix} \mathbf{r}_N \\ \mathbf{r}_I \\ \mathbf{u}_F \end{Bmatrix} = -\begin{bmatrix} \mathbf{0} \\ \mathbf{R}_I \\ \mathbf{0} \end{bmatrix} + \begin{bmatrix} \mathbf{0} \\ \mathbf{m}_{II}^{F} \\ \mathbf{m}_{FI} \end{bmatrix} \ddot{\mathbf{v}}_I + \begin{bmatrix} \mathbf{0} \\ \mathbf{c}_{II}^{F} \\ \mathbf{c}_{FI} \end{bmatrix} \dot{\mathbf{v}}_I + \begin{bmatrix} \mathbf{0} \\ \mathbf{k}_{II}^{F} \\ \mathbf{k}_{FI} \end{bmatrix} \mathbf{v}_I \tag{5.30}$$

where $\mathbf{M}$, $\mathbf{C}$ and $\mathbf{K}$ are the combined nonlinear mass, damping and stiffness matrix of the whole system, respectively.

It is important to note the similarities and differencies between Equations (5.26) and (5.30). First, the solution of Equation (5.30) consists of total displacements for the parts N and I of the system and displacements relative to the free-field motion of the part F of the system; whereas the solution of Equation (5.26) consists of the displacements relative to the scattered motion (added displacements). Second, the seismic input on the righthand side of Equation (5.30) depends on the free-field motion of the interface I of the original (unexcavated) site; whereas the seismic input on the righthand side of Equation (5.26) depends on the scattered motion of the interface I. Third, the submatrices on the righthand side of Equation (5.26) are

generally nonlinear; in the case of Equation (5.30) they are linear. Finally, since $\mathbf{r}_N=\mathbf{u}_N$ (similarly for the velocity and acceleration), by using the first of Equations (5.29), Equation (5.30) can be transformed into:

$$\mathbf{M}\begin{Bmatrix}\ddot{\mathbf{u}}_N\\ \ddot{\mathbf{u}}_I\\ \ddot{\mathbf{u}}_F\end{Bmatrix}+\mathbf{C}\begin{Bmatrix}\dot{\mathbf{u}}_N\\ \dot{\mathbf{u}}_I\\ \dot{\mathbf{u}}_F\end{Bmatrix}+\mathbf{K}\begin{Bmatrix}\mathbf{u}_N\\ \mathbf{u}_I\\ \mathbf{u}_F\end{Bmatrix}=-\begin{bmatrix}\mathbf{0}\\ \mathbf{R}_I\\ \mathbf{0}\end{bmatrix}+\begin{bmatrix}\mathbf{m}_{NI}\\ \mathbf{m}_{II}^N\\ \mathbf{0}\end{bmatrix}\ddot{\mathbf{v}}_I+\begin{bmatrix}\mathbf{c}_{NI}\\ \mathbf{c}_{II}^N\\ \mathbf{0}\end{bmatrix}\dot{\mathbf{v}}_I+\begin{bmatrix}\mathbf{k}_{NI}\\ \mathbf{k}_{II}^N\\ \mathbf{0}\end{bmatrix}\mathbf{v}_I \qquad (5.31)$$

Equation (5.31) clearly shows that the explanation for the difference between the scattered motion input in Equation (5.26) and free-field motion input in Equation (5.30) lies in the existence of the resulting interface force vector $\mathbf{R}_I$, and that either can be used for the analysis of locally nonlinear dam-foundation interaction systems.

5.4 Concluding Remarks

Different aspects of seismic input schemes for earthquake analysis of concrete gravity dam-foundation systems have been scrutinised in the previous sections. Here, the conclusions of the utmost importance for this and other works in this area are presented in the order in which they were treated through this Chapter.

<u>Free-field response of the site:</u>

a) If the boundary input scheme is to be used, a complete free-field analysis of the site has to be performed in order to obtain the far-field (boundary) input motions. The estimate of the whole free-field behaviour is often based only on the motion of a single point on the ground surface. In the current state-of-the-art analyses, stringent assumptions are needed. The simplest and the most popular of them is the standard deconvolution procedure which involves only SV-wave propagation.

b) If the interface input scheme is to be used, it suffices to know the free-field or scattered motions along the interface under consideration. The location of this interface depends not only on whether the structure is surface supported or embedded, but also on the location of possible nonlinearities.

Interaction mechanisms:

a) The standard division of interaction mechanisms into kinematic and inertial analysis phases was originally made for the complete method and boundary input scheme. However, the discussion can be extended to the substructure method and interface input scheme. The case of uniform (constant) free-field or scattered motions along the interface corresponds to the inertial interaction analysis.

Types of nonlinearities:

a) If the whole foundation behaves as a nonlinear domain, only the boundary input scheme may be used. The interface input scheme can be used only for local nonlinearities, i.e. if they occur in the dam and surrounding foundation.

Boundary input scheme:

a) The equations are formulated in terms of total motions and the proper far-field excitation should be determined out of a single surface record.

b) If the whole dam-foundation system is nonlinear, the equations simplify significantly in the case of uniform (constant) far-field motion. Then, the rigid body motion can be separated from the analysis because it does not induce any nonlinear behaviour.

c) For the linear dam-foundation system, nonuniform far-field motion can be included more easily into the analysis. If the boundary motion is uniform, the solution of the interaction problem can be obtained by using standard structural dynamics finite element packages.

d) There is no partition of the total motion in the boundary input scheme. The implementation of transmitting boundaries is therefore not straightforward and physically justified; because, in the case of earthquake loading, they must refer to the total minus free-field (or scattered) motion, not to the total motion which is used for this input scheme. For example, the numerical implementation of the viscous transmitting boundary in Equations (5.2) or (5.8) would create an additional radiation damping matrix, not fully compatible with the total motion formulation on the lefthand side of the respective equations. Moreover, the corresponding complete method of analysis would experience the difficulty of having to reconcile the definition of the far-field excitation and the existence of the transmitting boundary at the same location. In other words, a mechanism allowing the unaffected transmission of loading towards the structure, would have to be devised.

Interface input scheme:

a) The total motion is divided into the free-field (or scattered) and added component at the beginning of the analysis. The equations are formulated in terms of added motions only.

b) Nonuniform interface motions can be taken into account, but the assumption of uniform interface motion is here much more realistic than in the case of the far longer boundary in the boundary input scheme.

c) For the locally nonlinear dam-foundation system, the scattering problem has to be solved if the standard substructure method (Equation (5.26)) is used. If the Bielak-Christiano substructure method (Equation (5.30)) is used for the same purpose, the obtained results represent the total motion for the nonlinear part and interface, and motions relative to the free-field for the linear part of the foundation. The scattering problem need not be solved, and the price paid for this substitution of scattered motions with the free-field ones is that an additional, interface force vector, must be determined.

d) In Chapter 9, where concrete gravity dam-foundation systems will be actually analysed, priority will be given to Equation (5.26). If there are no nonlinearities immediately close to the interface *I*, it can be argued that the righthand side of Equation (5.26) is as constant as that of Equation (5.30). Futhermore, for the rock half-space foundation, there are no site amplification effects and any foundation interface is of the same order of rigidity as the dam. This enables the assumption that the scattered and free-field motions are reasonably similar and practically uniform. As for Equation (5.30), this amounts to neglecting the interface force vector term on its righthand side.

e) Most transmitting boundaries have been originally devised for the external dynamic loading, like machine foundation or blast loading. When, like in the case of earthquake excitation, the loading is transferred through the soil, the transmitting boundaries have to be formulated for the total minus free-field (or scattered) motion. This is precisely what Equations (5.16) and (5.26) state implicitly - if the damping matrix **C** on the lefthand side of these equations is constructed from radiation damping element matrices presented in Chapter 4, the transmitting boundary becomes appropriately associated with the added velocity vectors $\dot{\mathbf{u}}$ (total velocity vector $\dot{\mathbf{r}}$ minus free-field or scattered velocity vector $\dot{\mathbf{v}}$). This useful facility offered by the form of Equations (5.16) and (5.26) may be interpreted in another way: by employing the substructure method of analysis, the excitation of the total system has been 'taken out' of the foundation and reimposed as external loading for the interaction problem. Unfortunately, even if the substructure method is used, the location of transmitting boundaries is still not arbitrary and has to be determined independently. Building on general recommendations (Wolf, 1988), a detailed study about the location of the viscous transmitting boundary for concrete gravity dam-foundation systems will be carried out in Chapter 6. Its main objective will be to determine at what distance from the dam the standard

viscous transmitting boundary should be placed. From the analytical point of view, this is equivalent to finding the distance at which the far-field excitation of the free-field system (righthand side of Equation (5.13)) is equal to the far-field excitation of the total system (righthand side of Equation (5.14)).

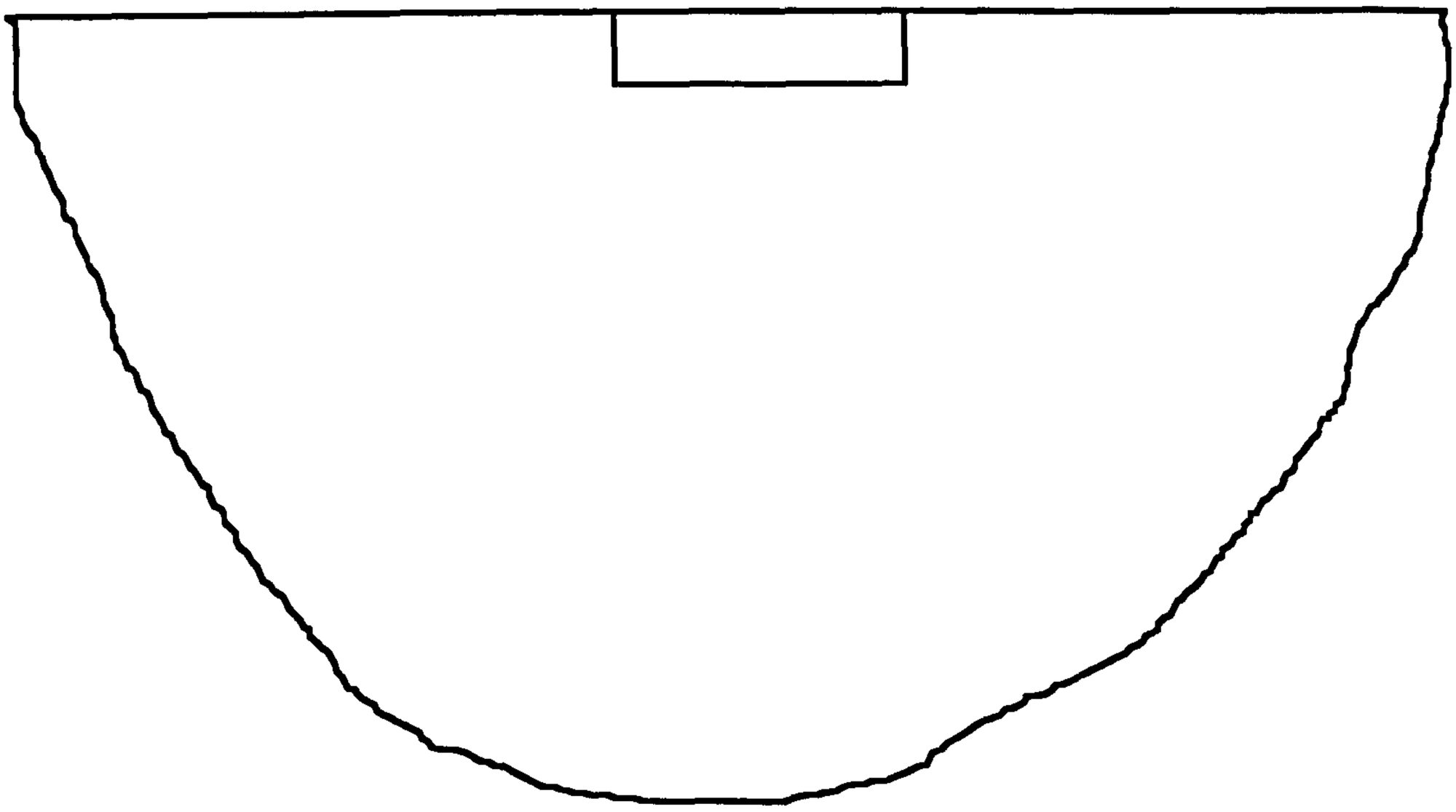

Figure 5.1a - Free-field problem of the site

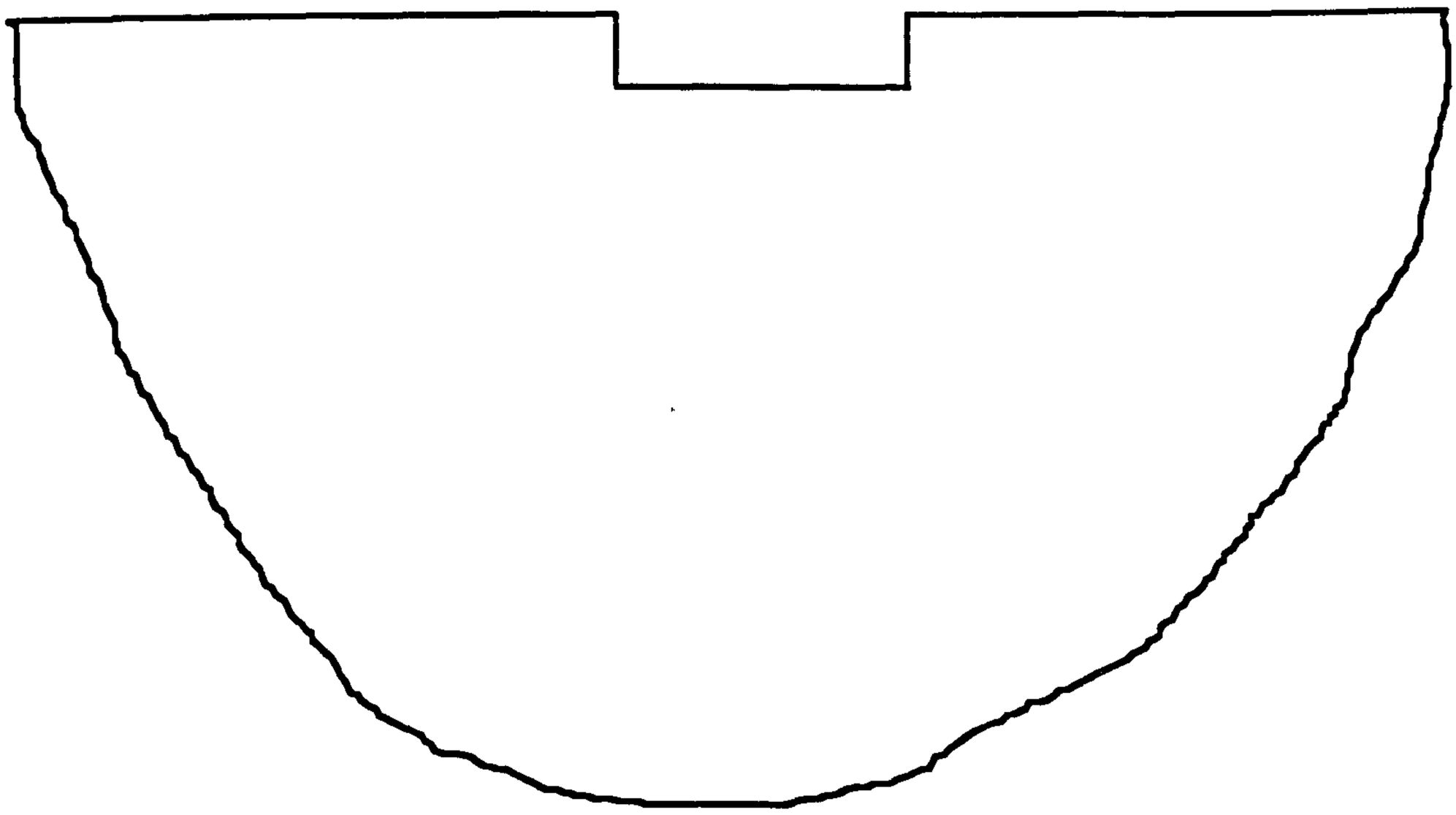

Figure 5.1b - Scattering problem of the site

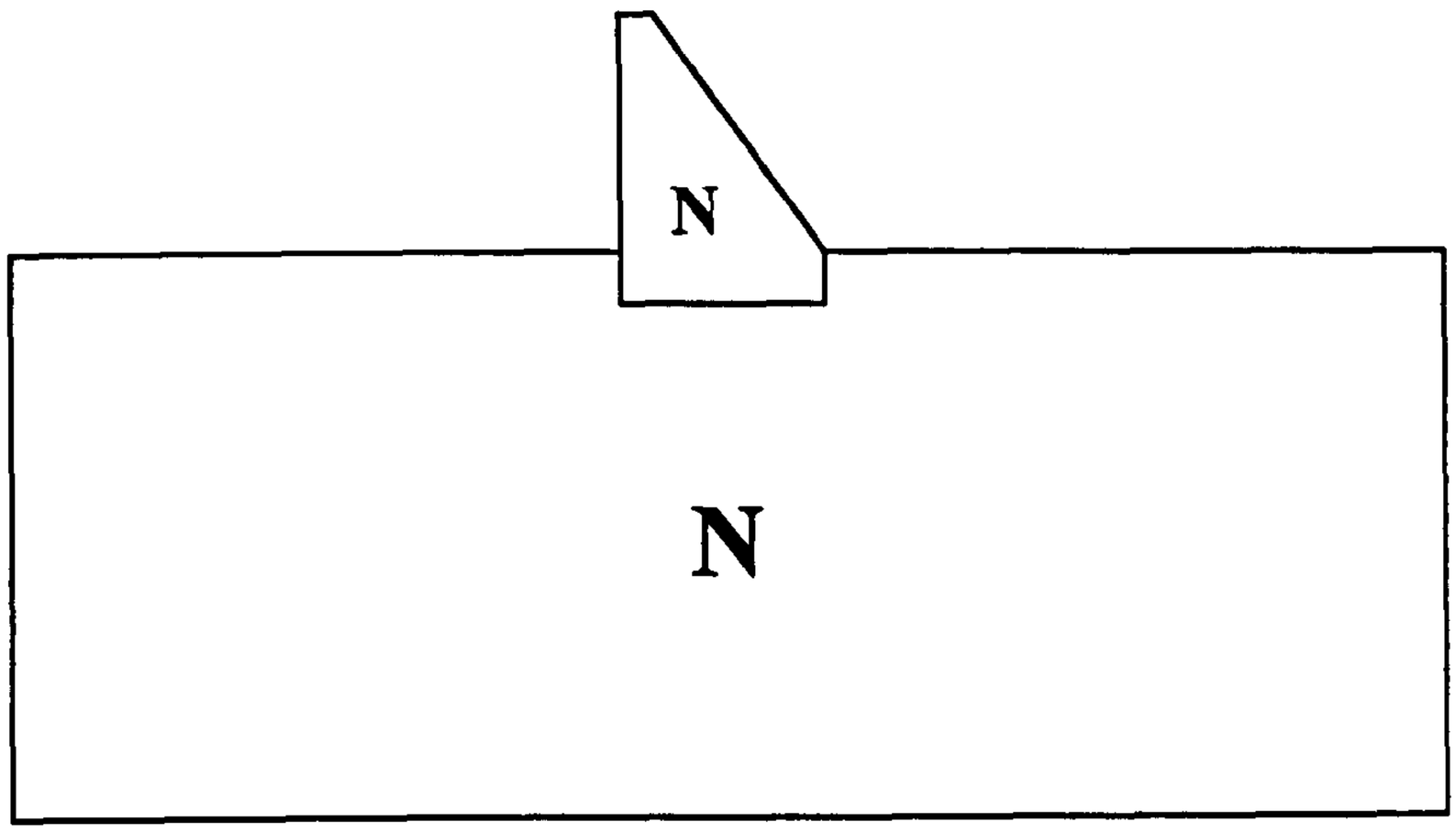

Figure 5.2a - Nonlinearities in the whole system

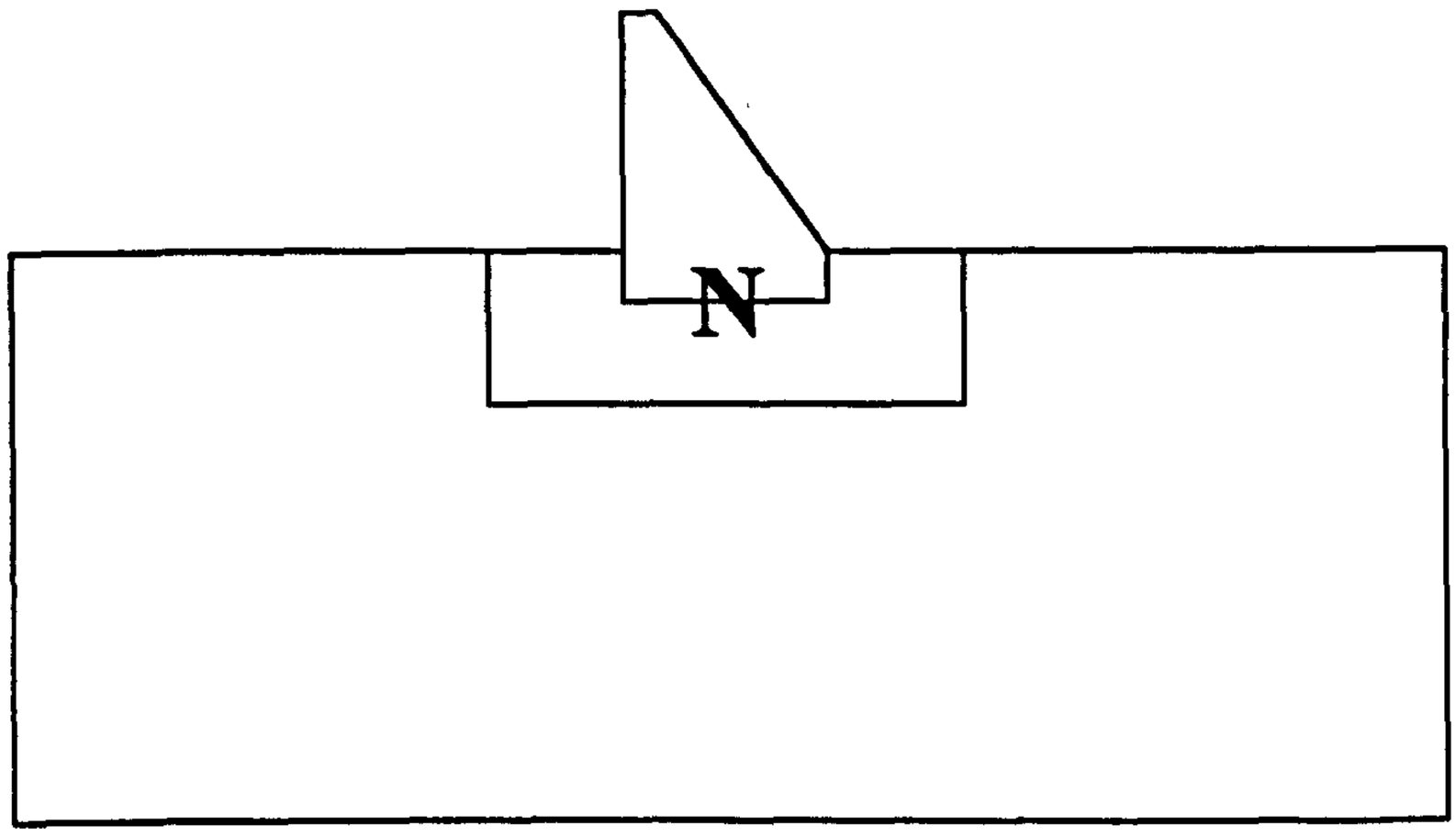

Figure 5.2b - Local nonlinearities

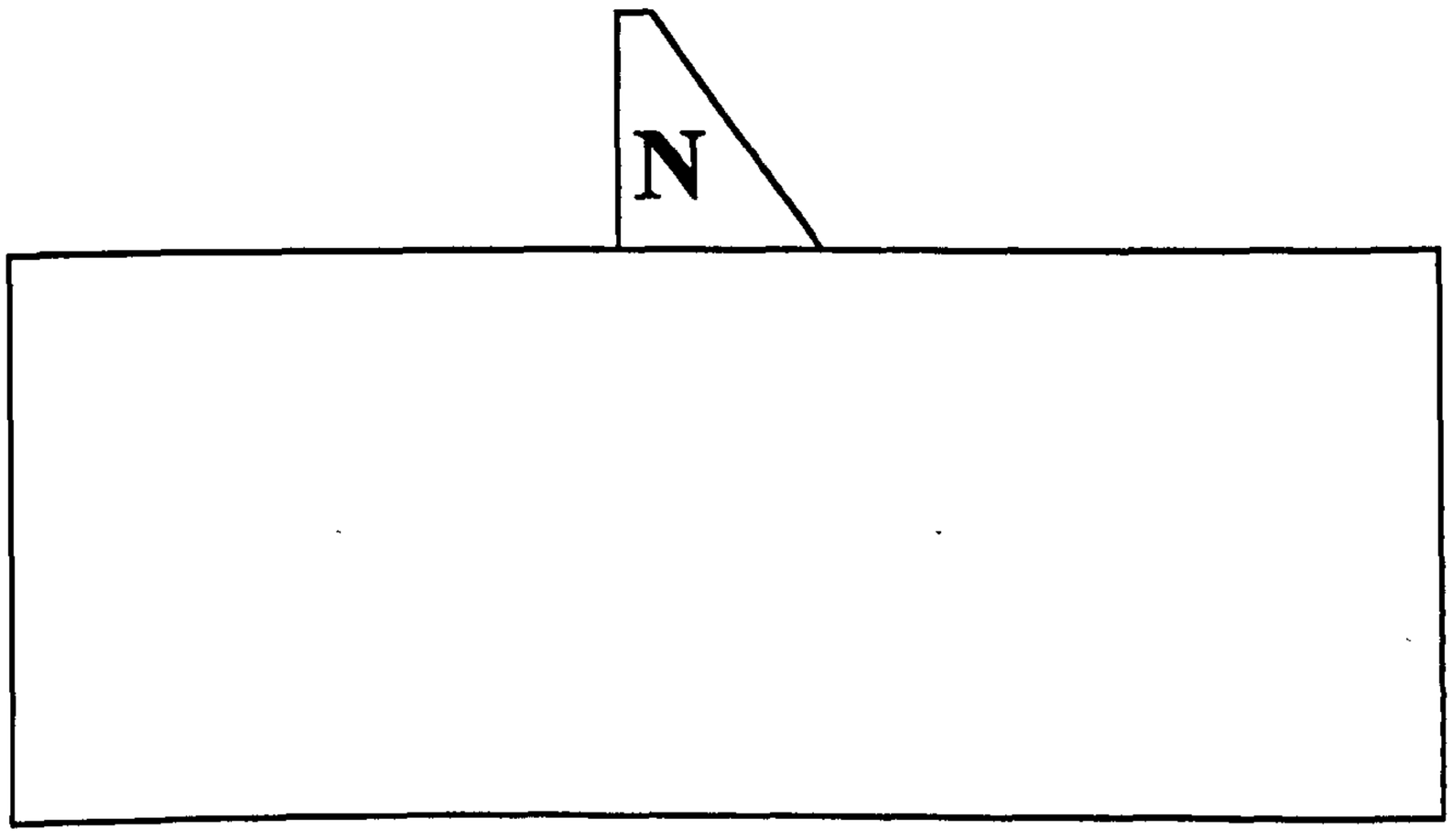

Figure 5.2c - Nonlinear dam and surface interface

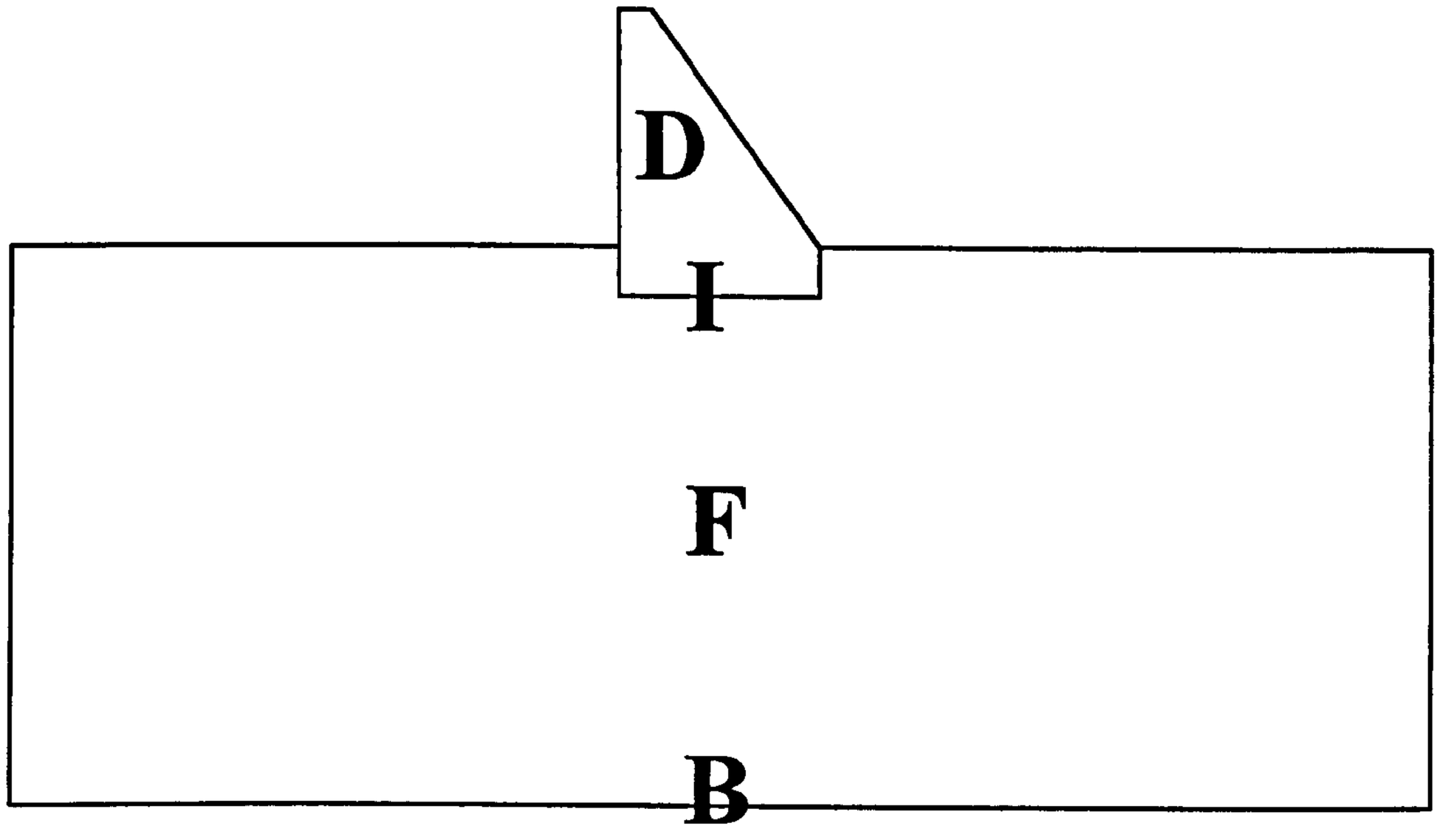

Figure 5.3 - Dam-foundation system: boundary input scheme

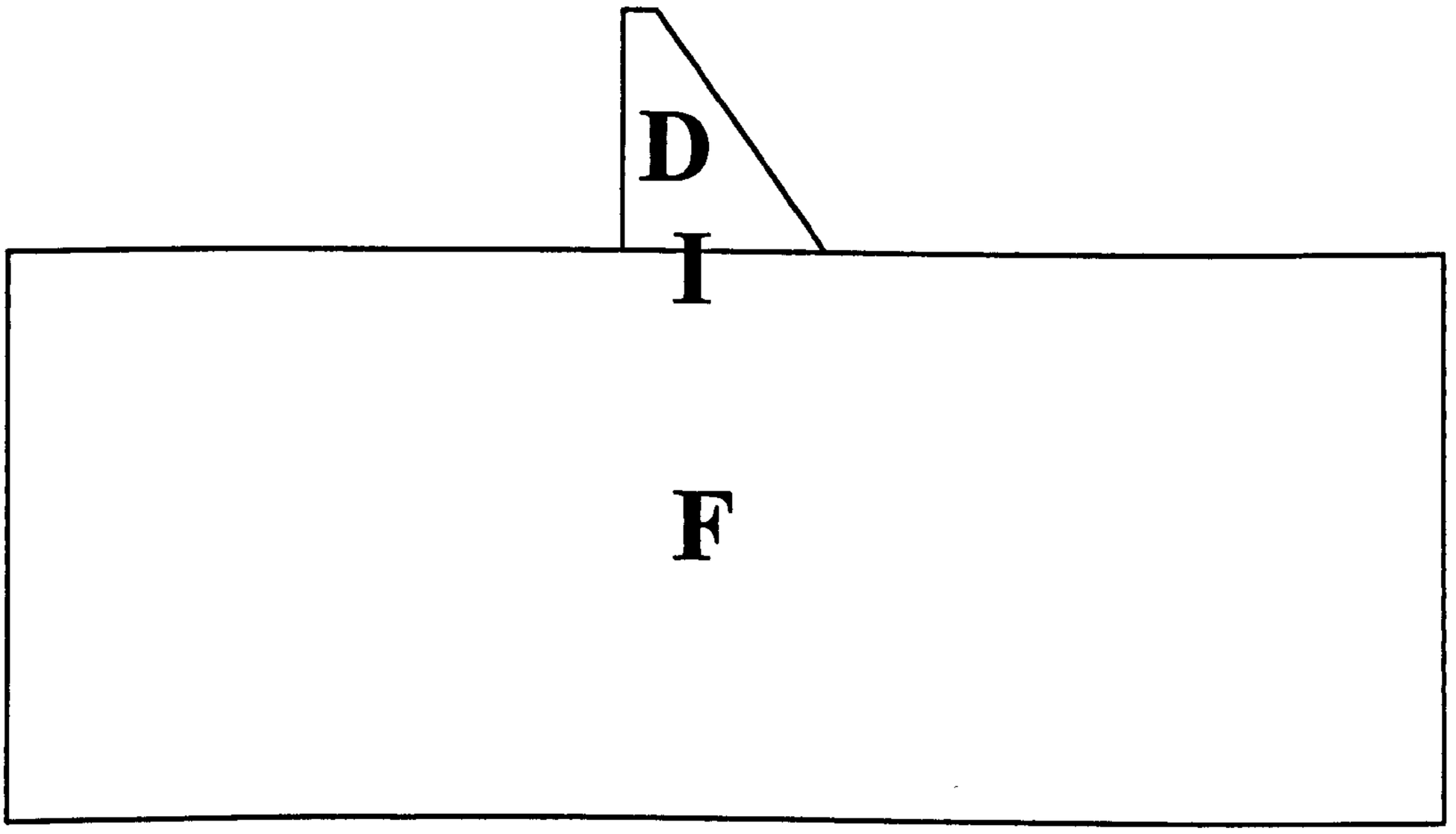

Figure 5.4 - Surface supported dam-foundation system: interface input scheme

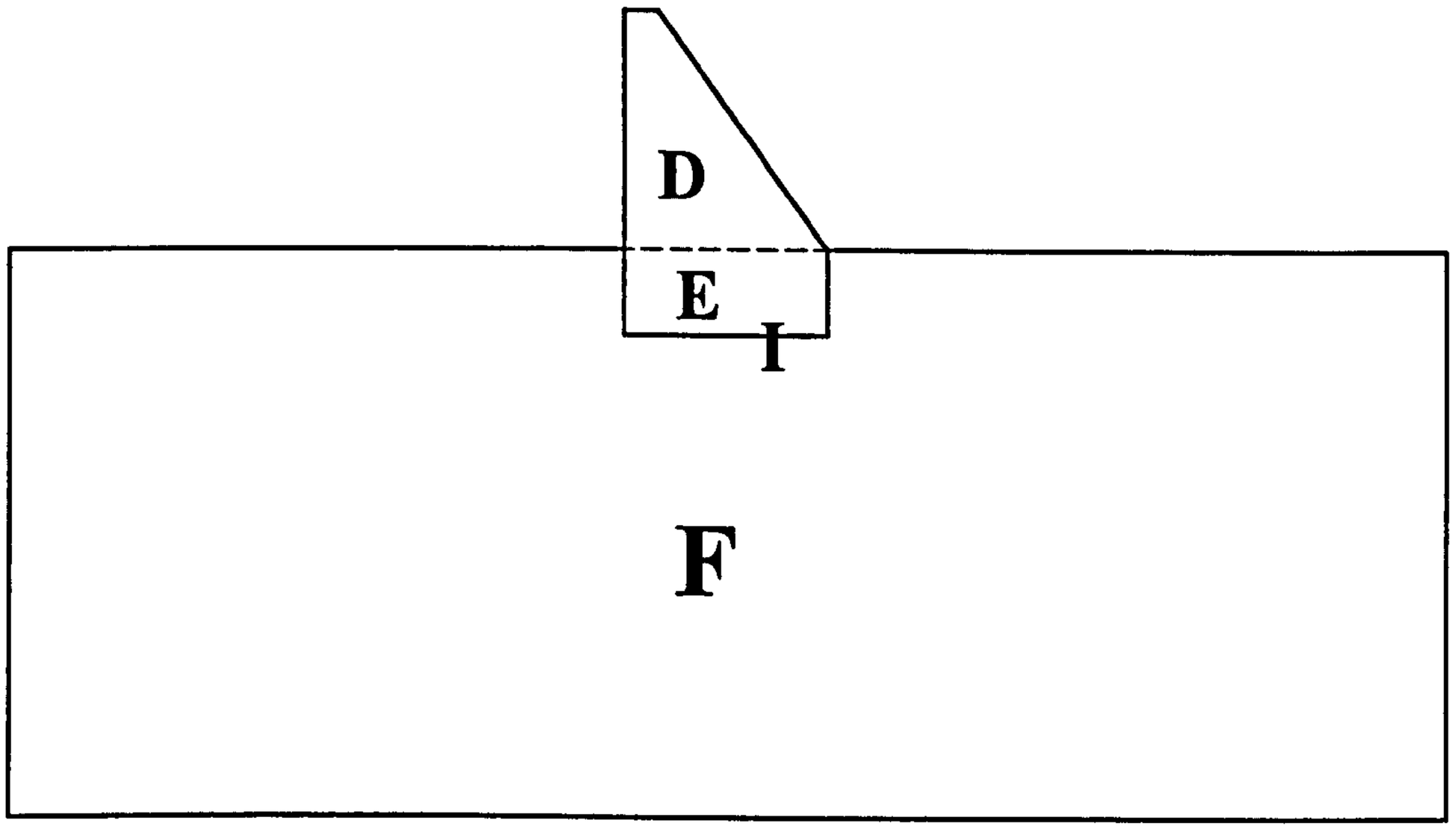

Figure 5.5 - Linear embedded dam-foundation system: interface input scheme

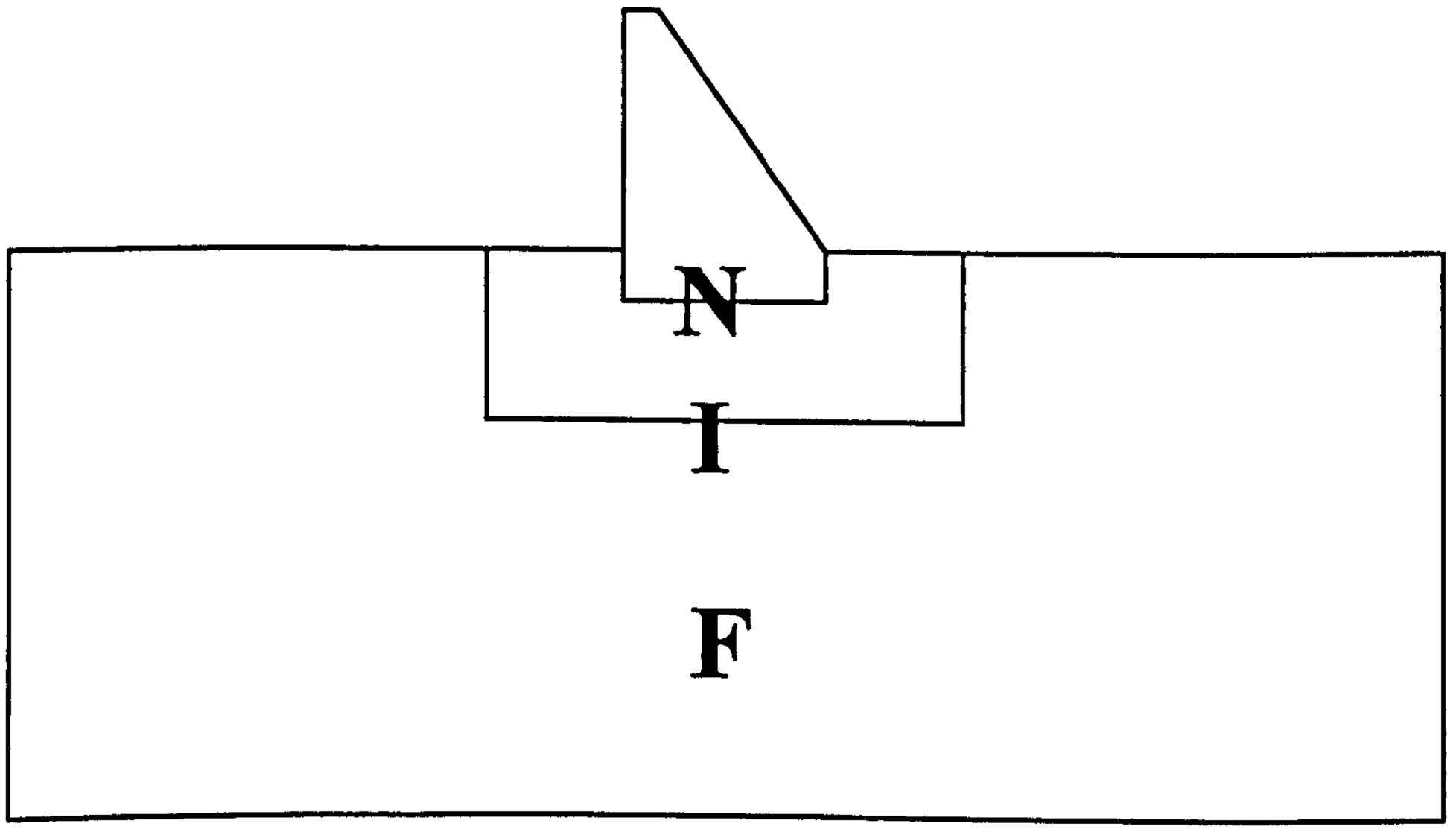

Figure 5.6 - Nonlinear embedded dam-foundation system: interface input scheme

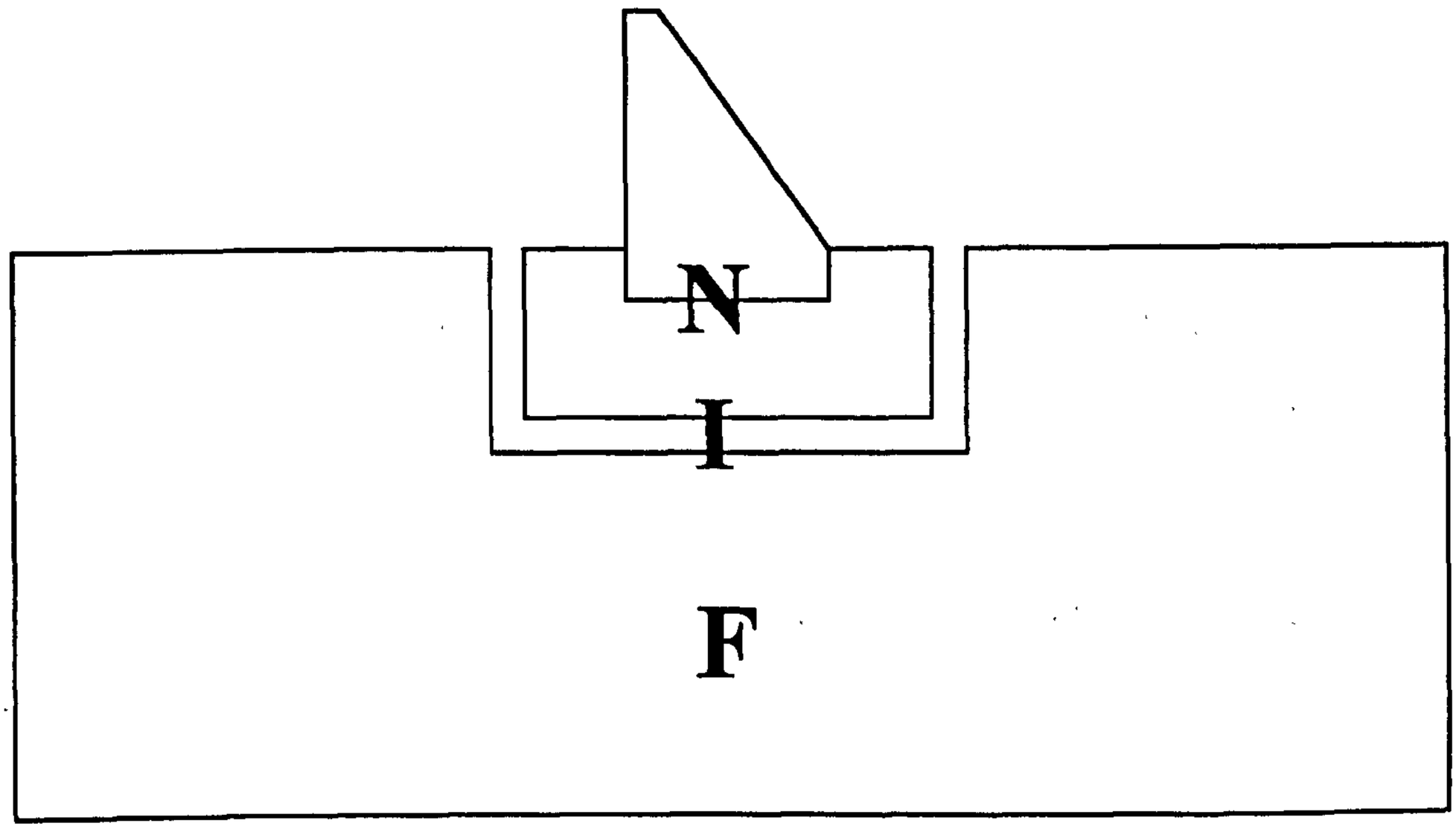

Figure 5.7 - Nonlinear embedded dam-foundation system:

Bielak-Christiano interface input scheme

Preliminary Linear Earthquake Analyses of Concrete Gravity Dam-Foundation Systems

The foundation part of the concrete gravity dam-foundation system was treated in Chapters 3 and 4. In Chapter 5, the dam was coupled with the foundation and dynamic equations for the combined system were presented. These equations were formulated in the time domain so they can be readily applied for both linear and nonlinear analyses.

In this Chapter, preliminary linear earthquake analyses of concrete gravity dam-foundation systems will be undertaken. The objectives are manyfold; from establishing the correct seismic input scheme for different foundation conditions, to recommending the size and fineness of the foundation finite element mesh. To achieve all this, several sets of analyses will be carried out using the finite element code SOLVIA (SOLVIA Engineering AB, 1989/92). First, two seismic input schemes (boundary and interface) will be compared for two different foundation conditions (rock layer and rock half-space). The practical significance of the research findings will be then illustrated on the example of earthquake analysis of a real dam. Finally, the finite element foundation discretisation will be examined as a function of radiation damping.

In order to enable the extension towards nonlinear analyses in Chapter 9, a procedure for combining the viscous transmitting boundary with static loading will be presented and tested at the end of this Chapter.

6.1 Evaluation of Seismic Input Schemes

To evaluate the correct seismic input scheme for different foundation conditions, three sets of analyses will be carried out. The common assumptions and explanations will be given in Subsection 6.1.1. In Subsection 6.1.2, two seismic input schemes (boundary and interface) will be compared for the case of an idealised concrete gravity dam on a rock layer. The response of the dam on a rock layer will be compared with the response of the dam on a rock half-space in Subsection 6.1.3; all by using the interface input scheme. In Subsection 6.1.4, two seismic input schemes (boundary with massless foundation and interface) will be compared for the case of a dam on the rock half-space. The conclusions on the seismic input scheme will be drawn in Subsection 6.1.5.

6.1.1 Assumptions and Explanations

There are several assumptions that are shared among the subsequent three sets of analyses (Subsections 6.1.2, 6.1.3 and 6.1.4). They will be stated and, where appropriate, explained in detail in this Subsection.

6.1.1.1 Geometry of the System

The finite element mesh of the idealised concrete gravity dam-foundation system is shown in Figure 6.1. It was assumed that the system is two dimensional and in the state of plane strain. The embedment of the dam is not considerable and the interface between the dam and the foundation can therefore be assumed as flat and at the ground level.

The dam is of idealised geometry - 50 m high, with a width of 50 m at the interface and 10 m at the top. It was modelled with 10 rows and 10 columns of four-noded

isoparametric finite elements. The rock foundation is a rectangular block, with a height of 50 m and width of 150 m. It was modelled with 30 rows and 10 columns of square four-noded isoparametric finite elements. The justification for this initial choice of the foundation element size is related to the material properties and will be given in Paragraph 6.1.1.2.

Two foundation conditions will be examined. In Subsection 6.1.2, the foundation is a rock layer lying on the basement rock, which means that a sharp geological discontinuity exists at the bottom of the foundation finite element mesh (line of nodes 1-31 in Figure 6.1). In this case, the left and right lateral boundaries of the foundation finite element mesh (lines of nodes 1-311 and 31-341, respectively) are free in the horizontal direction for the horizontal earthquake component and free in the vertical direction for the vertical earthquake component. On the other hand, in Subsection 6.1.4, the foundation in the form of the rock half-space will be considered. In Section 6.1.3, the two cases will be compared.

6.1.1.2 Linear Elastic Material Models

The linear elastic material model was assumed for both the dam and the foundation.

The modulus of elasticity of the dam was E_d=20 GPa, Poisson's ratio was μ_d=0.20, and mass density was ρ_d=2450 kg/m³. The Poisson's ratio of the foundation was μ_f =0.25 and its mass density was ρ_f=2450 kg/m³. In order to examine the influence of the flexibility of the foundation on the overall response of the system, two moduli of elasticity were used, E_f=5 GPa and E_f=20 GPa. The former represented a very soft foundation, almost the limiting case for concrete gravity dam foundations. The latter was interesting since it was the same modulus as for the dam concrete.

In Subsections 6.1.3 and 6.1.4, the foundation in the form of the rock half-space will be treated, necessitating the approximate modelling of radiation damping conditions at the edges of the foundation finite element mesh. Since wave-energy reflection or

non-reflection is a wave propagation phenomenon, it seemed reasonable to adopt the standard recommendations for the size of the foundation finite element mesh, as specified in Chapter 4 when dealing with wave propagation problems. Typically, uniform meshes are used and the size of the element is determined by dividing the smallest wavelength by a factor (usually between 8 and 12). The minimum wavelength, on the other hand, can be obtained by dividing the minimum velocity of seismic waves (usually S-waves) by the cut-off frequency present in the mesh (here 20 Hz, as will be shown in Paragraph 6.1.1.3).

The smallest foundation modulus (5 GPa) produced the minimum S-wave velocity (903.51 m/s), which suggested the choice of the element size in the range of 3.76-5.64 m. As mentioned in the previous Paragraph, the value of 5 m was chosen for all the analyses in the subsequent three Subsections.

6.1.1.3 Loading of the System

In this Chapter, only dynamic loading was considered.

For linear elastic models, the principle of superposition is valid, which means that different loads can be analysed independently, one by one. The response to the sum of loads is equal to the sum of the responses to each of the loads. According to this principle, the earthquake loading can be analysed on its own. In order to produce a realistic load combination, the obtained results can later be added to the results due to any other load.

Here, it was assumed that the surface free-field acceleration record is known and that only the horizontal component is significant. The time history of the record is in the form of the Ricker wavelet with the peak amplitude of 0.5g

$$\ddot{v}(t) = -0.5g\left(1-2\tau^2\right)e^{-\tau^2} \tag{6.1}$$

in which τ is the parameter

$$\tau = \frac{t - t_s}{t_0} \tag{6.2}$$

where t is time; t_s is the time instant which controls the duration of the wavelet by specifying the occurence of its maximum peak (set here to 0.2 s); and t_0 is the parameter which controls the frequency content of the excitation (set here to $1/7\pi$ s). The positive unit Ricker wavelet is shown in Figure 6.2a. However, it is important to keep the negative sign in Equation (6.1) because the negative main peak of the acceleration wavelet (direction downstream to upstream) corresponds to the positive (direction upstream to downstream) main peaks of both the inertial force and displacement.

The Fourier transform of the Ricker wavelet can be expessed in the closed form

$$F(\omega) = 2\sqrt{\pi}\, t_0\, e^{-i\omega t_s} \frac{\omega^2 t_0^2}{4} e^{-\frac{\omega^2 t_0^2}{4}} \tag{6.3}$$

whose real part, imaginary part and modulus are shown in Figure 6.2b. While the parameter t_s=0.2 s can be identified in Figure 6.2a as the time at which the maximum peak of the wavelet occurs, the parameter t_0 can be observed only in Figure 6.2b. Its setting to the value of $1/7\pi$ s means that the dominant frequency is at about 7 Hz and that the frequency of excitation is in the range of 0 Hz to 20 Hz (the so-called cut-off frequency).

Furthermore, it was assumed that the earthquake motion is uniform. For the boundary input scheme this means that the motion along the basement rock is uniform while for the interface input scheme this means that the motion along the dam-foundation interface is uniform.

In addition to the dynamic earthquake excitation, reservoir-dam interaction was modelled by the Westergaard added mass technique (Westergaard, 1933; Greeves, 1991).

6.1.1.4 Damping of the System

Two main forms of damping exist in concrete gravity dam-foundation systems.

First, internal damping arises due to energy dissipation in the material itself (dam concrete or foundation rock). One convenient form of internal damping is the so-called Rayleigh damping. In the finite element formulation, the Rayleigh damping matrix **C** of the whole system is expressed as

$$\mathbf{C} = \alpha\mathbf{M} + \beta\mathbf{K} \tag{6.4}$$

where **M** and **K** are the mass and stiffness matrix of the system, respectively; and α and β are the parameters which can be determined if two damping ratios for the two control frequencies are known (Clough & Penzien, 1975). This form of damping will be used in the case of the dam on the rock layer, where it represents the only source of damping (Subsections 6.1.2 and 6.1.3). In order to enable a proper comparison, Rayleigh damping will also be used for the dam on the rock half-space in Subsection 6.1.3, as one of the two sources of damping. For all the cases, setting the two damping ratios to 0.05 (5%) for the control frequencies of 2.715 Hz and 18.806 Hz produced the parameters α=1.491 and β=0.0007395356, ensuring a fair distribution of damping over the frequency range of interest (Figure 6.3).

Second, external, radiation damping arises due to energy radiating away from the dam, which is particularly important in the case of the half-space foundation. This form of damping was described in detail in Chapters 3 and 4, where it was suggested that the standard viscous transmitting boundary could be successfully applied in the dam-foundation interaction analyses. The standard viscous transmitting boundary will be used in the case of the dam on the rock half-space, where it represents one of the two sources of damping (Subsections 6.1.3 and 6.1.4). Its handling in the finite element computations was already specified in Chapter 4. The internal damping of the system is not included so that the radiation damping effects can be emphasised to their extremes.

6.1.1.5 Solution of the Dynamic Equations

The fact that only linear earthquake analyses were carried out in this Chapter enabled the use of simplified dam-foundation interaction equations. Equation (5.8) was used for the boundary input scheme and Equation (5.21) was used for the interface input scheme. They were both solved through implicit, direct integration, by employing the Newmark constant-average-acceleration method (with Newmark parameters γ =0.5 and β=0.25). The time step was adopted according to the standard wave propagation criterion, by dividing the cut-off period with a factor greater than 10 (usually 12). Since the cut-off period (for the cut-off frequency of 20 Hz) is 0.05 s, the time step of 0.004 s was chosen for all the analyses.

Although the solutions for the dam on the rock layer (Subsection 6.2) could have been obtained by employing the computationally less expensive modal superposition method, for the sake of comparison it was decided to use the direct integration method throughout. It was explained in Chapters 3 and 4 why the modal superposition method cannot be used for the analyses where radiation damping is present.

Initially, it was thought that slight numerical damping (the Newmark parameters γ> 0.5 and β>(γ+0.5)/4, as explained in Chapter 3 and applied in Chapter 4) might help with the numerical solution of the problem. However, the results of the analyses have shown that variation of the Newmark parameters had little or no effect on the solution. This fact was not unexpected since the main benefit of numerical damping is the reduction of high-frequency oscillations, which do not appear for dynamic excitations with the relatively narrow frequency range (e.g. earthquakes).

The solution of dynamic equations such as Equations (5.8) and (5.21) necessarily produces a large amount of data. It was therefore decided to use only two response time-histories as representative for the whole analysis. The first one is the horizontal displacement at the upstream face of the top of the dam (node 441 in Figure 6.1) and the second one is the vertical stress at the heel of the dam, just above the dam-

foundation interface (node 342 in Figure 6.1). The choice of the representative stress in the finite element node implies the extrapolation from the values at the element integration points.

6.1.2 Dam on a Rock Layer

In this Subsection, the results of the boundary and interface input scheme are compared in the earthquake response analysis of the concrete gravity dam on a rock layer.

It was described in detail in Chapter 5 that two seismic input schemes can be applied for the time-domain linear earthquake response analysis of concrete gravity dam-foundation systems: boundary and interface. When a sharp geological discontinuity exists at a reasonable depth below the ground level, the underlying rock formation can be regarded as a basement rock (line of nodes 1-31 in Figure 6.1) which means that the foundation behaves like a rock layer. Under these conditions, both input schemes can be used.

For the boundary input scheme, and according to Equation (5.8), the earthquake acceleration has to be specified at the boundary (basement rock). Unfortunately, the seismic records are available, if at all, only at the ground level and a free-field analysis of the site has to be performed in order to determine the motions at the boundary. As explained in Chapter 5, the present state-of-the-art two dimensional free-field site analysis requires stringent assumptions, of which certainly the most popular one is the standard deconvolution procedure with SV-wave propagation. Nevertheless, if the known surface free-field acceleration record is applied at the basement rock, it is thought that the site amplification effects would render the results of the analysis unacceptable. Such a behaviour was predicted in Chapter 5, based on the theoretical considerations. To illustrate this, the representative horizontal displacement time-history is shown alongside other solutions in Figures

6.4a and 6.5a for the foundation moduli of E_f=20 and 5 GPa, respectively. Also, the representative vertical stress time-history is shown alongside other solutions in Figures 6.4b and 6.5b for the foundation moduli of E_f=20 and 5 GPa, respectively.

The advantage of the boundary input scheme in the case of the dam on a rock layer is that standard structural dynamics finite element packages can be used. In order to keep this facility, an approximate method, the so-called massless foundation input scheme, was suggested by Clough (1980). The known surface free-field acceleration record is still prescribed at the basement rock, but the mass of the foundation is assigned the zero value. The massless medium reduces the latter's influence on the wave propagation mechanism and it was thought that the obtained response was a reasonably good approximation of the real response of the dam. Unfortunately, if this scheme is applied, only the dam response results are meaningful. Similar to the original boundary input scheme, the representative horizontal displacement time-history is shown in Figures 6.4a and 6.5a, while the representative vertical stress time-history is shown in Figures 6.4b and 6.5b, for the foundation moduli of E_f=20 and 5 GPa, respectively.

On the other hand, the same problem may be modelled by using the interface input scheme according to Equation (5.21), which, within the limits of its own assumptions, offers the exact solution. The only disadvantage of the interface input scheme is the form of its Equation (5.21), for it cannot be readily used within a general purpose finite element code like SOLVIA (SOLVIA Engineering AB, 1989/92). The code was therefore adapted to create the forcing function on the righthand side of Equation (5.21). As in the other two cases, the chosen horizontal displacement time-history is shown in Figures 6.4a and 6.5a, while the chosen vertical stress time-history is shown in Figures 6.4b and 6.5b, for the foundation moduli of E_f=20 and 5 GPa, respectively.

6.1.3 Dam on a Rock Layer and Dam on a Rock Half-Space: Comparison

In this Section, the response of the dam on a rock layer is compared with the response of the dam on a rock half-space. The interface input scheme was used for both analyses.

Apart from the boundary conditions, the two models under investigation are the same and follow the descriptions given in Subsection 6.1.1. For the dam on a rock layer, a basement rock (line of nodes 1-31 in Figure 6.1) exists at the foundation depth equal to the height of the dam. The nodes 1-31 are therefore fixed, which, according to the explanations given in Chapters 3 and 4, enables almost complete energy reflection at the boundary. The results for this model were taken from the previous Section. For the dam on a rock half-space, semi-infinity of the foundation and the corresponding energy radiation was modelled by the standard viscous transmitting boundary.

The representative horizontal displacement time-histories are shown in Figures 6.6a and 6.7a, while the representative vertical stress time-histories are shown in Figures 6.6b and 6.7b, for the foundation moduli of E_f=20 and 5 GPa, respectively.

6.1.4 Dam on a Rock Half-Space

In this Section, the results of the boundary input scheme with massless foundation are compared with the results of the interface input scheme for the earthquake response analysis of the concrete gravity dam on a rock half-space.

The two seismic input schemes for time-domain linear earthquake response analysis of concrete gravity dam-foundation systems, boundary and interface, were analytically described in Chapter 5 and applied to the dam on the rock layer in Subsection 6.1.2. According to the theoretical considerations in Chapter 5, it was concluded that the interface input scheme is the only appropriate one to be used for dams on rock half-space foundations. Nevertheless, it was attempted here to use the boundary input

scheme with massless foundation. By comparing its results with the results of the proper interface input scheme it may be established whether this method, although theoretically unfounded, is capable of producing meaningful results.

The representative horizontal displacement time-histories are shown in Figures 6.8a and 6.9a, while the representative vertical stress time-histories are shown in Figures 6.8b and 6.9b, for the foundation moduli of E_f=20 and 5 GPa, respectively.

6.1.5 Concluding Remarks on the Seismic Input Scheme

The concluding remarks in this Subsection are based on the results presented in the previous three Subsections and concern the type and choice of the seismic input scheme.

The standard boundary input scheme cannot be used for dams on a rock layer unless the free-field analysis of the site is carried out and the excitation of the basement rock is fully determined. If the surface records are applied at the basement rock, the results are unacceptably high due to site amplification effects (Figures 6.4 and 6.5). This happens irrespective of the foundation flexibility.

In some cases, the boundary input scheme with massless foundation can be used for dams on a rock layer. The correlation with the exact interface input scheme demonstrates that better agreement is achieved for the more rigid foundation conditions (E_f=20 GPa in Figures 6.4a and 6.4b). On the other hand, the agreement is worse for the more flexible foundation conditions (E_f=5 GPa in Figures 6.5a and 6.5b), which corroborates the assumption that the interaction effects are more pronounced in this case.

The response of the dam on a rock layer is completely different from the response of the dam on a rock half-space (Figures 6.6 and 6.7). This is not unexpected, since the systems are physically different and the presence of the radiation damping in the latter considerably reduces the response. Under no circumstances can one case be

substituted with the other, nor can the results of one be interpreted as the results of the other.

The radiation damping in the case of dams on rock half-spaces is stronger for the more flexible foundation (E_f=5 GPa in Figures 6.7 and 6.9).

The irregular oscillations (oscillations that do not follow the pattern of the Ricker wavelet) are visible for the more flexible foundations (E_f=5 GPa) in the case of the boundary input scheme with massless foundation. For the dam on a rock half-space, these oscillations are noticed for both displacements and stresses (Figures 6.9a and 6.9b), whereas for the dam on a rock layer, the oscillations are confined to the stresses (Figure 6.5b). In the last case, they can be observed even in the case of the interface input scheme. Fortunately, the irregular oscillations are not present in the most realistic case (dam on a rock half-space) in conjunction with the appropriate seismic input scheme (interface input scheme). This will be further investigated in Section 6.3.

For the dam on a rock half-space, the results produced by the interface input scheme are always smaller than those produced by the boundary input scheme with massless foundation (Figures 6.8 and 6.9). Again, better correlation is achieved for the more rigid foundation (E_f=20 GPa in Figure 6.8). It seems acceptable to use the boundary input scheme scheme with massless foundation for the foundations equal or more rigid than the dam. Unfortunately, if this scheme is applied, only the dam response results are meaningful and only linear analyses can be carried out. On the other hand, for the more flexible foundation (E_f=5 GPa in Figure 6.9), the differences are more pronounced and the interface input scheme is the only alternative. Furthermore, the irregular oscillation discussed in the previous paragraph and observed when the massless foundation input scheme was used, are bound to corrupt the response due to real earthquake records, where they could not be so easily identified.

6.2 Example of a Linear Earthquake Concrete Gravity Dam-Foundation Analysis

This Section presents the results of a seismic analysis of a realistic concrete gravity dam. The chosen model was based on an actual UK dam.

6.2.1 Linear Elastic Material Models for the Dam-Foundation System

A linear elastic material model was assumed for both the mass concrete and the rock foundation.

The modulus of elasticity of the dam was estimated to be E_d=30 GPa; Poisson's ratio μ_d=0.20, and mass density ρ_d=2380 kg/m³. The modulus of elasticity of the foundation was estimated to be E_f=22 GPa. Due to uncertainty of the estimate procedure, a modulus of E_f=10 GPa was also used for comparison purposes. The Poisson's ratio of the foundation was estimated to be μ_f=0.25 and its mass density ρ_f =2800 kg/m³.

6.2.2 Geometry of the Dam-Foundation System

A single block of the dam was analysed. The breadth of the block was 14.17 m and it was assumed to be in a state of plane stress. The final finite element mesh of the dam-foundation system, adopted according to the results of preliminary frequency and response spectrum analyses, is shown in Figure 6.10, where the thick lines denote the interface between the dam and the foundation.

It is well-known that frequency analyses of structure-foundation systems are heavily influenced by the amount of foundation taken into account. The larger the foundation, the lower the frequencies. In order to minimise these effects and to

determine the minimum size and fineness of the foundation mesh, preliminary modal and response spectrum analyses were all conducted with a massless foundation.

First, two foundation meshes were examined; one extended approximately one height of the dam upstream, downstream and underneath the dam, while the second was three times bigger. Preliminary modal analyses have shown that the resulting frequencies for the two meshes were very close and that the mode shapes corresponded to each other. Since the smaller mesh produced the first, dominant frequency closer to the maximum ordinates of the earthquake spectrum (to be used in subsequent response spectrum analyses), it was recommended for further use.

Once the size of the foundation finite element mesh had been established, it was decided to assess its accuracy due to discretisation by carrying out preliminary response spectrum analyses. Initially, two meshes were examined. The coarser mesh had 8 elements along the width of the dam and the finer one had 16. Both meshes were subjected to the UK hard ground spectrum (Principia Mechanica Ltd., 1981) with 5% damping (Figure 6.11). The horizontal component of the spectrum was scaled to a peak ground acceleration of 0.3g while the vertical component was taken as two thirds of the horizontal one over the entire frequency range. Although the frequencies, mode shapes and displacements produced by the two meshes were also compared, the main criterion for the decision regarding their accuracy was the stress distribution around the interface between the dam and the foundation. It was finally decided to adopt a mesh 'in between' the two previously described. This mesh had 12 elements along the width of the dam and is shown in Figure 6.10. Its largest foundation element size was about 4 m, which is acceptable even according to the wave propagation criterion presented in Paragraph 6.1.1.2 and should be able to satisfy the most stringent requirements for modelling the radiation damping.

The possibilities of achieving good results with more economical foundation finite element meshes will be further investigated in Section 6.3.

6.2.3 Loading of the Dam-Foundation System

Both static and earthquake loads were considered in the finite element analysis of the dam. However, since the analyses were all linear and in order to ease the comparison with the idealised dam treated in the previous Section, only the results due to seismic loads will be presented.

The earthquake load was modelled through the response spectrum shown in Figure 6.11, which served as a basis for response spectrum analyses. Twelve (6 horizontal and 6 vertical) spectrum compatible synthetic accelerograms with the peak ground acceleration of 0.3g and 0.2g, respectively, were also created to provide a basis for time-history analyses. Only a small selection of the results from the latter set of analyses will be presented.

For full reservoir conditions, in addition to the dynamic earthquake excitation, reservoir-dam interaction was modelled using the Westergaard added mass technique.

6.2.4 Damping of the Dam-Foundation System

For time-history analyses, two forms of damping were considered: internal and radiation. One set of analyses was conducted only with internal damping (as typically done in standard time-domain earthquake dam-foundation analyses) and the other set was conducted with both kinds of damping. The former case implies the existence of a fully reflecting foundation boundary (e.g. basement rock) while the latter implies the existence of an unbounded rock half-space.

Rayleigh damping according to Equation (6.4) was chosen to represent the internal damping of the dam-foundation system. For each of the four analytical models (E_f=10 GPa and reservoir empty, E_f=10 GPa and reservoir full, E_f=22 GPa and reservoir empty, E_f=22 GPa and reservoir full), a set of Rayleigh damping parameters α (mass proportional term) and β (stiffness proportional term) was constructed with both control frequencies fixed at 5%.

The standard viscous transmitting boundary in the form of concentrated viscous dashpots was chosen to represent the radiation damping. For each of the two foundation conditions (E_f=10 GPa and E_f=22 GPa), a pair of viscosity coefficients (normal and tangential to the boundary) was calculated according to Equation (4.6).

6.2.5 Solution of the Dynamic Equation

Following the conclusions given in Subsection 6.1.5 and having in mind that only linear earthquake analyses were considered, it was decided to use the simplified dam-foundation interaction equation for the boundary input scheme with massless foundation. In other words, Equation (5.8) with a massless foundation was used for the dam on the rock layer (internal damping only, no radiation damping due to reflection from the artificial boundaries) as well as for the dam on the rock half-space (both internal and radiation damping present).

The dynamic equations were solved through implicit, direct integration, using the Newmark constant-average-acceleration method (with Newmark parameters γ=0.5 and β=0.25) and with the time step of 0.01 s.

6.2.6 Some Results and Concluding Remarks

Only the horizontal displacement time-history at the upstream face of the top of the dam will be presented here. Also, only the results for the full reservoir conditions will be covered (BEELAB, 1993/94).

For the dam-foundation system subjected to the synthetic accelerograms of earthquake no. 1 (its unit horizontal and vertical components are shown in Figures 6.12a and 6.12b, respectively), the representative time-histories for the first 4 s and for the foundation moduli of E_f=22 and 10 GPa are shown in Figures 6.13a and 6.13b.

In order to sudy the damping mechanism more carefully, the dam-foundation system was subjected to the horizontal accelerogram in the form of Ricker wavelet (shown in Figure 6.2a), whose peak was scaled to 0.3g for this exercise. The application of the Ricker wavelet instead of the real earthquake record facilitated the observation of the amplitude decay, which is of primary importance when damping is concerned. In addition to the examination of the radiation damping, different forms of Rayleigh damping (mass proportional only, stiffness proportional only and full) were also investigated. The representative time-histories with the full Rayleigh damping demonstrating the effect of the radiation damping are shown in Figures 6.14a and 6.15a for the foundation moduli of E_f=22 and 10 GPa, respectively. The representative time-histories with no radiation damping demonstrating the effects of different types of the Rayleigh damping are shown in Figures 6.14b and 6.15b for the foundation moduli of E_f=22 and 10 GPa, respectively. The same results, but with radiation damping included, are shown in Figures 6.14c and 6.15c.

The comparison between Figures 6.14a and 6.15a (dam subjected to Ricker wavelet acceleration) and Figures 6.13a and 6.13b (dam subjected to synthetic earthquake acceleration) demonstrates that the same conclusion can be drawn from either of these pairs; namely, that the radiation damping is far too important to be neglected. This also means that the Ricker wavelet may be used for qualitative investigations into seismic behaviour of concrete gravity dam-foundation systems.

For the system under examination, the radiation damping is greater than the full Rayleigh damping constructed with 5% of the critical damping at the chosen control frequencies.

The non-smooth parts of the response (particularly visible in the case of E_f=10 GPa) are due to the application of the boundary input scheme with massless foundation and are expected to disappear with the application of the interface input scheme, as explained in Subsection 6.1.5.

Rayleigh damping exhibits greater importance when considered on its own, without the radiation damping.

The mass proportional Rayleigh damping part is very close to the full Rayleigh damping while the stiffness proportional Rayleigh damping part is very close to the non-damped case. This means that the internal, Rayleigh damping for concrete gravity dam-foundation systems is indirectly and almost entirely governed by the mass of the system.

6.3 Rock Half-Space Foundation Discretisation

The previous Sections have clearly indicated the importance of the radiation damping and have offered conclusions about the application of the appropriate seismic input scheme. However, in the case of a concrete gravity dam on a rock half-space foundation, no definite answers were given to the questions regarding the size of the foundation finite element mesh and the size of the foundation finite elements.

All the previous analyses in this Chapter were performed with uniform foundation finite element meshes of fixed size. The typical size of the element was determined according to the wave propagation criterion, which is a correct but uneconomic solution. The size of the mesh itself was determined either arbitrarily (Section 6.1) or according to the properties of the seismic loading (Section 6.2). In this Section, a detailed investigation into rock half-space foundation discretisation will be undertaken in order to reach conclusions about the foundation size and necessary fineness of the mesh. Ideally, these conclusions should only be functions of the foundations properties.

6.3.1 Assumptions and Explanations

Several assumptions common for the subsequent analyses are summarised in this Subsection. Frequent reference will be made to detailed explanations in Subsection 6.1.1.

6.3.1.1 Geometry of the System

It was assumed that the system is two-dimensional and in the state of plane strain.

The embedment of the dam is not considerable and the dam-foundation interface was therefore assumed as flat and at the ground level.

The geometry and discretisation of the dam were as explained in Subsection 6.1.1 and depicted in Figure 6.1. A rock half-space foundation was modelled by a rectangular block equipped with the standard viscous transmitting boundary at the edges of the foundation mesh in order to model the radiation damping. The size of the foundation block was varied in multiples of the height of the dam H. Hence, the height of the foundation block was xH (x is the variable parameter) and its width was $(2x+1)H$.

6.3.1.2 Linear Elastic Material Models

A linear elastic material model was assumed for both the dam and the foundation. The modulus of elasticity of the dam was E_d=20 GPa; the Poisson's ratio was μ_d =0.20, and mass density was ρ_d=2450 kg/m³. The Poisson's ratio of the foundation was μ_f=0.25 and its mass density was ρ_f=2450 kg/m³. The only variable parameter was the most influential one - the foundation modulus of elasticity. The values of E_f=5, 10, 20 and 40 GPa were examined.

For the reasons explained in Section 6.1, the element size within uniform foundation finite element meshes was adopted according to the wave propagation criterion. Again, the smallest foundation modulus (5 GPa) controlled the smallest element size

and the value of 5 m was chosen for all the preliminary analyses. This decision will be reviewed in Subsection 6.3.3.

Fortunately, the conclusions reached with the linear elastic models should be valid for any local nonlinear analysis (see Chapter 7). The occurence of nonlinearities will only increase the number of energy-consuming mechanisms and the conclusions would remain conservative. Radiation damping is a global effect which must be artificially simulated for all bounded domains (linear or nonlinear) which are otherwise unbounded in reality.

6.3.1.3 Loading of the System

Only the dynamic loading in the form of a Ricker wavelet was considered. The peak amplitude was scaled to 0.5g while the other parameters were set according to the explanations in Subsection 6.1.1. It was assumed that only the horizontal component is significant and that the earthquake motion is uniform along the dam-foundation interface (since the interface input scheme was used).

In addition to the dynamic earthquake excitation, the dam-reservoir interaction was modelled through the Westergaard added mass technique.

6.3.1.4 Damping of the System

No internal damping was considered for any of the subsequent analyses. In this way, the effects of the radiation damping were emphasised to their extremes.

Moreover, the standard proportional Rayleigh damping according to Equation (6.4) is not good enough because it cannot take into account the nonproportional damping arising from the coupling of the dam and the foundation (Léger & Boughoufalah, 1989). As already mentioned, the external, radiation damping was represented with the standard viscous transmitting boundary.

6.3.1.5 Solution of the Dynamic Equations

The previous studies have confirmed that the interface input scheme is the only reliable input scheme because it is not influenced by the foundation properties and does not cause irregular oscillations. Since the earthquake analyses in this Section are linear, the interface input scheme was represented by Equation (5.21) and solved through direct integration, using the Newmark constant-average-acceleration method. The time step was adopted according to the standard wave propagation criterion mentioned in Subsection 6.1.1, bringing about the value of 0.004 s. Furthermore, the interface input scheme enforces the viscous transmitting boundary to react only to the total minus free-field motion, as explained in Chapter 5.

The analyses lasted slightly longer than in the previous Sections. Here, they ended at t=1.5 s in order to allow the remaining reflections from the viscous transmitting boundaries to come back into the area of dominant interest (dam and the surrounding foundation). This was true even for the largest foundation meshes.

In this Section, the same time-histories were monitored as in Section 6.1, i.e. the horizontal displacement at the upstream face of the top of the dam and the vertical stress at the heel of the dam. For both time-histories, MAX (absolute maximum) and SRSS (square root of the sum of the squares) values were identified and calculated in order to quantify and ease the comparison.

6.3.2 Size of the Foundation Finite Element Mesh

In time-domain analyses of concrete gravity dams founded on rock half-space foundations, some kind of local approximation of energy radiation conditions is necessary. If the standard viscous transmitting boundary is used for this purpose, recommendations regarding the extent of the foundation mesh that should be taken into account have not been published so far. In other words, the location of the viscous transmitting boundary is not arbitrary and should be determined in advance.

From an analytical point of view, the fact that the dynamic interaction equation of the substructure method is used (Equation (5.21)), implies that this quest is equivalent to finding the distance at which the far-field excitation of the free-field is equal to the far-field excitation of the whole system (righthand sides of Equations (5.13) and (5.14), respectively).

Herein, the investigation into the size of the foundation mesh was carried out according to Paragraph 6.3.1.1, by varying the parameter x. The values of 0.5, 1, 2, 3, 4, 5 and 6 were used for all four different foundation conditions. The representative time-histories for the three smallest values of x are shown in Figures 6.16, 6.17, 6.18 and 6.19 for the foundation moduli of E_f=5, 10, 20 and 40 GPa, respectively. The time-histories for higher values of x are very close to the time-histories for x=2 and are therefore not shown. Instead, the full set of MAX and SRSS values for all the values of x and for all the foundation moduli is shown in Table 6.1. The graphical equivalent of this Table was obtained by normalising the values to x=6 and by averaging the four sets of valus for all four foundation conditions, which is depicted in Figure 6.20.

An attempt was made to improve the standard viscous transmitting boundary by using the Rayleigh viscous transmitting boundary defined for the first natural frequency of the system, as described in Chapter 4. Many variations of this approach were tested: constant dampers all around the mesh; dampers linearly interpolated along lateral foundation sides; dampers linearly interpolated between mid-points of the lateral foundation sides and highest foundation points. None of these solutions has proved worthy of the extra effort since the obtained results were negligibly different from those already presented.

The review of Figures 6.16-6.20 (particularly the last one) reveals several conclusions which can be formulated as practical recommendations. First, it is obvious that the importance of the radiation damping decreases with the increase of the foundation modulus. Consequently, for the limit case of the rigid foundation, there would be no

radiation damping at all. Second, the x-values for which the maxima in Figure 6.20 occur increase with the increase of the foundation modulus. Finally, the first value of x that yields acceptable results is x=2. However, the lines immediately left to this value are very steep which renders this choice somewhat unreliable and the value of x=3 can be recommended as a general 'rule of thumb' for a wide range of foundation conditions.

6.3.3 Size of the Foundation Finite Elements

Similar to the overall size of the foundation finite element mesh, recommendations regarding the foundation finite element size for time-domain analyses of concrete gravity dams founded on rock half-spaces have never been previously published. Therefore, all the analyses so far were conducted by obeying the strict wave propagation rule for finite element size.

Once the minimum acceptable size of the foundation finite element mesh has been established (Subsection 6.3.2), further analyses can be carried out in order to investigate the aspects of finite element microidealisation, namely the optimal size and shape of the finite elements. Since the same results were observed for all four foundation conditions, only the results for E_f=10 GPa will be presented. The representative time-histories for two uniform meshes (one with element size of 5 m and the other with element size of 25 m) and one nonuniform mesh (depicted in Figure 6.21) are shown in Figures 6.22a and 6.22b. The results produced by the first and by the third mesh are practically indistinguishable. The corresponding MAX and SRSS values are shown in Table 6.2.

Both Figure 6.22 and Table 6.2 clearly indicate that the solution with large elements (25 m) throughout the foundation mesh is not good. On the other hand, the nonuniform mesh seems like the best solution. Without jeopardising the accuracy, its computational economy is much better than that of the fine uniform mesh (element

size 5 m). If fine elements are kept close to the dam-foundation interface area, the performance of the viscous transmitting boundary does not seem to be affected by the coarse elements at the edges of the foundation mesh (30 and 35 m). Moreover, the size of the elements of the nonuniform mesh increases as the distance from the dam increases. This helps in preserving the density of the outgoing radiation energy, which is constantly reduced by encountering the ever-increasing volume of the foundation. Therefore, it may be concluded that sufficiently large and appropriately designed nonuniform meshes can be recommended for earthquake analysis of concrete gravity dams lying on rock half-space foundations.

6.3.4 Comparison with the Frequency-Domain Analysis

The validity of the conclusions drawn in the previous Subsections can be verified by comparing the results of a time-domain and frequency domain analysis.

The time-domain analysis was carried out according to the recommendations and explanations given in this Section. The nonuniform foundation mesh (Figure 6.21) with E_f=10 GPa was used. The frequency domain analysis was carried out using the computer program EAGD84 (Fenves & Chopra, 1984) where the dam is modelled by standard finite elements while the rock half-space foundation is modelled by frequency dependent force-displacement (impedance) functions at the dam-foundation interface. Two main advantages of this procedure are that there is no need to discretise the foundation and that the energy radiation conditon is implicitly satisfied. However, since the computation has to be performed in the frequency domain, the program can be neither applied nor extended to nonlinear analyses.

At this stage, for the linear analyses, the dam-foundation system had to be examined for empty reservoir conditions because of the inherent differences in modelling the dam-reservoir interaction. Also, since EAGD84 eliminates rigid body displacement of the dam-foundation interface (which is not true for SOLVIA time-domain

analyses), the comparison between the displacements is not as straightforward as for the stresses (where only relative displacements are important). Therefore, Figure 6.23 shows the representative stress time histories for the two linear (SOLVIA time-domain and EAGD84 frequency-domain) analyses. Their comparison demonstrates that the time-domain analysis adequately models the radiation damping and that the implementation of the conclusions drawn in this Section about the rock half-space discretisation produces accurate results.

6.4 Combining a Viscous Transmitting Boundary with Static Loading

All the analyses in this Chapter were carried out for earthquake loading only. Radiation damping was represented with the viscous transmitting boundary in the form of viscous dashpots at the edges of the foundation mesh, as symbolically depicted in Figure 6.24a. Since all the models were linear, the results due to dynamic loading can be superimposed to the results due to static loading in order to obtain the combined results. Unfortunately, the viscous transmitting boundary cannot support static loading (detailed explanations are given in Chapter 4) and it is not possible to analyse the system shown in Figure 6.24a for the combined loading.

On the other hand, in nonlinear analyses, the principle of superposition of the loads is not valid. All the loads (static and dynamic) have to analysed simultaneously because the nonlinear mechanisms are defined for total values (e.g. displacements, strains, stresses). As the next logical step of this work is to carry out the nonlinear analyses in Chapter 9, a special procedure should be divised to ensure the simulataneous action of loads while still preserving the effects of the viscous transmitting boundary. Conveniently, this procedure can be tested on a linear analysis where the obtained results must be exactly the same as those obtained through the superposition.

The procedure presented here consists of two steps, which is in agreement with the realistic loading scenario. First, the static loads (typically dead weight and hydrostatic pressure, as symbolically shown in Figure 6.24b) are applied to the mesh which, in comparison with the one in Figure 6.24a, has another outer layer of foundation elements. The boundary forces acting at this last layer of elements are noted and memorised. In the second step, the earthquake loading (symbolically shown as the horizontal load in the centre of gravity of the dam depicted in Figure 6.24c) acts together with the previously defined static loads and the boundary forces memorised in the first step. These forces are now applied with the negative sign to counteract the effect of the static loads. The stiffness of the outer layer of foundation elements is removed, maintaining only its damping in the form of Equations (4.3) or (4.6). The latter kind of damping is equivalent to the viscous dashpots used for dynamic-only analysis shown in Figure 6.24a.

The finite element code SOLVIA (SOLVIA Engineering AB, 1989/92) was adapted to accommodate the described numerical procedure. A number of tests were conducted by carring out linear analyses and all the obtained results have appeared indistinguishable from those obtained by applying the principle of superposition. For this reason, their graphical comparison is not shown on this occasion. However, the full importance of this procedure will become obvious in the realms of nonlinear analyses, in Chapter 9.

6.5 Concluding Remarks

Most of the relevant conclusions have already been presented in the previous Sections, alongside the corresponding analyses. In this Section, only the most important findings will be summarised.

A product of the substructure method of earthquake analysis of general structure-foundation systems in the time domain, the interface input scheme, has emerged as the only seismic input alternative which can be used under all circumstances for concrete gravity dams lying on rock half-space foundations. On the other hand, the boundary input scheme with massless foundation can be used only for a very limited number of cases.

Even if the substructure method of analysis is used (and consequently the interface input scheme), the size of the rock half-space foundation finite element mesh is not arbitrary. The mesh which extends approximately 3 heights of the dam upstream, downstream and underneath the dam, can be recommended.

With respect to accuracy and computational economy, the optimal way to discretise the dam-foundation finite element mesh is to design it in accordance with the expected local nonlinearities in the dam and around the dam-foundation interface (as will be explained in Chapters 7 and 9), and gradually to increase the size of the elements with the increase of distance from the dam.

The comparison between the time domain and frequency domain analysis of a concrete gravity dam-foundation systems has shown that the former adequately models the radiation damping if the two previous recommendations are followed.

The solution for combining the viscous transmitting boundary and static loading was found and tested. It will be further applied for nonlinear analyses in Chapter 9.

E_f [GPA]	x	u_{MAX} [mm]	u_{SRSS} [mm]	σ_{MAX} [MPa]	σ_{SRSS} [MPa]
5	0.5	7.173	32.666	1.239	4.848
	1	8.282	40.242	1.374	5.864
	2	8.528	45.813	1.328	6.008
	3	8.529	45.356	1.324	5.827
	4	8.529	44.284	1.324	5.737
	5	8.529	43.909	1.324	5.752
	6	8.529	44.382	1.324	5.811
10	0.5	8.240	34.062	1.749	6.937
	1	9.567	43.946	2.055	9.133
	2	10.019	54.424	2.076	10.199
	3	10.032	52.316	2.051	9.850
	4	10.032	50.648	2.050	9.525
	5	10.032	49.732	2.050	9.439
	6	10.032	49.892	2.050	9.561
20	0.5	8.932	36.499	2.171	9.469
	1	10.307	49.254	2.599	13.167
	2	10.906	62.122	2.761	16.182
	3	10.952	63.564	2.727	16.136
	4	10.954	61.278	2.717	15.401
	5	10.954	59.401	2.716	14.941
	6	10.954	58.582	2.716	14.816
40	0.5	9.378	40.940	2.500	12.547
	1	10.550	57.212	2.919	17.915
	2	11.208	75.703	3.169	23.557
	3	11.325	80.761	3.185	24.811
	4	11.338	79.358	3.166	24.157
	5	11.339	76.221	3.159	23.114
	6	11.339	73.996	3.158	22.446

Table 6.1 - MAX and SRSS values for different foundation sizes

Elements	u_{MAX} [mm]	u_{SRSS} [mm]	σ_{MAX} [MPa]	σ_{SRSS} [MPa]
Uniform 5m	10.032	52.316	2.051	9.850
Uniform 25m	9.548	47.291	2.187	10.927
Nonuniform	10.012	51.853	2.051	9.788

Table 6.2 - MAX and SRSS values for E_f=10GPa and different element sizes

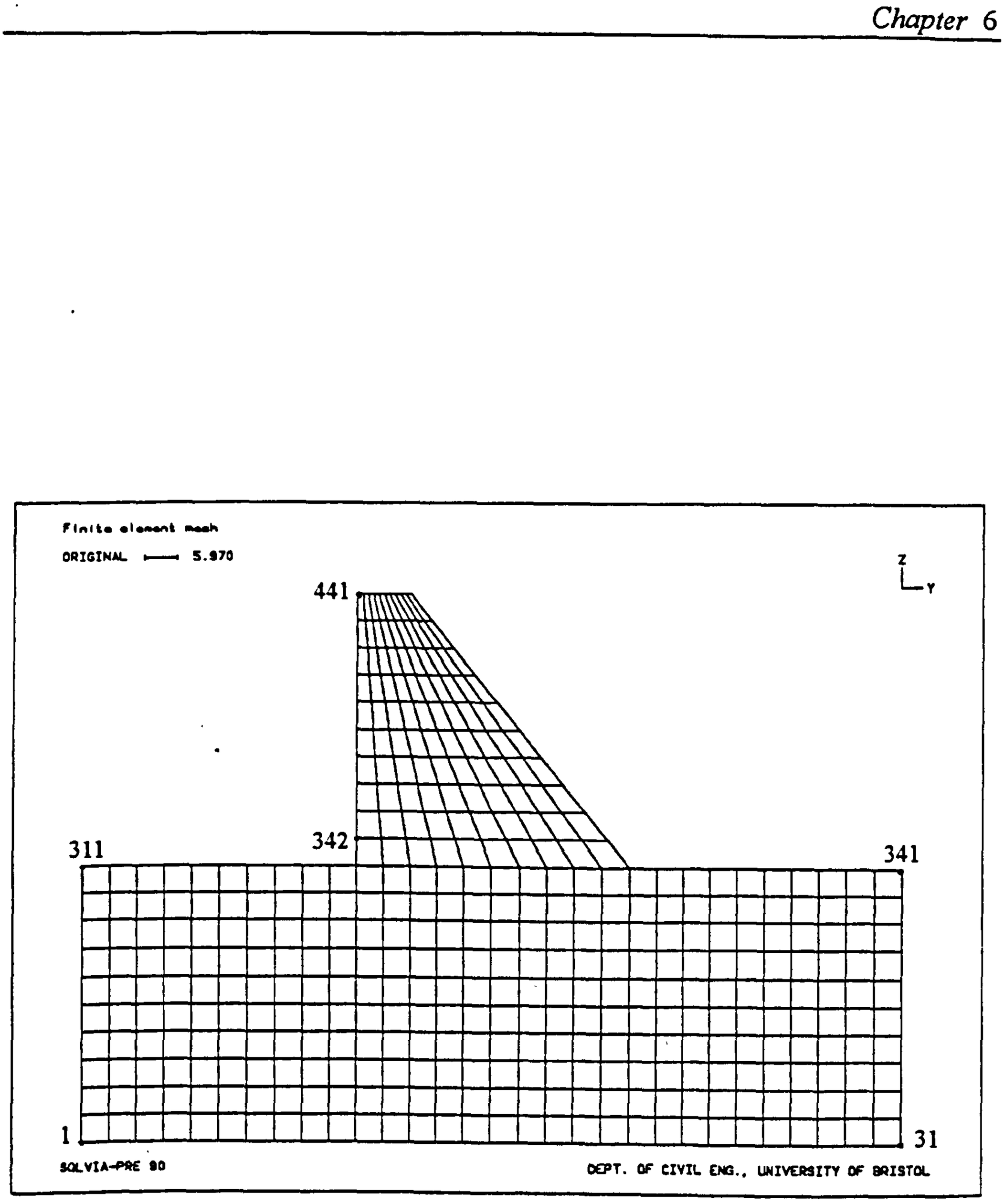

Figure 6.1 - Finite element mesh of the concrete gravity dam-foundation system

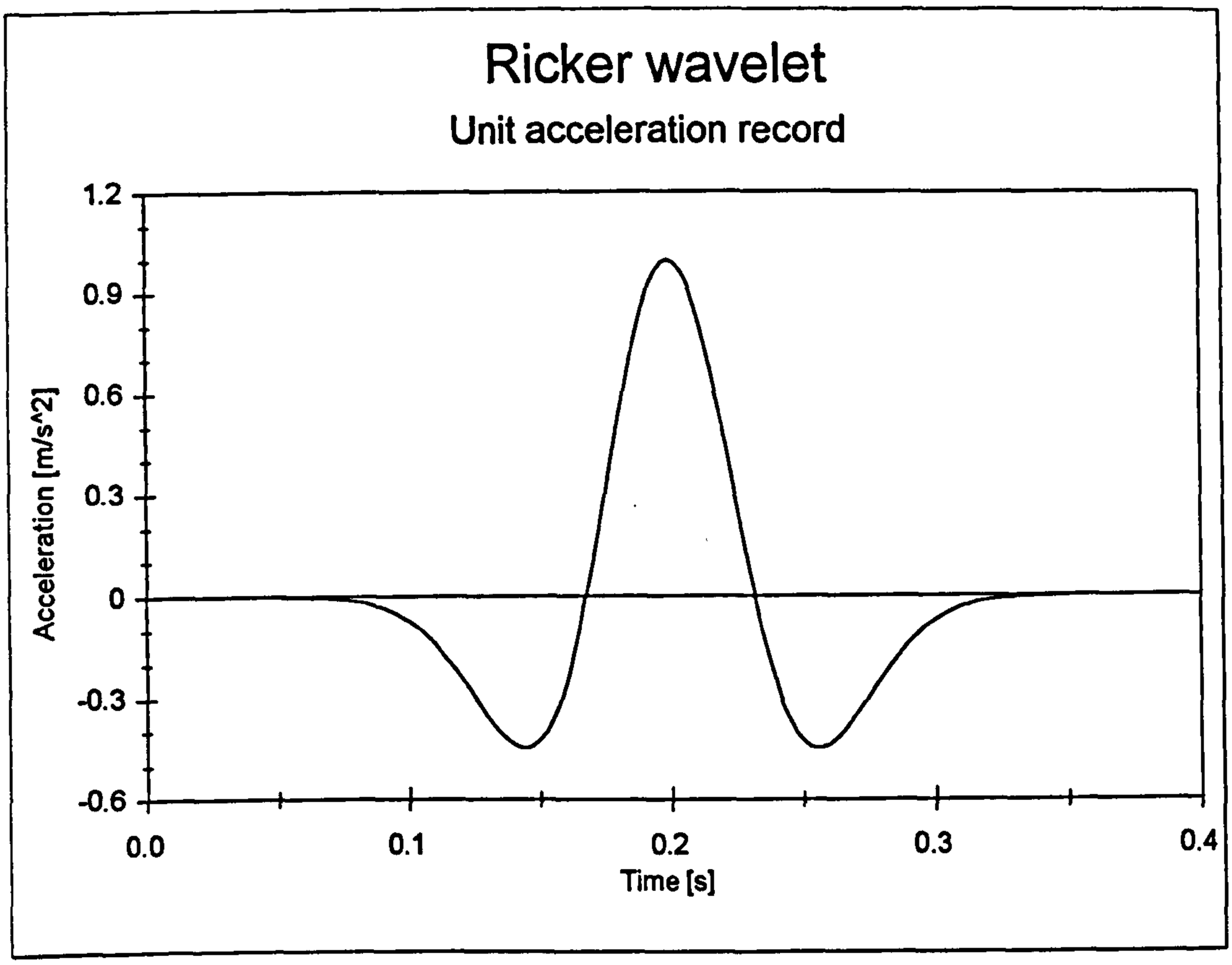

Figure 6.2a - Positive unit Ricker wavelet

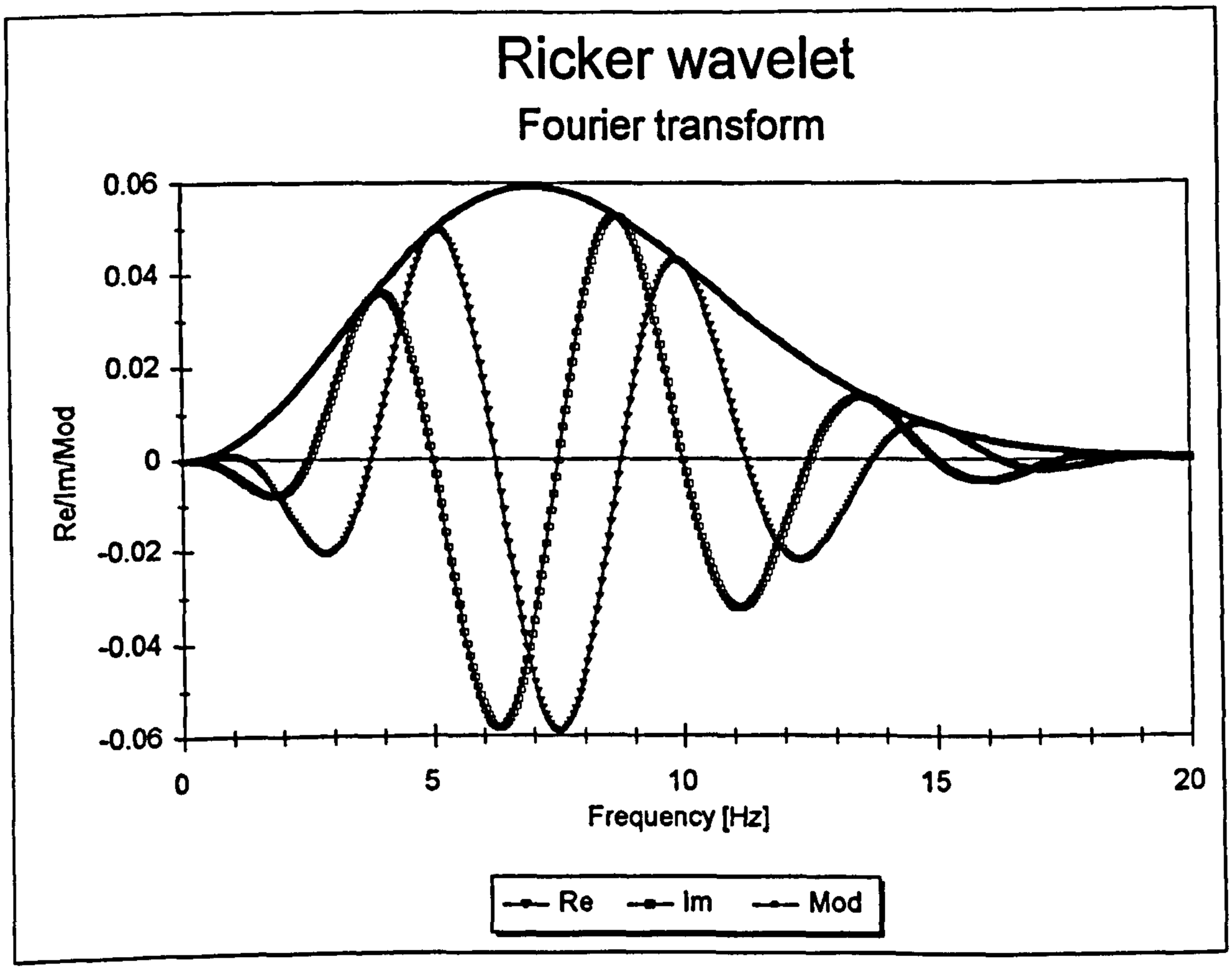

Figure 6.2b - Fourier transform of the Ricker wavelet

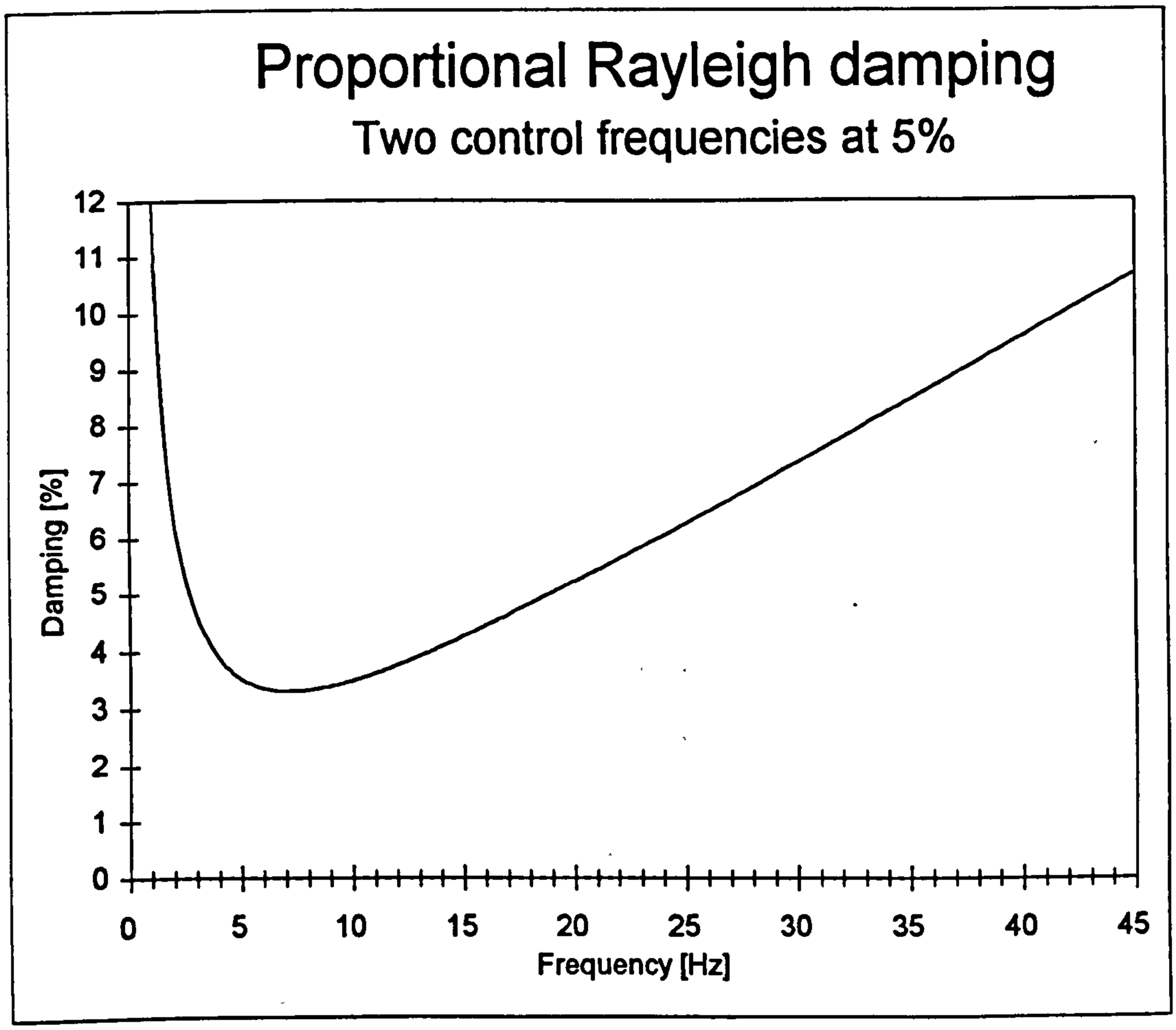

Figure 6.3 - Rayleigh damping of the concrete gravity dam-foundation system

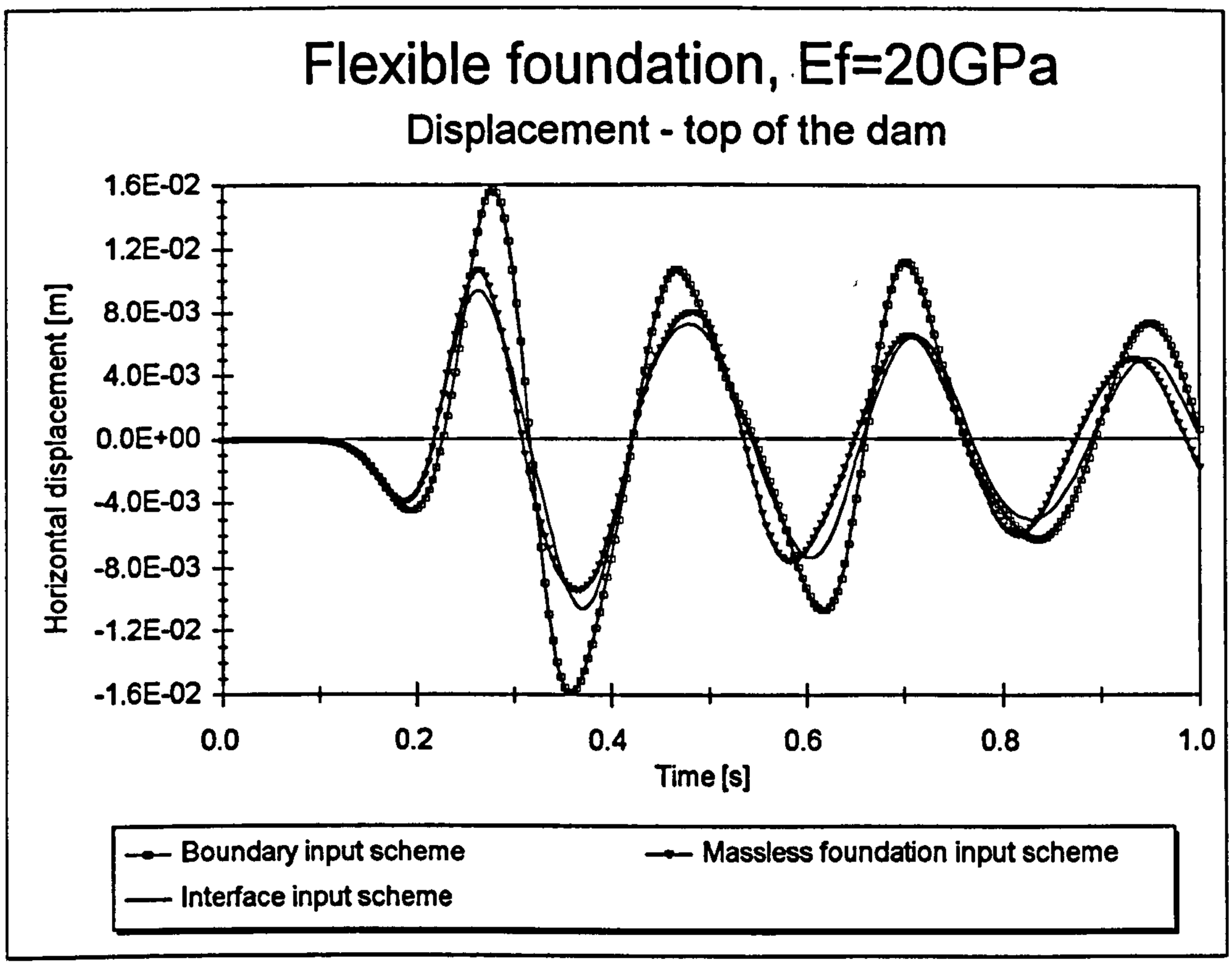

Figure 6.4a - Displacement of the top of the dam (rock layer, E_f=20 GPa)

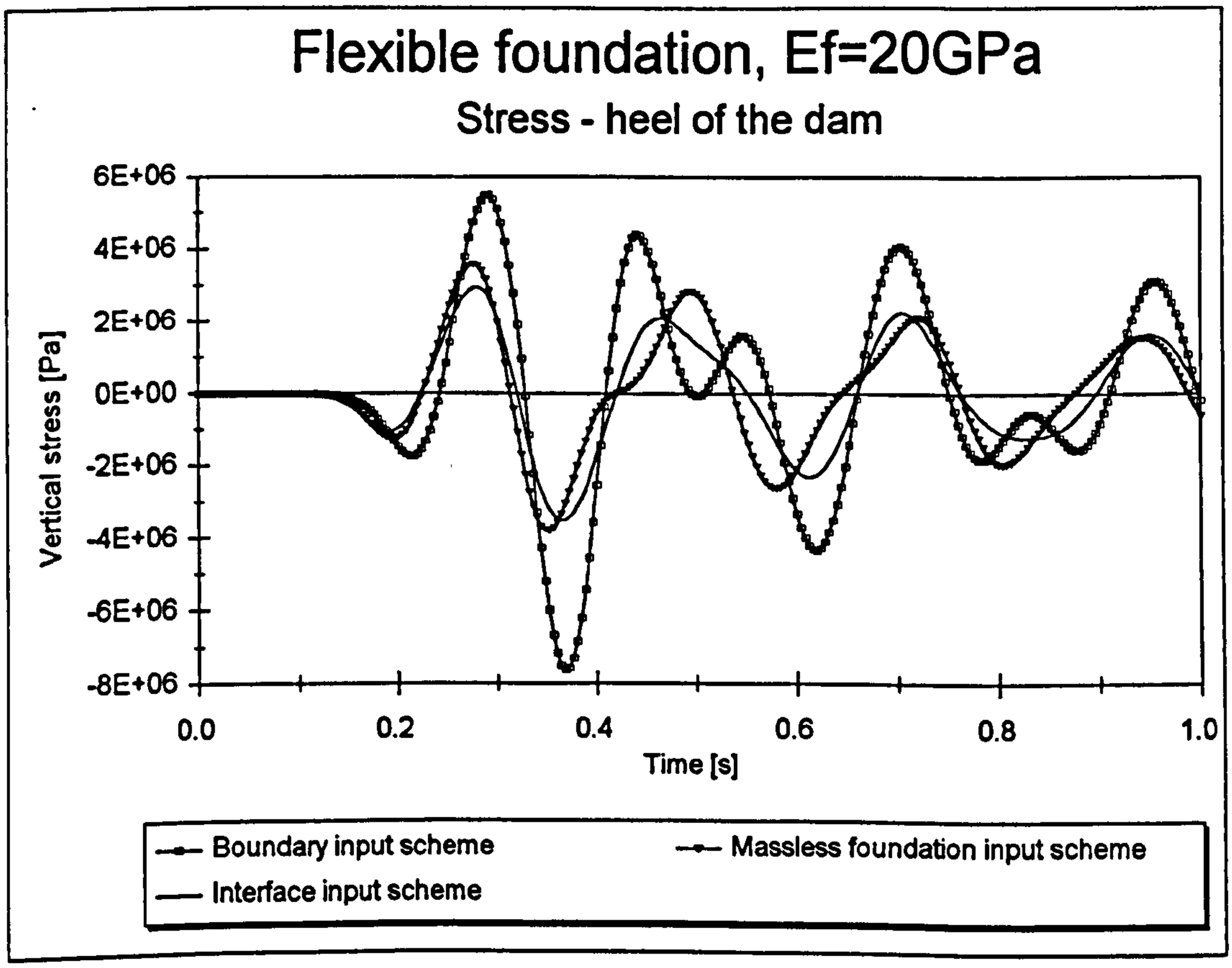

Figure 6.4b - Stress at the heel of the dam (rock layer, E_f=20 GPa)

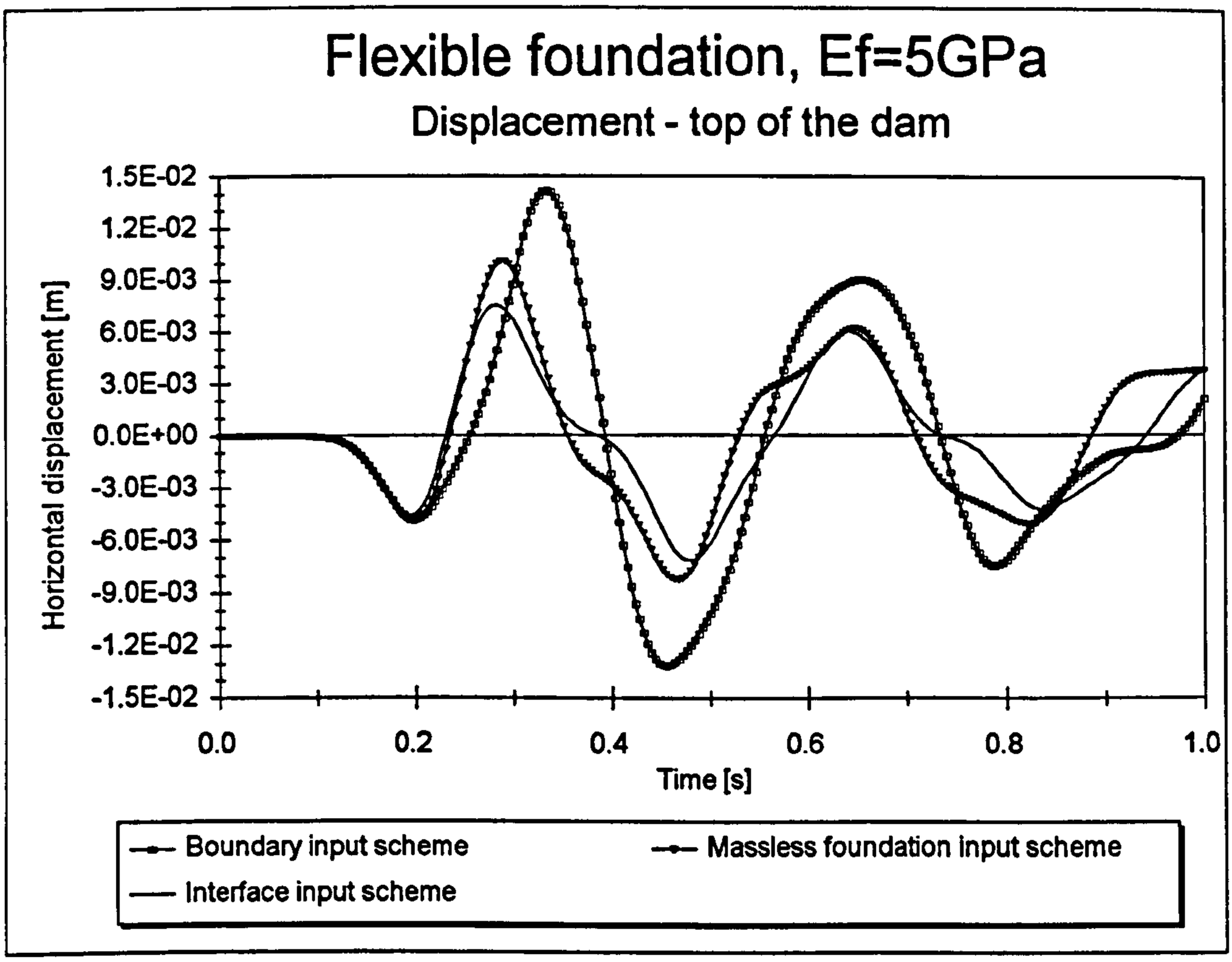

Figure 6.5a - Displacement of the top of the dam (rock layer, E_f=5 GPa)

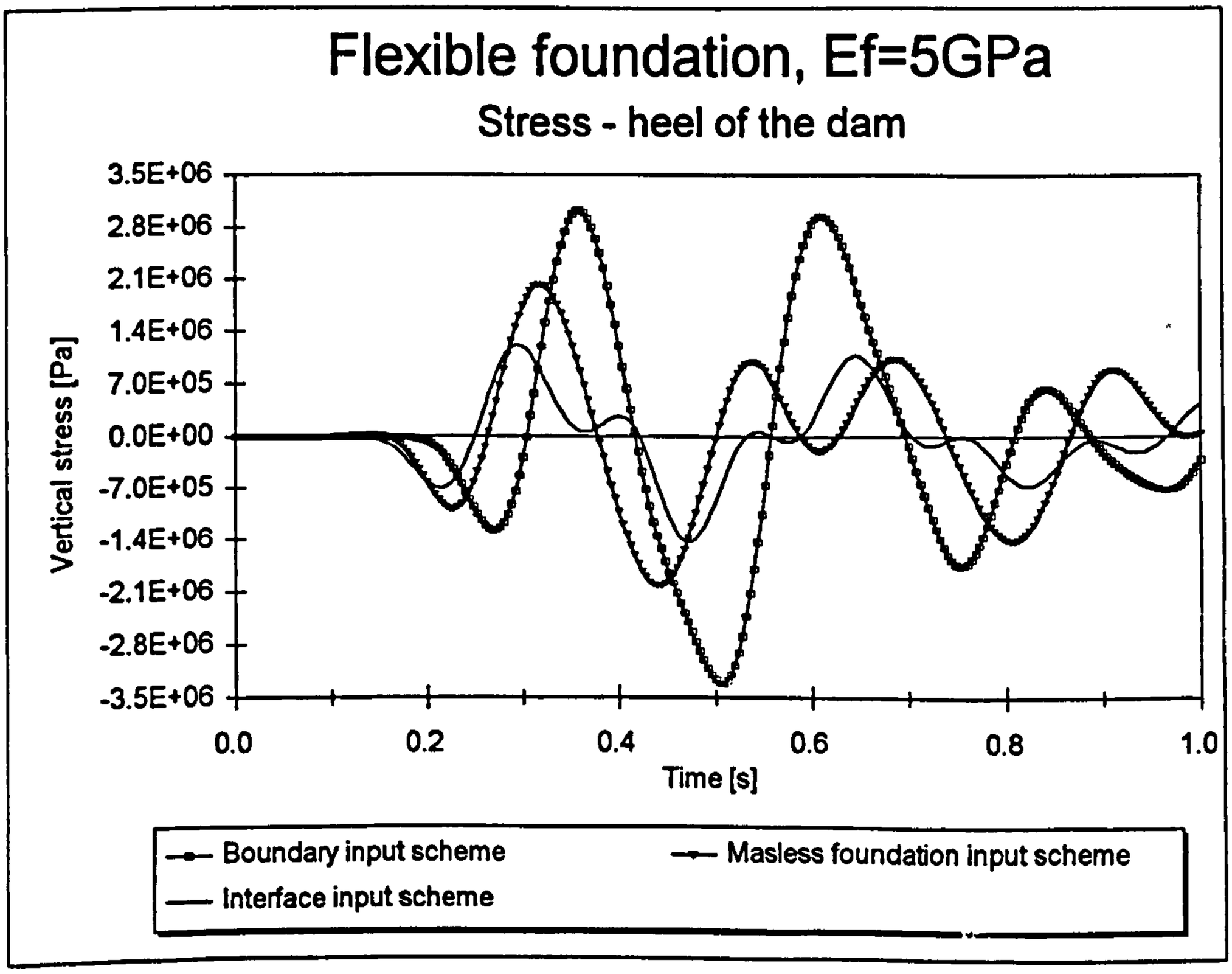

Figure 6.5b - Stress at the heel of the dam (rock layer, E_f=5 GPa)

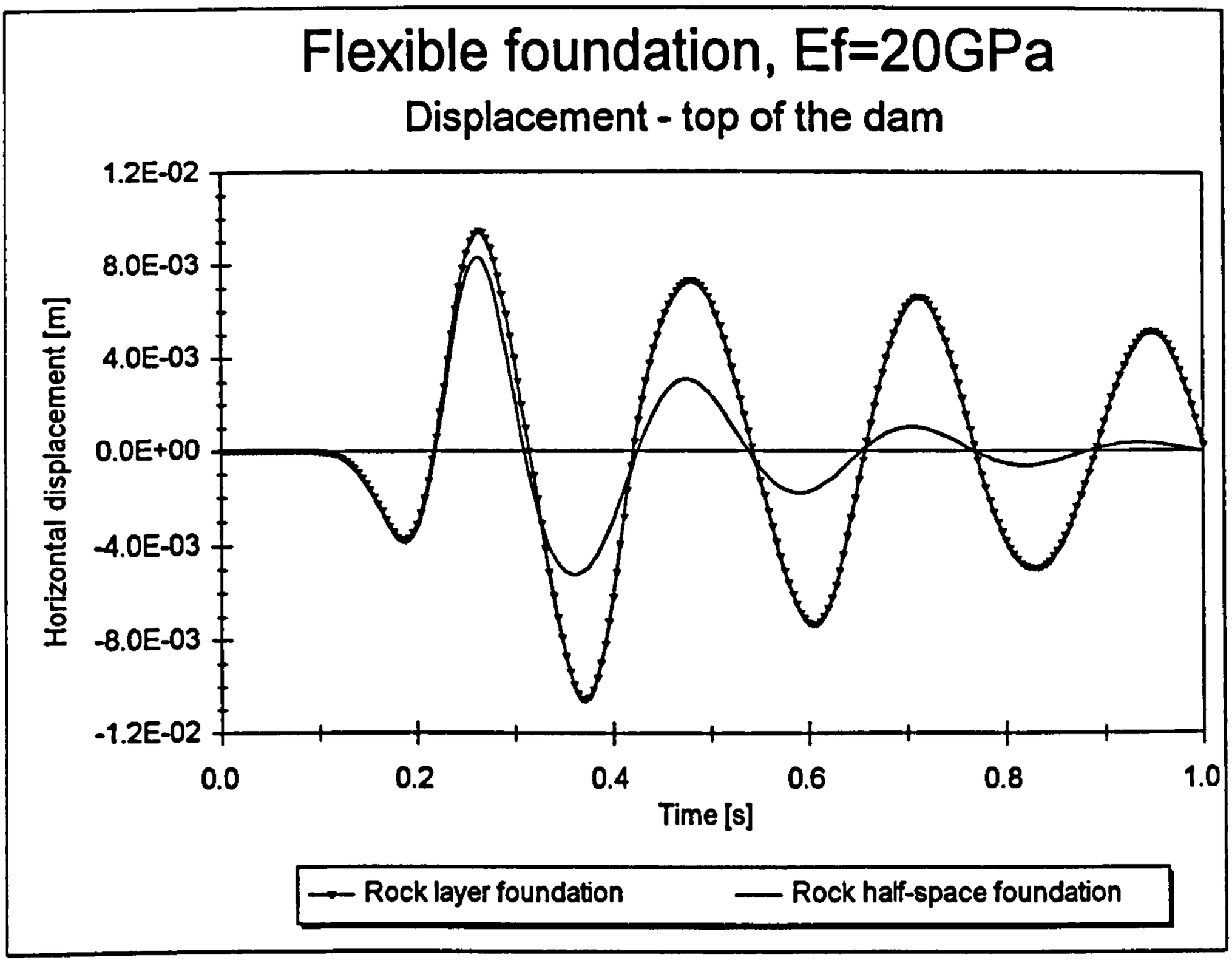

Figure 6.6a - Displacement of the top of the dam (E_f=20 GPa)

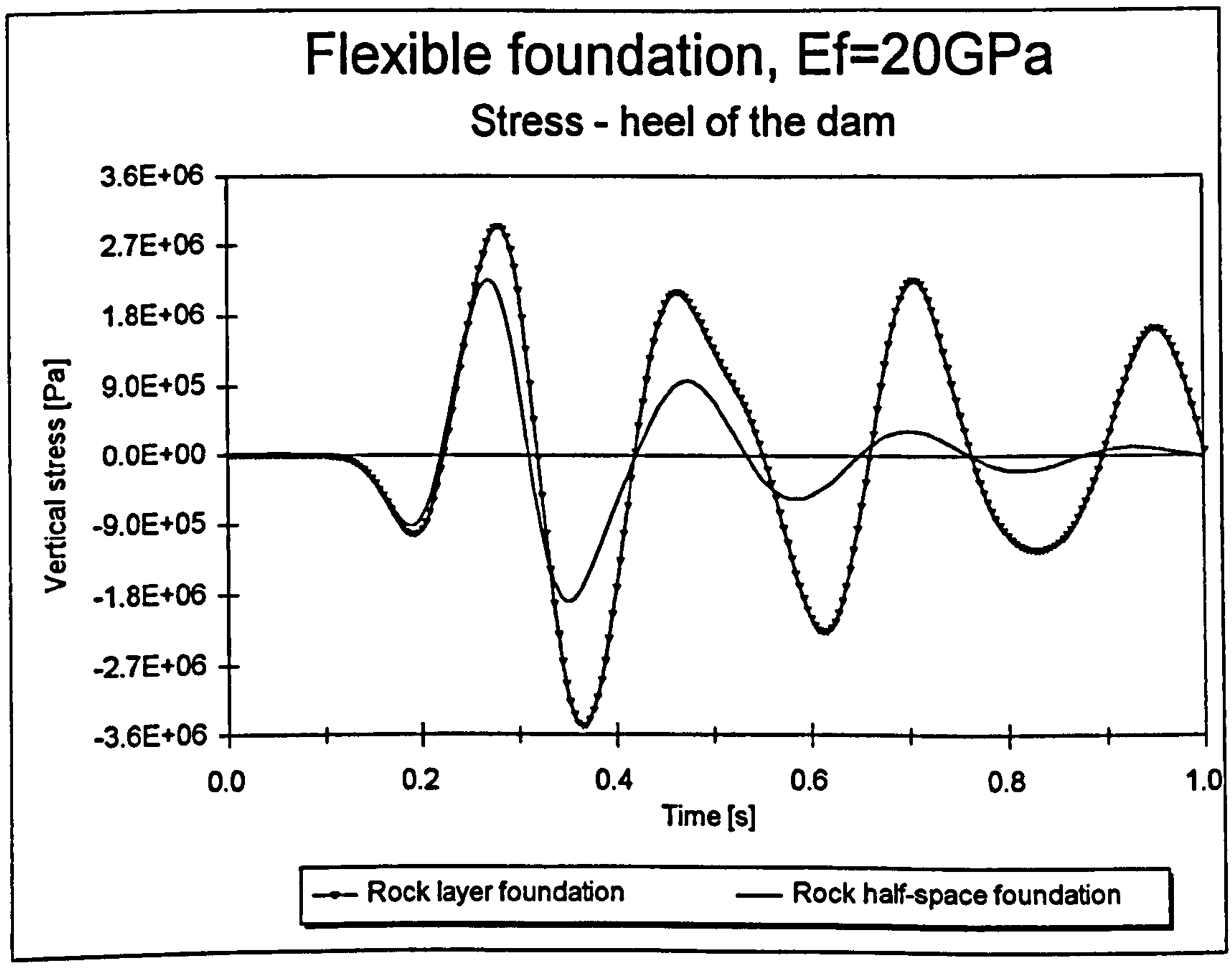

Figure 6.6b - Stress at the heel of the dam (E_f=20 GPa)

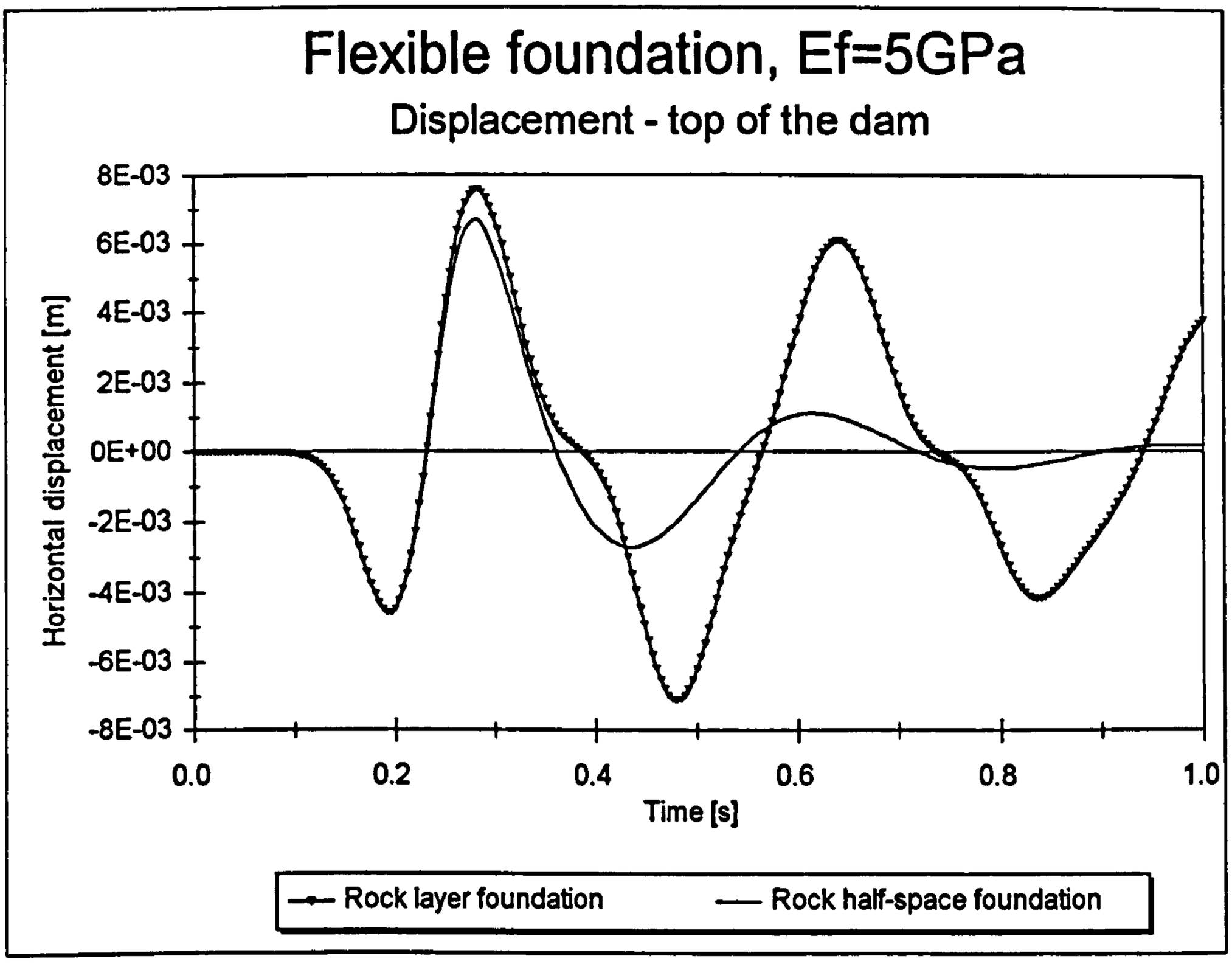

Figure 6.7a - Displacement of the top of the dam (E_f=5 GPa)

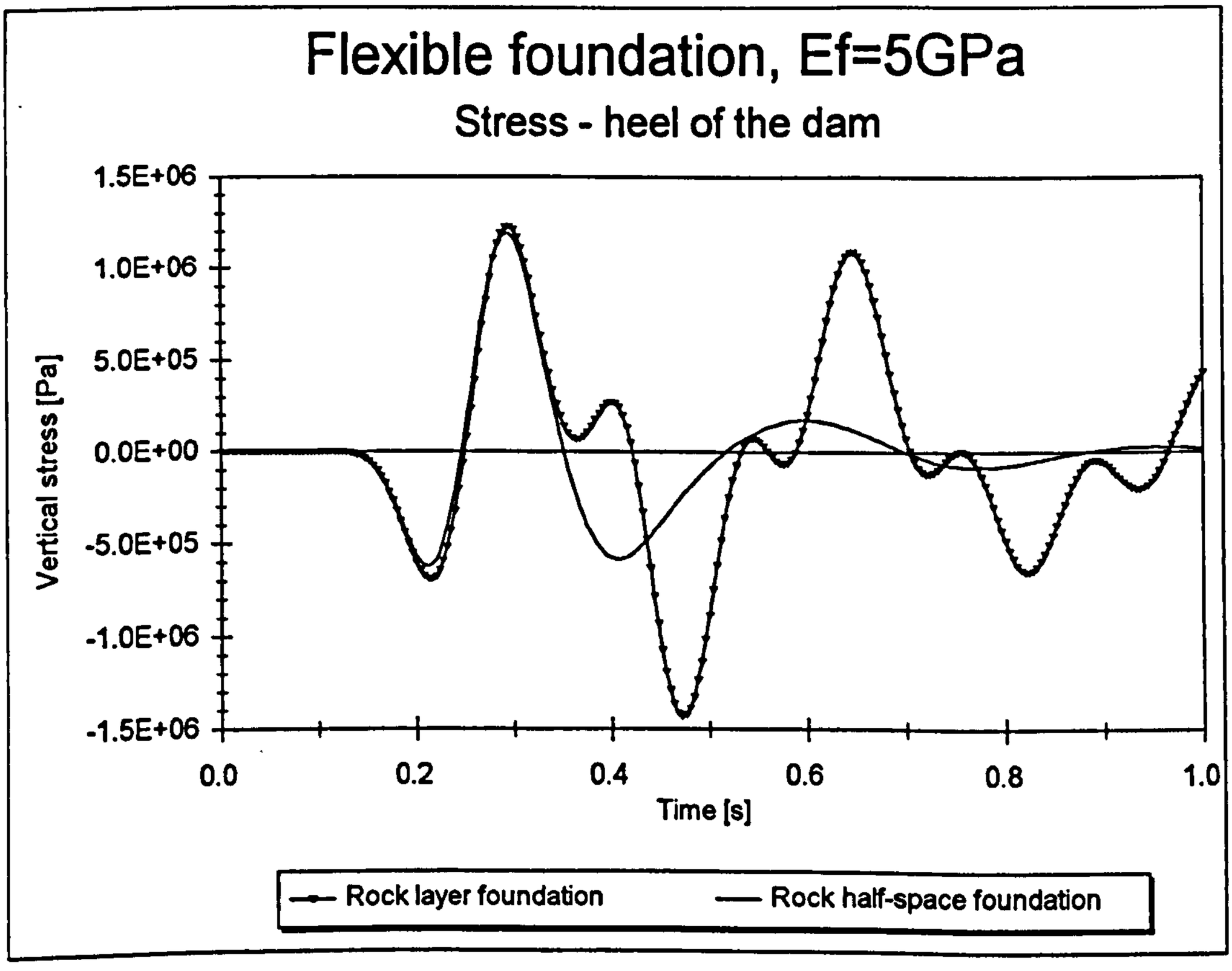

Figure 6.7b - Stress at the heel of the dam (E_f=5 GPa)

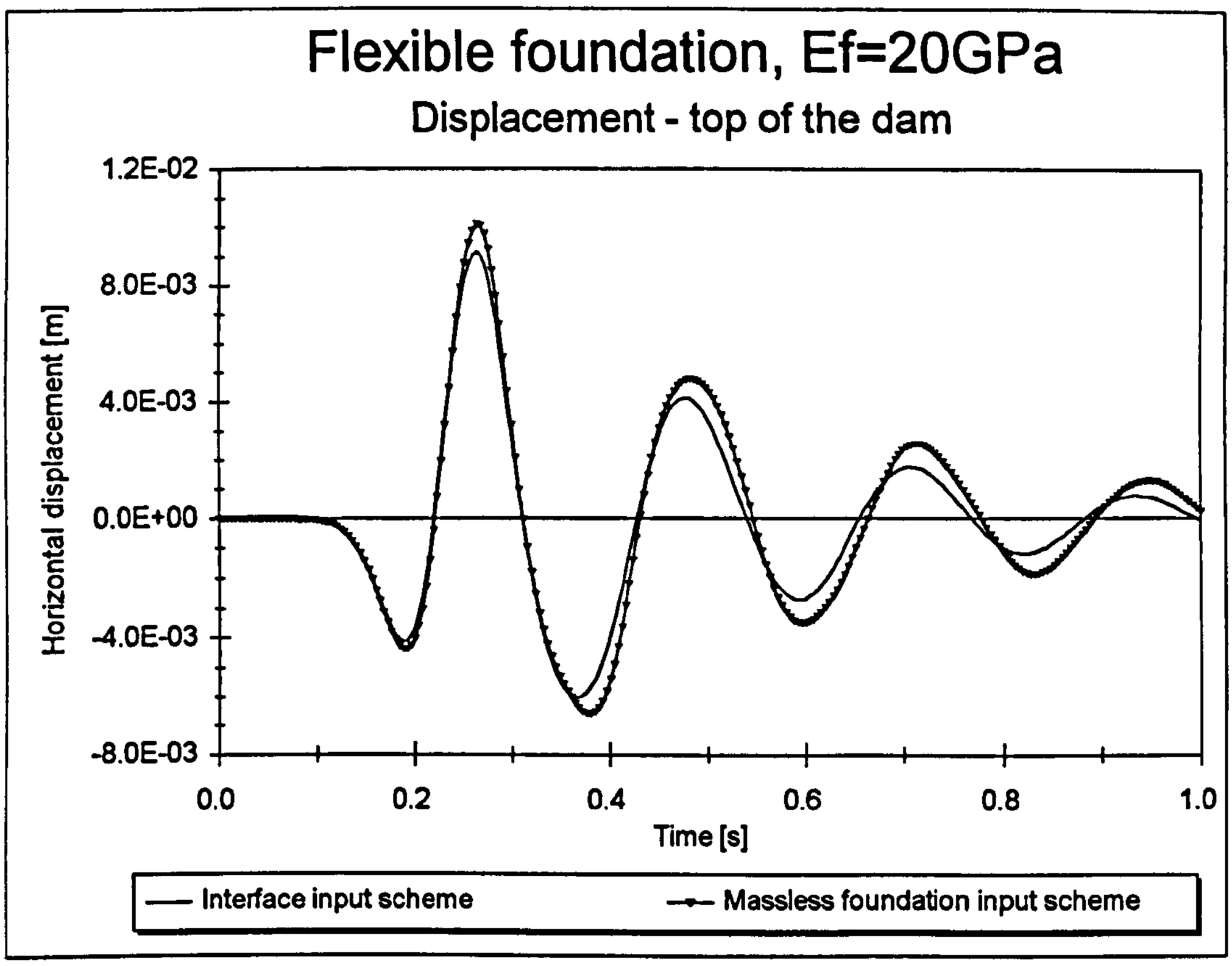

Figure 6.8a - Displacement of the top of the dam (rock half-space, E_f=20 GPa)

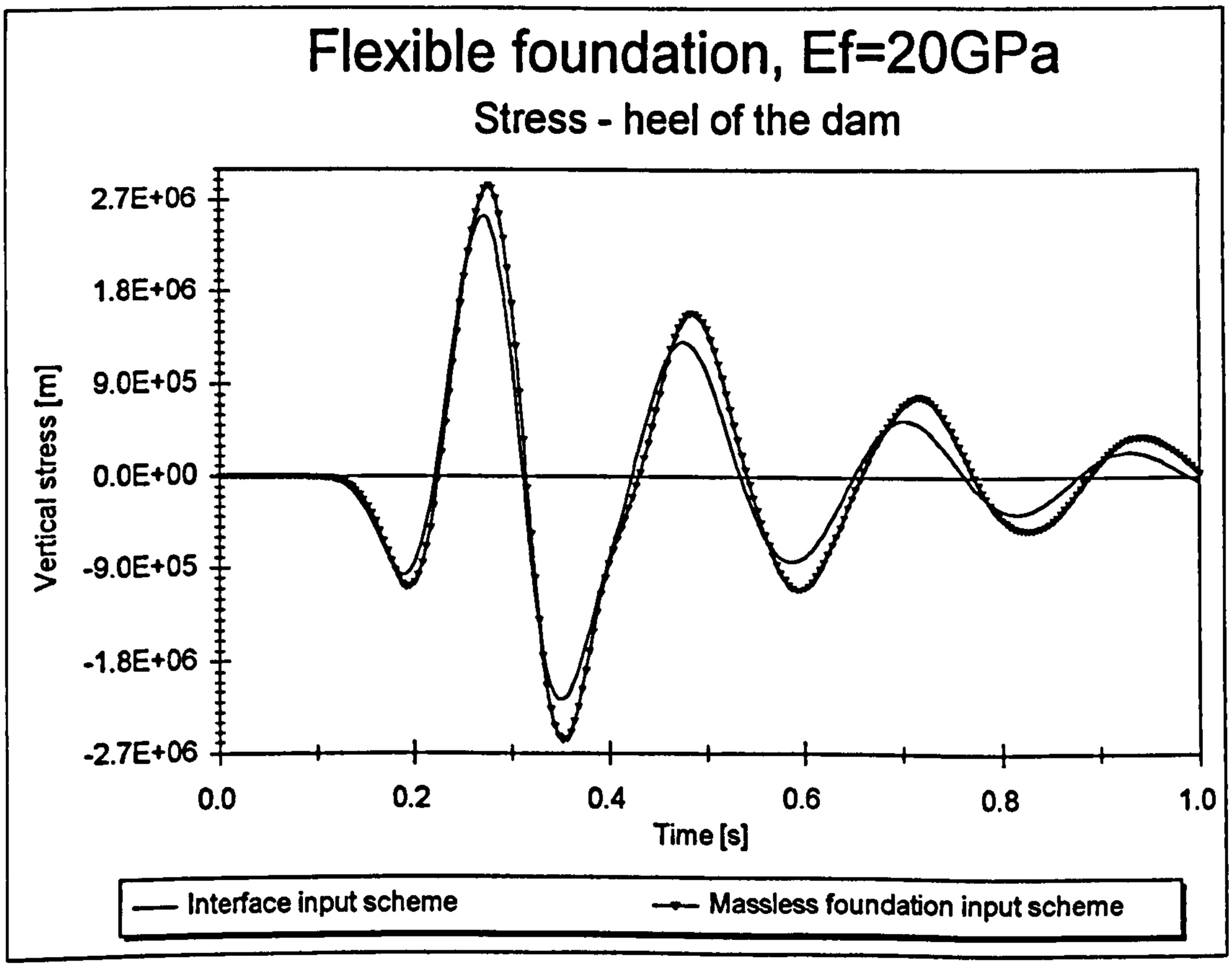

Figure 6.8b - Stress at the heel of the dam (rock half-space, E_f=20 GPa)

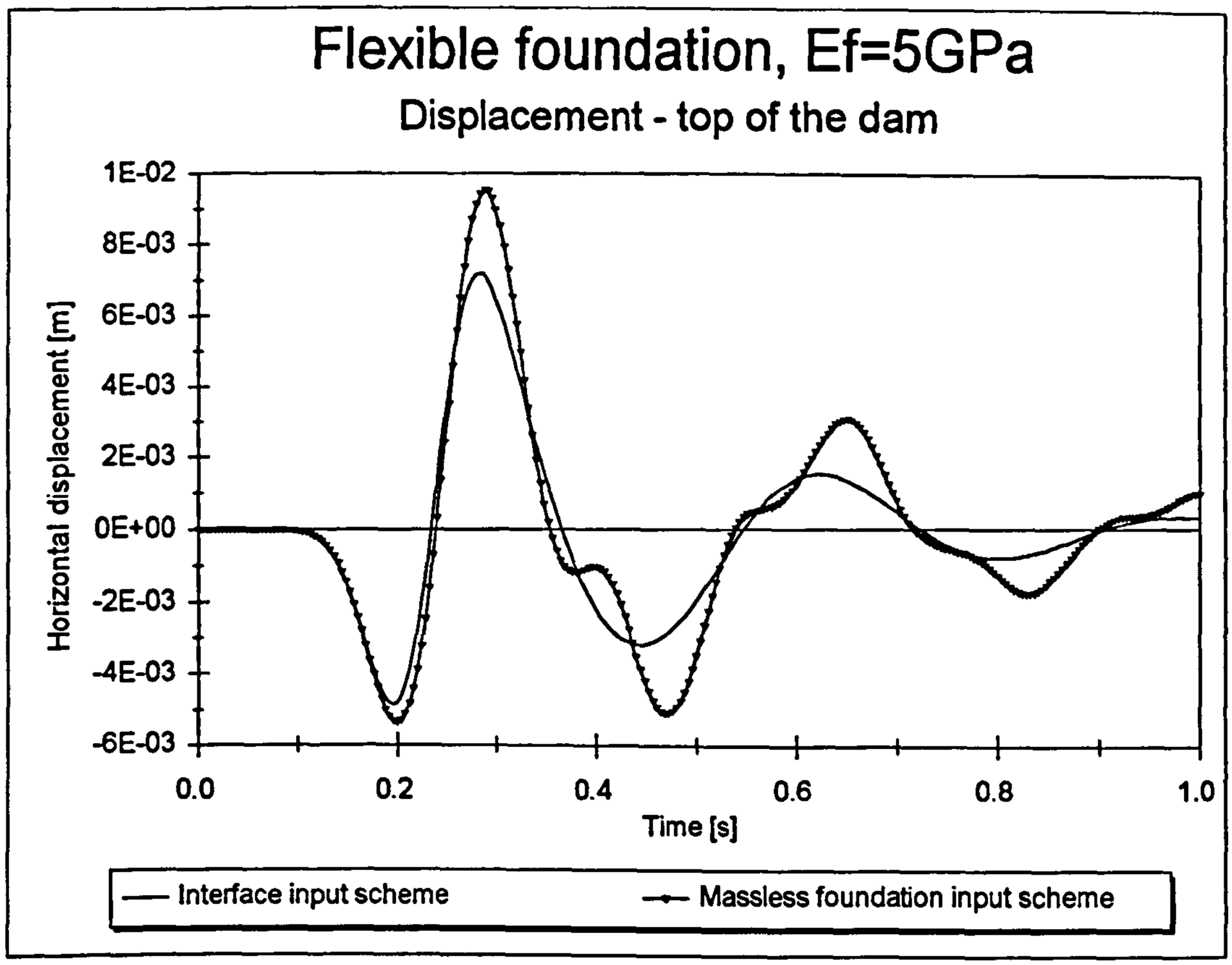

Figure 6.9a - Displacement of the top of the dam (rock half-space, E_f=5 GPa)

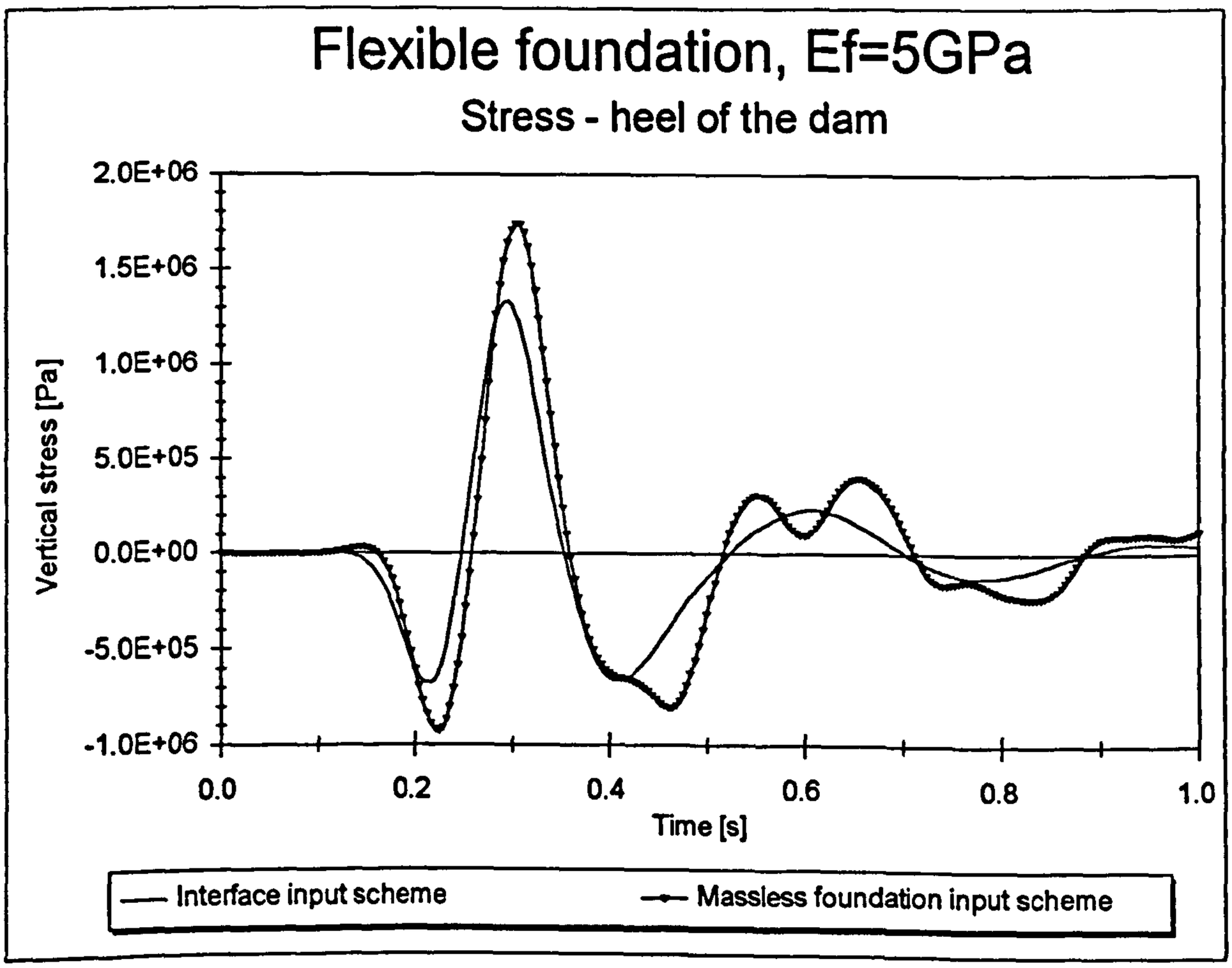

Figure 6.9b - Stress at the heel of the dam (rock half-space, E_f=5 GPa)

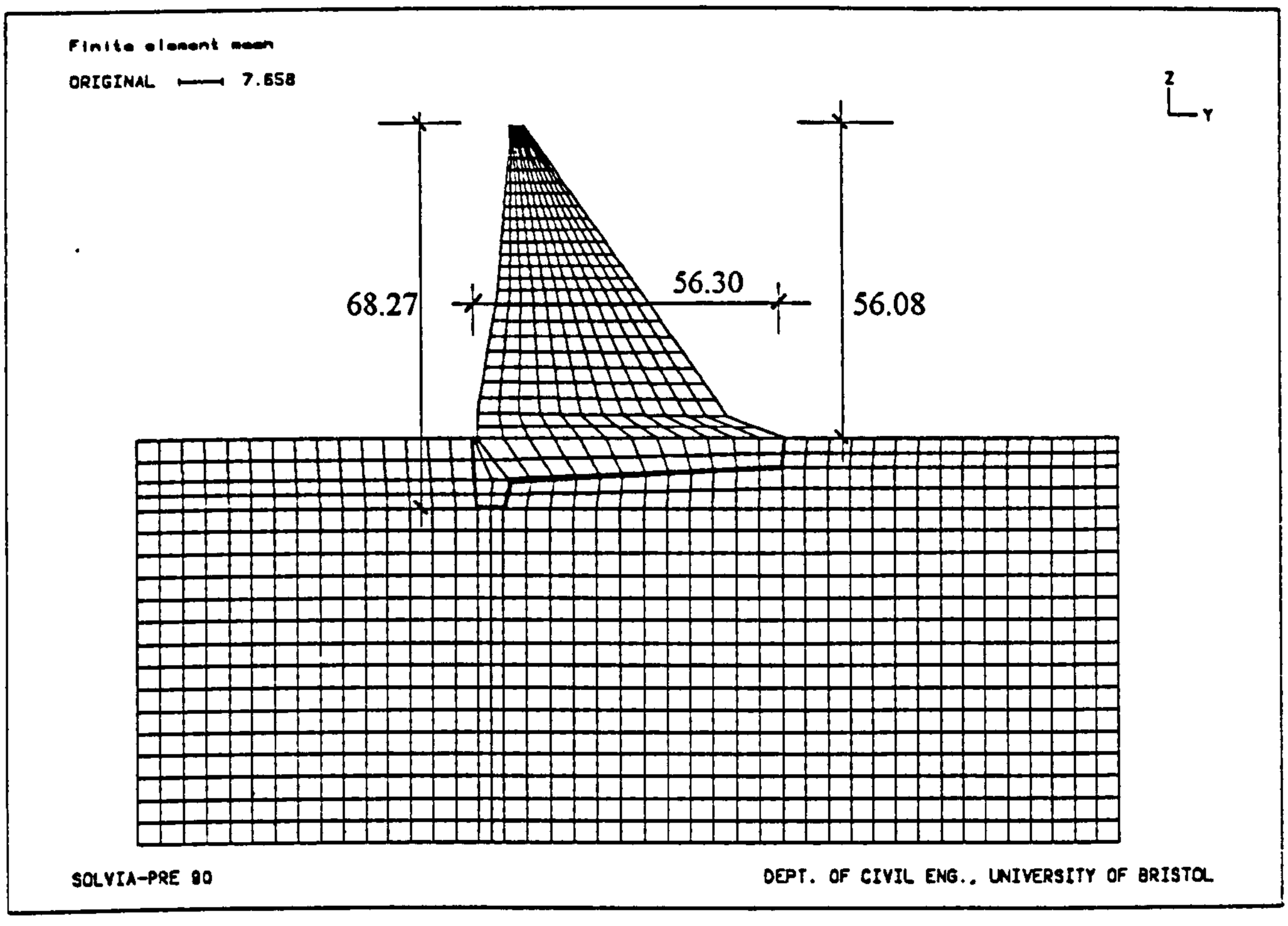

Figure 6.10 - Finite element mesh of the realistic dam-foundation system

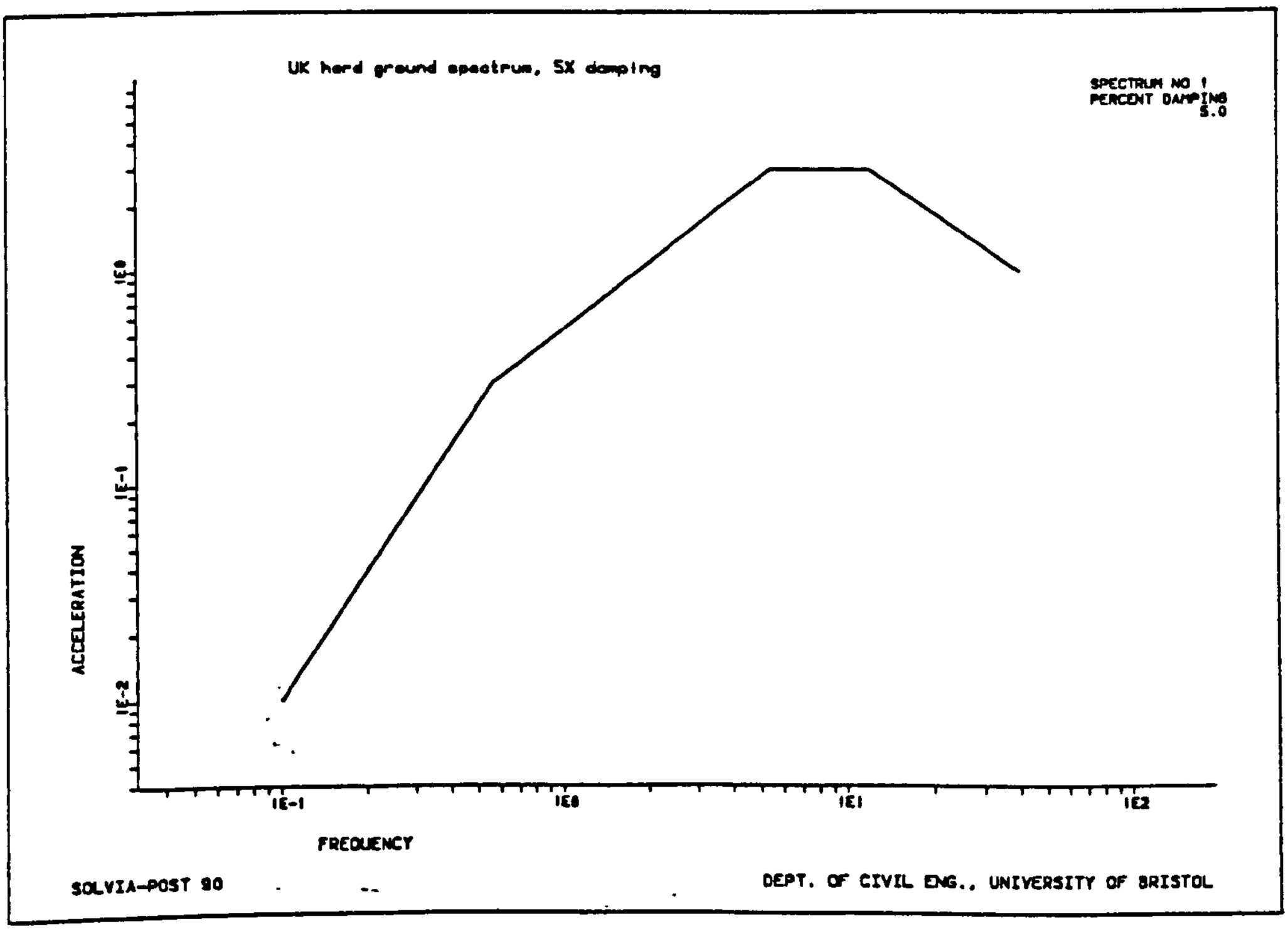

Figure 6.11 - UK hard ground spectrum with 5% damping

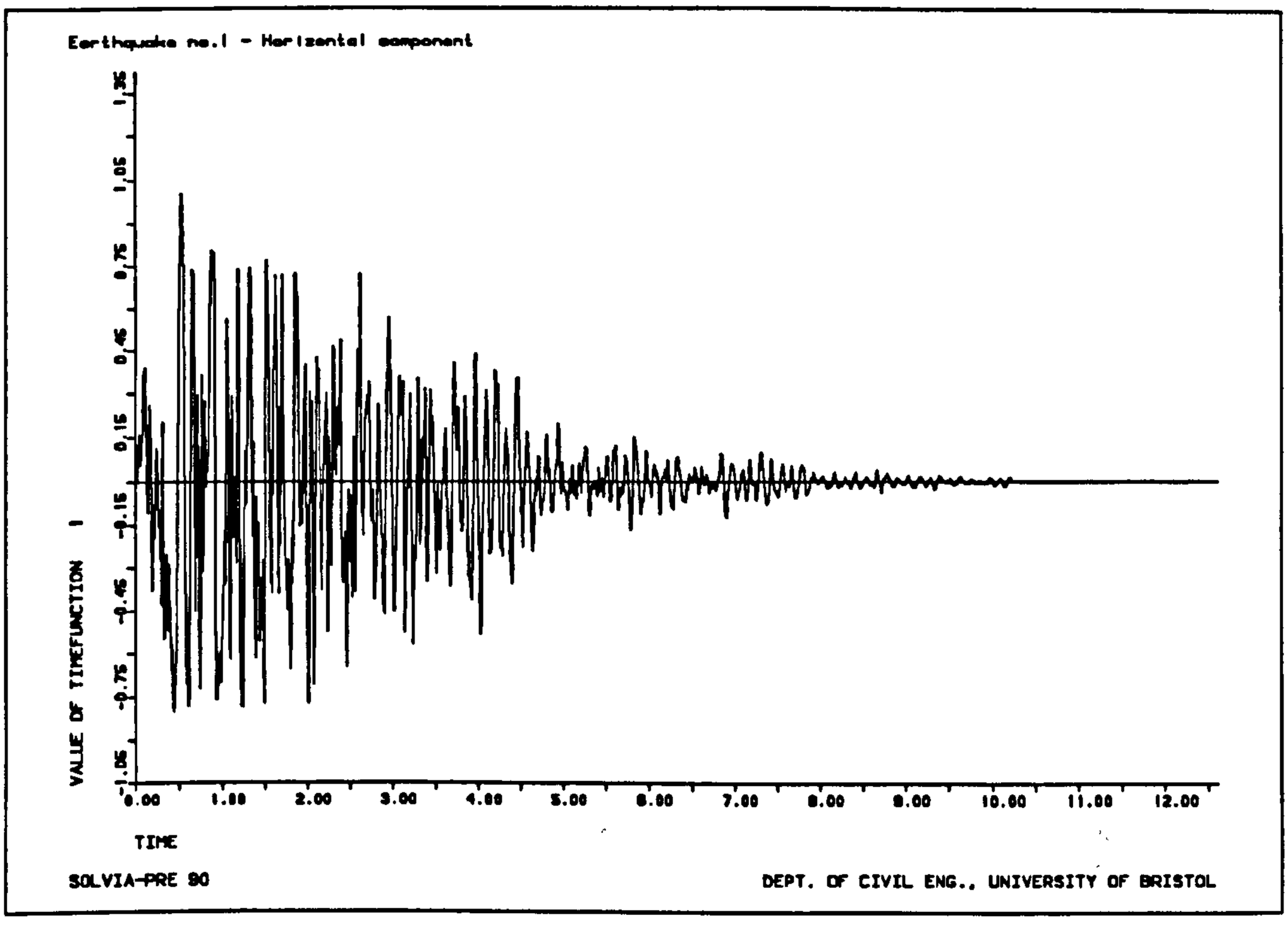

Figure 6.12a - Spectrum compatible unit horizontal acceleration time history

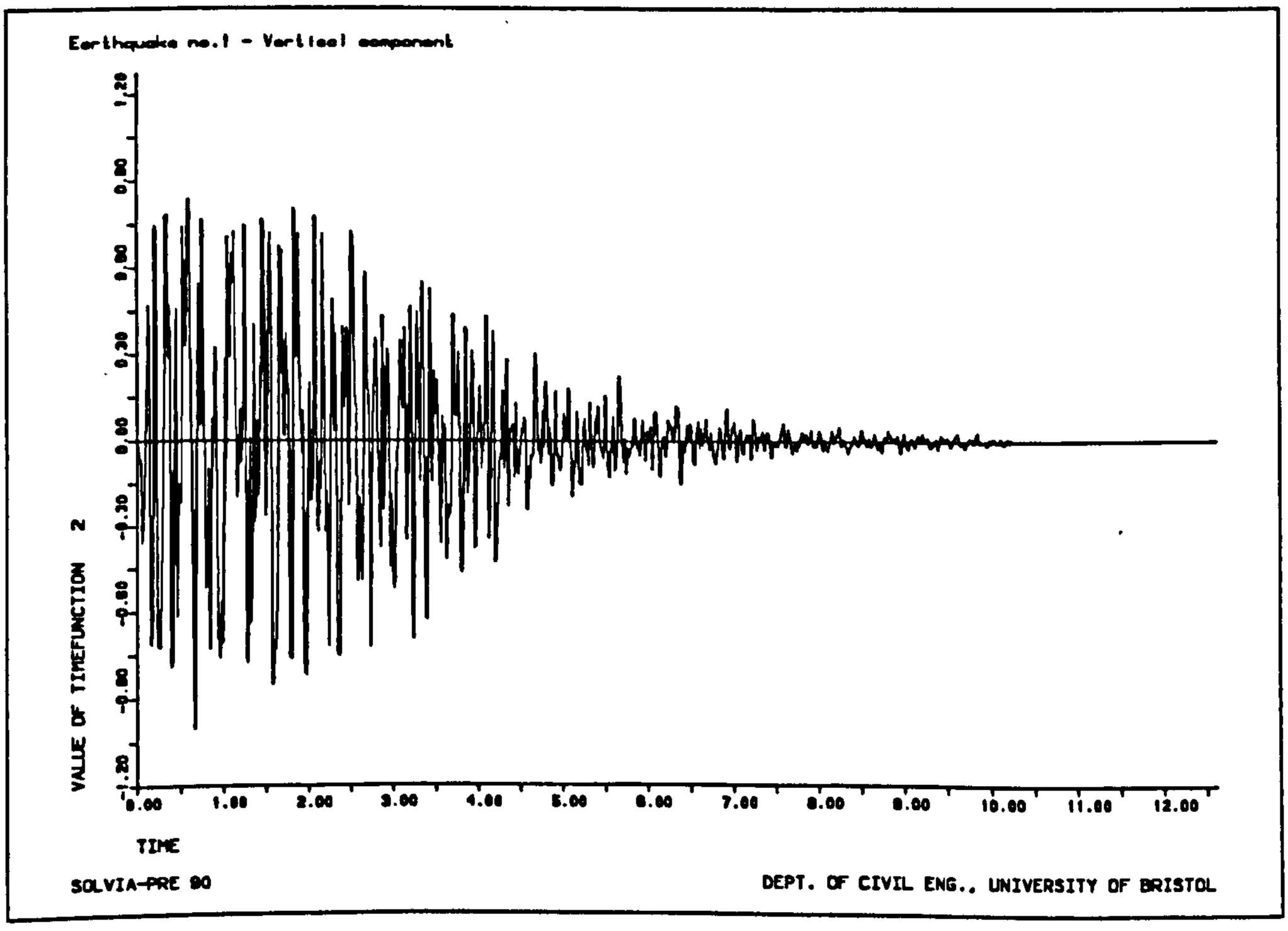

Figure 6.12b - Spectrum compatible unit vertical acceleration time history

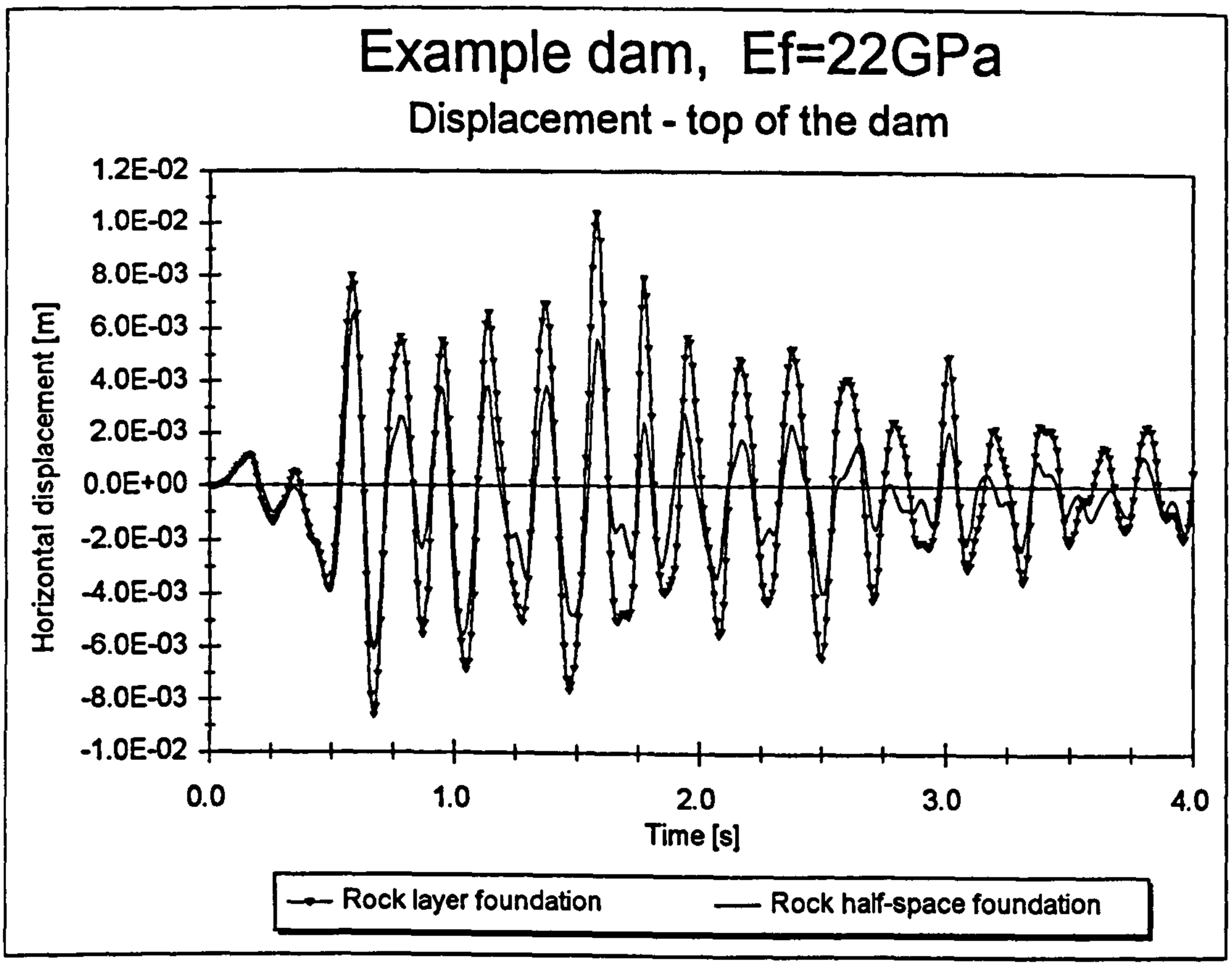

Figure 6.13a - Displacement of the top of the dam (E_f=22 GPa)

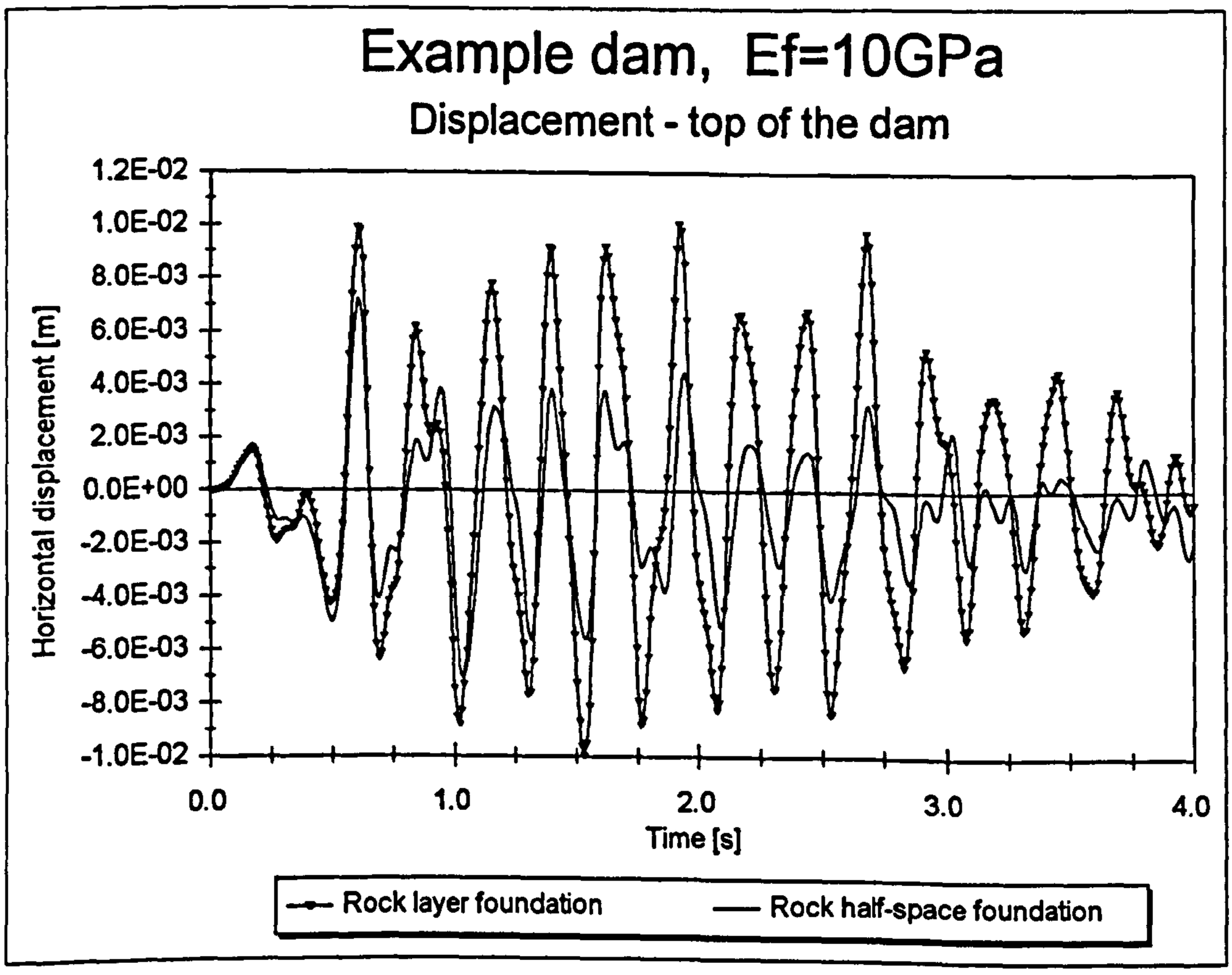

Figure 6.13b - Displacement of the top of the dam (E_f=10 GPa)

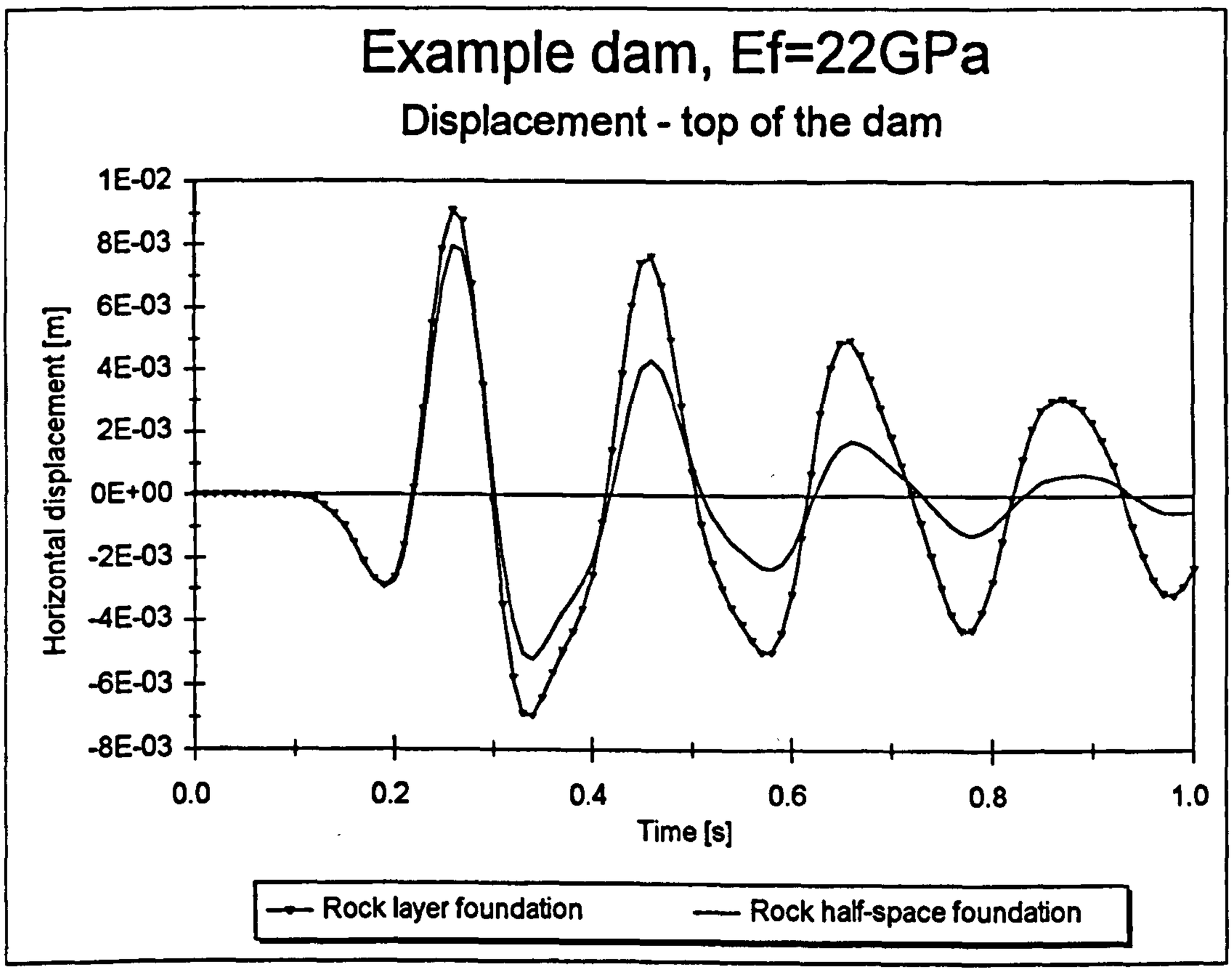

Figure 6.14a - Dam displacement (full Rayleigh damping, E_f=22 GPa)

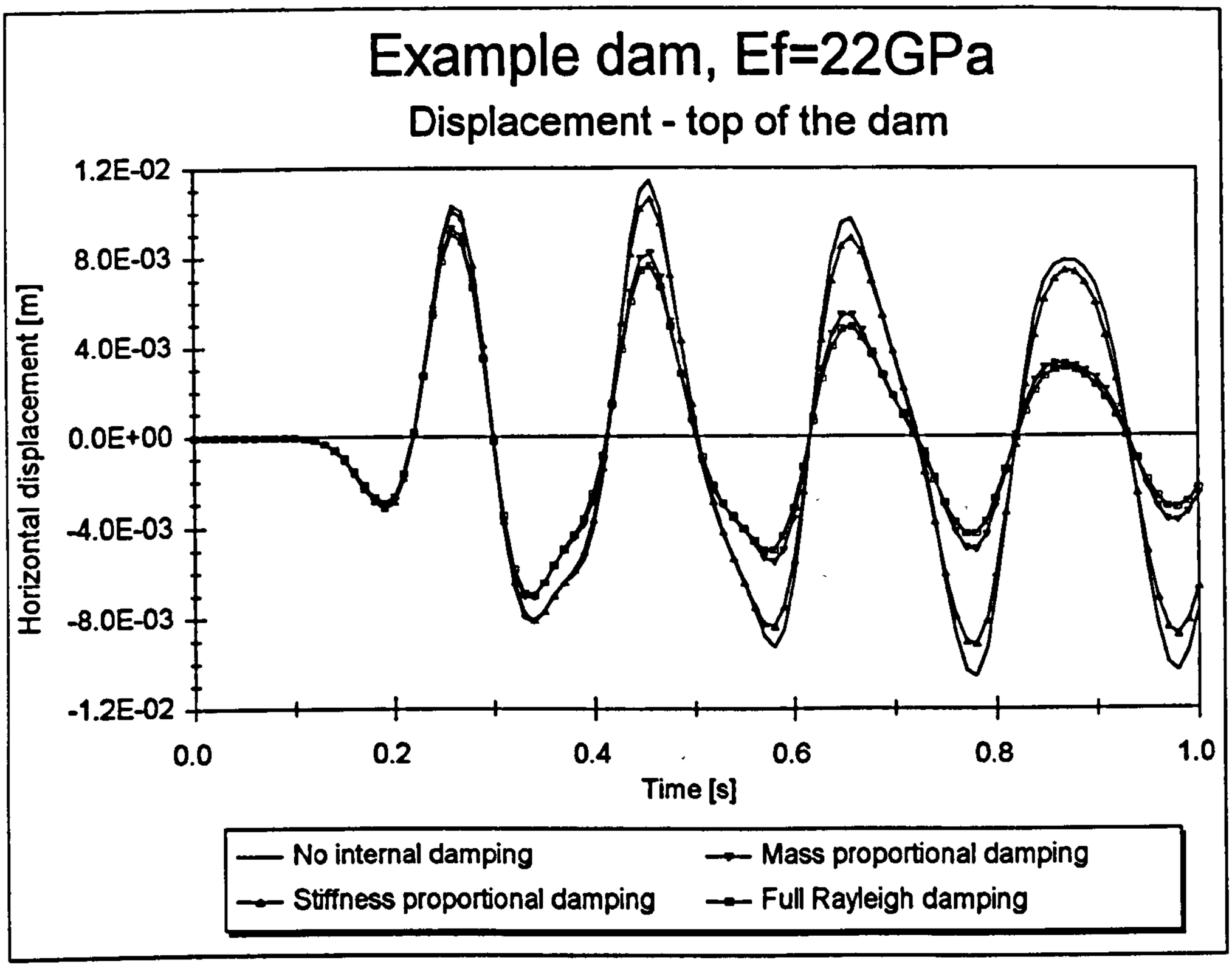

Figure 6.14b - Dam displacement (no radiation damping, E_f=22 GPa)

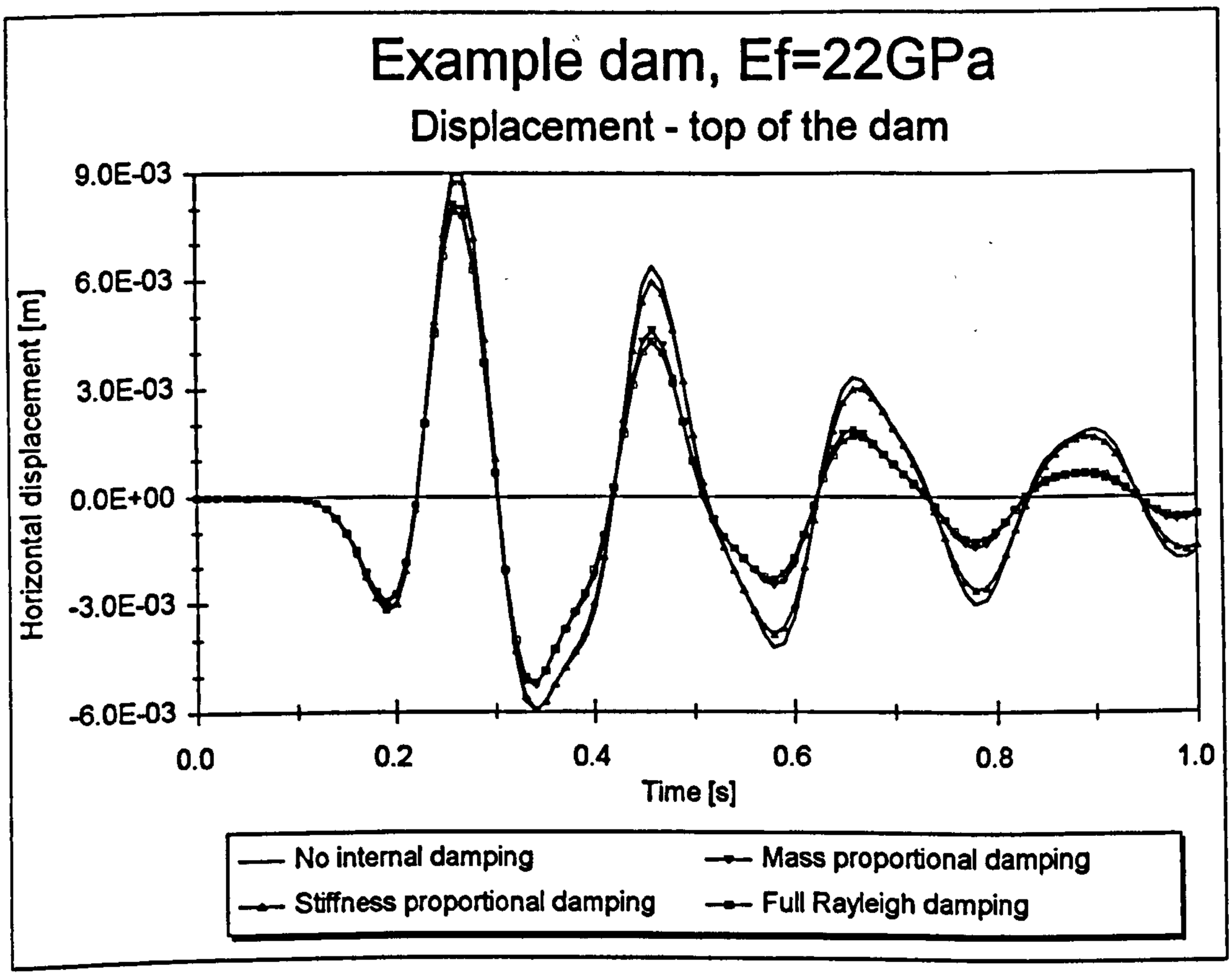

Figure 6.14c - Dam displacement (with radiation damping, E_f=22 GPa)

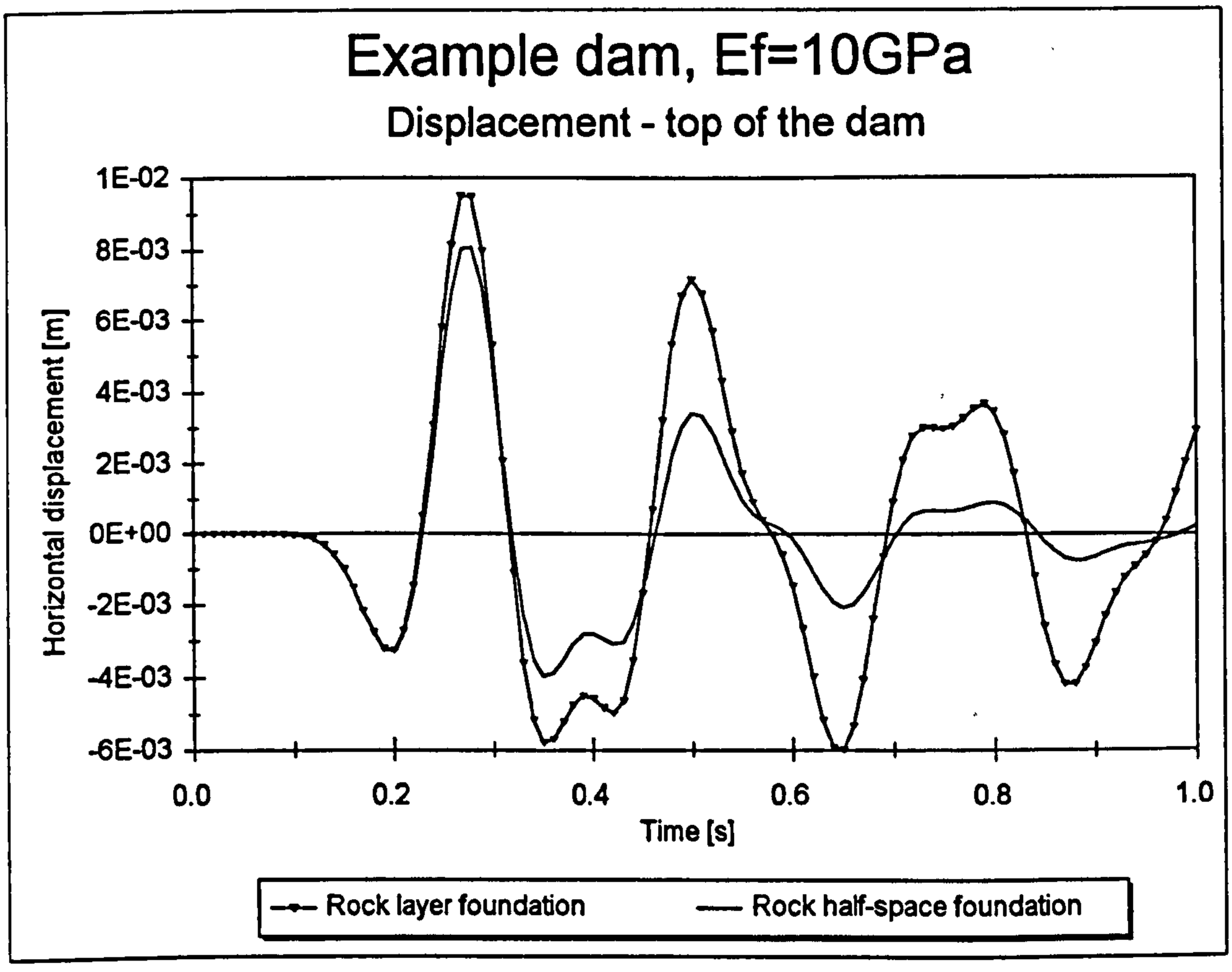

Figure 6.15a - Dam displacement (full Rayleigh damping, E_f=10 GPa)

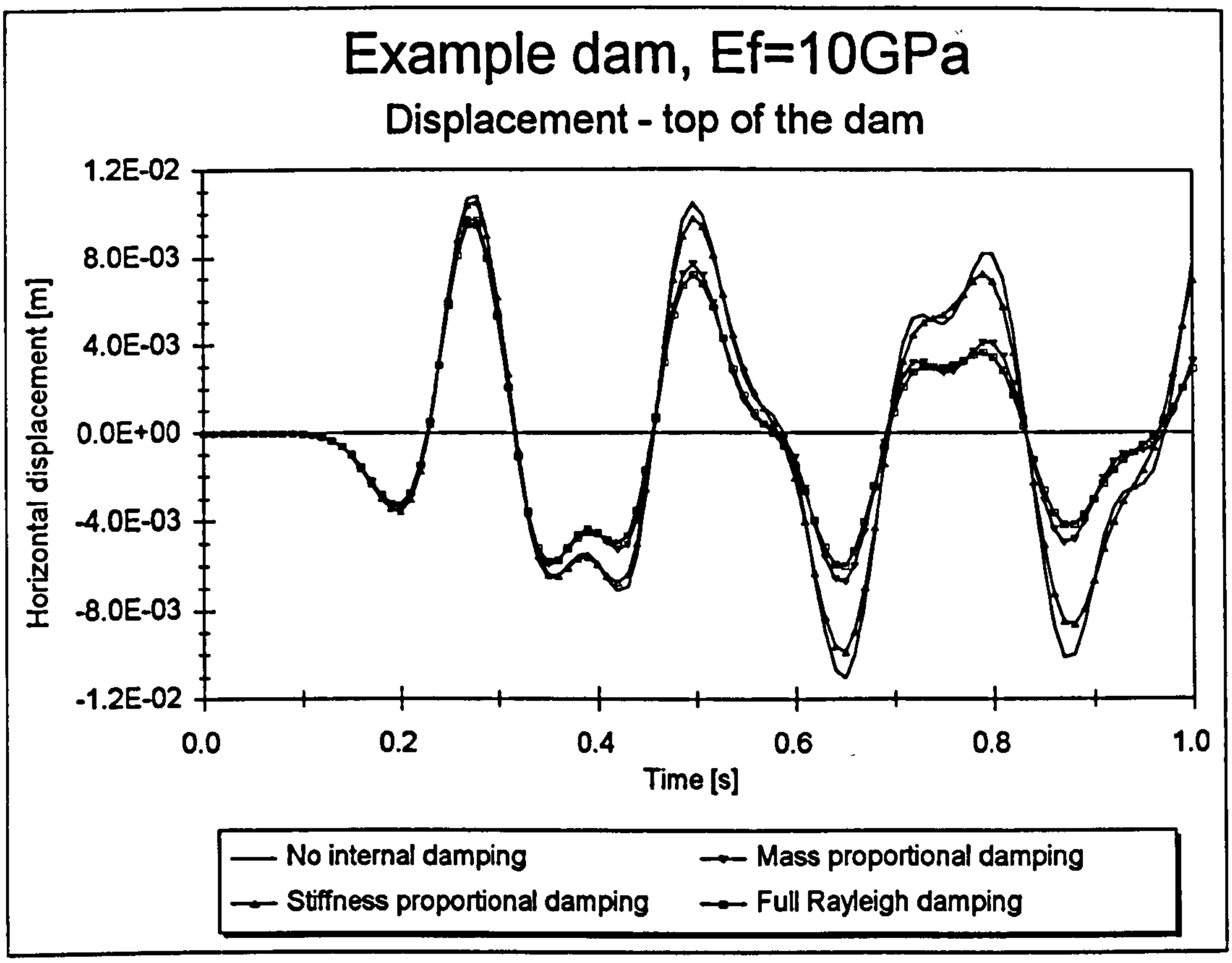

Figure 6.15b - Dam displacement (no radiation damping, E_f=10 GPa)

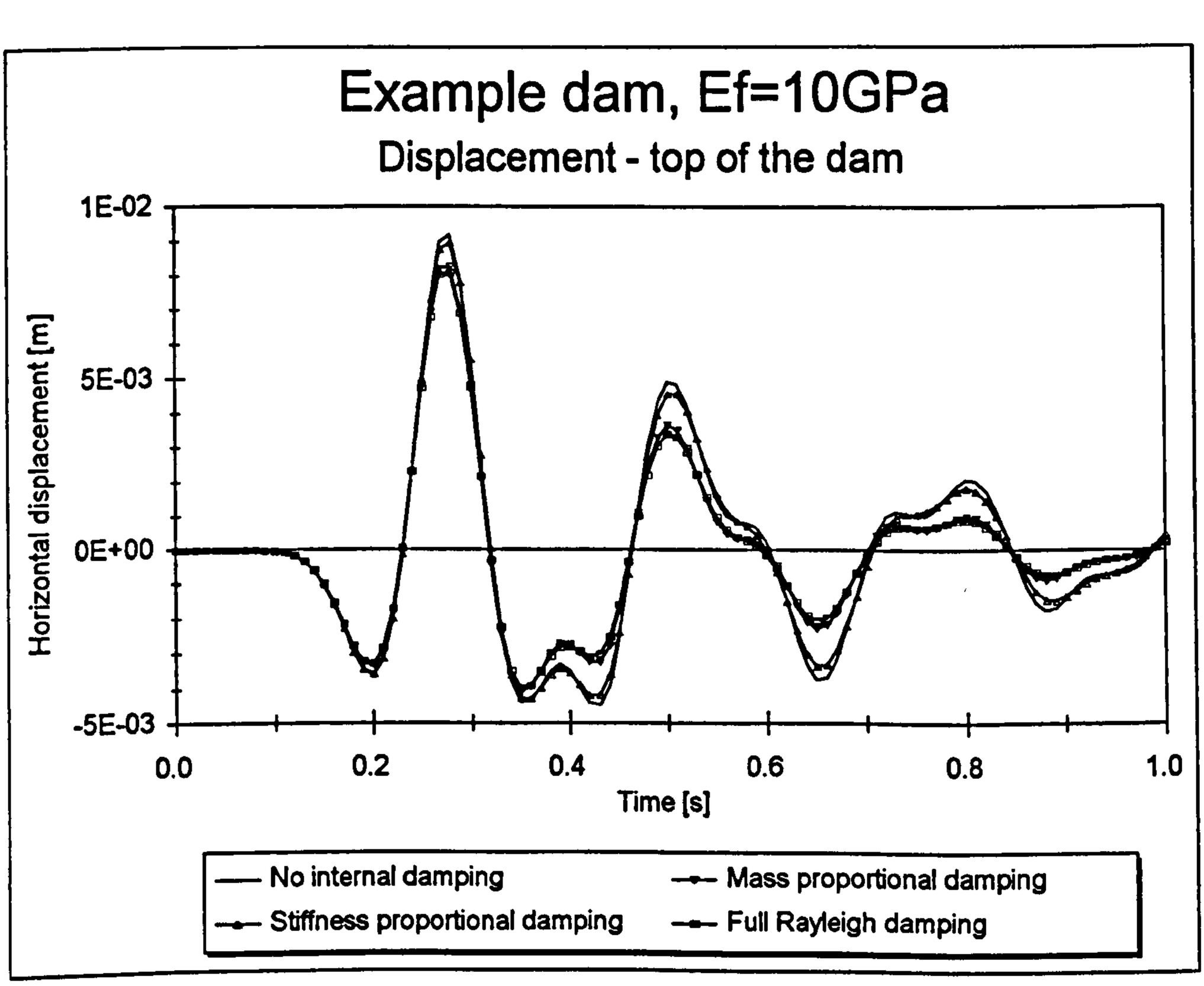

Figure 6.15c - Dam displacement (with radiation damping, E_f=10 GPa)

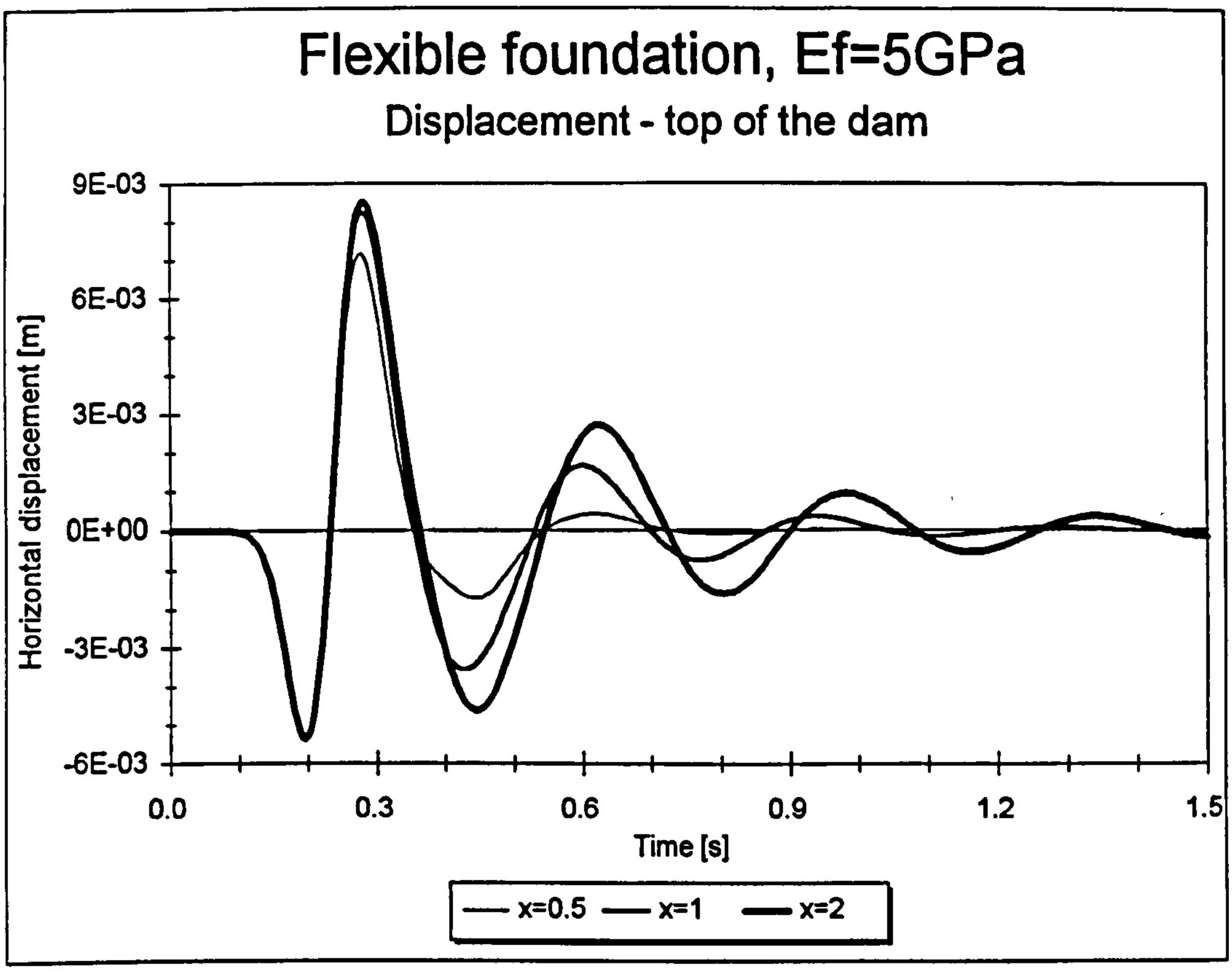

Figure 6.16a - Top displacement for different foundation sizes (E_f=5 GPa)

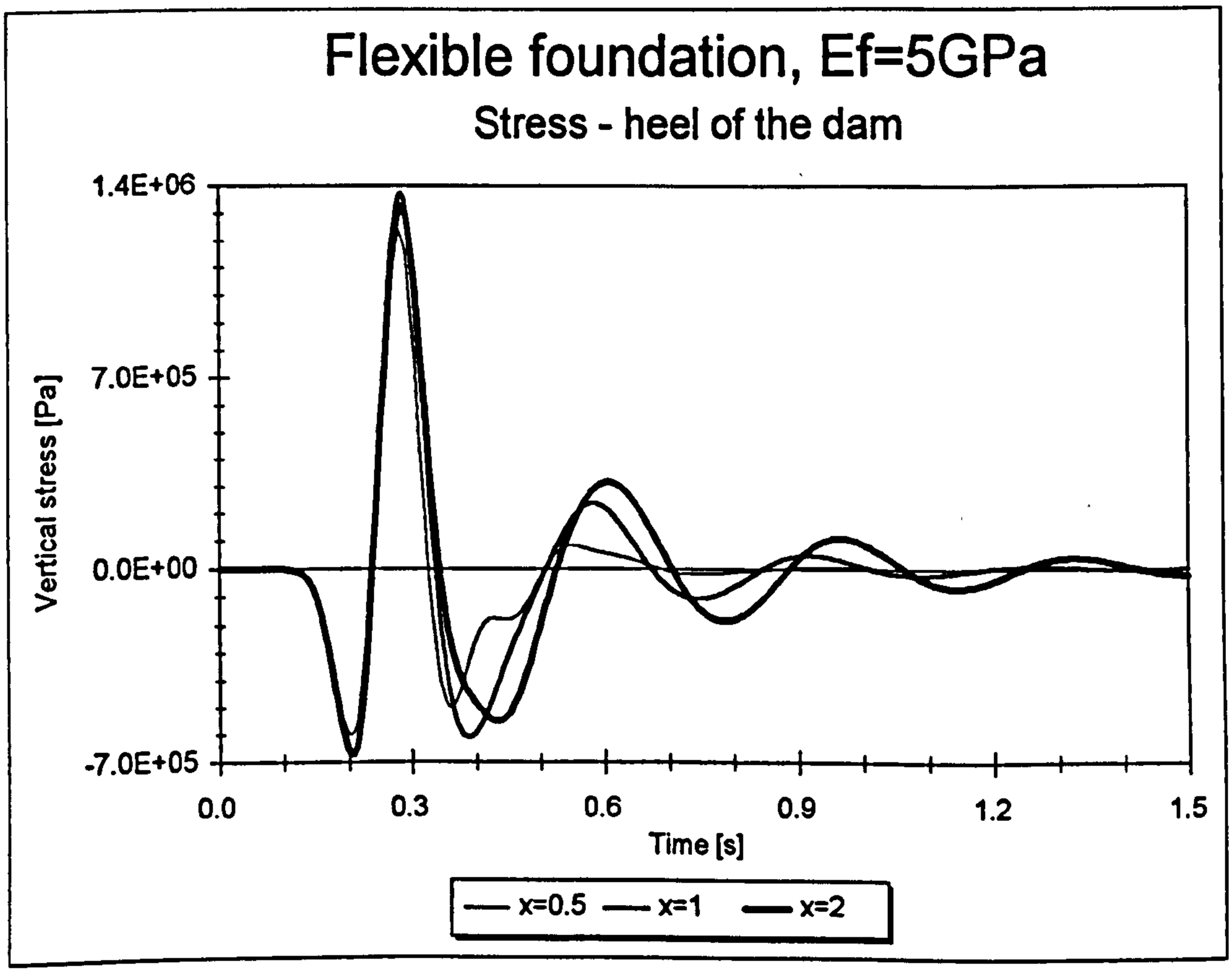

Figure 6.16b - Heel stress for different foundation sizes (E_f=5 GPa)

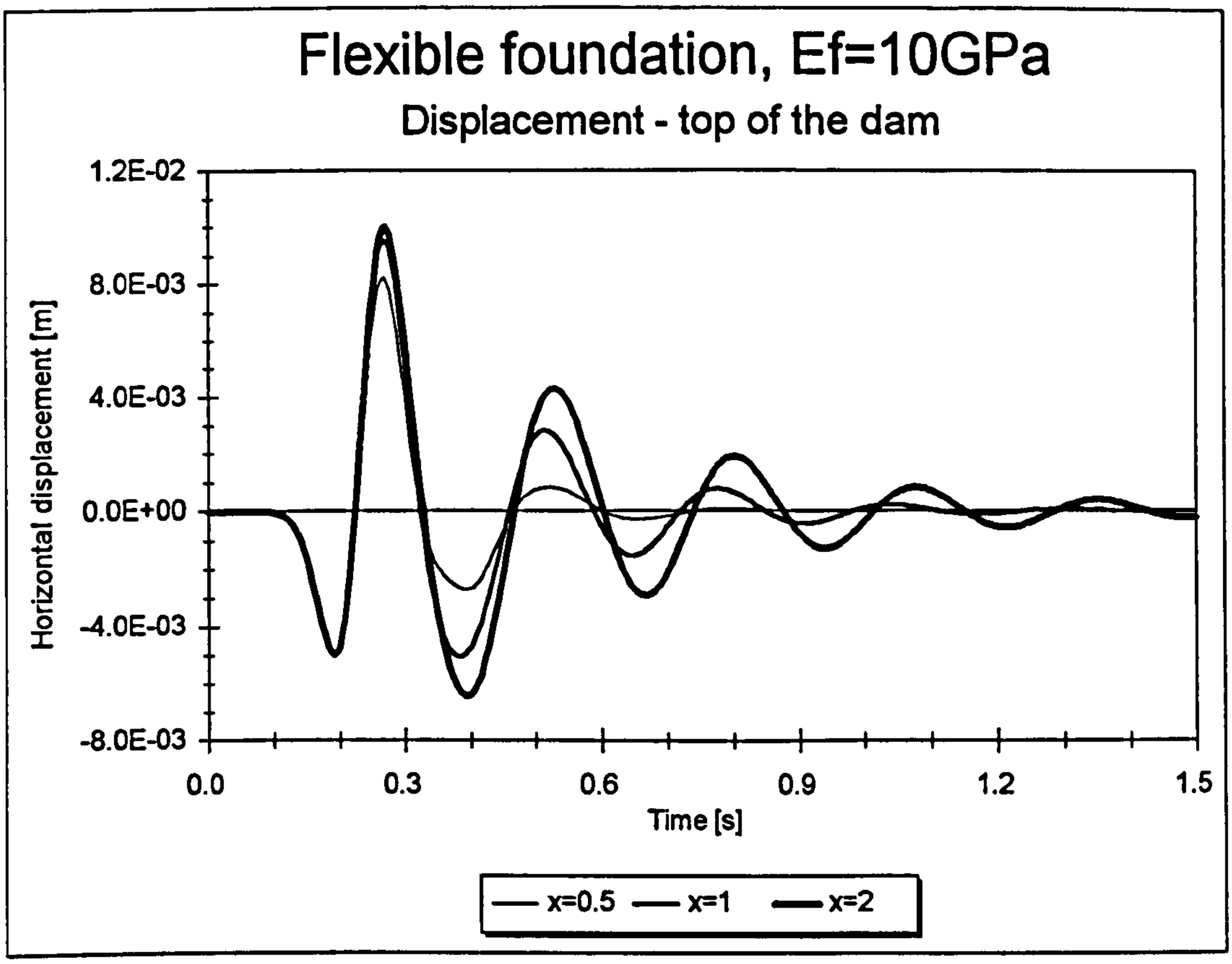

Figure 6.17a - Top displacement for different foundation sizes (E_f=10 GPa)

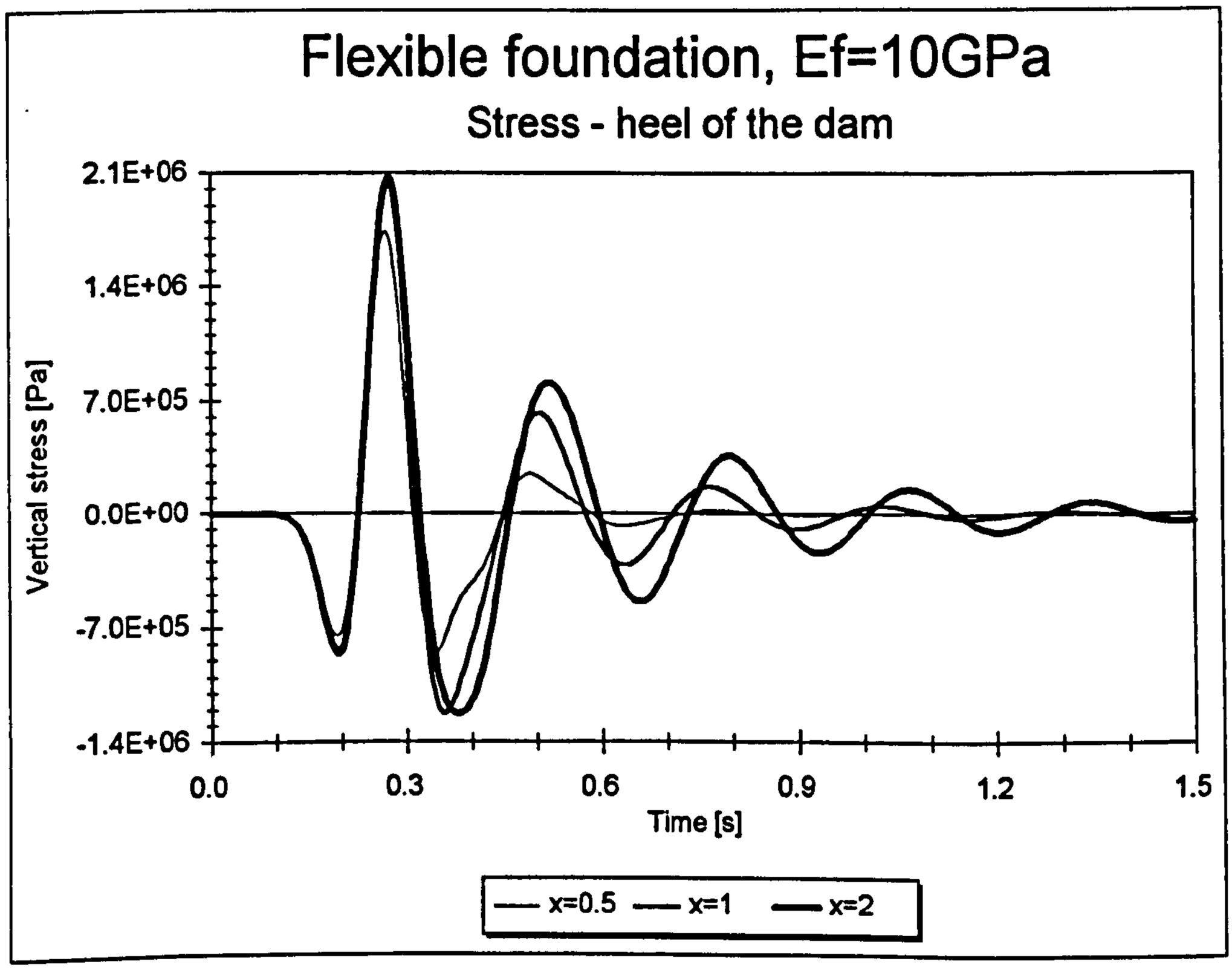

Figure 6.17b - Heel stress for different foundation sizes (E_f=10 GPa)

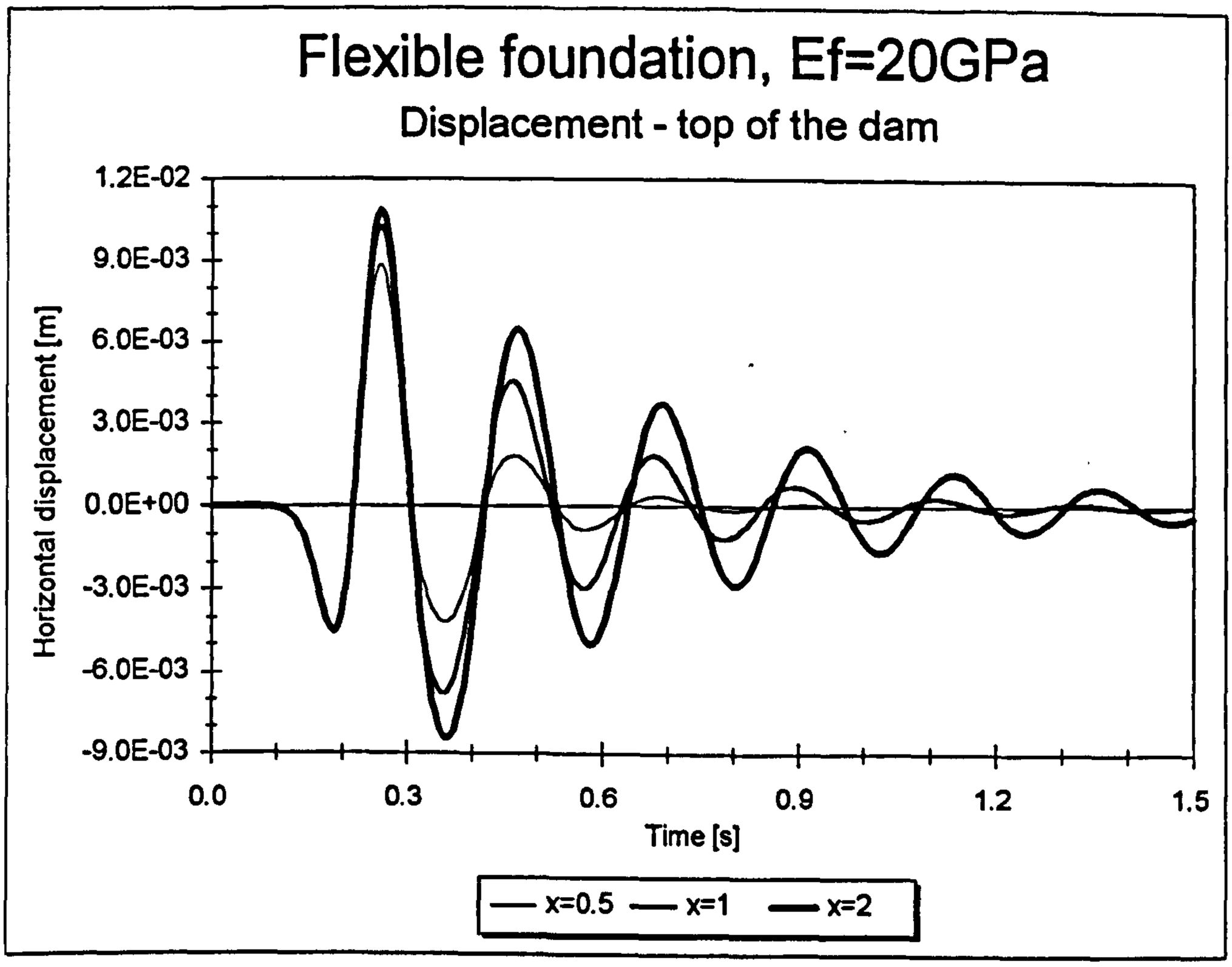

Figure 6.18a - Top displacement for different foundation sizes (E_f=20 GPa)

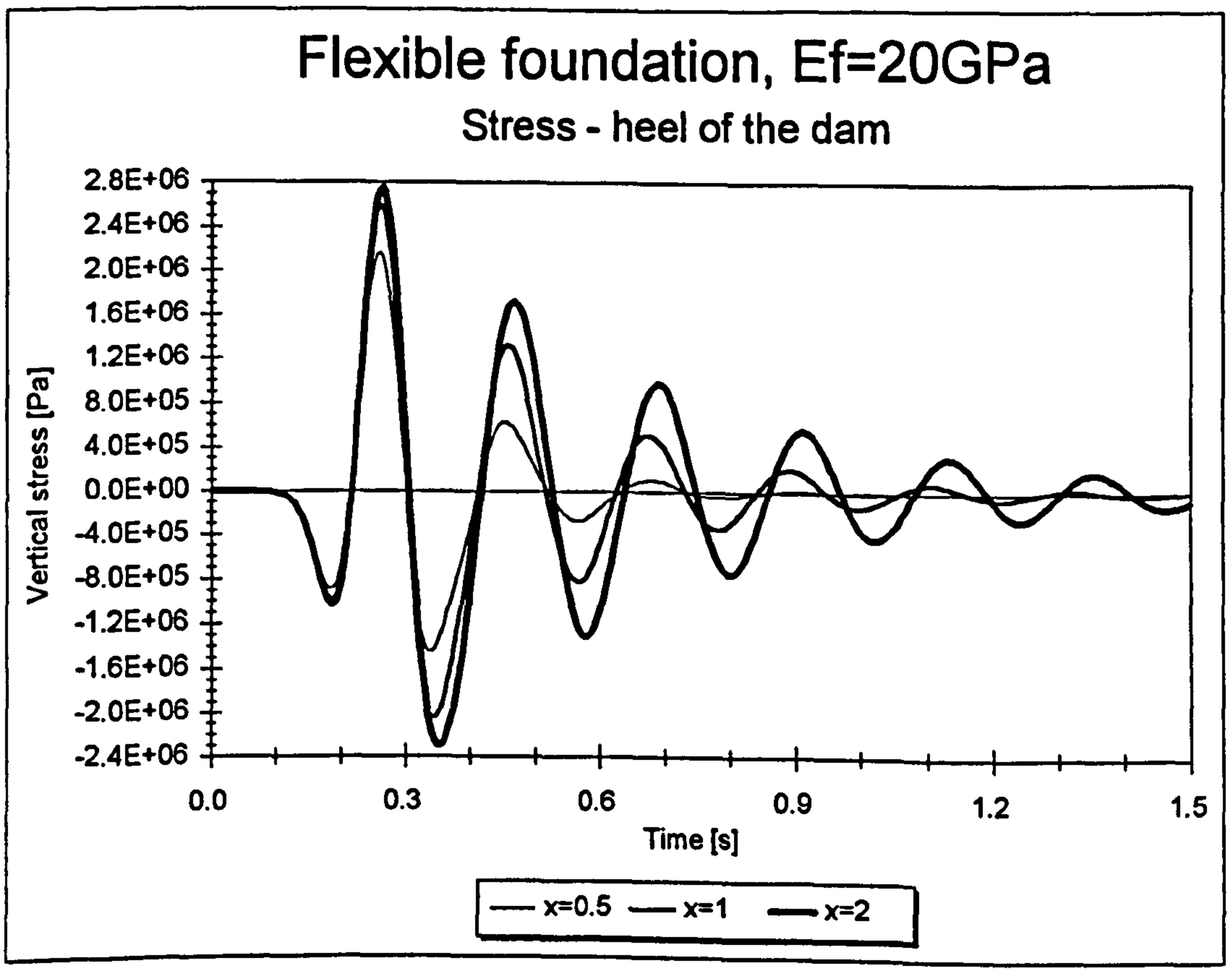

Figure 6.18b - Heel stress for different foundation sizes (E_f=20 GPa)

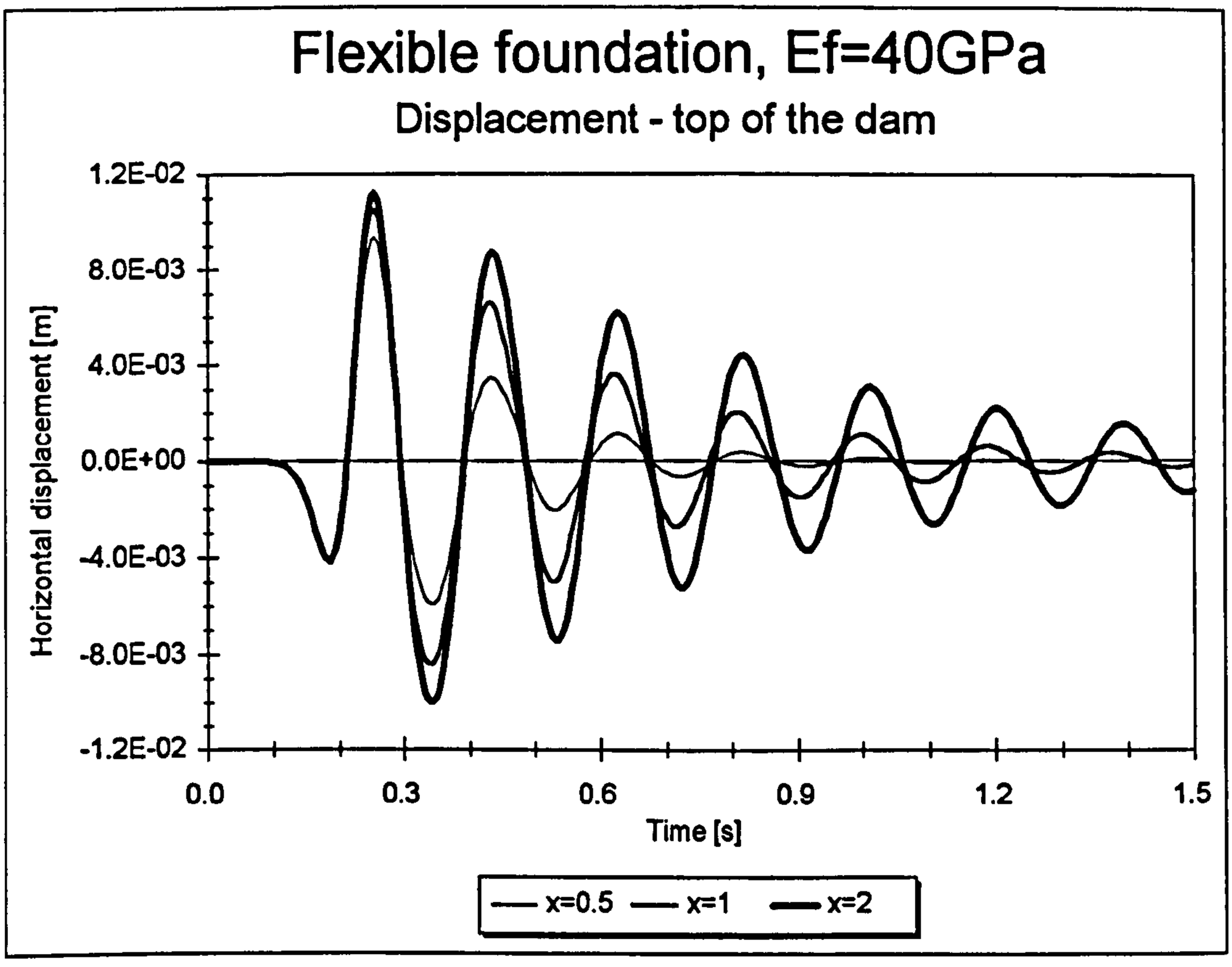

Figure 6.19a - Top displacement for different foundation sizes (E_f=40 GPa)

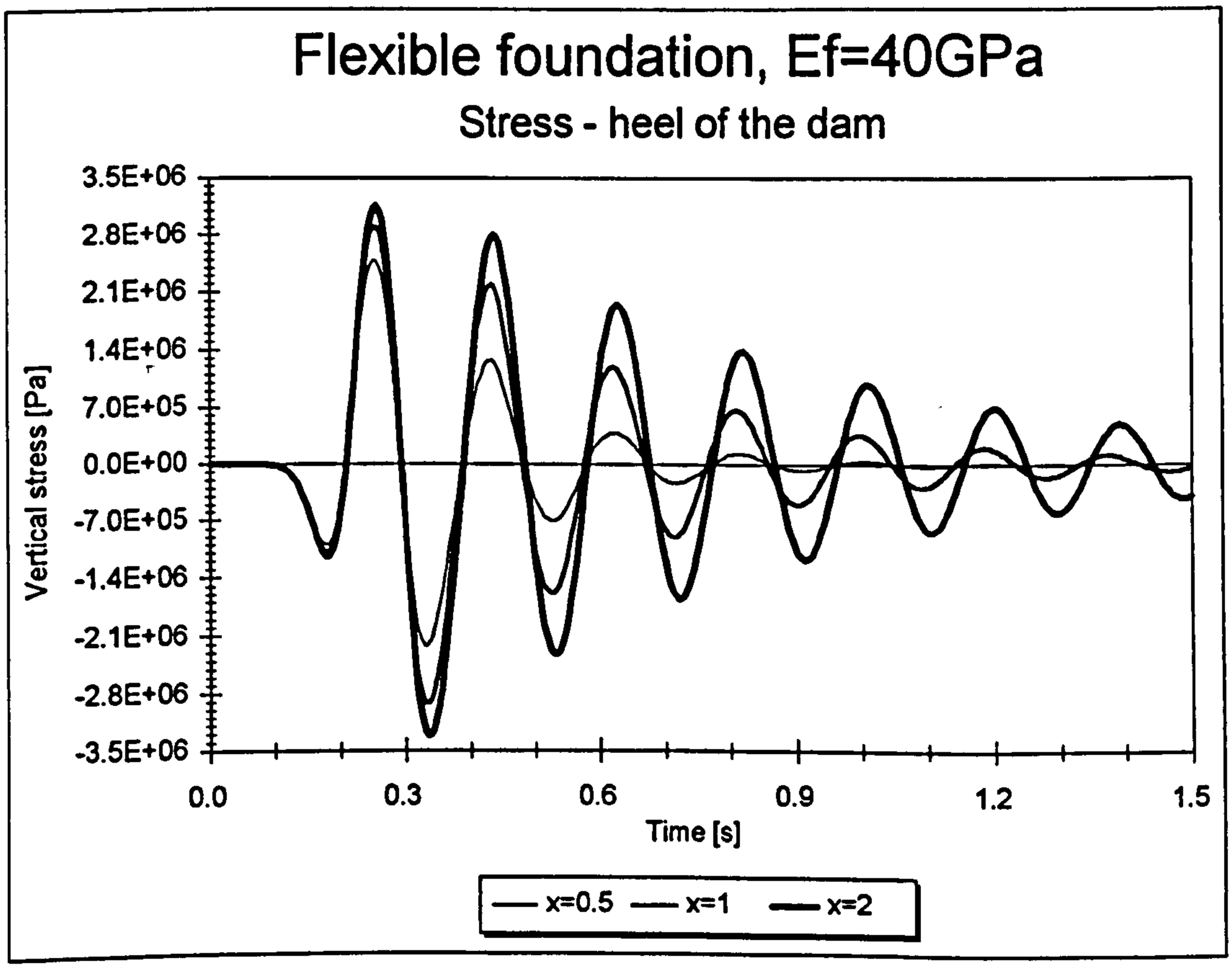

Figure 6.19b - Heel stress for different foundation sizes (E_f=40 GPa)

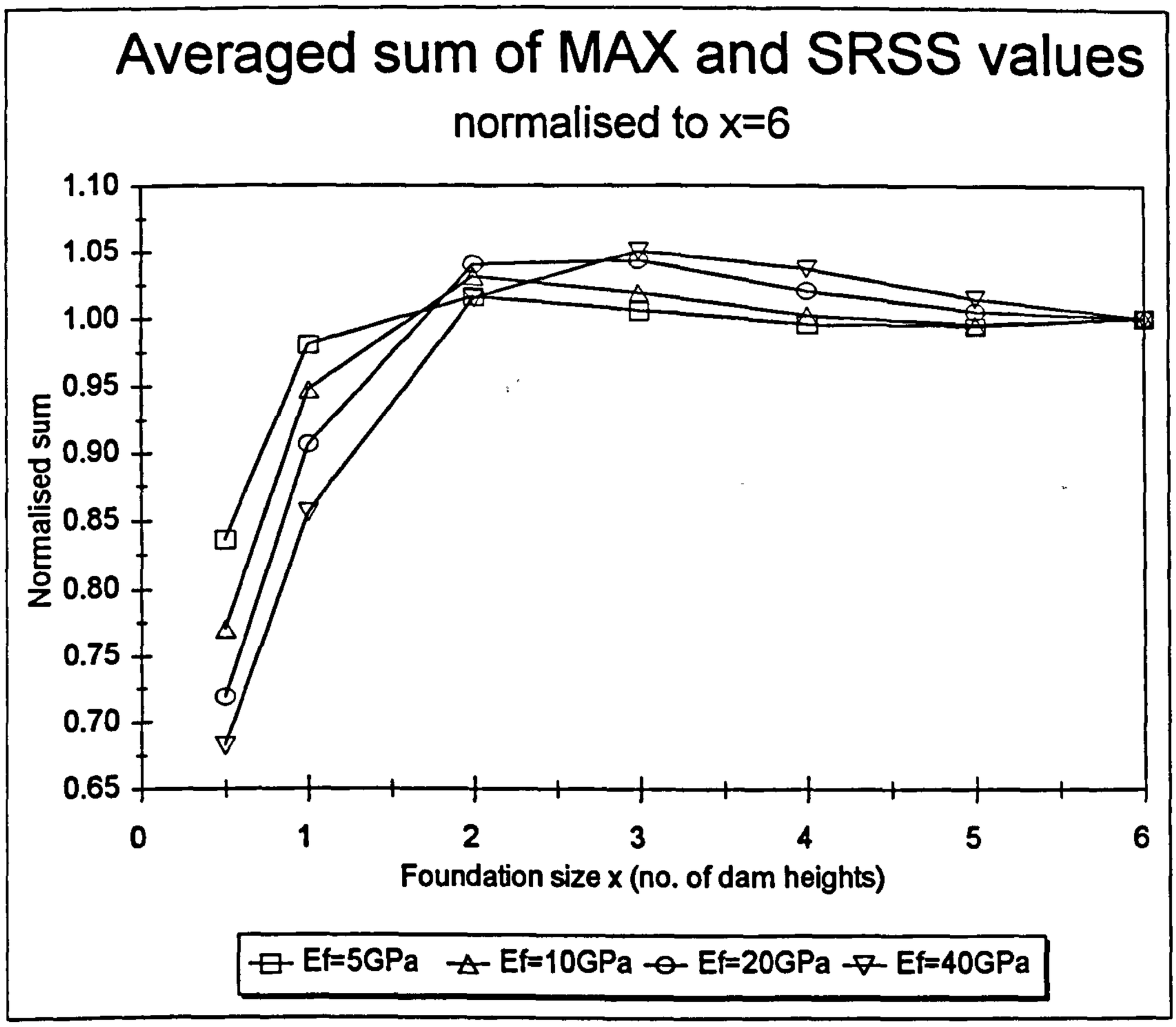

Figure 6.20 - Normalised average sum of MAX and SRSS values

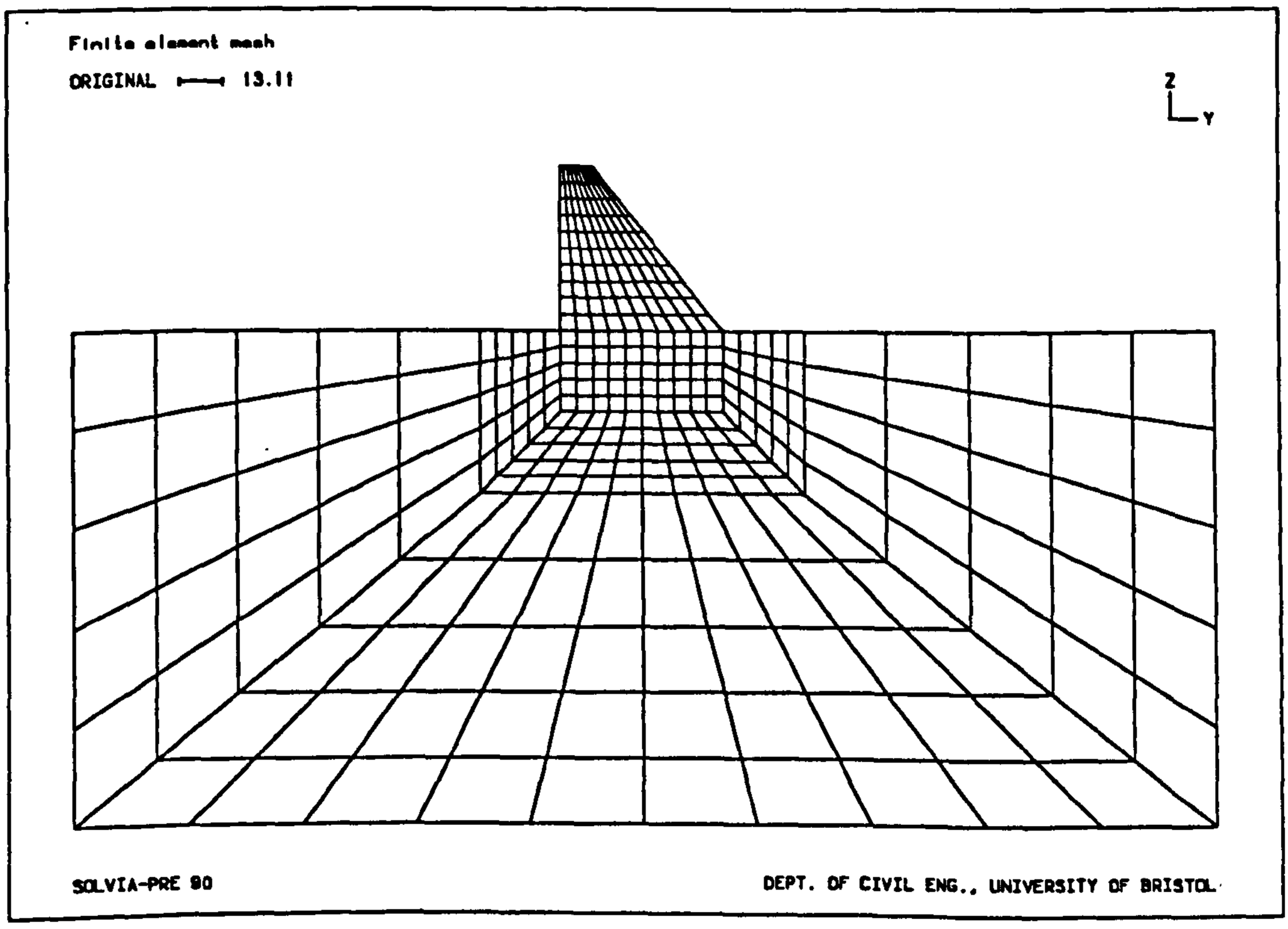

Figure 6.21 - Finite element mesh with nonuniform foundation elements

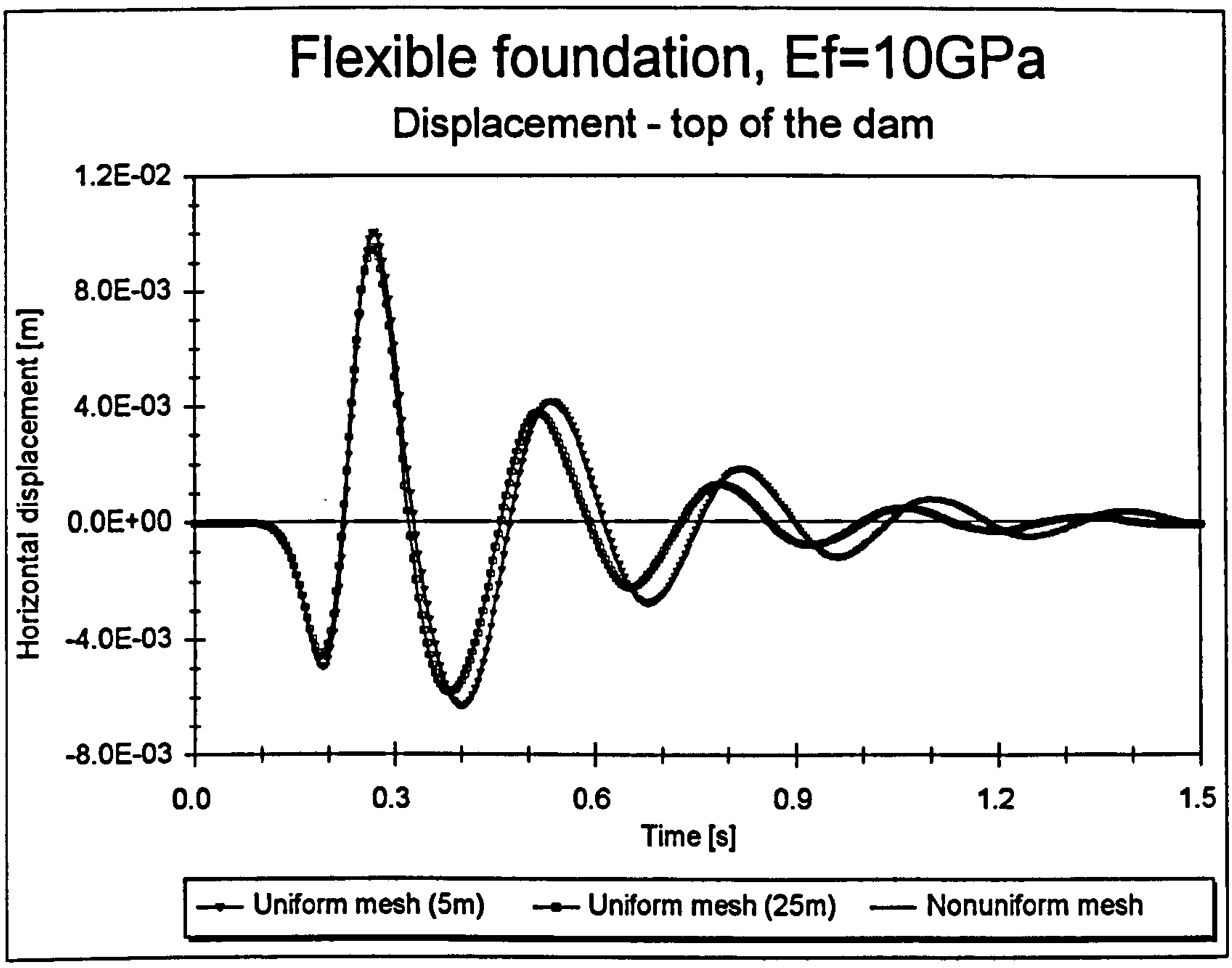

Figure 6.22a - Top displacement for different element sizes (E_f=10 GPa)

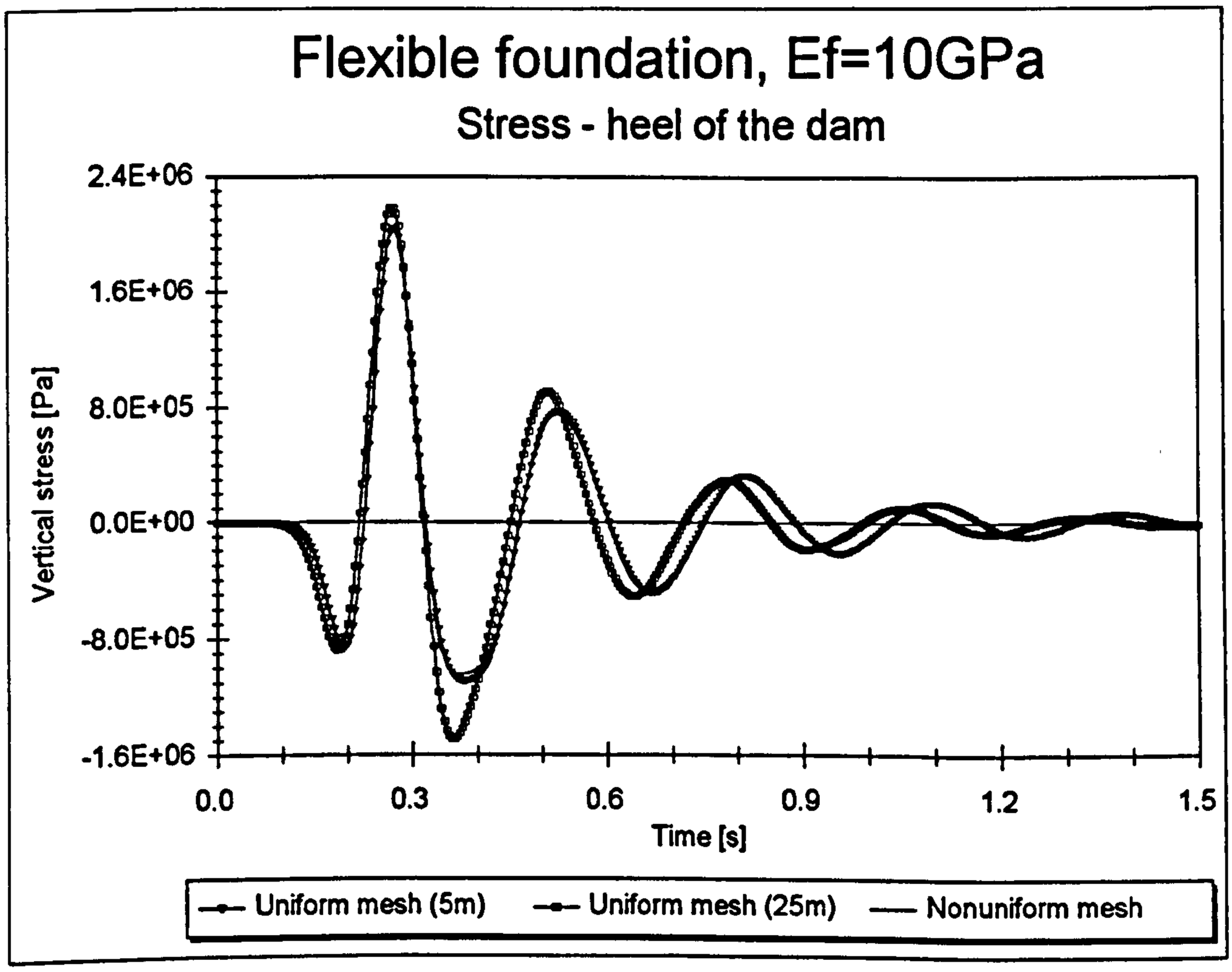

Figure 6.22b - Heel stress for different element sizes (E_f=10 GPa)

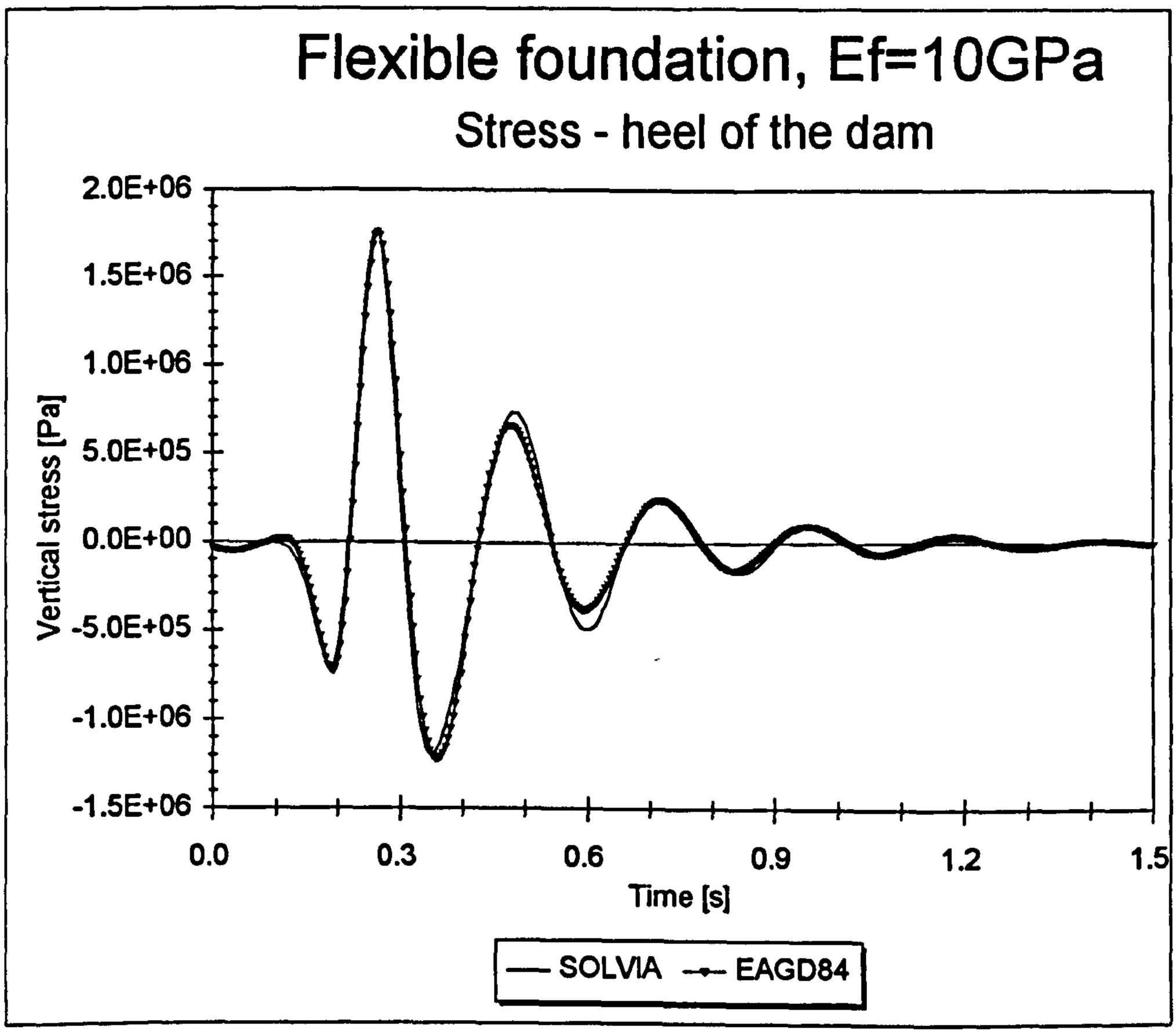

Figure 6.23 - Heel stress for time and frequency domain analysis (E_f=10 GPa)

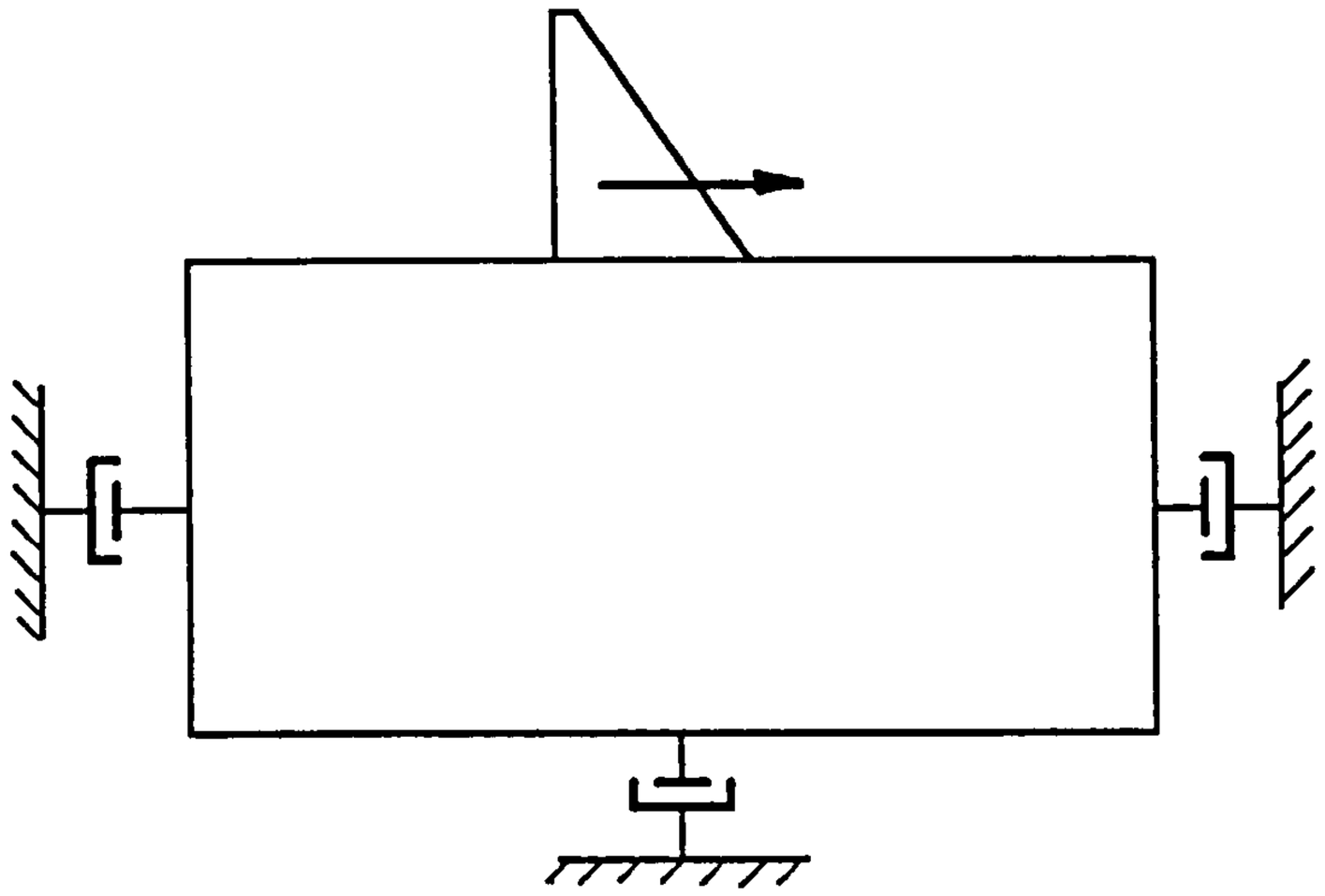

Figure 6.24a - Viscous transmitting boundary with dynamic loading

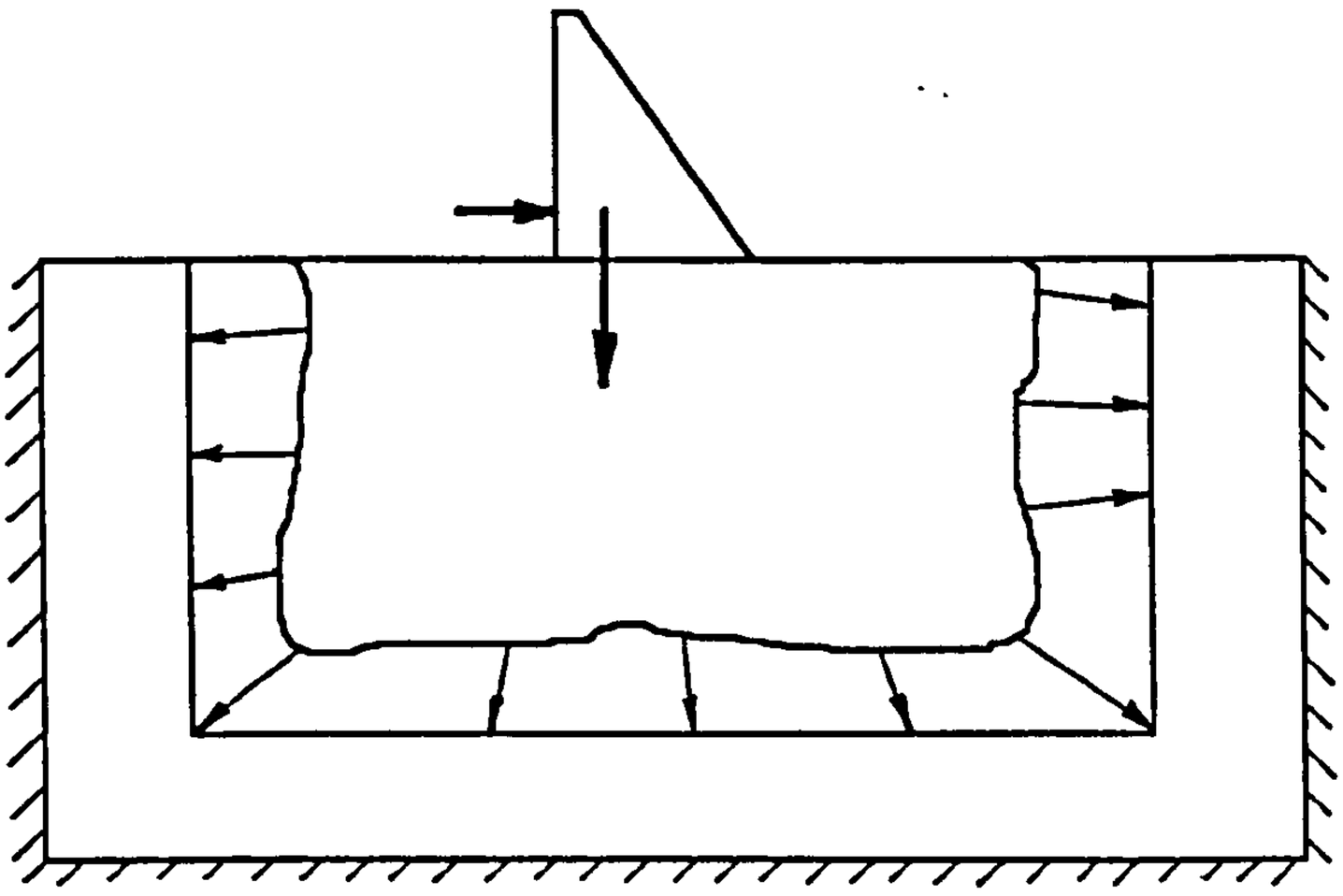

Figure 6.24b - Determination of boundary forces due to static loading

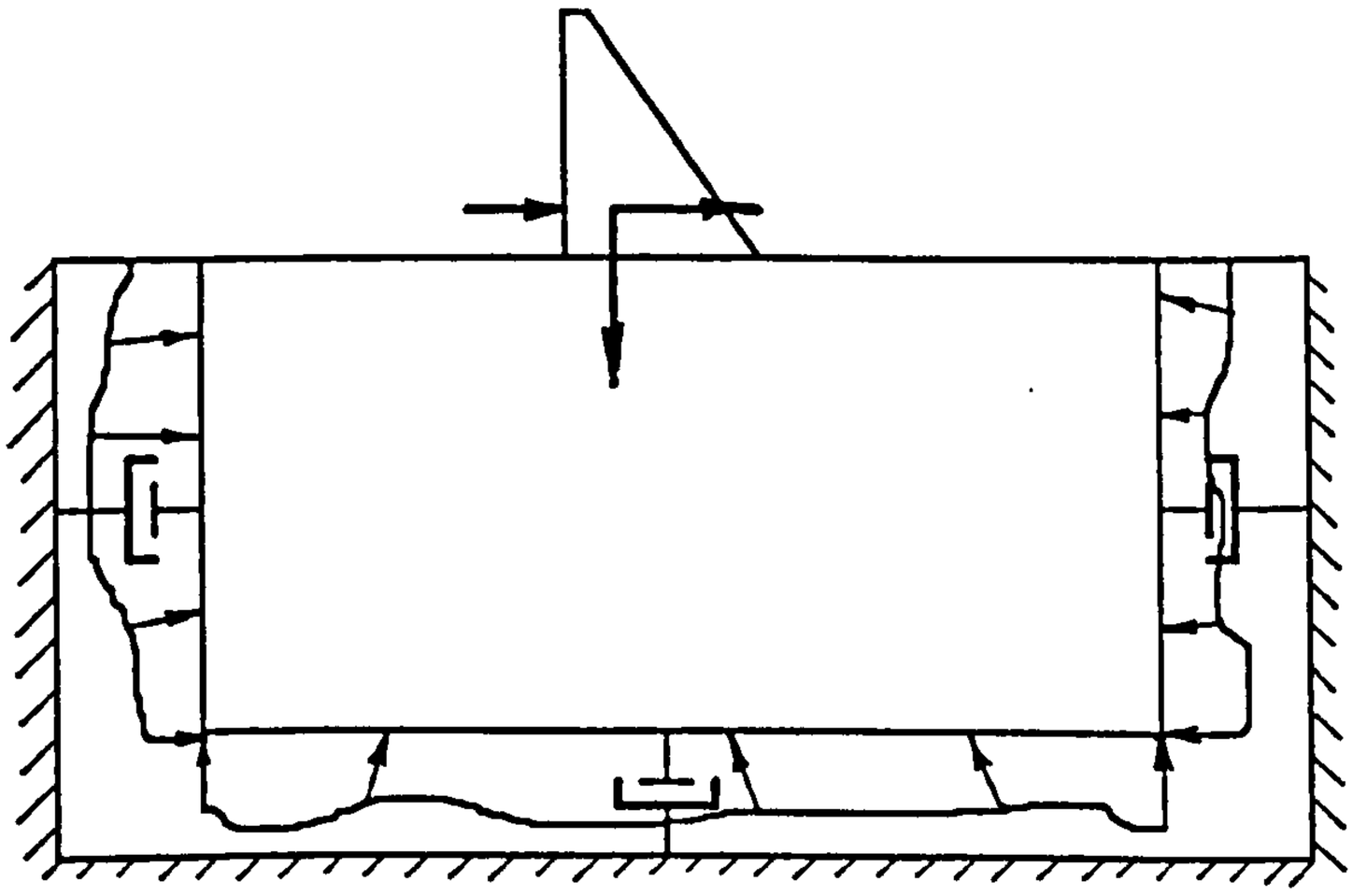

Figure 6.24c - Viscous transmitting boundary with combined loading and boundary forces

Nonlinearities of Concrete Gravity Dam-Foundation Systems: Theory

After presenting the dynamic equations for concrete gravity dam-foundation interaction in Chapter 5, preliminary linear elastic analyses were carried out in Chapter 6. They have established recommendations about the type of the seismic input, size of the foundation finite elements and overall size of the foundation finite element mesh. Having so equipped the numerical model, the stage is set for the introduction of possible nonlinearities.

Concrete gravity dams are practically always founded on rock. This means that only two materials should be investigated: mass concrete and rock. On the other hand, the nature of the whole dam-foundation system suggests that the likeliest nonlinearities belong either to the limited tension or contact categories. Although both may be formulated by using the Boundary Element Method (Cruse, 1979; Pekau et al., 1991; Becker, 1992), only the Finite Element Method formulations will be presented in this Chapter. First, nonlinearities will be classified and described by exploiting the differences and similarities between the dam concrete and rock. Second, several possibilities for representing limited tension nonlinearities will be examined, emphasising those that will eventually be used in Chapters 8 and 9.

7.1 Dam Concrete and Rock: Differences and Similarities

The nonlinear behaviour of concrete gravity dam-foundation systems can be classified according to the location of nonlinearities - above and below the ground level, and according to the type of nonlinearities - contact and limited tension nonlinearities.

7.1.1 Contact Nonlinearities

Various physical discontinuities which can be found above and below the ground level of concrete dam-foundation rock systems give rise to contact nonlinear behaviour.

Above the ground level, this is typically represented by contact (or joint) problems between gravity dam monoliths or arch dam cantilevers. The material discontinuities are usually due to zonation of mass concrete throughout the dam. The corresponding variation of properties (concrete density, modulus of elasticity, etc.) is inherent in the discretised, finite element approach, and therefore does not create any nonlinearities.

Below the ground level, material discontinuities are even more important and should be carefully determined through field investigation. Nevertheless, for the same reasons as above the ground level, this kind of discontinuity does not cause nonlinear behaviour. As for physical discontinuities, on one hand, the influence of numerous fissures, joints and occasionally faults in the rock is so important that it actually governs the behaviour of the rock mass. On the other hand, the dam-foundation interface is a predetermined discontinuity between two different materials and with practically unknown bonding characteristics. However, these phenomena can all be regarded as contact problems because the modes of deformation are analogous: joint shearing, joint opening and joint closing correspond to interface sliding (slipping), interface debonding (dam uplifting) and interface rebonding, respectively.

After realising in the late Fifties and Sixties that Rock Mechanics is a separate discipline, the importance of rock discontinuities was acknowledged (Jaeger, 1979;

Goodman, 1980) and subjected to a thorough investigation (Goodman, 1976). Various numerical models for the local treatment of major discontinuities, the so-called joint elements, were suggested. The element initially proposed for rock joints by Goodman et al. (1968) was later implemented by Toki et al. (1981) for soil-structure interface. Other widely used joint elements were originally devised by Ghaboussi et al. (1973) and Desai et al. (1984). At the global level, major discontinuities can be modelled by employing the Lagrange multiplier technique which mathematically couples two domains by ensuring compatibility of their displacements (Chaudhary & Bathe, 1986).

7.1.2 Limited Tension Nonlinearities

Both mass concrete and rock have relatively low tensile strengths and are not able to withstand high (sometimes hardly any) tensile stresses. Cracking may occur, particularly under extreme loading conditions (earthquake, flooding with dam overflow, etc.), creating the so-called limited tension nonlinear behaviour. Cracks can be found both above (body of the dam) and below ground level (dam embedment and rock foundation). The second case is further complicated by the fact that it is not known a priori whether cracking would develop in the concrete, rock or at the interface between the two.

In compression, the nonlinear behaviour of mass concrete and rock can also be observed. Constitutive models are dependent on the speed of initial loading (in this case, the initial static loading of the dam-foundation system) and possible subsequent loading cycles (in this case, the only realistic cyclic loading is earthquake loading). Furthermore, when exposed to very high compressive stresses, crushing of the material may occur, producing yet another nonlinearity. However, for concrete gravity dams (and to a lesser extent for concrete arch dams), the working compressive stresses in the dam and foundation under normal loading conditions are well below the compressive strengths of mass concrete and rock. The reason for this

lies in the design stage since concrete gravity dams are intentionally designed as structures with considerable reserves of compressive capacity. In other words, the range of working compressive stresses is on the linear part of the stress-strain curve, allowing the assumption of linear elastic behaviour for mass concrete and rock in compression. The previous remarks are valid not only for the normal loading conditions, but may be extended to combined static and earthquake loading (Zienkiewicz et al, 1986). Unfortunately, the scarcity of experimental data is a limiting factor for the full interpretation of cyclic loading effects on dam-foundation systems. The necessary data would have to be collected either from large-scale laboratory, dynamic, mass concrete tests, or from the existing dams subjected to sufficiently strong dynamic excitation. Until such data are available, it is not clear whether the extrapolation of uniaxial test results (Zienkiewicz et al., 1981; Bicanic & Zienkiewicz, 1983) is a reliable procedure.

7.1.3 The Practical Choice

When conducting nonlinear analyses of concrete gravity dams, contact nonlinearities above the ground level are rarely treated (not so in the case of arch dams), and the usual practice follows one of two approaches:

a) Greater importance is assigned to contact nonlinearities. This approach is justified in the case of foundation discontinuities, where the 'weak points' (important rock joints or faults) are known in advance. As for the contact at the dam-foundation interface, some researchers have argued that the dam-foundation interface is a potential crack at a known location (Léger & Katsouli, 1989; Ibrahimbegovic & Wilson, 1990; Léger et al., 1991). However, if one bears in mind all the beneficial effects of a realistic dam-foundation interface (considerable roughness and friction mobilisation, geometrical complexity, presence of a cutoff, etc.), it becomes clear that its failure is not as

straightforward as in the case of typical soil-structure interaction problems where the contact is much poorer.

b) Greater importance is assigned to limited tension nonlinearities. A dam-foundation system is typically considered as perfectly bonded and can therefore be treated with standard continuum mechanics equations. Eventually, cracks may appear anywhere in the system (Vargas-Loli & Fenves, 1989; El-Aidi & Hall, 1989; Bhattacharjee & Léger, 1993; Waggoner et al., 1993).

The previous discussion shows that the choice between the two approaches almost entirely depends on the state of the dam-foundation bond. If strong, cracking can be expected in the surrounding materials (dam embedment concrete and/or foundation rock), which then becomes the situation explained in approach *(b)*. If the bond is weak, the crack would initiate and propagate exactly at the interface, which is the situation explained in approach *(a)*. Interestingly, a nonlinear analysis that combines the two approaches has not yet been reported.

Herein, it will be assumed that the dam-foundation interface is perfectly bonded. Neither foundation nor interface contact nonlinearities will be treated, allowing only for the limited tension nonlinear behaviour. In order to eliminate possible cracking nonlinearities in the upper parts of the dam (usually due to the abrupt change of geometry at the downstream face), the cross section of the dam above the ground level will be idealised. A simple trapezoidal shape will be assumed for all the analyses in Chapters 8 and 9. Therefore, the problems associated with the neck of the dam (e.g. the Koyna dam case) will be avoided and the nonlinear phenomena will be predetermined to occur in the lower parts of the dam (particularly the heel of the dam), dam embedment, dam-foundation interface and the surrounding rock foundation.

7.2 No-Tension Material

Zienkiewicz et al. (1968) made probably one of the first departures from linear elastic theory by introducing an idealised material incapable of withstanding any tensile principal stresses. They called it a no-tension material and applied it to rock (Zienkiewicz, 1968; Zienkiewicz et al. 1968). At the time when the model was first proposed, only computer codes with the assumption of linear elastic material behaviour were available, and the authors used an iterative procedure. If it converges, the no-tension state can ultimately be obtained, which means that the system is capable of sustaining the imposed loads only by compression. On the other hand, the non-convergent process would imply the system's proneness to failure.

This iterative procedure will be explained here on a concrete gravity dam-foundation system shown in Figure 7.1. There are three essential steps which correspond to the appropriate parts of that figure:

a) The dam-foundation system subjected to known static forces and initial in situ stresses is analysed assuming linear elastic material behaviour of the mass concrete and rock. The region in which the principal tensile stresses developed is noted (shaded area in Figure 7.1a).

b) As the materials are not capable of withstanding any tension, the tensile region is eliminated and its effect on the rest of the system is represented with the equivalent external forces (outward arrows in Figure 7.1b).

c) Since the forces from step *(b)* do not exist in reality, their effect has to be compensated by the effect of the forces acting in the opposite direction (inward arrows in Figure 7.1c). The original system, with the different loading only, is reanalysed. It is expected that the tensions will develop once again, but this time on a smaller scale.

In order to obtain a complete set of the 'relaxed tension' results after the first iteration, the results from steps *(b)* and *(c)* should be superimposed. The iterative process is continued by repeating steps *(b)* and *(c)* until convergence is achieved, creating the no-tension state.

The described procedure, initially called by its authors 'the stress transfer method', served later as a basis for closely related, but more widely applicable inital stress method (Zienkiewicz & Taylor, 1991). Their mutual essence is that for every iteration, the same stiffness matrix is used, considerably improving the economy of the required number of linear elastic analyses. Unfortunately, this set of analyses cannot be reformulated as an explicit stress-strain relation, but the nearest analogy is that of the zero cut-off tensile stress for tensile strains (Zienkiewicz et al., 1970). The uniaxial representation of this criterion is shown in Figure 7.2a. Although the stress-strain relationship is not unique (all positive strains correspond to one, zero stress), the problem is still path independent and the strain returns to zero upon removal of the load. This characteristic of the model enables the instantaneous application of the total static load.

Alternatively, uniaxial stress-strain behaviour may be considered as path dependent (the strain depends not only on the stress level but also on the stress history, i.e. on whether the loading or unloading branch is considered). For this case, shown in Figure 7.2b, a somewhat modified procedure is necessary (Venturini, 1983). Application of the total load should be carried out in increments.

The importance of path dependent stress-strain behaviour lies in the fact that it provides a link between early, standard no-tension elastic analyses (no-tension elasticity) and later extentions towards the theory of plasticity (no-tension plasticity). Their similarities will be identified in Section 7.3, after considering the main concepts of limited tension elasto-plasticity and elasto-viscoplasticity.

The inital no-tension material was widely used in the past and thought to have given good approximations to the real behaviour of mass concrete and rock (Pande et al.,

1990; Zienkiewicz & Taylor, 1991). However, from the point of view of this work, its main drawback is that it is impractical, if not impossible, to use it for the kind of earthquake analyses that will be carried out in Chapter 9. The conditions under which the related limited and no-tension plasticity models can be used for nonlinear analyses of concrete dam-foundation systems will be explored in greater detail in Section 7.3.

Moreover, it should be emphasised that no-tension elasticity (a similar conclusion will be reached for no-tension plasticity in Section 7.3) acts like a distributor of nonlinearities. In other words, instead of being able to observe the expected cracking pattern, the analyst is confronted with comparatively larger zones that indicate certain, usually stress dependent, levels of material damage.

7.3 Elasto-Plasticity and Elasto-Viscoplasticity

The theories of plasticity and viscoplasticity are vast subjects and cannot be treated in great detail. Despite the fact that they cover various engineering materials, only aspects relevant to the numerical modelling of concrete and rock for the purpose of analyses of dam-foundation systems will be presented here. If the behaviour of materials prior to yielding is elastic, the theories are then called elasto-plasticity and elasto-viscoplasticity, respectively. Herein, only the special case of linear elastic behaviour prior to yielding will be treated. Alternative assumptions (e.g. nonlinear elasticity) are possible, but this particular one is in line with the discussion and conclusions from Section 7.1.

7.3.1 Elasto-Plasticity

Although the behaviour of concrete dam-foundation systems is not one-dimensional, the basic concepts of elasto-plasticity can be introduced more easily within the framework of uniaxial material behaviour.

The simplest idealised uniaxial elastoplastic behaviour, identical in tension and in compression, is shown in Figure 7.3a. The behaviour is purely elastic up to the yield stress σ_y, after which the strain continues to increase and after which it is not possible to recover the original unstrained state of the material. If the load is removed (dashed line in Figure 7.3a), the plastic strain ε^p remains; and the total deformation consists of elastic and plastic components. In other words, the behaviour is path dependent, which is completely analogous to the situation presented in Figure 7.2b. Indeed, Figure 7.2b can be obtained from Figure 7.3a by translating the coordinate system to the point where the yield tensile stress is zero and by assuming that the yield compressive stress is extremely high. It is in this way that no-tension plasticity is introduced.

One possible refinement of the model is to introduce material hardening or softening. The effects of the former on the stress-strain behaviour are shown in Figure 7.3b, where it can be seen that σ_y does not correspond to the maximum possible stress but merely denotes the beginning of plastic flow. In other words, the yield stress of the material increases (or decreases for the case of softening) with the increase of plastic strain.

Although the generalisation of plasticity concepts and the extention to multiaxial (biaxial or triaxial) states of stress and strain is not straightforward, the underlying principles are same. The stress-strain relationship prior to yielding can once again be assumed as linear elastic. The plastic yield of the material cannot be represented as simply as in the uniaxial case (Figure 7.3a)

$$\sigma - \sigma_y = 0 \tag{7.1}$$

and the more general yield criterion F needs to be postulated. Obviously, the criterion will depend on the stresses, but should not depend on the choice of coordinate axes or their possible transformation. Therefore, it is essential not to define the yield criterion as a function of stress components, but as a function of quantities which do not change with coordinate transformation. Such quantities are

called invariants of stress and can be found tabulated together with the invariants of strain in many textbooks which cover this subject (e.g. Pande et al., 1990).

In the uniaxial case, it was implicitly assumed that once the plastic strain is initiated, it develops in the same direction as the applied stress. For any multiaxial case, where all plastic strain components exist, the direction of the plastic strain vector is not known. However, it can be determined by defining the so-called flow rule as

$$d\varepsilon^p = d\lambda \frac{\partial Q(\sigma)}{\partial \sigma} \tag{7.2}$$

where Q is the plastic potential function - a scalar function of the stress vector σ, and where d is used to denote various infinitesimal increments. Consequently, $d\varepsilon^p$ is the vector of plastic strain increments and $d\lambda$ is an incremental proportionality constant which can be determined when deriving a complete stress-strain relation for an elasto-plastic material (Pande et al., 1990). If the plastic potential function is assumed to be the same as the yield criterion ($Q = F$), the flow rule is called associated. Otherwise, the flow rule is nonassociated.

Finally, the material hardening or softening for multiaxial situations are defined similarly as in the uniaxial case - as the dependence of the yield criteria on some parameters. In this respect, the general yield criterion F may be written as

$$F = F(\sigma, k) \tag{7.3}$$

where σ is the vector of stresses and k is a hardening (or softening) parameter. k is often expressed as a function of the invariants of plastic strains (e.g. principal plastic strains, which is analogous to the uniaxial case), but many other alternatives have also been reported (Pande et al., 1990; Zienkiewicz & Taylor, 1991).

7.3.1.1 Some Yield Criteria

After having covered all the important features of multiaxial elasto-plasticity, some of the best known yield criteria for isotropic materials will be presented:

1) *Tresca yield criterion.* Does not incorporate friction in the yield model. Primarily used for metal plasticity and theoretically can be used for nonfrictional soils. Therefore, the criterion is of little practical interest to the present study.

2) *Von Mises yield criterion.* Does not incorporate friction in the yield model. Primarily used for metal plasticity and theoretically can be used for nonfrictional soils. Therefore, the criterion is of little practical interest to the present study.

3) *Mohr-Coulomb yield criterion.* Does incorporate friction in the yield model and can therefore be used for any material where the friction plays an important role. Following the form of Equation (7.3), the Mohr-Coulomb yield criterion can be given as

$$F = \frac{I_1}{3}\sin\phi + \sqrt{J_2}\left(\cos\theta_0 - \frac{1}{\sqrt{3}}\sin\theta_0\sin\phi\right) - c\cos\phi = 0 \qquad (7.4)$$

where c and ϕ are the material cohesion and angle of friction, respectively. If c and ϕ are constant, the material is perfectly plastic (i.e. there are no hardening or softening effects). On the other hand, c and ϕ may not be constant and may depend on a hardening (or softening) parameter k, as explained for Equation (7.3). I_1, J_2 and θ_0 are the invariants of stress as follows (Pande et al., 1990)

$I_1 = \sigma_1 + \sigma_2 + \sigma_3 = \sigma_x + \sigma_y + \sigma_z$ First invariant of stress

$J_2 = S_1S_2 + S_2S_3 + S_3S_1$ Second invariant of deviatoric stress

where S_1, S_2 and S_3 are principal deviatoric stresses

$$S_1 = \sigma_1 - \sigma_m \qquad S_2 = \sigma_2 - \sigma_m \qquad S_3 = \sigma_3 - \sigma_m$$

in which $\sigma_m = I_1/3$ is the hydrostatic part of the stress tensor;

$$\theta_0 = \frac{1}{3}\arcsin\left(-\frac{3\sqrt{3}J_3}{2J_2^{1.5}}\right) \qquad \text{Lode's angle}$$

Lode's angle is the angular form of the third invariant of deviatoric stress

$$J_3 = S_1 S_2 S_3$$

and it varies between -30° and +30°.

4) *Drucker-Prager yield criterion.* Does incorporate friction in the yield model and can therefore be used for any material where the friction plays an important role. Following the form of Equation (7.3), Drucker-Prager yield criterion can be given as

$$F = \alpha I_1 + \sqrt{J_2} - K = 0 \qquad (7.5)$$

where α and K are the parameters which depend on the cohesion c and angle of friction ϕ. One possibility is that c and ϕ are constant, in which case the material is perfectly plastic. On the other hand, c and ϕ may depend on a hardening (or softening) parameter k, as explained for Equations (7.3) and (7.4).

In their original work, Drucker and Prager tried to match the Mohr-Coulomb yield criterion for plane strain conditions which led to the following expressions for α and K (Venturini, 1983)

$$\alpha = \frac{\tan\phi}{\sqrt{9+12\tan^2\phi}} \qquad K = \frac{3c}{\sqrt{9+12\tan^2\phi}} \qquad (7.6)$$

Two alternative expressions are (Venturini, 1983)

$$\alpha = \frac{2\sin\phi}{\sqrt{3}(3-\sin\phi)} \qquad K = \frac{6c\cos\phi}{\sqrt{3}(3-\sin\phi)} \qquad (7.7)$$

$$\alpha = \frac{2\sin\phi}{\sqrt{3}(3+\sin\phi)} \qquad K = \frac{6c\cos\phi}{\sqrt{3}(3+\sin\phi)} \qquad (7.8)$$

All the yield criteria mentioned so far can be presented graphically as yield surfaces in the principal stress space, as shown in Figure 7.4 (originally from Zienkiewicz &

Taylor, 1991). In this Figure, some important aspects of the four elastoplastic yield criteria can be observed:

The Tresca and von Mises yield surfaces are parallel to the axis $\sigma_1=\sigma_2=\sigma_3$ which means that the corresponding criteria do not depend on the hydrostatic stress component.

When the angle of friction ϕ is taken as zero, the Mohr-Coulomb and Drucker-Prager yield surfaces degenerate into Tresca and von Mises yield surfaces, respectively.

The von Mises and Drucker-Prager yield surfaces are smooth. Since every point is uniquely defined, from the numerical point of view it is easier to deal with them than with the other two yield surfaces.

The Drucker-Prager yield surface coincides with the outer apices of the Mohr-Coulomb hexagonal yield pyramid if the parameters α and K are set according to Equation (7.7). It coincides with the inner apices if the same parameters are set according to Equation (7.8) (Venturini, 1983).

5) *Ottosen yield criterion.* This perfectly plastic yield criterion with an associated flow rule, originally proposed for plain concrete by Ottosen, has recently been applied as the damage model for concrete gravity dams under increased static loading (Gioia et al., 1992). The application of this limited tension plasticity approach substituted the local effects of cracking with a suitable global constitutive law for the material under consideration. As a result, comparatively larger plastified (damaged) zones are observed. The main argument for following such a procedure was to avoid the difficulties inherent in the smeared and discrete representations of fracture (Rots, 1991; Gioia et al., 1992).

7.3.1.2 The ADINA Improved Drucker-Prager Model

Theoretically, all the yield mechanisms presented so far are not bound in the principal stress space, i.e. no matter how high the hydrostatic stress is, the material will not

yield. In order to allow for yielding under hydrostatic loading, the so-called cap models (where the cap is nothing else but the basis of a particular surface) were introduced. Bathe et al. (1980) suggested a convenient yield model (Figure 7.5) based on the Drucker-Prager surface with isotropic hardening, but improved with cap (hydrostatic) yielding in compression and with a tension cut-off limit (Bathe et al., 1980; Bathe, 1982).

The model was implemented into a general purpose finite element code ADINA (ADINA Engineering, 1984), from where it was inherited by the finite element code SOLVIA (SOLVIA Engineering AB, 1989/92). Since SOLVIA will be the main computational tool in Chapters 8 and 9, at this stage it is important to note that apart from standard mechanical properties (Young's modulus, Poisson's ratio and density), three sets of data are required for the full definition of the model.

1) Parameters α and K for the definition of the standard Drucker-Prager yield function (Figure 7.5), according to Equations (7.5)-(7.8)

2) Parameters for the definition of the cap yield function and determination of its position I_1^a (Figure 7.5) on the negative (compression) axis of the first stress invariant I_1.

3) Parameter T for the definition of the tension cut-off limit (Figure 7.5) on the positive (tension) axis of the first stress invariant I_1.

7.3.2 Elasto-Viscoplasticity

In the theory of elasto-plasticity, due to total time independence, a solution outside the yield surface is not admissible and the strain increments $d\varepsilon^p$ in Equation (7.2) are generated instantaneously with the load causing yielding. In other words, the plastic strain rate $\dot{\varepsilon}^p$ iz zero for stresses below the yield stress, but once it develops (at the moment of yielding), it is both indeterminate and redundant.

Similarly, in the theory of elasto-viscoplasticity, the viscoplastic strain rate $\dot{\varepsilon}^{vp}$ is zero if the stress state is inside or on the yield surface. In those cases, the behaviour is elastic. On the other hand, and contrary to elasto-plasticity, the viscoplastic strain rate develops only when the stress state is outside the yield surface F, in which case it can be written as

$$\dot{\varepsilon}^{vp} = \mu\Phi(F)\frac{\partial Q}{\partial \sigma} \tag{7.9}$$

where μ is the fluidity (Venturini, 1983; Pande et al., 1990) or viscosity (Zienkiewicz & Taylor, 1991) parameter which can be adopted either as a constant (e.g. 1 in Pande et al., 1990) or as a variable (Zienkiewicz et al., 1981); $\Phi(F)$ is a monotonic function of the yield function F, sometimes F itself (Pande et al., 1990); and where the rest of the symbols are as explained for Equation (7.2).

A good comparison of the theories of elasto-plasticity and elasto-viscoplasticity was tabulated by Pande et al. (1990). It is worth noting that the concepts of yield function (yield surface), flow rule and hardening rule apply to both of them. However, for the former, the load increments must be small since the state outside the yield surface is not admissible. For the latter, loads need not be applied in small increments unless the elasto-plastic solution is to be obtained as the limit case. Since the problems of elasto-viscoplasticity are time dependent, the appropriate time step should be used. Some useful selection and convergence criteria are given by Venturini (1983).

Examples of viscoplastic material modelling in geomechanics within the finite and boundary element method formulations were presented by Venturini (1983). Plain concrete, subjected to earthquake conditions, was treated by assuming elasto-viscoplastic behaviour in compression and by extrapolating uniaxial test results (Zienkiewicz et al., 1981; Bicanic & Zienkiewicz, 1983). More importantly, the authors have applied their model to concrete gravity dam monoliths. Unfortunately, they have failed to describe the behaviour in tension and correlation between limited tension elasto-viscoplasticity and cracking mechanisms.

7.4 Smeared Cracking

The smeared crack approach is one of the possibilities for representing the fracture of brittle materials such as mass concrete and rock. It is thought to be the simplest to implement into finite element computations because it is based on the concepts of continuum mechanics and the description of cracking through nonlinear constitutive relations.

7.4.1 Basic Smeared Crack Model

Prior to cracking, the material is usually considered as isotropic and linear elastic. For each time step, the principal stresses are monitored either in every element integration point or averaged for the whole element. For this model, cracking occurs when the maximum principal stress exceeds the tensile strength of the material. Although the cracks are not dimensionally present in the finite element mesh (i.e. their length or width cannot be observed or known), it is assumed that they are straight and perpendicular to the direction of the maximum principal stress. Furthermore, since all the calculations are done for the integration points only, the precise crack location is not known, necessitating the assumption that cracking is evenly distributed (smeared) throughout the element.

Immediately after cracking, the so far isotropic material model is replaced by an anisotropic constitutive model. This model with practically zero stiffness normal to the crack and possible shear transfer across the crack can be expressed in the local coordinate system as

$$\begin{Bmatrix} \Delta\sigma_n \\ \Delta\sigma_t \\ \Delta\tau_{nt} \end{Bmatrix} = \begin{bmatrix} 0 & 0 & 0 \\ 0 & E & 0 \\ 0 & 0 & \eta_s G \end{bmatrix} \begin{Bmatrix} \Delta\varepsilon_n \\ \Delta\varepsilon_t \\ \Delta\gamma_{nt} \end{Bmatrix} \tag{7.10}$$

where Δ denotes the incremental values, n the direction normal to the crack, t the tangential direction (aligned with the crack); and where E is the modulus of elasticity; G is the shear modulus; and η_s is the shear retention (or shear stiffness reduction) factor. The vectors on the lefthand and righthand side of (7.10) represent the incremental stress and strain vectors, respectively. Originally, it was thought that the retention of some shear capacity ($\eta_s G$), can simulate aggregate interlock and can help with the prediction of subsequent cracks, nonorthogonal to the initial one (Norman & Anderson, 1985).

Among many implementations of the basic smeared crack model into nonlinear finite element codes, only two are mentioned here. Bathe and Ramaswamy (1979) incorporated the model into ADINA, calling it the ADINA Concrete model (ADINA Engineering, 1984), while Greeves (1991) did the same for NONSAP (Bathe et al., 1974). The former model had many other useful features: taking into account multiaxial stress conditions and failure surfaces in tension and compression, a possibility of compression crushing and strain softening in compression, etc. Mlakar (1987) used this model when investigating nonlinear earthquake response of concrete gravity dams on rigid foundations. Although his work showed very important effects of concrete gravity dam cracking, the main drawbacks of the basic smeared crack model became obvious.

First, the model is not able to localise the cracked zones following the crack tip. The cracks are spread over several elements in width, causing so-called diffusion of cracking. Second and more important, the model is mesh dependent. Since the tensile strength of the material is the only criterion for the inititation and propagation of cracking, as soon as a crack in an element has initiated; the load required to propagate it further to the surrounding, so far uncracked elements, depends on the size of the cracked element. The smaller its size, the smaller the load required for crack propagation. In other words, the use of coarse finite element meshes might overestimate the energy that causes fracture, which is not on the safe side.. Although

remedies such as reduction of the tensile strength may help, being as arbitrary as they are, they do not provide a clear answer to this problem.

Another phenomenon, somewhat related to the abovementioned diffusion of cracking, is stress locking. When comparing smeared and discrete crack models, Rots (1991) realised that for the former model, spurious tensile stresses remained locked-in at either side of the already separated crack. He also discovered that the phenomenon was irrespective of the mesh fineness and element type, concluding that the explanation probably lies in the finite element displacement compatibility, inherently assumed in all smeared crack models and analyses.

7.4.2 Smeared Crack Band Model

Clearly, the mesh dependence of the basic smeared crack model, as discussed above, is a major flaw. One way of avoiding this problem was formulated by Bazant and Cedolin (1979). In addition to the tensile stress or strain cracking criterion, they introduced a fracture mechanics criterion based on the energy needed for crack extension. Their model was called the crack band model because it enforced the preservation of energy of the propagating band of smeared cracks. This preservation of energy can also be associated with the phenomenon of strain softening in tension.

7.4.2.1 Some Crack Band Models

Based on the original idea, different variations of the crack band model were suggested. Vargas-Loli & Fenves (1989) incorporated one of them into their own nonlinear finite element code. A somewhat modified version was reported by El-Aidi & Hall (1989). Both pairs of authors investigated nonlinear earthquake response of concrete gravity dams on rigid foundations, and both claimed to have eliminated mesh dependence. On the other hand, diffusion of cracking either remained a problem (Vargas-Loli & Fenves, 1989), or was eliminated by user interaction and

decision-making at every iteration (El-Aidi & Hall, 1989). In the latter case, stress locking was also observed and attributed to the viscous damping mechanism which was chosen linearly proportional to the linear elastic stiffness matrix. The mass proportional term was omitted with the argument that it provides artificial stability to the portion of the dam above the crack. Consequently, any damping was removed from elements after cracking.

7.4.2.2 The Improved ADINA Concrete Model

The main purpose of this work is to show how limited tension (cracking) numerical procedures can be incorporated into nonlinear concrete gravity dam-foundation interaction problems, and not to evaluate their relative quality. Drawing conclusions from the above overview, it seems that sufficiently good results may be obtained by using the crack band (strain softening) model, provided that the internal viscous damping mechanism is handled properly (El-Aidi & Hall, 1989; Bhattacharjee & Léger, 1993).

As explained in Subsection 7.4.1, the original basic smeared crack ADINA Concrete model was mesh dependent and therefore not entirely satisfactory. However, the model was considerably improved (Bathe et al., 1989) and implemented into later versions of the finite element code ADINA, from where it was inherited by the latest version of the finite element code SOLVIA (SOLVIA Engineering AB, 1992). Since SOLVIA will be the main computational tool in Chapters 8 and 9, the main features of the model will be presented now, particularly emphasising the improvements regarding tensile cracking and strain softening.

The improved ADINA Concrete material model is based on a uniaxial stress-strain relation, whose tensile part is shown in Figure 7.6. Multiaxial stress conditions and failure surfaces in tension and compression are taken into account. A great advantage of the model is that it can be used for both mass concrete and rock.

According to what has been said earlier, the behaviour of concrete gravity dam-foundation systems in compression is largely linear elastic and the compression parameters of the model must be calibrated appropriately. Apart from the standard mechanical properties (modulus of elasticity at zero strain, Poisson's ratio and mass density), the data defining the uniaxial stress-strain curve in compression are:

σ_c - the uniaxial maximum compressive stress (negative)

ε_c - the uniaxial compressive strain at σ_c (also negative)

σ_u - the uniaxial ultimate compressive stress (negative)

ε_u - the uniaxial compressive strain at σ_u (also negative)

For the definition of the compression failure envelopes of the material, the ratio β between principal stresses σ_{p2} and σ_{p3}, together with 24 discrete stress values is used (Bathe et al., 1989; SOLVIA Engineering AB, 1989/92):

σ_{p11}, σ_{p12}, σ_{p13}, σ_{p14}, σ_{p15}, σ_{p16},

σ_{p311}, σ_{p321}, σ_{p331}, σ_{p341}, σ_{p351}, σ_{p361},

σ_{p312}, σ_{p322}, σ_{p332}, σ_{p342}, σ_{p352}, σ_{p362},

σ_{p313}, σ_{p323}, σ_{p333}, σ_{p343}, σ_{p353}, σ_{p363}

where the first row represents the six ratios σ_{p1}/σ_c for which the discrete two-dimensional failure envelopes for additional stresses σ_{p2} and σ_{p3} are input. These envelopes are then given by the six failure stress values σ_{p3}/σ_c for the stress magnitudes $\sigma_{p2}=\sigma_{p1}$ (second row), $\sigma_{p2}=\beta\sigma_{p3}$ (third row) and $\sigma_{p2}=\sigma_{p3}$ (fourth row).

In tension, failure occurs when the tensile stress in a principal stress direction exceeds the tensile failure stress. Under uniaxial conditions (Figure 7.6), after reaching the uniaxial cut-off tensile stress σ_t, linear strain softening begins: as the strain increases from ε_t to $\kappa\varepsilon_t$, the stress decreases to zero value. The strain softening mechanism preserves the fracture energy of the material, G_f, by equating it to the area under the lines

$$\frac{\kappa \varepsilon_t \sigma_t}{2} l = G_f \tag{7.11}$$

where l is the characteristic length of the finite element. Equation (7.11) actually eliminates the mesh dependence of this numerical model. Different values of the fracture energy of dam concrete have been suggested and used: G_f = 75 N/m (Vargas-Loli & Fenves, 1989), G_f in the range of 150 and 250 N/m (Linsbauer, 1990), G_f = 150 N/m (Bhattacharjee & Léger, 1993), experimental values of 175, 235 and 257 N/m (Brühwiler & Wittmann, 1990), etc. Once the fracture energy of dam concrete and rock is known or adopted, two computational procedures can be recommended:

a) If the finite element mesh is predetermined, the strain softening parameter κ is obtained from equation (7.11).

b) If the strain softening diagram is known for the concrete under investigation, and may be approximated with linear strain softening mechanism (as in Figure 7.6), the finite element mesh is designed according to Equation (7.11).

The normal stiffness reduction factor following tensile failure is η_n. Although its value is practically zero (the top left element of the constitutive matrix in Equation (7.10)), a non-zero value is usually adopted to avoid numerical instability. The shear stiffness reduction factor is η_s.

Of course, all the presented material data may be corrected to take into account strain-rate effects due to dynamic, earthquake loading. This is usually done through the dynamic magnification factor. Bhattacharjee & Léger (1993) have used the value of 1.20 (i.e. 20 per cent magnification due to dynamic effects).

7.4.3 Coaxial Rotating Smeared Crack Model

The models treated in Subsections 7.4.1 and 7.4.2 were all based on the fixed single smeared crack concept. For a particular point, this means that the crack direction is

set (fixed) at the first moment for which the maximum principal stress exceeds the tensile strength of the material. Subsequent loading can cause cracking only in the direction perpendicular to the first one.

In reality, however, it is more likely that the subsequent loading will cause tensile principal stresses in some other directions, i.e. that the axes of principal stress will rotate after the formation of the initial crack. Therefore, the introduction of many nonorthogonal cracks at the same point is required. This approach, called the fixed multidirectional smeared crack concept (Rots, 1991), comprises of new crack initiations whenever the angle of inclination between the existing cracks and the current direction of the principal stress exceeds a certain angle.

For static loading and for the allowable angle of inclination equal to 0, Rots (1991) developed a limiting case of the previous concept. Since the angle is 0, the principal stress axes rotate continuously after the initial cracking has occured. As opposed to the fixed concept (both single and multidirectional), where an explicit shear capacity term is defined for every fixed plane of cracking (Equation (7.10)); the new concept requires an implicit shear term which would enforce the continuous coaxiality of principal stress and strain. For his simple static examples, Rots (1991) concluded that the fixed single crack concept is too stiff and that the best results are achieved when using the coaxial rotating concept or the fixed multidirectional concept with negligible shear retention factors η_s. The stress locking effects were present in all three approaches. Since the examples were static, there was no viscous damping to influence this phenomenon.

Bhattacharjee and Léger (1993) have applied the coaxial rotating smeared crack model when investigating the seismic cracking of gravity dams on rigid foundations. The authors argued that the unfavourable characteristics of the simpler smeared crack models (mesh dependence, diffusion of cracking, stress locking) can be eliminated by following their approach and by carefully choosing the viscous damping mechanism. The latter was taken as time dependent and linearly proportional to the nonlinear

stiffness matrix. The mass proportional term was omitted once again. It is interesting to note that when the damping was changed to be linearly proportional to the linear elastic stiffness matrix, considerable crack diffusion was noted. This finding corroborates the fact that the material viscous damping mechanism is the main reason for diffused crack patterns. Therefore, if material damping is handled appropriately, the smeared crack band model (e.g. the improved ADINA Concrete model) might be as successful as the more complicated coaxial rotating smeared crack model.

7.5 Discrete Cracking

The discrete crack approach is another possibility for representing the fracture of brittle materials such as mass concrete and rock. When a criterion for initiation or further propagation of cracks is satisfied, the elements are physically separated. Since such an approach does not correspond to the continuum mechanics nature of the standard displacement finite element formulation, computationally expensive remeshing for each crack configuration is necessary.

Probably the main advantage of the discrete representation of fracture is that it does not suffer from stress locking (Rots, 1991) and that the precise crack geometry can be easily determined by following the interelement path. In that sense, the discrete crack approach resembles the formulation of joint (interface) elements, which are typically used for describing contact nonlinearities. While both approaches treat the problem as a discontinuum, the cracks in the joint element formulation are predefined at the place whose location is based on the analyst's judgement (e.g. dam-foundation interface).

Similarly, in what was probably the first application of the discrete crack approach to statically loaded concrete structures (Ngo & Scordelis, 1967), the location of the

cracks was predetermined. With the improvement of the model, this requirement was abandoned and cracking criteria were introduced. Building on the concepts of discrete cracking, Skrikerud & Bachmann (1986) developed a procedure for dynamically loaded, unreinforced concrete structures, incorporating the conditions for initiation, extension, closure and reopening of cracks, as well as the possible stress transfer due to aggregate interlock. Assuming a rigid foundation, they applied their model to the seismic analysis of Koyna dam.

According to the present developments in this area, the future of the discrete crack model is seen in combinations with the fracture mechanics approach.

7.6 Fracture Mechanics Approach

Fracture mechanics (Broek, 1978) is a vast subject and only some aspects relevant to the numerical modelling of concrete and rock for the purpose of analyses of dam-foundation systems will be mentioned here.

Rather than dealing with stress or strain-based criteria, fracture mechanics treats the crack propagation by concentrating on the energy considerations and stress intensity factors. By not putting standard engineering values (displacement, stress) in the forefront, the applications of fracture mechanics in dam engineering did not gain much popularity until recently, when an ongoing debate was initiated (Bazant, 1990; Gioia et al., 1992; Tardieu & Londe, 1992; Bazant, 1993). Furthermore, most of the work has been done for static and monotonic loading conditions, requiring further efforts in the area of dynamic (seismic) loading.

Two approaches are usually considered: linear elastic fracture mechanics (LEFM) and nonlinear fracture mechanics (NLFM). The choice between the two largely depends on the fracture process zone, which is the zone where the cracking currently occurs. Gioia et al. (1992), without quoting the type of loading, were of the opinion

that for dam concrete it suffices to use the LEFM because the fracture process zone (roughly the size of the aggregates, approximately 0.2m) is small compared to the size of the whole structure. On the other hand, Bhattacharjee & Léger (1993) claimed that nonlinear behaviour in the fracture process zone is always significant for concrete normally used in dams. They further specified that neglecting this nonlinearity (i.e. using the LEFM) is adequate for very slowly applied loads on one side and for impulsive loads on the other side. In the intermediate range, for quickly applied loads and seismic loads, the NLFM is more appropriate.

An interesting comparison between the no-tension plasticity model (Section 7.3) and LEFM approach was made for the case of Koyna dam with rigid foundation conditions under increasing hydrostatic pressure (Gioia et al., 1992). The main conclusion was that the no-tension analysis is not guaranteed to be always safe, as taken for granted for so many years.

Probably the first combination of the fracture mechanics approach and two cracking models (Sections 7.4 and 7.5, respectively) was the introduction of the smeared crack band model, where a simple energy criterion (Equation (7.11)) was added to help eliminate the mesh dependence of the basic smeared crack model. Later, Chapuis et al. (1985) used the LEFM approach in a hybrid smeared-discrete crack model of Pine Flat dam on the rigid foundation. Droz (1987) used the LEFM propagation criterion in conjunction with smeared cracks based on the discontinuous finite element shape functions. In this way, he discretised the smeared crack model, making it conceptually closer to the discrete crack approach. Finally, Ayari & Saouma (1990) applied the LEFM approach to the discrete seismic crack model of Koyna dam on the rigid foundation. As for the application of NLFM models in cracking analyses of concrete dams, only a few papers have so far been accepted for publication (Bhattacharjee & Léger, 1993).

7.7 Concluding Remarks

One of the essential prerequisites for carrying out a valid nonlinear (static and/or dynamic) concrete dam-foundation interaction analysis by means of numerical finite element modelling is to describe correctly the behaviour of the materials under consideration (mass concrete and rock). After the detailed discussions in the previous sections, several aspects deserve to be emphasised and clarified:

a) The most important common property of the two materials is their ability to withstand relatively high compressive stresses but only low tensile stresses.

b) One of the major differences between concrete and rock is that the latter exists long before the structure. Consequently, the rock has substantial loading history which is registered in the form of initial stresses whose distribution can be either measured or assumed. These stresses should be accommodated to represent the starting point for any combined dam-foundation interaction analysis.

c) Without being much mistaken, it may be assumed that the behaviour of mass concrete and rocks in compression is linear elastic. This holds for both static and dynamic (earthquake) conditions. Extensive testing and experimenting on cyclic loading of mass concrete is required before more complicated numerical models are recommended. Due to exclusive dependency on the site location, such an approach cannot be followed in the case of rocks, where significant investigations can be undertaken only once the future dam site is chosen.

d) Only nonlinear models can successfully describe the behaviour of dam concrete and rock in tension, the so-called limited tension behaviour. When the tensile strength is negligible, a special case of no-tension behaviour arises. The limited tension behaviour of mass concrete and rocks can be modelled in two ways. The first is to adopt either the limited tension elasticity or limited tension plasticity

approach. The second way is to deal with rock and concrete by emphasising their brittleness and by examining their possible fracture scenarios. This is typically done by using one or more of the three concepts: smeared cracking, discrete cracking and fracture mechanics criteria.

e) If applied properly, limited tension elasticity and limited tension plasticity may perform well in cracking analyses of dam-foundation systems under static loading. The solution is obtained either through iterations (path independent limited tension elasticity) or incremental analysis (path dependent limited tension plasticity). Of course, the choice of a yield function with adequately limited behaviour in tension is assumed in the latter case. However, for dynamic loading, there are some problems that require special attention. At the yield load, plastic strain increments are generated instantaneously and progress of yielding is simultaneous (nonpropagating) at all points of the endangered area. Once the plastic flow has occured, the system cannot reconstitute itself. To the contrary, in reality, the damaged (cracked) region can be reconstituted under earthquake loading because the cracks may close upon the reapplication of the sufficiently high compressive stresses. In other words, although the phenomena such as crack opening and crack propagation are similar to limited tension plastic yielding in a sense that they both describe some kind of damage due to limited tension behaviour, it is not possible to model probable subsequent cyclic crack closure and reopening with the latter. In an attempt to apply the elasto-perfect plastic material model for the soil in the earthquake soil-structure interaction analysis (Toki & Miura, 1983), it was noted that the damaged (plastified) region had progressed further and further with every time step. This behaviour may indeed be justifiable for truly 'plastic' materials such as soils, but is certainly not appropriate for predominantly 'brittle' materials such as rocks and mass concrete. Therefore, the main conclusion is that limited tension plasticity

models are not convenient for expressing the dynamic tensile behaviour of rock and concrete.

f) The smeared cracking method is a very useful representation of the fracture of dam-foundation systems. Unfortunately, only dams on rigid foundations have been treated so far. The standard drawbacks of the original procedure (mesh dependence, crack diffusion and stress locking) can be circumvented to some extent by adding energy based criteria for cracking and by controlling the internal viscous damping of the system.

g) The discrete cracking method requires constant finite element remeshing.

h) Particularly in the past ten years, the concepts of linear elastic fracture mechanics have found their application in the cracking analyses of concrete dams. They were considered on their own and in combination with smeared and discrete crack models. The application of fracture mechanics to the coupled dam-foundation systems would be much more difficult, primarily because of the enormous versatility of rocks and broad variation of their numerous parameters.

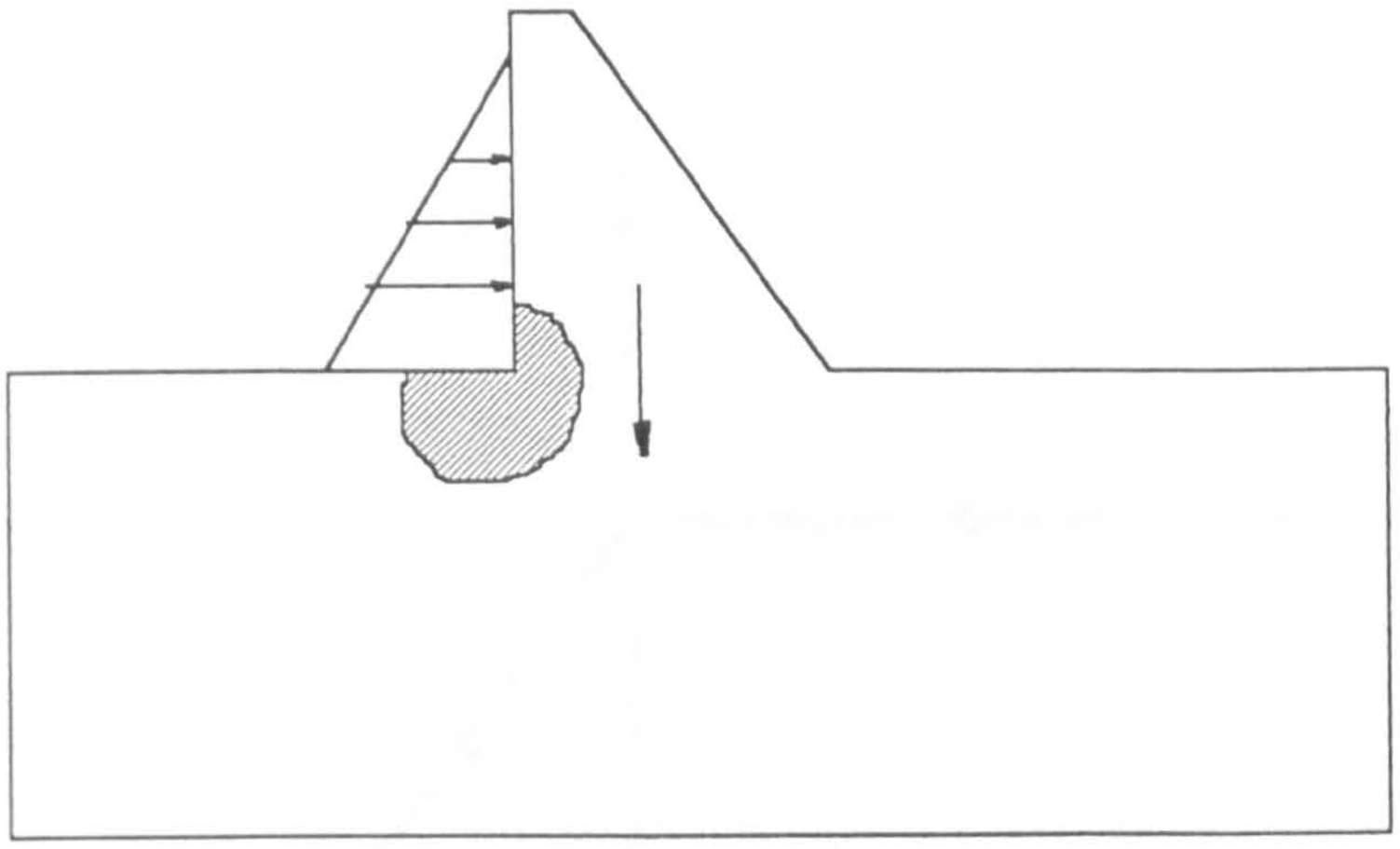

Figure 7.1a - Initial tensile region of the dam-foundation system

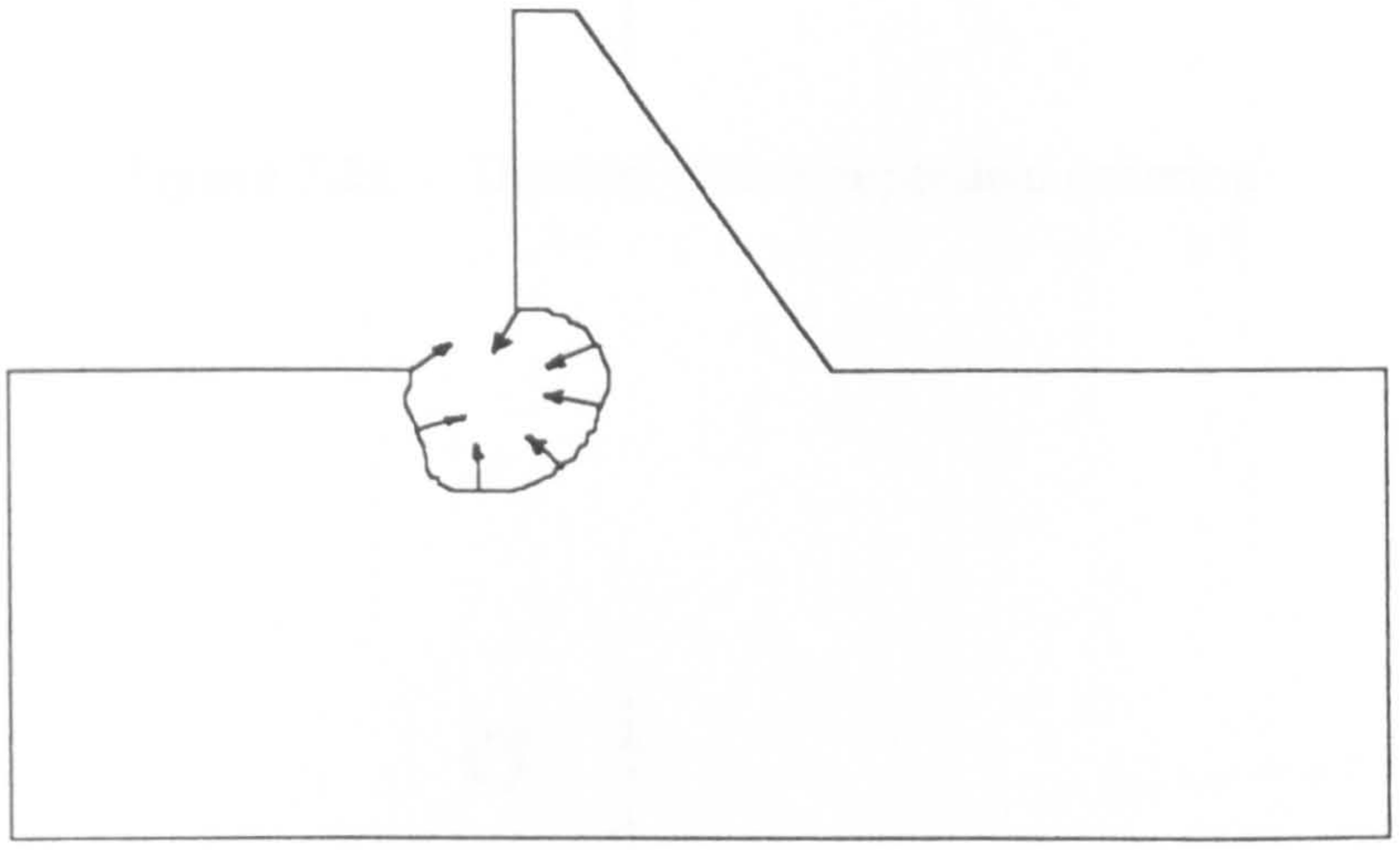

Figure 7.1b - Elimination of tensile stresses

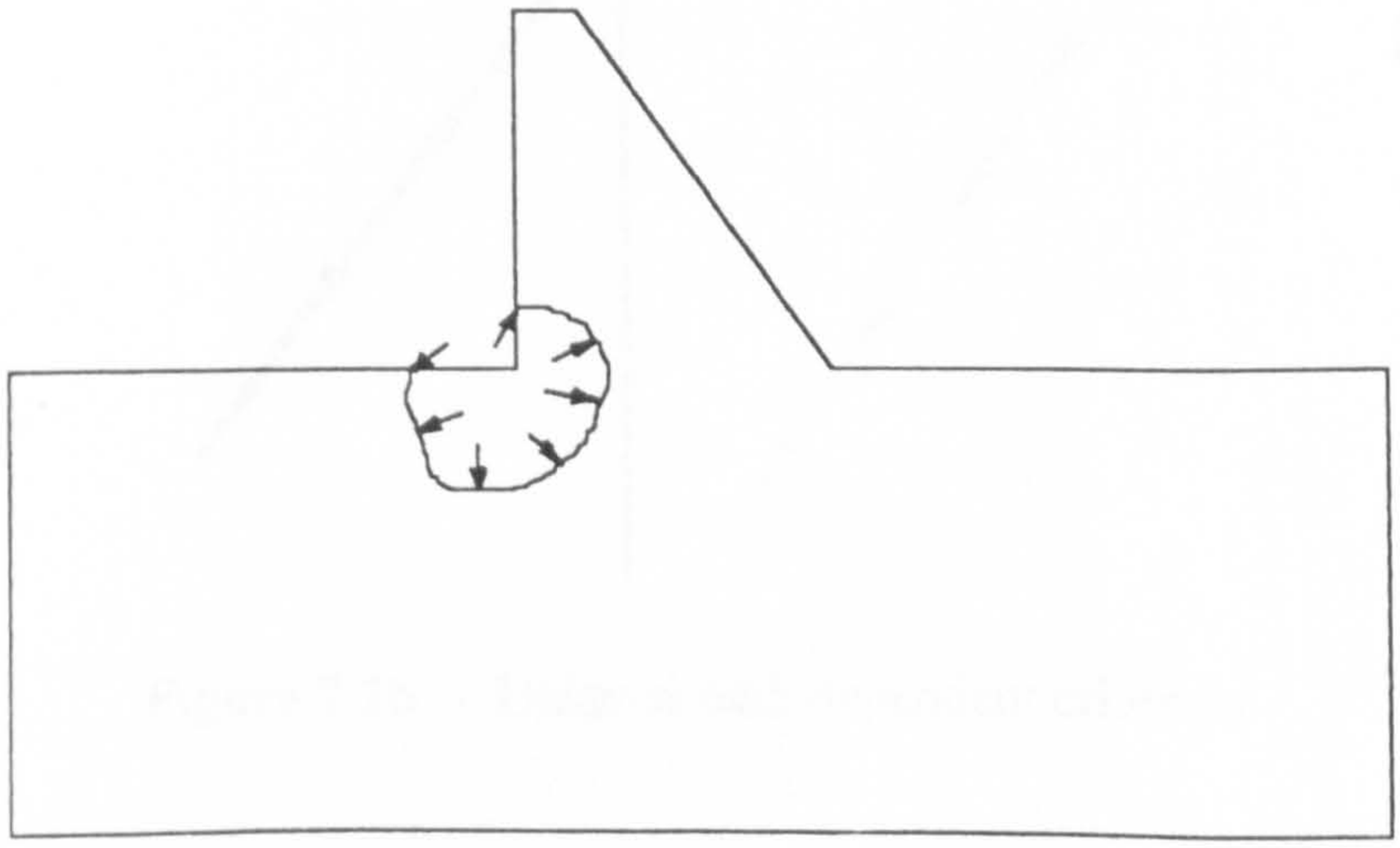

Figure 7.1c - Reanalysis of the system

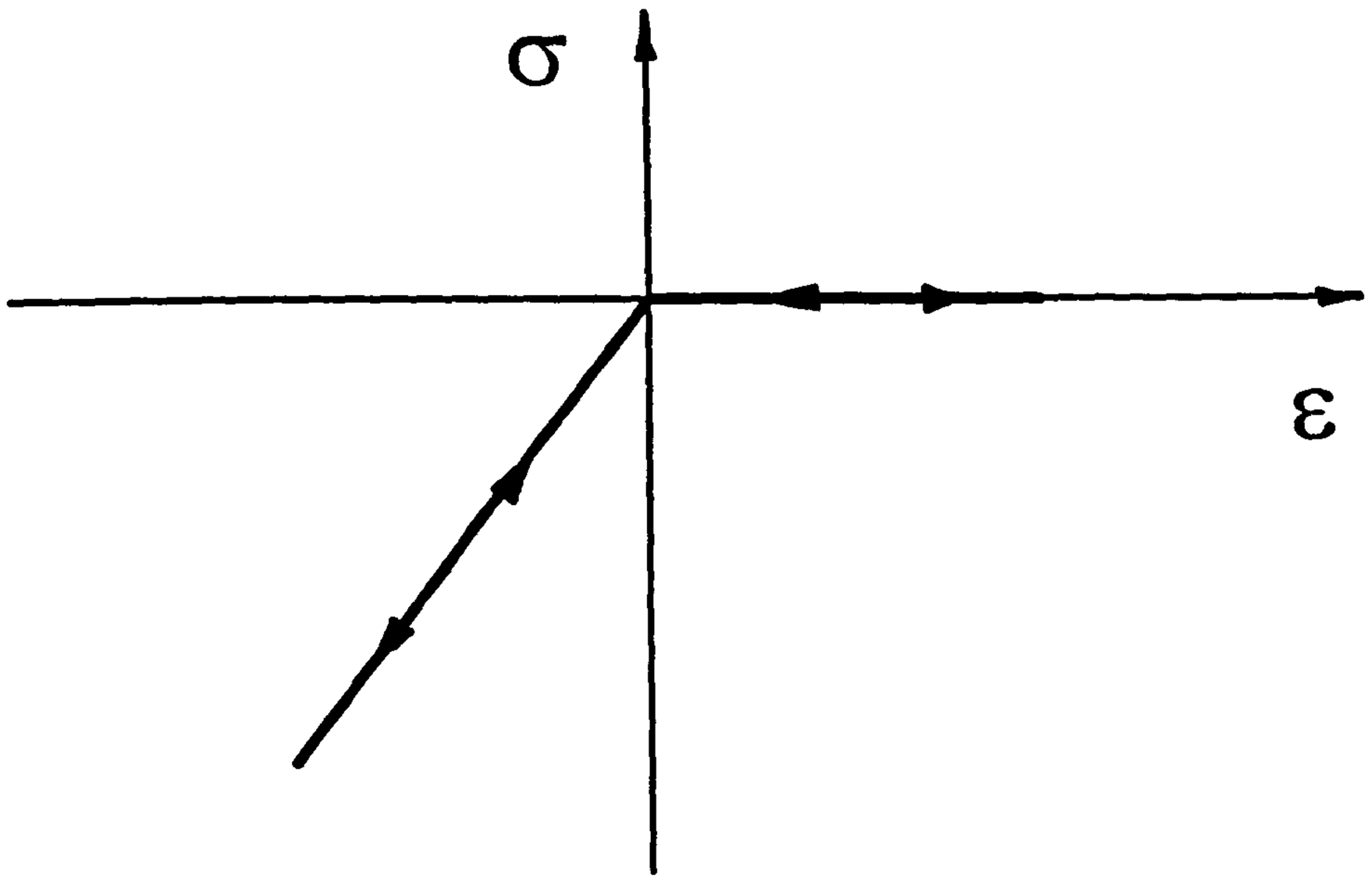

Figure 7.2a - Uniaxial path independent criterion

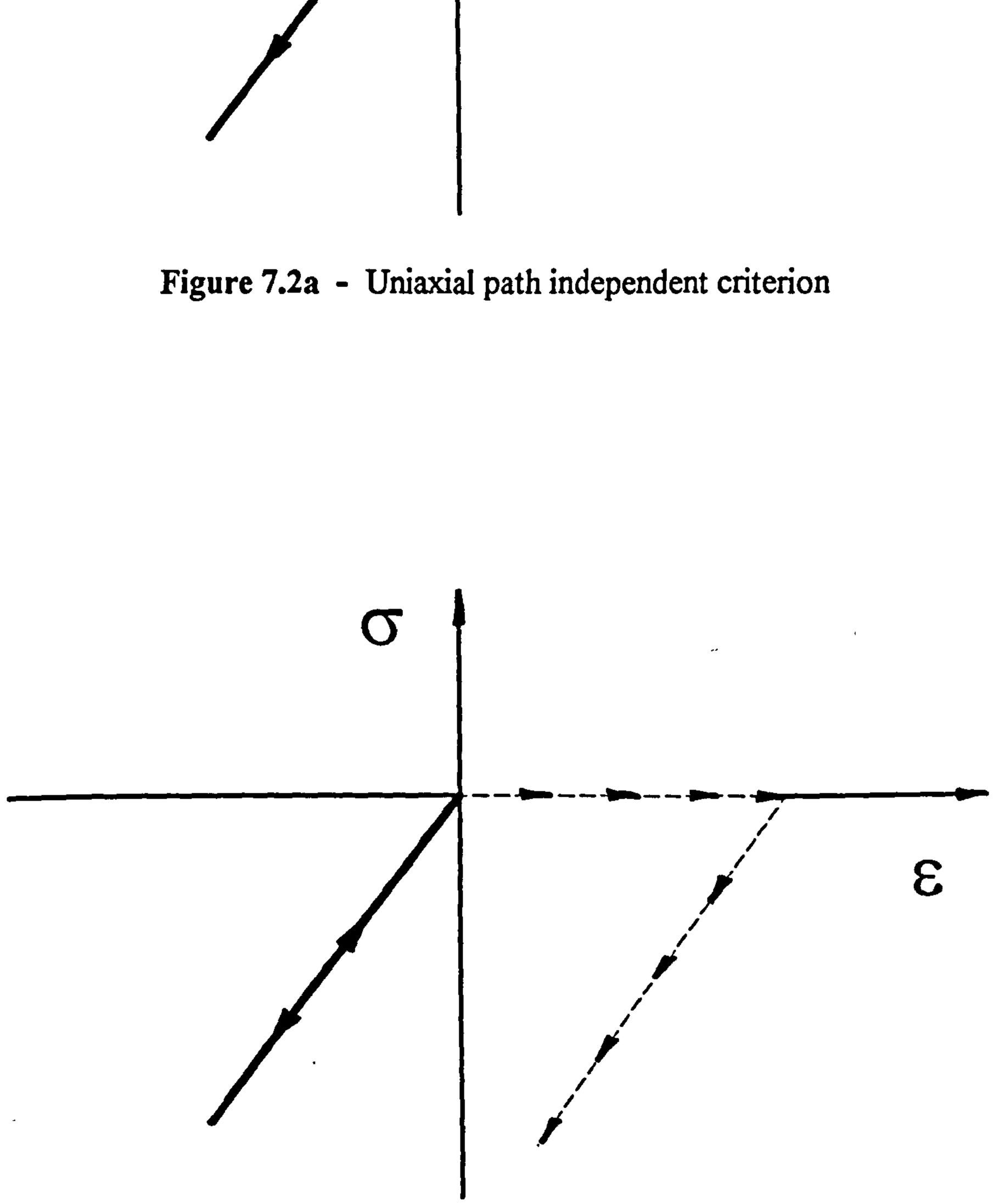

Figure 7.2b - Uniaxial path dependent criterion

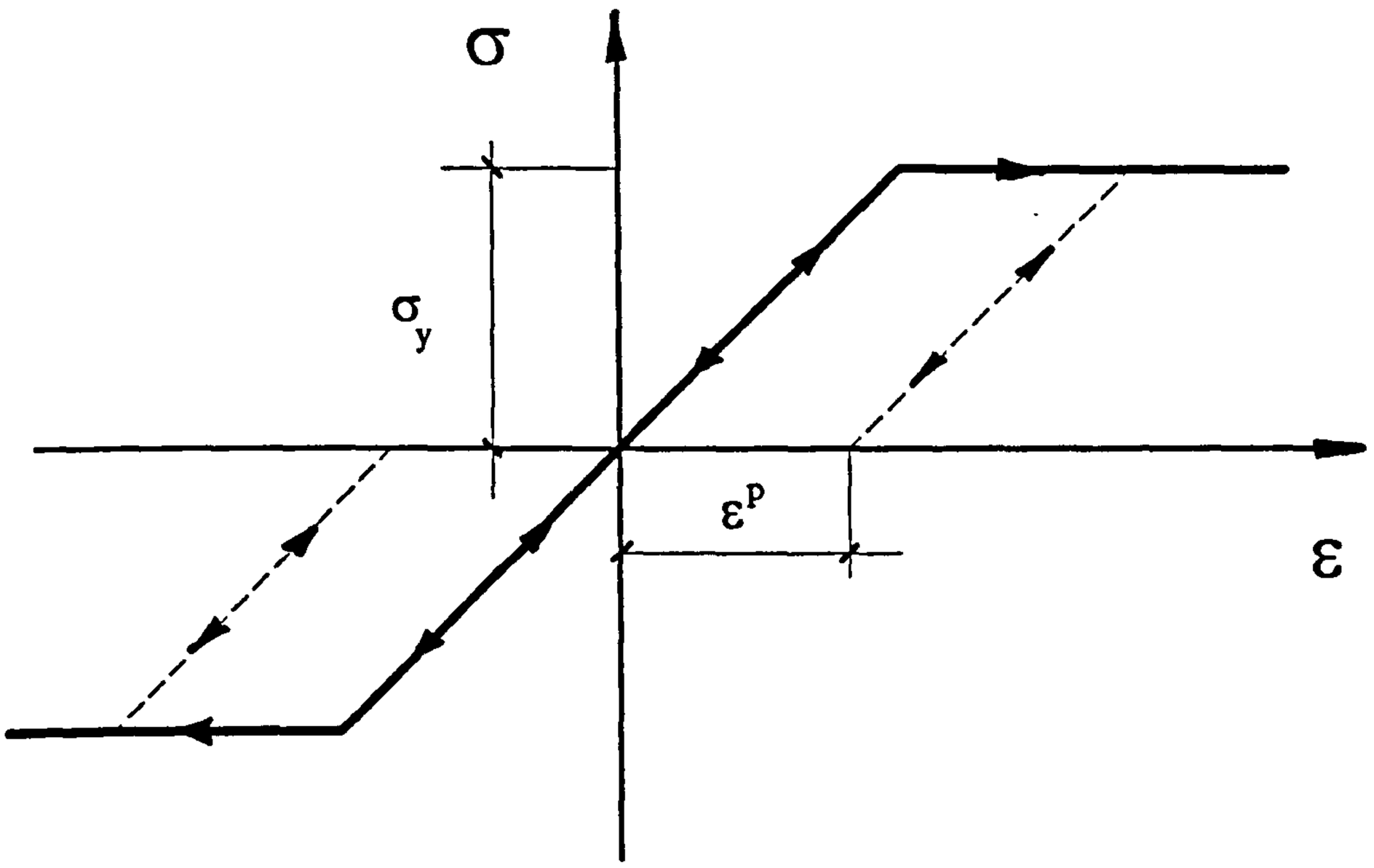

Figure 7.3a - Uniaxial elasto-perfect plastic behaviour

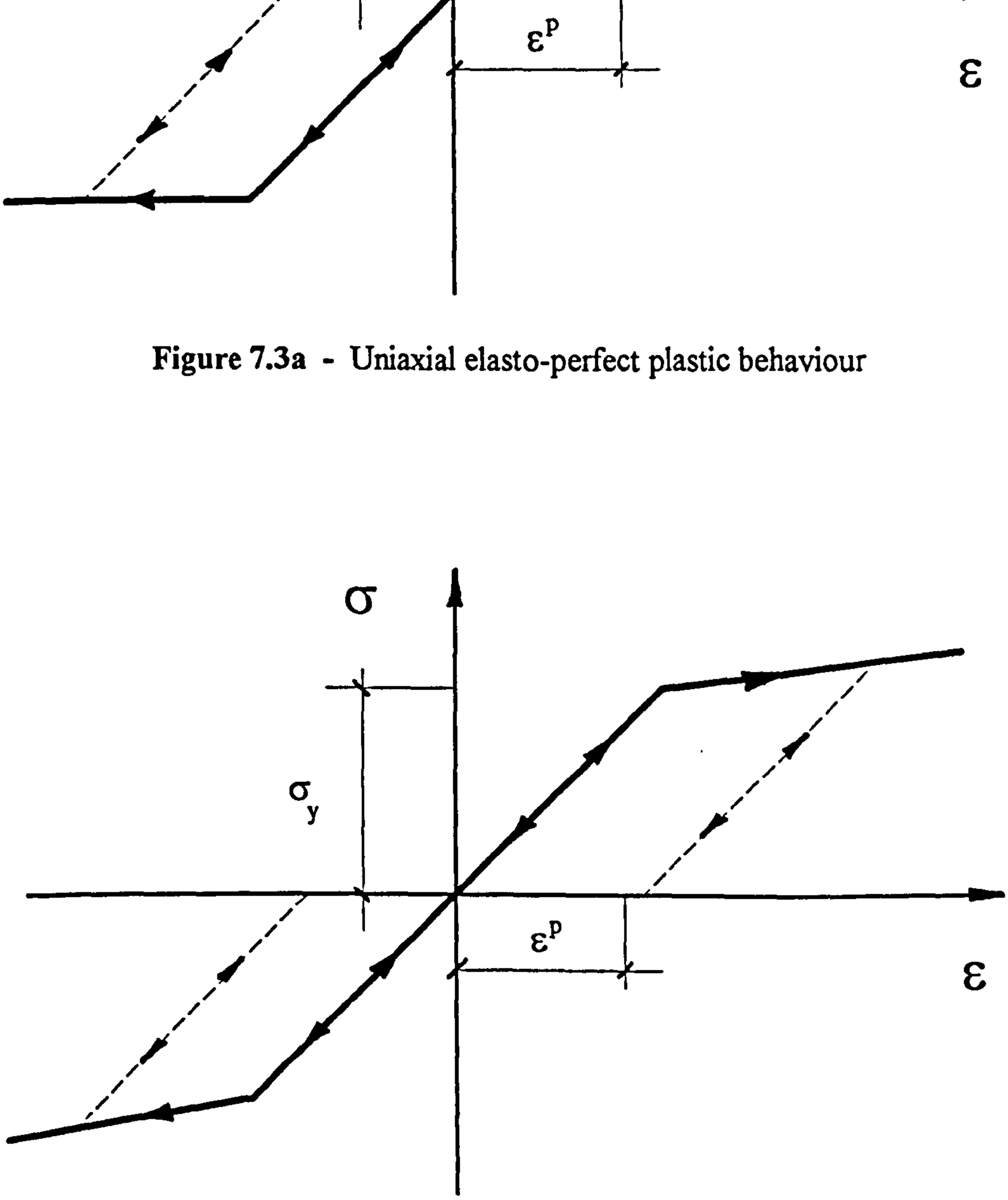

Figure 7.3b - Uniaxial elasto-plastic behaviour with hardening

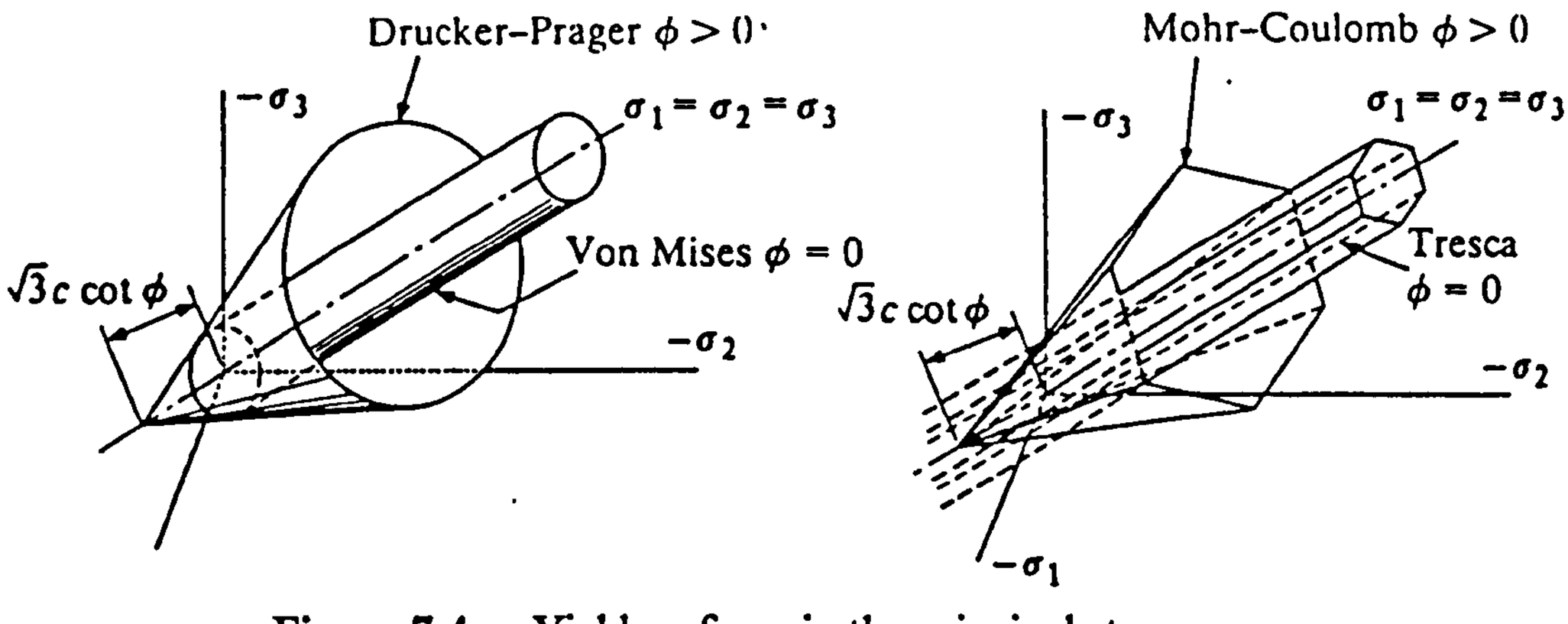

Figure 7.4 - Yield surfaces in the principal stress space

(Zienkiewicz & Taylor, 1991)

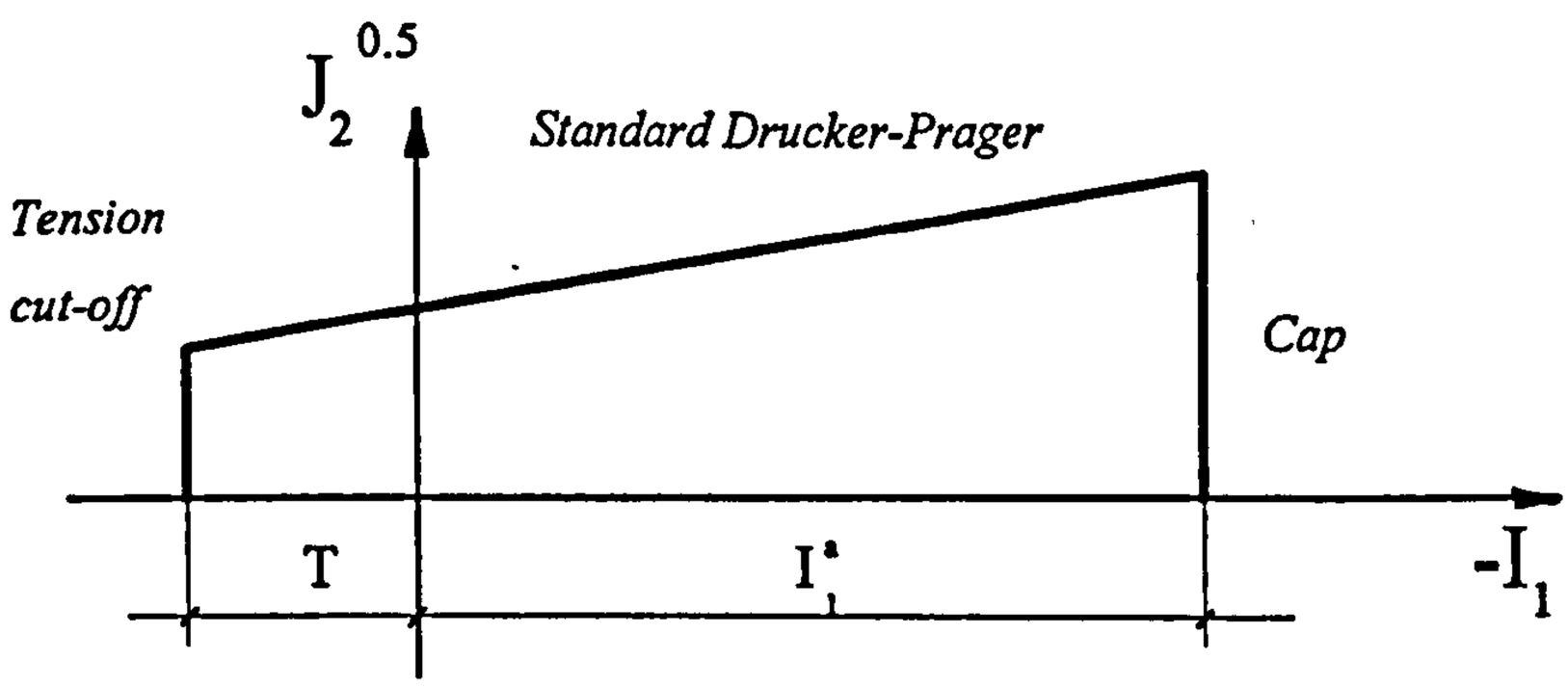

Figure 7.5 - Improved Drucker-Prager yield surface in the stress invariant plane

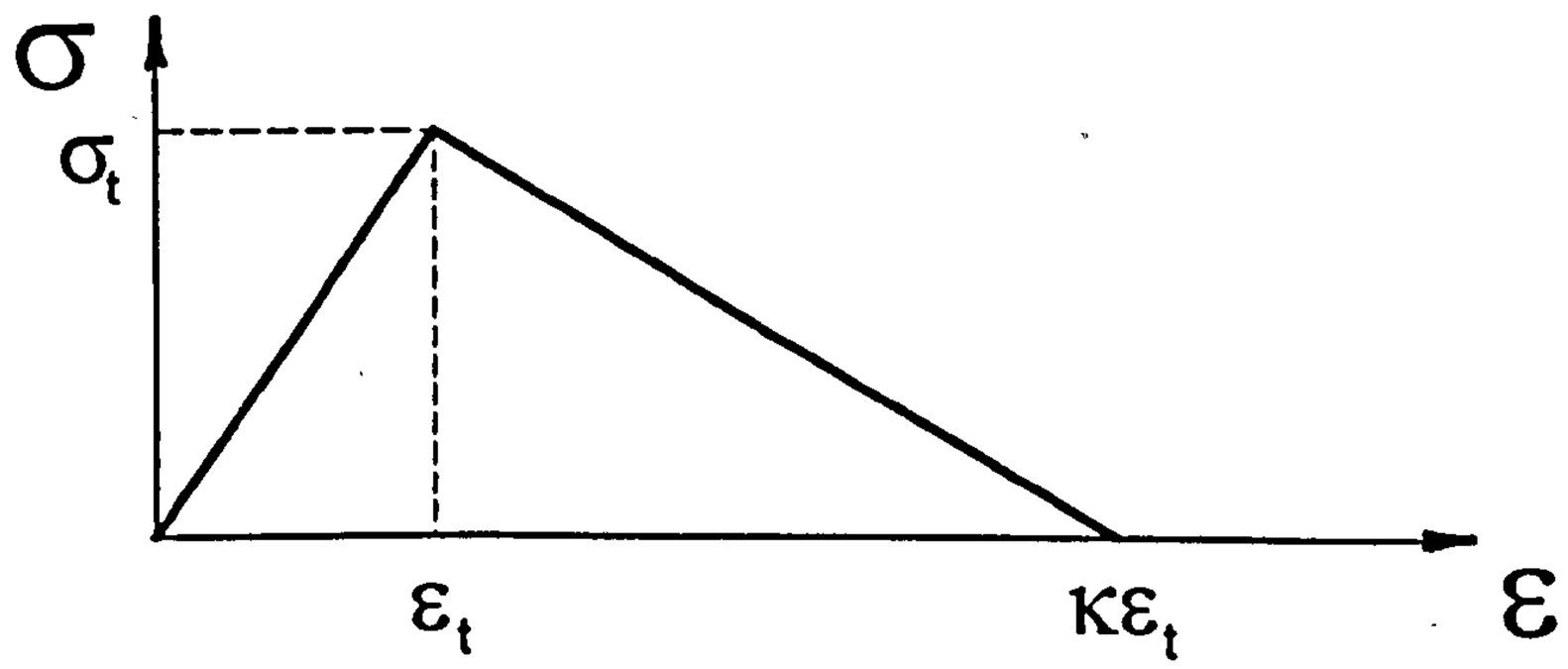

Figure 7.6 - Strain softening for the ADINA concrete model in uniaxial tension

Nonlinear Static Analyses of Concrete Gravity Dam-Foundation Systems

Under normal loading conditions, the behaviour of concrete gravity dam-foundation systems designed according to standard procedures can be described by a linear elastic material model. The nonlinear behaviour is expected only under extreme loading conditions. Typical nonlinearities which may develop were mentioned and classified in the previous Chapter. Different analytical formulations for the limited tension nonlinearities were emphasised.

The load level required to induce nonlinear behaviour is usually caused either by increased static loading or by earthquake loading. While the latter will be investigated in the next Chapter, the former will be treated in this one. The loading will be provided by continuously increasing the reservoir water level, as in the case of dam overflow. Two basic foundation conditions will be examined: rigid and flexible.

At first sight, the nonlinear static behaviour is not relevant to the nonlinear earthquake behaviour of concrete gravity dam-foundation systems. Nevertheless, apart from offering a deeper, general understanding about these systems, the importance of this Chapter is twofold. First, it serves as a calibration test for the numerical models presented in Chapter 7; and second, by carrying out static nonlinear analyses until collapse, different modes of failure can be identified, which facilitates their recognition in the more complicated, dynamic analyses of Chapter 9.

All the analyses were performed using the finite element code SOLVIA (SOLVIA Engineering AB, 1989/92).

8.1 Rigid Foundation

The rigid foundation case implies that the foundation is much more (infinitely) stiffer than the dam. In reality, this is seldom true and this model is therefore regarded as the upper limit for the behaviour of dams on flexible foundations. After the summary about the model, the results and conclusions will be presented.

8.1.1 Assumptions and Explanations

The important assumptions and explanations relevant to the numerical modelling of concrete gravity dams on rigid foundations are summarised here.

8.1.1.1 Geometry of the Dam

It was assumed that the dam is in the state of plane strain and that the dam-foundation interface is flat and at the ground level. Rigid foundation conditions were imposed by restraining horizontal and vertical displacements at the interface level. The dam was of idealised geometry, 50m high, with the width of 40m at the interface and 5m at the top. It was modelled with 25 rows and 10 columns of 4-noded isoparametric elements, totalling to 250 finite elements in the dam (Figure 8.1). This simplified and idealised geometry was deliberately chosen to avoid possible nonlinearites at the neck of the dam, usually due to a change in the downstream slope of the dam. With the present geometry, the nonlinearities were bound to occur around the foundation interface.

8.1.1.2 Loading of the Dam

The loading of the dam comprised the dead weight (taken as mass-proportional loading) and upstream hydrostatic pressure (taken as element pressure loading) which

increased in 7 load increments from 20m below to 50m above the crest of the dam. Although such a loading scenario is not realistic (overflowing of the dam equal to the height of the dam), it provided sufficient horizontal force for the initiation and propagation of limited tension nonlinearities.

8.1.1.3 Material Models

Three different formulations were used for material modelling of mass concrete of the dam: linear elastic, limited tension plasticity and smeared cracking. Since the two latter formulations are nonlinear, it was reasonable to expect that their responses would be substantially different from the first one. Nevertheless, a comparison of all three formulations is very useful because the linear elastic solution represents a lower limit for the nonlinear analyses.

Linear elastic model

The linear elastic model was used for the dam analyses in Chapter 6 and it suffices here to state only its main properties. The modulus of elasticity of the dam was E_d=20 GPa, Poisson's ratio was μ_d=0.20, and mass density was ρ_d=2450 kg/m^3.

Limited tension plasticity model

Strictly speaking, mass concrete is a brittle material rather than elasto-plastic. However, it was mentioned in Chapter 7 that limited tension plasticity models may be used for modelling the expected fracture of mass concrete, provided that they are interpreted as damage models. The yield function controls the inititation and extention of damaged zones which may be interpreted as zones susceptible to cracking. Here, the ADINA improved Drucker-Prager model, described in Paragraph 7.3.1.2, was used. The yielding parameters were set in a way which guaranteed linear elastic behaviour in compression (inside the failure surface) and nonlinear behaviour only in tension. In order to investigate its influence on the

nonlinear phenomena, the tensile strength σ_t of the dam concrete was varied and given values of 2, 1, 0.5 and 0.2 MPa.

The basic properties of the model were equal to those of the linear elastic model and remained unaltered for all the analyses:

E_d=20 GPa μ_d=0.20 ρ_d=2450 kg/m³

The parameters for the definition of the cap yield function (Subsection 7.3.1) were also unaltered for all the analyses. By setting W to -0.1 and D to -1, it was ensured that the position of the compression cap throughout the analyses remained very close to its initial position of I_1^a=-20 MPa. On the positive part of the first stress invariant axis, the tensile cap (tension cut-off limit) was set to T=20 MPa, which meant that the yielding was fully governed by the standard Drucker-Prager yield cone.

The definition of the standard Drucker-Prager yield function, given by Equation (7.5), depends on the uniaxial compressive strength σ_c and uniaxial tensile strength σ_t of the dam concrete. In the first step, the cohesion c and the angle of friction ϕ were expressed in terms of these uniaxial strengths (Pande et al., 1990) as

$$c=\frac{\sigma_t}{2\sqrt{n}}=\frac{\sigma_c\sqrt{n}}{2} \qquad \sin\phi=\frac{1-n}{1+n} \tag{8.1}$$

where n is the ratio of absolute strength values σ/σ_c. Once the cohesion and the angle of friction were known, the parameters of the Drucker-Prager yield function, α and K, were obtained from Equations (7.6) - (7.8). For all cases, it was assumed that σ_c=-0.001E_d, i.e. -20 MPa. For different values of σ_t, Equations (8.1) and (7.6) produced the following values:

$$\sigma_t = 2\,\text{MPa} \Rightarrow \alpha = 0.25 \qquad K = 1.64\,\text{MPa}$$

$$\sigma_t = 1\,\text{MPa} \Rightarrow \alpha = 0.27 \qquad K = 0.84\,\text{MPa}$$

$$\sigma_t = 0.5\,\text{MPa} \Rightarrow \alpha = 0.28 \qquad K = 0.43\,\text{MPa}$$

$$\sigma_t = 0.2\,\text{MPa} \Rightarrow \alpha = 0.284 \qquad K = 0.17\,\text{MPa}$$

Smeared cracking model

In this study, the improved ADINA concrete model, described in Paragraph 7.4.2.2, was used to represent the smeared cracking phenomena. Again, the parameters were set in a way which guaranteed linear elastic behaviour in compression and up to the cracking point in tension.

The basic properties of the model were equal to those of the linear elastic model and remained unaltered for all the analyses. The modulus of elasticity at zero strain for the dam was E_d=20 GPa, Poisson's ratio was μ_d=0.20, and mass density was ρ_d =2450 kg/m^3.

Other parameters that remained unaltered for all the analyses were σ_c , the uniaxial maximum compressive stress (negative); ε_c, the uniaxial compressive strain at σ_c; σ_u, the uniaxial ultimate compressive stress (negative); ε_u, the uniaxial ultimate compressive strain; β, the principal stress ratio; and 24 discrete stress values for the definition of the compression failure envelopes (guaranteeing linear elastic behaviour in compression):

$$\sigma_c = -20\text{MPa} \qquad \varepsilon_c = -0.20\% \qquad \sigma_u = -19\text{MPa} \qquad \varepsilon_u = -0.27\%$$

$$\beta = 0.75 \quad \sigma_{p11} = 0.0 \quad \sigma_{p12} = 0.3 \quad \sigma_{p13} = 0.6 \quad \sigma_{p14} = 0.9 \quad \sigma_{p15} = 1.2 \quad \sigma_{p16} = 1.5$$

$$\sigma_{p311} = 1.0 \quad \sigma_{p321} = 2.0 \quad \sigma_{p331} = 3.0 \quad \sigma_{p341} = 4.0 \quad \sigma_{p351} = 5.0 \quad \sigma_{p361} = 6.0$$

$$\sigma_{p312} = 1.25 \quad \sigma_{p322} = 2.5 \quad \sigma_{p332} = 3.75 \quad \sigma_{p342} = 5.0 \quad \sigma_{p352} = 6.25 \quad \sigma_{p362} = 7.5$$

$$\sigma_{p313} = 1.2 \quad \sigma_{p323} = 2.4 \quad \sigma_{p333} = 3.6 \quad \sigma_{p343} = 4.8 \quad \sigma_{p353} = 6.0 \quad \sigma_{p363} = 7.2$$

The stiffness reduction factor following tensile failure was set to η_n=0.0001, while the shear stiffness reduction factor was initially set to η_s=0.5. The variation of the latter was examined in the wider range (0.01 to 0.5) and it was found out that this parameter was of no decisive importance to the overall solution.

As already mentioned, the only parameter that changed for each analysis was the uniaxial cut-off tensile stress, σ_t. The values of 2, 1, 0.5 and 0.2 MPa were investigated.

8.1.2 Results of the Analyses

The results of the analyses are presented for each particular material model and for 8 loading states because the nonlinear static analyses were conducted in 7 load increments. The loading state when the water in the reservoir was 20m below the crest is marked as state 1. Continuing correspondingly with the numbering, the state when the water in the reservoir reached its highest level (50m above the crest) is marked as state 8.

8.1.2.1 Linear Elastic Model

For the linear elastic model, the horizontal displacements u of the upstream face of the top of the dam (node 276 in Figure 8.1) were:

water	-20	-10	0	10	20	30	40	50
state	1	2	3	4	5	6	7	8
u [mm]	-1.37	-0.53	1.40	4.17	6.94	9.72	12.49	15.26

Among many possibilities for the description of the behaviour of the dam on the whole, it was decided here to present only the results which are comparable with the subsequent nonlinear results. First, the zones where the principal stresses were in tension (i.e. greater than zero) are shown in Figure 8.2a. These zones correspond to the initial steps of the no-tension analyses (Section 7.2). Obviously, they increase with the increase in water level, which is also shown in Figure 8.2a. According to the discussion conducted in Paragraph 8.1.1.3 and for the modulus of elasticity equal to 20 GPa, it was reasonable to assume that the uniaxial tensile strength is 2 MPa. This

enabled the second representation of the overall behaviour of the dam - the zones where the tensile principal stresses were greater than 0.9 of the tensile strength (1.8 MPa). For different water levels, these zones are shown in Figure 8.2b. To some extent, they describe the limited tension behaviour of the dam and may be interpreted as damage-prone zones, i.e. zones susceptible to cracking. In order to enable the comparison between different material models, similar results will be presented for the two nonlinear models.

8.1.2.2 Limited Tension Plasticity Model

For the limited tension elasto-plastic model, the horizontal displacements *u* (in mm) of the upstream face of the top of the dam (node 276) depend on the tensile strength of the mass concrete:

water	-20	-10	0	10	20	30	40	50
state	1	2	3	4	5	6	7	8
$u(\sigma_t$=2MPa)	-1.37	-0.55	1.32	4.10	6.88	9.77	12.83	16.20
u(σ_t=1MPa)	-1.37	-0.55	1.32	4.12	7.08	10.43	14.70	21.25
u(σ_t=0.5MPa)	-1.37	-055	1.32	4.21	7.51	12.44	23.27	58.46
$u(\sigma_t$=0.2MPa)	-1.37	-0.55	1.34	4.42	9.33	25.26		

Some of the displacements from the previous table are graphically compared with the linear elastic displacements in Figure 8.3.

As the water level increases, the damaged zones also increase in size. This is shown in Figures 8.4a, 8.4b, 8.4c and 8.4d for uniaxial concrete tensile strengths of 2, 1, 0.5 and 0.2 MPa, respectively. The term damaged zone is again used to define a zone where the principal tensile stresses were greater than 0.9 of the tensile strength (1.8, 0.9, 0.45 and 0.18 MPa, respectively).

8.1.2.3 Smeared Cracking Model

For the smeared cracking model, the horizontal displacements u (in mm) of the upstream face of the top of the dam (node 276) also depend on the tensile strength of the mass concrete:

water	-20	-10	0	10	20	30	40	50
state	1	2	3	4	5	6	7	8
$u(\sigma_t$=2MPa)	-1.37	-0.55	1.33	4.12	6.92	9.90	13.47	28.30
$u(\sigma_t$=1MPa)	-1.37	-0.55	1.33	4.15	7.28	13.23	19.73	
$u(\sigma_t$=0.5MPa)	-1.37	-0.55	1.33	4.30	9.57	22.97		
$u(\sigma_t$=0.2MPa)	-1.37	-0.55	1.35	4.68	10.41			

Some of the displacements from the previous table are graphically compared with the linear elastic displacements in Figure 8.5.

As the water level increases, the damaged zones also increase in size. This is shown in Figures 8.6a, 8.6b, 8.6c and 8.6d for uniaxial concrete tensile strengths of 2, 1, 0.5 and 0.2 MPa, respectively. The term damaged zone is here used to define a zone of cracked elements.

8.1.3 Conclusions from the Rigid Foundation Analyses

The analyses conducted in this Section have demonstrated that the limited tension nonlinearities are highly dependent on the tensile strength (Figures 8.3, 8.4, 8.5, 8.6).

The damaged zone predicted by the linear elastic model is completely different from the damaged zone predicted by the two nonlinear models. The former spreads mainly into the body of the dam, towards the top, but very little along the base (Figure 8.2b). The latter spreads mainly along the base so that its failure is the cause of the failure of the whole dam (Figures 8.4 and 8.6). In other words, the extrapolation of

linear elastic results to reach the conclusions about the failure mechanism would be misleading.

The displacements produced by the limited tension elasto-plastic model are smaller than the displacements produced by the smeared cracking model. Although the damaged zones are of similar spreading pattern, the zones predicted by the limited tension plasticity model spread into the body of the dam for lower tensile strengths (Figures 8.4). Since such behaviour is not realistic and since the plasticity model with low tensile strengths is typically used to represent the no-tension solution for concrete gravity dams, the validity of this solution is seriously compromised.

8.2 Flexible Foundation

In this case, the influence of the foundation on the nonlinear behaviour of the whole dam-foundation system can be investigated by varying the stiffness of the foundation, i.e. its modulus of elasticity. After the summary about the models, the results and conclusions will be presented.

8.2.1 Assumptions and Explanations

The important assumptions and explanations relevant to the numerical modelling of concrete gravity dams on flexible foundations are summarised here.

8.2.1.1 Geometry of the System

It was assumed that the dam and the foundation block are in the state of plane strain. The dam-foundation interface is flat and at the ground level. The geometry of the dam was as specified in Section 8.1. The rock foundation was considered as a rectangular block, with the height of 150m (equal to 3 heights of the dam) and with

the width of 340m (3 heights of the dam upstream and downstream from the dam). The foundation block was modelled with 250 finite elements which increased in size as the distance from the dam increased. Anticipating the initiation and extention of major nonlinearities in the area where the mesh is the finest (around the dam-foundation interface), this idealisation was also in line with the recommendations arising from the radiation damping studies performed in Chapter 6 (Simic, 1993c), which altogether enabled the use of the similar mesh for dynamic nonlinear analyses in Chapter 9. The full finite element mesh for the present study is shown in Figure 8.7.

8.2.1.2 Loading of the System

The loading of the dam-foundation system was as described in Section 8.1. It was assumed that the deformations of the foundation had already taken place prior to construction of the dam. Therefore, the density of the foundation was given a zero value because the dead weight was taken as the mass-proportional loading.

8.2.1.3 Material Models

As in the rigid foundation case, three different formulations were used for material modelling of the dam and foundation: linear elastic, limited tension plasticity and smeared cracking. Material models of the dam were as described in Paragraph 8.1.1.3. The foundation flexibility was varied by prescribing the values of 5, 10, 20 and 40 GPa to its modulus of elasticity E_f. For nonlinear models, the uniaxial compressive strength σ_c and uniaxial tensile strength σ_t of the foundation were set to:

$$\sigma_c = -0.001E_f \qquad \sigma_t = 0.0001E_f \tag{8.2}$$

Linear elastic model

The modulus of elasticity of the foundation was variable as described above, its density was always 0, and its Poisson's ratio was μ_f=0.25 for all the cases.

Limited tension plasticity model

In order to reduce the number of analyses, the uniaxial tensile strength of dam concrete was set to 2 MPa (contrary to the rigid foundation case, where it was varied in a given range). On the other hand, the rock foundation modelled by the ADINA improved Drucker-Prager model partly depends on the uniaxial compressive and tensile strengths. The parameters that remained unaltered for all the analyses were:

$$\mu_f = 0.25 \qquad \rho_f = 0\ \mathrm{kg/m^3} \qquad W_f = -0.1 \quad D_f = -1 \quad \alpha_f = 0.25$$

The strength-dependent parameters changed for each analysis and were calculated according to Equations (8.2), (8.1) and (7.6):

$$E_f = 5\mathrm{GPa} \;\Rightarrow\; K_f = 0.41\,\mathrm{MPa} \quad T_f = -I_{1f}^a = 5\mathrm{MPa}$$

$$E_f = 10\mathrm{GPa} \;\Rightarrow\; K_f = 0.82\,\mathrm{MPa} \quad T_f = -I_{1f}^a = 10\mathrm{MPa}$$

$$E_f = 20\mathrm{GPa} \;\Rightarrow\; K_f = 1.64\,\mathrm{MPa} \quad T_f = -I_{1f}^a = 20\mathrm{MPa}$$

$$E_f = 40\mathrm{GPa} \;\Rightarrow\; K_f = 3.28\,\mathrm{MPa} \quad T_f = -I_{1f}^a = 40\mathrm{MPa}$$

Smeared cracking model

As in the previous set of nonlinear analyses, it was assumed that the uniaxial tensile strength of dam concrete is 2 MPa. On the other hand, the rock foundation modelled by the improved ADINA concrete model partly depends on the uniaxial tensile strength and stress-strain behaviour in compression. The foundation parameters that were equal to those of the dam (Section 8.1.1) and remained unaltered for all the analyses were the principal stress ratio β, 24 discrete stress values for the definition of the compression failure envelopes, two stiffness reduction factors (η_n and η_s), and two strains (ε_c and ε_u). The other two parameters that remained unaltered for all the analyses were:

$$\mu_f = 0.25 \qquad \rho_f = 0\mathrm{kg/m^3}$$

The shape of the rock foundation stress-strain curve in compression was the same as that of the dam concrete. This was accomplished by fixing the strain parameters and

by changing the stress parameters proportionally to the foundation modulus of elasticity and uniaxial tensile strength:

$$E_f = 5\text{GPa} \quad \Rightarrow \quad \sigma_c = -10\sigma_t = -5\text{MPa} \quad \sigma_u = -4.75\text{MPa}$$

$$E_f = 10\text{GPa} \quad \Rightarrow \quad \sigma_c = -10\sigma_t = -10\text{MPa} \quad \sigma_u = -9.5\text{MPa}$$

$$E_f = 20\text{GPa} \quad \Rightarrow \quad \sigma_c = -10\sigma_t = -20\text{MPa} \quad \sigma_u = -19\text{MPa}$$

$$E_f = 40\text{GPa} \quad \Rightarrow \quad \sigma_c = -10\sigma_t = -40\text{MPa} \quad \sigma_u = -38\text{MPa}$$

8.2.2 Results of the Analyses

The results of this study will be presented in a similar way as for the rigid foundation case in Subsection 8.1.2. Again, all 8 loading states should be observed, but this time for four foundation conditions.

8.2.2.1 Linear Elastic Model

For the linear elastic model, the horizontal displacements u (in mm) of the upstream face of the top of the dam (node 276 in Figure 8.7) were:

water	-20	-10	0	10	20	30	40	50
state	1	2	3	4	5	6	7	8
u(E_f=5GPa)	-2.42	1.79	8.74	17.62	26.49	35.36	44.24	53.11
u(E_f=10GPa)	-2.09	0.36	4.71	10.47	16.23	21.99	27.75	33.51
u(E_f=20GPa)	-1.72	-0.06	3.09	7.40	11.72	16.03	20.34	24.66
u(E_f=40GPa)	-1.54	-0.29	2.24	5.80	9.37	12.93	16.50	20.06

The increase in size of the damaged zones with the increase in water level is shown in Figures 8.8a, 8.8b, 8.8c and 8.8d for the foundation moduli of 5, 10, 20 and 40 GPa, respectively. The term damaged zones is used to define a zone where the principal

tensile stresses were greater than 0.9 of the smaller of the two assumed tensile strengths (0.45, 0.9, 1.8 and 1.8 MPa, respectively).

8.2.2.2 Limited Tension Plasticity Model

For the limited tension elasto-plastic model, the horizontal displacements *u* (in mm) of the upstream face of the top of the dam (node 276 in Figure 8.7) were:

water	-20	-10	0	10	20	30	40	50
state	1	2	3	4	5	6	7	8
u(E_f=5GPa)	-2.87	1.13	7.82	16.60	26.65	39.78	59.35	126.3
u(E_f=10GPa)	-2.09	0.36	4.71	10.47	16.52	23.10	30.73	39.80
u(E_f=20GPa)	-1.72	-0.06	3.09	7.40	11.72	16.26	21.06	26.34
u(E_f=40GPa)	-1.54	-0.29	2.24	5.80	9.37	13.12	17.04	21.35

The increase in size of the damaged zones with the increase in water level is shown in Figures 8.9a, 8.9b, 8.9c and 8.9d for the foundation moduli of 5, 10, 20 and 40 GPa, respectively. The term damaged zones is used to define a zone where the principal tensile stresses were greater than 0.9 of the smaller of the two tensile strengths (0.45, 0.9, 1.8 and 1.8 MPa, respectively).

8.2.2.3 Smeared Cracking Model

For the smeared cracking model, the horizontal displacements *u* (in mm) of the upstream face of the top of the dam (node 276 in Figure 8.7) were:

water	-20	-10	0	10	20	30	40	50
state	1	2	3	4	5	6	7	8
u(E_f=5GPa)	-2.87	1.20	7.97	16.97	30.49	45.93	68.08	

u(E_f=10GPa)	-2.09	0.38	4.76	10.56	16.77	24.47	38.13	53.51
u(E_f=20GPa)	-1.72	-0.05	3.11	7.44	11.79	16.57	22.76	33.68
u(E_f=40GPa)	-1.54	-0.29	2.25	5.83	9.42	13.30	18.37	29.54

For the foundation moduli of 5, 10, 20 and 40 GPa, the propagation of the crack for the last four available loading states is presented in Figures 8.10, 8.11, 8.12 and 8.13, respectively. The cracked elements are black.

In this case, the term damaged zone may be used to define a zone of cracked elements. In order to enable the comparison with other material models and previous results, the increase in size of these zones with the increase in water level is shown in Figures 8.14a, 8.14b, 8.14c and 8.14d for the foundation moduli of 5, 10, 20 and 40 GPa, respectively.

8.2.3 Conclusions from the Flexible Foundation Analyses

For all material models, the displacements of the dam-foundation system decrease as the foundation modulus of elasticity increases, with the rigid foundation case acting as the lower limit.

The damaged zone predicted by the linear elastic model is completely different from the damaged zone predicted by the two nonlinear models. The former spreads mainly into the upstream region of the foundation (Figures 8.8) while the latter spreads mainly into the part of the foundation underneath the dam (Figures 8.9 and 8.14). This means that the linear elastic model cannot be used to identify the parts of the dam-foundation system which are prone to damage.

The displacements produced by the limited tension elasto-plastic model are smaller than the displacements produced by the smeared cracking model. The damaged zones are of similar spreading pattern and two basic failure modes can be identified (Figures 8.9 and 8.14). For $E_f < E_d$, the damage is not located around the dam-foundation

interface. Non-horizontal cracking in the foundation is observed. On the other hand, for $E_f \geq E_d$, the damage tends to be located around the dam-foundation interface, with horizontal cracking. This behaviour is consistent with the behaviour of the rigid foundation case, where $E_f \gg E_d$, i.e. where $E_f \rightarrow \infty$.

Closely related to the previous conclusion is the conclusion about the overall stability of the system: the softer the foundation, the greater the displacements of the dam and the higher the angles of the main cracking with respect to the dam-foundation interface. In other words, the cases where the foundation is very rigid are more dangerous from the stability point of view because rigid-body sliding will potentially occur through a much smaller volume of material (dam-foundation interface rather than the whole foundation).

8.3 Water Penetration into Open Cracks

The analyses in the previous Sections have shown that the cracking of dam-foundation systems occurs under higher-than-normal static loading. The cracking was observed either in the dam (for $E_f \geq E_d$) or in the foundation (for $E_f < E_d$). Once the cracks are open on the upstream face of the dam-foundation system, it is highly likely that the water will penetrate into the system and cause new loading distribution. However, the minimum size of the crack opening which allows for water intrusion is not known. Two basic scenarios for water penetration can be foreseen: when the foundation is permeable and when the foundation is impermeable.

8.3.1 Permeable Foundation

In the case of very quick reservoir filling, the water pressure load is generated both on the upstream face of the dam and the reservoir bottom (Figure 8.15). Later, steady-state seepage would be established, changing the loading pattern. If no uplift

reduction measures have been undertaken, and providing that the distribution of uplift pressure in the foundation is linear, the loading on the dam would look like in Figure 8.16a. The existence of uplift reduction measures (drainage, grout curtain, etc.) changes the load distribution by reducing, if not eliminating the uplift pressure, leading to loading on the dam similar to that in Figure 8.16b. Furthermore, if dam concrete is assumed permeable (i.e. there is no drainage in the dam), the same discussion applies for any horizontal section of the dam. Uplift pressure is generated and can be evaluated accurately by constructing a flow net. The usual simplification in traditional gravity dam design (USBR, 1976) is to assume a linear distribution along the section, as shown in Figure 8.17a. Alternatively, if drainage exists in the dam, a typical uplift diagram would be reduced and would look like the one in Figure 8.17b.

For the cases described in Section 8.2, cracking of the dam-foundation systems occurs and the loading pattern becomes even more complicated. If the main crack is horizontal (typically for $E_f \geq E_d$), the loading distribution changes from that in Figure 8.16a to the one in Figure 8.18a. On the other hand, if the main crack is inclined (like in Figure 8.18b, typical for $E_f < E_d$), this would influence the seepage in the foundation, altering the flow net to the extent which would have to be evaluated by carrying out a new, independent seepage analysis.

8.3.2 Impermeable Foundation

In the unlikely event of a realistically impermeable foundation, seepage through the foundation never occurs, and the pressure on the reservoir bottom, shown in Figure 8.15, is never relieved. Another scenario that falls into this category is the case for which the seepage occurs and for which it may be assumed that the uplift has been fully eliminated under the dam (the limit case of Figure 8.16b). Although this scenario is not conservative, because the probability of drainage clogging or grout material rinsing increases with the duration of dam exploitation, it has to be investigated since

it corresponds to the previous static analyses, where no uplift forces have been taken into account.

If horizontal cracking occurs, the loading is entirely due to water pressure and not to seepage. For an open crack in Figure 8.19a, a negative vertical hydrostatic pressure is created on the upper face of the crack and acts on the dam. An equivalent positive loading is created on the lower face of the crack and acts on the foundation. The subsequent behaviour of the crack can be examined by using many theories: Linsbauer (1985, 1990) has used fracture mechanics principles. In reality, uplift reduction measures (which must exist for this cracking scenario) may relieve some of the newly created negative vertical pressure, but it is not known to what extent. If inclined cracking occurs (typically for $E_f < E_d$), the hydrostatic load distribution can be drawn easily (Figure 8.19b). Again, properly working uplift reduction measures may relieve a part of the hydrostatic pressure created on the faces of the crack. Clearly, shifting of the crack away from the horizontal direction decreases this potential ability of pressure reduction.

Although it was already mentioned that the scenario described in this Subsection is not conservative, there are three reasons which corroborate its use in the subsequent analyses. First, the loading pattern is considerably simpler. Second, the qualitative behaviour is similar to that of the permeable foundation case, allowing for the extension of conclusions to both cases. Finally, earlier investigations have shown that the effects of seepage flow are of minor (in some cases negligible) importance when compared to the effects of water penetration (Rescher, 1990). Moreover, the analyses in Section 8.2 have demonstrated that the cases for which $E_f < E_d$ exhibit higher displacements and produce inclined cracks in the foundation, whereas the cases for which $E_f \geq E_d$ exhibit smaller displacements and produce horizontal cracks at the dam-foundation interface. Under all these circumstances, it was decided to evaluate only the effects of water penetration for the limit case of the rigid foundation ($E_f \rightarrow \infty$) and for the tensile strength of 2 MPa.

8.3.3 Computational Procedure

A combined incremental-iterative computational procedure able to deal with water penetration into open cracks is introduced in this Subsection. The procedure consisted of the following steps:

a) Whenever a crack in the smeared cracking model of the dam is observed, the hydrostatic water pressure is updated to include the upward vertical pressure in the crack. It is assumed that the full vertical water pressure is immediately generated in even the narrowest part of the crack opening.

b) For the same loading increment, an iterative solution is sought to establish whether the crack propagation for this load level is convergent and what is the final crack length.

c) The new loading increment is applied only if the crack length has converged for the previous increment. The whole procedure is repeated again, starting with step *(a)*.

For the new computational procedure, the horizontal displacements u^{wp} of the upstream face of the top of the dam (node 276 in Figure 8.1) were given in the third row of the following table:

water	-20	-10	0	10	20	30	40	50
u [mm]	-1.37	-0.55	1.33	4.12	6.92	9.90	13.47	28.30
u^{wp} [mm]	-1.37	-0.55	1.33	4.12	7.01	10.79	35.86	

The results of the new procedure (water penetration effects included) can be compared with the previous results of the same system with no water penetration effects (Paragraph 8.1.2.3). For the latter case, the appropriate horizontal displacements of the node 276 were repeated in the second row of the table above. The graphical comparison between the two solutions is presented in Figure 8.20a. Similarly, the increase in size of the cracked zones with the increase in water level

(water penetration effects included) is shown in Figure 8.20b, which can be compared with Figure 8.6a (no water penetration effects). It may be concluded that for this case, the effect of water penetration is roughly equivalent to the effect of the upstream reservoir being 10 m higher than the real one.

8.4 Concluding Remarks

The significance of the conclusions drawn from the studies carried out in this Chapter is twofold. Primarily, they answer various questions about the stability of concrete gravity dam-foundation systems under increased static loading. More importantly from the point of view of this whole work, they identify types of failure and their location, which was covered in detail in Subsections 8.1.3 and 8.2.3.

Under normal static loading, a properly designed concrete gravity dam on a sound rock foundation possesses a considerable reserve of structural stability. Consequently, nonlinear behaviour is encountered only when the dam-foundation system is severely overloaded.

Failure mechanisms of concrete gravity dam-foundation systems can be studied only by using nonlinear computational models (unlike linear models which are used for the description of the behaviour under normal exploitation). By providing the required levels of overloading and carrying out the nonlinear analyses until collapse, important lessons are learnt about different modes of failure and identification of the most vulnerable parts of the system. Once their location is known, it is easier to devise remedies that can be undertaken in order to reduce the damage and avoid serious consequences associated with dam failure.

For all the cases considered in this Chapter, the linear elastic computational model is the lower limit for the nonlinear computational models, and therefore a useful check.

Nonlinear numerical models should be carefully calibrated to account for the predominantly linear elastic behaviour in compression and predominantly nonlinear behaviour in tension. The proof that this requirement was achieved is that the response of the nonlinear models for lower loading states is either identical or negligibly different from the response of the linear models.

Limited tension nonlinearities are highly dependent on the tensile strength, which was demonstrated in Section 8.1. Since the tensile strength of mass concrete in dams is usually estimated and rarely experimentally determined, special care should be taken when making these estimates. Small changes of the estimated value cause drastic changes in the behaviour.

When the limited tension elasto-plastic model is employed, the damage of the dam-foundation system occurs due to yielding at the tensile part of the Drucker-Prager yielding surface and not due to yielding at the tensile cap.

The smeared cracking model is better suited for modelling limited tension nonlinearities of concrete dam-foundation systems than the elasto-plastic model. If the latter model is used, it is only possible to obtain the potential extent of the damaged zones and the precise location of the crack cannot be determined, rendering the model not fully reliable. Therefore, in Chapter 9, where earthquake nonlinear analyses will be undertaken, only the smeared cracking model will be used.

If water is allowed to penetrate the cracks open due to the overloading, the stability of the dam is additionally endangered.

For this particular case and for the assumption of the immediate generation of full vertical water pressure in even the tiniest of the crack openings, the effect of the water penetration is roughly equivalent to the effect of the upstream reservoir being 10 m higher than the real one.

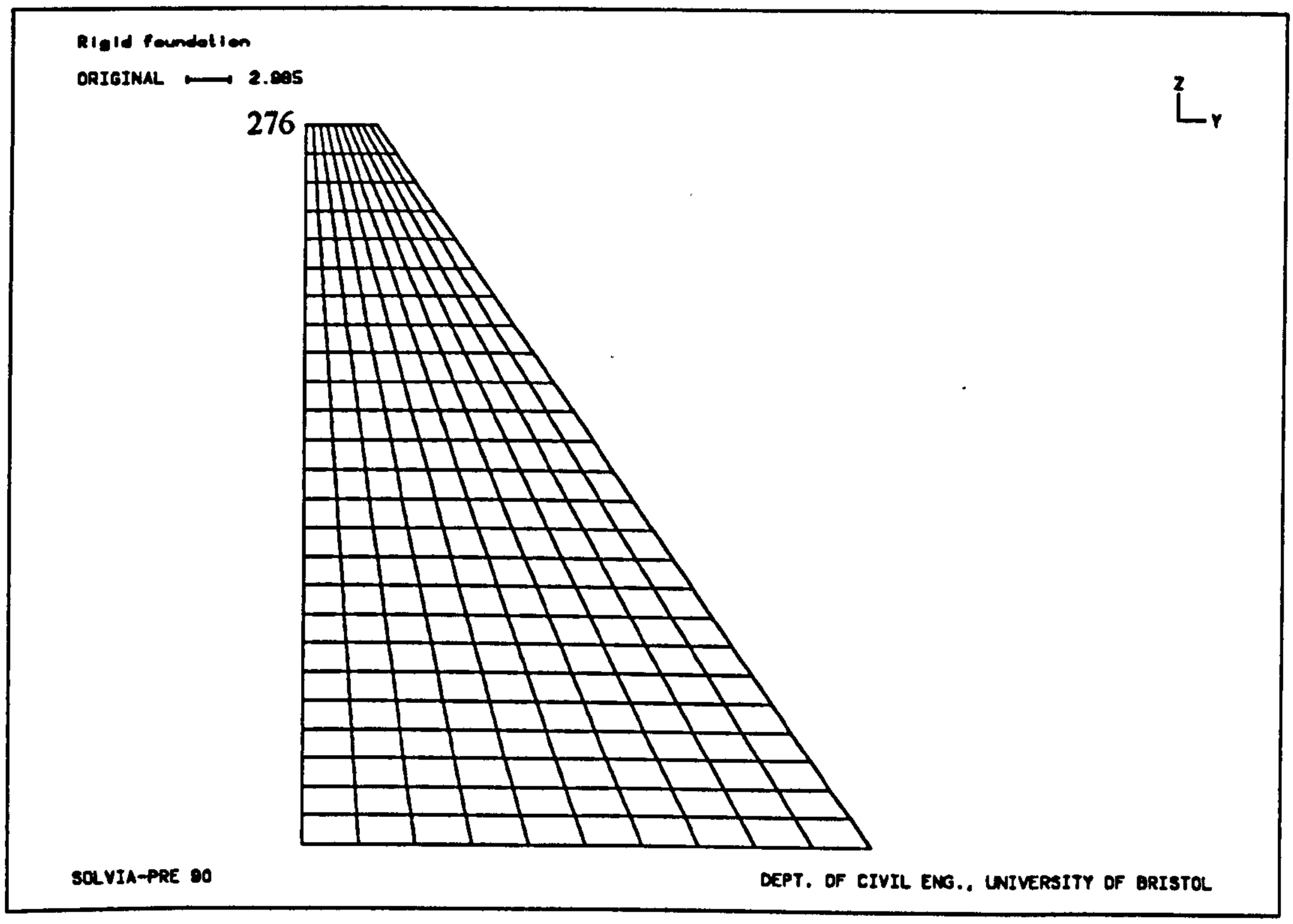

Figure 8.1 - Finite element mesh of the concrete gravity dam

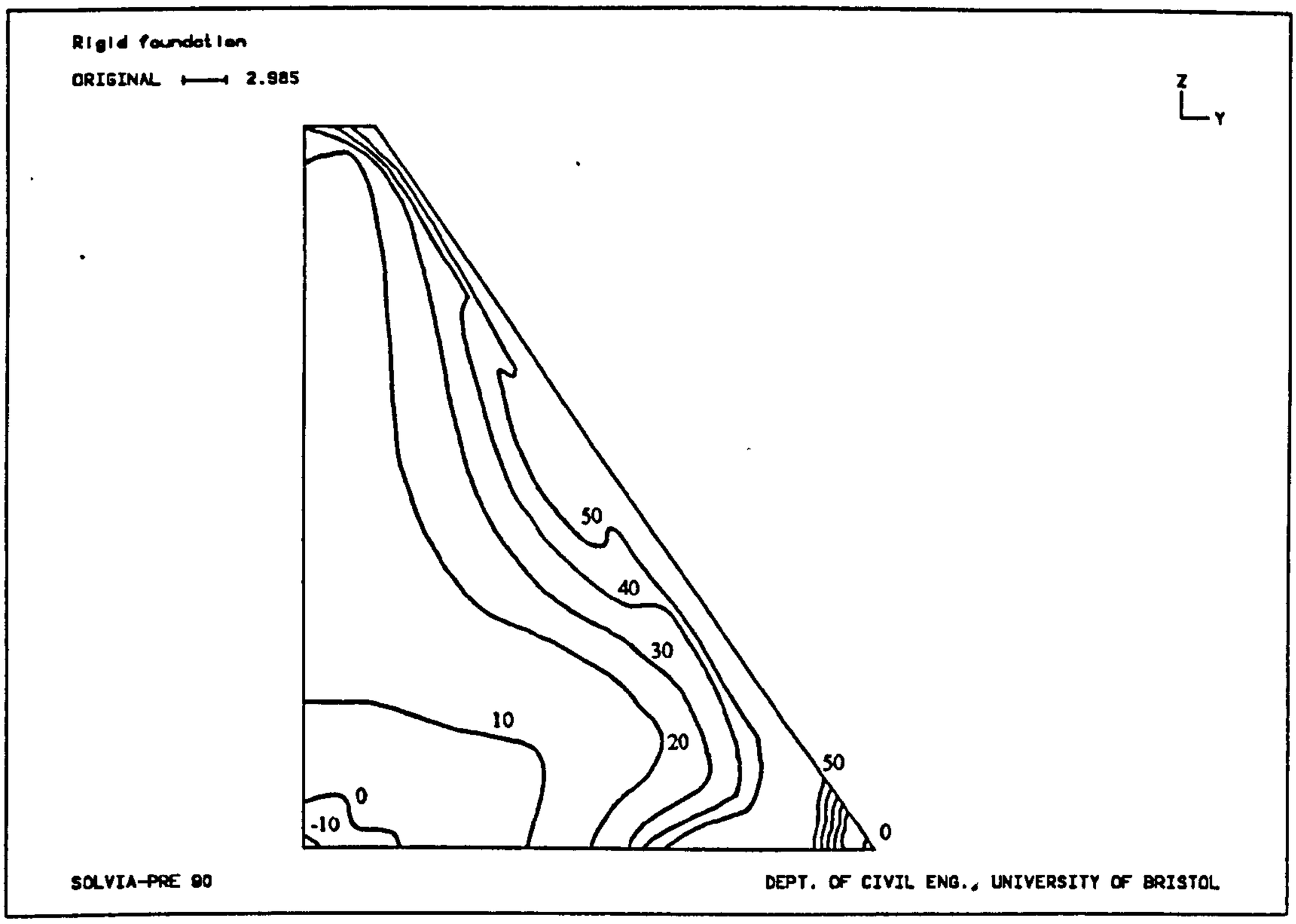

Figure 8.2a - Zones of tensile principal stresses for different water levels

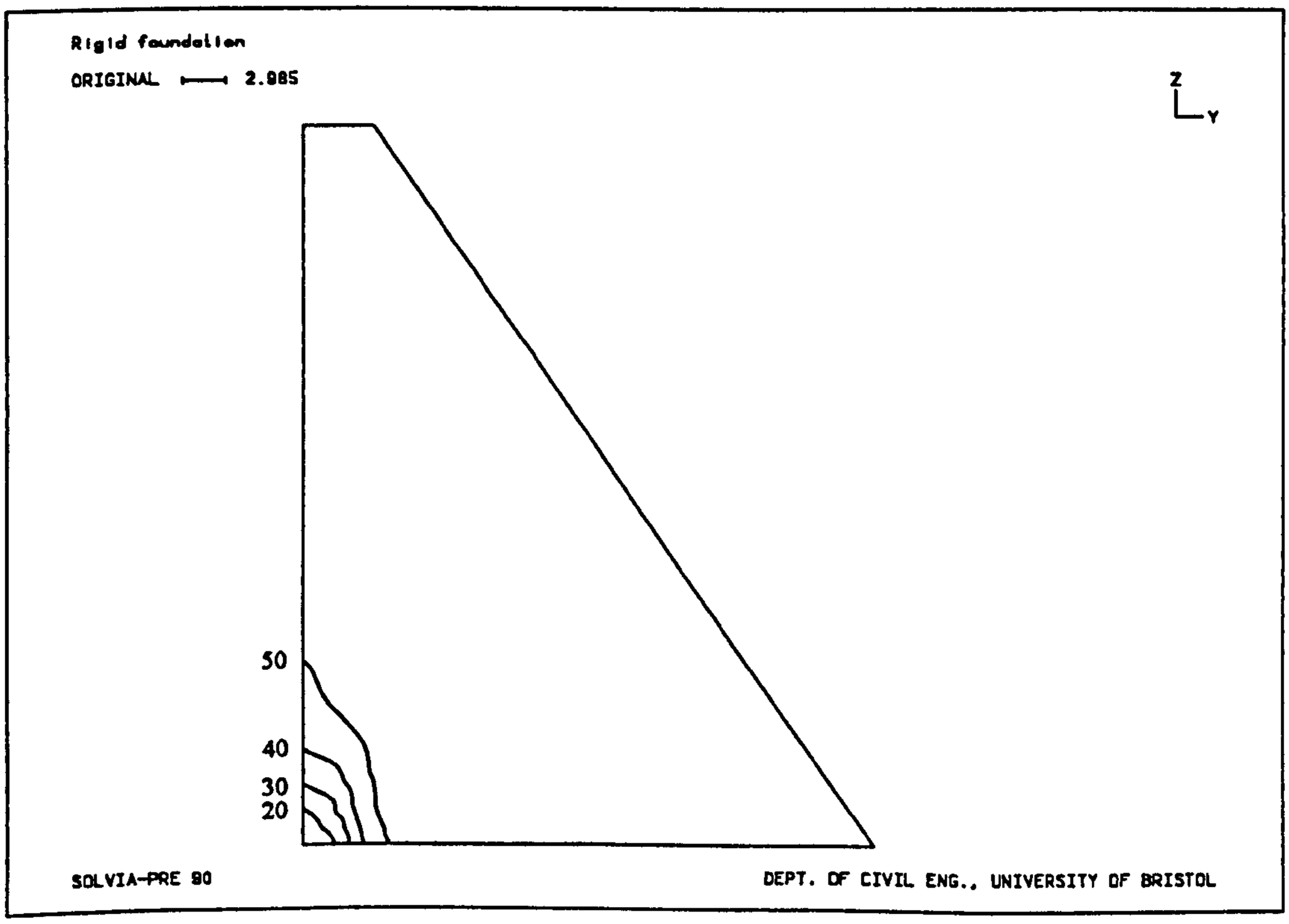

Figure 8.2b - Damaged zones for different water levels (linear elastic model)

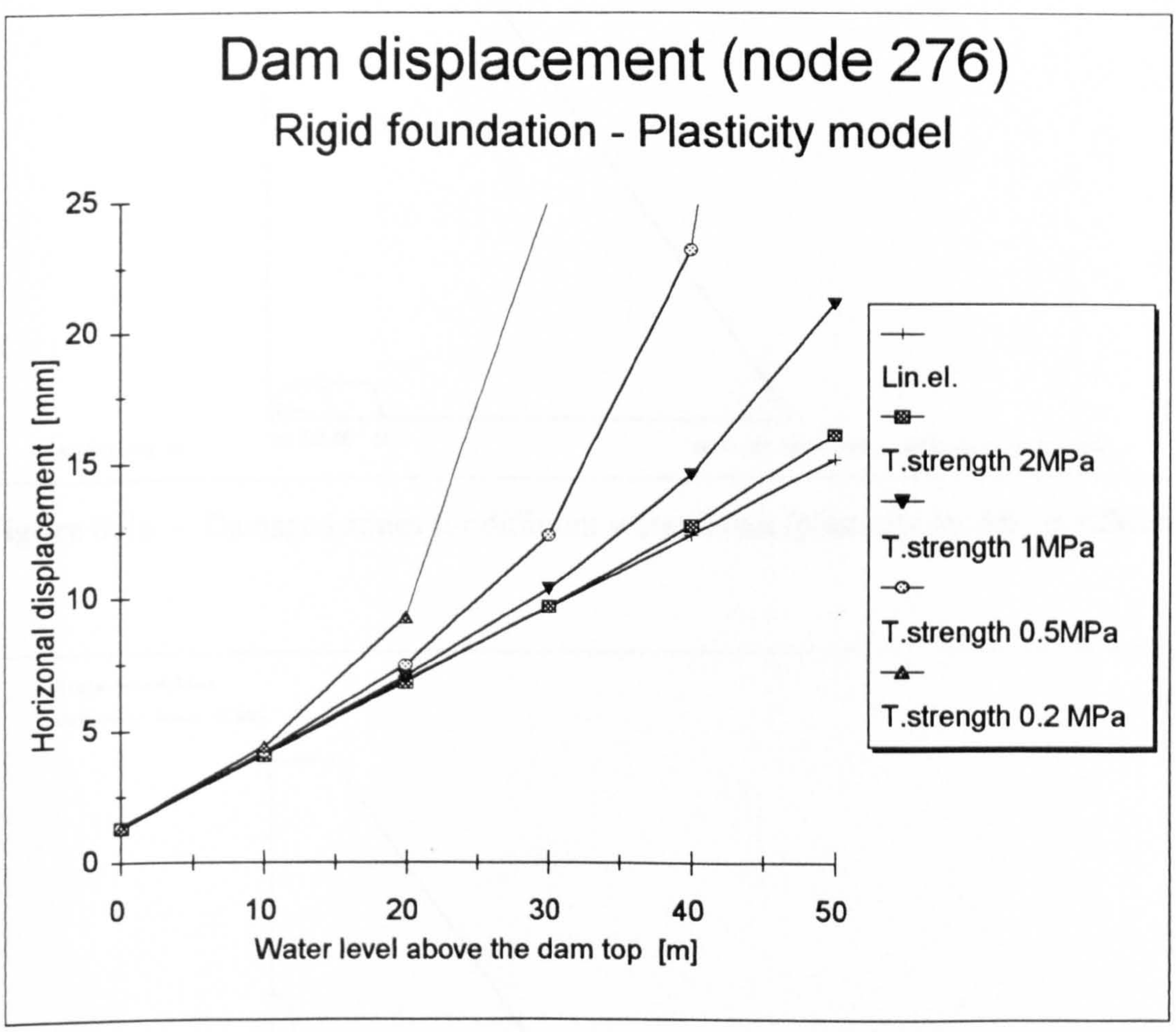

Figure 8.3 - Displacement of the top of the dam

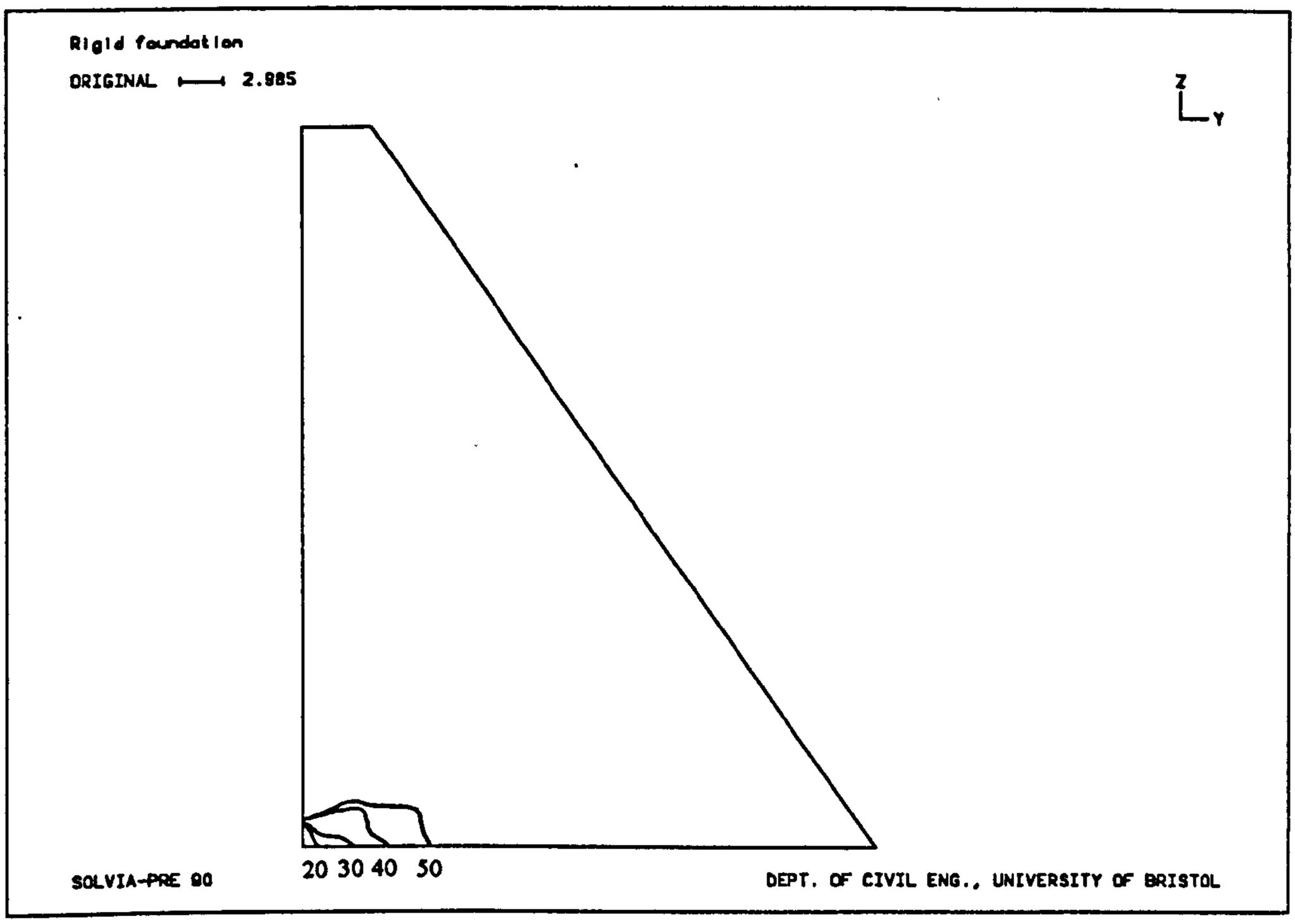

Figure 8.4a - Damaged zones for different water levels (plasticity model, σ_t=2MPa)

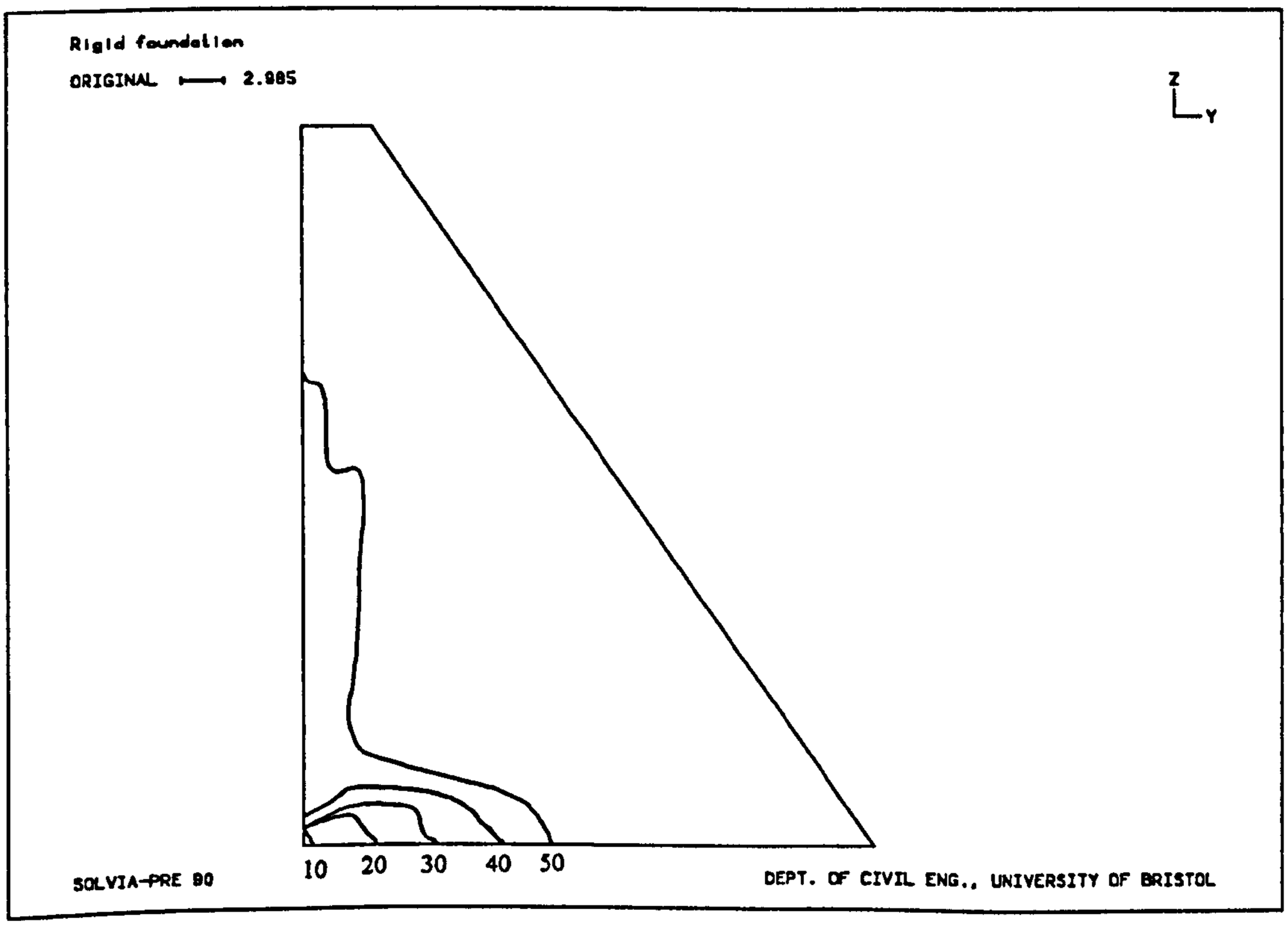

Figure 8.4b - Damaged zones for different water levels (plasticity model, σ_t=1MPa)

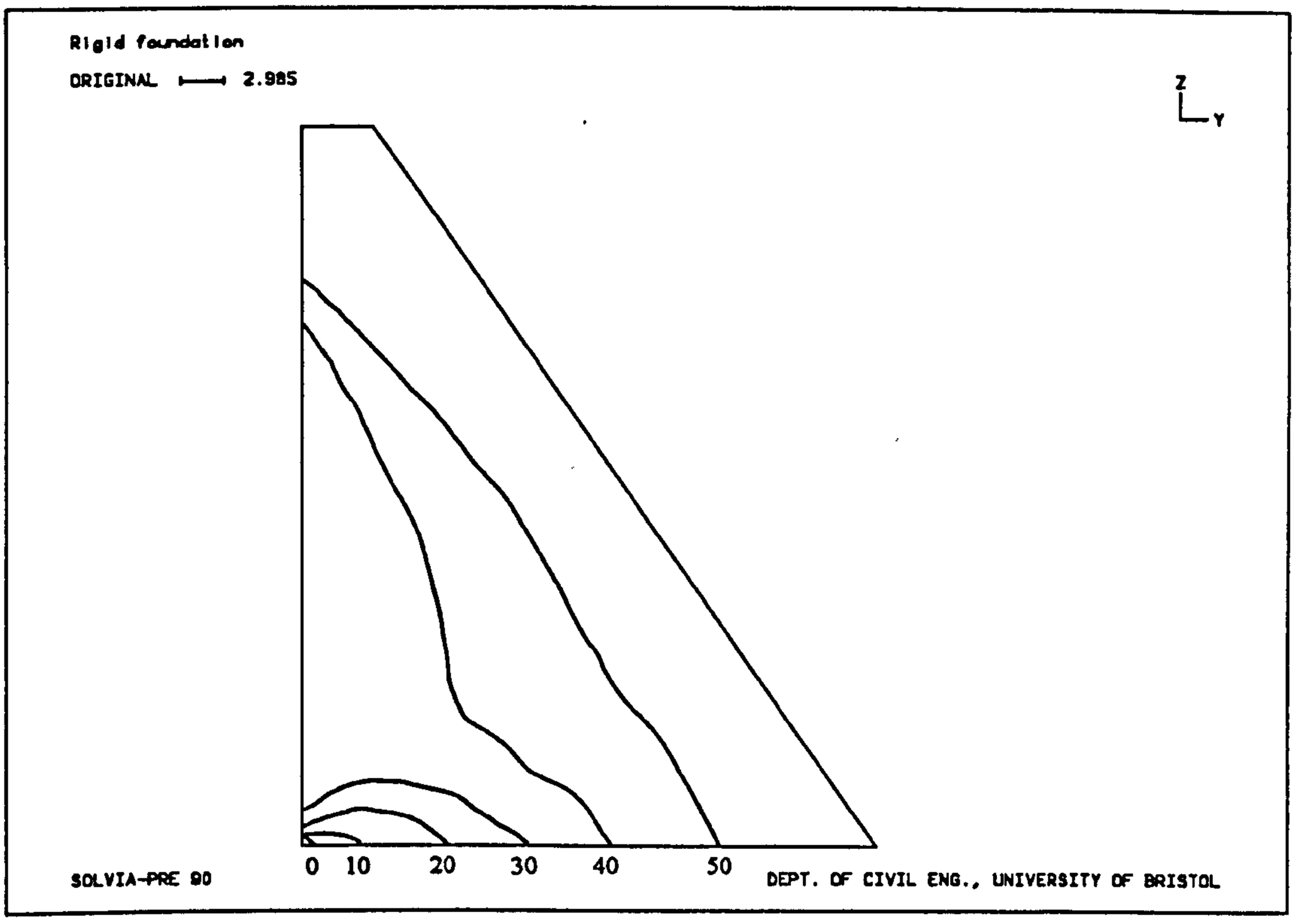

Figure 8.4c - Damaged zones for different water levels (plasticity model, σ_t=.5MPa)

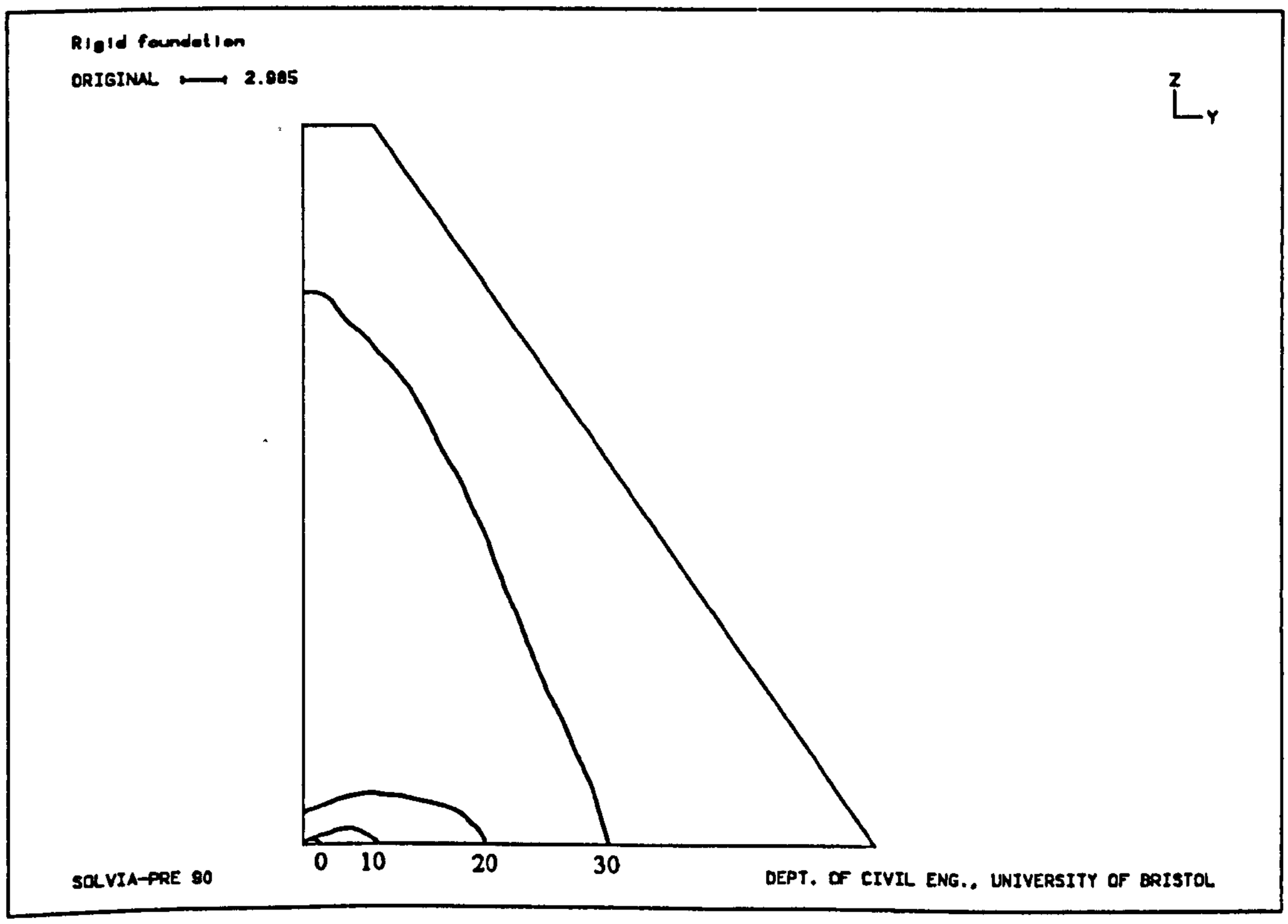

Figure 8.4d - Damaged zones for different water levels (plasticity model, σ_t=.2MPa)

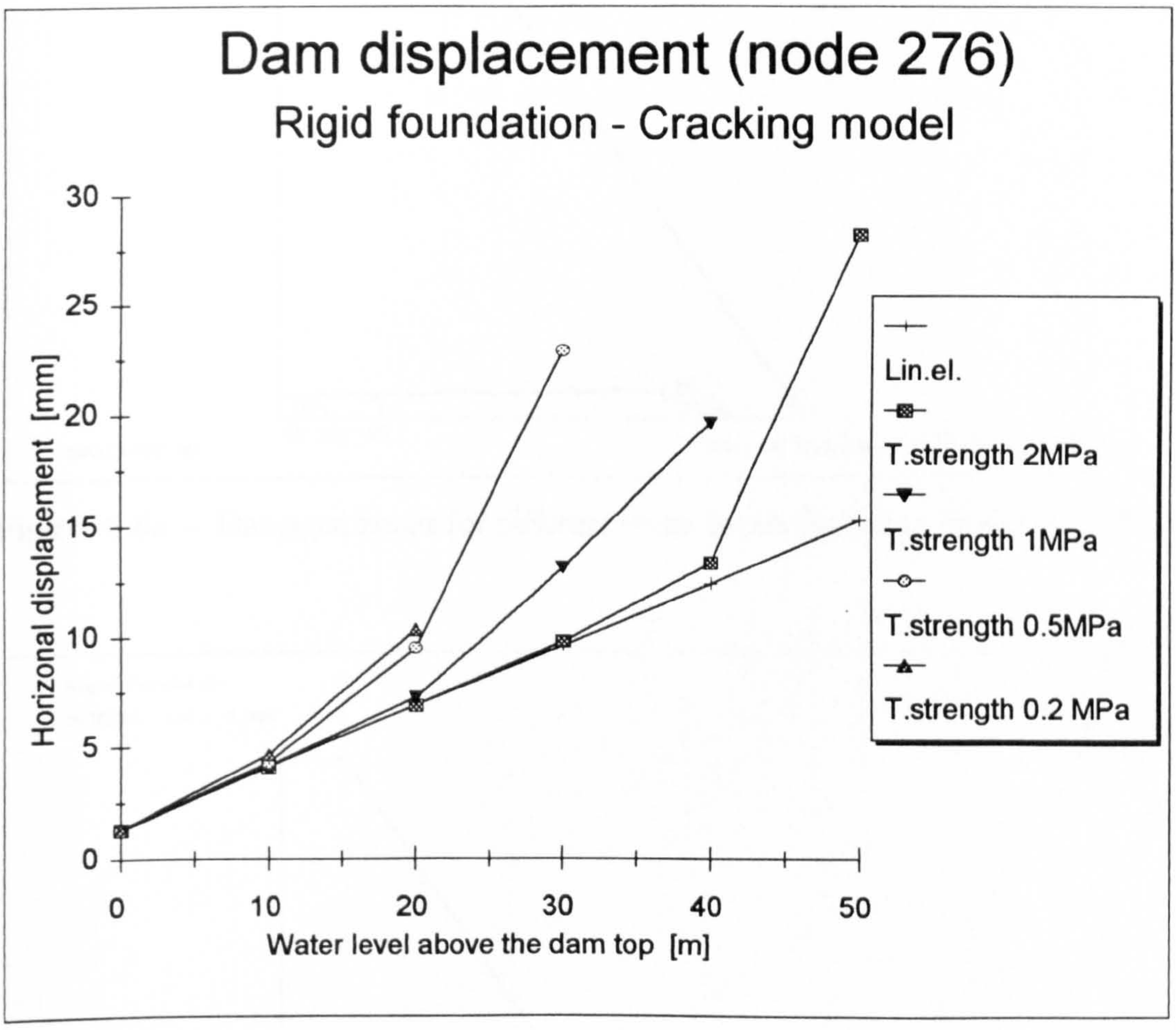

Figure 8.5 - Displacement of the top of the dam

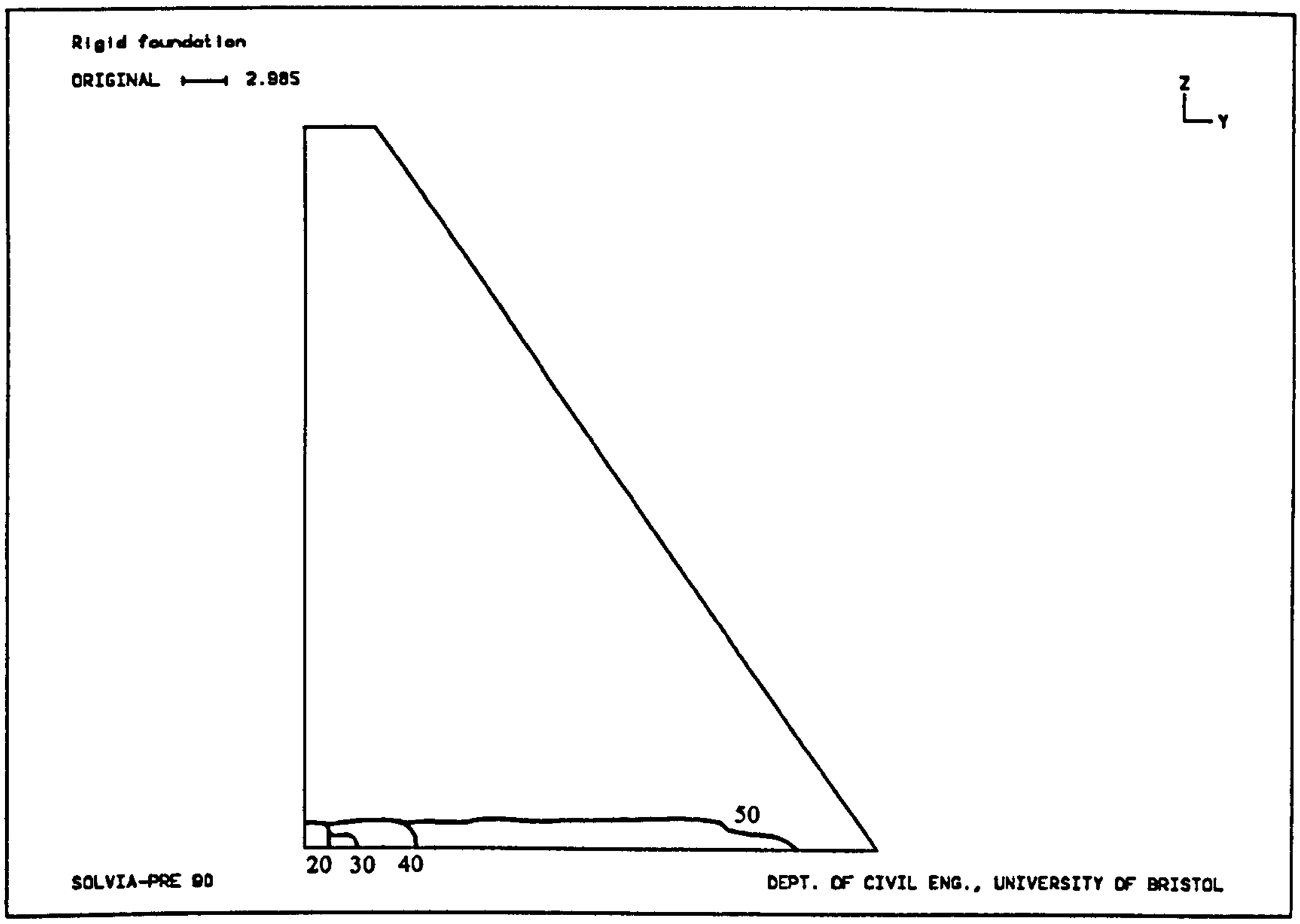

Figure 8.6a - Damaged zones for different water levels (cracking model, σ_t=2MPa)

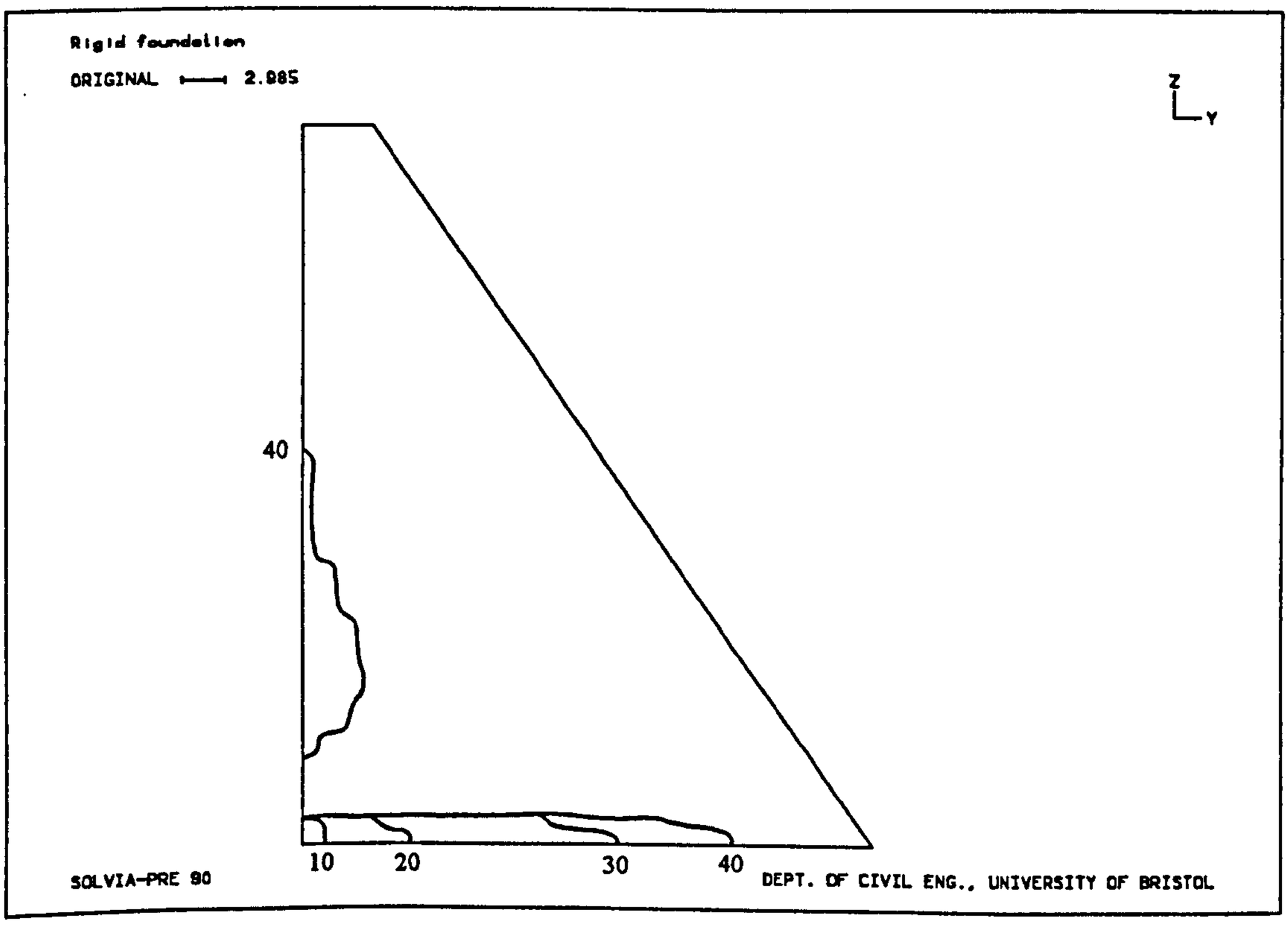

Figure 8.6b - Damaged zones for different water levels (cracking model, σ_t=1MPa)

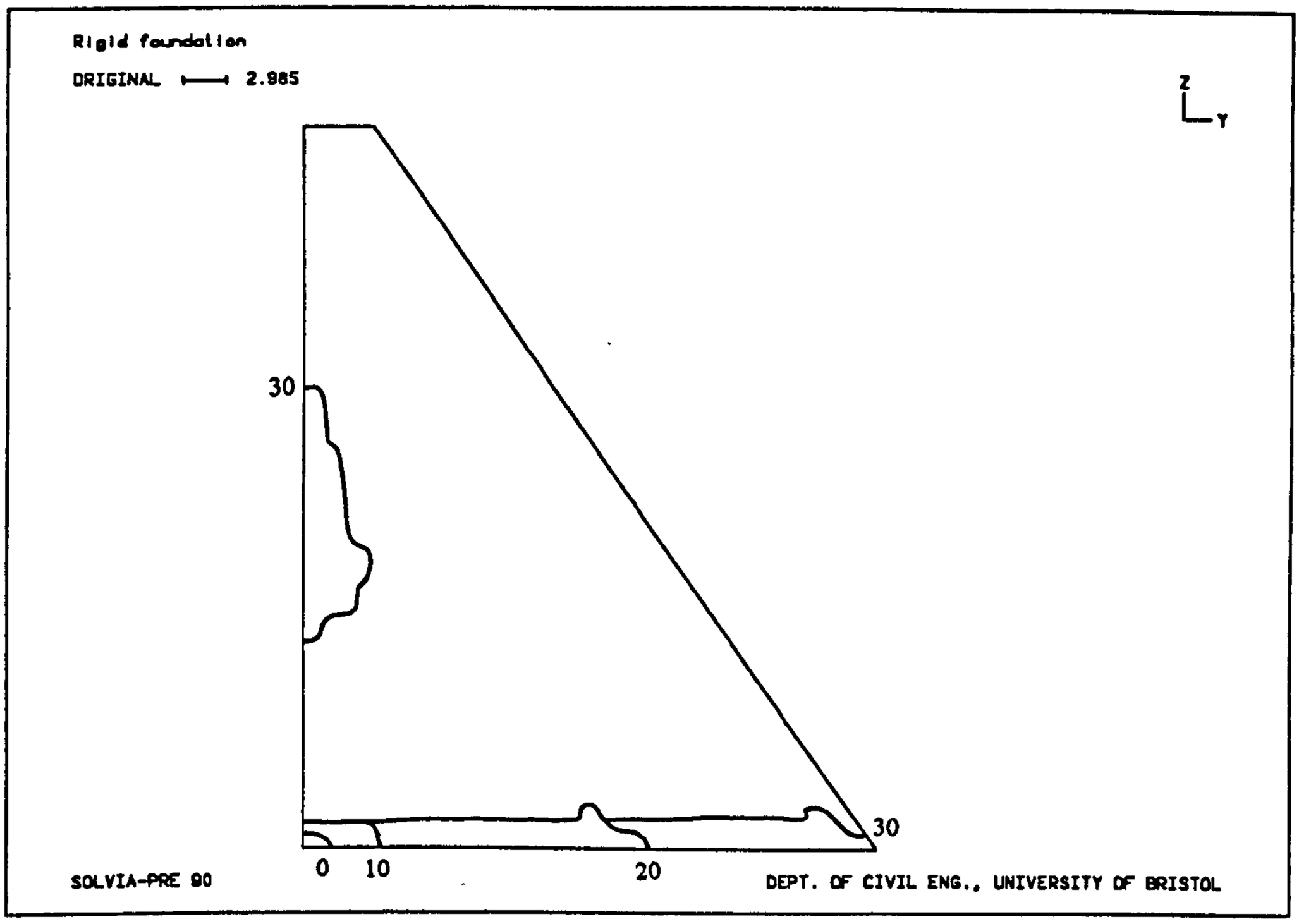

Figure 8.6c - Damaged zones for different water levels (cracking model, σ_t=.5MPa)

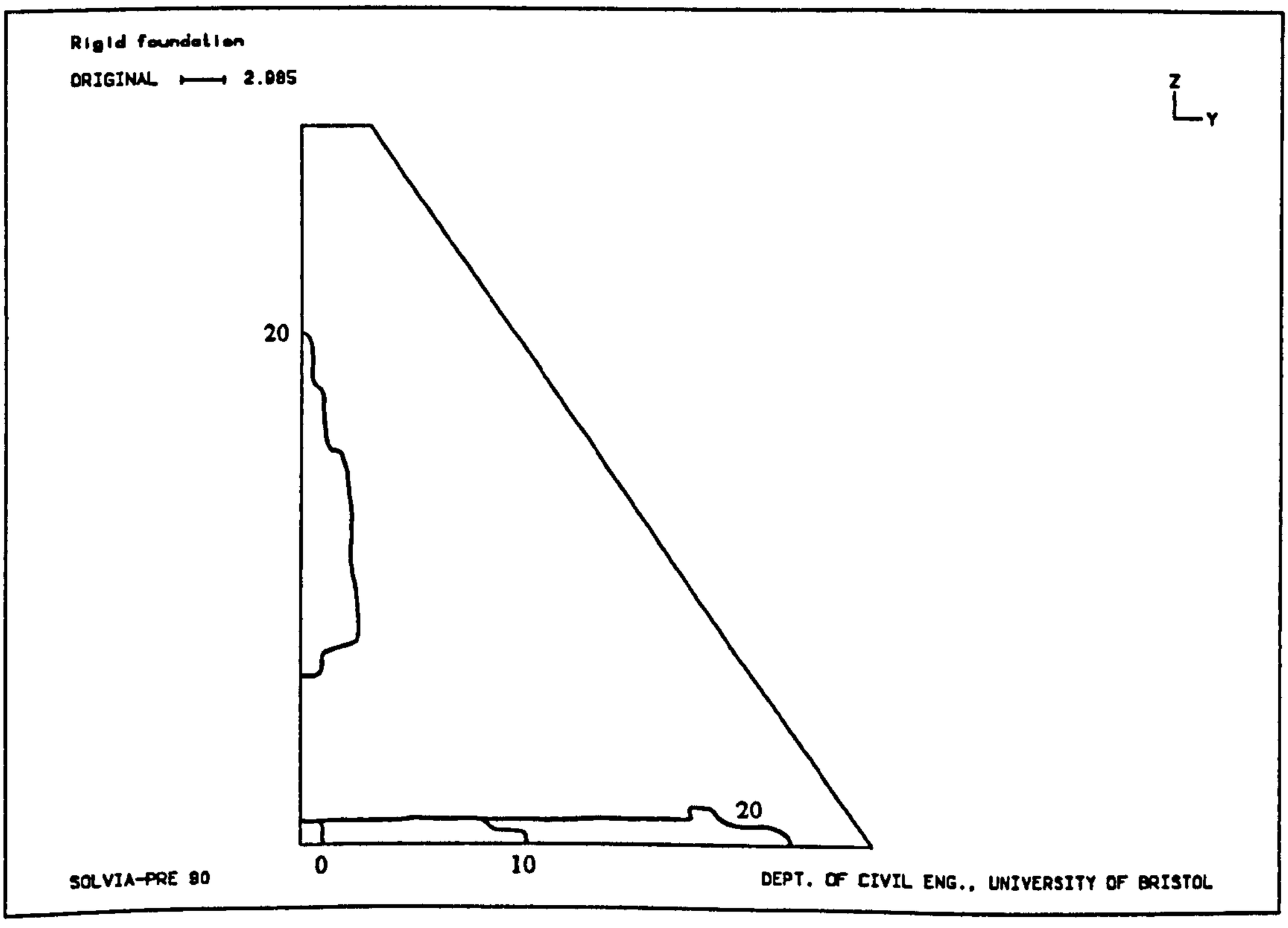

Figure 8.6d - Damaged zones for different water levels (cracking model, σ_t=.2MPa)

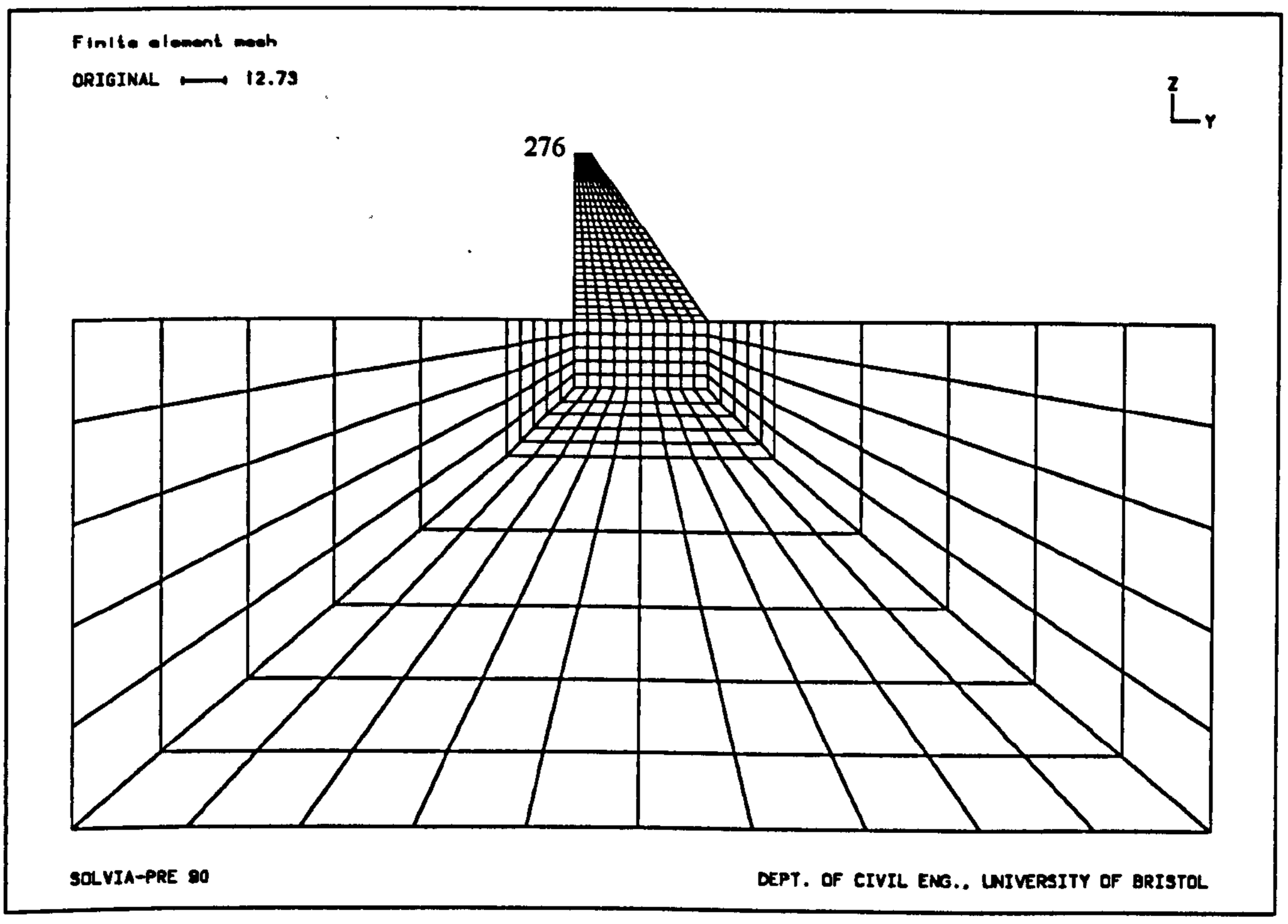

Figure 8.7 - Finite element mesh of the concrete gravity dam-foundation system

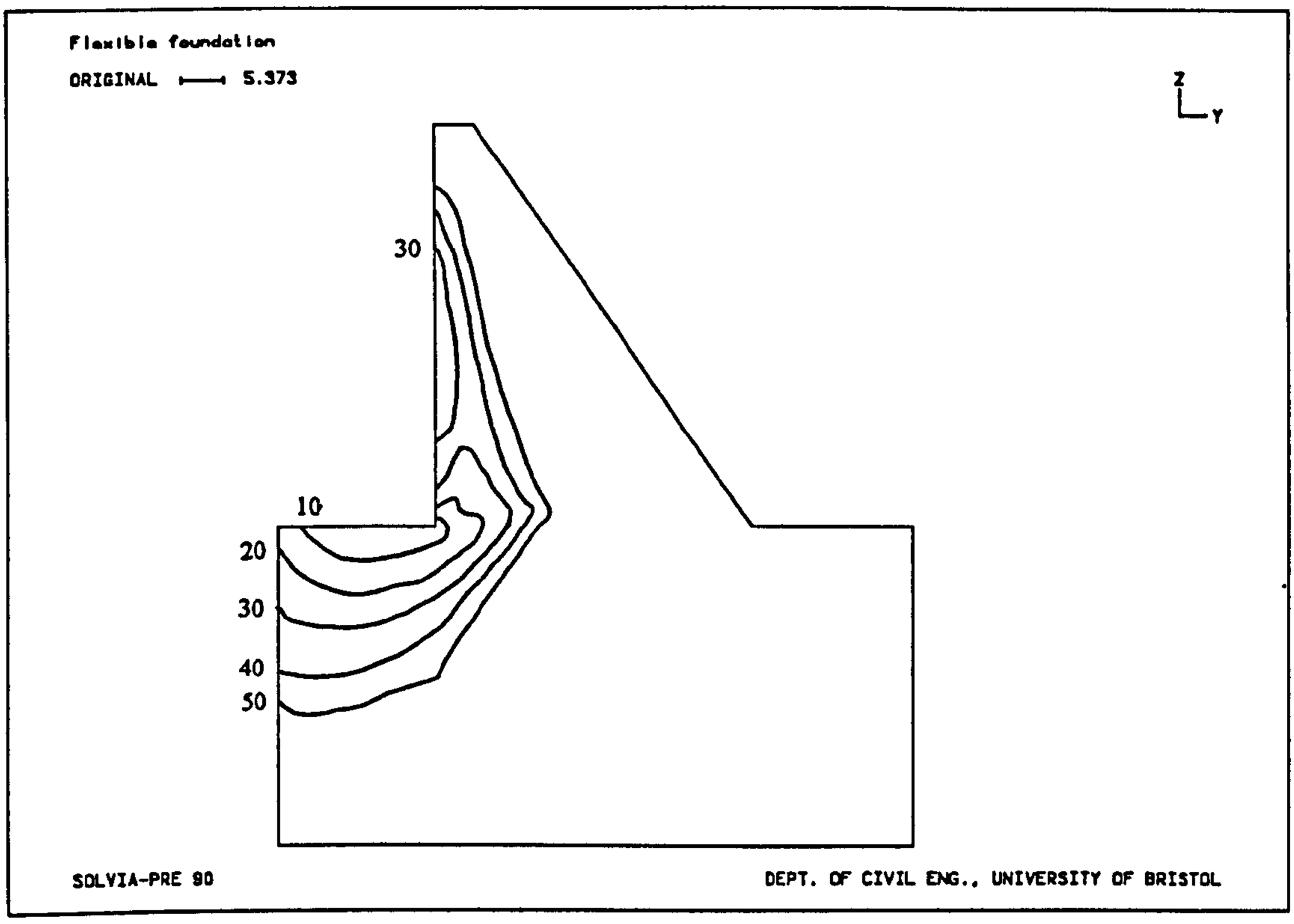

Figure 8.8a - Damaged zones for different water levels (linear model, E_f=5GPa)

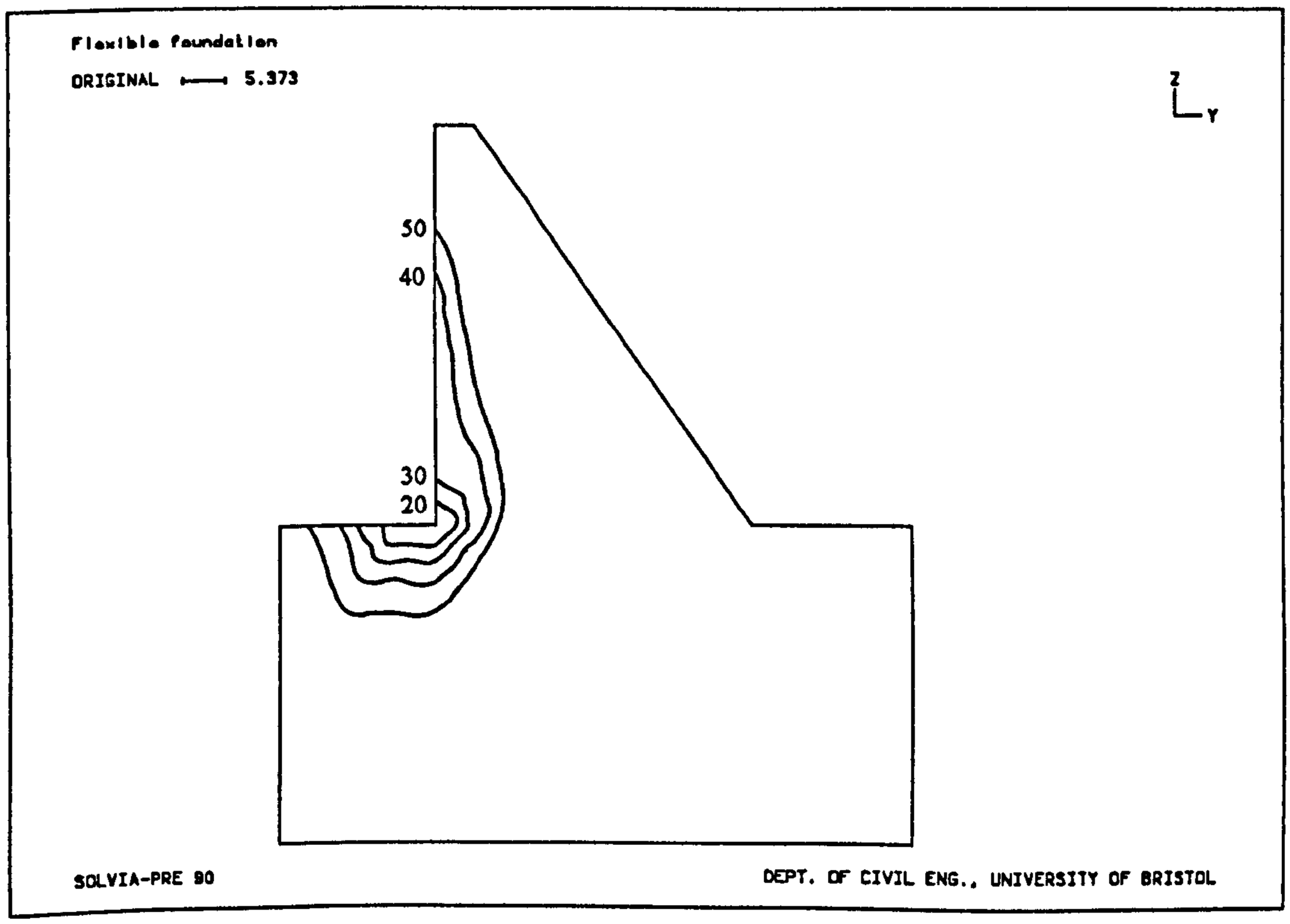

Figure 8.8b - Damaged zones for different water levels (linear model, E_f=10GPa)

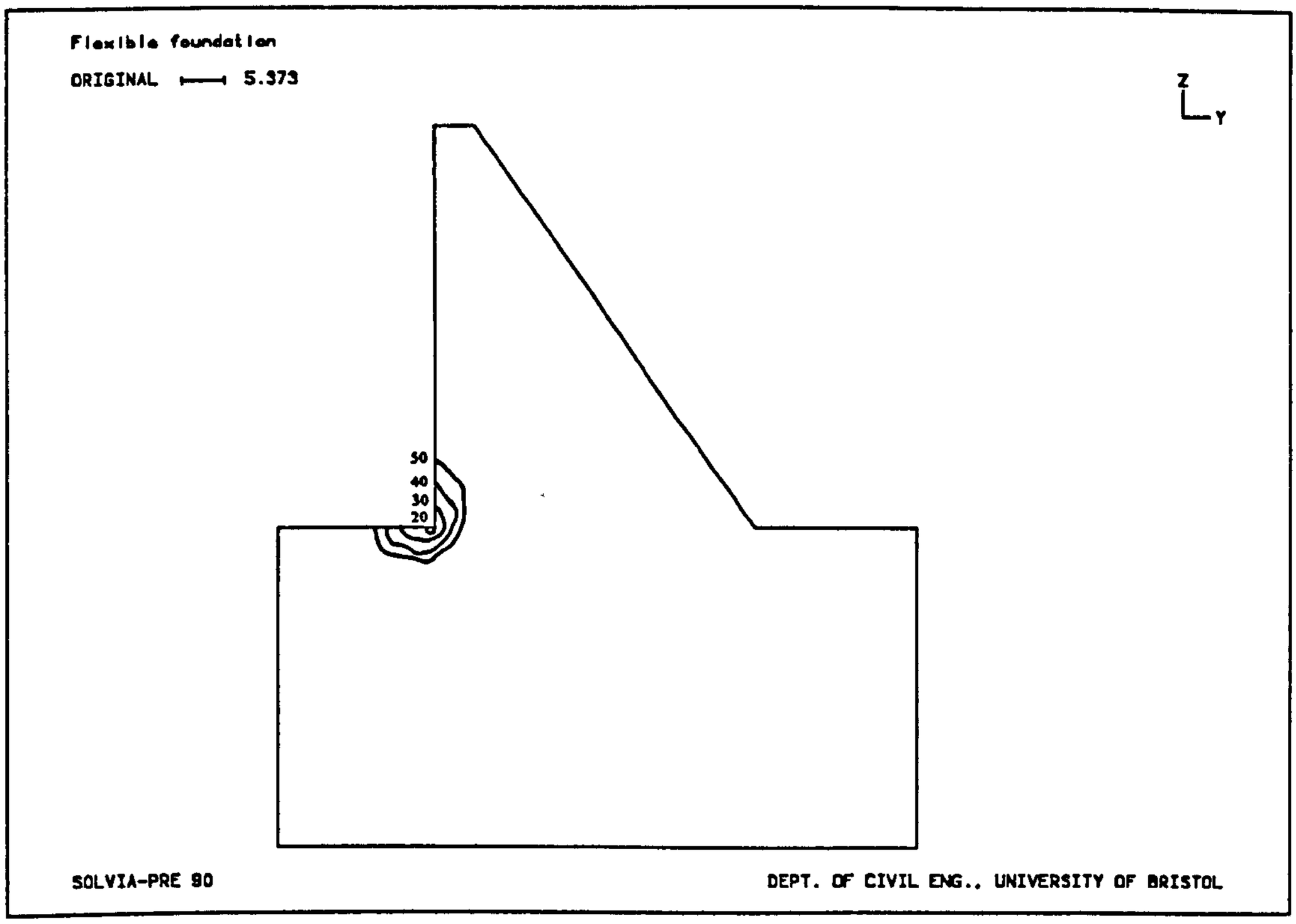

Figure 8.8c - Damaged zones for different water levels (linear model, E_f=20GPa)

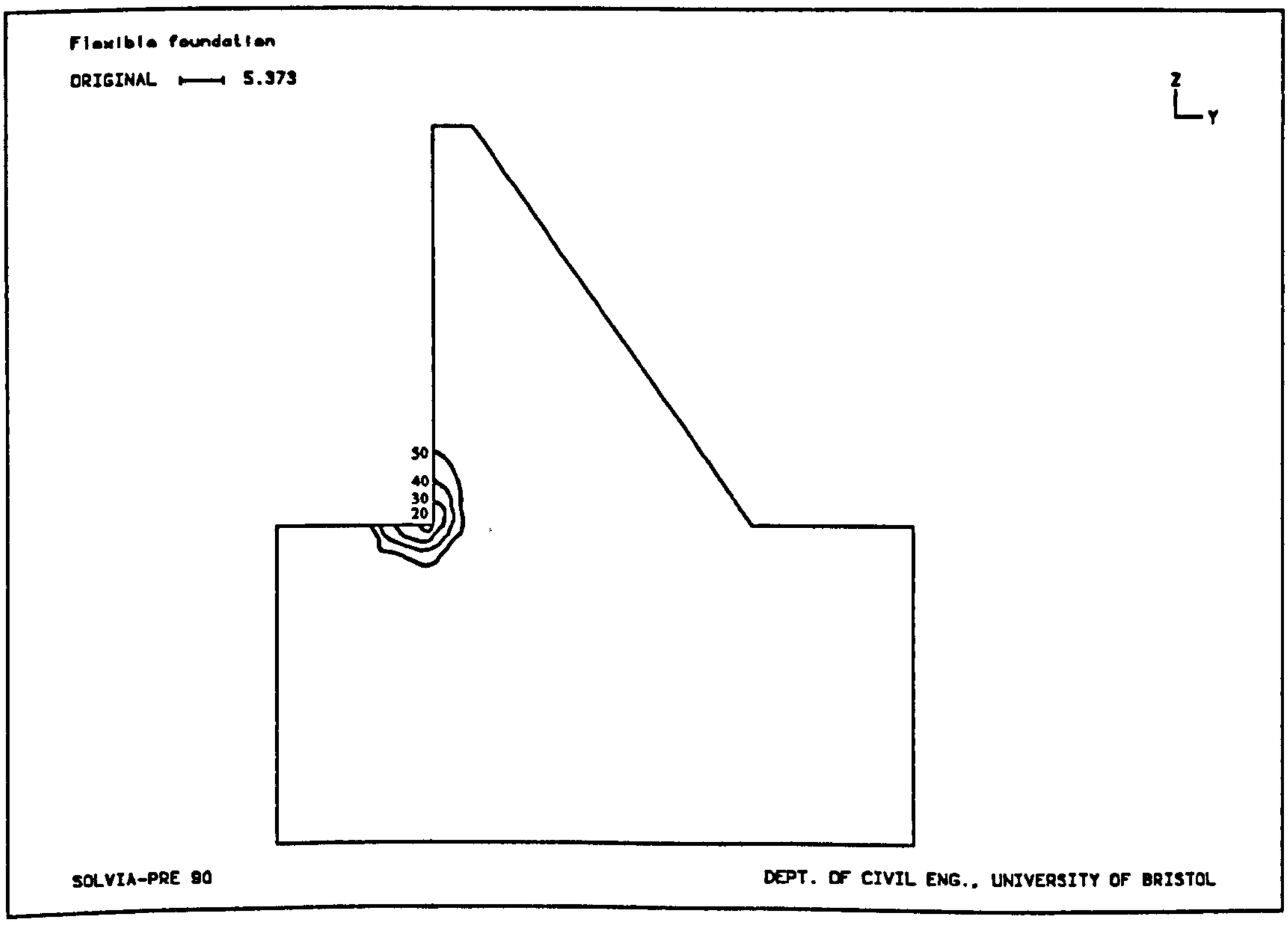

Figure 8.8d - Damaged zones for different water levels (linear model, E_f=40GPa)

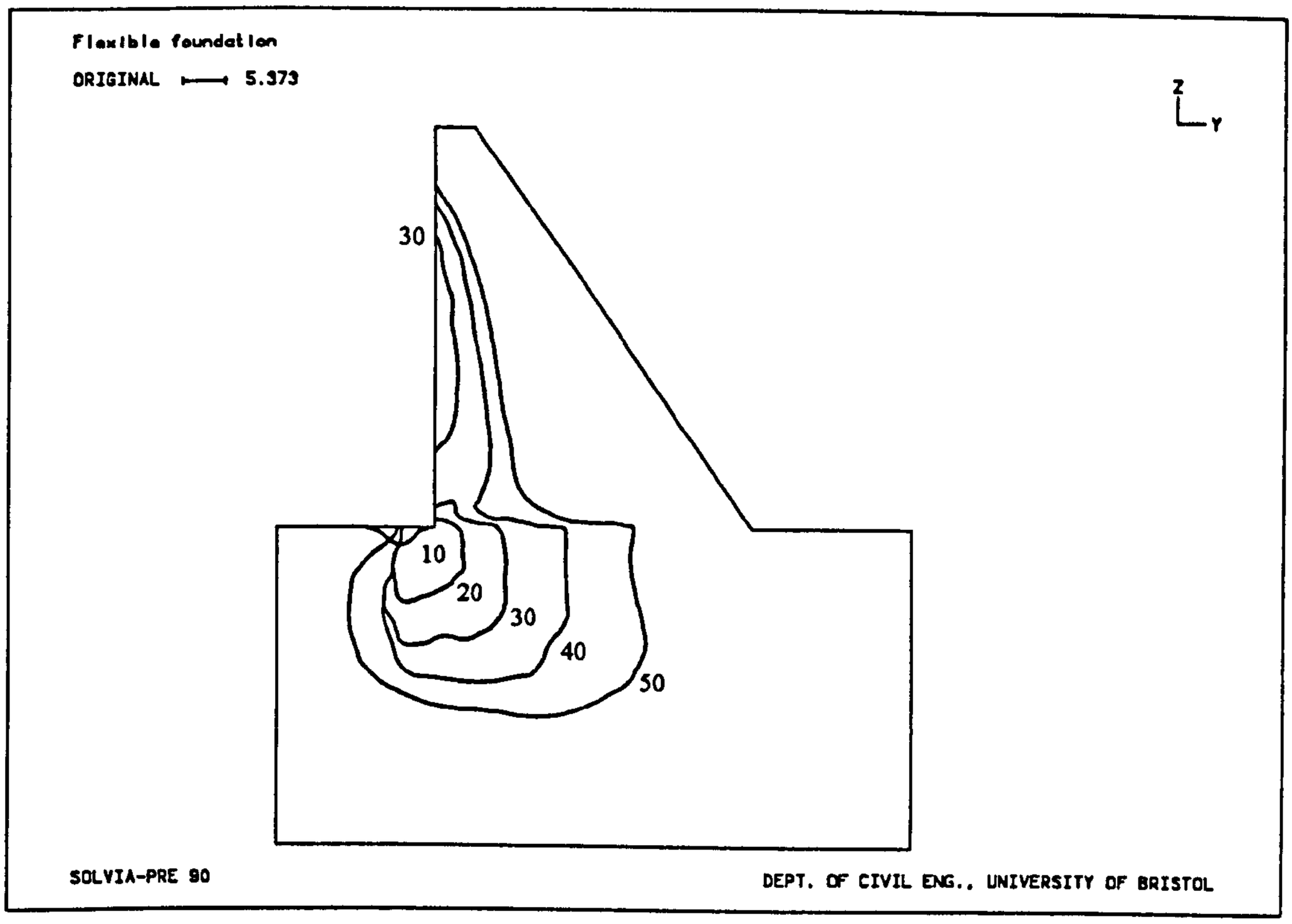

Figure 8.9a - Damaged zones for different water levels (plasticity, E_f=5GPa)

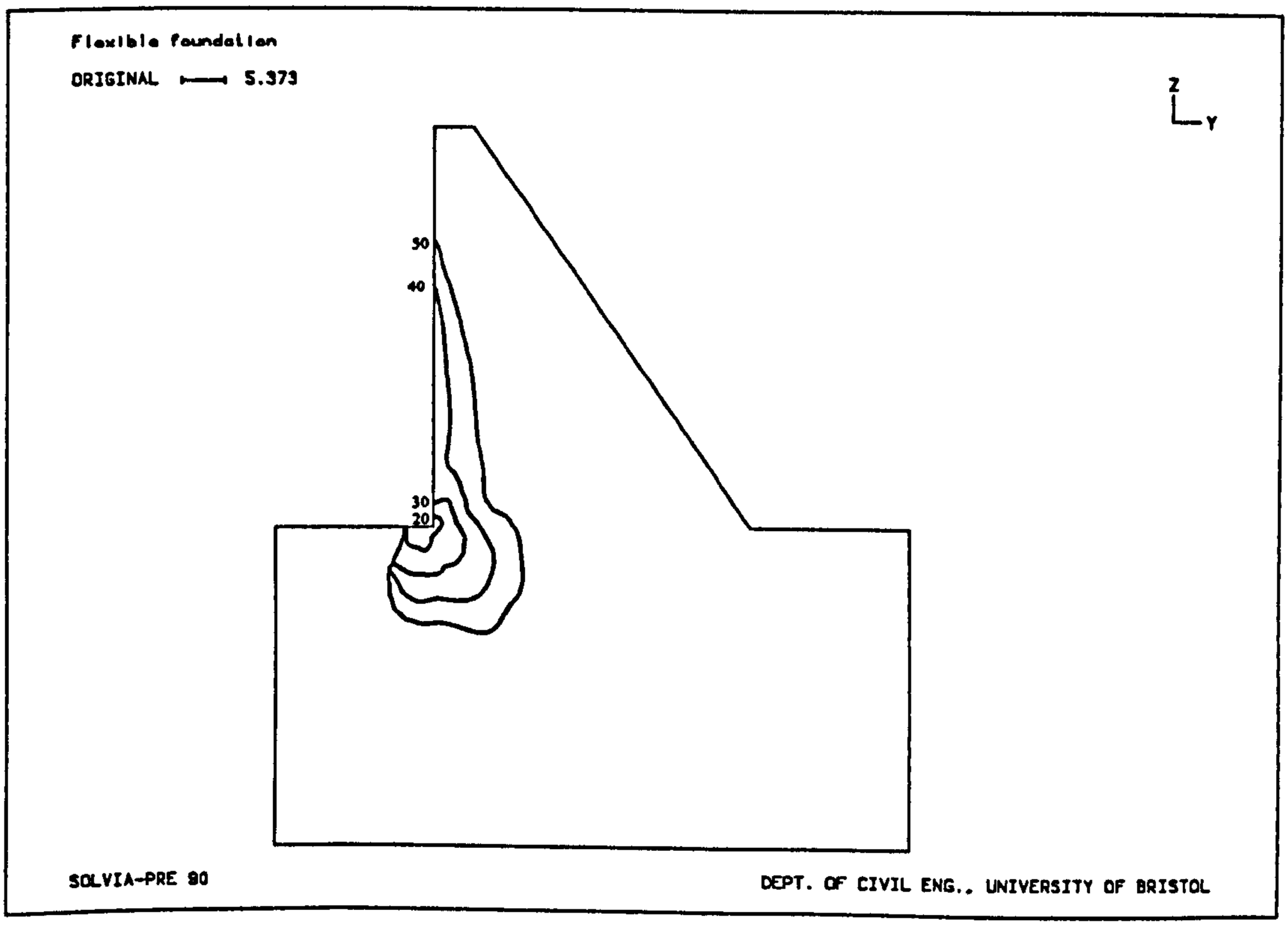

Figure 8.9b - Damaged zones for different water levels (plasticity, E_f=10GPa)

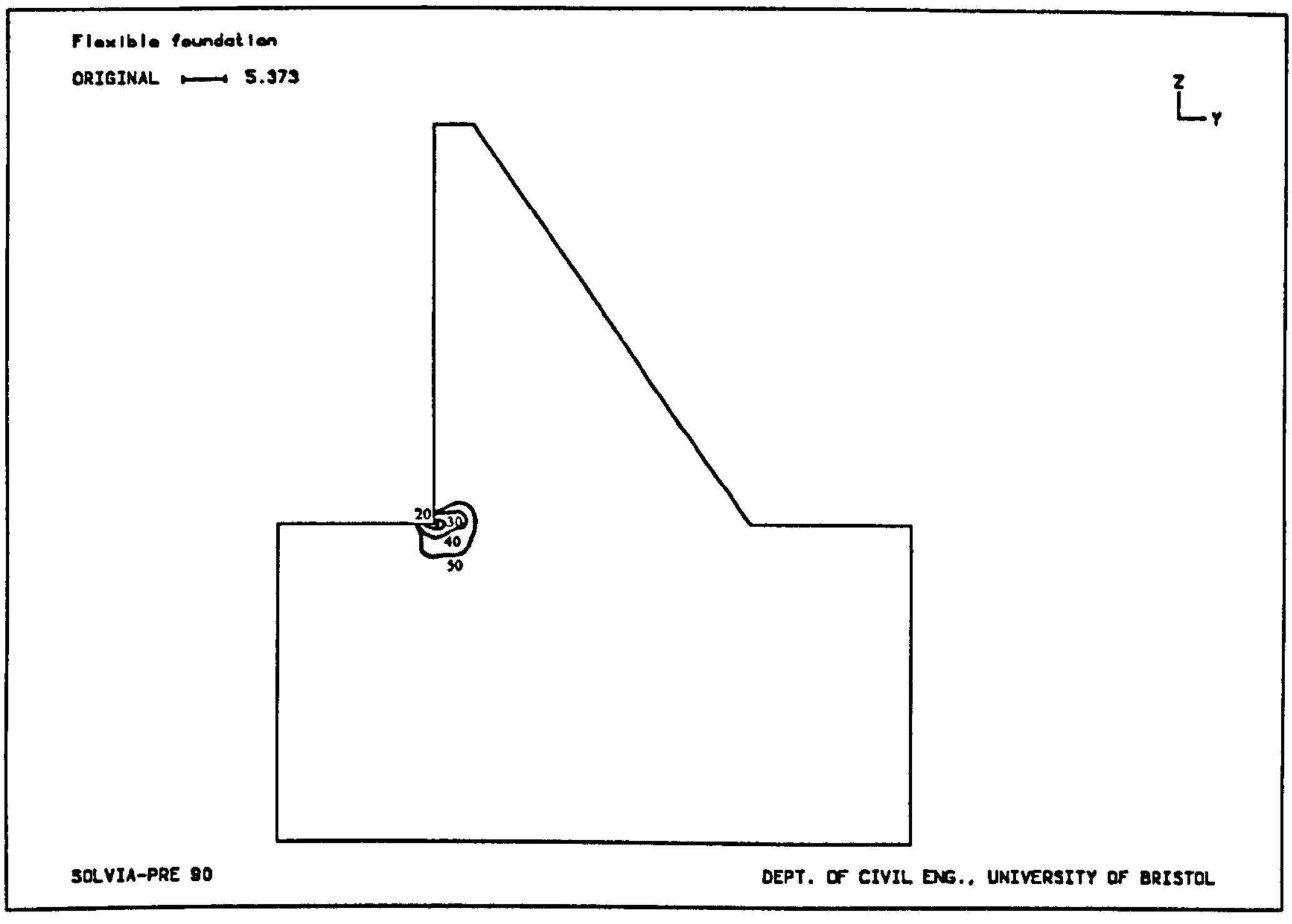

Figure 8.9c - Damaged zones for different water levels (plasticity, E_f=20GPa)

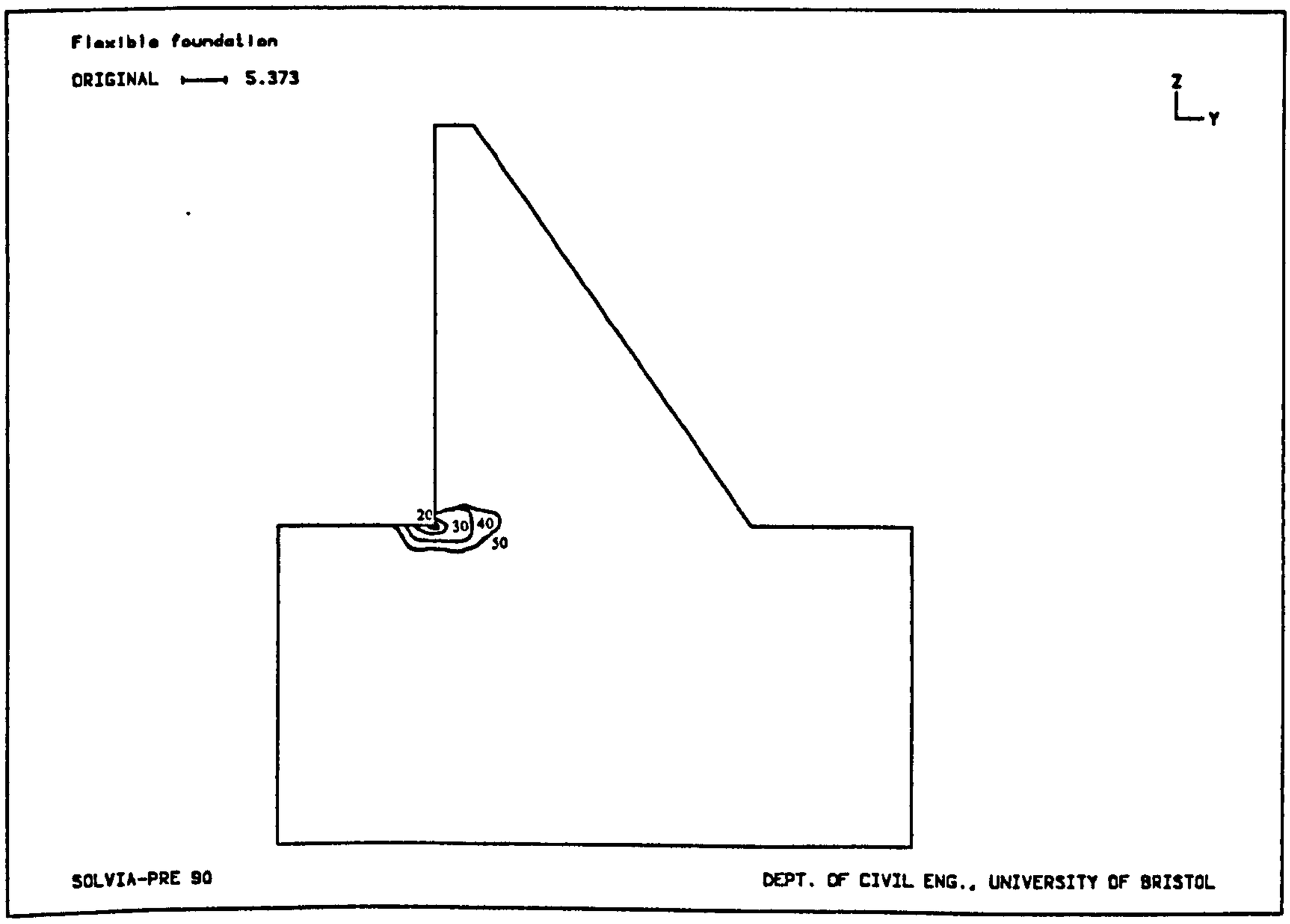

Figure 8.9d - Damaged zones for different water levels (plasticity, E_f=40GPa)

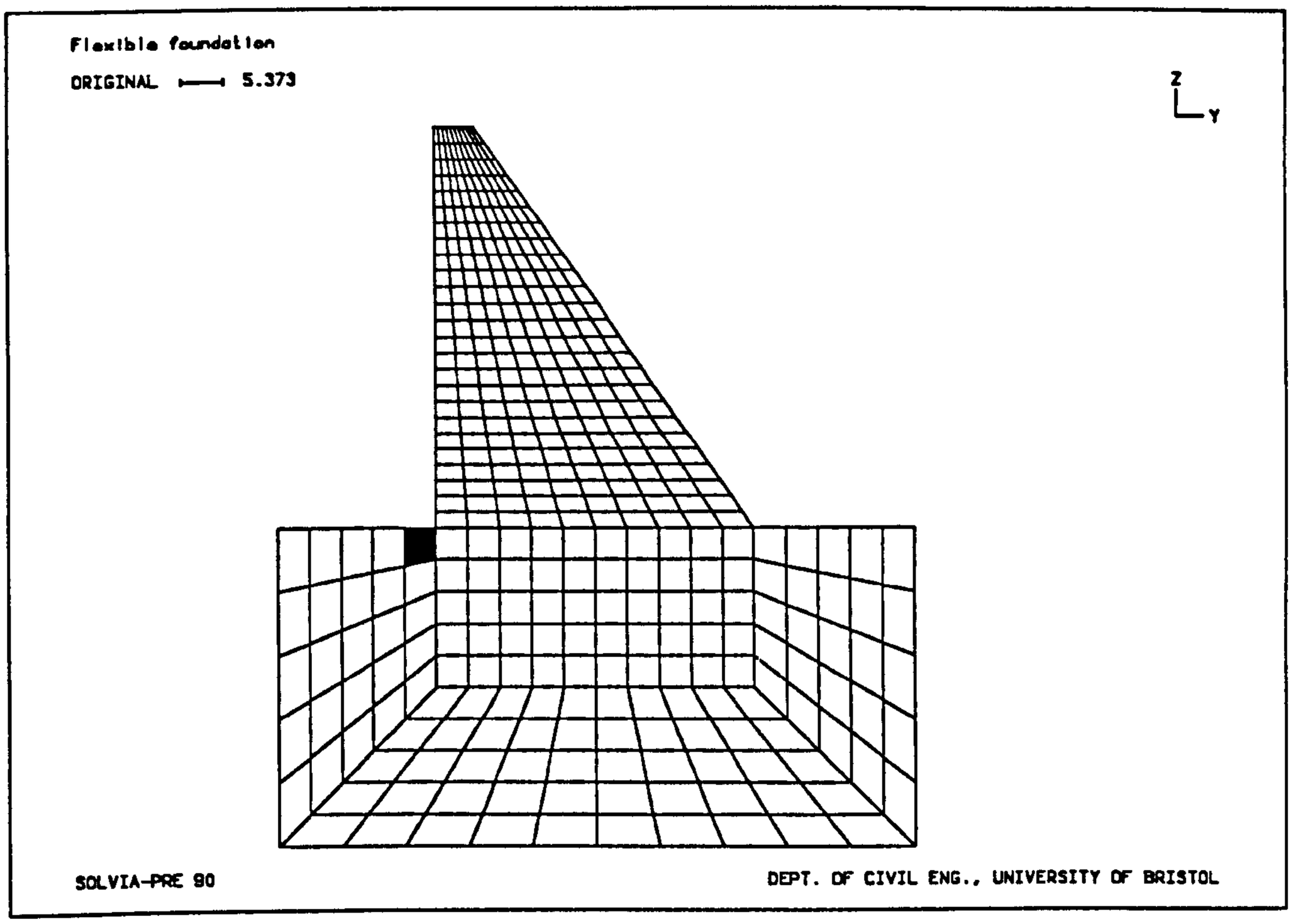

Figure 8.10a - Cracking pattern for water level 10 (E_f=5GPa)

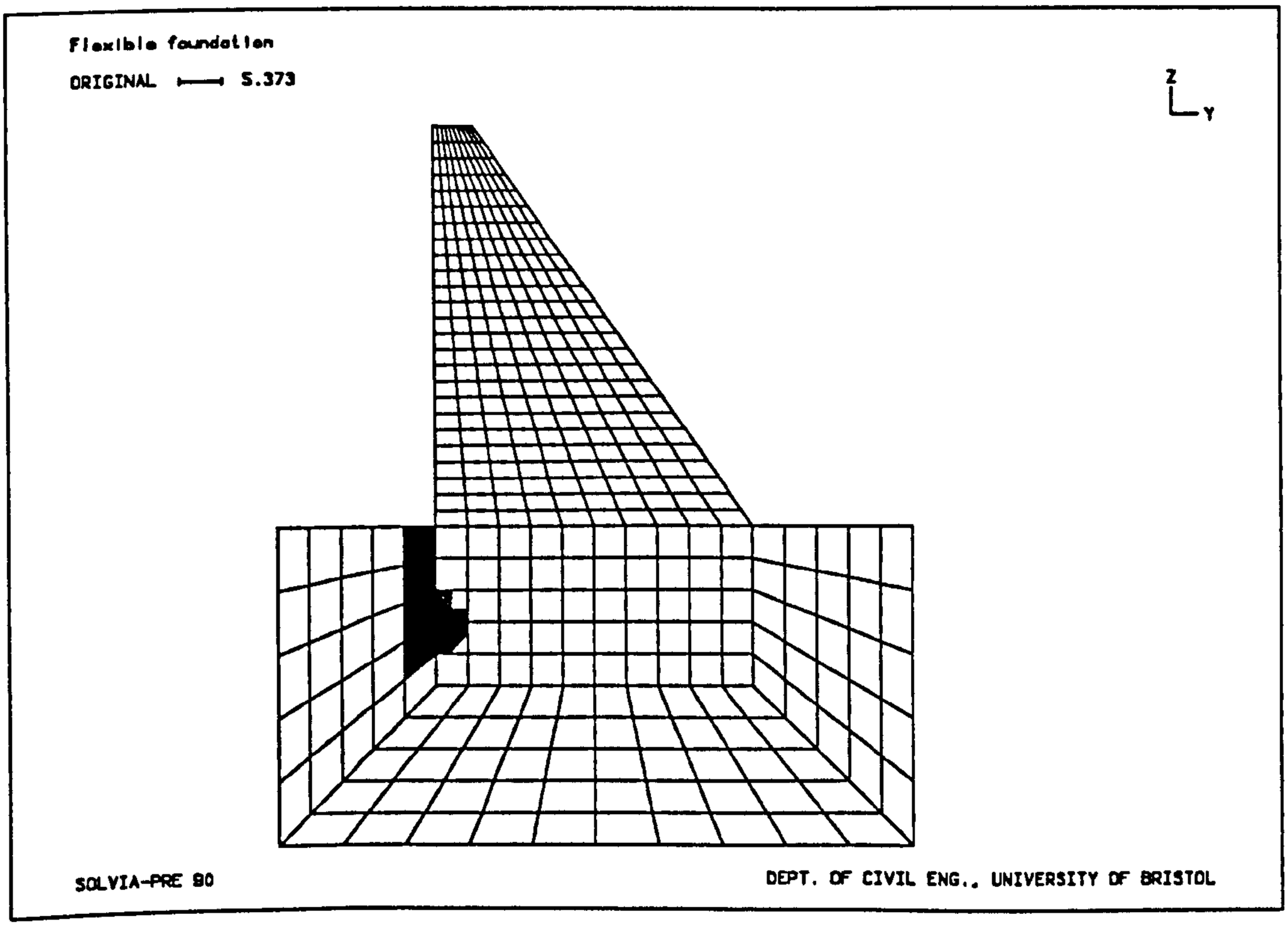

Figure 8.10b - Cracking pattern for water level 20 (E_f=5GPa)

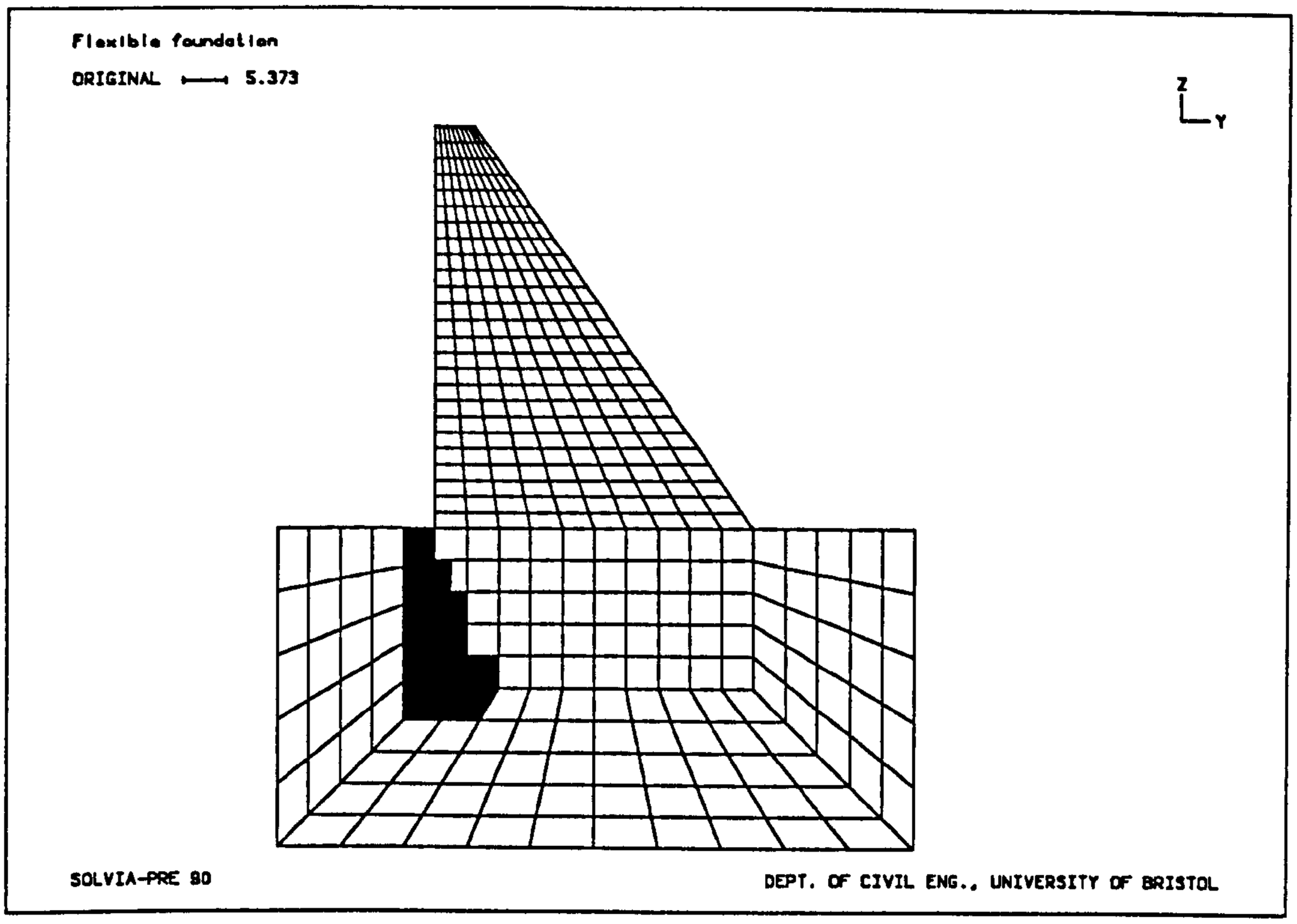

Figure 8.10c - Cracking pattern for water level 30 (E_f=5GPa)

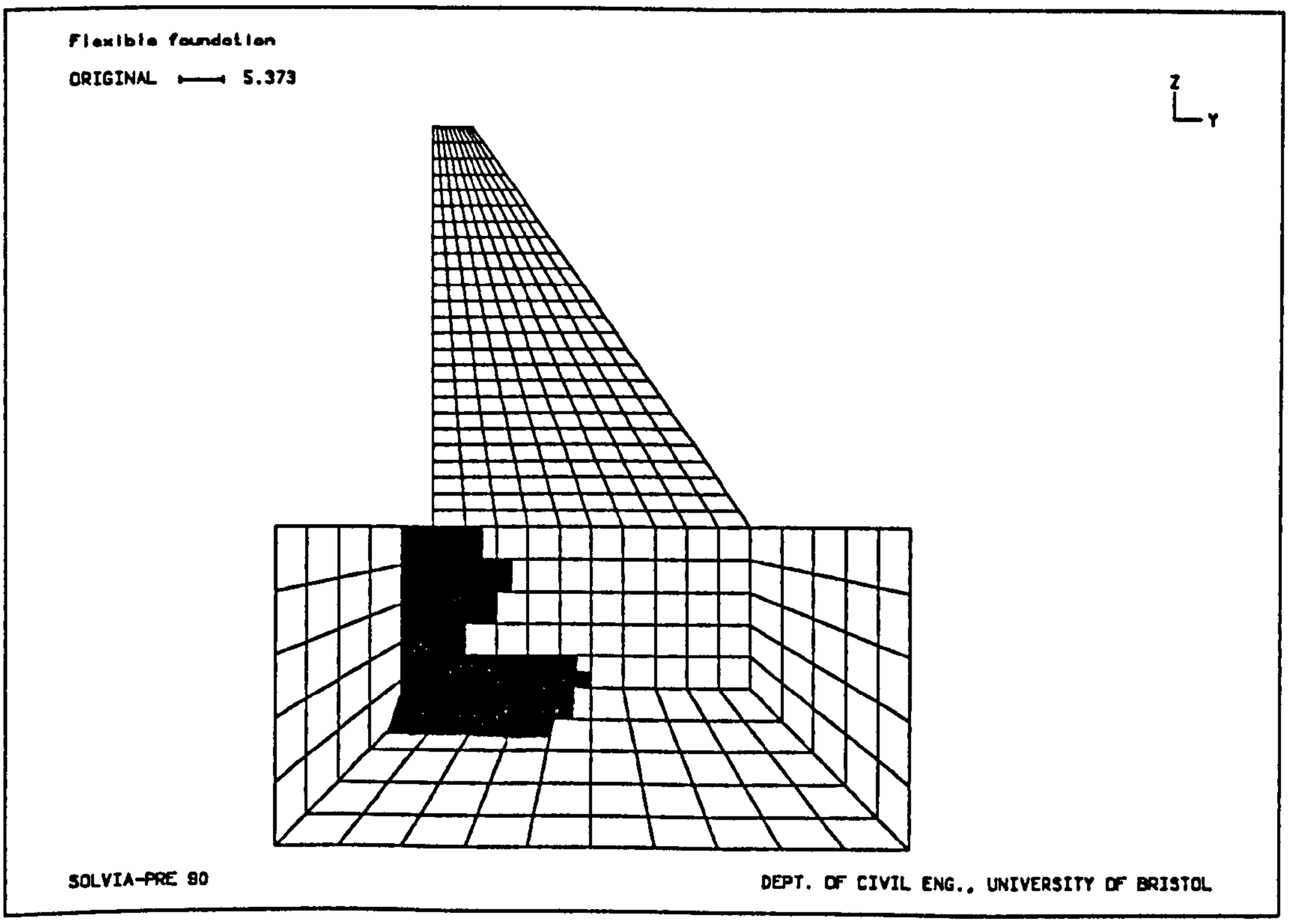

Figure 8.10d - Cracking pattern for water level 40 (E_f=5GPa)

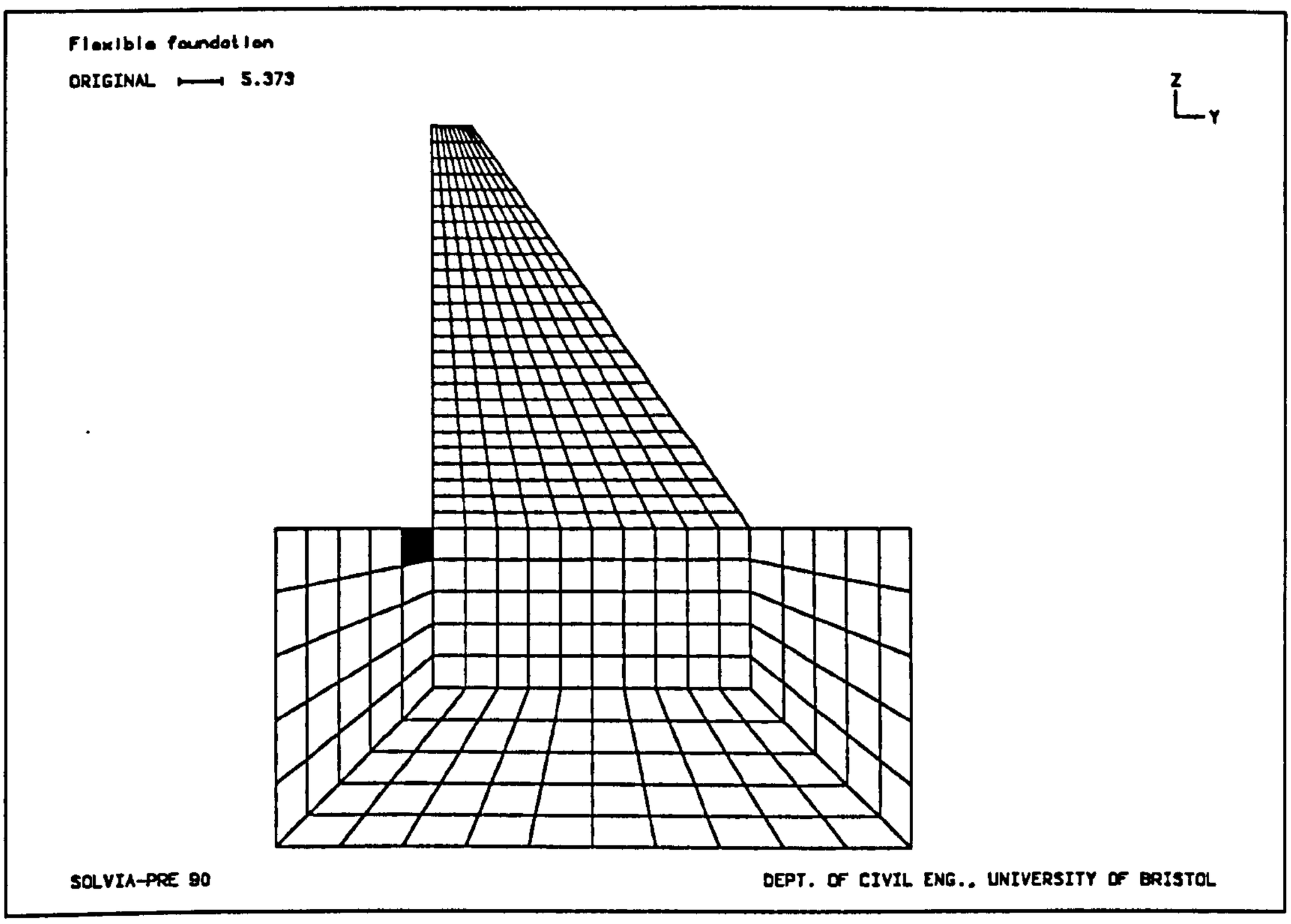

Figure 8.11a - Cracking pattern for water level 20 (E_f=10GPa)

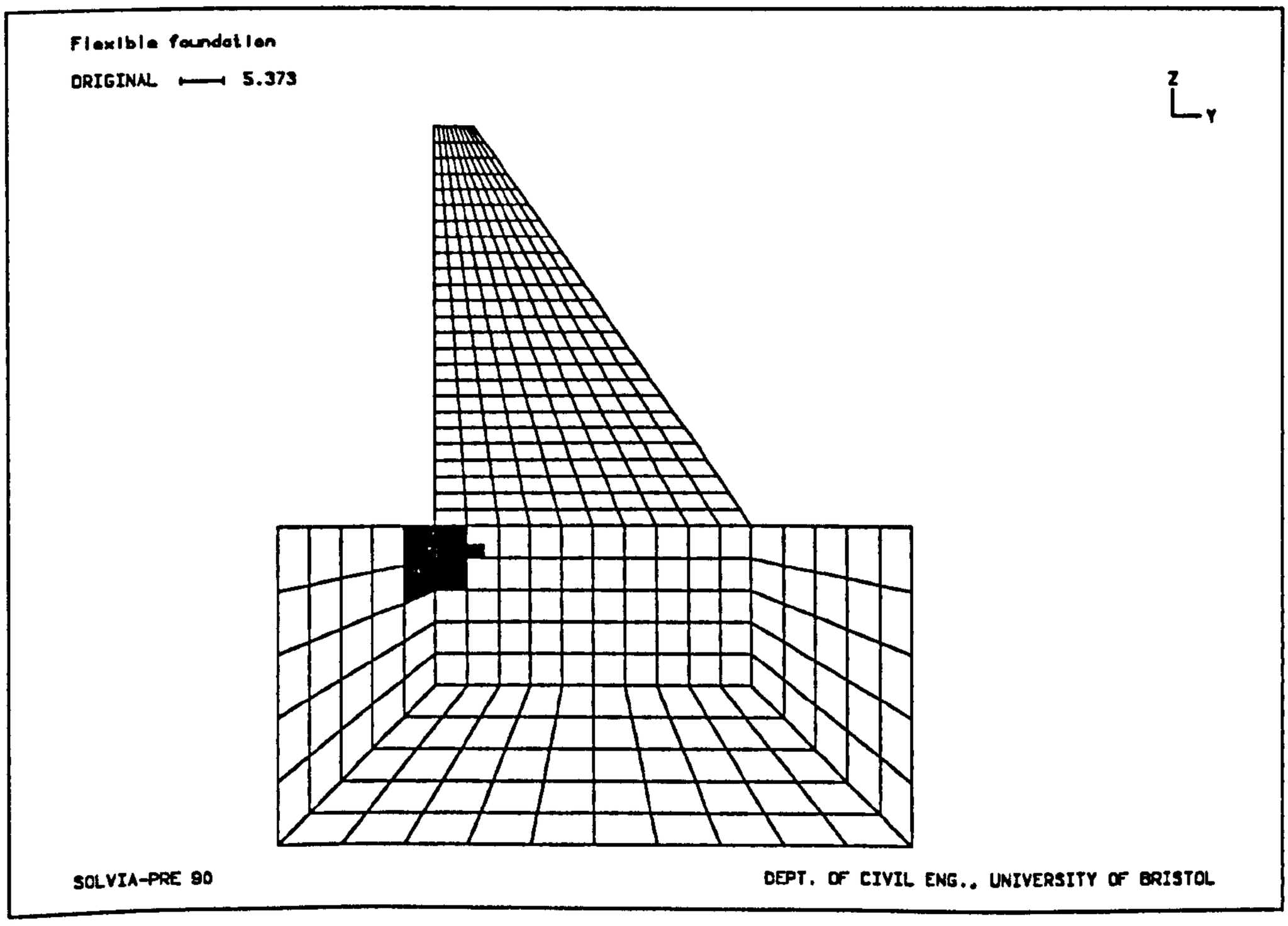

Figure 8.11b - Cracking pattern for water level 30 (E_f=10GPa)

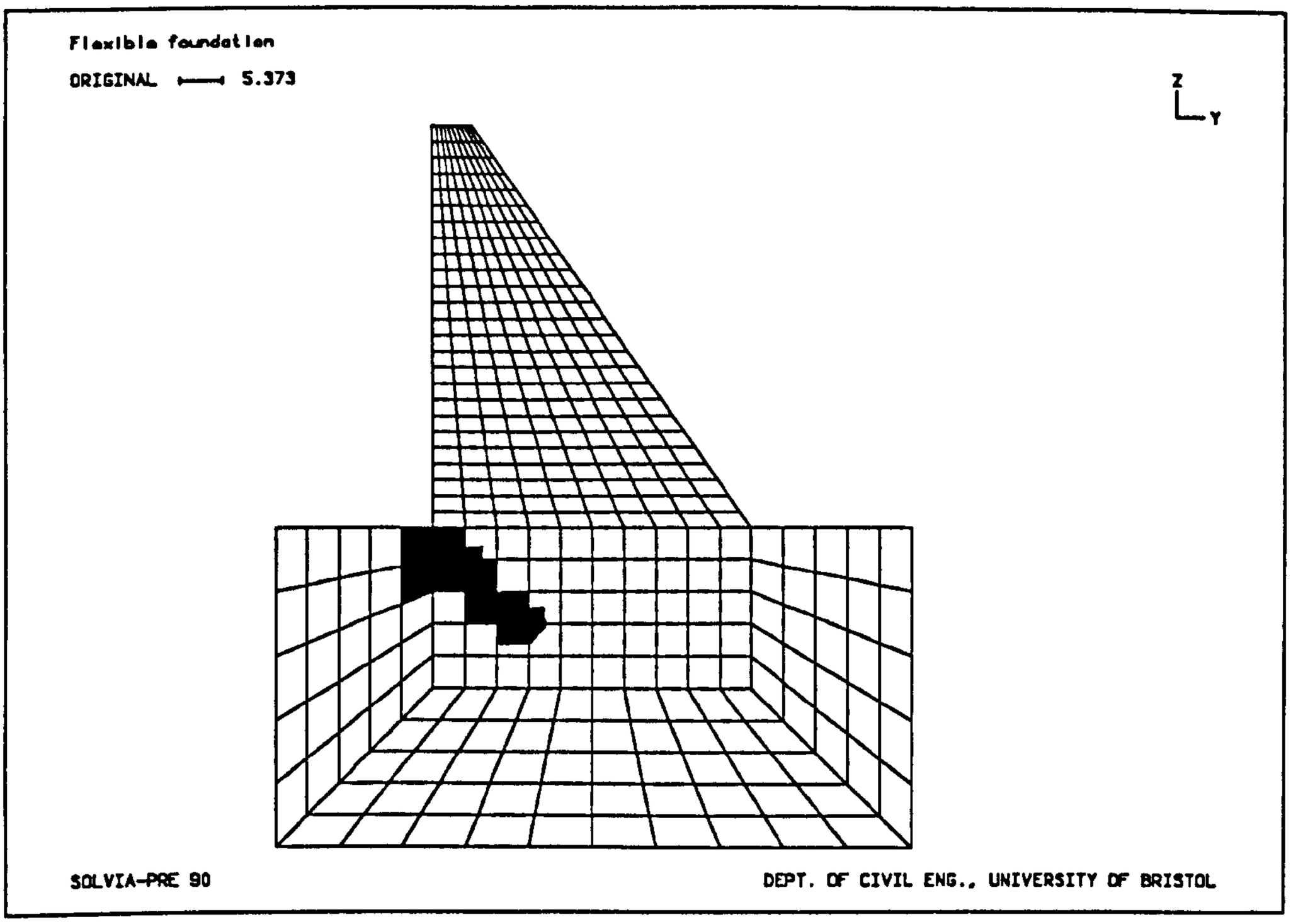

Figure 8.11c - Cracking pattern for water level 40 (E_f=10GPa)

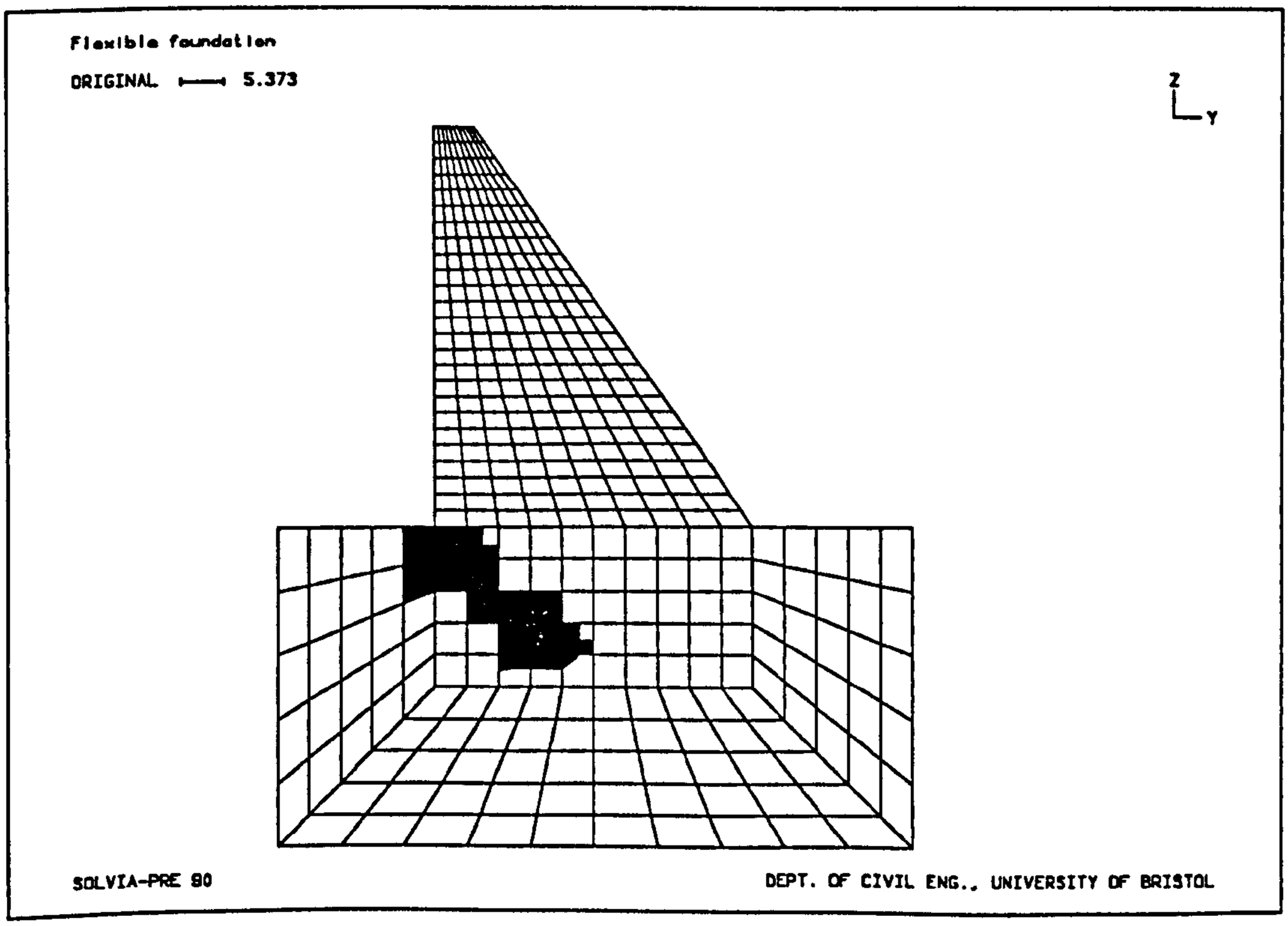

Figure 8.11d - Cracking pattern for water level 50 (E_f=10GPa)

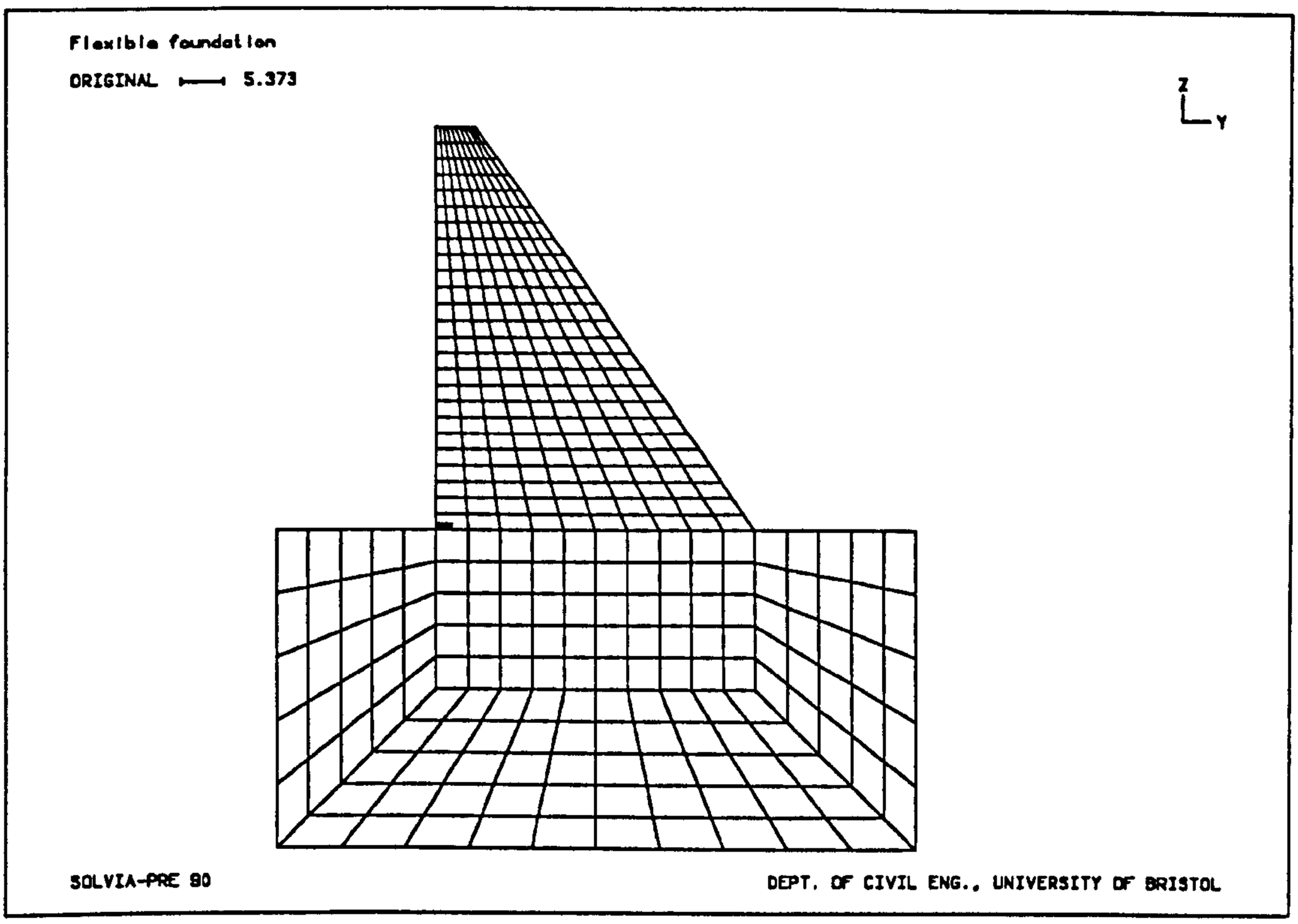

Figure 8.12a - Cracking pattern for water level 20 (E_f=20GPa)

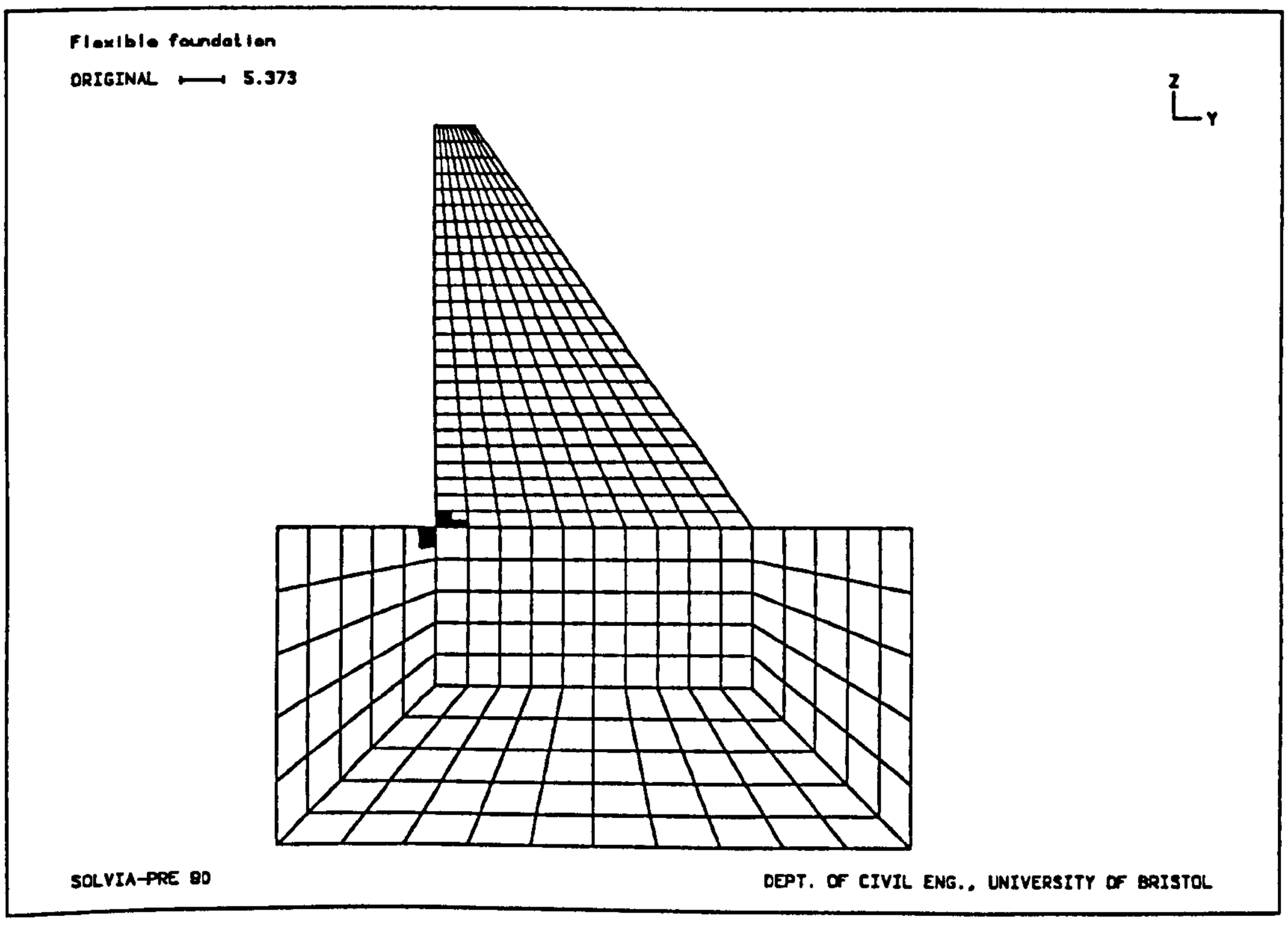

Figure 8.12b - Cracking pattern for water level 30 (E_f=20GPa)

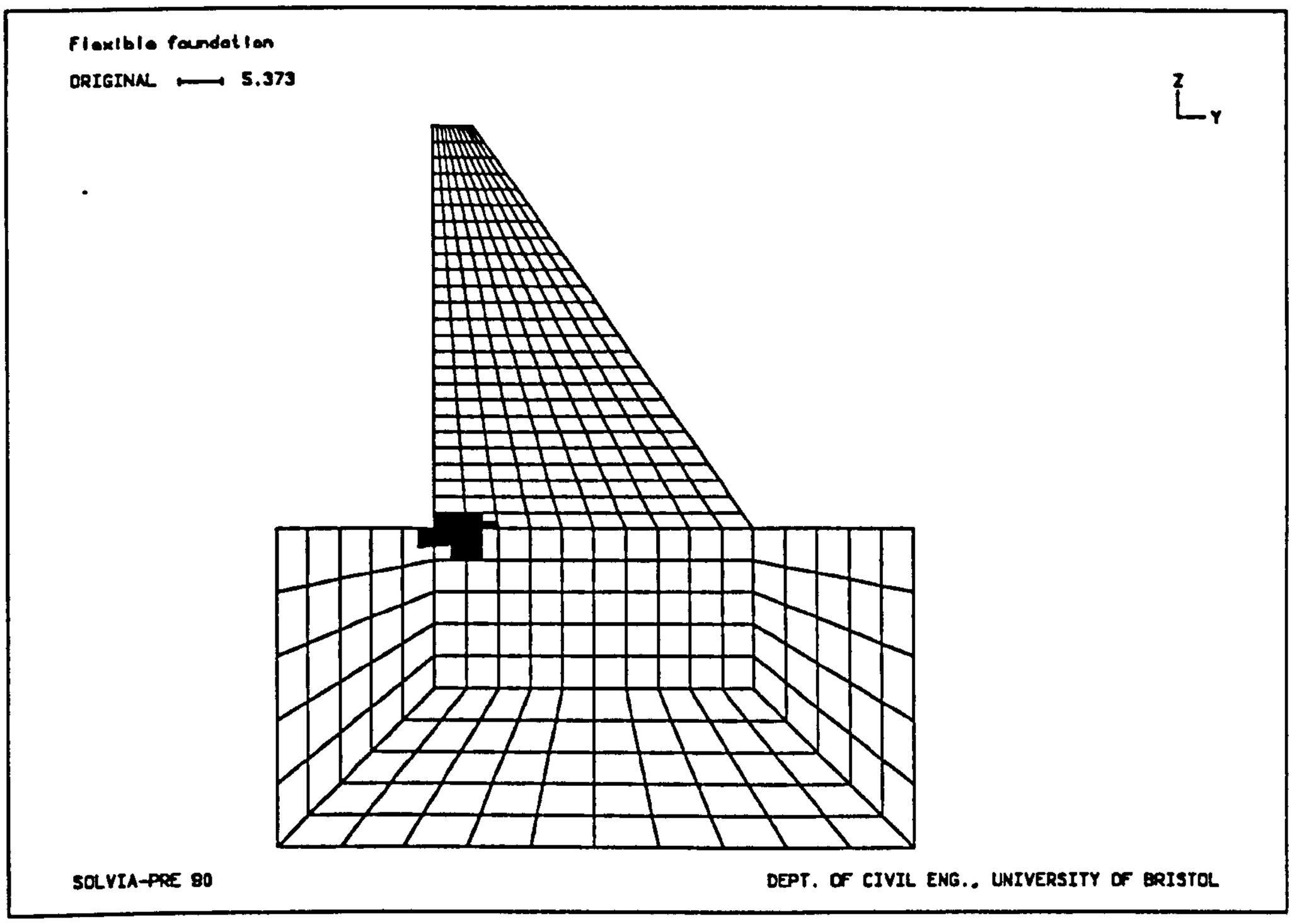

Figure 8.12c - Cracking pattern for water level 40 (E_f=20GPa)

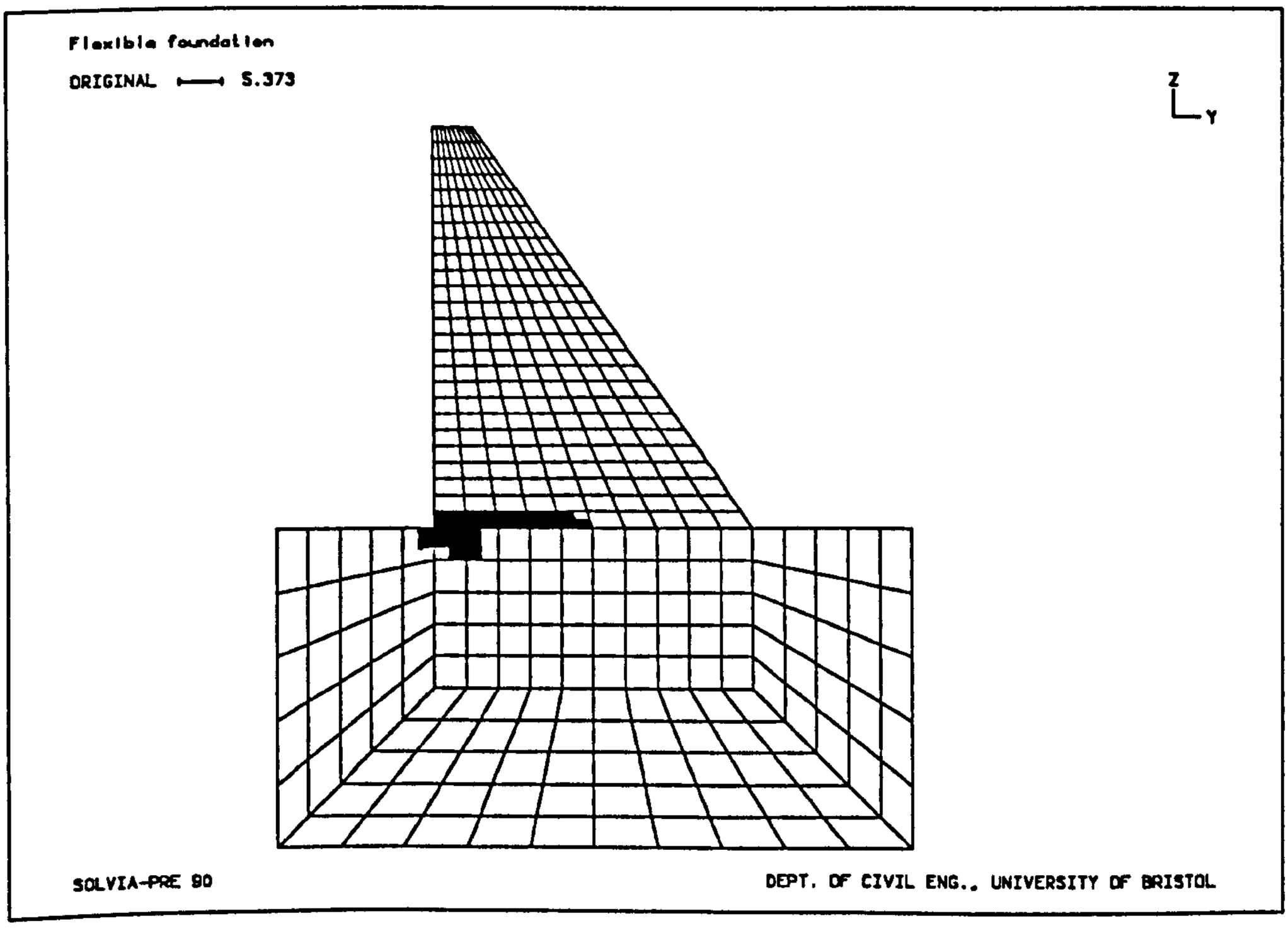

Figure 8.12d - Cracking pattern for water level 50 (E_f=20GPa)

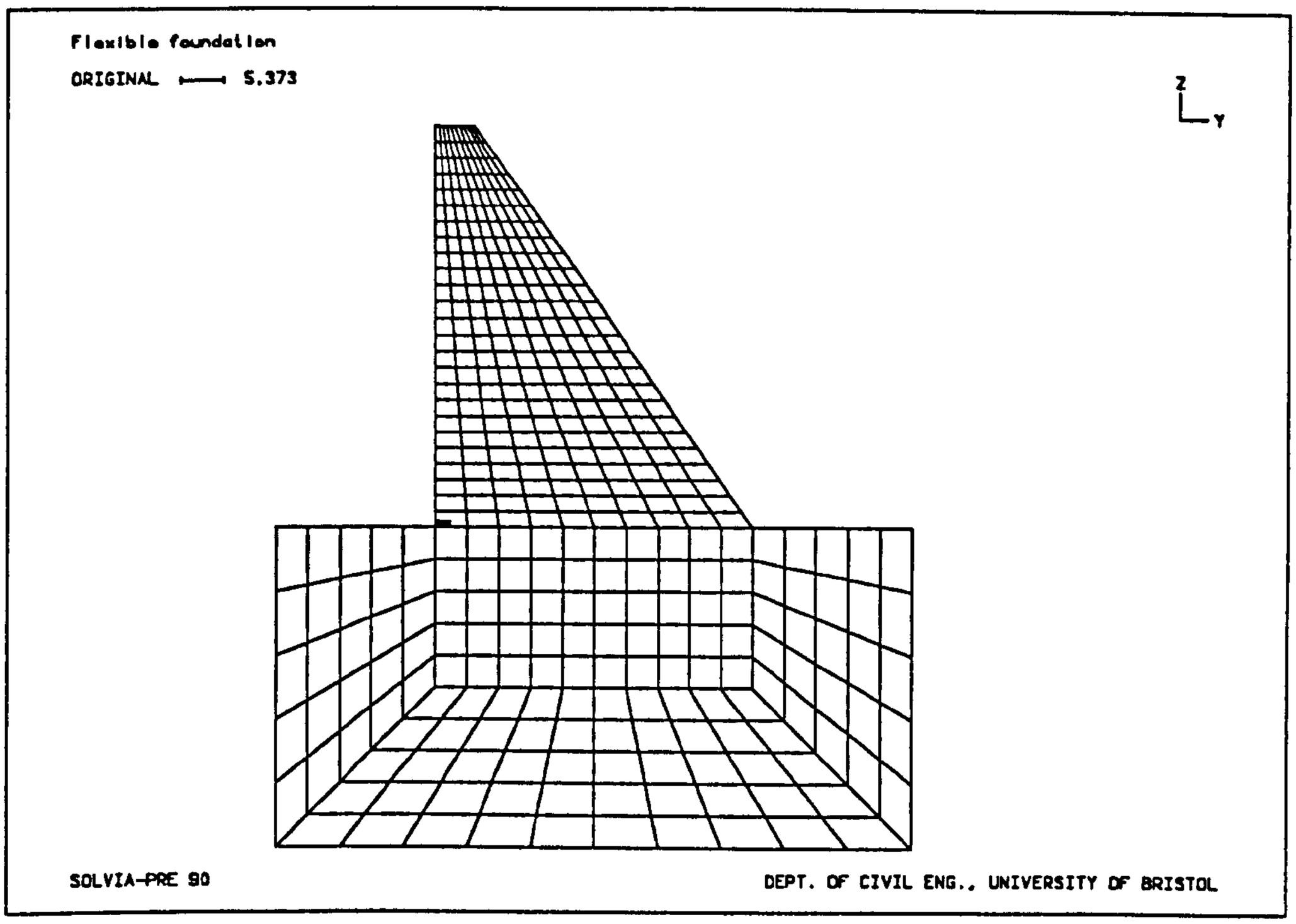

Figure 8.13a - Cracking pattern for water level 20 (E_f=40GPa)

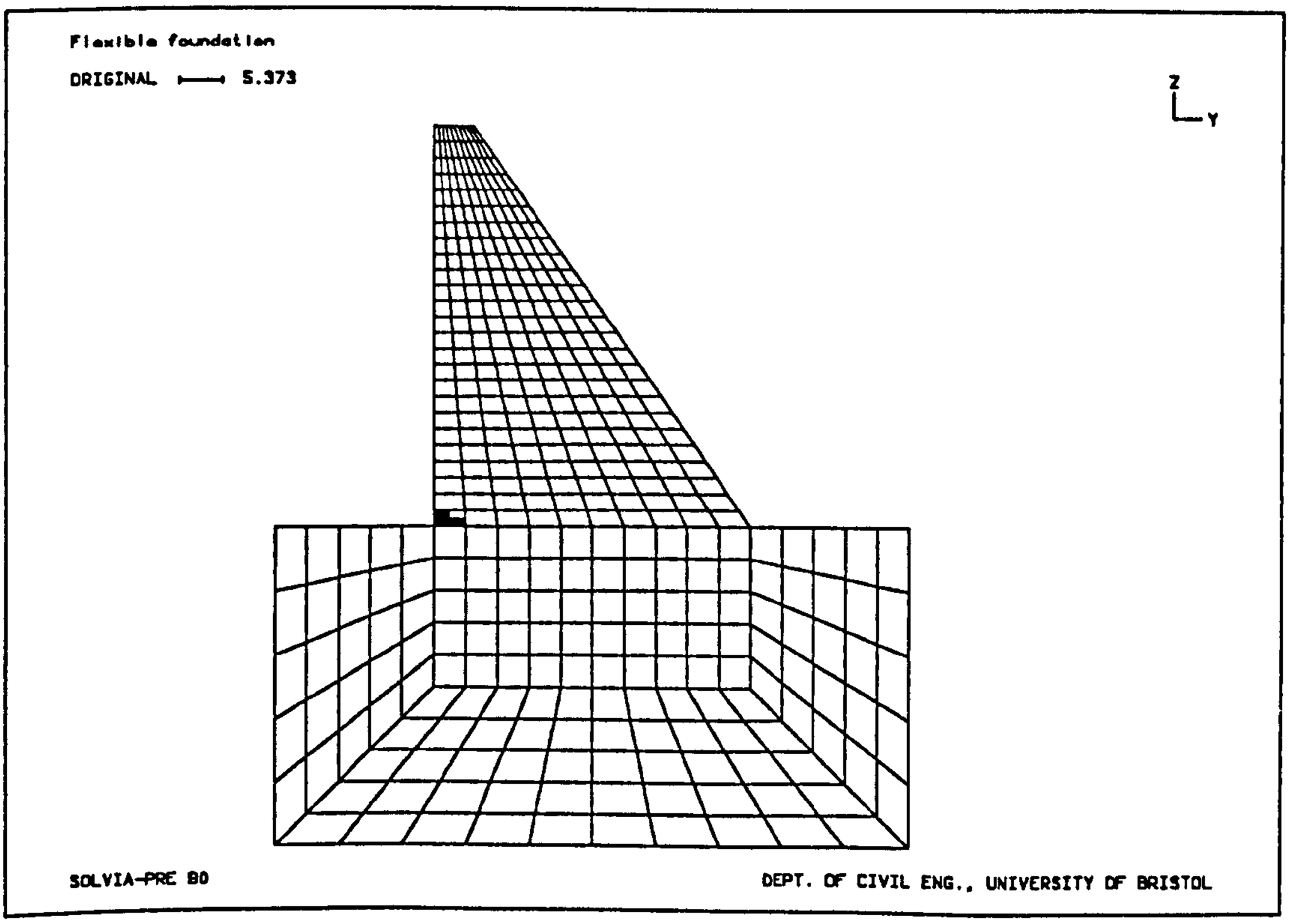

Figure 8.13b - Cracking pattern for water level 30 (E_f=40GPa)

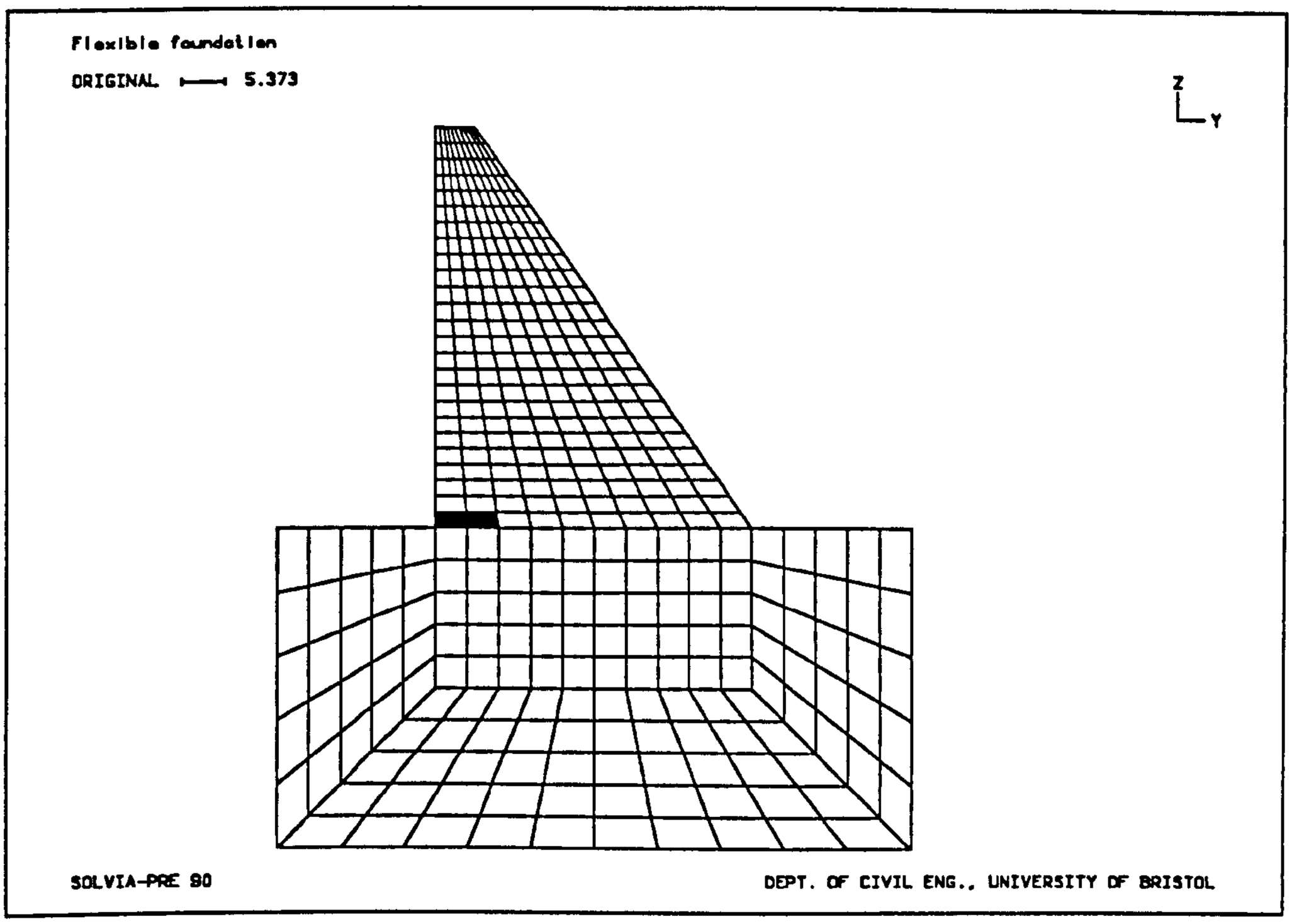

Figure 8.13c - Cracking pattern for water level 40 (E_f=40GPa)

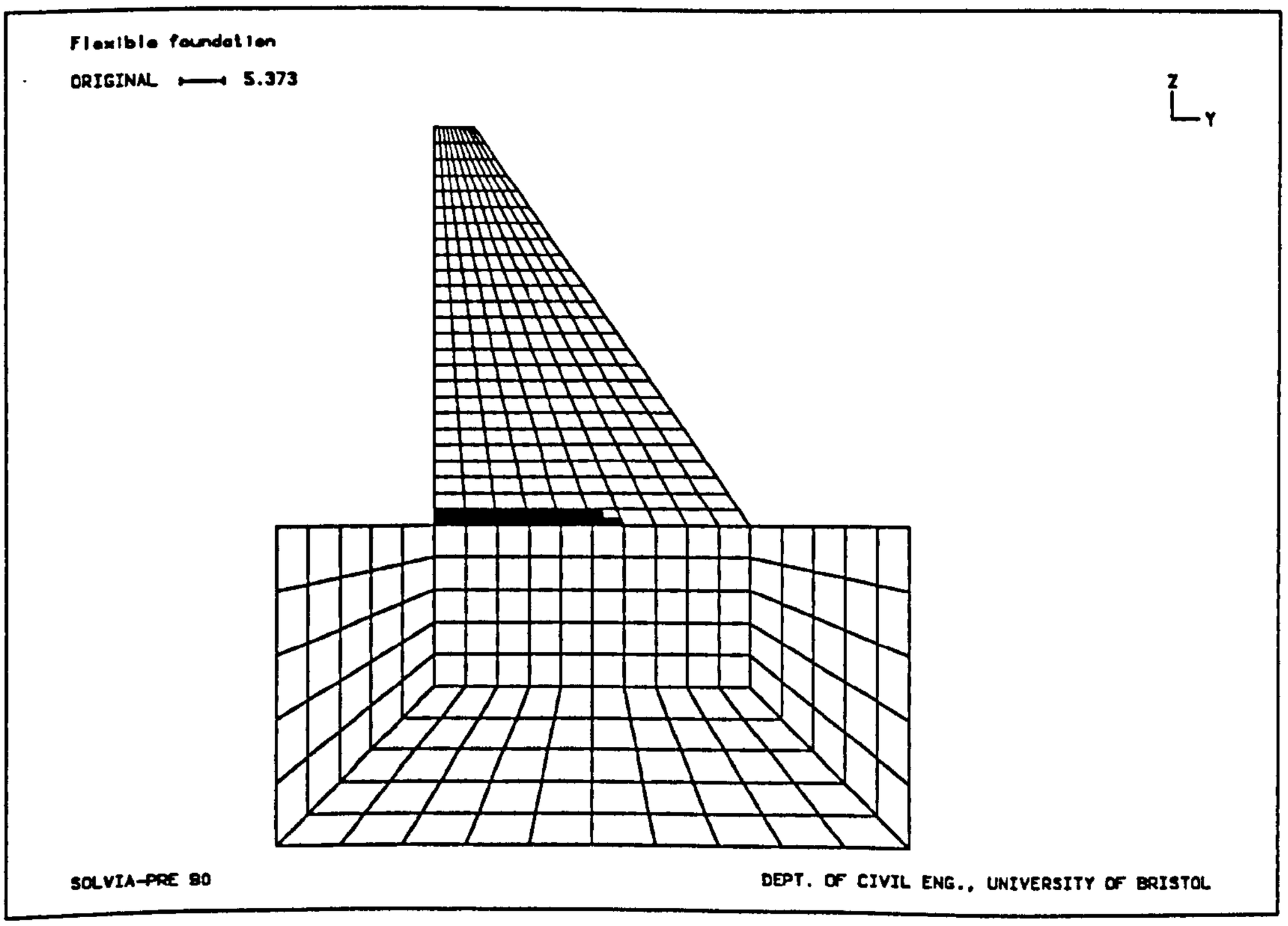

Figure 8.13d - Cracking pattern for water level 50 (E_f=40GPa)

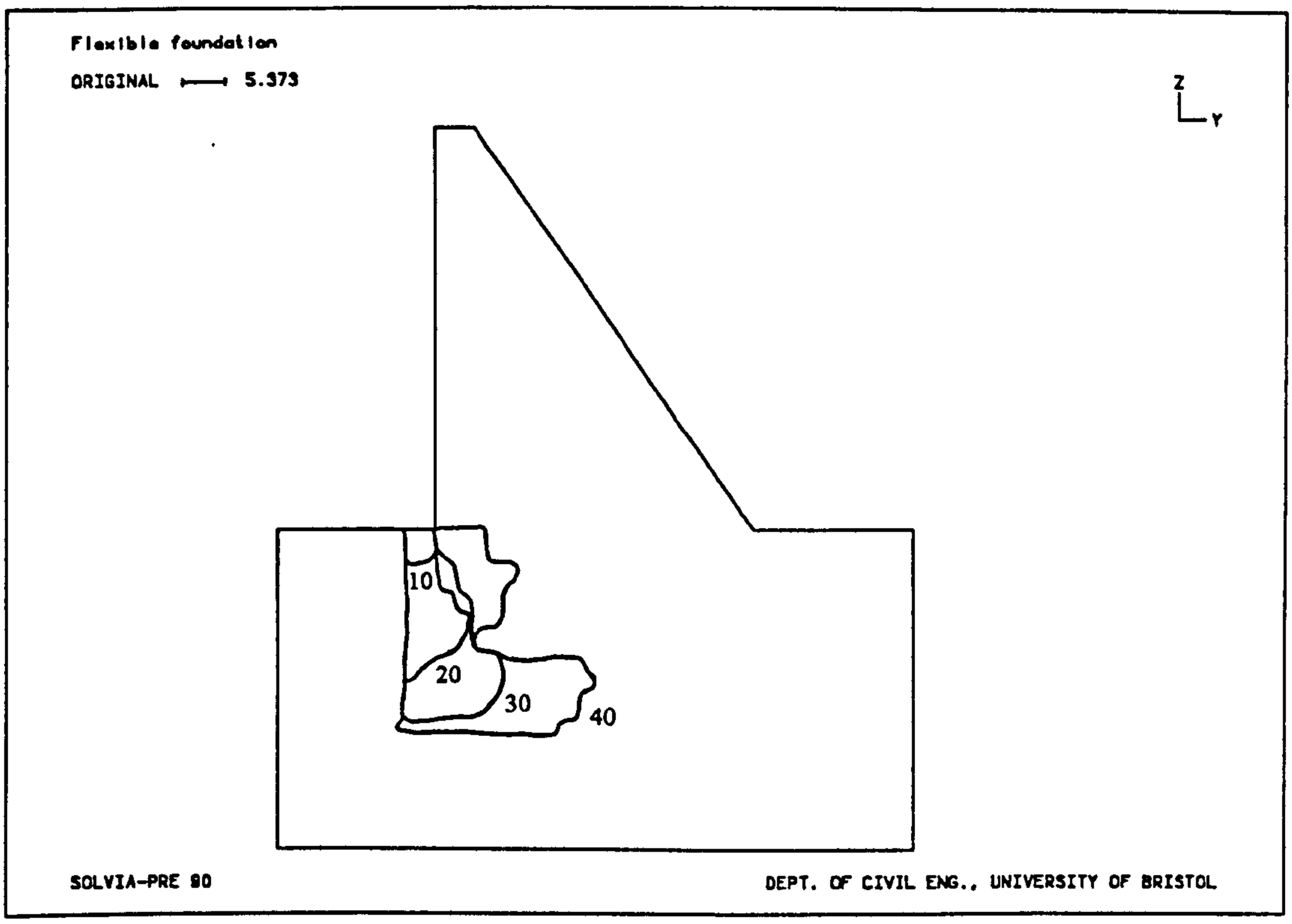

Figure 8.14a - Damaged zones for different water levels (cracking, E_f=5GPa)

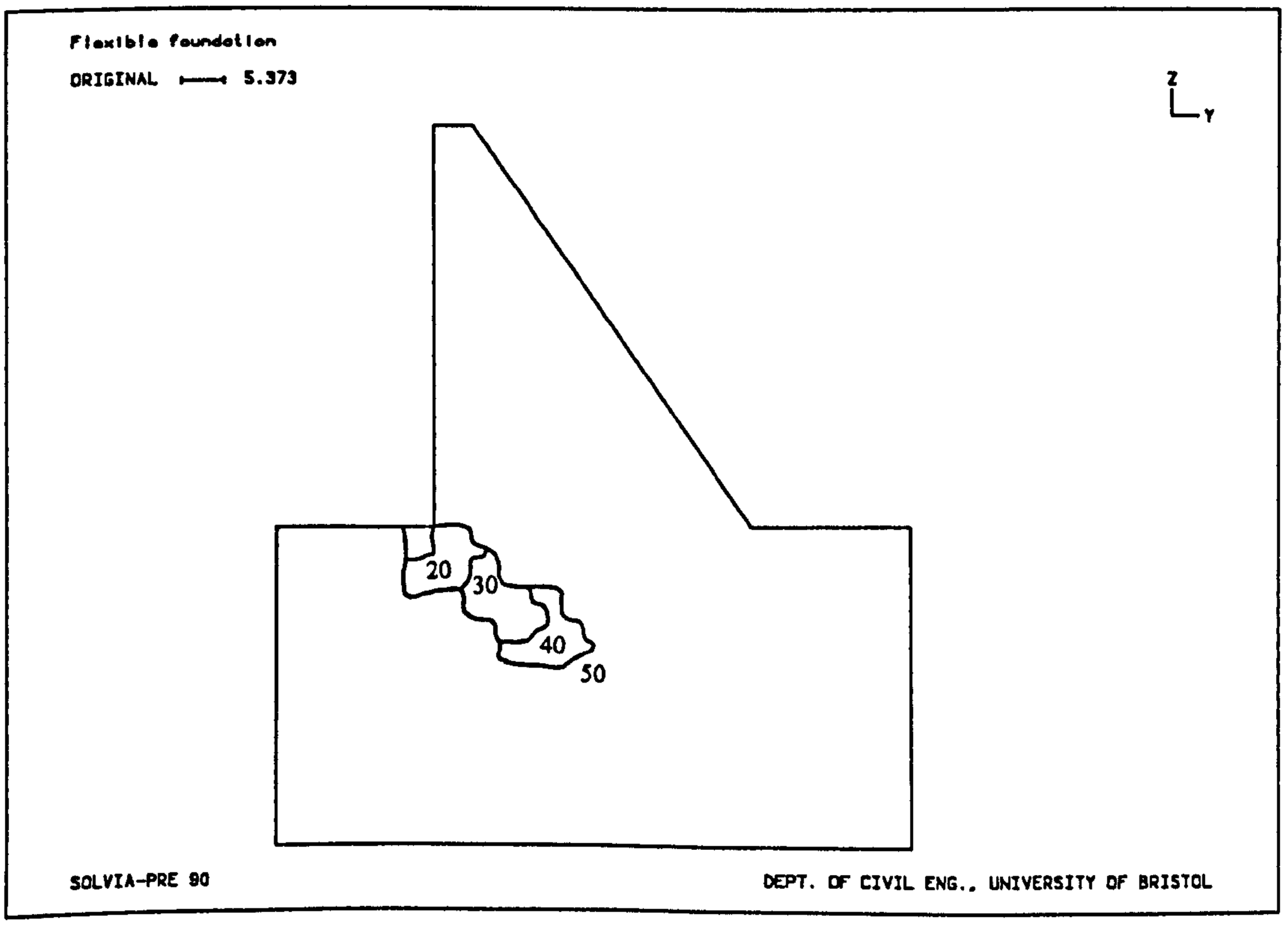

Figure 8.14b - Damaged zones for different water levels (cracking, E_f=10GPa)

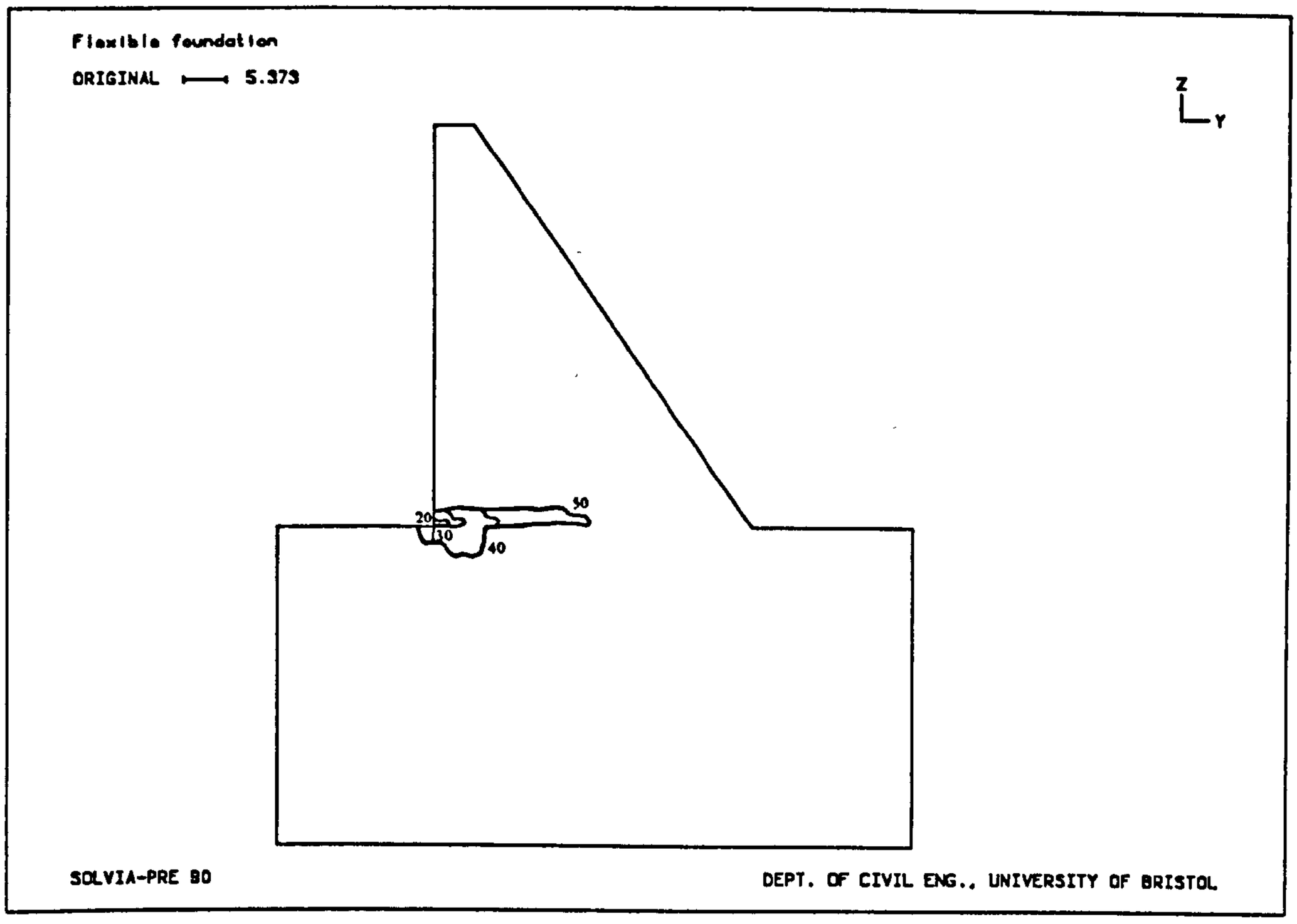

Figure 8.14c - Damaged zones for different water levels (cracking, E_f=20GPa)

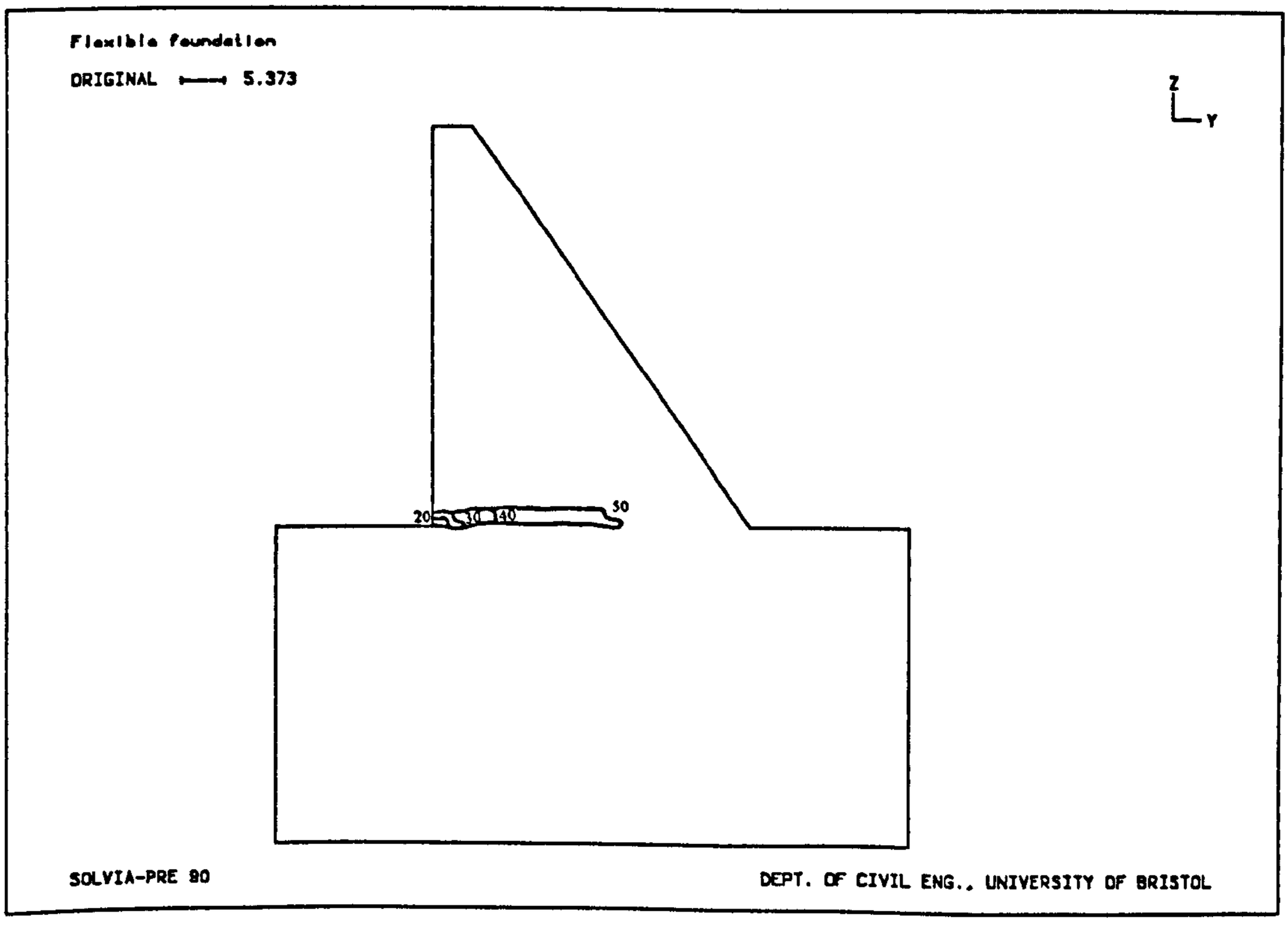

Figure 8.14d - Damaged zones for different water levels (cracking, E_f=40GPa)

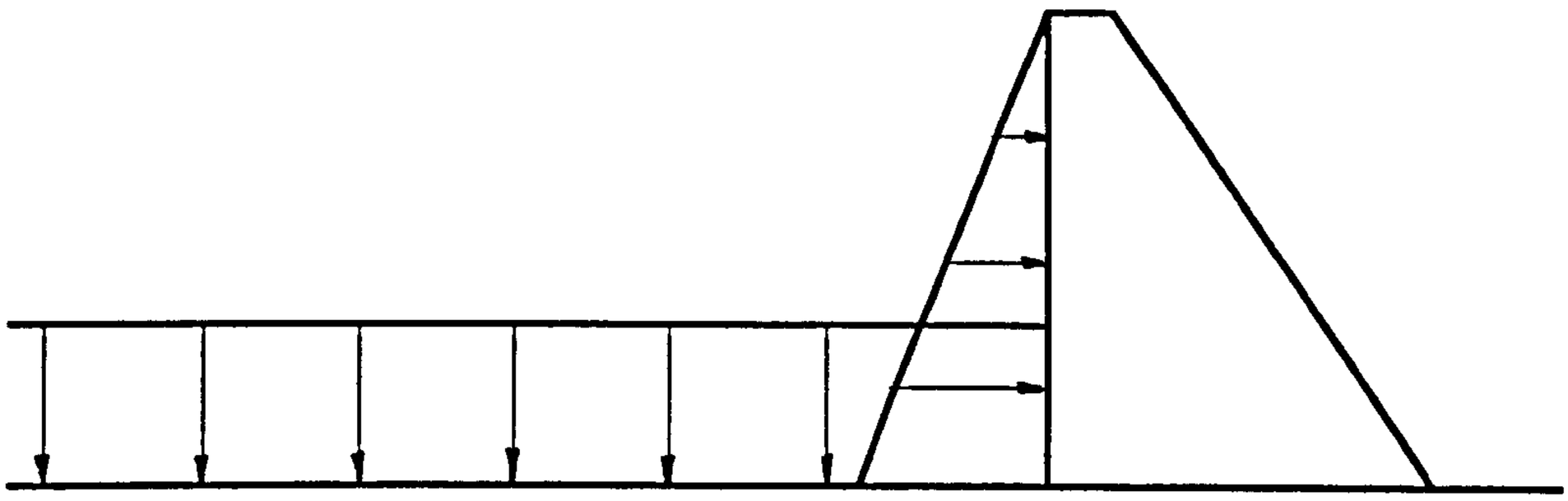

Figure 8.15 - Water pressure for quick reservoir filling

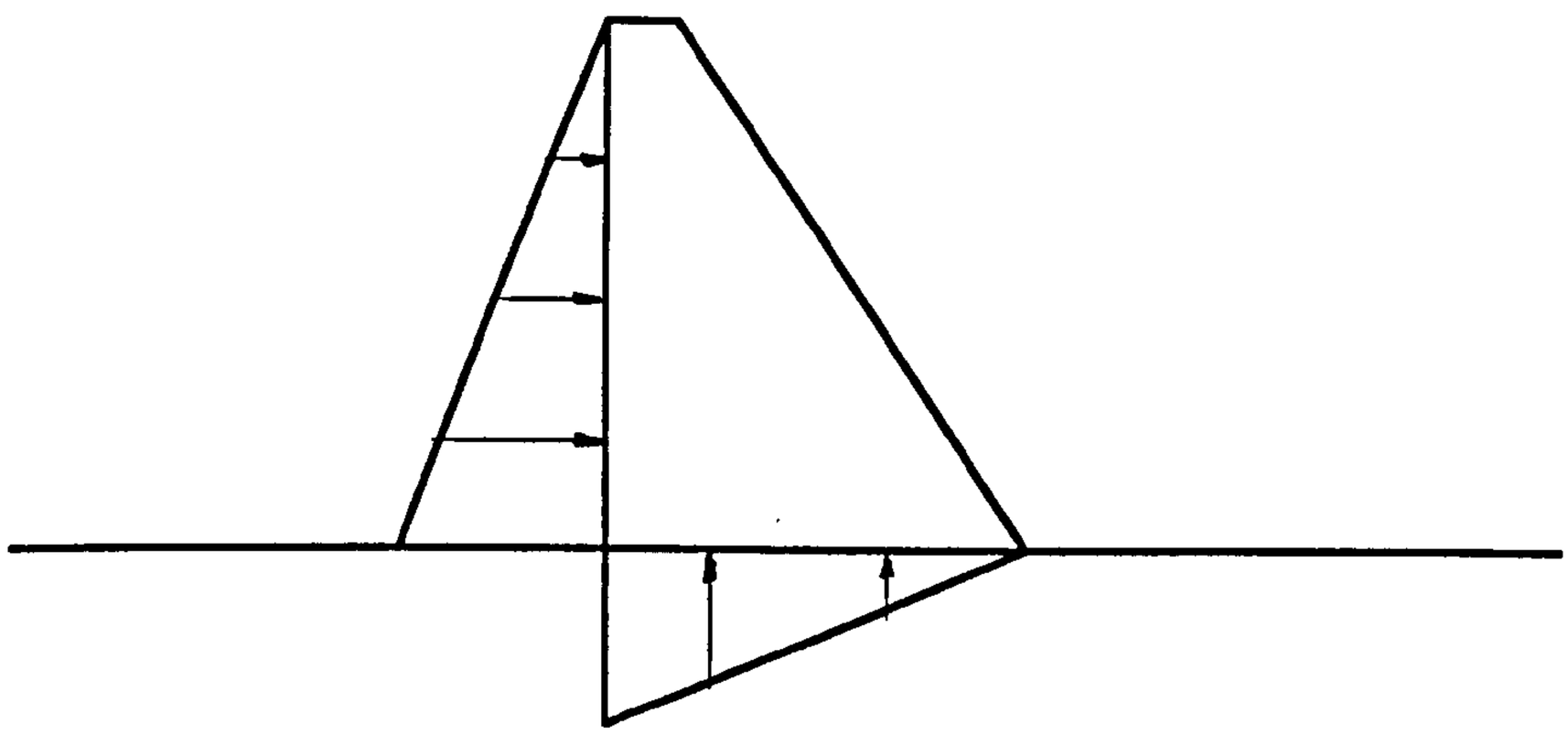

Figure 8.16a - Water pressure and uplift without reduction measures

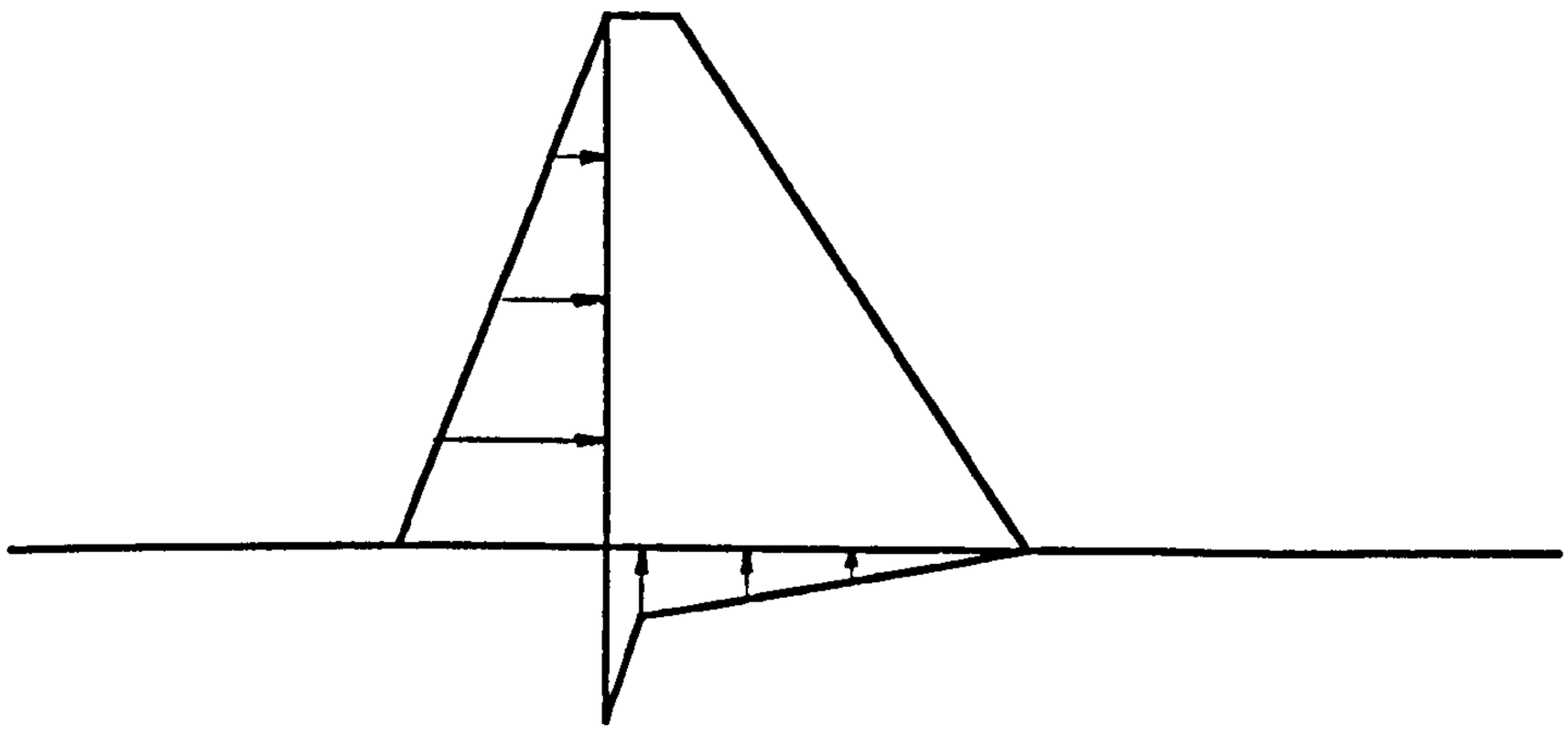

Figure 8.16b - Water pressure and uplift with reduction measures

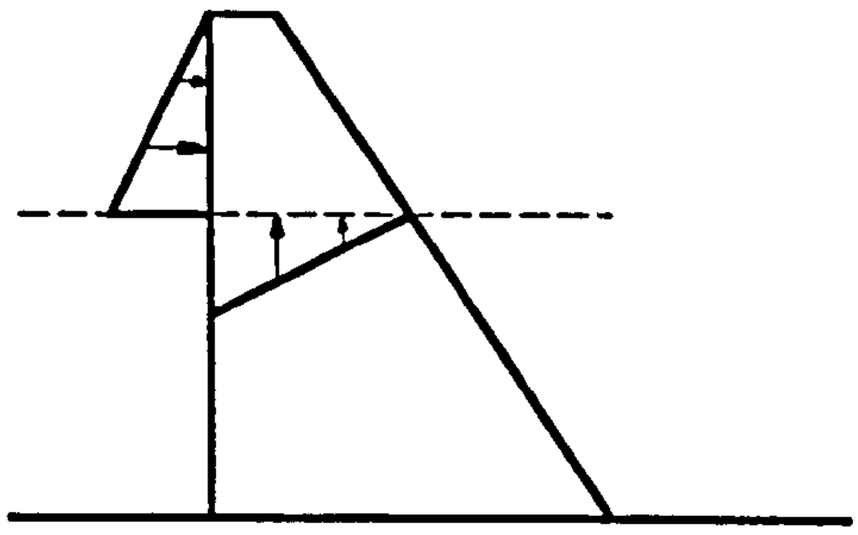

Figure 8.17a - Uplift in the dam without drainage

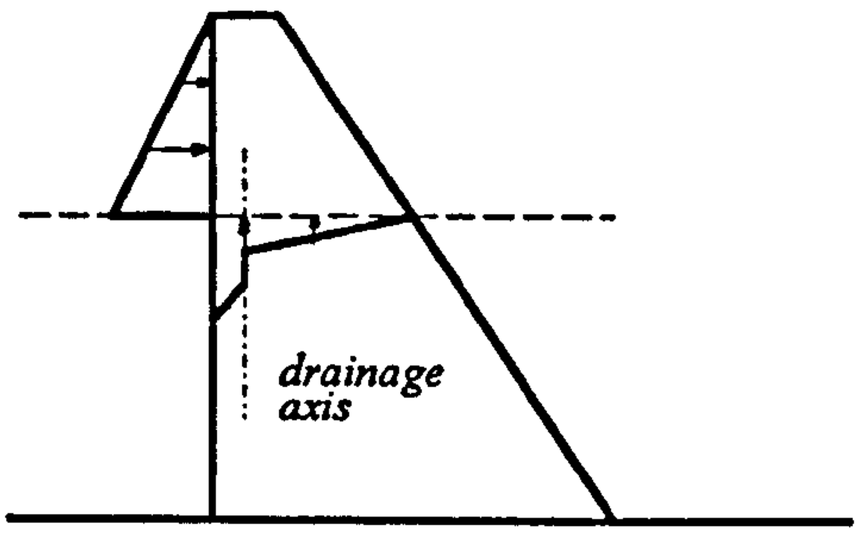

Figure 8.17b - Uplift in the dam with drainage

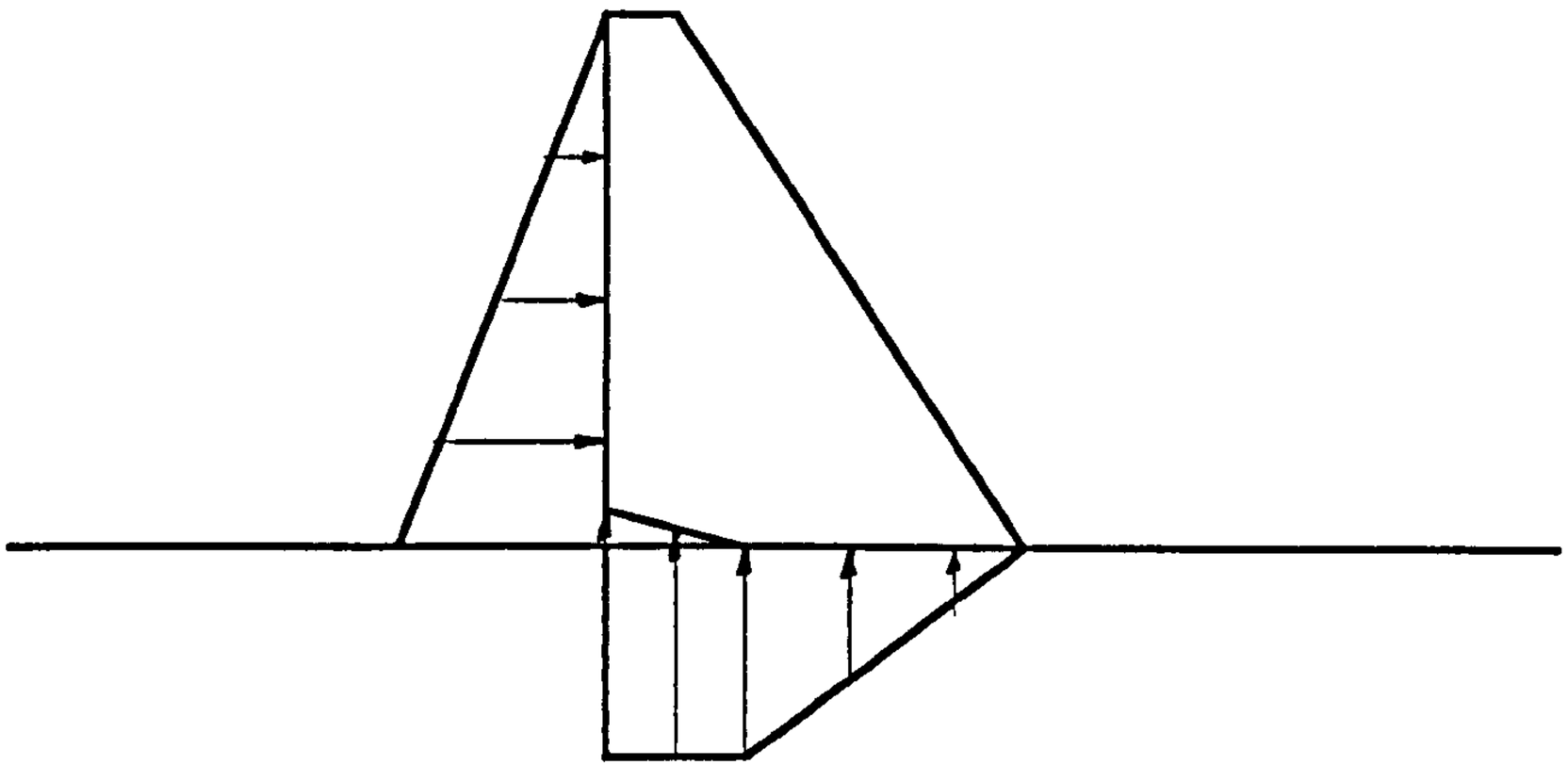

Figure 8.18a - Water pressure and uplift with a horizontal crack

Figure 8.18b - Non-horizontal crack in the foundation

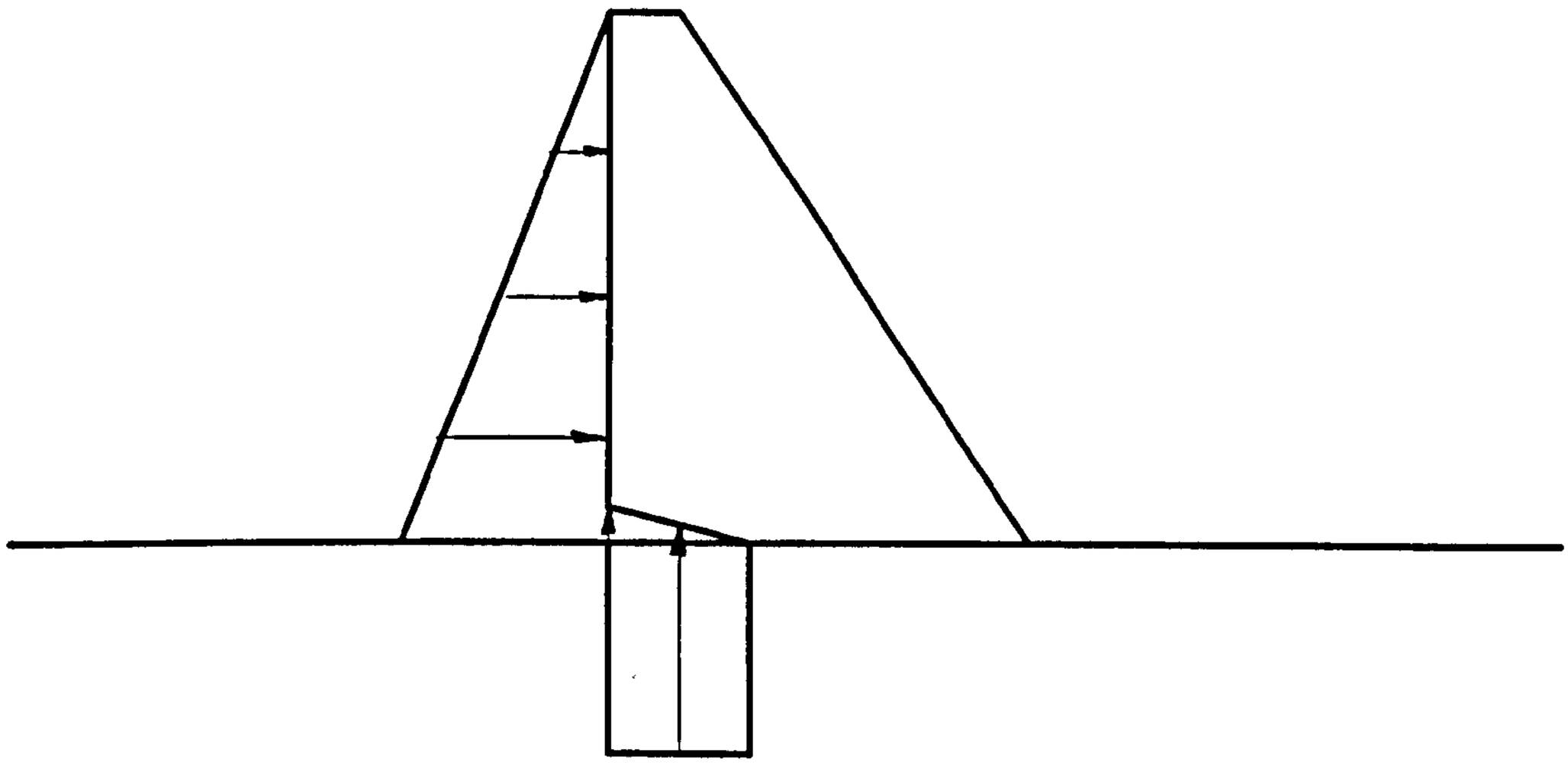

Figure 8.19a - Water pressure for a horizontal crack (impermeable foundation)

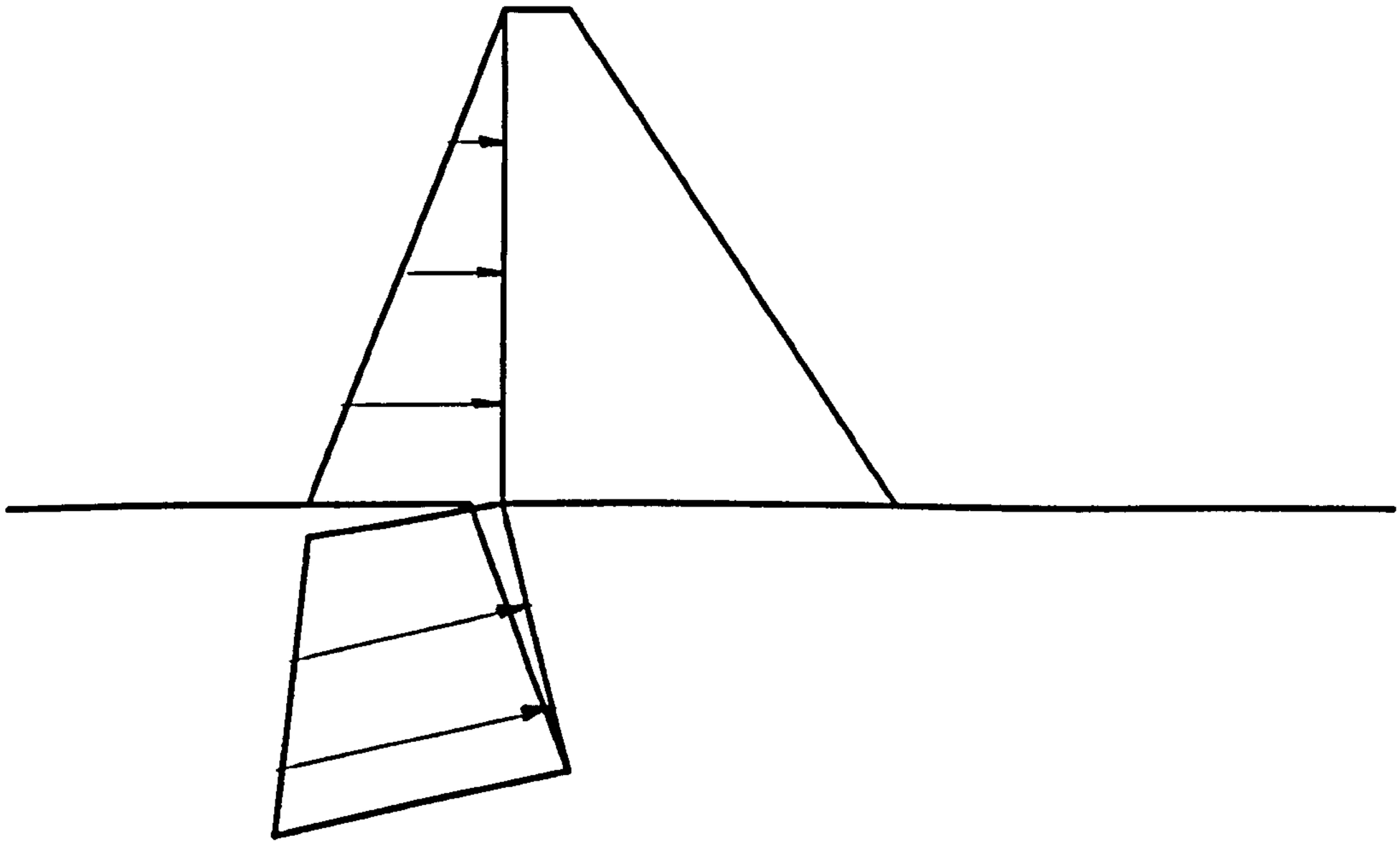

Figure 8.19b - Water pressure for a non-horizontal crack (impermeable foundation)

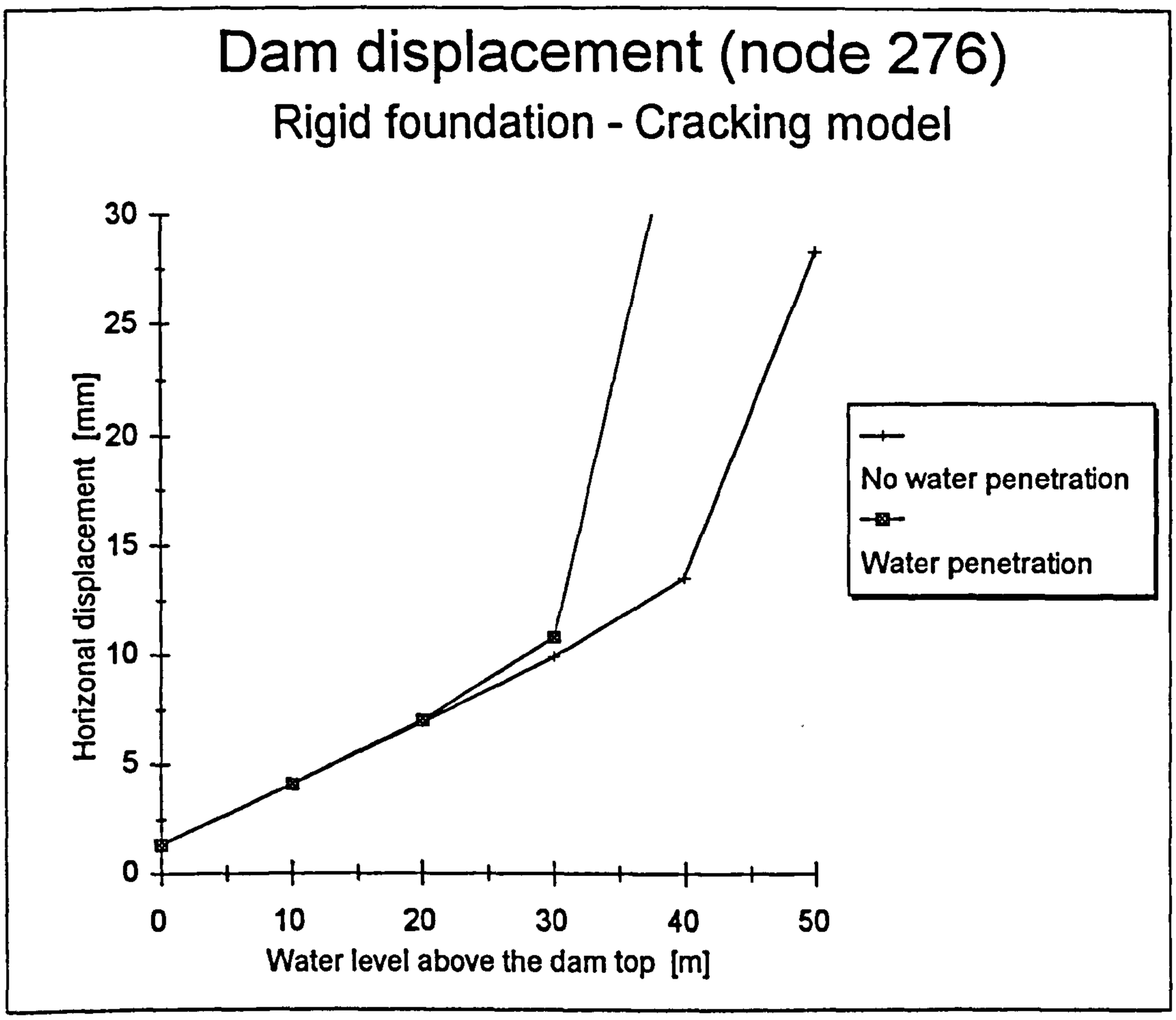

Figure 8.20a - Displacement of the top of the dam

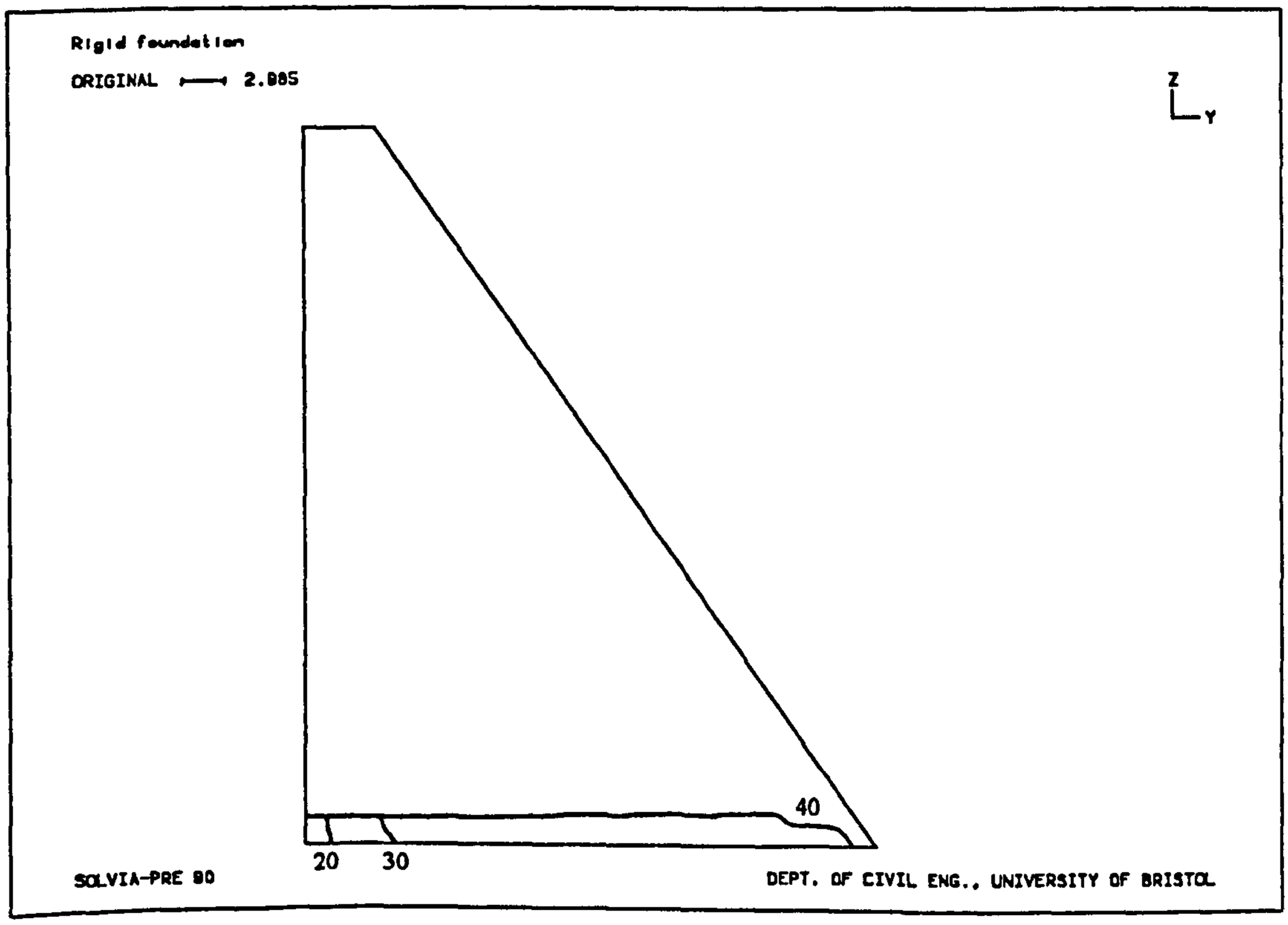

Figure 8.20b - Damaged zones for different water levels (with water penetration)

Nonlinear Earthquake Analyses of Concrete Gravity Dam-Foundation Systems

Dynamic equations for concrete gravity dam-foundation interaction were presented in Chapter 5. Preliminary linear elastic analyses, carried out in Chapter 6, have established the proper seismic input scheme, size of the foundation finite elements and overall size of the foundation finite element mesh. Dam concrete and foundation rock nonlinearities were classified and described in Chapter 7.

In this Chapter, the actual nonlinear earthquake analyses of concrete gravity dam-foundation systems will be undertaken for five different foundation conditions. The analyses are based on a procedure which, to the best of author's knowledge, has never been applied before. It does not require a free-field analysis of the site, successfully approximates the energy radiation condition and allows for the nonlinearities to occur both in the dam and foundation. These nonlinearities are due to limited tension behaviour and were described in Paragraph 7.4.2.2.

In order to discuss the results of the nonlinear analyses and reach conclusions about possible failure modes of dam-foundation systems, a comparison with adequate linear elastic analyses is necessary. Both types will be performed using the finite element code SOLVIA (SOLVIA Engineering AB, 1989/92). This code is a derivative of the general purpose finite element code ADINA (ADINA Engineering, 1984), and has been specially adapted by the author to treat coupled problems (according to equations and explanations given in Chapters 5 and 6).

9.1 Linear Elastic Analyses

For a proper comparison between linear and nonlinear dam-foundation analyses, the seismic input mechanisms have to be adjusted as described in Chapter 5. After presenting the basic details on geometry, material modelling, loading and solution of the equations, this adjustment will be explained by discussing the results of linear elastic analyses. The extension towards nonlinear analyses then becomes straightforward and will be elaborated in Section 9.2.

9.1.1 Geometry of the System

The complete finite element mesh of the concrete gravity dam-foundation system is shown in Figure 9.1. It was assumed that the system is in a state of plane strain and that the dam-foundation interface is flat and at the ground level. The dam is of idealised geometry - 50 m high, with a width of 40 m at the interface and 5 m at the top. It was modelled with 250 four-noded isoparametric finite elements. The rock foundation was considered as a rectangular block, with a height of 150 m (equal to 3 heights of the dam) and with a width of 340 m (3 heights of the dam upstream and downstream from the dam). The foundation block was modelled with 250 four-noded isoparametric finite elements which increase in size as the distance from the dam increases. Radiation damping was modelled with the viscous transmitting boundary, localised at the far end of the foundation (12 bottom and 10 side elements).

9.1.2 Linear Elastic Material Models

The modulus of elasticity of the dam was taken as E_d=20 GPa; Poisson's ratio was μ_d =0.20, and mass density was ρ_d=2450 kg/m^3. The foundation flexibility was varied by prescribing the values of 5, 10, 20 and 40 GPa to its modulus of elasticity, E_f. The rigid foundation condition ($E_f \rightarrow \infty$ GPa) was also investigated. The Poisson's

ratio of the foundation was taken as μ_f=0.25, and its mass density was ρ_f=2450 kg/m^3.

9.1.3 Loading of the System

The static loading of the system comprised of the dead weight of the dam and upstream hydrostatic pressure for water level at the top of the dam. It was assumed that the deformations of the foundation had already taken place prior to construction of the dam and therefore only the dead weight of the dam was taken into account. In addition to these loads, concentrated forces counteracting the effect of static loads were applied at the nodes between the foundation and elements representing the viscous transmitting boundary (this is because the viscous transmitting boundary cannot support the static load).

A linear elastic analysis of the dam-foundation system can be carried out according to Equations (5.16), (5.21) and (5.26), where the dynamic loading is represented by the righthand side. Apart from the property submatrices, knowledge of the earthquake acceleration, velocity and displacement record along the interface I is required for the first and the last of these Equations. The assumption that the motion records along the interface I are uniform was reasonable in the case of a rock foundation. Furthermore, it was assumed that the interface acceleration record is horizontal and in the form of the Ricker wavelet

$$\ddot{v}_I = -a\left(1-2\left(\frac{t-t_s}{t_0}\right)^2\right)e^{-\left(\frac{t-t_s}{t_0}\right)^2} \qquad (9.1)$$

where a is the amplitude (set to 0.5g); t is time; t_s is the time instant for which the wavelet has its maximum (set to 0.2 s); and t_0 is the parameter which governs the frequency range of the excitation. If t_0 is set to $1/7\pi$, the frequency range is between 0 and 20 Hz, with the dominant frequency of about 7 Hz. The unit Ricker wavelet (a=1) with the appropriate velocity and displacement records is shown in Figure 9.2.

The main peak of the Ricker wavelet is negative (direction downstream to upstream), which causes a positive (direction upstream to downstream) main inertial force and displacement.

There are several reasons why Ricker motion records were used for the dynamic analysis instead of real earthquake ones: the importance and effects of the radiation damping can be spotted more easily; the swinging cracking pattern is followed without any difficulties; the duration of the analysis is much shorter; and the results of the application of real earthquake records do not change any of the conclusions reached through the application of Ricker wavelet records (as will be demonstrated later in the Chapter).

In addition to the dynamic excitation expressed by the righthand side of Equations (5.16), (5.21) and (5.26), the reservoir-dam interaction was modelled using the Westergaard added mass technique (Westergaard, 1933; Taylor et al., 1994).

9.1.4 Solution of the Linear Dam-Foundation Interaction Equations

Investigations by other researchers into seismic cracking of concrete gravity dams on rigid foundations were mentioned in Chapter 7. They have all used different forms of viscous, stiffness-proportional internal damping, arguing that mass-proportional damping provides artificial stability to the parts of the dam above the main cracks. After a recent discovery about the responsibility of the internal viscous damping model for the diffused crack patterns (Bhattacharjee & Léger, 1993), it was decided here to abandon this damping model altogether. Such an approach is justified by the fact that internal damping is not the only source of damping in interaction systems, where external, radiation damping also exists (not so in the rigid foundation case). More importantly, it was demonstrated in Chapter 6 that for concrete gravity dam-foundation systems, the contribution of the radiation damping by far outweighs the contribution of the internal viscous damping (Simic, 1993d). Consequently, the

second term on the righthand side of Equations (5.16) and (5.26) vanishes, while the second term on the lefthand side of these Equations contains only the nonproportional, radiation damping part. The Equations are then solved through implicit, direct integration. The Newmark constant-average-acceleration method was used with the time step of 0.004 s. To ease the comparison, this time step was adopted as equal to that for the nonlinear analyses, for which the explanation will be given in Section 9.2.

9.1.5 Results of the Linear Analyses

In Chapter 6, preliminary linear analyses of concrete dam-foundation systems were carried out using the equation for the dynamic component of motion, i.e. Equation (5.21). Unfortunately, this Equation is valid only for linear systems because the partition expressed by Equation (5.17) can only be made by assuming the validity of the superposition principle. For nonlinear systems, Equation (5.16) and (5.26) have to be used. For a correct comparison, these Equations then have to be applied even when analysing the corresponding linear systems.

SOLVIA, as a general purpose finite element code is not able to deal with dynamic interaction Equations like (5.16) or (5.26). It was decided to adapt the code by calculating the righthand side of these Equations, which is equivalent to determining and applying the force time histories in the appropriate nodes. Obviously, such an intervention in the numerical procedure has to be tested.

9.1.5.1 Adaptation of the Finite Element Code for Ground Level Interfaces

The first part of the test consisted of comparing the results of Equations (5.16) and (5.21) for ground level interfaces, i.e. for surface supported dams. The comparison was made for a foundation modulus of E_f=40 GPa and three characteristic points shown in Figure 9.1. The first point belongs to the dam, the second to the flat

interface and the third to the foundation (finite element nodes 276, 6 and 310, respectively). In the case of a uniform interface earthquake motion, the partition of these displacements can be expressed according to Equations (5.11) and (5.17):

$$\begin{Bmatrix} r_{276} \\ r_6 \\ r_{310} \end{Bmatrix} = \begin{Bmatrix} 0 \\ v_6 \\ v_{310} \end{Bmatrix} + \begin{Bmatrix} u_{276}^{rb} \\ 0 \\ 0 \end{Bmatrix} + \begin{Bmatrix} u_{276}^{d} \\ u_6^{d} \\ u_{310}^{d} \end{Bmatrix} \tag{9.2}$$

Application of Equation (5.21) results in the dynamic displacements. For the three characteristic points, they are presented by the last vector in Equation (9.2) and shown in Figures 9.3a, 9.3b and 9.3c, respectively. Since the interface earthquake motion is uniform, the pseudostatic displacements are equal to rigid body displacements of the dam. Therefore, $u_{276}^{rb}=v_6$, as the node 6 lies on the interface. The added displacement for the dam (node 276) can be obtained by adding the two terms: u_{276}^{d} and u_{276}^{rb}. The latter term (with unit amplitude) was already depicted in Figure 9.2c . Equation (9.2) also demonstrates that the added displacements for the interface (node 6) and foundation (node 310) are equal to the dynamic displacements.

On the other hand, application of the described numerical procedure in the form of Equation (5.16) results directly in the added displacements. The added dam displacement for node 276 is shown in Figure 9.4. The added displacements for nodes 6 and 310 are exactly the same as those in Figures 9.3b and 9.3c. Since the absolute compatibility between the application of Equations (5.21) and (5.16) is observed, it may be concluded that the numerical adaptation procedure for the latter had been carried out successfully and that it yields accurate results.

9.1.5.2 Adaptation of the Finite Element Code for Deep Interfaces

The second part of the testing of the numerical procedure consisted of comparing the results of Equations (5.16) and (5.26). The latter Equation was derived to

accommodate deep interfaces and is particularly important because it permits the extension towards problems where nonlinearities are encountered both in the dam and surrounding foundation. The comparison is made for four different foundation conditions (foundation moduli of E_f=5, 10, 20 and 40 GPa). In addition to other points in Figure 9.1, the vertical stress in the lower left integration point of the lowest row of elements at the heel of the dam (point A in Figure 9.1) will be observed. In the case of uniform interface earthquake motion (the interface is in this case presented with thicker lines in Figure 9.1), the partition of the relevant displacements can be expressed according to Equation (5.25):

$$\begin{Bmatrix} r_{276} \\ r_{310} \\ r_F \end{Bmatrix} = \begin{Bmatrix} 0 \\ v_{310} \\ v_F \end{Bmatrix} + \begin{Bmatrix} u_{276} \\ u_{310} \\ u_F \end{Bmatrix} \tag{9.3}$$

It is important to note that this time, the comparison between Equations (5.16) and (5.26) should not yield equivalent results as they have different physical meanings. The former uses the free-field input mechanism where the motion is applied at the surface interface (e.g. node 6). The latter uses the scattered input mechanism where the motion is applied at the deep interface (e.g. node 310). The difference between the two approaches is in a way a measure of the arising kinematic interaction, which was elaborated in Chapter 5.

According to Equations (9.2) and (9.3), the results of both procedures for the dam are total displacements. For the same input motion in both cases, the displacements in node 276 are shown in Figures 9.5a, 9.6a, 9.7a and 9.8a for the foundation moduli of E_f=5, 10, 20 and 40 GPa, respectively. Similarly, the stresses in the dam are the total stresses. The vertical stresses in point A are shown in Figures 9.5b, 9.6b, 9.7b and 9.8b for the foundation moduli of E_f=5, 10, 20 and 40 GPa, respectively.

For the nodes lying at the ground level (e.g. node 6), the result of the scattered input scheme is the total displacement. The result of the free-field input scheme for the same node is the added motion to which the free-field displacement (Figure 9.2c)

must be superimposed for a valid comparison. Thus obtained displacements are shown in Figure 9.8c for the foundation modulus of E_f=40 GPa.

Figures 9.5 - 9.8 are illustrative in many ways. First, they show the extent of the error made when the real scattered motion is not known and is substituted with the free-field motion. Second, the extent of that error increases for more flexible foundation conditions, which is well in line with the expectation expressed in Chapter 5. The more flexible the foundation, the greater the interaction effects. Finally, by comparing Figures 9.8a and 9.8c (similar comparisons can be made for other foundation conditions, still reaching the same conclusions), it is clear that the contribution of the free-field displacement can hardly be felt at the top of the dam, while it forms a major peak at the interface. Obviously, none of these conclusions could have been reached if the analysis had been conducted in terms of dynamic displacements only, as typically done for structural dynamics problems.

Since the comparison between the application of Equations (5.16) and (5.26) is satisfactory and logical, it may be concluded that the numerical adaptation procedure for the latter had been carried out successfully. Ideally, its accuracy should be tested through an independent analysis.

9.2 Nonlinear Analyses

After adapting the SOLVIA finite element code for the treatment of deep interfaces, the extension towards nonlinear analyses is straightforward.

9.2.1 Geometry of the System

Everything that has been said about the geometry of the system in Section 9.1 is also applicable for nonlinear analyses. It should only be added that the simplified and

idealised geometry of the dam was deliberately chosen to avoid possible (and indeed common) nonlinearities at the neck of the dam, usually due to the abrupt change of the downstream slope (e.g. the Koyna dam case). With the present geometry, the nonlinearities are most likely to occur around the dam-foundation interface, where the mesh has been appropriately refined. The foundation mesh becomes coarser as the distance from the dam increases, which is in line with the recommendations made in Chapter 6 and the extensive radiation damping study (Simic, 1993c; Simic & Taylor, 1994).

The downstream slope of 1:0.7 corresponds well to the slope of Bristol EERC model tests on the shaking table (Mir & Taylor, 1994) and to the slope of a real dam monitored and analysed by the Bristol EERC (Taylor et al., 1994).

9.2.2 Nonlinear Material Models

The basic properties of the nonlinear material models are equal to those of the linear elastic models in Subsection 9.1.2. The modulus of elasticity at zero strain for the dam was taken as E_d=20 GPa; Poisson's ratio was μ_d=0.20, and mass density was ρ_d =2450 kg/m^3. The foundation flexibility was varied by prescribing the values of 5, 10, 20 and 40 GPa to its modulus of elasticity, E_f. The Poisson's ratio of the foundation was taken as μ_f=0.25, and its mass density was ρ_f=2450 kg/m^3.

The nonlinearities in the dam and foundation were allowed to occur above the interface marked with thicker lines in Figure 9.1, and they were due to limited tension behaviour of concrete dam-foundation systems. The model itself was described in detail in Chapter 7. Its properties defining the uniaxial stress-strain curve, for both dam and foundation, were

$$\sigma_c = -0.001E \quad \varepsilon_c = -0.20\% \quad \sigma_u = -0.00095E \quad \varepsilon_u = -0.27\% \quad \sigma_t = 0.0001E$$

where σ_c is the uniaxial maximum compressive stress (negative); ε_c is the uniaxial compressive strain at σ_c; σ_u is the uniaxial ultimate compressive stress (negative); ε_u

is the uniaxial ultimate compressive strain; σ_t is the uniaxial cut-off tensile stress; and E is the modulus of elasticity (of either the dam concrete or foundation rock).

For the definition of the compression failure envelopes of the mass concrete and rock, the following principal stress ratio β and 24 discrete stress values were used:

β=0.75 $\sigma_{p11} = 0.0$ $\sigma_{p12} = 0.3$ $\sigma_{p13} = 0.6$ $\sigma_{p14} = 0.9$ $\sigma_{p15} = 1.2$ $\sigma_{p16} = 1.5$

$\sigma_{p311} = 1.0$ $\sigma_{p321} = 2.0$ $\sigma_{p331} = 3.0$ $\sigma_{p341} = 4.0$ $\sigma_{p351} = 5.0$ $\sigma_{p361} = 6.0$

$\sigma_{p312} = 1.25$ $\sigma_{p322} = 2.5$ $\sigma_{p332} = 3.75$ $\sigma_{p342} = 5.0$ $\sigma_{p352} = 6.25$ $\sigma_{p362} = 7.5$

$\sigma_{p313} = 1.2$ $\sigma_{p323} = 2.4$ $\sigma_{p333} = 3.6$ $\sigma_{p343} = 4.8$ $\sigma_{p353} = 6.0$ $\sigma_{p363} = 7.2$

The parameters presented so far were calibrated in a way which ensures that the dam-foundation system behaves like a linear elastic system in compression and up to the cracking point in tension.

The stiffness reduction factor following tensile failure was set to η_n=0.0001, and the shear stiffness reduction factor was set to η_s=0.5. This applied to both the dam and foundation.

It was assumed that all the given material data are appropriately set for the dynamic, earthquake loading, i.e. that the strain-rate effects (usually taken through the dynamic magnification factor) have already been accounted for.

9.2.3 Loading of the System

Everything mentioned in Section 9.1 is also applicable to nonlinear analyses. The earthquake load in the form of a Ricker wavelet with the amplitude of 0.5g was again combined with basic static (dead weight and hydrostatic) loads. The effects of water penetration into open cracks were completely disregarded due to the oscillatory nature of earthquake loading and due to the quick opening and closing of the cracks.

9.2.4 Solution of the Nonlinear Dam-Foundation Interaction Equations

As indicated in Section 9.1, the dynamic interaction equation with nonproportional damping (Equation (5.26)) was solved through implicit, direct integration. In this case, the dynamic equation is nonlinear, and the BFGS matrix update method with line searches and energy convergence criterion (SOLVIA Engineering AB, 1989/92) was employed to solve iteratively the equilibrium equations. The Newmark constant-average-acceleration method was used. The choice of the time step was governed by crack propagation. It was desirable to have small time steps because the number of newly cracked finite elements per time step should be kept as low as possible (ideally one). For an average cracked finite element size and with recent information on crack propagation velocity in concrete (Curbach & Eibl, 1990), it was decided to use the time step of 0.004 s.

9.2.5 Results of the Nonlinear Analyses

The results of the nonlinear analyses are presented through total horizontal displacement time-histories of the upstream face of the dam top (node 276). Five time-histories (for five different foundation conditions, E_f=5, 10, 20, 40 and ∞ GPa) are shown in comparison with linear time-histories in Figures 9.9a, 9.10a, 9.11a, 9.12a and 9.13a, respectively. For each of these five cases, cracking patterns at up to three time instants are shown in Figures 9.9, 9.10, 9.11, 9.12 and 9.13. Cracked elements are black.

For the foundation with E_f=5 GPa, after initial opening of the crack, at t=0.412 s the crack is still fully open (Figure 9.9b). After the reversal of loading, a small part of the crack is closed at t=0.560 s (Figure 9.9c). Towards the end of the analysis, the crack remains open at t=1.000 s (Figure 9.9d).

For the foundation with E_f=10 GPa, after initial opening of the crack, the crack is still open at t=0.328 s (Figure 9.10b). After the reversal of loading, the crack is fully

closed at t=0.380 s (not shown). At t=0.568 s, the crack is reopened (Figure 9.10c); and closed again at t=0.720 s (not shown) after the second reversal of loading. At t=1.500 s, the crack is open again (Figure 9.10d). The observed cracking pattern for this foundation condition does not match the corresponding one from Chapter 8 (Figure 8.11), contrary to all other cases. Therefore, by increasing the amplitude of the acceleration from 0.5g to 0.75g, the influence of the level of earthquake loading to the cracking pattern can be investigated. After the initial opening of the crack, the cracks are still open at t=0.284 s (Figure 9.10e). Apart from the main foundation crack, superficial cracking at the upstream face of the dam is also observed. Later in time, at t=0.580 s, the main crack propagates further into the foundation, while the superficial dam cracks extend only slightly (Figure 9.10f). The upstream dam cracks are closed, but the main crack remains open at t=1.500 s (Figure 9.10g). The cracking pattern for the increased earthquake loading reveals that the main direction of cracking dips into the foundation at an angle of approximately 45° to the ground surface, rather than staying vertical as in Figures 9.10b - 9.10d. This is consistent with Figure 8.11 and conclusions from Chapter 8.

For the foundation with E_f=20 GPa and acceleration amplitude of 0.5g , after initial opening of the crack, the crack is still open at t=0.292 s (Figure 9.11b). After the reversal of loading, the crack is fully closed at t=0.332 s (not shown). At t=0.464 s, the crack is reopened (Figure 9.11c), only to be closed again at t=0.576 s (not shown) after the second reversal of loading.

For the foundation with E_f=40 GPa, after initial opening of the crack, the crack is still open at t=0.280 s (Figure 9.12b). Apart from the main crack, superficial cracking at the upstream face of the dam can also be observed. After the reversal of loading, all the cracks are fully closed at t=0.324 s (not shown). At t=0.496 s, the cracks are reopened with the main one having propagated even further into the dam (Figure 9.12c). All the cracks are closed again at t=0.548 s (not shown) after the second reversal of loading.

For the rigid foundation (E_f=∞ GPa), after initial opening of the crack, the upstream crack is still open at t=0.272 s (Figure 9.13b). At t=0.308 s, the upstream crack is fully closed (not shown). After the first reversal of loading, the upstream crack is still fully closed, but superficial cracking at the downstream face of the dam can be observed at t=0.356 s (Figure 9.13c). At t=0.456 s, the upstream crack is reopened and has propagated much further into the dam (Figure 9.13d). The upstream crack is closed again and the downstream one reopened at t=0.560 s (not shown because the cracking pattern is equal to that at t=0.356 s) after the second reversal of loading.

In order to investigate further the influence of the level of loading to the cracking pattern of the dam on a rigid foundation, the peak acceleration amplitude was decreased from 0.5g to 0.3g. The initial opening of the crack at the the upstream face, at t=0.228 s, is not larger than one quarter of the element (Figure 9.14a). After the first reversal of loading, at t=0.340 s (not shown), the small upstream crack is closed. Later in time, the upstream crack reopens and extends to one half of the element at t=0.408 s (Figure 9.14b). The crack is even longer at t=0.436 s (Figure 9.14c), but closes at t=0.520 s (not shown). Towards the end of the analysis, the crack reaches its maximum length of two and a half elements at t=1.380 s (Figure 9.14c). The comparison between the cracking patterns for the peak acceleration amplitudes of 0.5g and 0.3g (shown in Figures 9.13 and 9.14, respectively) indicates that the propagation of the main, upstream crack is considerably reduced in the latter case and that the downstream cracking does not appear.

So far, only horizontal earthquake loading was considered. Although this component is expected to be the most significant, the influence of the vertical component should also be investigated. In the nonlinear analysis, the principle of superposition is not valid and the combined solution due to both components has to be examined independently. First, the dam on the rigid foundation was subjected to the vertical earthquake with the acceleration amplitude of 0.333g, which is equal to 2/3 of the horizontal component. This ratio corresponds to the measured data as well as to

standard recommendations for dam analysis in earthquake conditions (Charles et al., 1991). The linear and nonlinear horizontal displacement time-histories of the upstream face of the dam top (node 276) are shown together in Figure 9.15. The time-histories are identical and no cracking appears for the whole duration of the analysis. Second, the horizontal and vertical earthquake components are applied together. Again, the representative result is the horizontal displacement of the node 276, depicted in Figure 9.16a for the linear and nonlinear analysis. In the latter case, the cracking patterns are deliberately shown for t=0.272 s (Figure 9.16b), t=0.356 s (Figure 9.16c) and t=0.456 s (Figure 9.16d); so they may be compared with cracking patterns for the horizontal earthquake only (Figures 9.13b - 9.13d). The influence of the addition of the vertical component can also be evaluated in Figure 9.17, where two nonlinear time-histories of the node 276 are shown together. It is clear that in this case the vertical earthquake component does not contribute significantly to seismic cracking patterns and that general conclusions about the cracking behaviour of this concrete gravity dam may be reached by considering horizontal earthquake records only.

It was explained in Subsection 9.1.3 why the earthquake loading was taken in the form of the Ricker wavelet. The suitability of this simplified loading and its ability to match the important aspects of linear elastic dam-foundation systems subjected to real earthquakes was confirmed in Chapter 6. Herein, the comparison will be made for the dam in the nonlinear range by examining cracking patterns due to the Ricker wavelet and real earthquake loading. For the latter, the dam on the rigid foundation was subjected to an artificially created earthquake acceleration record, generated for the Bristol EERC shaking table tests of concrete gravity dam models (Mir & Taylor, 1994). The acceleration record used for Model 4 and transformed to prototype scale (Mir, 1994) was for this purpose scaled to the peak acceleration amplitude of about 0.5g, so that both its amplitude and frequency content correspond to those of the Ricker wavelet. The unit acceleration record is shown in Figure 9.18. The

comparison between linear and nonlinear horizontal displacements of the node 276 is shown for an interesting time interval in Figure 9.19a. The initial opening of the crack occurs at about t=4.404 s (Figure 9.19b). At t=4.424 s, the crack is closed (not shown). After the first substantial reversal of loading (horizontal displacement in Figure 9.19a is approximately -1.2 cm), at t=4.464 s, the upstream crack is still closed, but superficial cracking at the downstream face of the dam can be observed (Figure 9.19c). At t=4.584 s, after the first substantial 'positive' loading (horizontal displacement in Figure 9.19a is approximately 1.2 cm), the upstream crack is reopened and has propagated much further into the dam (Figure 9.19d). A similar cracking pattern can be observed for the second substantial 'positive' loading, at t=6.024 s (horizontal displacement in Figure 9.19a is approximately 1.5 cm). The upstream crack is reopened again and even longer than before (Figure 9.19e). The observed behaviour is similar to that under the Ricker wavelet loading in Figure 9.13. This suggests that a simple loading such as Ricker wavelet can be successfully used for the investigation into seismic cracking of concrete gravity dams.

9.3 Concluding Remarks

So far, seismic cracking analyses of concrete gravity dams have mostly been performed with rigid foundation conditions, as elaborated in Chapter 7. This Chapter has shown that this procedure is very conservative and that if the precise location and level of cracking are required, the only alternative is to conduct a full analysis for the flexible foundation case.

Another very important conclusion is in connection with the dynamic dam-foundation interaction equations, presented in Chapter 5. They were successfully implemented into an existing finite element code (SOLVIA) and their results were verified on a number of linear elastic numerical tests. The confidence gained through these tests

has enabled further applications in nonlinear cracking analyses of dam-foundation systems.

The comparison between the Ricker wavelet and real earthquake analysis has demonstrated that the former may be used for qualitative description of cracking patterns of concrete gravity dams. In other words, the conclusions drawn from the analyses with the loading in the form of the Ricker wavelet can be successfully extrapolated to the analyses with real earthquake loadings. Of course, one cannot fully substitute the other, and in practice, preference should be given to the latter whenever reliable information on earthquake motions are available. For a successful extrapolation of conclusions, it is necessary to emphasise once again some properties of the Ricker wavelet. As described in Chapter 6, the frequency content of the Ricker wavelet is between 0 and 20 Hz, with the dominant frequency of 7 Hz. This dominant loading frequency is reasonably close to expected first natural frequencies of the examined dam-foundation systems (3 to 8 Hz), which means that the higher natural frequencies can also be excited by the Ricker wavelet loading. However, it is likely that the variation of dominant loading frequency will have some effect on the overall response of the system and the conclusions should be interpreted bearing this in mind.

For all foundation conditions, the nonlinear displacements (i.e. the displacements of the cracked system) are smaller than the linear displacements (i.e. the displacements of the linear elastic, noncracked system). The cracking may be therefore regarded as the energy-consuming mechanism.

For all foundation conditions, the frequency content of the presented displacements indicates that the frequency of the cracked dam-foundation system is smaller than the frequency of the equivalent linear, noncracked system. The cracked systems have experienced a loss in stiffness, which is proportional to the frequency.

For the rigid foundation case, the level of cracking is by far the most extensive and in very good agreement with the Bristol EERC shaking table tests (Mir & Taylor, 1994).

If the load level is reduced (peak acceleration amplitude reduced from 0.5g to 0.3g) the cracking of the downstream face disappears completely.

For the rigid foundation case, the dam subjected to the scaled vertical earthquake component does not exhibit any cracking. The observed difference in results between the application of the combined vertical and horizontal earthquake components and the application of the horizontal component only is not significant from the practical point of view. This supports the view that seismic cracking behaviour of concrete gravity dams may well be understood by considering horizontal records only. Similar conclusions can be reached for flexible foundation cases as they are generally less prone to cracking.

For the flexible foundation cases, the level of cracking is much less extensive. This indicates that the simpler, rigid foundation case is on the 'safe side', but also that the full nonlinear, flexible foundation analysis is the only alternative if rigorous conclusions on crack location and extent are sought.

The two conclusions above are closely related to the presence of radiation damping. In the rigid foundation case, there is no radiation damping at all - the vibration energy is reflected from the rigid base and remains trapped inside the system. In the flexible foundation case, radiation damping is present - a part of the vibration energy is transmitted away from the dam. The 'softer' the foundation, the greater the radiation damping.

Among the four presented flexible foundation cases, cracking is less severe for the cases where E_f=10 and 20 GPa. Cracking is more pronounced for the cases where E_f=5 and 40 GPa.

No single flexible foundation case exhibits cracking of the downstream face. This conclusion has wider implications on the stability of dams with more realistic cross-sections (e.g. where the neck of the dam exists). The simplified rigid foundation

analysis might show cracking at the downstream face of the neck, while in reality, due to foundation flexibility, the stresses might be relieved and no cracking occur.

For all foundation conditions except for the softest foundation (E_f=5 GPa), the cracks open, close and reopen again, following the general pattern of the main oscillation. For the softest foundation, due to the high level of radiation damping and loading in the form of the Ricker wavelet, there is insufficient 'restoring energy' which would close the main crack, and it remains open throughout the time span of the analysis.

In cases for which $E_f < E_c$, the principal direction of cracking is non-horizontal. This direction is vertical for E_f=5 GPa, and slightly inclined for E_f=10 GPa. If the level of loading is further increased, the ultimate failure mode would be the failure of the foundation.

In cases for which $E_f \geq E_c$, the principal direction of cracking is horizontal. If the level of loading is further increased, the ultimate failure mode would be the failure of the dam-foundation interface. The overall stability of the dam is in greater danger.

The conclusions presented in this Section were based on the particular dam geometry, foundation conditions and earthquake records. Ideally, they should all be confirmed in a more detailed study using a number of different dam geometries, foundation conditions and real earthquake records. By solving and explaining some important analytical problems that might be encountered in concrete dam-foundation interaction analyses, this work has paved the way for such a study.

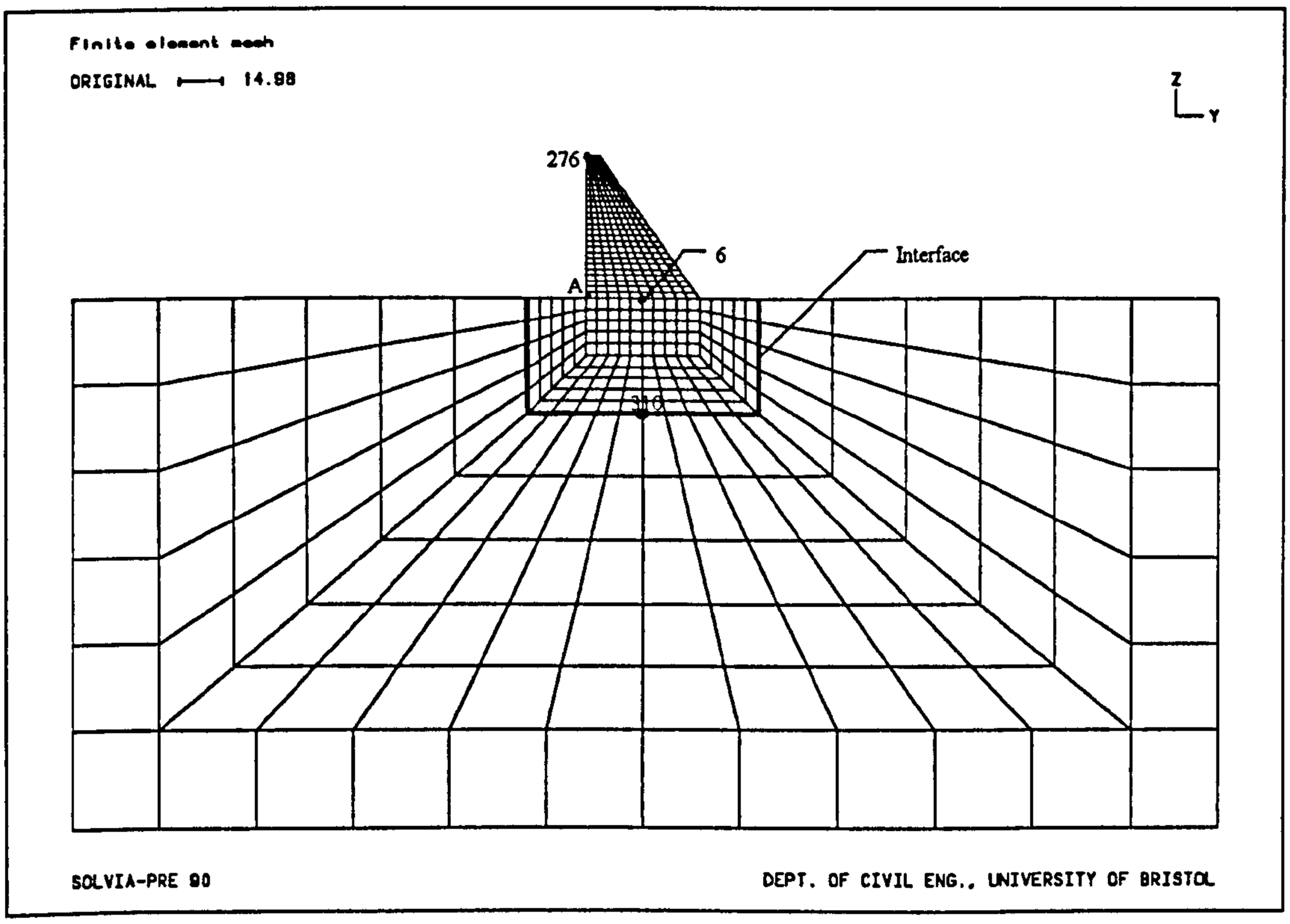

Figure 9.1 - Finite element mesh of the concrete gravity dam-foundation system

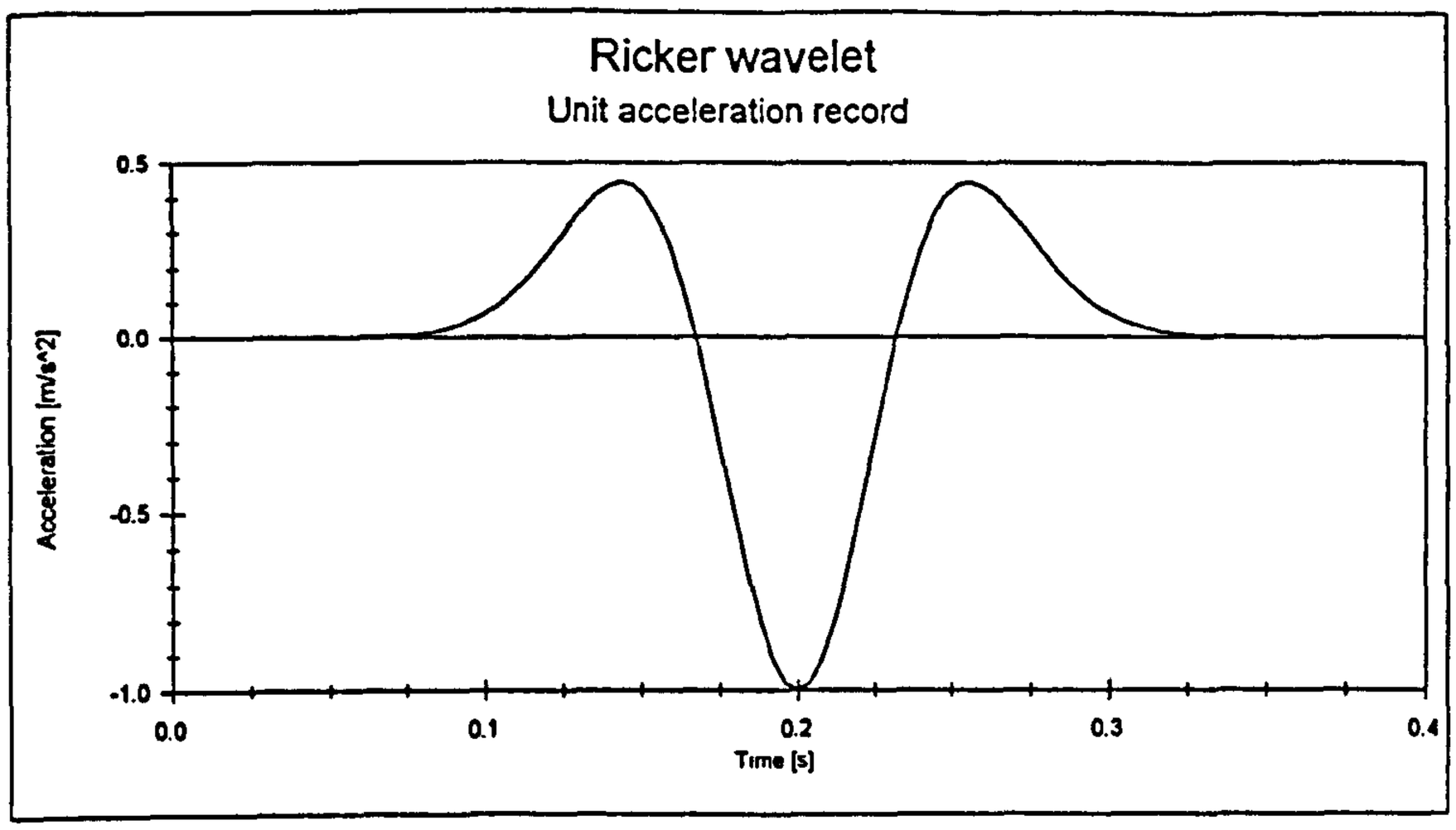

Figure 9.2a - Acceleration record

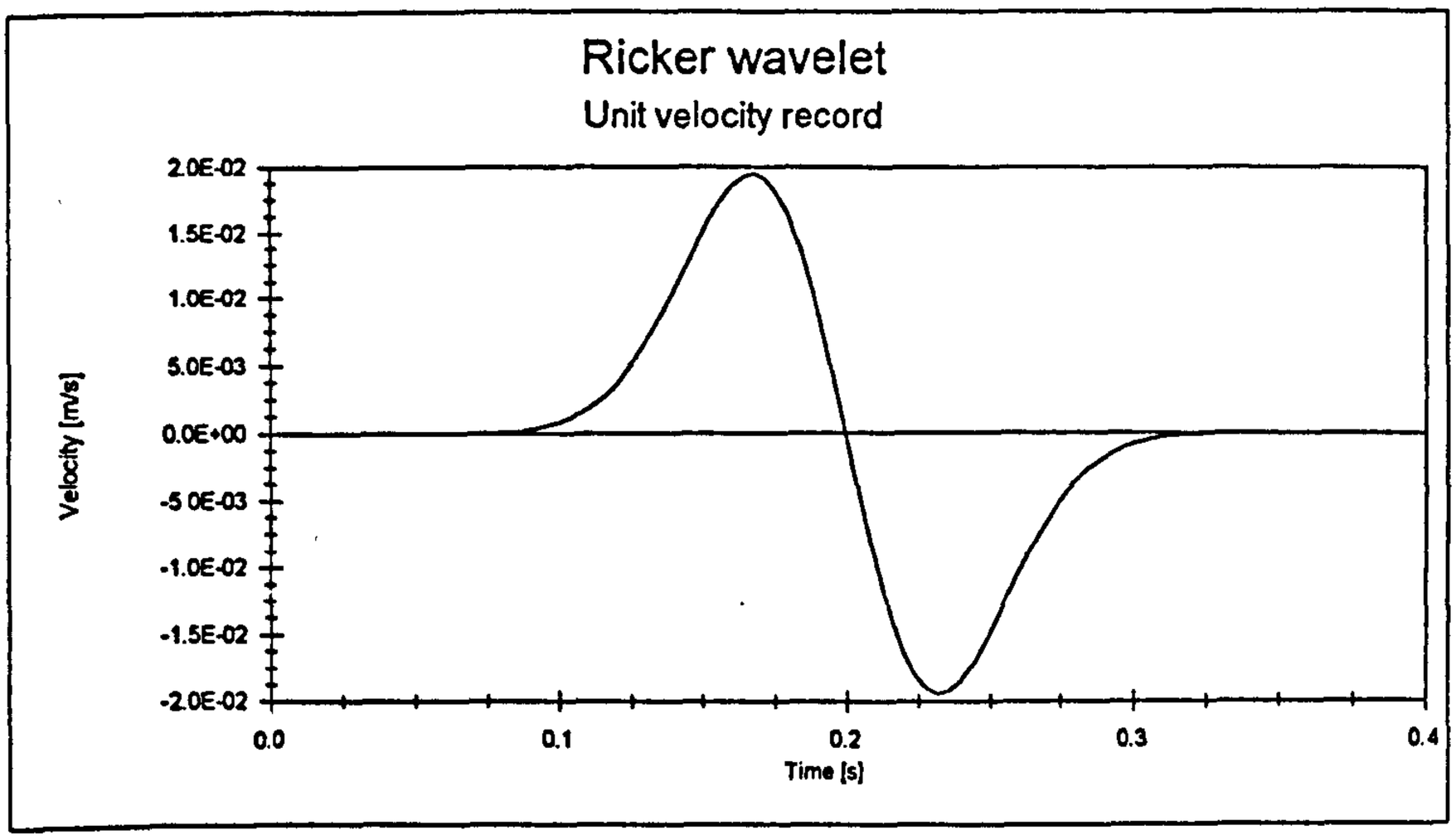

Figure 9.2b - Velocity record

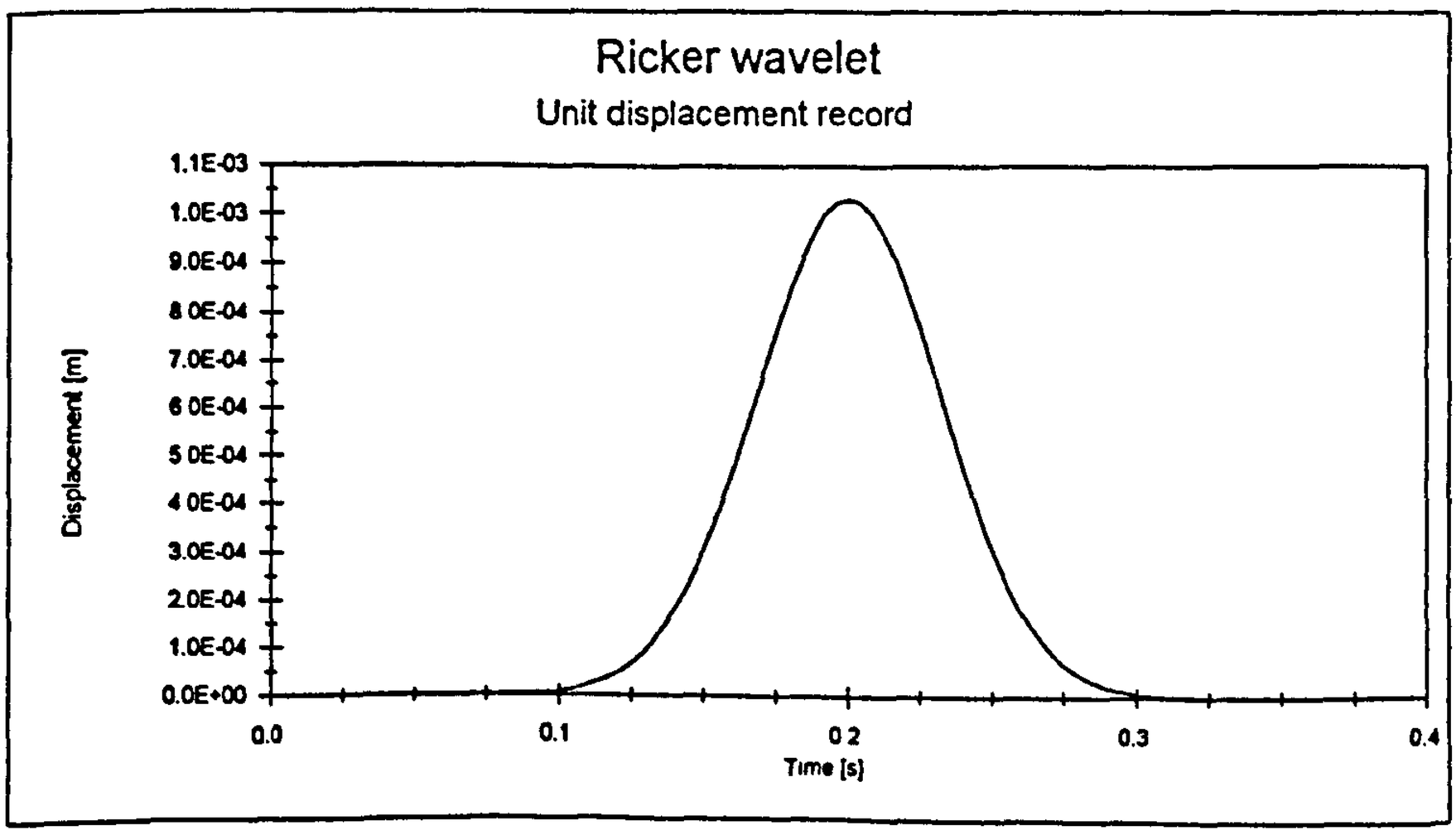

Figure 9.2c - Displacement record

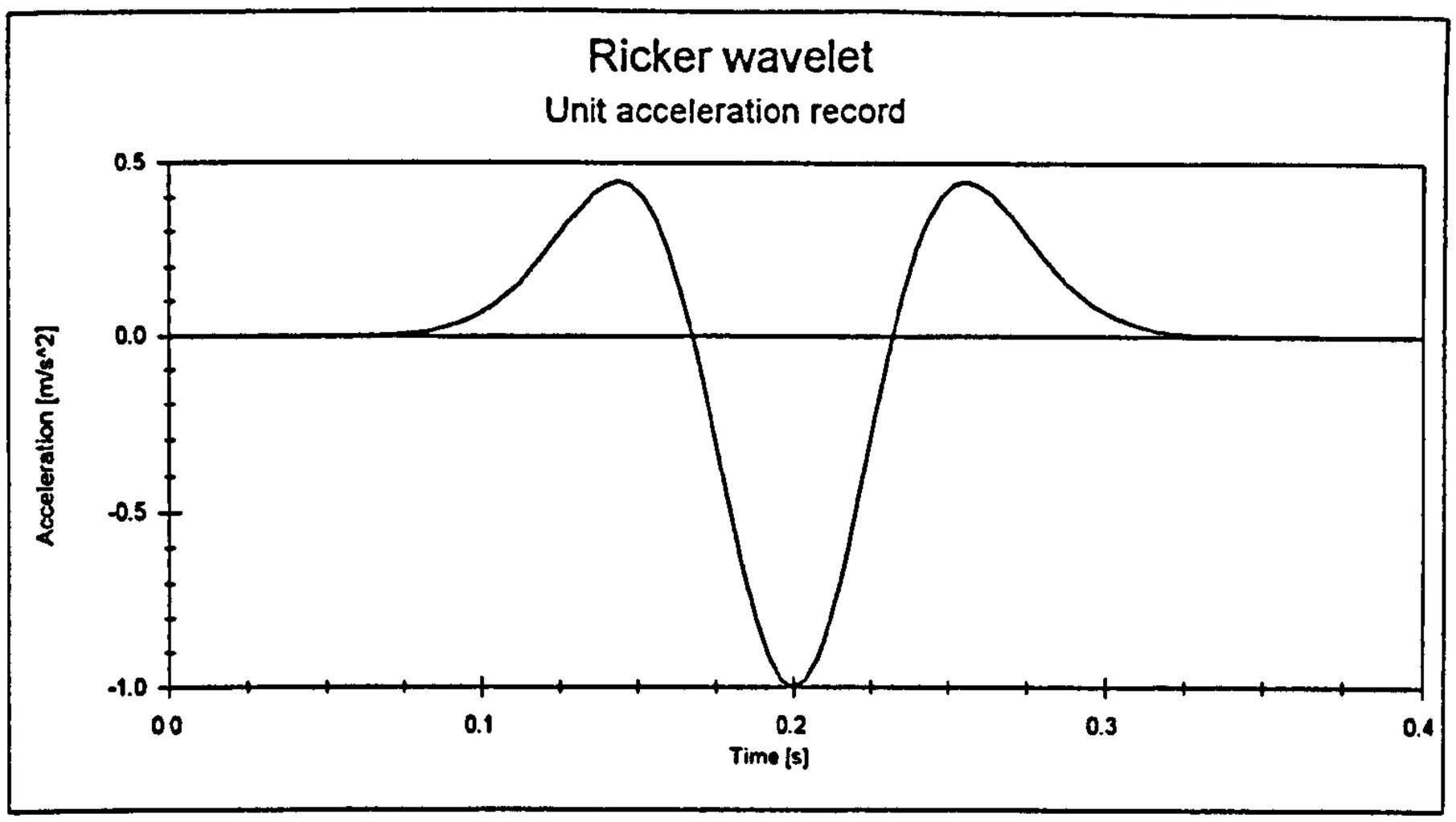

Figure 9.2a - Acceleration record

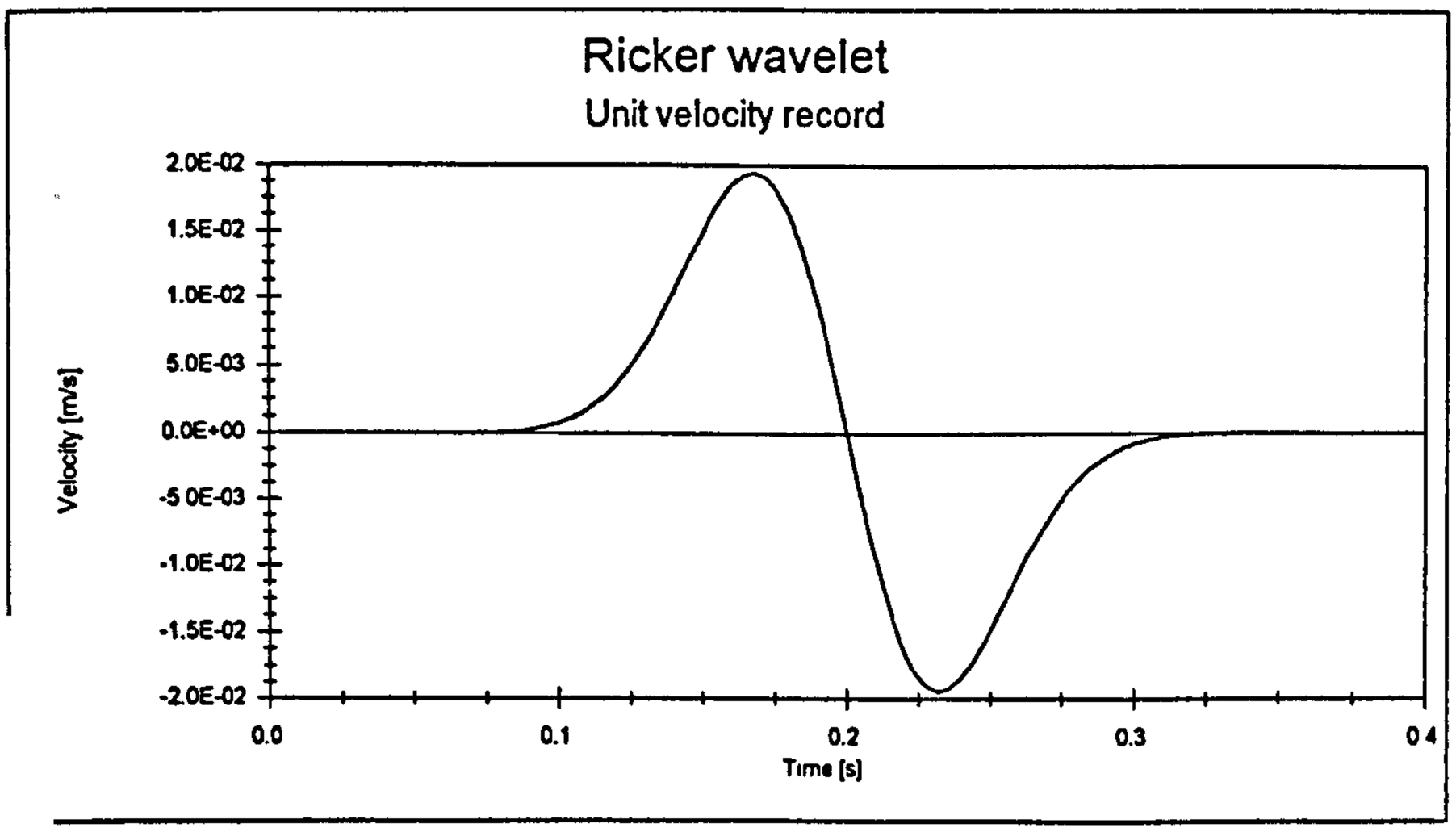

Figure 9.2b - Velocity record

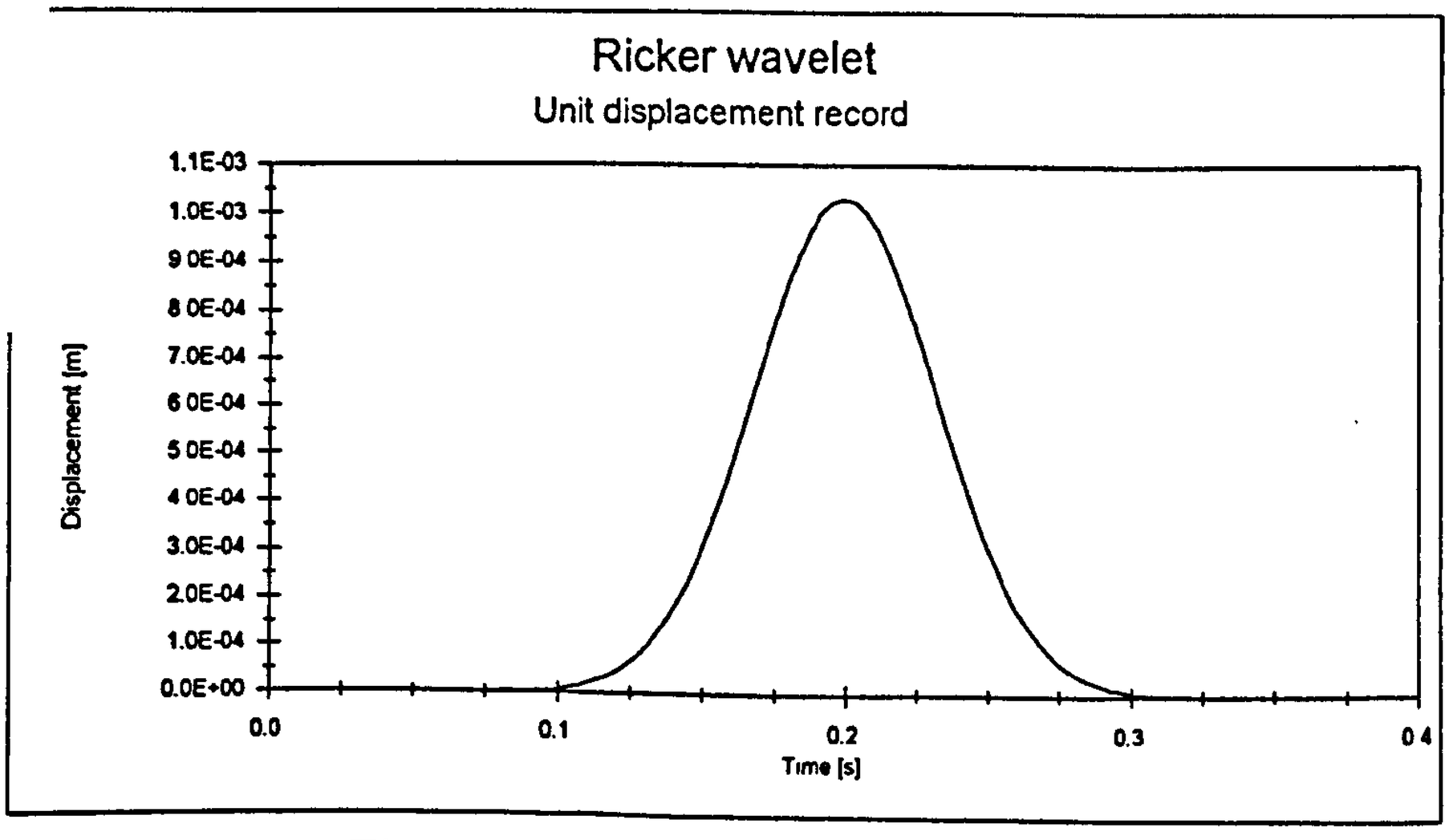

Figure 9.2c - Displacement record

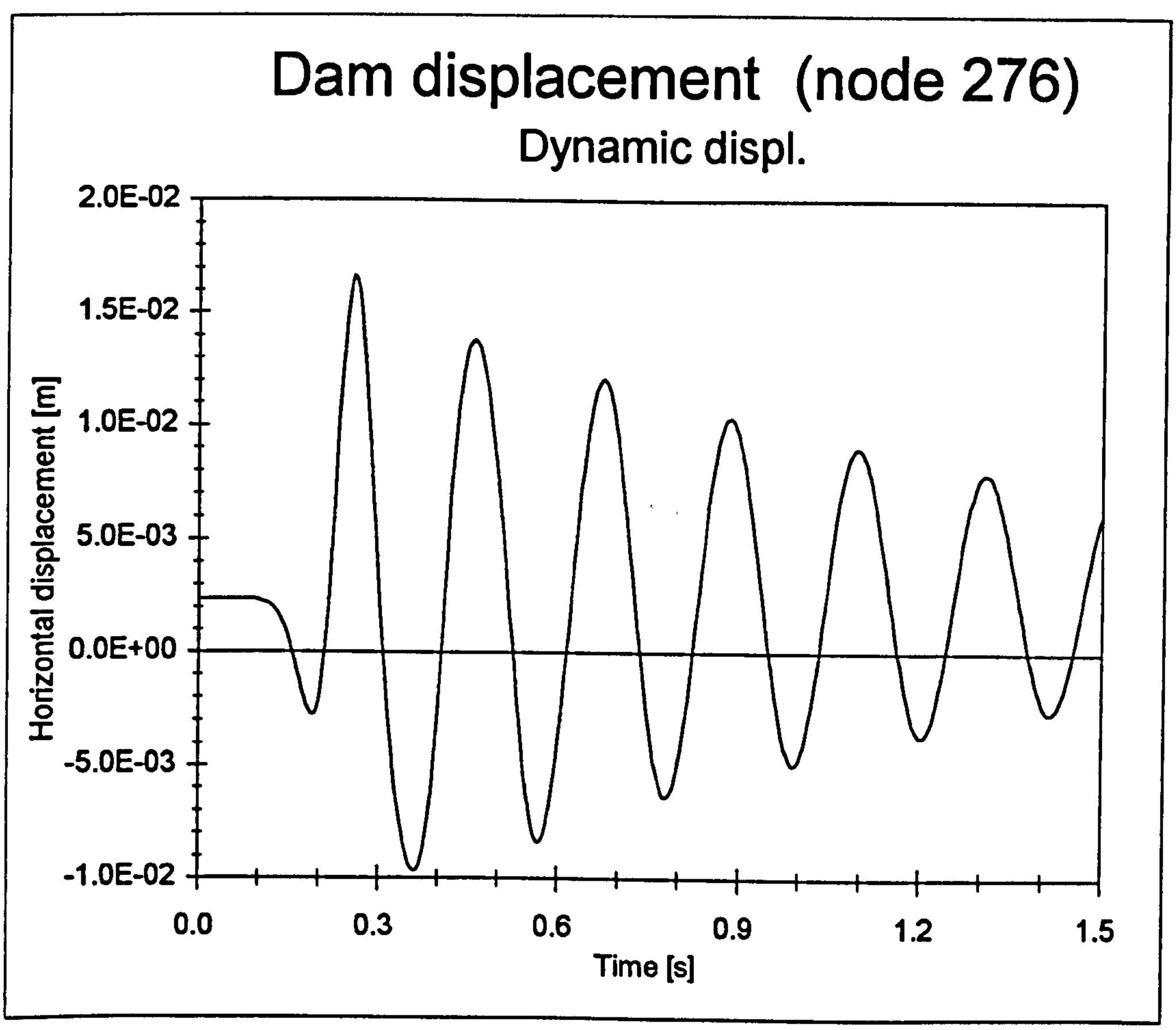

Figure 9.3a - Dynamic displacement of the top of the dam

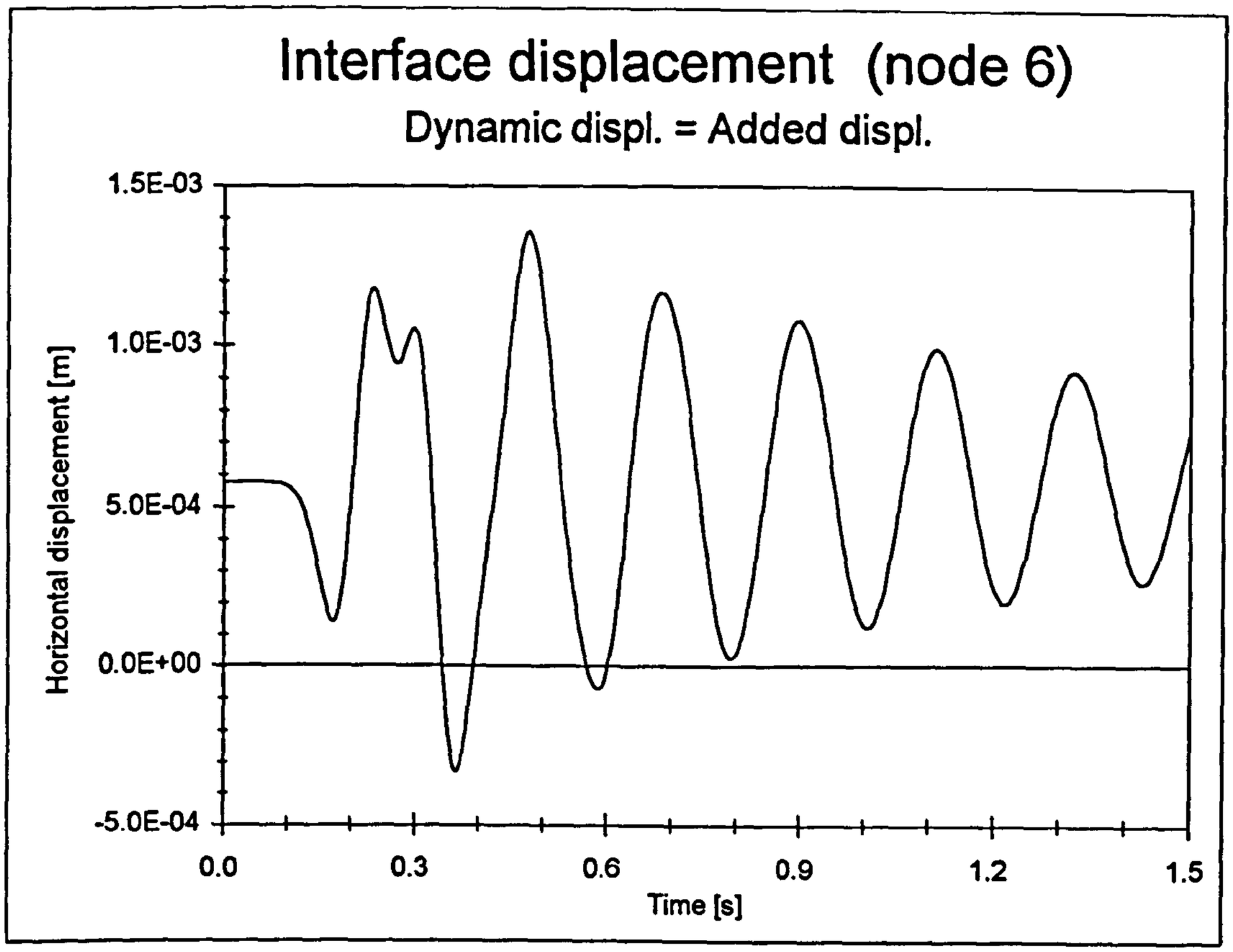

Figure 9.3b - Dynamic displacement of the interface

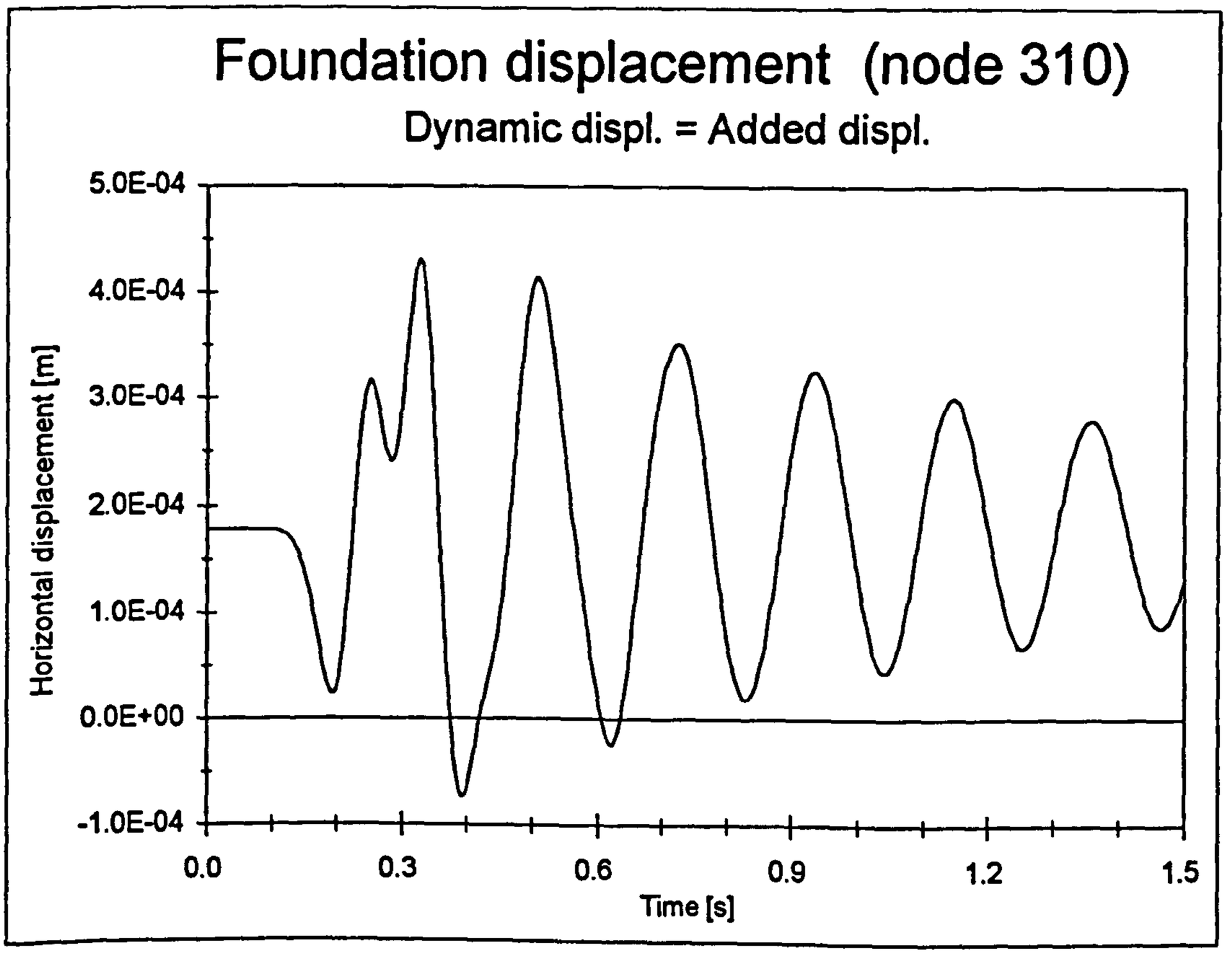

Figure 9.3c - Dynamic displacement of the foundation

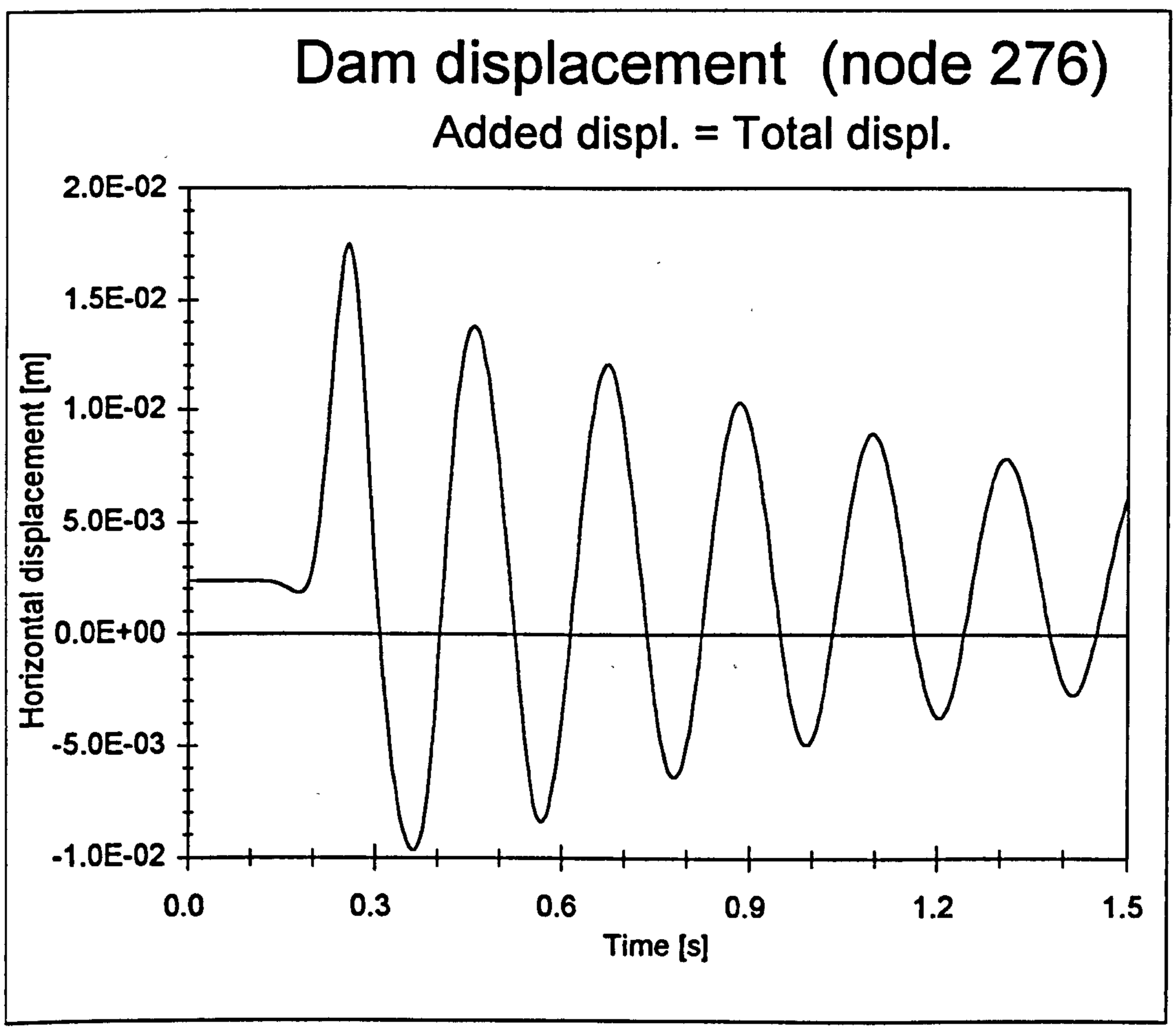

Figure 9.4 - Added (total) displacement of the top of the dam

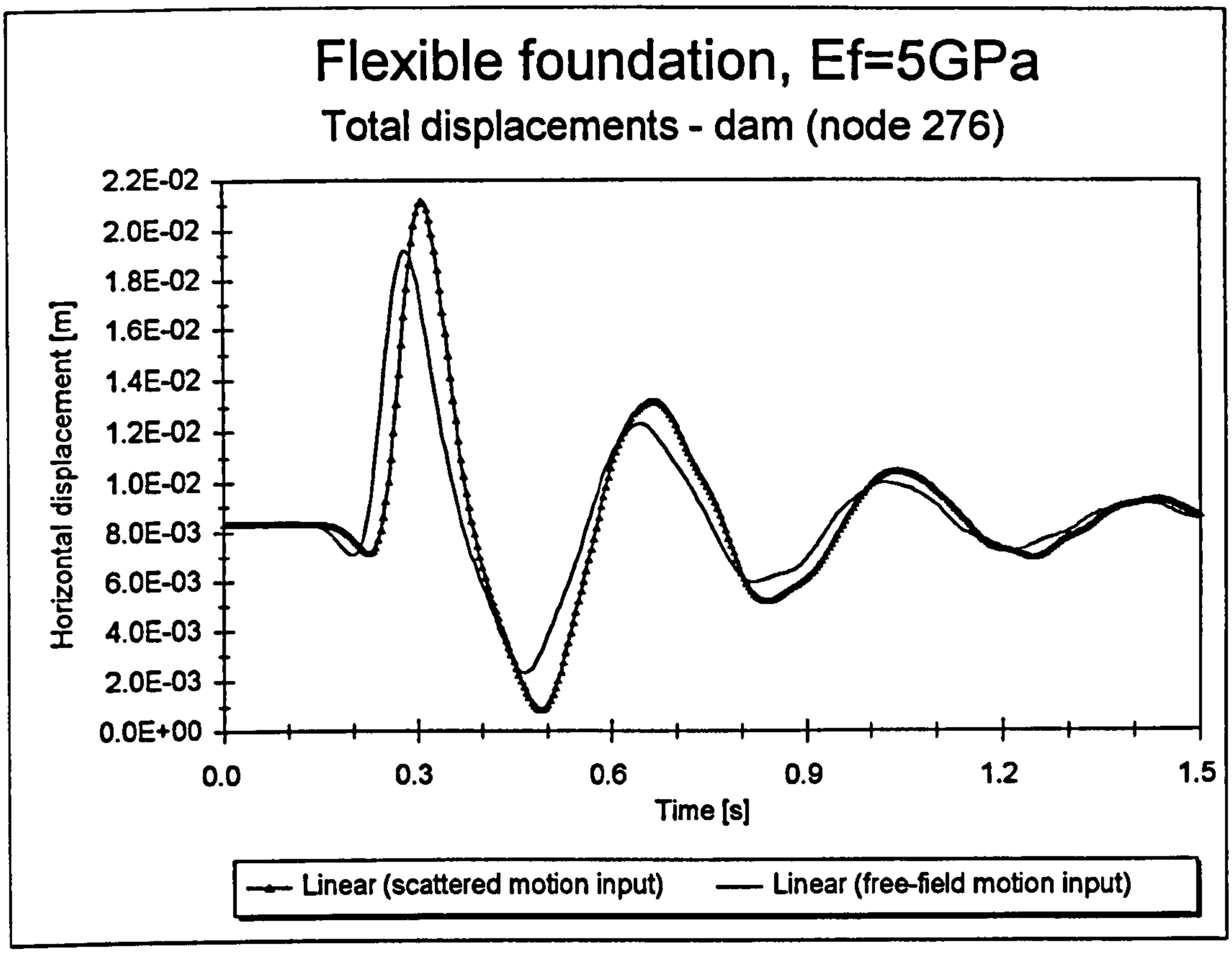

Figure 9.5a - Total displacement of the top of the dam

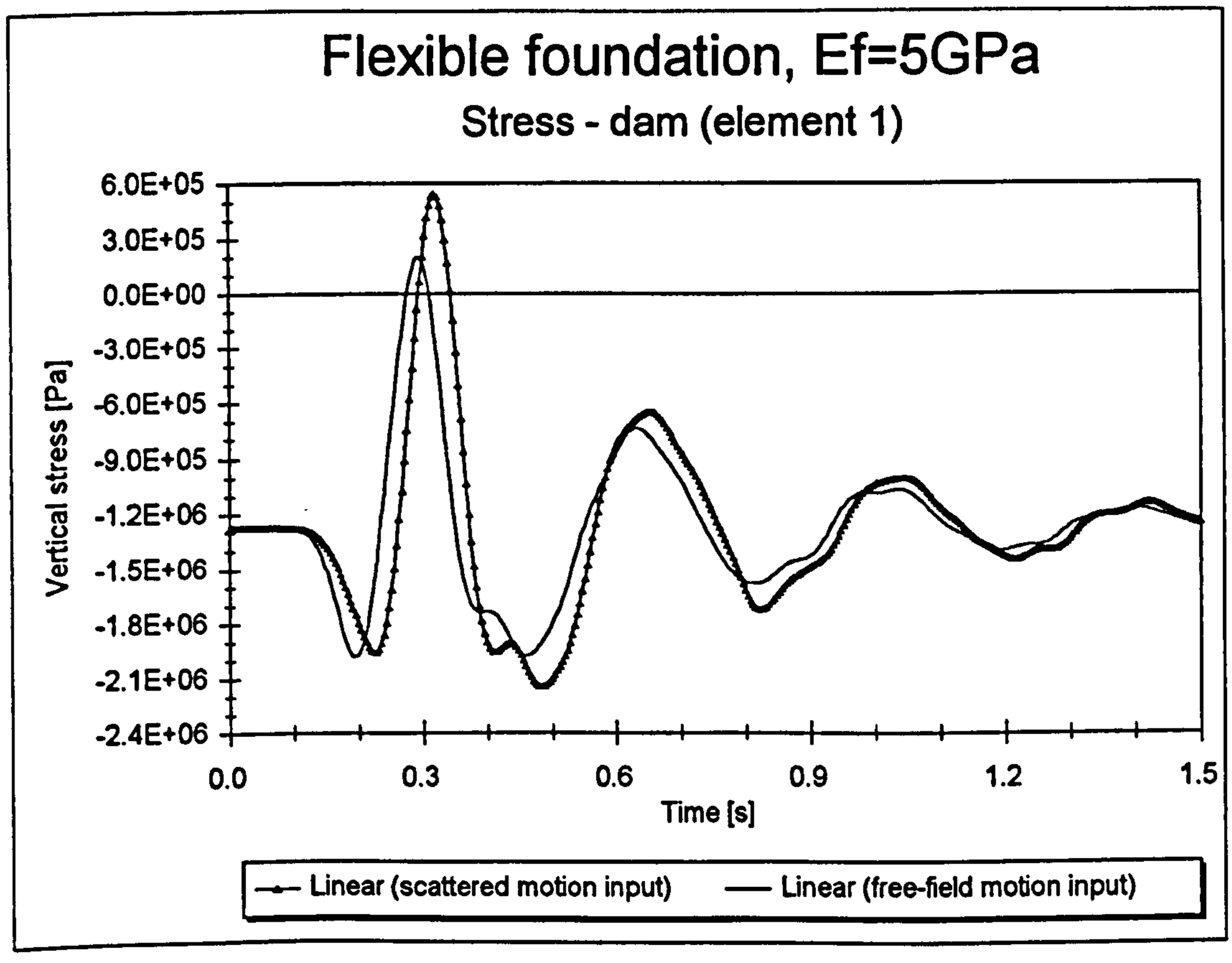

Figure 9.5b - Stress at the heel of the dam

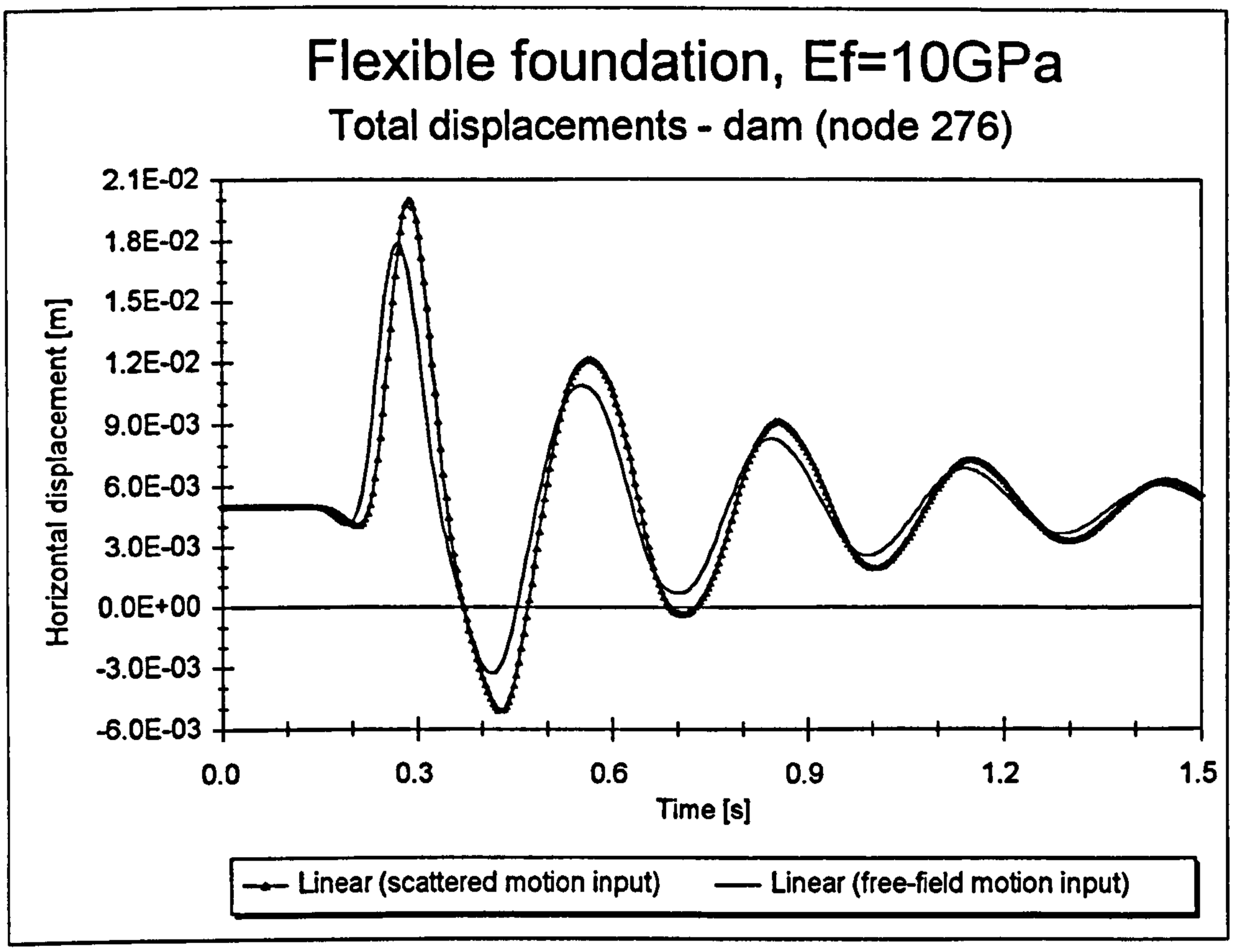

Figure 9.6a - Total displacement of the top of the dam

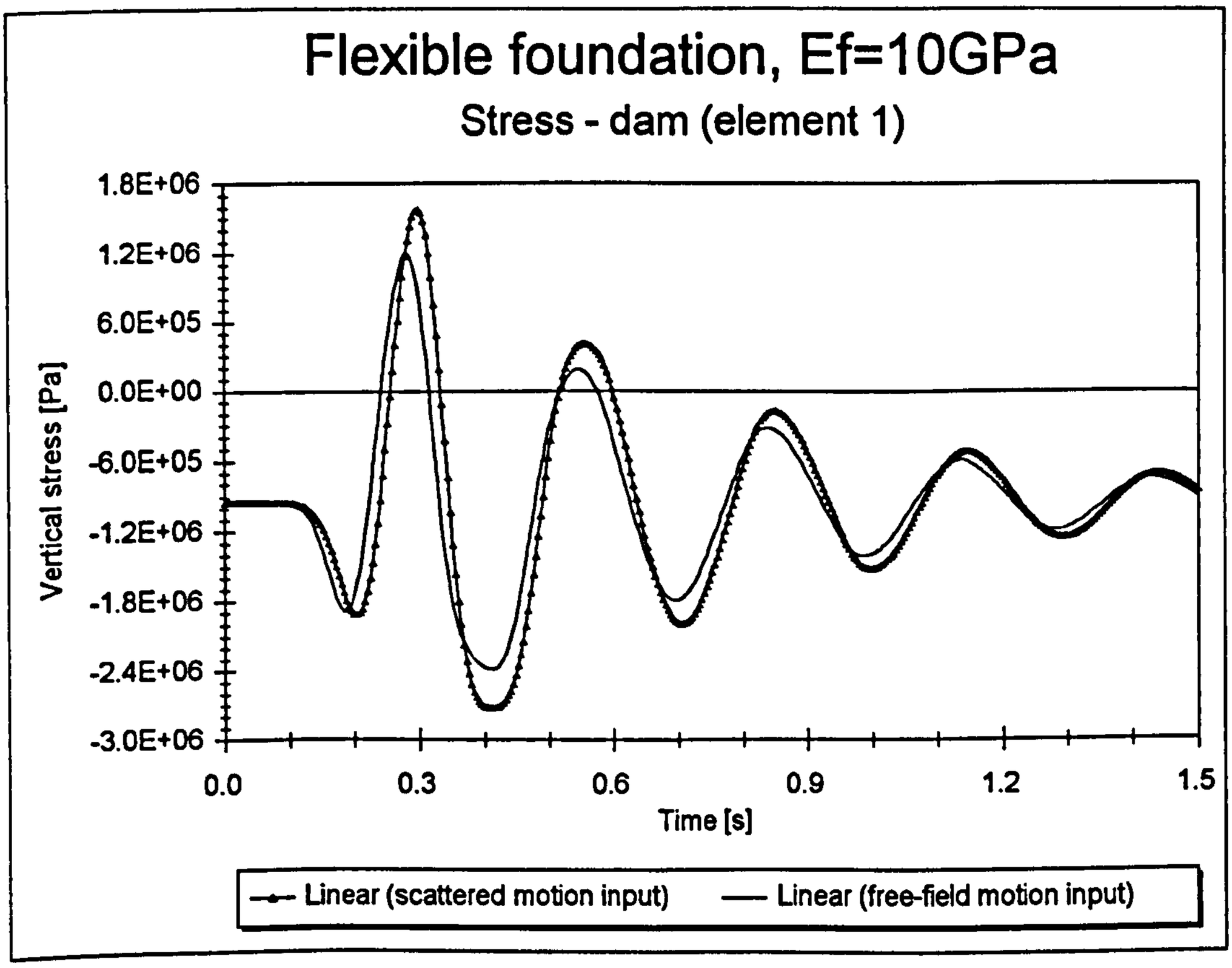

Figure 9.6b - Stress at the heel of the dam

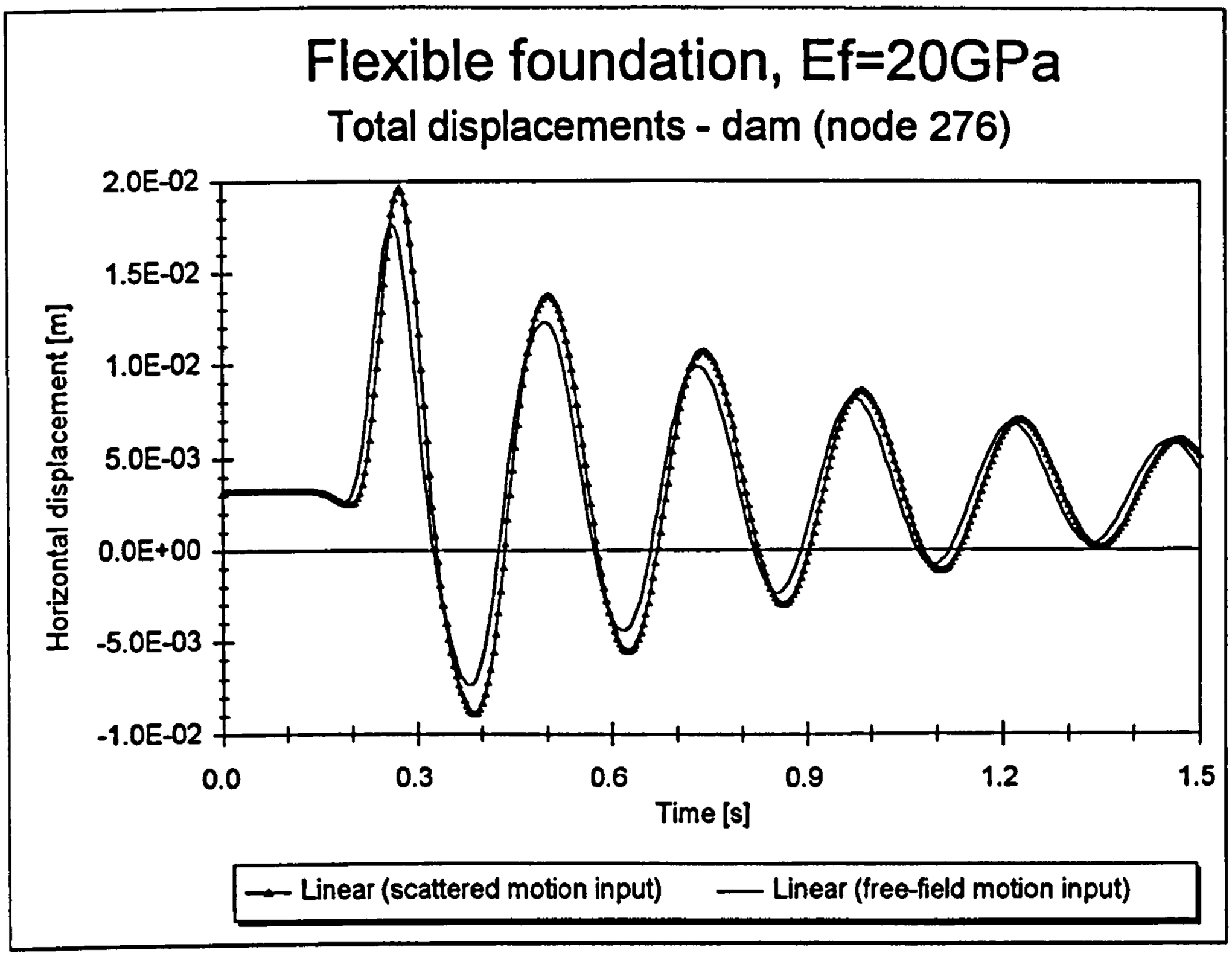

Figure 9.7a - Total displacement of the top of the dam

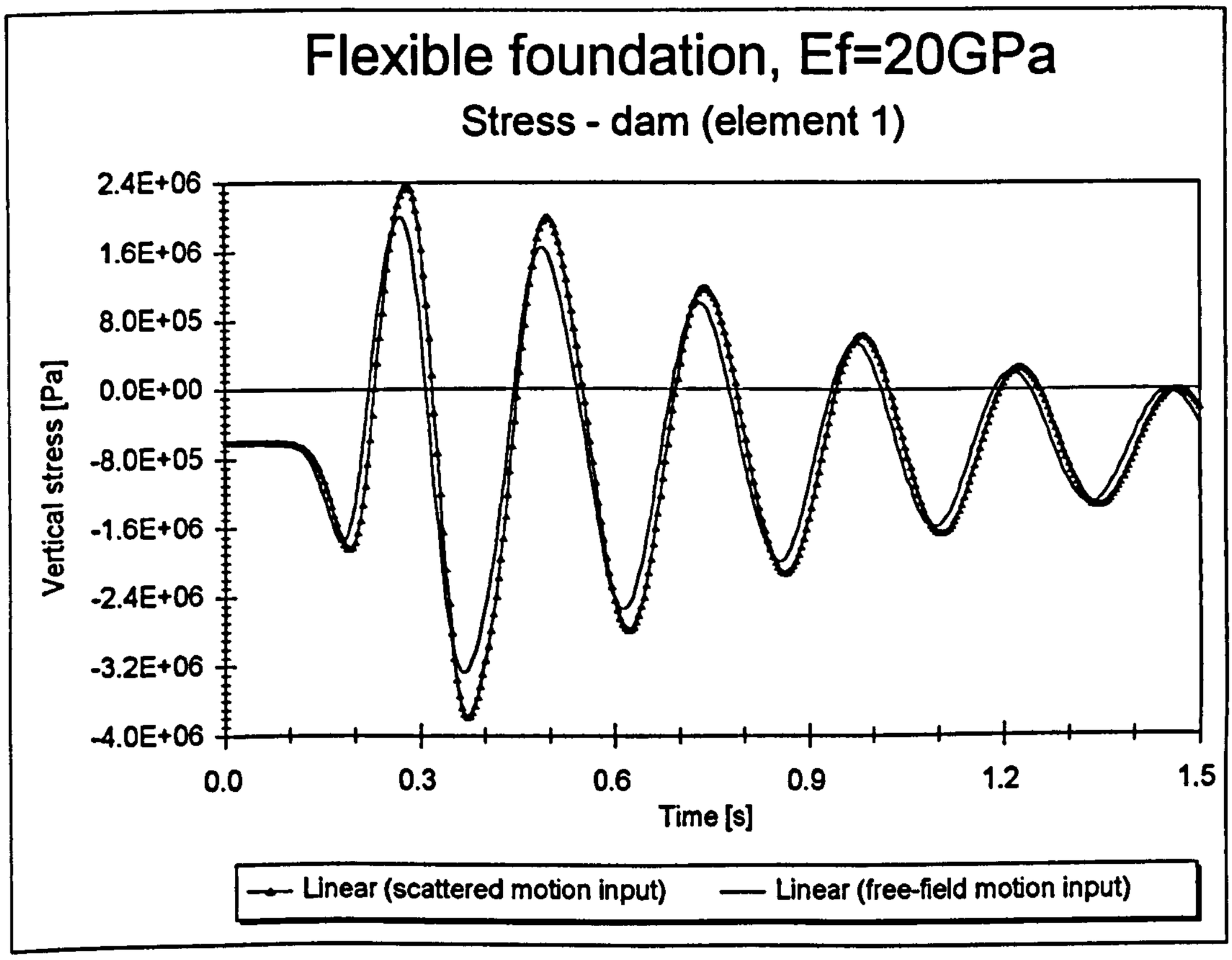

Figure 9.7b - Stress at the heel of the dam

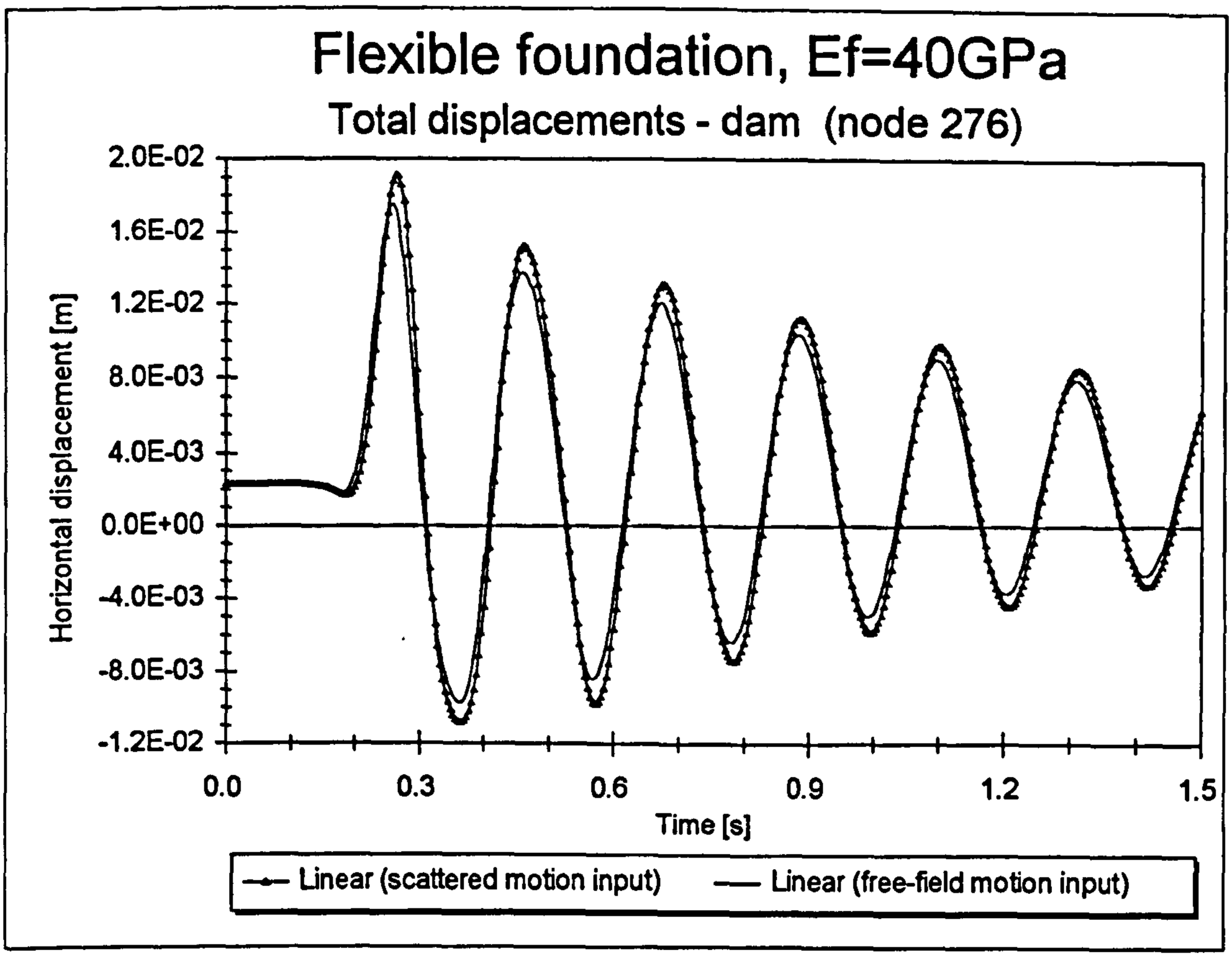

Figure 9.8a - Total displacement of the top of the dam

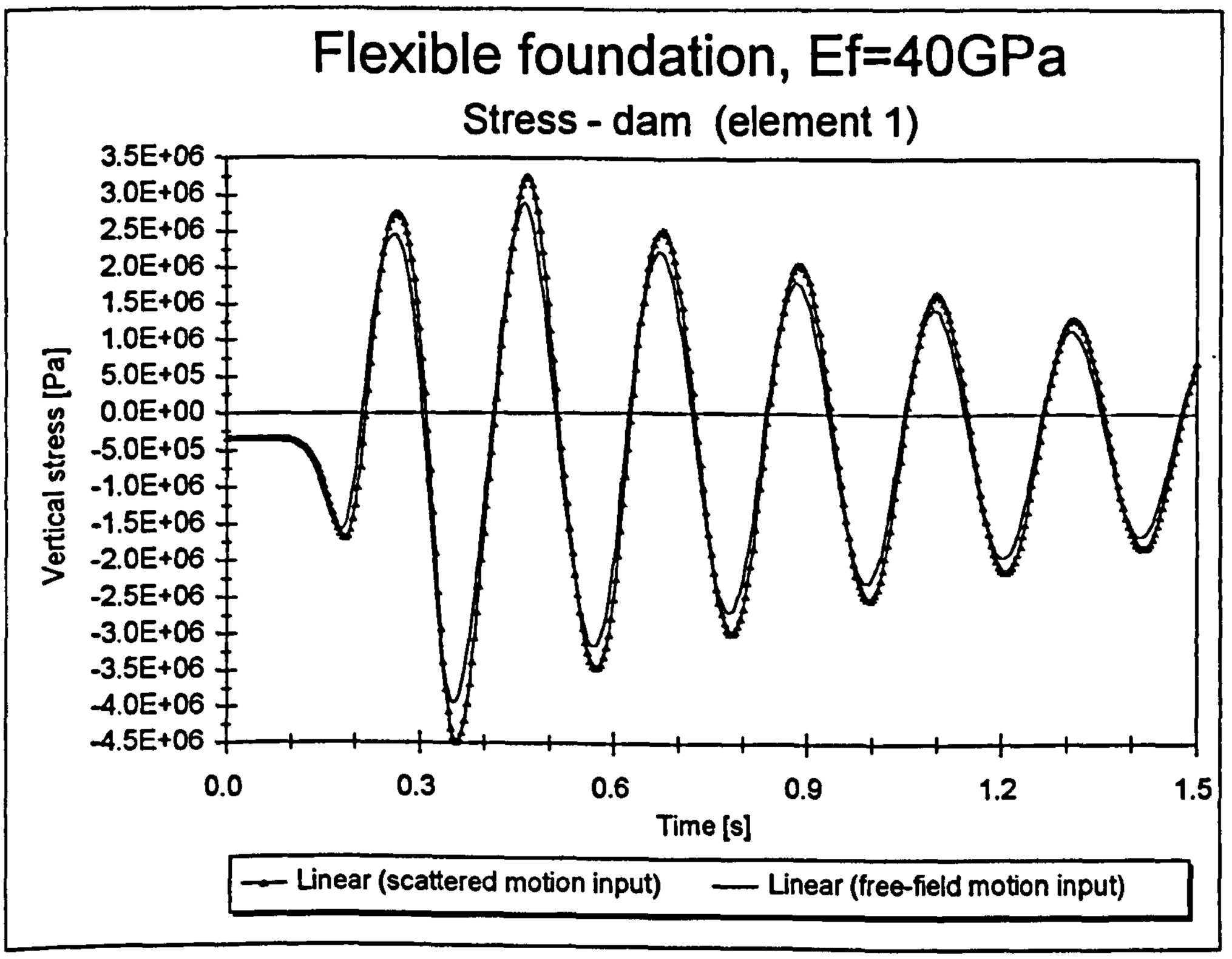

Figure 9.8b - Stress at the heel of the dam

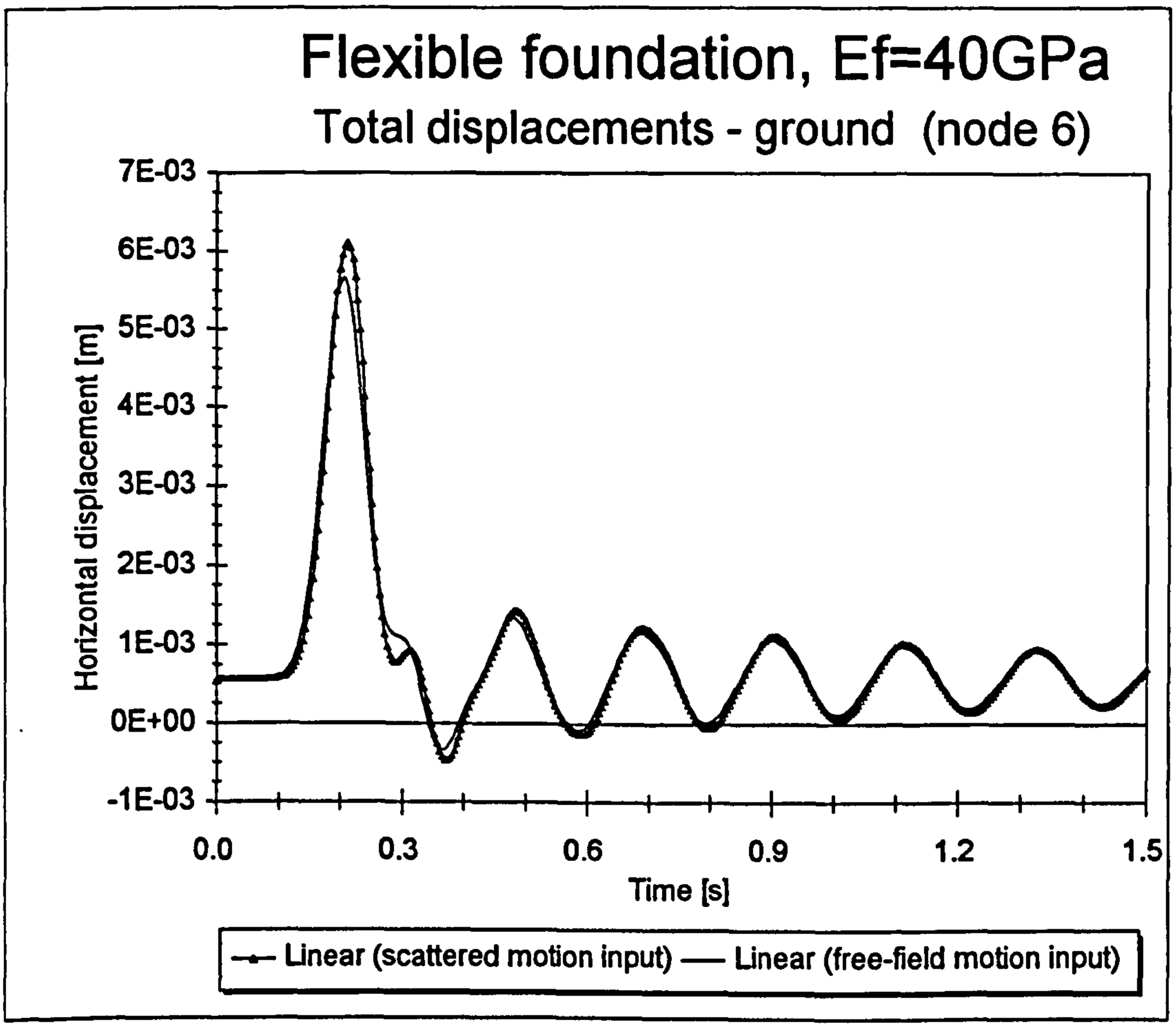

Figure 9.8c - Total displacement of the dam-foundation interface

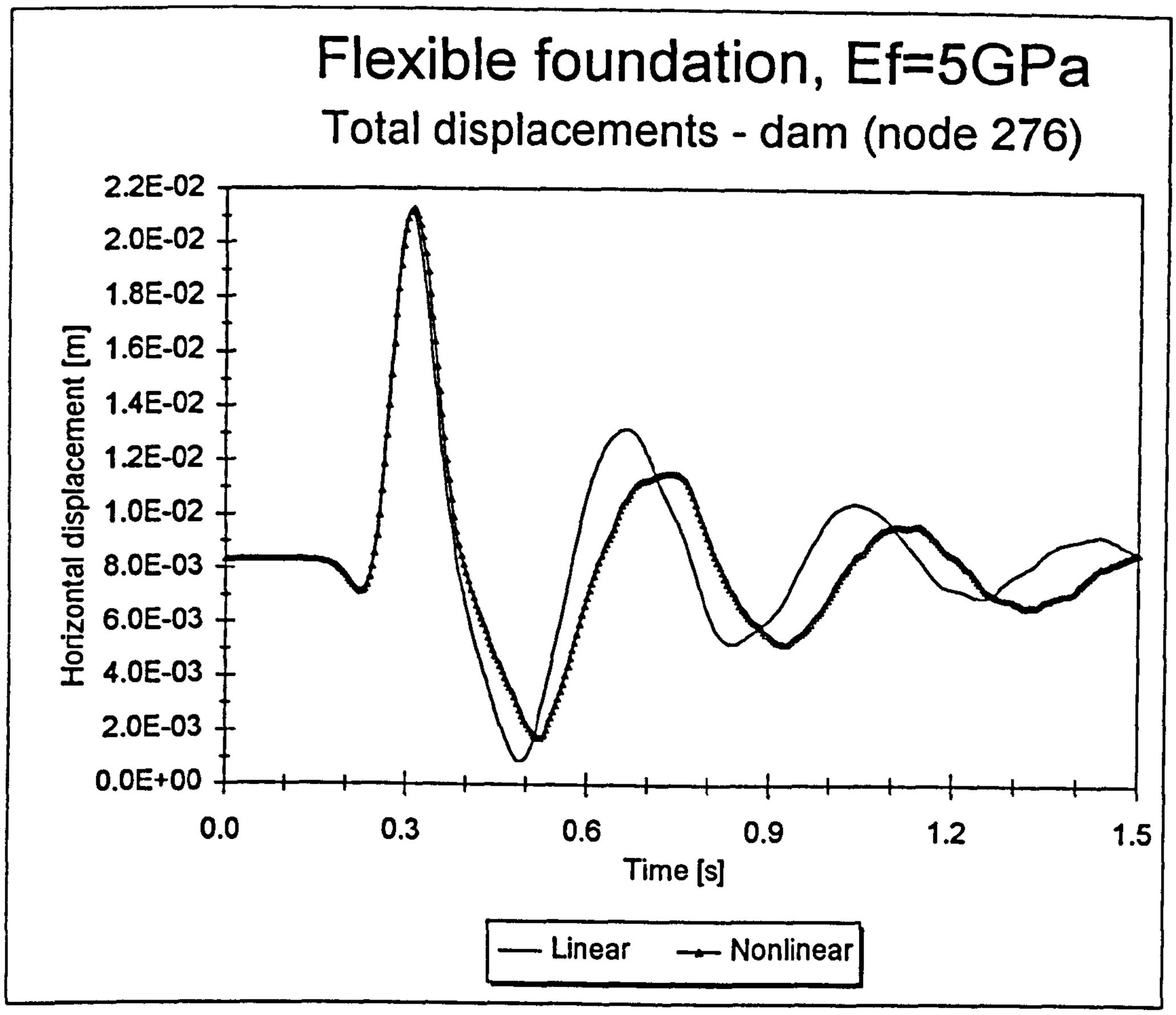

Figure 9.9a - Total displacement of the top of the dam

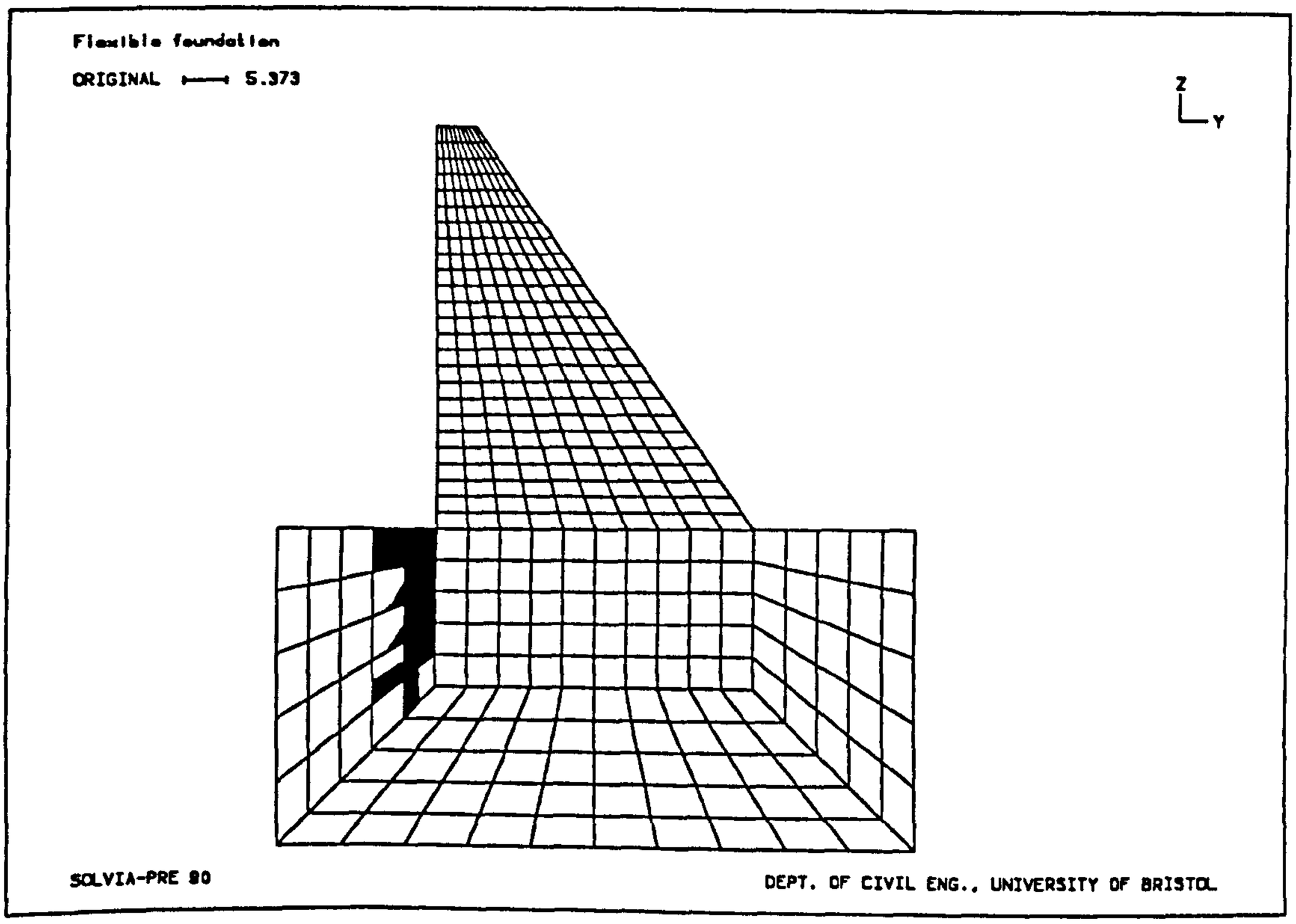

Figure 9.9b - Cracking pattern at t=0.412 s (E_f=5 GPa)

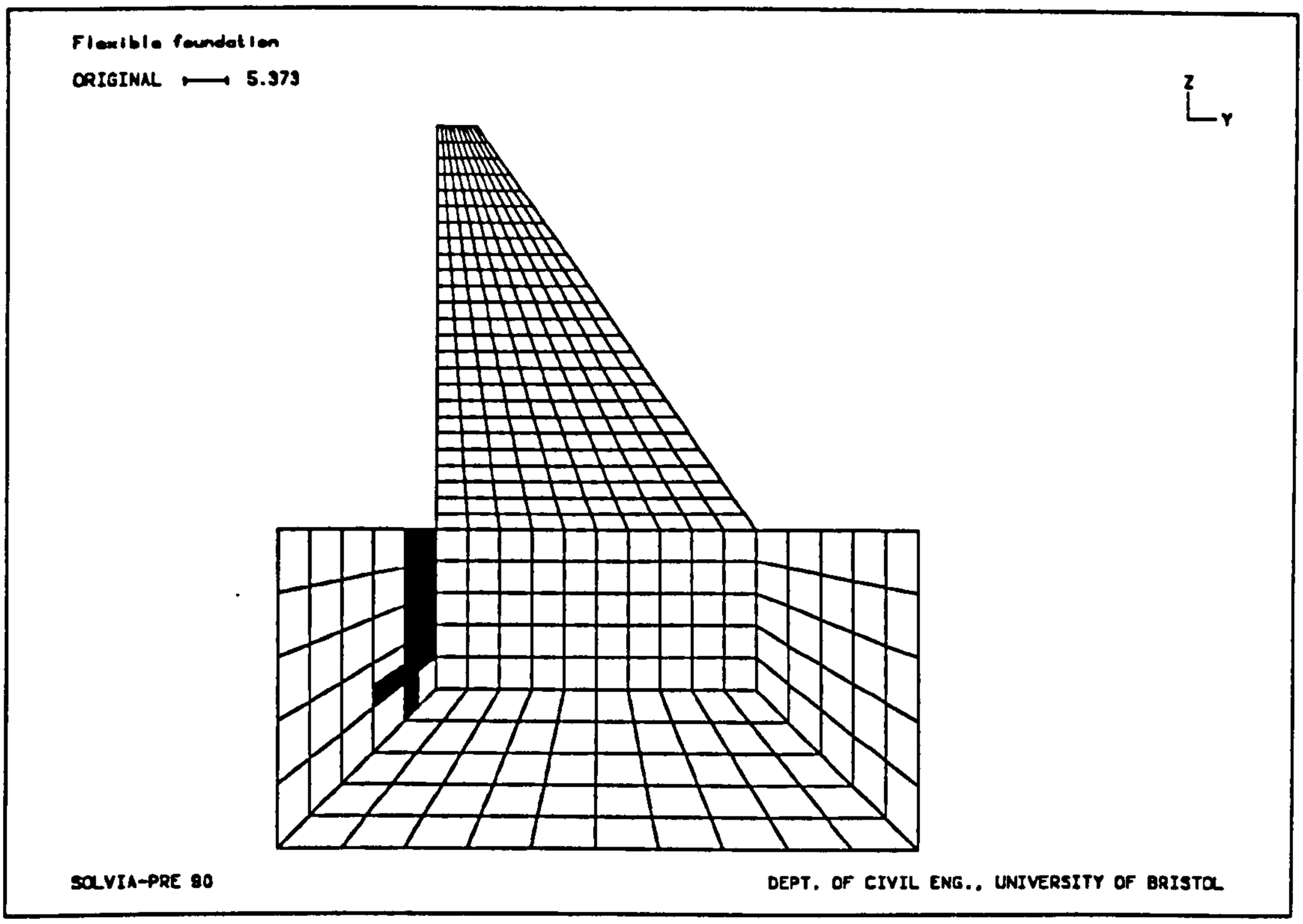

Figure 9.9c - Cracking pattern at t=0.560 s (E_f=5 GPa)

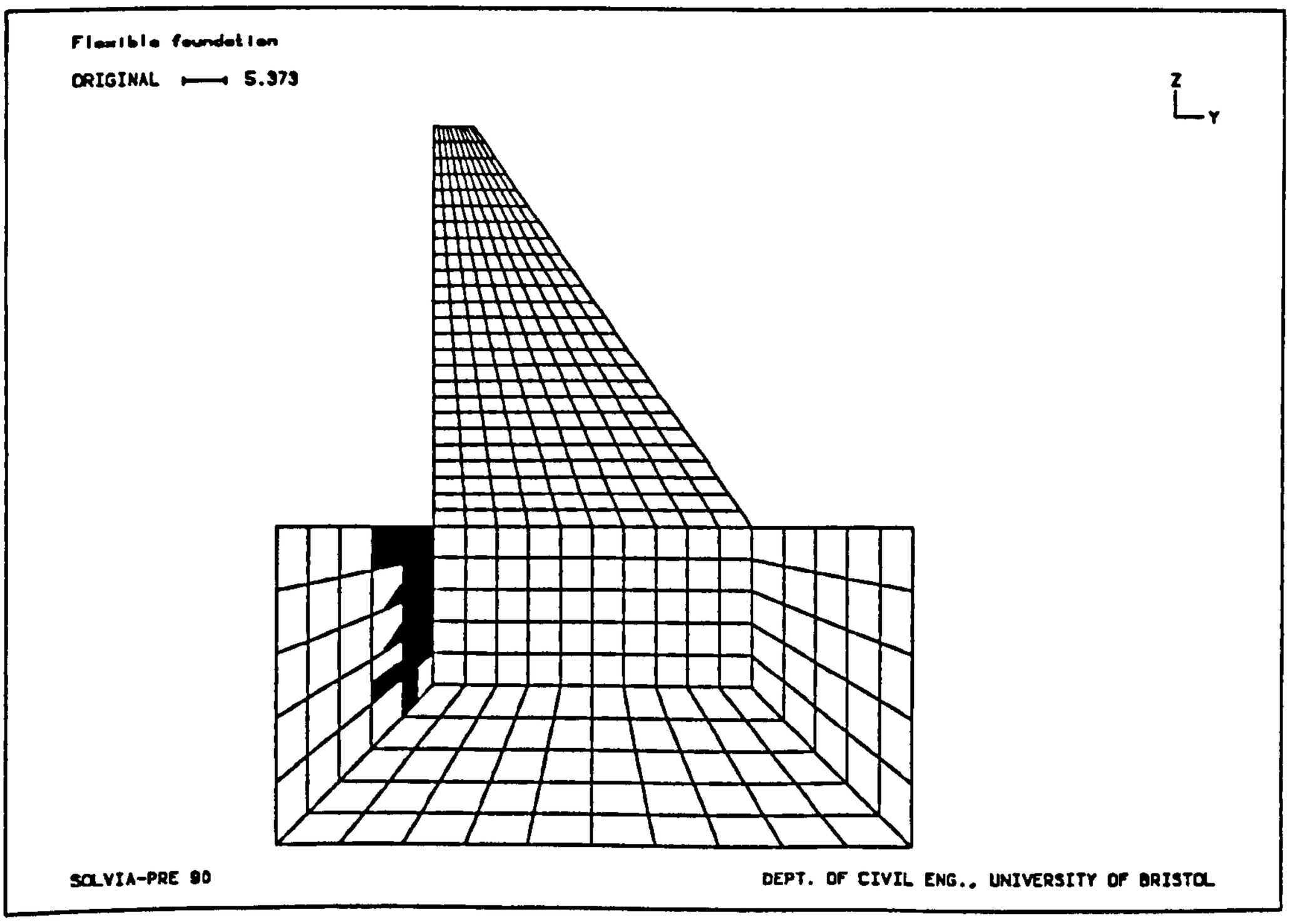

Figure 9.9d - Cracking pattern at t=1.000 s (E_f=5 GPa)

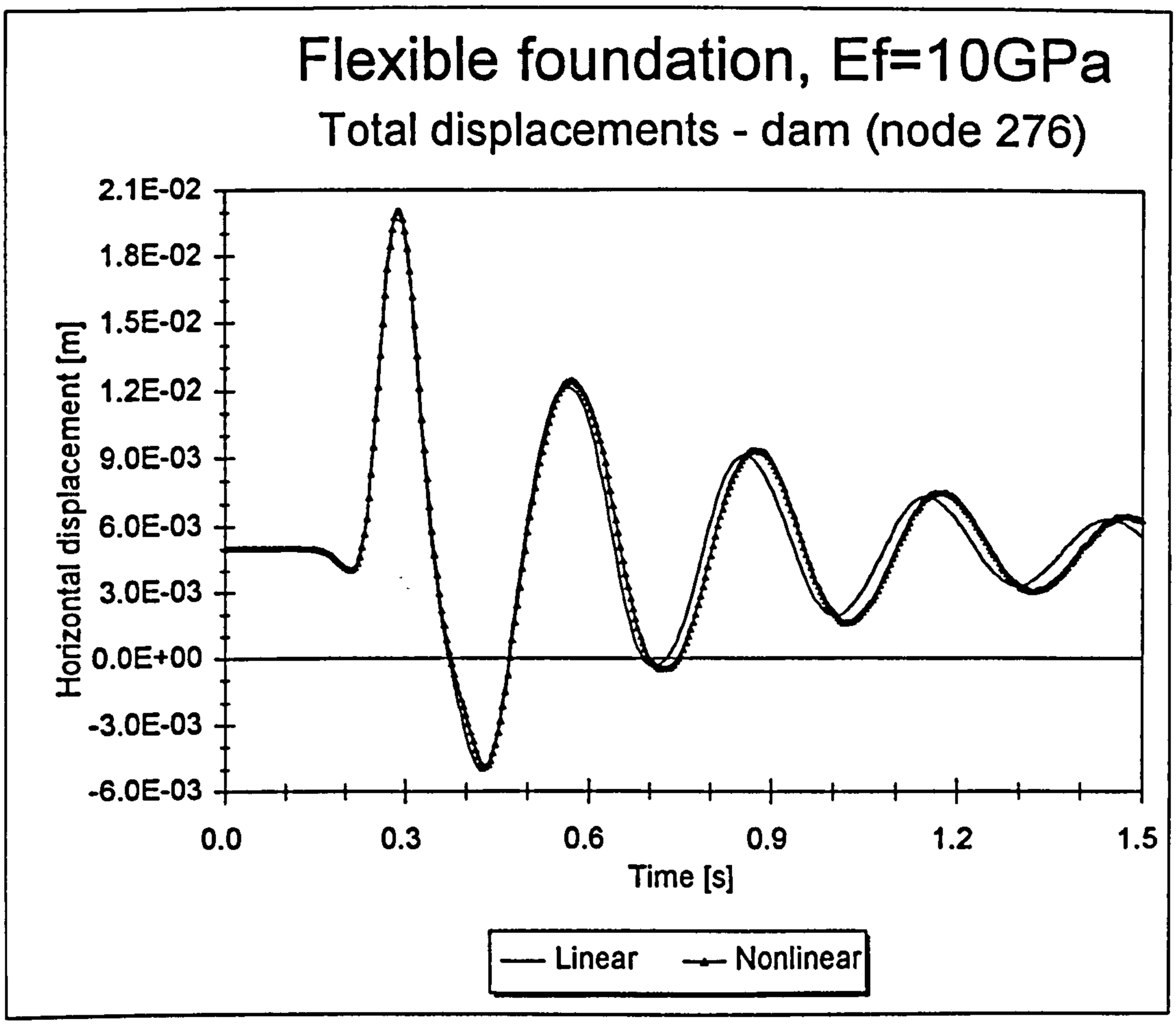

Figure 9.10a - Total displacement of the top of the dam

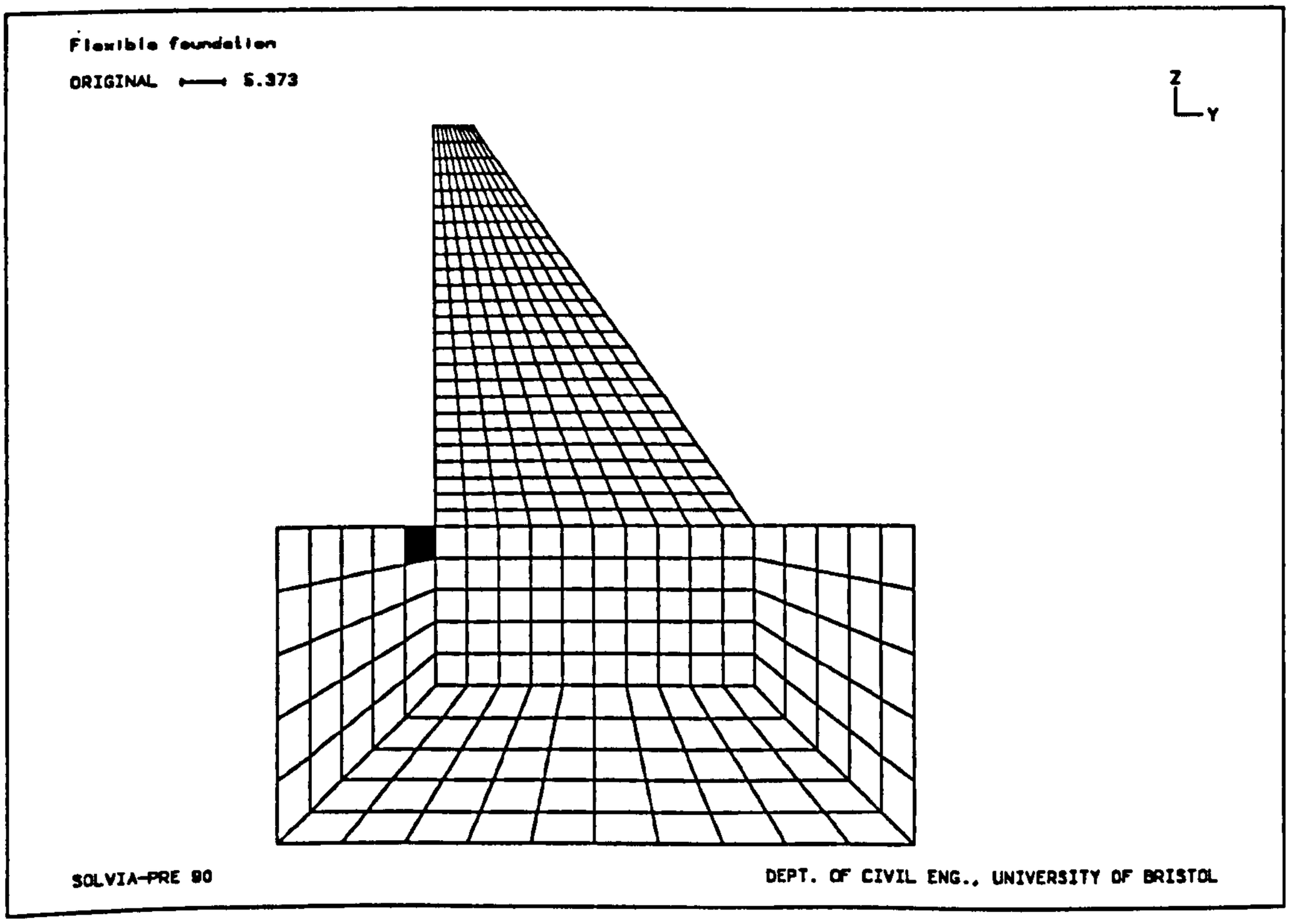

Figure 9.10b - Cracking pattern at t=0.328 s (E_f=10 GPa)

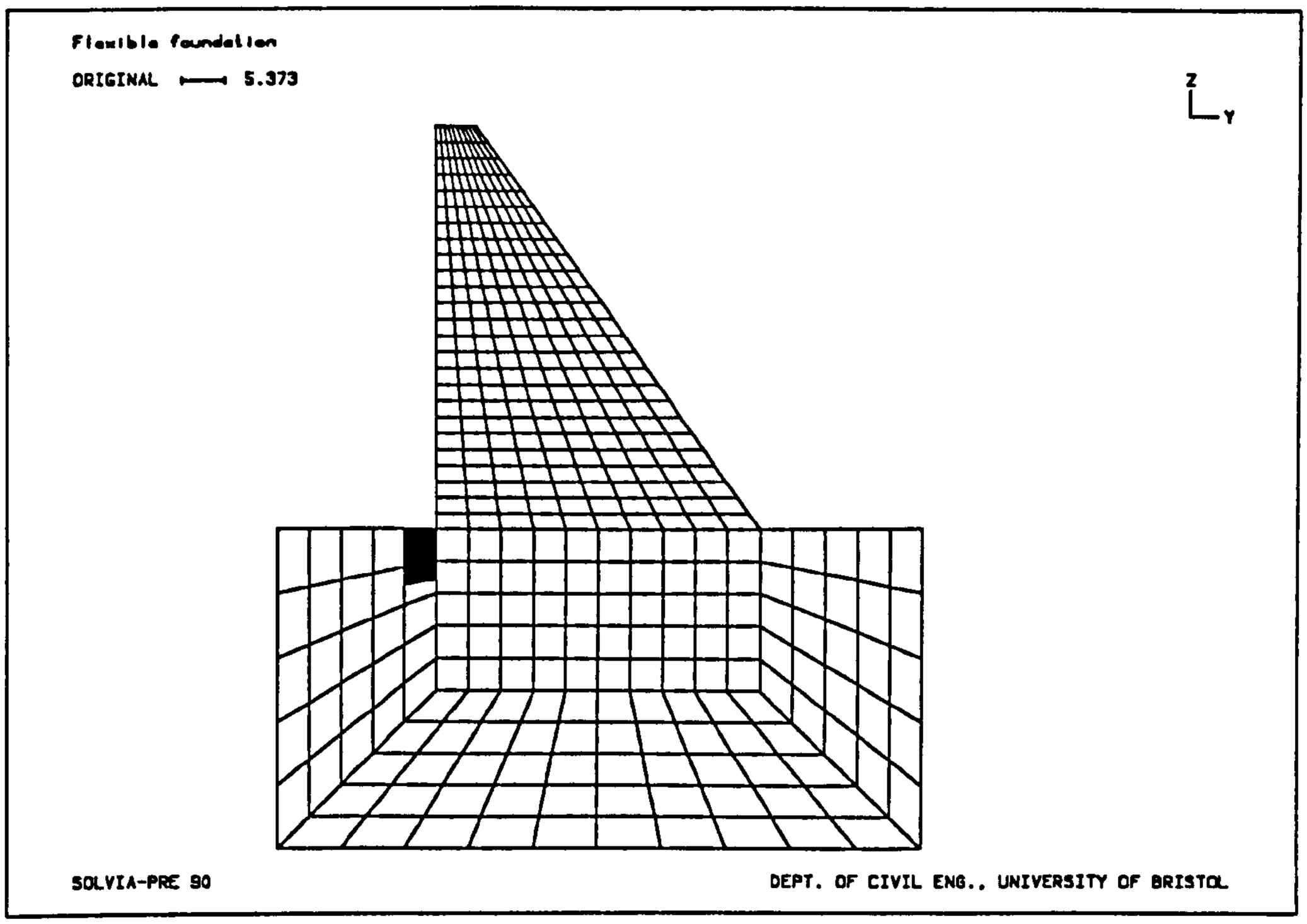

Figure 9.10c - Cracking pattern at t=0.568 s (E_f=10 GPa)

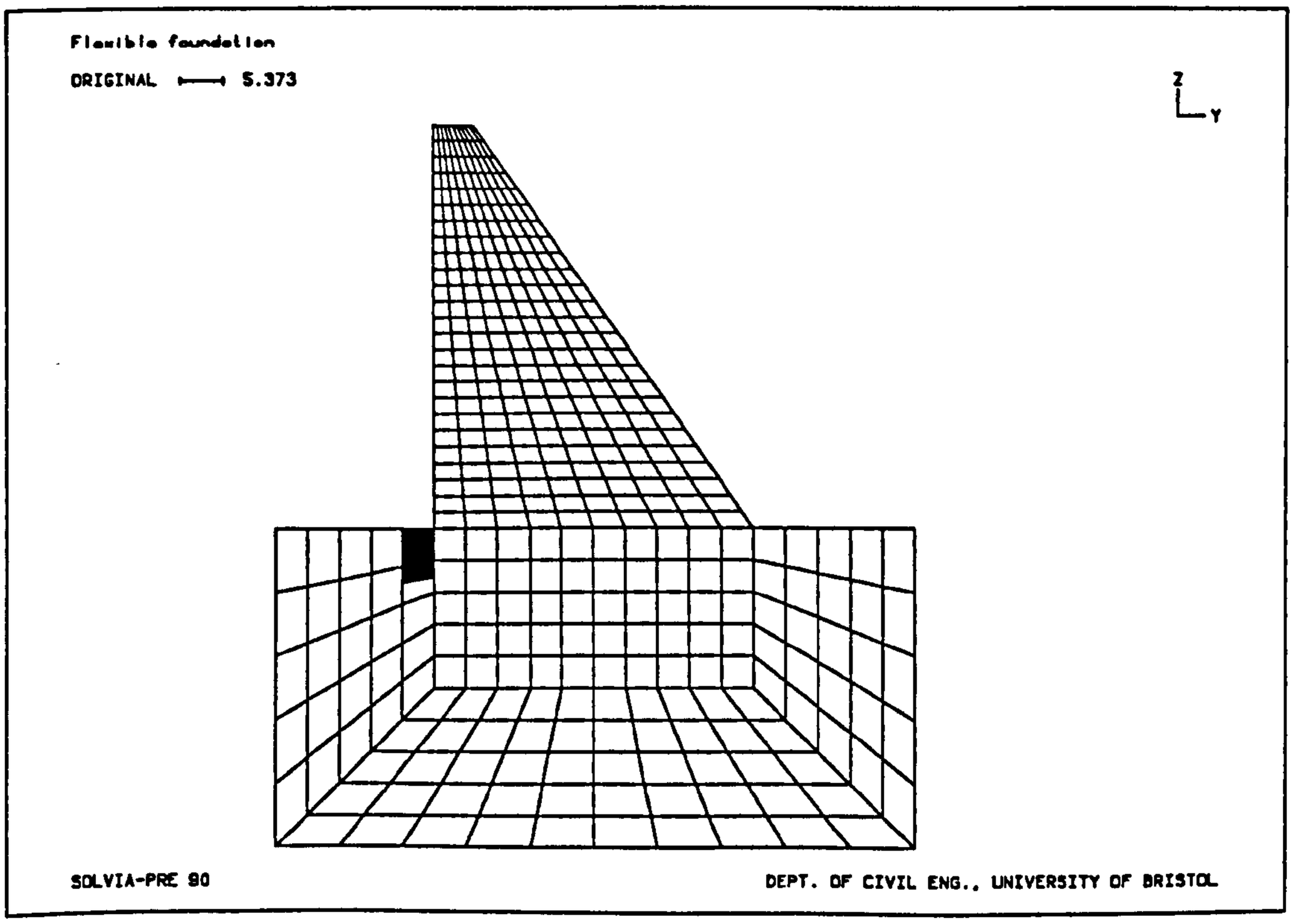

Figure 9.10d - Cracking pattern at t=1.500 s (E_f=10 GPa)

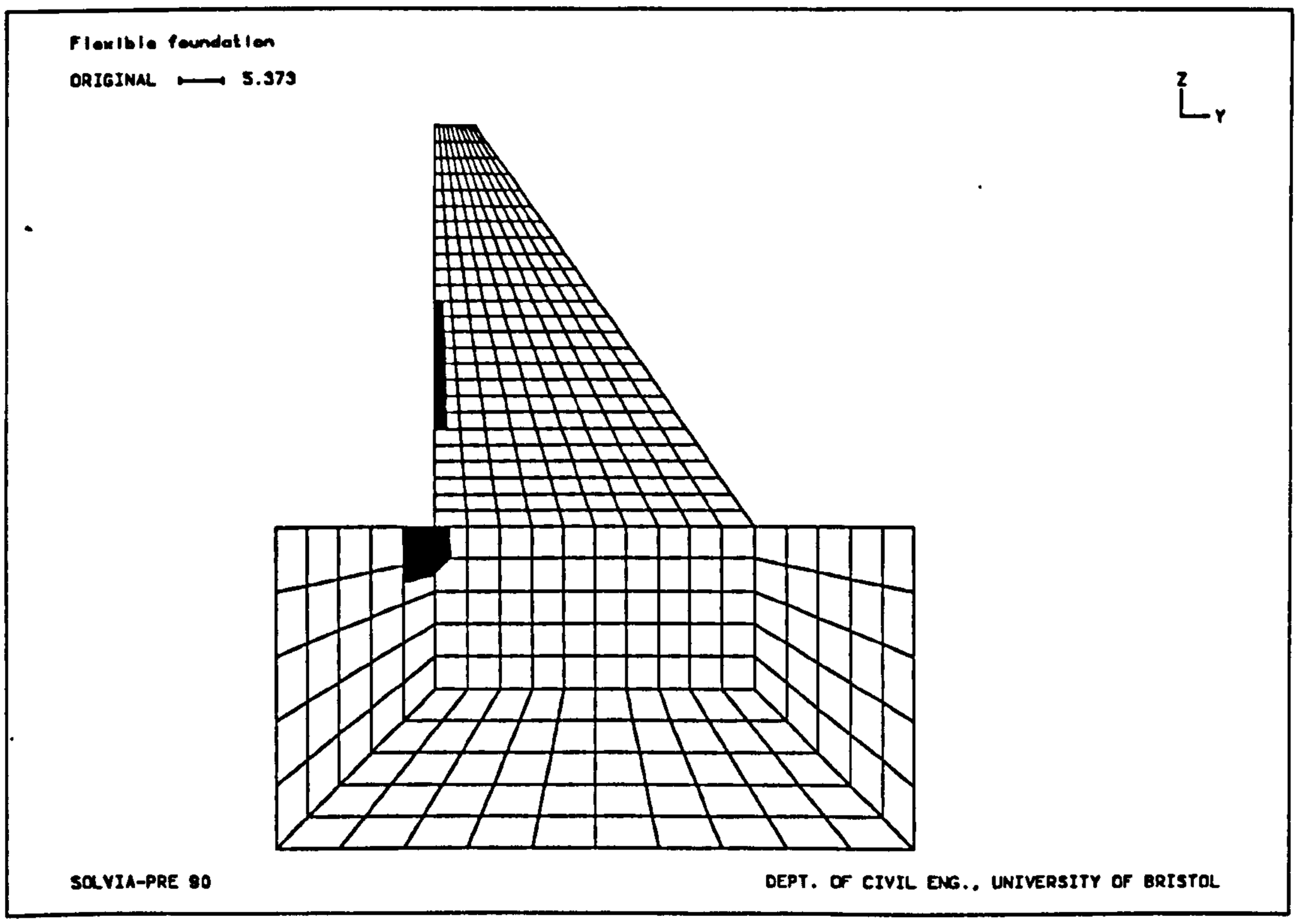

Figure 9.10e - Cracking pattern for increased loading at t=0.284 s (E_f=10 GPa)

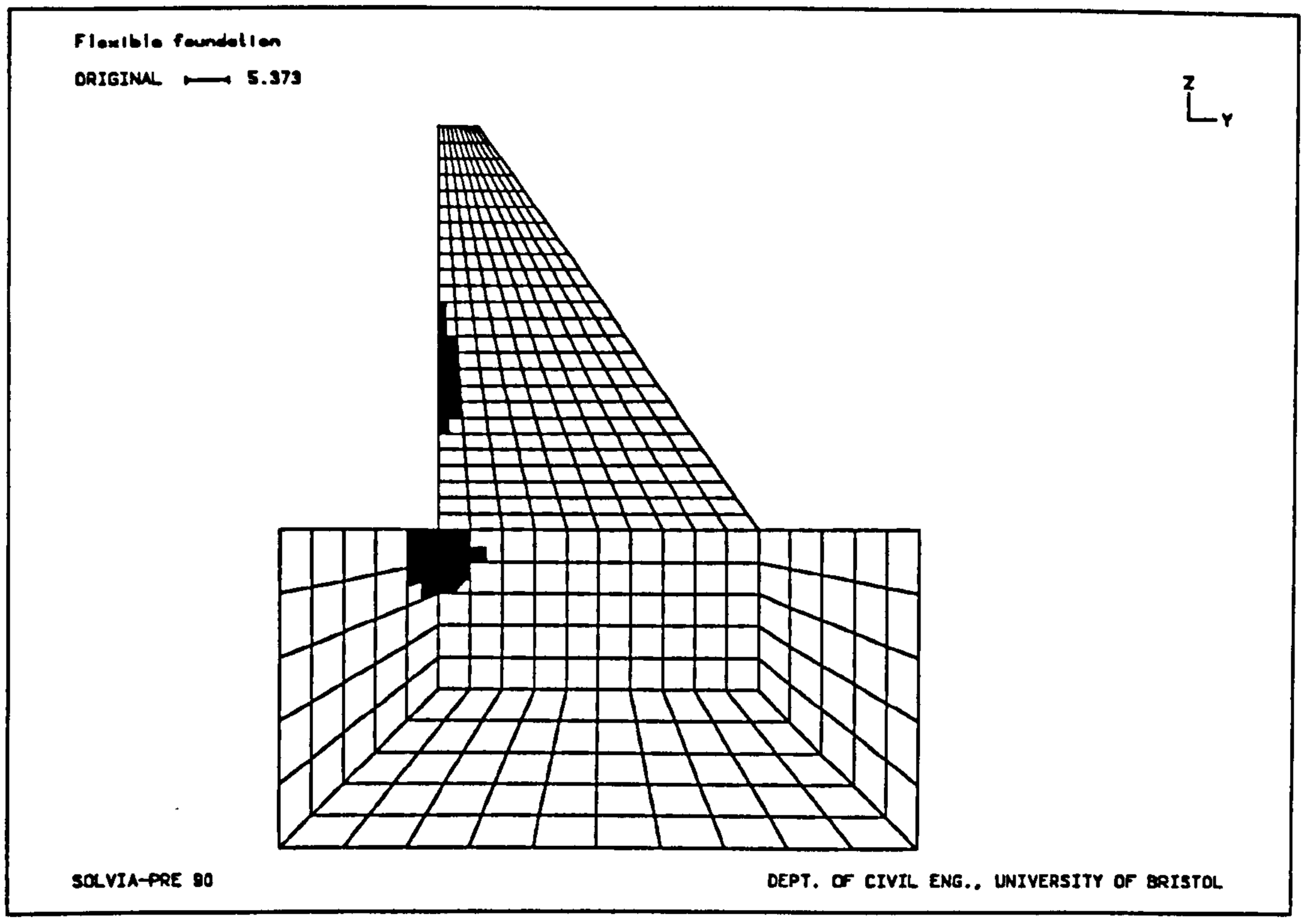

Figure 9.10f - Cracking pattern for increased loading at t=0.580 s (E_f=10 GPa)

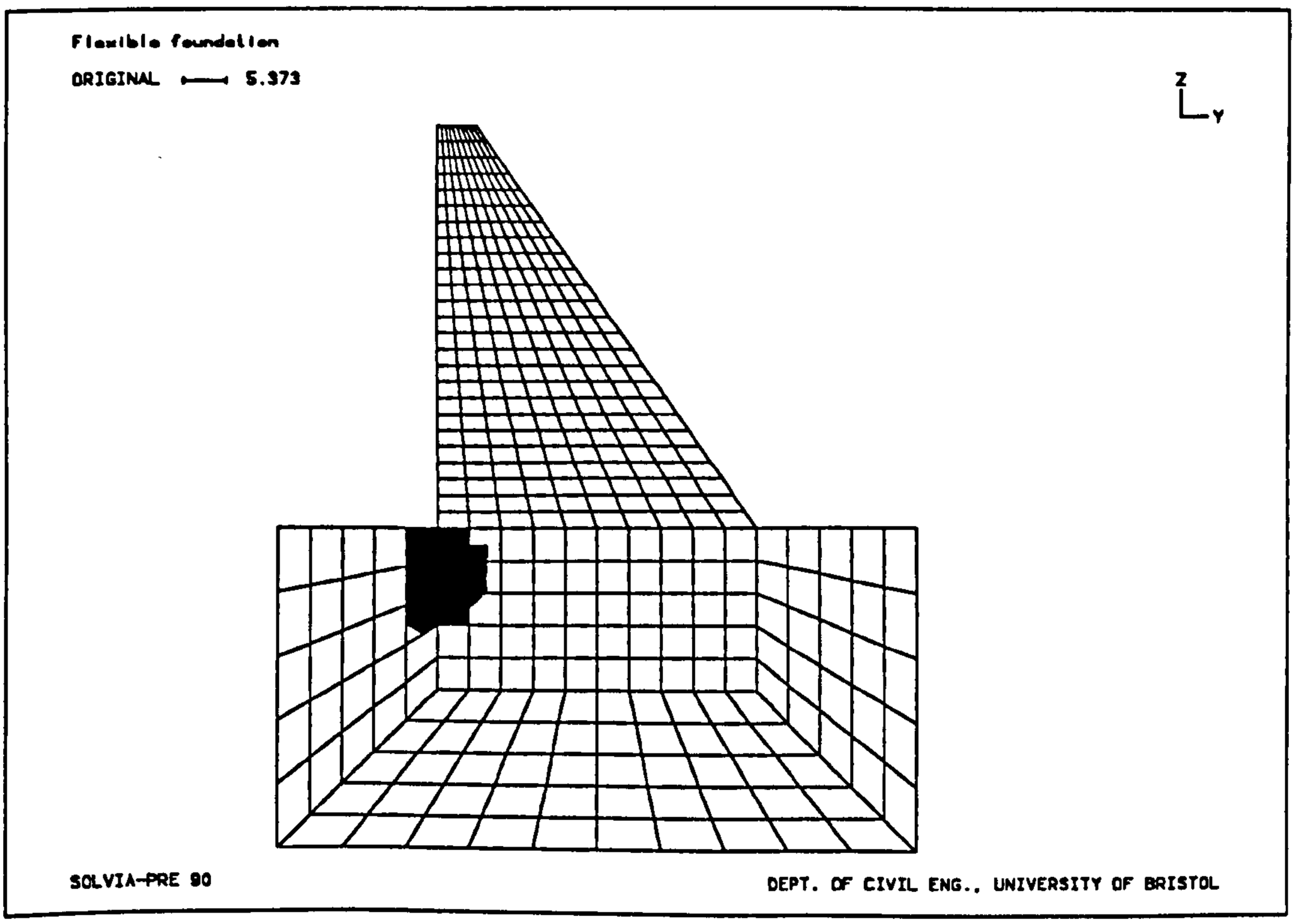

Figure 9.10g - Cracking pattern for incresed loading at t=1.500 s (E_f=10 GPa)

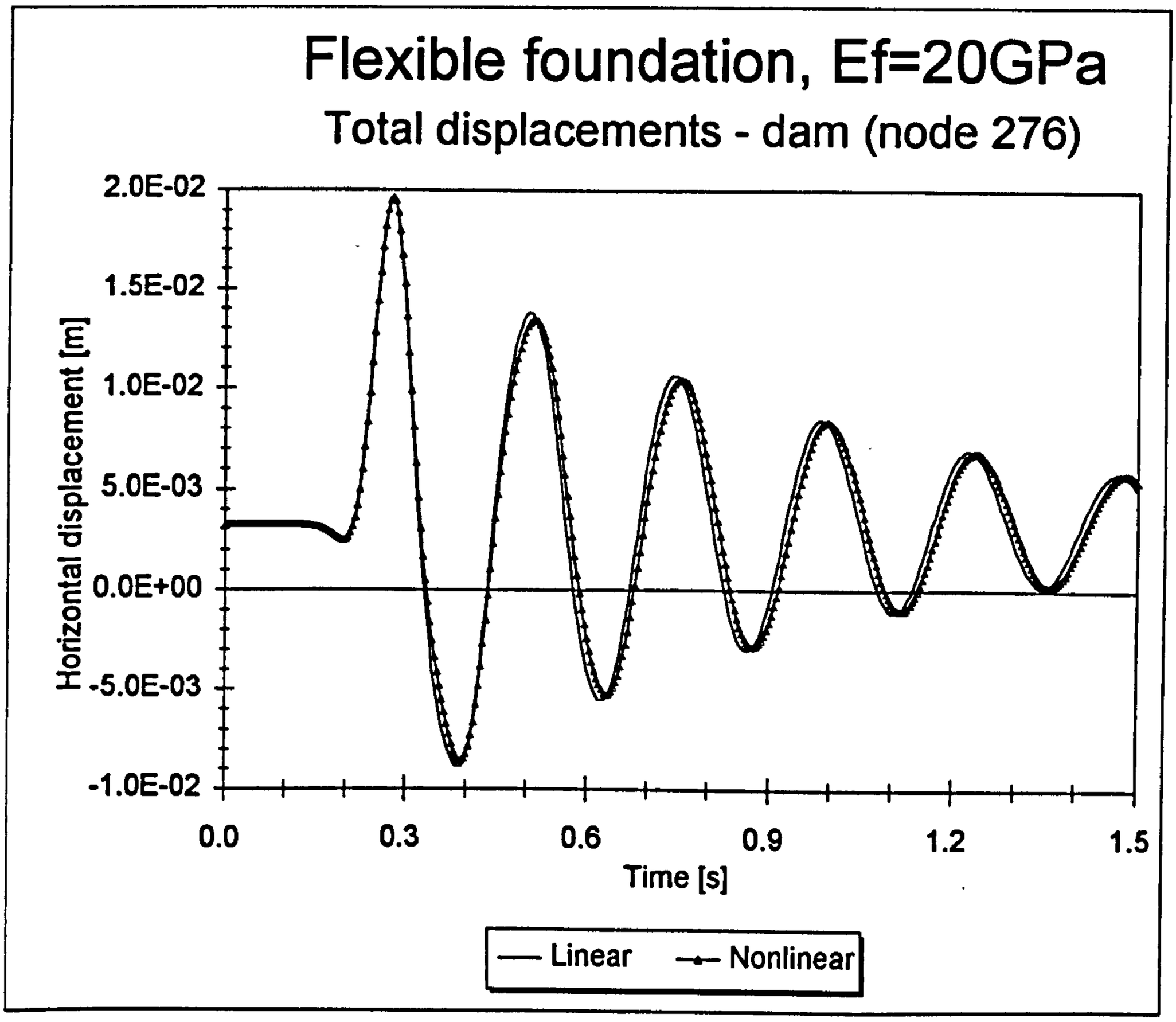

Figure 9.11a - Total displacement of the top of the dam

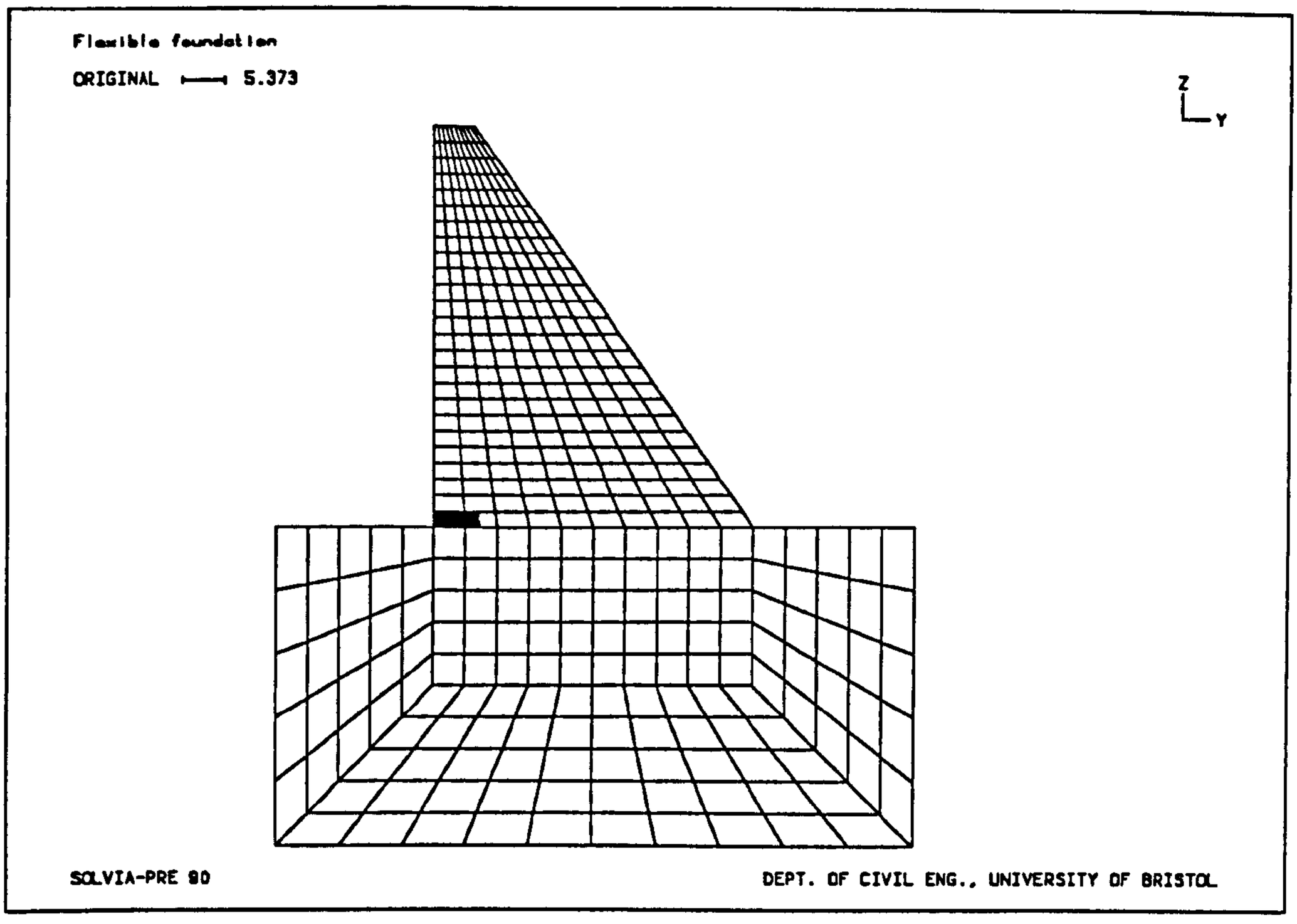

Figure 9.11b - Cracking pattern at t=0.292 s (E_f=20 GPa)

Figure 9.11c - Cracking pattern at t=0.464 s (E_f=20 GPa)

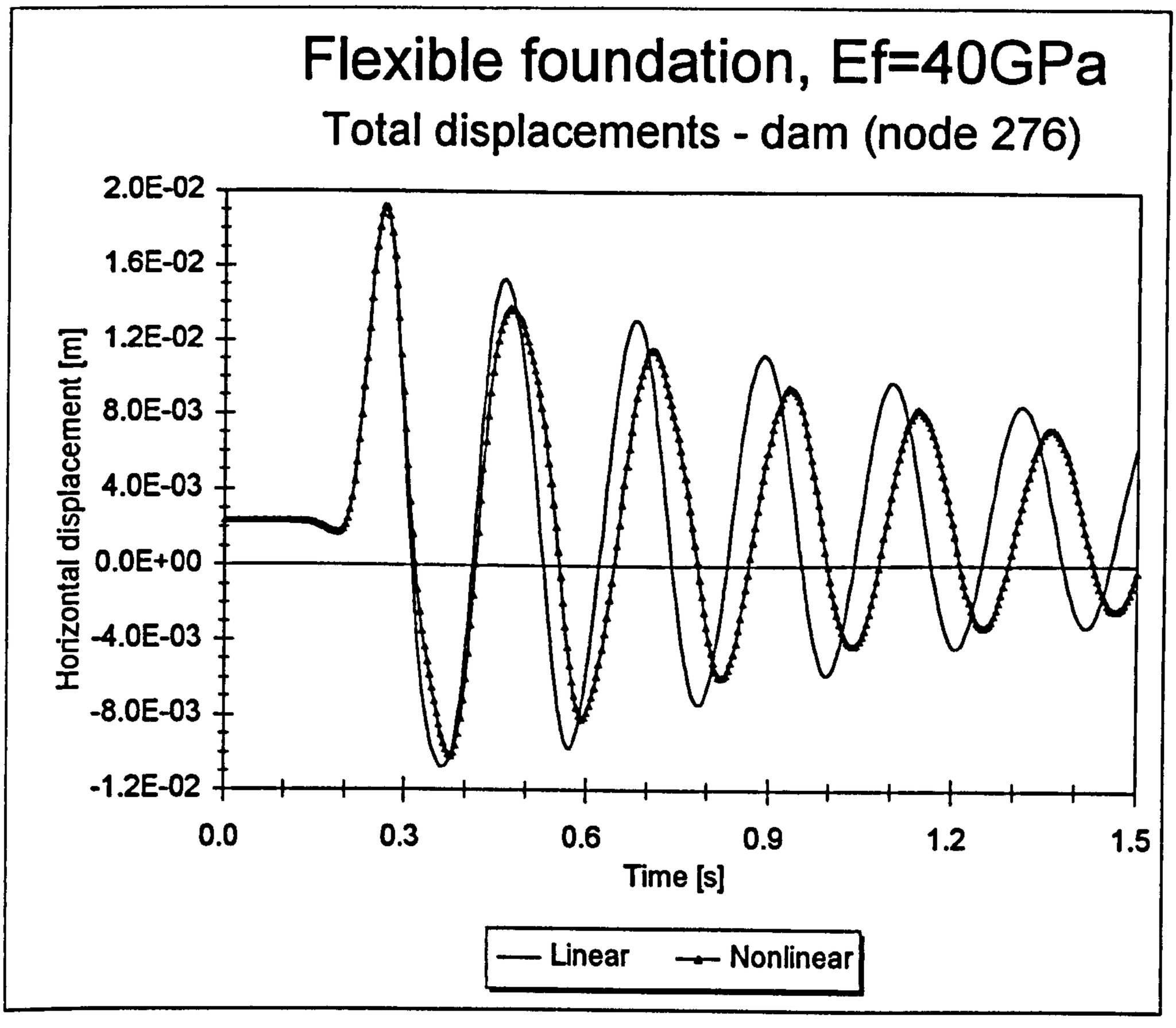

Figure 9.12a - Total displacement of the top of the dam

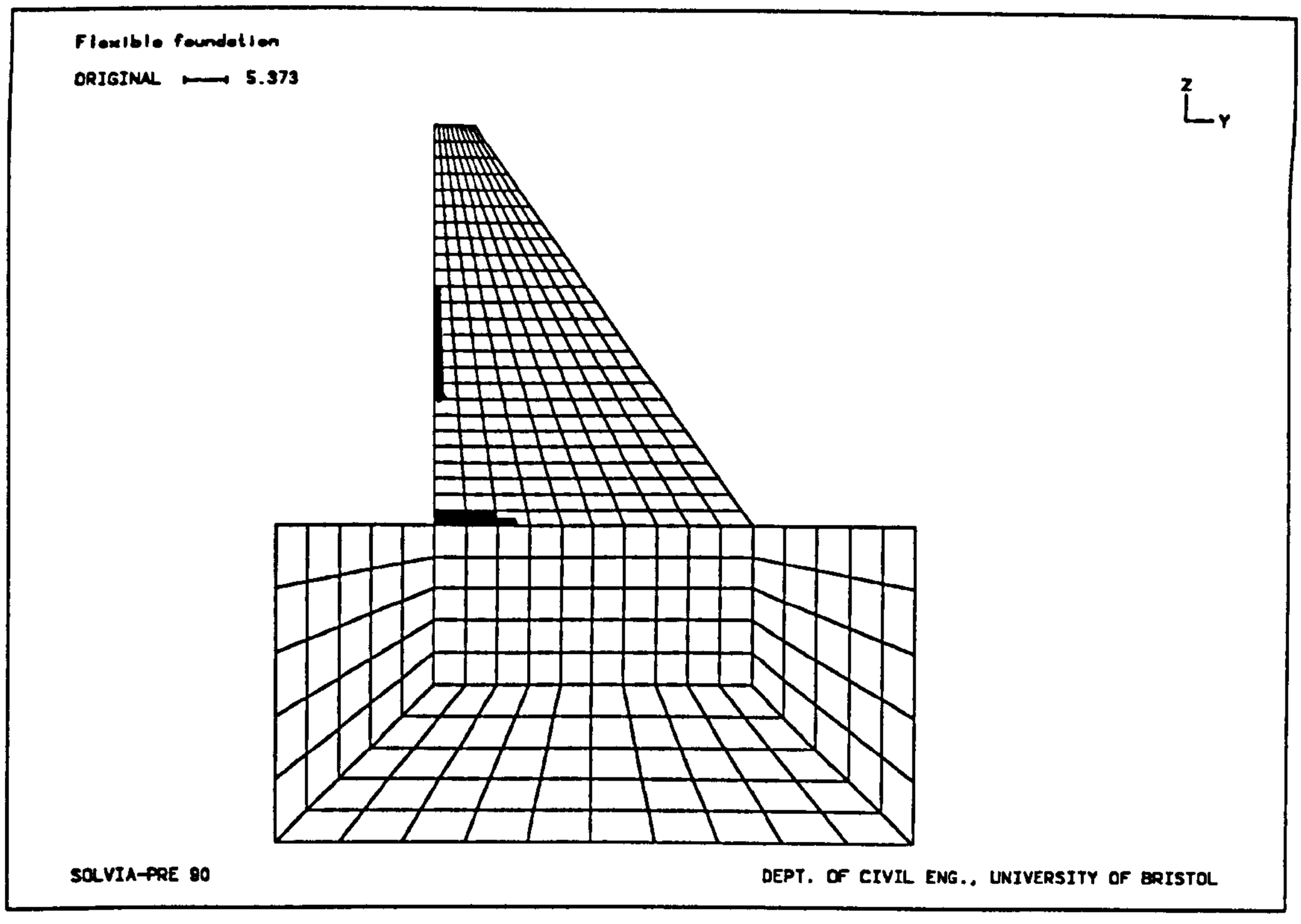

Figure 9.12b - Cracking pattern at t=0.280 s (E_f=40 GPa)

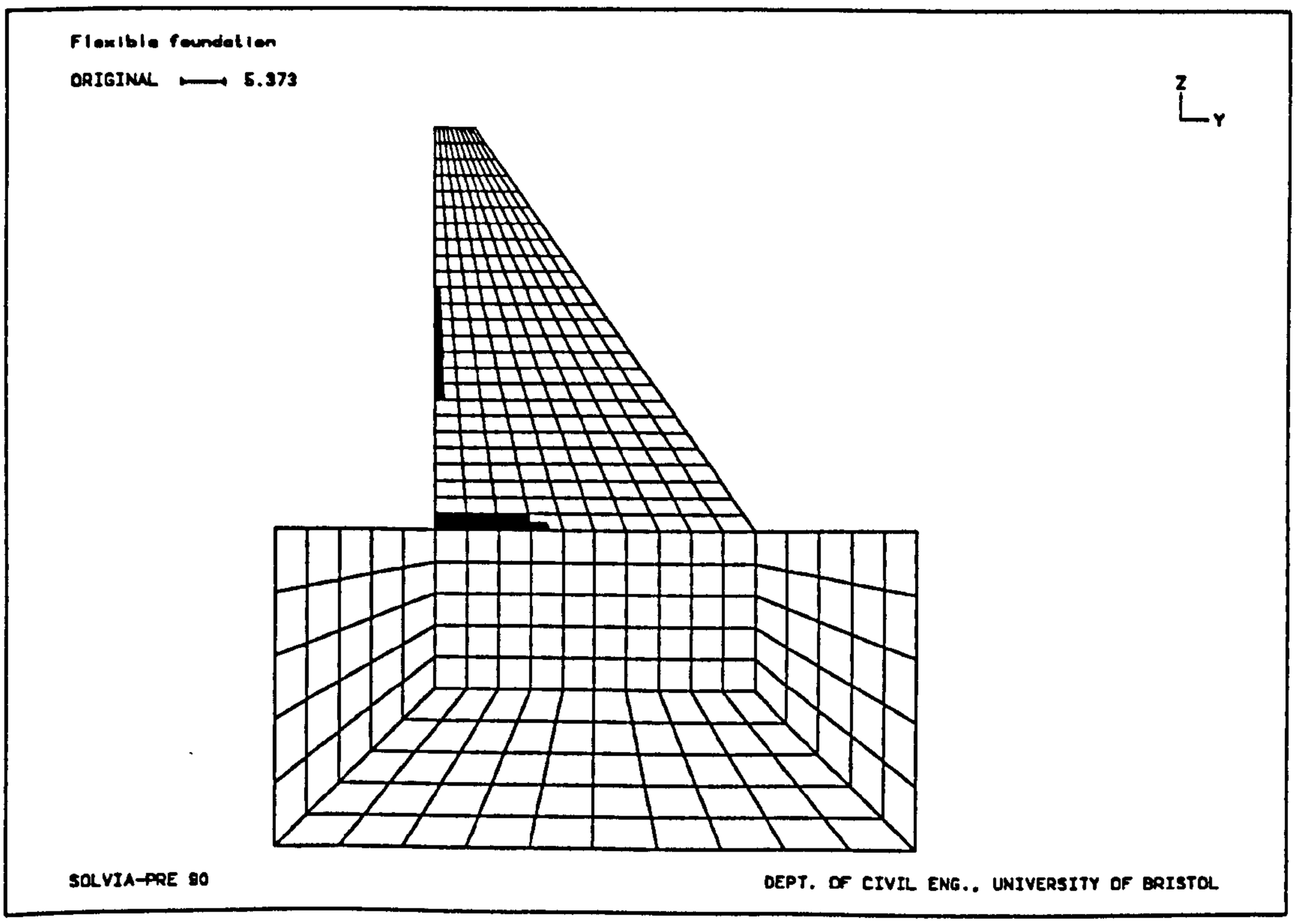

Figure 9.12c - Cracking pattern at t=0.496 s (E_f=40 GPa)

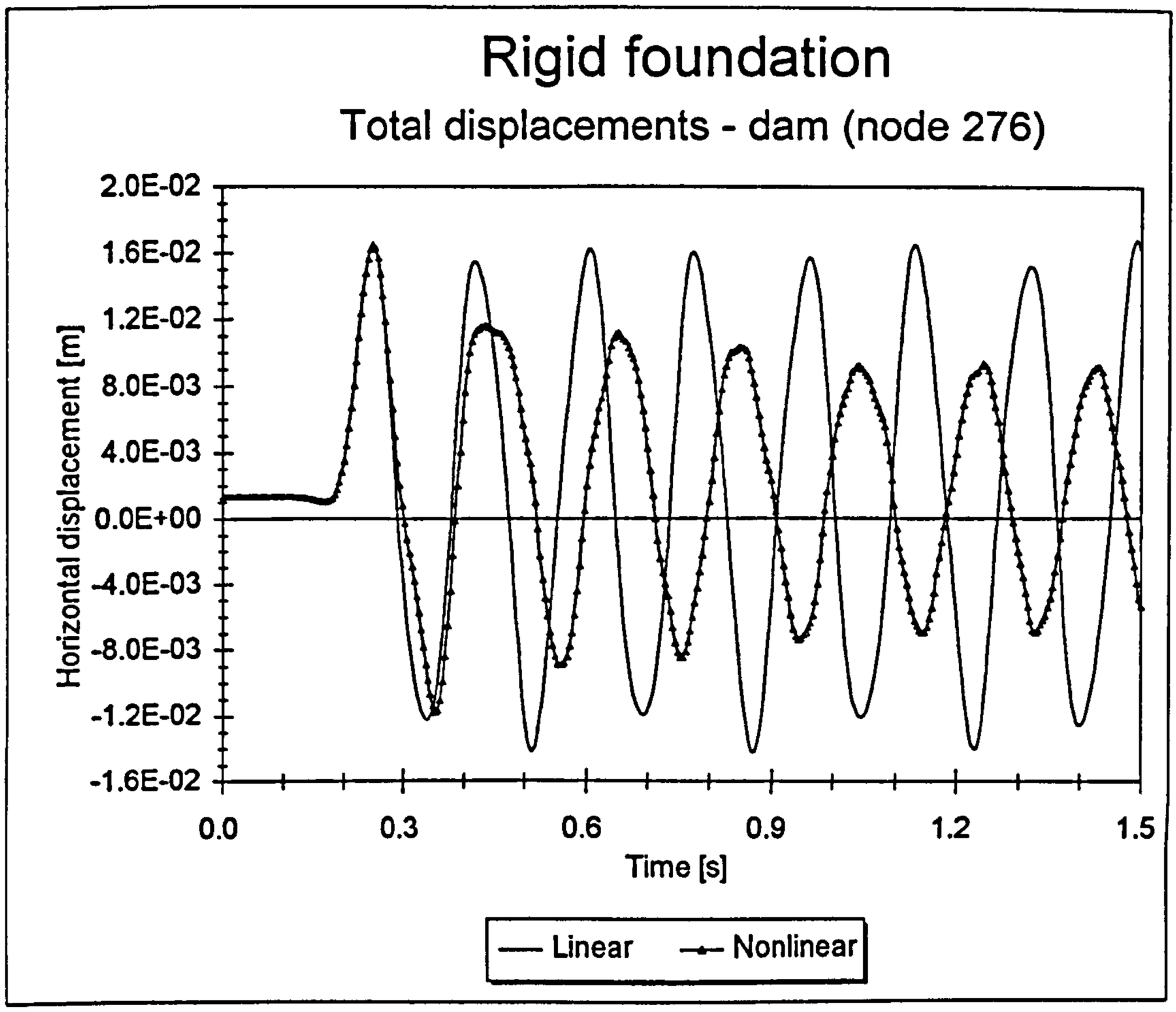

Figure 9.13a - Total displacement of the top of the dam

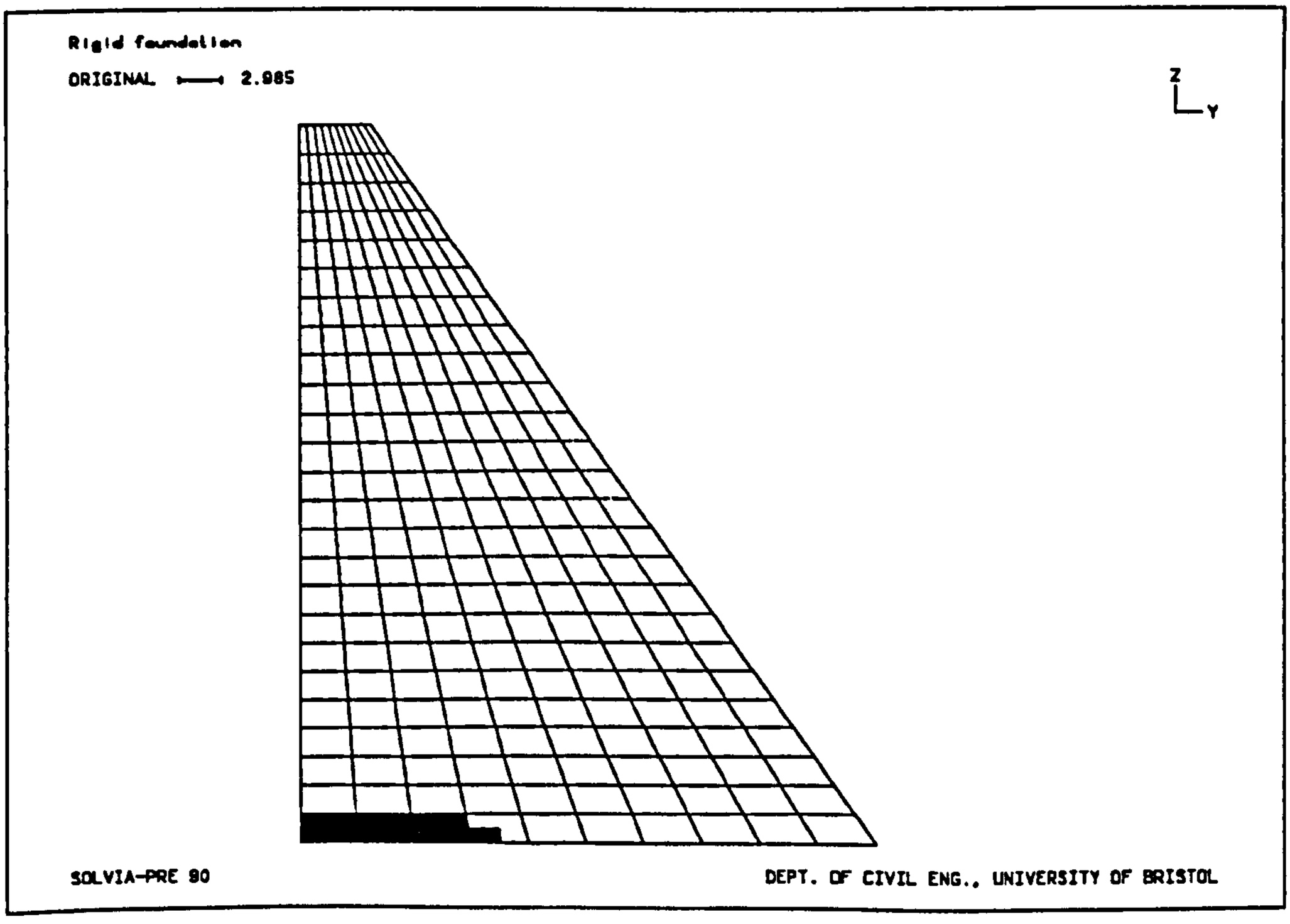

Figure 9.13b - Cracking pattern at t=0.272 s (E_f=∞ GPa)

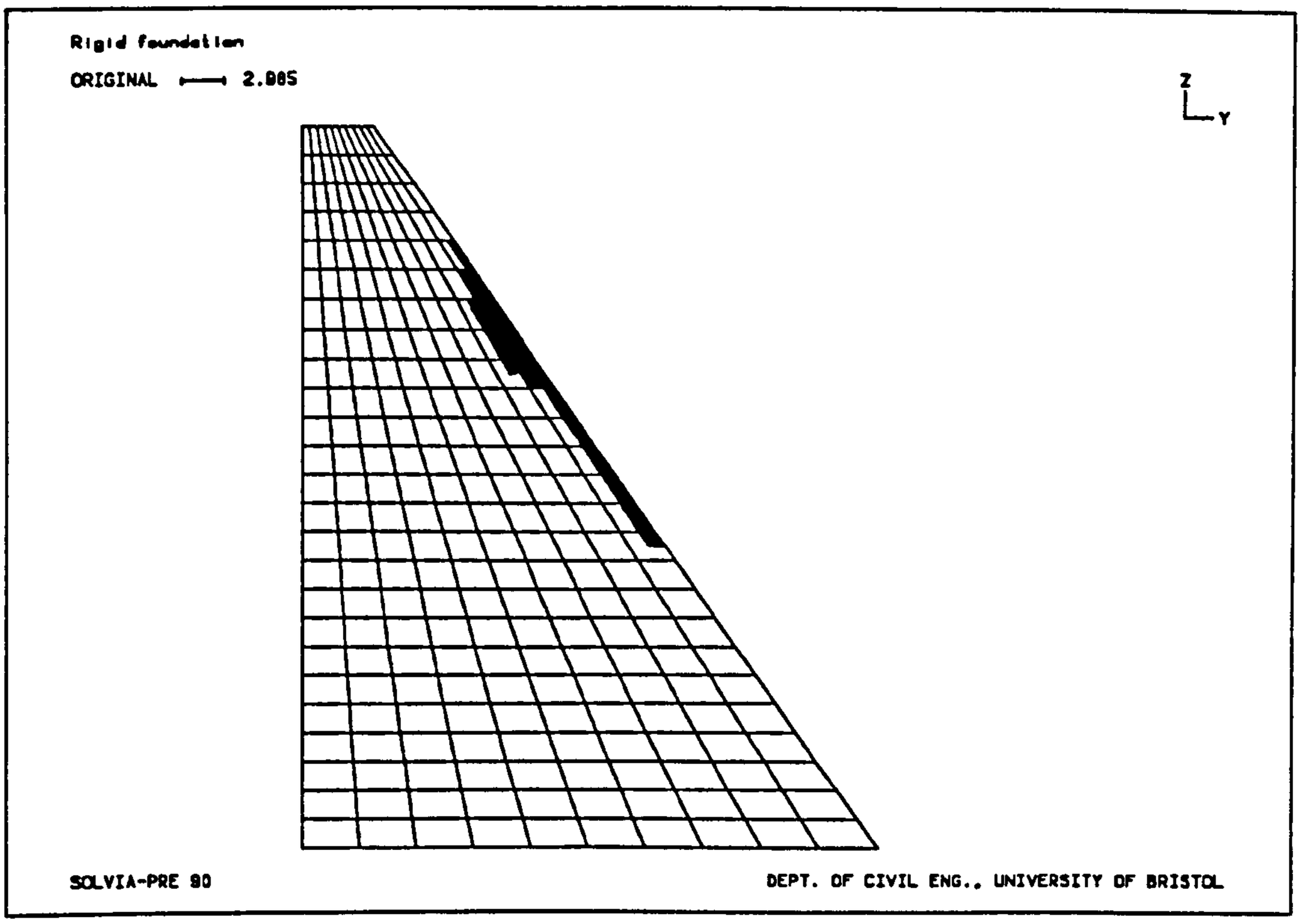

Figure 9.13c - Cracking pattern at t=0.356 s (E_f=∞ GPa)

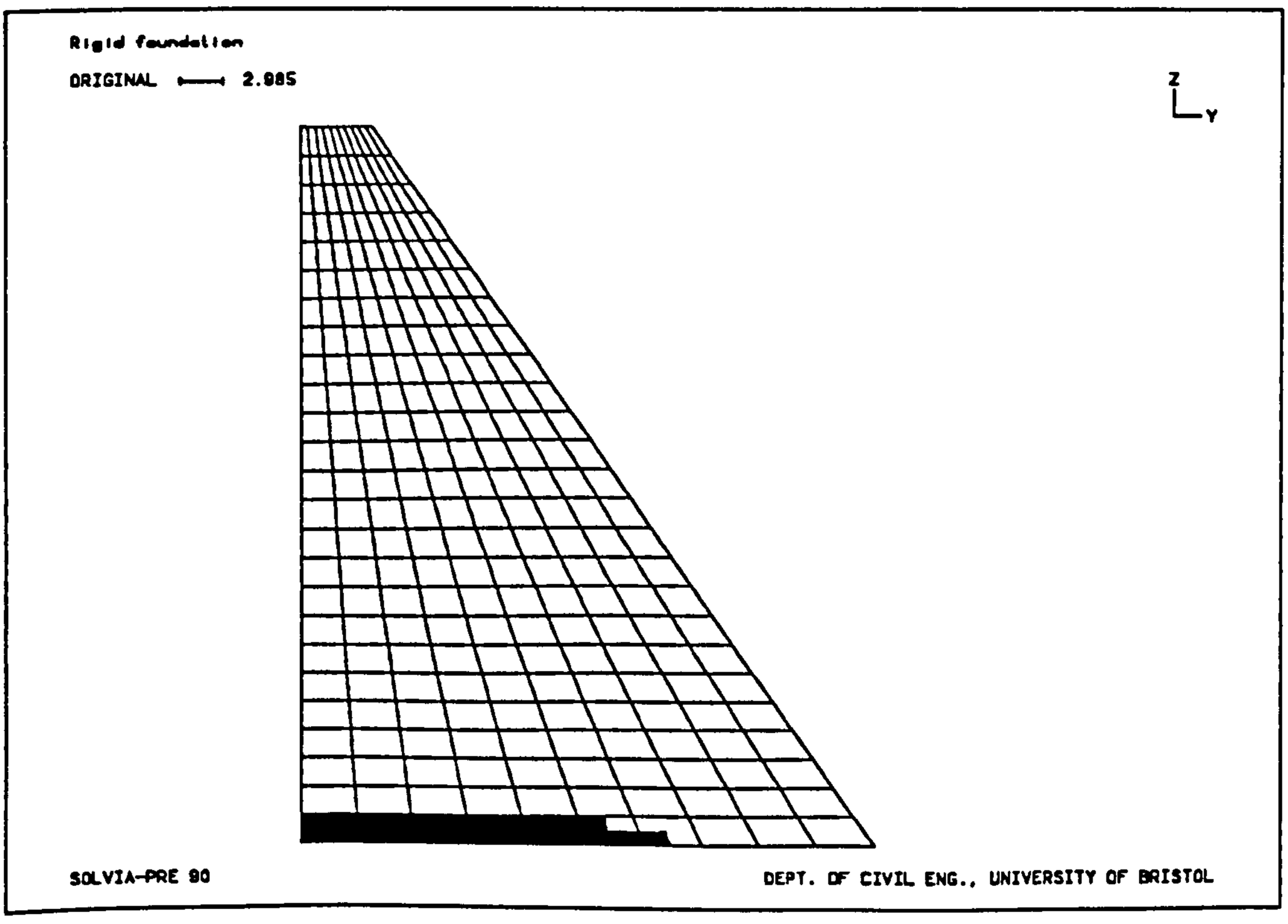

Figure 9.13d - Cracking pattern at t=0.456 s (E_f=∞ GPa)

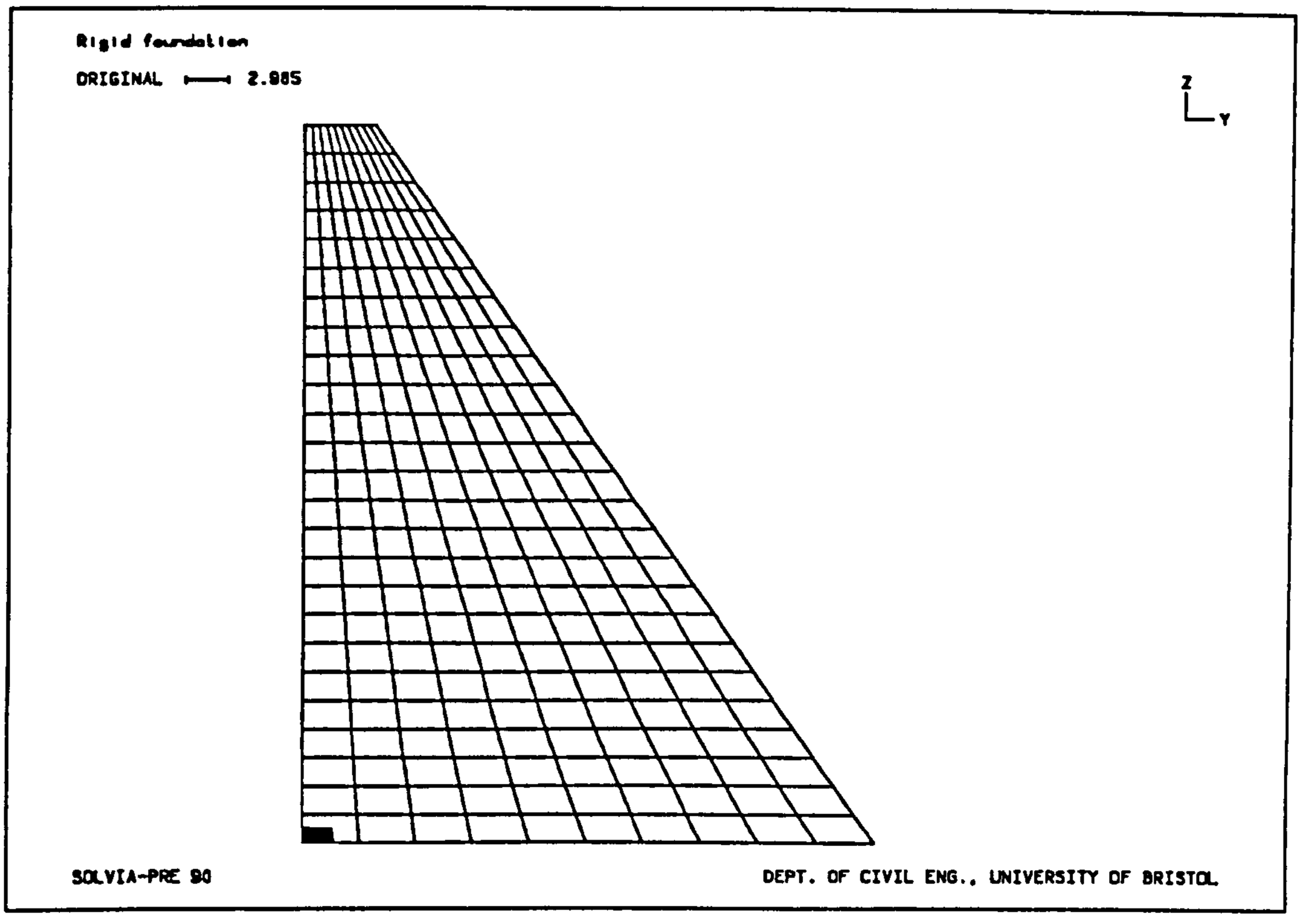

Figure 9.14a - Cracking pattern for reduced loading at t=0.228 s (E_f=∞ GPa)

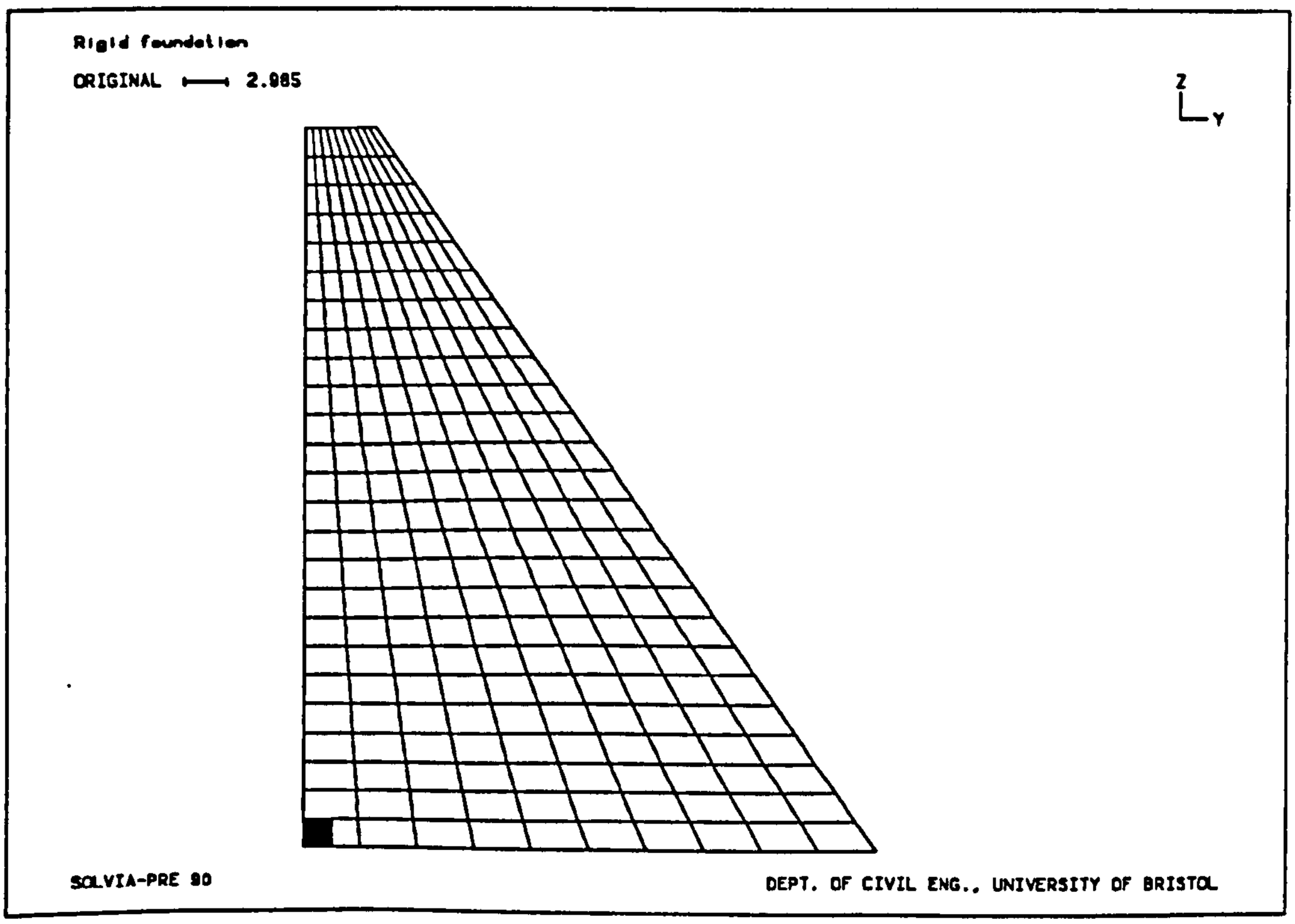

Figure 9.14b - Cracking pattern for reduced loading at t=0.408 s (E_f=∞ GPa)

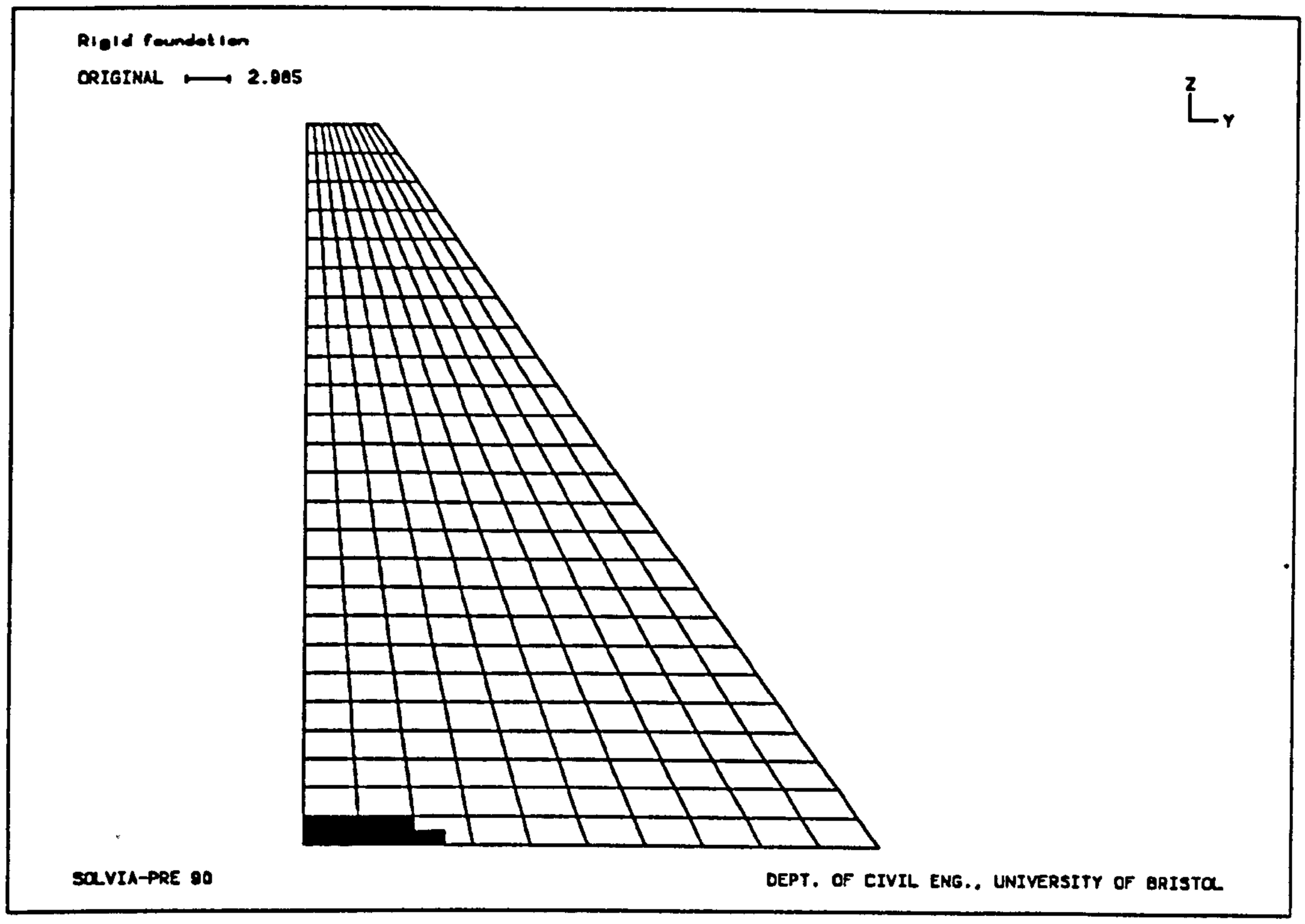

Figure 9.14c - Cracking pattern for reduced loading at t=0.436 s (E_f=∞ GPa)

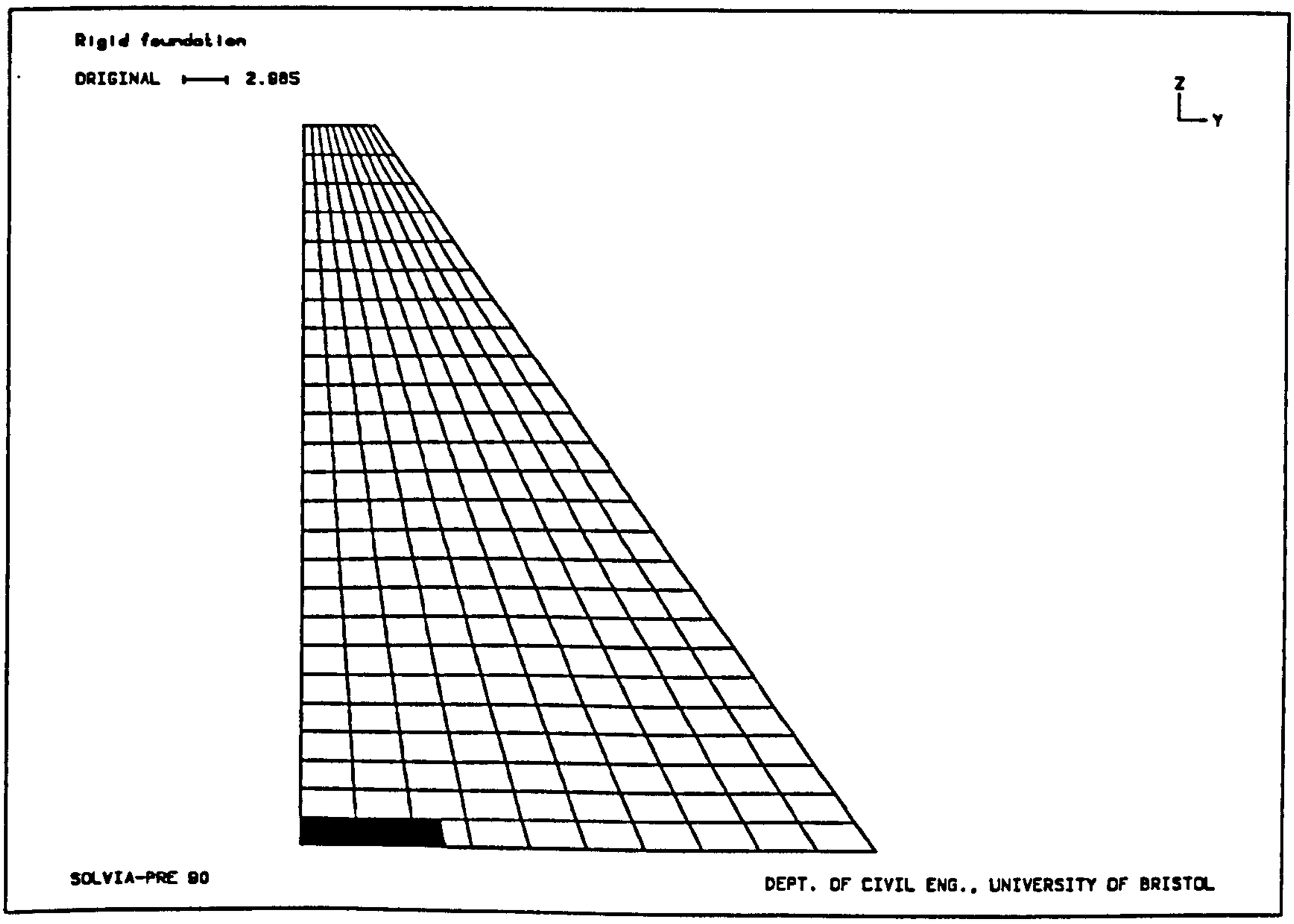

Figure 9.14d - Cracking pattern for reduced loading at t=1.380 s (E_f=∞ GPa)

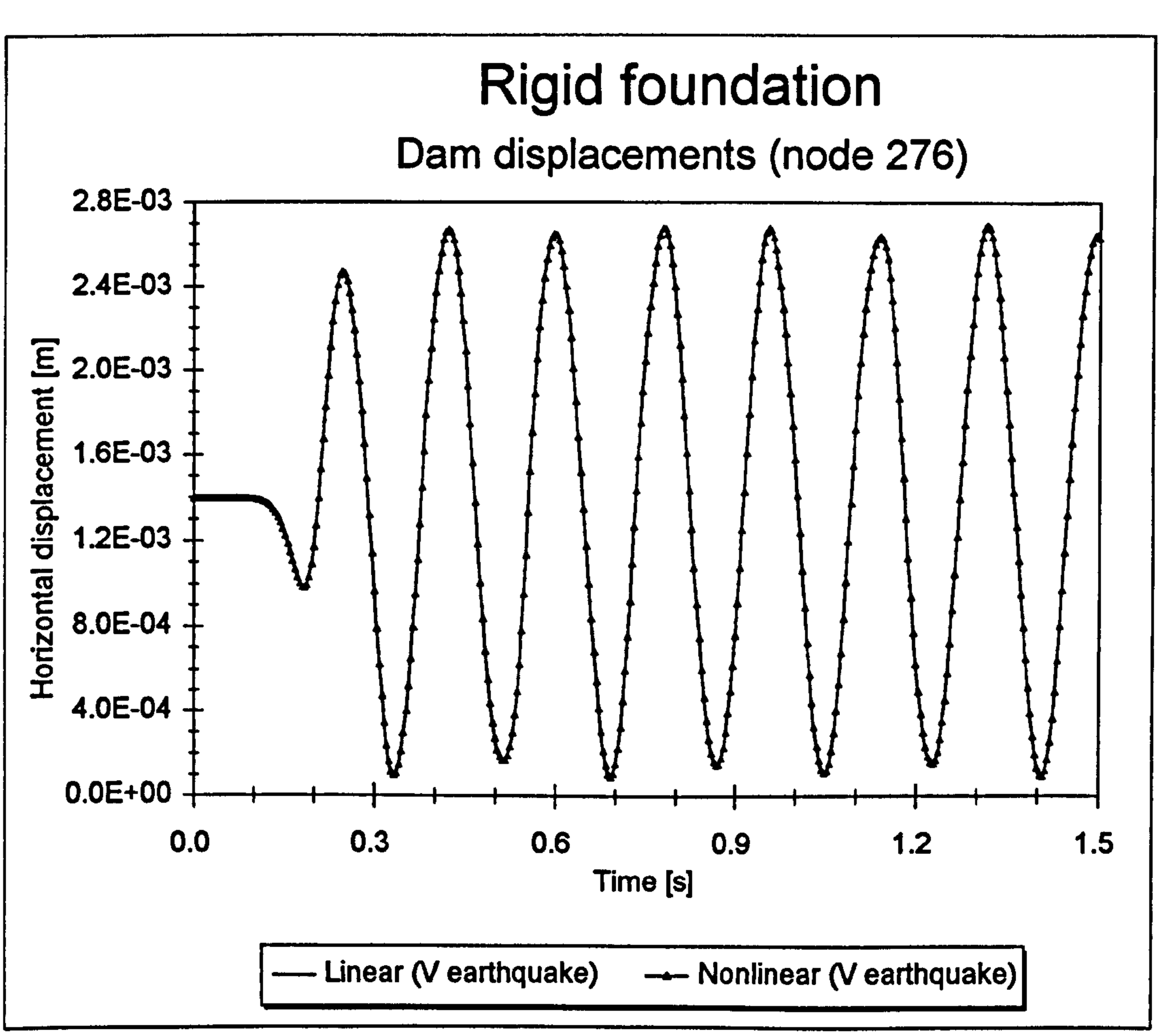

Figure 9.15 - Displacement of the top of the dam due to vertical earthquake

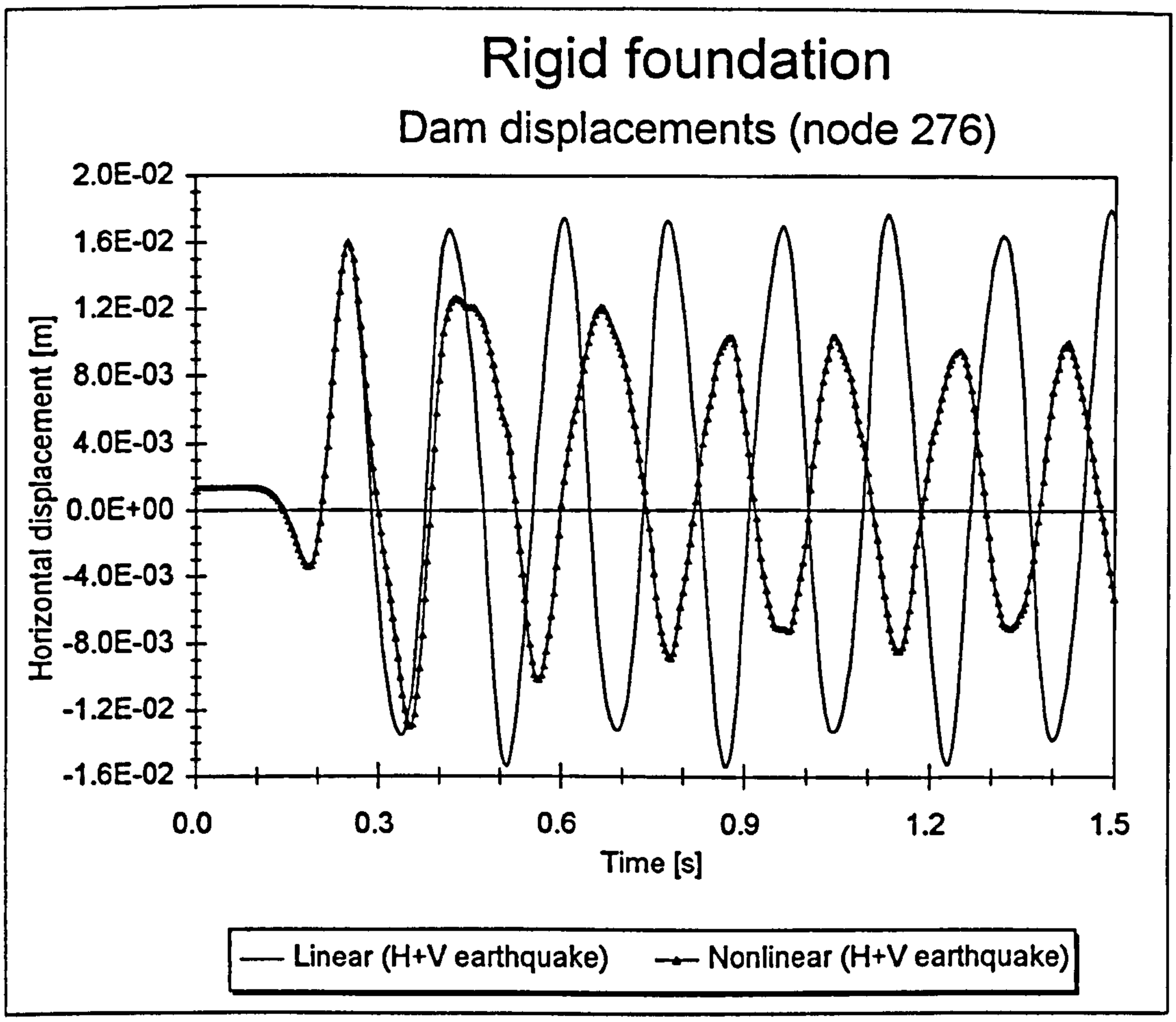

Figure 9.16a - Displacement due to combined horizontal and vertical earthquake

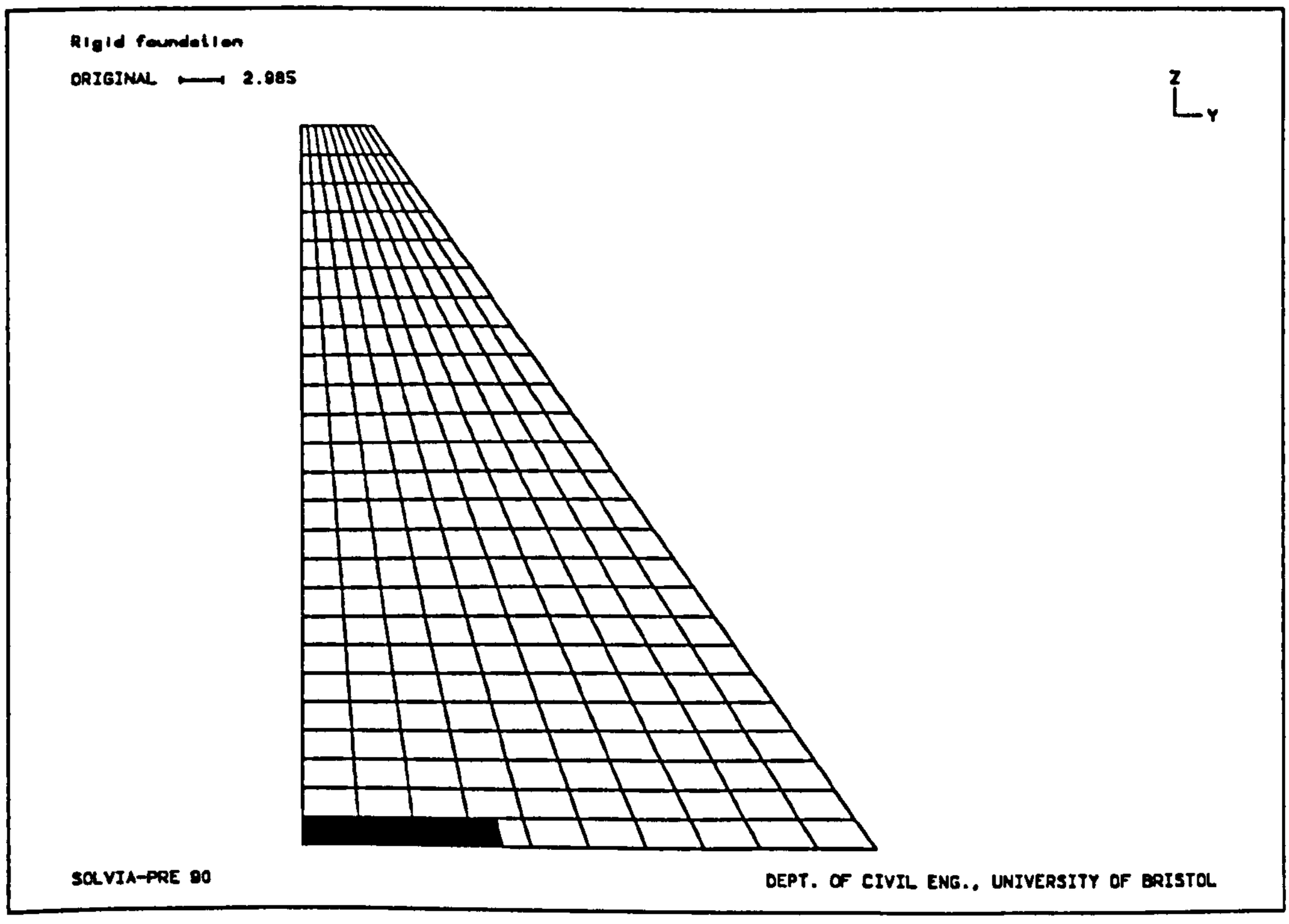

Figure 9.16b - Cracking pattern for combined earthquake at t=0.272 s (E_f=∞ GPa)

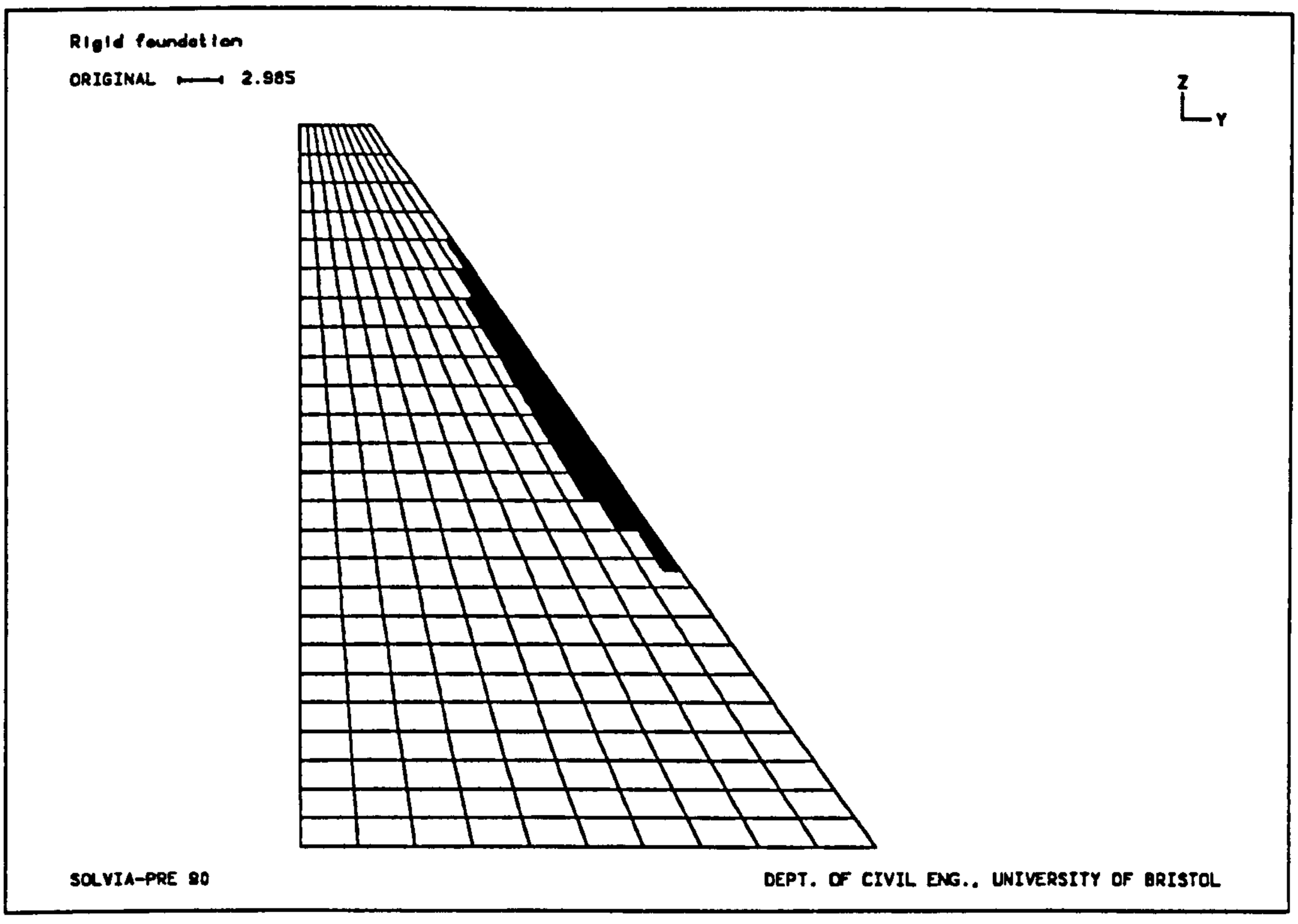

Figure 9.16c - Cracking pattern for combined earthquake at t=0.356 s (E_f=∞ GPa)

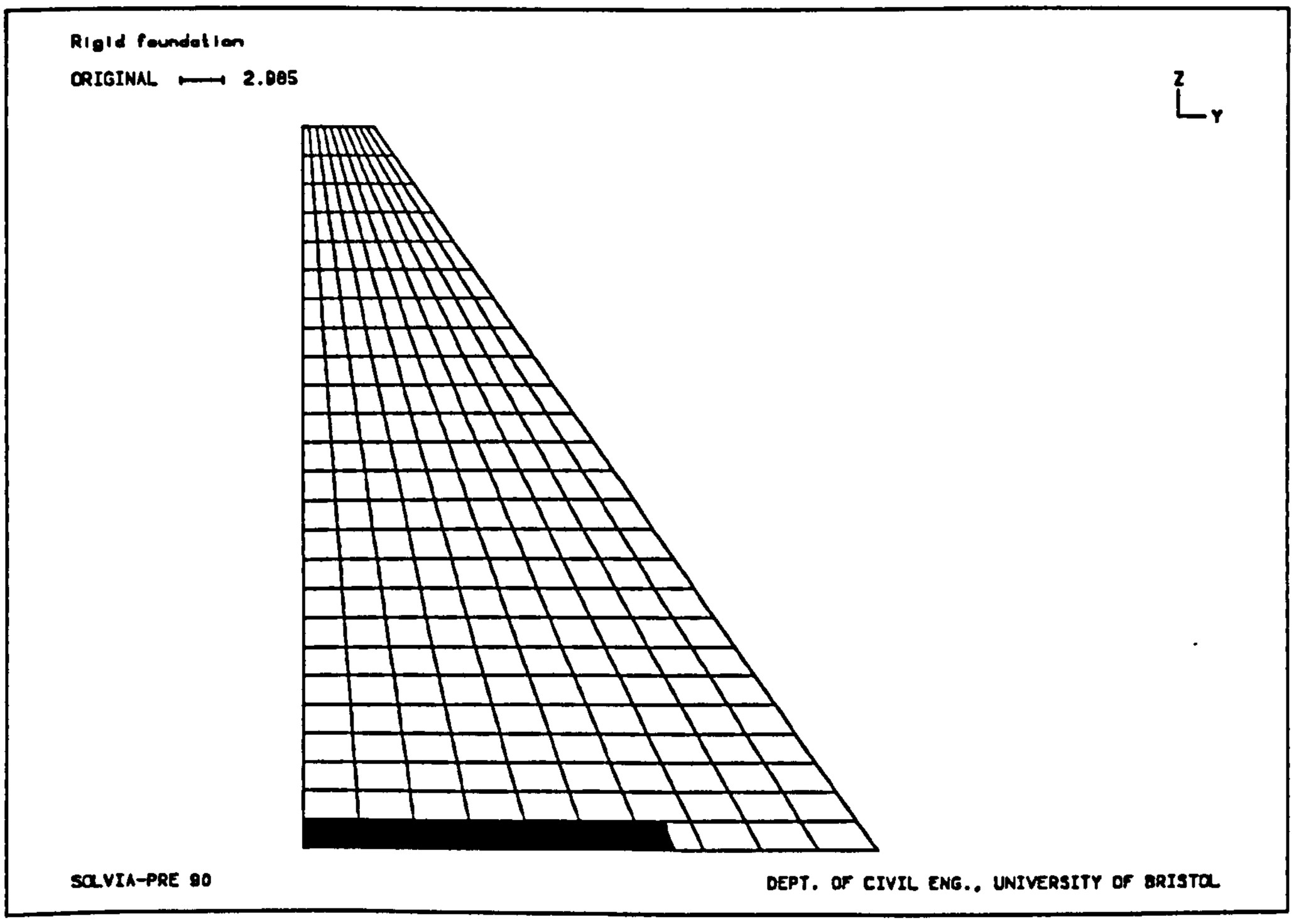

Figure 9.16d - Cracking pattern for combined earthquake at t=0.456 s (E_f=∞ GPa)

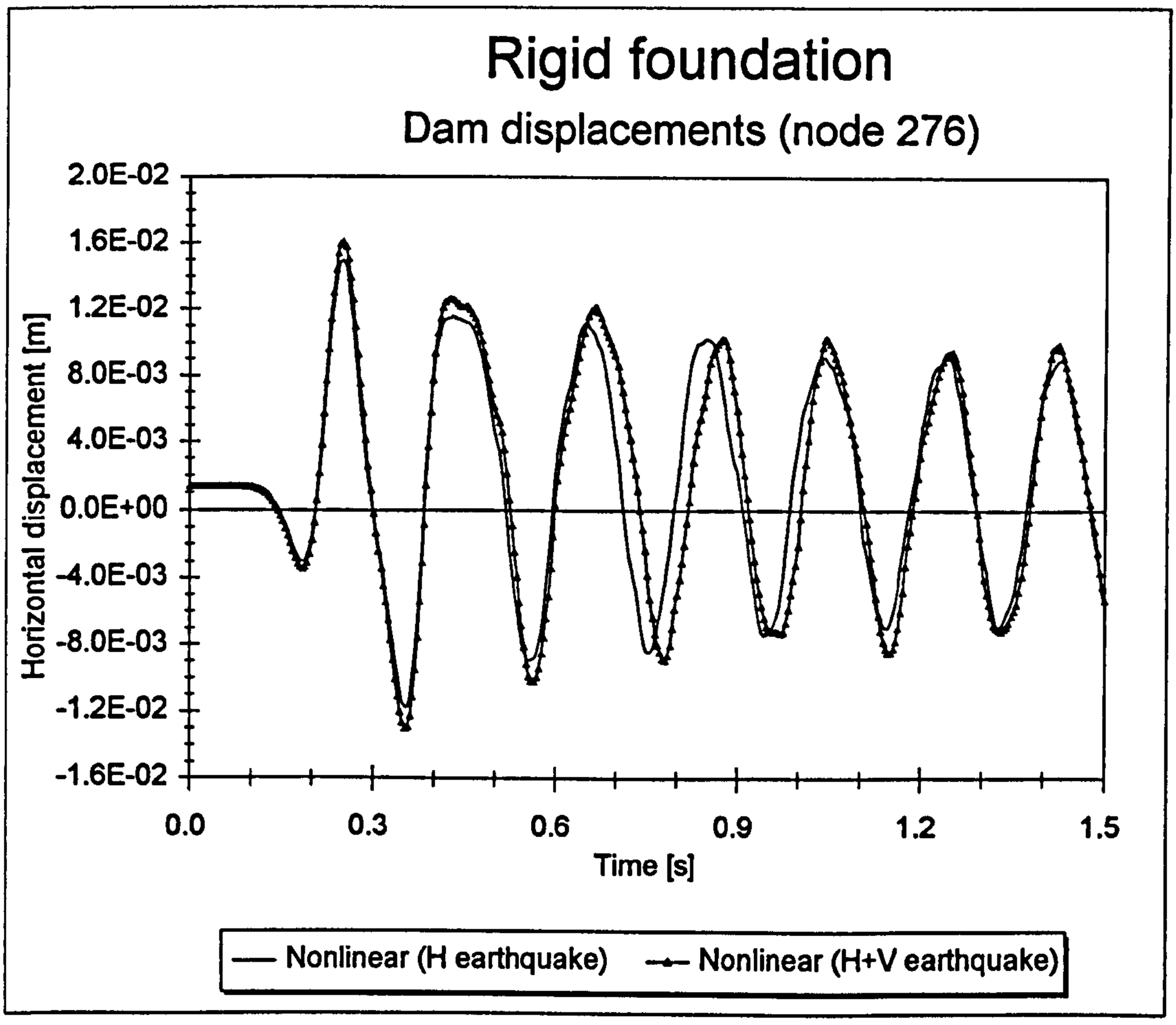

Figure 9.17 - Displacement due to combined and horizontal earthquake

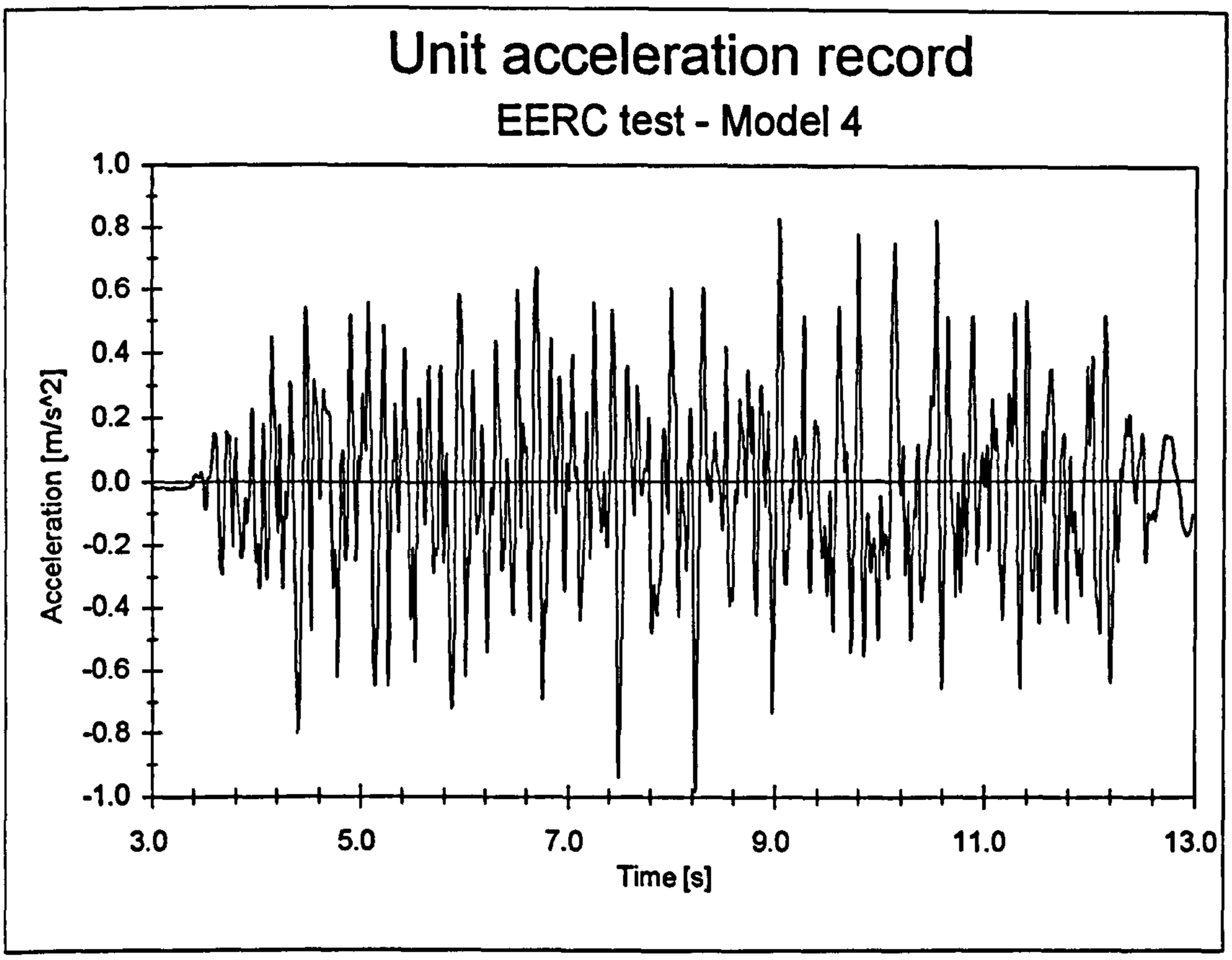

Figure 9.18 - Earthquake unit acceleration record

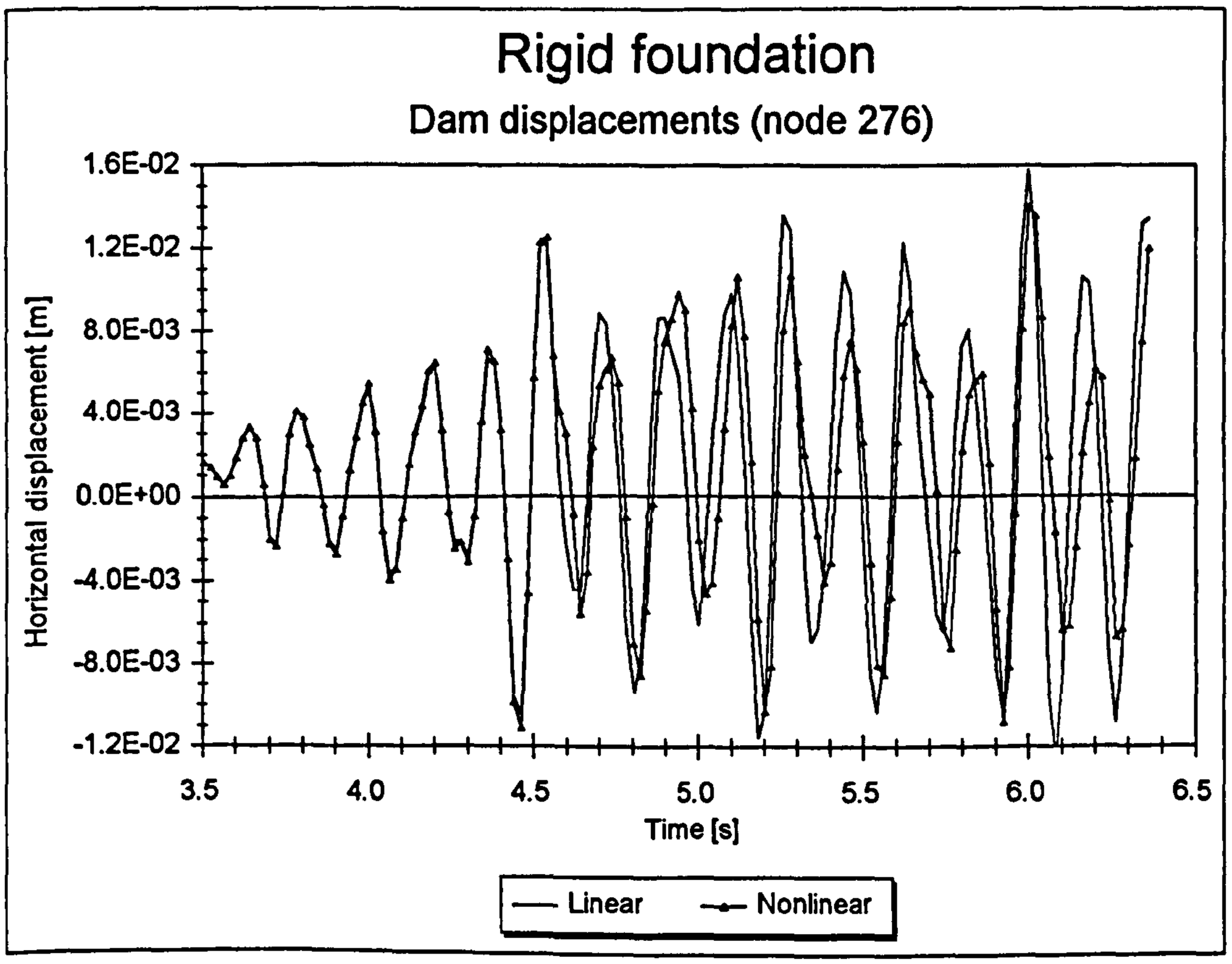

Figure 9.19a - Displacement of the top of the dam due to Model 4 earthquake

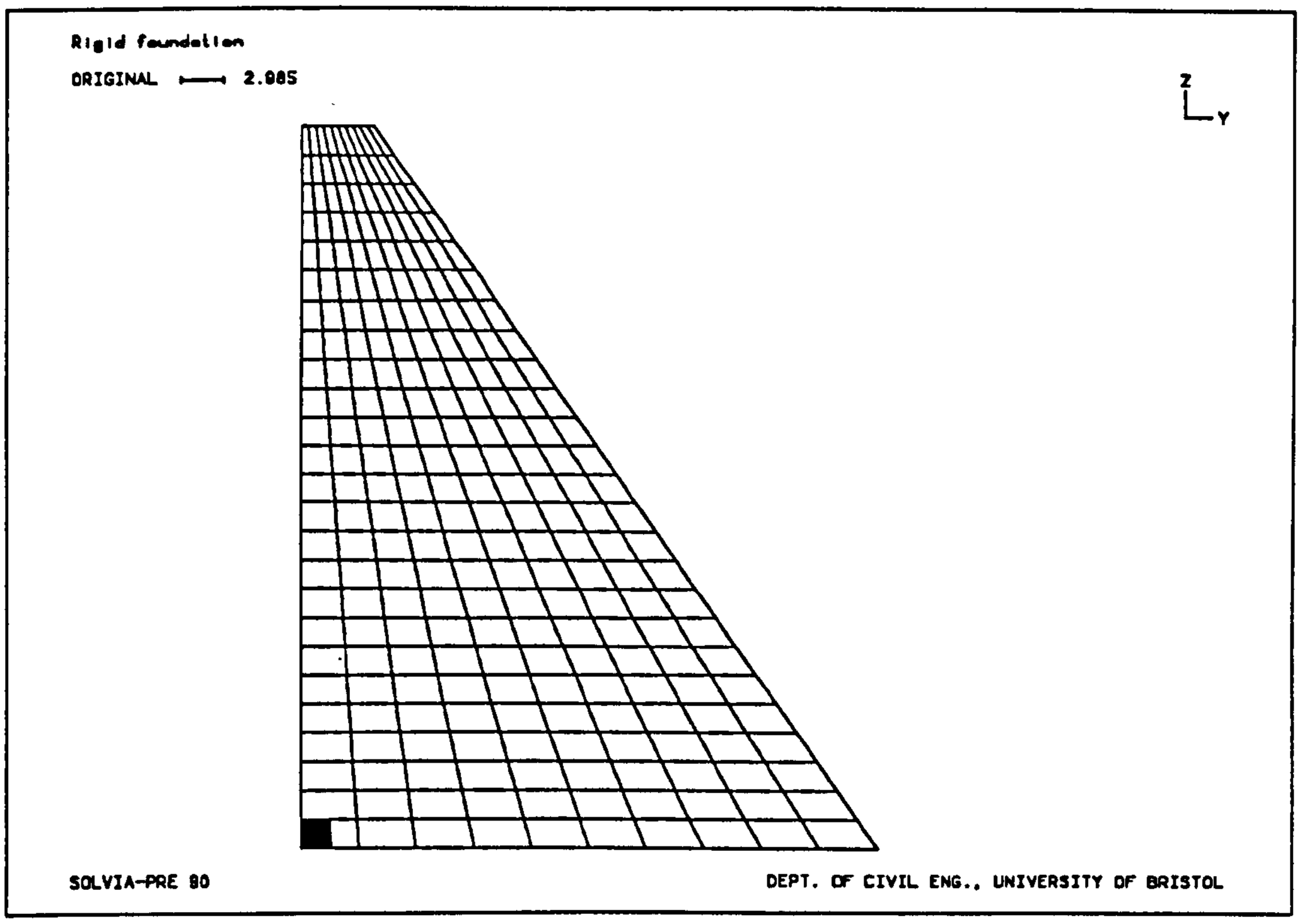

Figure 9.19b - Cracking pattern for Model 4 earthquake at t=4.404 s (E_f=∞ GPa)

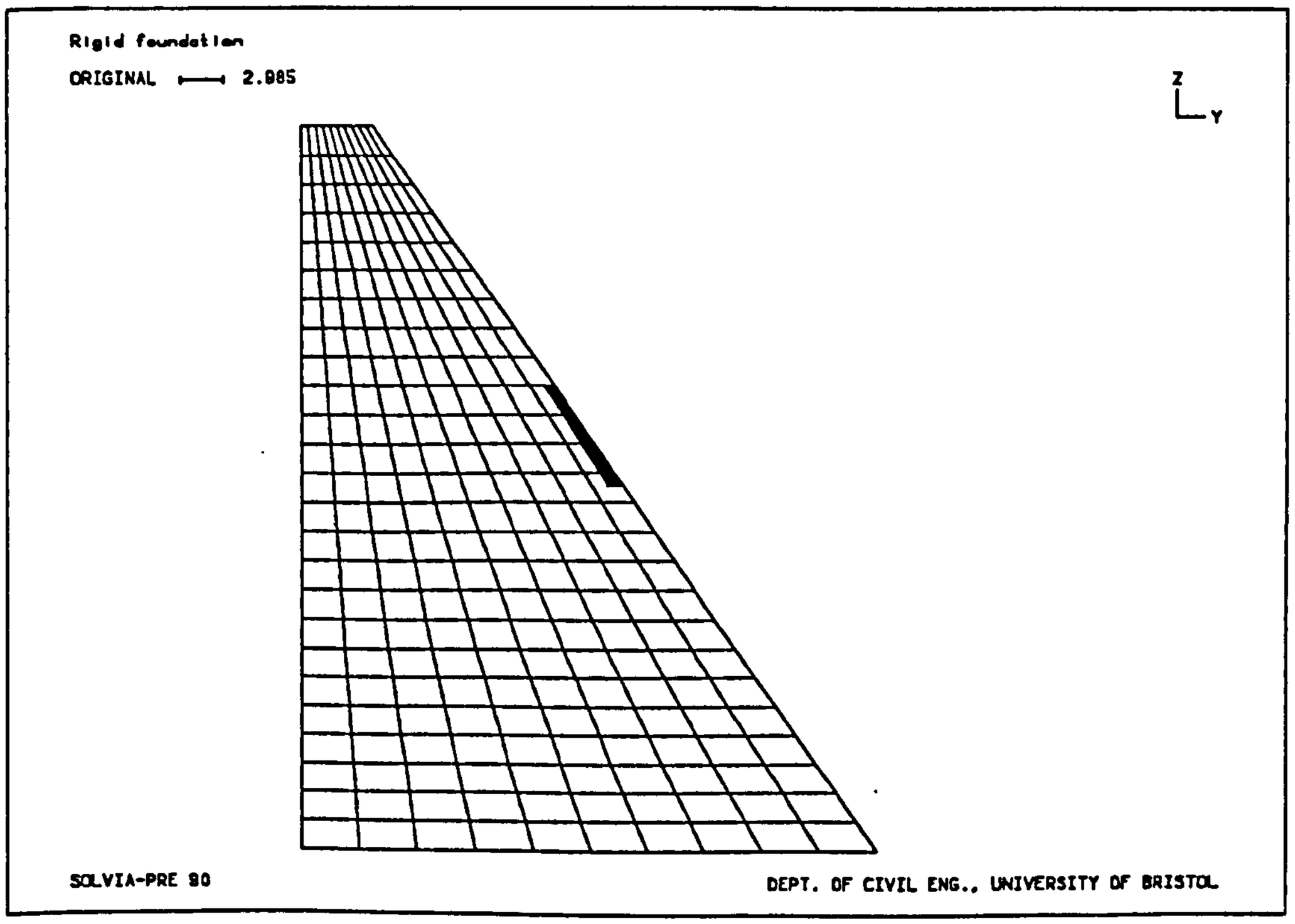

Figure 9.19c - Cracking pattern for Model 4 earthquake at t=4.464 s (E_f=∞ GPa)

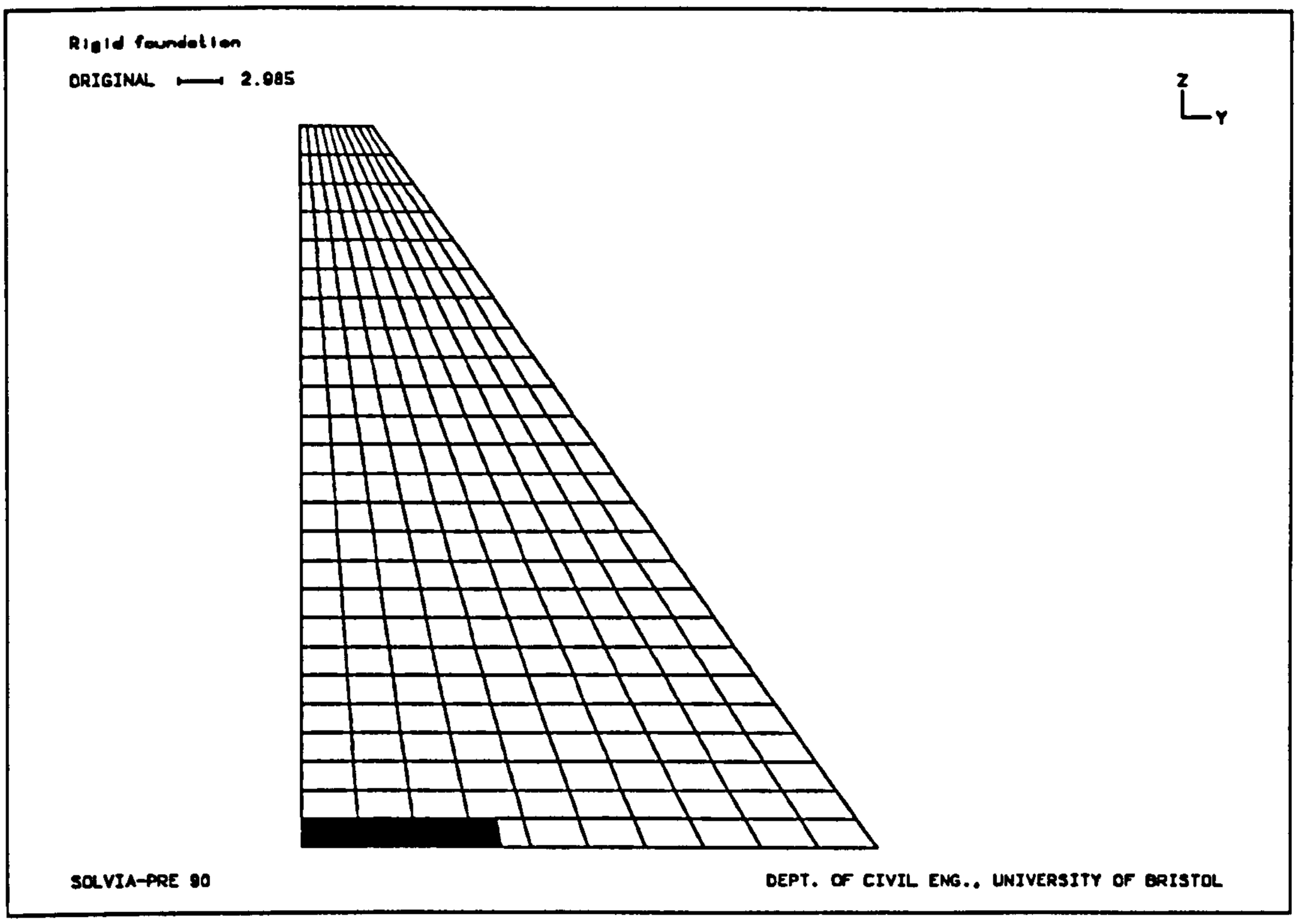

Figure 9.19d - Cracking pattern for Model 4 earthquake at t=4.584 s (E_f=∞ GPa)

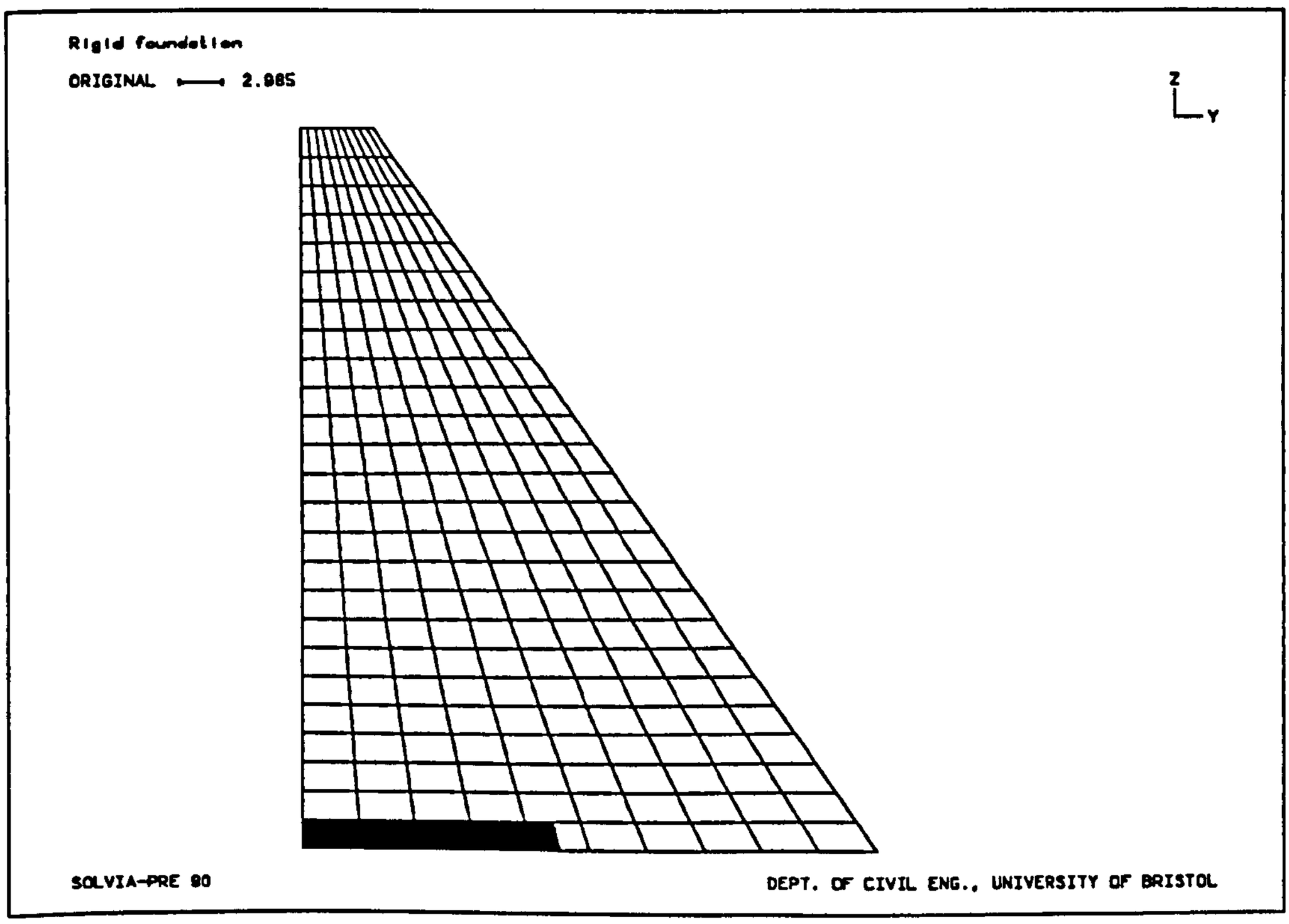

Figure 9.19e - Cracking pattern for Model 4 earthquake at t=6.024 s (E_f=∞ GPa)

Conclusions and Further Work

A comprehensive research project in the area of concrete gravity dams is currently being conducted at the Earthquake Engineering Research Centre (EERC) of Bristol University. The work presented in this thesis was an integral part of this wider project, but also a self-contained study into earthquake behaviour and analysis procedures for concrete gravity dam-foundation systems.

The thesis was divided into ten Chapters. After setting research objectives and defining the structure of the thesis in Chapter 1, Chapter 2 reviewed the present knowledge about earthquake analysis of concrete gravity dams and outlined the research strategy through a practising dam engineer's point of view. The final aim of the work was formulated as a quest for a coherent methodology for carrying out nonlinear earthquake analyses of concrete gravity dams with the appropriate modelling of energy radiation and seismic input. Chapters 3 to 8 have followed a step by step approach to this quest. Finally, in Chapter 9, the ultimate aim was fulfilled. Each of the Chapters contained its own, detailed set of intermediate conclusions. Here, only the most important ones will be emphasised. In addition, recommendations for further work will be made.

10.1 Summary

In order to facilitate the drawing of main conclusions in the following Section, the whole research work is summarised here by listing its crucial steps:

1) In earthquake analyses of concrete gravity dam-foundation systems, geological conditions at real dam sites often require the modelling of semi-infinite foundations. In order to verify simple computational models, prior to any further, more complicated, interaction analyses, Green's functions for the two-dimensional infinite and half-space elastodynamic problems were presented in the first part of Chapter 3. They were later used as theoretical solutions in the test comparison with approximate, numerical solutions in Chapter 4.

2) The relevant aspects of modelling unbounded media (i.e. infinite and semi-infinite half-space) with the Finite Element Method were mentioned in the second part of Chapter 3. It was explained that the unbounded nature of these problems and the need to model the energy radiation condition require the use of special boundary conditions, the so-called transmitting boundaries. In most circumstances, their implementation is associated with the direct integration of the equations of motion. Therefore, suitable algorithms for direct time integration were classified, emphasising the common problems such as finite time rise of real step discontinuities, overshooting, and spurious oscillations. Methods for the reduction of overshooting and spurious oscillations were reviewed, especially detailing the introduction of numerical (algorithmic) damping.

3) Also in Chapter 3, it was pointed out why it was not clear whether the problem of earthquake dam-foundation interaction falls into the wave propagation or structural dynamics category. Numerical studies which finally solve this dilemma were presented later, in Chapter 6.

4) After reviewing the best known local transmitting boundaries and overviewing numerical examples in the literature, the viscous transmitting boundary was recommended in Chapter 4 for further application in dam-foundation interaction problems. Advantages and disadvantages of the viscous transmitting boundary were stated.

5) To confirm the suitability of the viscous transmitting boundary to model the energy radiation condition, the boundary was subjected to stringent infinite and half-space foundation tests in the second part of Chapter 4. Although the tests were standard wave propagation problems with sharp and discontinuous wave fronts, the boundary performed very well.

6) In Chapter 5, the problem of concrete gravity dam-foundation interaction was extracted from the general soil-structure interaction problem. The differences and similarities between the free-field and scattering problem were noted. Finally, two methods of interaction analysis, complete and substructure, were reviewed by presenting rigorous mathematical formulations of their respective seismic input schemes (boundary and interface). In this process, some common terminological confusions and misuses were addressed and alternative terms were suggested.

7) An important discussion on the relationship between the seismic input scheme and the transmitting boundary was carried out in Chapter 5. By employing the substructure method of analysis, the earthquake excitation of the total system is 'taken out' of the foundation and reimposed in the form of external loading for the interaction problem. The transmitting boundary then correctly responds to the total minus free-field (or total minus scattered motion), but its location is still not known and has to be determined independently. A detailed study on the location of the viscous transmitting boundary for concrete gravity dam-foundation systems was carried out later, in Chapter 6.

8) In Chapter 6, preliminary linear earthquake analyses of concrete gravity dam-foundation systems were carried out. The first set of conclusions concerned the type and choice of the seismic input scheme. The second set of conclusions in Chapter 6 were reached by conducting the earthquake analysis of a real concrete gravity dam. The finite element foundation discretisation (i.e. the size of the foundation finite element mesh and the size of the foundation finite elements) was examined as a function of radiation damping, also in Chapter 6. The objective of determining at what distance from the dam the standard viscous transmitting boundary should be placed, was from the analytical point of view equivalent to finding the distance at which the far-field excitation of the free-field system is equal to the far-field excitation of the total system.

9) The comparison between the time domain and frequency domain analysis of a concrete gravity dam-foundation system, conducted in Chapter 6, has indicated that radiation damping in time domain analyses is adequately modelled if the recommendations formulated in the same Chapter are followed.

10) In order to enable the extension towards nonlinear analyses in Chapter 9, a procedure for combining the viscous transmitting boundary with static loading was devised and tested at the end of Chapter 6.

11) Chapter 7 introduced possible nonlinearities of the mass concrete and rock. An important discussion was conducted, distinguishing between the contact and limited tension nonlinearities. Practical choices were suggested. Possibilities for representing limited tension nonlinearities were particularly examined (namely no-tension, elasto-plastic and elasto-viscoplastic materials, and smeared, discrete and fracture mechanics approaches to cracking), emphasising those that will eventually be used in the subsequent Chapters. In all cases, it was assumed that the behaviour of mass concrete and rock in compression is linear elastic.

12) In Chapter 8, nonlinear static analyses of concrete gravity dam-foundation systems were carried out. The objectives of the analyses were the calibration of

nonlinear material models and identification of different modes of failure. The loading required to induce the nonlinear behaviour was provided by continuously increasing the reservoir water level.

13) At the end of Chapter 8, two basic scenarios for the likely penetration of water into open cracks were discussed. For one of them, a simple, novel incremental-iterative computational procedure was proposed and tested.

14) The final aim of this whole work was achieved in Chapter 9, when a set of nonlinear earthquake analyses of concrete gravity dam-foundation systems were carried out. The analyses were based on a novel procedure which does not require a free-field analysis of the site, successfully approximates the energy radiation condition and allows for the nonlinearities to occur both in the dam and foundation.

15) The results of the nonlinear analyses were compared with the results of the appropriate linear analyses. Both were performed by using the finite element code SOLVIA, a derivative of the general purpose finite element code ADINA. In order to treat the coupled, interaction problems, SOLVIA was specially adapted and tested by the author. One of the main advantages of this adaptation was the possibility to assess the contribution of different displacement components, created by the partition of the displacement vector, which is inherent in the substructure method of analysis.

10.2 Conclusions

Each of the Chapters in this thesis contained a set of detailed, intermediate conclusions. The most important ones are emphasised in this Section.

- The viscous transmitting boundary can be recommended for application in dam-foundation interaction problems. The only serious drawback of the boundary is the inability to support static loads.
- For wave propagation problems with viscous transmitting boundaries, the performance of the implicit, Newmark, direct integration algorithm was better than the performance of the explicit, central difference algorithm.
- Internal Rayleigh damping cannot be used as a substitute for radiation damping.
- The interface input scheme is the only seismic input alternative which can be used for concrete gravity dams lying either on rock layer or rock half-space foundations.
- The standard boundary input scheme cannot be used for dams on the rock layer unless the free-field analysis of the site is carried out and the excitation of the basement rock is fully determined.
- The response of the dam on the rock layer is completely different from the response of the dam on the rock half-space. Under no circumstances can one case be substituted with the other, nor can the results of one be interpreted as the results of the other.
- Only in some cases, can the boundary input scheme with a massless foundation be used for dams lying on the rock layer or the rock half-space. As a rough guide, it seems acceptable to use the boundary input scheme with a massless foundation for foundation stiffness equal to or more rigid than the dam.
- For the analysed system, the radiation damping was greater than for full Rayleigh damping constructed with 5% critical damping at the chosen control frequencies. The mass proportional Rayleigh damping part was very close to the full Rayleigh damping, while the stiffness proportional Rayleigh damping part was very close to the non-damped case.

- The Ricker wavelet may be used for qualitative investigations into seismic behaviour of concrete gravity dam-foundation systems. Although some conclusions may be extrapolated, in practice, preference should be given to analyses with real earthquake records whenever reliable information on earthquake motions are available.

- A foundation finite element mesh which extends approximately 3 heights of the dam upstream, downstream and underneath the dam, is acceptable for a wide range of foundation conditions.

- With respect to accuracy and computational economy, the optimal way to discretise the dam-foundation finite element mesh is to design it in accordance with the expected local nonlinearities in the dam and around the dam-foundation interface, and gradually to increase the size of the elements with increasing distance from the dam.

- In order to enable the extension towards nonlinear analyses, a procedure devised to combine the viscous transmitting boundary with static loading performed very well.

- Limited tension nonlinearities are highly dependent on tensile strength. Since the tensile strength of the mass concrete in dams is usually estimated and rarely experimentally determined, special care should be taken when making these estimates. Small changes of the estimated value cause drastic changes in the response and behaviour of the dam-foundation system.

- A smeared cracking model is better suited for modelling limited tension nonlinearities of concrete dam-foundation systems than an elasto-plastic model.

- For both the rigid and flexible foundation static analyses of concrete gravity dam-foundation systems, the damaged zones predicted by the linear elastic model were different from the damaged zones predicted by the two nonlinear models. This proves that the linear elastic model cannot be used to identify parts

of the dam-foundation system prone to damage and that the extrapolation of linear elastic results to reach the conclusions about the failure mechanisms is misleading.

- For nonlinear static analyses of concrete gravity dam-foundation systems, the damaged zones produced by the elasto-plastic and smeared cracking model were similar and two basic modes of failure were identified. When the modulus of elasticity of the foundation was smaller than the modulus of elasticity of the dam, inclined cracks propagated from the heel of the dam into the foundation. When the modulus of elasticity of the foundation was equal or greater than the modulus of elasticity of the dam, the cracking tended to propagate horizontally along the dam-foundation interface.

- If water is allowed to penetrate into the cracks open due to overloading, the stability of the dam is additionally endangered. For the considered case and for the assumption of immediate generation of full vertical water pressure in even the tiniest of the crack openings, the effect of the water penetration is roughly equivalent to the effect of the upstream reservoir being 10 m higher than in reality.

- For nonlinear earthquake analyses of the concrete gravity dam on a rigid foundation, the level of cracking was by far the most extensive and in very good agreement with Bristol EERC shaking table tests. For the flexible foundation cases, the level of cracking was less extensive. This indicates that the simpler, rigid foundation case is conservative and that a nonlinear analysis with flexible foundation conditions is the only alternative if rigorous conclusions on crack location and extent are needed.

- The seismic cracking of concrete gravity dam-foundation systems may be regarded as an energy-consuming mechanism, strongly dependent on tensile strength. After cracking, systems experience a loss in stiffness. The influence of the horizontal earthquake component is dominant.

- For nonlinear earthquake concrete gravity dam-foundation analyses and the modulus of elasticity of the foundation smaller than the modulus of elasticity of the dam, the principal direction of cracking is non-vertical. This direction is vertical for the lowest foundation modulus (E_f=5 GPa), and inclined for the intermediate foundation modulus (E_f=10 GPa). If the level of loading were further increased, the ultimate failure mode would be the failure of the foundation. In cases for which the modulus of elasticity of the foundation is equal to or greater than the modulus of elasticity of the dam, the principal direction of cracking is horizontal. If the level of loading were further increased, the ultimate failure mode would be the failure of the dam-foundation interface. The overall stability of the dam is in greater danger as the potential sliding surface is much shorter.

10.3 Recommendations for Further Work

Although the work presented in this thesis is complete, its findings and conclusions generate a wide range of possibilities for further work. This can be divided into three main categories: analytical work, work on the computational aspects, and experimental work.

10.3.1 Analytical Work

- The present investigation has concentrated on moderately high (≈50 m) concrete gravity dams of given geometry. As cross-sections of the majority of these dams throughout the world do not vary considerably, there is a limited number of behaviour patterns and modes of failure. It is believed that the conclusions about the behaviour patterns and modes of failure reached in this thesis are fairly typical, but to confirm this, further parametric studies are needed. Since the

majority of important analytical problems have already been solved and explained in the previous Chapters, future parametric studies would not be difficult to conduct. The likely variables could be the height of the dam, geometry of the cross-section, earthquake input, concrete and rock strengths, etc.

- A detailed discussion on the relationship between contact and limited tension nonlinearities was given in Chapter 7, and it was explained why only the latter were treated in this thesis. It was also concluded that the properties of contact nonlinearities in the foundation rock (e.g. length and width of joints and faults) are so random that they have to be addressed if and when they appear. In contrast, the predetermined discontinuity between the dam and the foundation is always present. Although it is not yet clear under what circumstances its behaviour becomes nonlinear, it can be foreseen that the bond between the two materials plays the most important role. Further studies are needed to determine in which cases the contact nonlinearity between the dam and the foundation becomes more important than limited tension nonlinearities. The simplest way to achieve this would be to consider concrete gravity dam-foundation systems as contact nonlinear problems where the bond between the two can be examined by varying some simple properties (e.g. coefficient of friction). After carrying out earthquake analyses, peak ground accelerations (PGAs) that cause the occurence of the nonlinearity would be noted, and the relationship between these PGAs and coefficients of friction could be easily established. Similar relationships could be established for limited tension nonlinearities, where PGAs and tensile strengths could be correlated. By comparing the two, it can be concluded in what cases a particular nonlinear model is more likely to affect the dam-foundation system.

10.3.2 Work on the Computational Aspects

- It was mentioned in Chapter 1 that one of the aims of the research in Bristol is to produce a comprehensive finite element code which would include all the recent research findings. In this thesis, like in the one which treated concrete dam-reservoir interaction (Greeves, 1991), the existing finite element computer codes were adapted to accommodate the required alterations. Now, having all the 'ingredients' for a full nonlinear, dam-foundation-reservoir interaction analysis, a special purpose finite element code can be written.

10.3.3 Experimental Work

- Parallel to this research project, shaking table scale model tests of concrete gravity dam monoliths were conducted in laboratory conditions (Mir, 1994), providing valuable information. They were particularly useful as a comparison for rigid foundation cases presented in this thesis. If this kind of work is extended to treat flexible foundation cases, experimental models could be used to evaluate the numerical modelling techniques and to validate the computer code mentioned in the previous Subsection.

- The dam engineering community currently lacks reliable data on the properties and behaviour of mass concrete, typically used in concrete gravity dams. The present state-of-the-art envisages the extrapolation of one-dimensional or, at best, two-dimensional data. This problem is particularly sensitive in the case of older dams, where ageing effects have to be taken into account and where limited information had been archived. Further research in this area can be conducted either through testing of the existing built-in mass concrete or through large-scale tests in laboratory conditions.

Aboudi, J. (1971) Numerical simulation of seismic sources, *Geophysics*, **36**, 810-821.

Aboudi, J. & Benveniste, Y. (1975) The nonlinear Lamb problem, *Comp. Meth. Appl. Mech. Eng.*, **6**, 319-334.

Aboudi, J. (1976) Two-dimensional wave propagation in a nonlinear elastic half-space, *Comp. Meth. Appl. Mech. Eng.*, **9**, 25-46.

Achenbach, J.D. (1973) *Wave Propagation in Elastic Solids*, North-Holland Publishing Co..

ADINA Engineering (1984) Automatic dynamic incremental nonlinear analysis users manual, *Report AE 84-1*, ADINA Engineering, USA.

Aki, K. & Richards, P.G. (1980) *Quantitative Seismology, Vol.I*, W.H.Freeman & Company.

Al-Hunaidi, M.O., Towhata, I. & Ishihara, K. (1990) Silent boundary for time domain wave motion analyses based on direct energy deletion, *Soil Dyn. Earthquake Eng.*, **9**, 85-95.

Antes, H. (1985) A boundary element procedure for transient wave propagations in two-dimensional isotropic elastic media, *Fin. Elem. Anal. Des.*, **1**, 313-322.

Ayari, M.L. & Saouma, V.E. (1990) A fracture mechanics based seismic analysis of concrete gravity dams using discrete cracks, *Eng. Fracture Mech.*, **35**, 587-598.

Aydinoglu, M.N. (1980) Unified formulations for soil-structure interaction, *Proc. 7th World Conf. Earthquake Eng.*, Istanbul, Turkey, **6**, 121-128.

Bathe, K.-J., Wilson, E.L. & Iding, R.H. (1974) NONSAP - a structural analysis program for static and dynamic response of nonlinear systems, *Report No.*

UC/SESM 74/03, Structural Engineering and Structural Mechanics, University of California, Berkeley, California.

Bathe, K.-J. & Ramaswamy, S. (1979) On three-dimensional nonlinear analysis of concrete structures, *Nuc. Eng. Des.*, **52**, 385-409.

Bathe, K.-J., Snyder, M.D., Cimento, A.P. & Rolph, W.D.III (1980) On some current procedures and difficulties in finite element analysis of elastic-plastic response, *Comput. Struct.*, **12**, 607-624.

Bathe, K.-J. (1982) *Finite Element Procedures in Engineering Analysis*, Prentice-Hall.

Bathe, K-J., Walczak, J, Welch, A. & Mistry, N. (1989) Nonlinear analysis of concrete structures, *Comput. Struct.*, **32**, 563-590.

Bayo, E. & Wilson, E.L. (1983) Numerical techniques for the evaluation of soil-structure interaction effects in the time domain, *Report No. UCB/EERC 83/04*, Earthquake Engineering Research Center, University of California, Berkeley, California.

Bayo, E. & Wilson, E.L. (1984) Finite element and Ritz vector techniques for the solution to three-dimensional soil-structure interaction problems in the time domain, *Eng. Comput.*, **1**, 298-311.

Bazant, Z.P. & Cedolin, L. (1979) Blunt crack band propagation in finite element analysis, *J. Eng. Mech. ASCE*, **105**, 297-315.

Bazant, Z.P. (1990) A critical appraisal of 'no-tension' dam design: a fracture mechanics viewpoint, *Dam Eng.*, **I**, 237-247.

Bazant, Z.P. (1993) Technical Note, *Dam Eng.*, **IV**, 59.

Becker, A.A. (1992) *The Boundary Element Method in Engineering - A complete course*, McGraw-Hill.

BEELAB (1993/94) *Documentation for Project SWH493*, BEELAB, Bristol.

Belytschko, T., Holmes, N. & Mullen, R. (1975) Explicit integration - stability, solution properties, cost, pp. 1-21 in *Finite Element Analysis of Transient Nonlinear Structural Behaviour*, ASME.

Bhattacharjee, S.S. & Léger, P. (1993) Seismic cracking and energy dissipation in concrete gravity dams, *Earthquake Eng. Struct. Dyn.*, **22**, 991-1007.

Bicanic, N. & Zienkiewicz, O.C. (1983) Constitutive model for concrete under dynamic loading, *Earthquake Eng. Struct. Dyn.*, **11**, 689-710.

Bielak, J. & Christiano, P. (1984) On the effective seismic input for non-linear soil-structure interaction systems, *Earthquake Eng. Struct. Dyn.*, **12**, 107-119.

Broek, D. (1978) *Elementary Engineering Fracture Mechanics*, Sijthoff & Noordhoff.

Brühwiler, E. & Wittmann, F.H. (1990) Failure of dam concrete subjected to seismic loading conditions, *Eng. Fracture Mech.*, **35**, 565-571.

Chakrabarti, P. & Chopra, A.K. (1973) Earthquake analysis of gravity dams including hydrodynamic interaction, *Earthquake Eng. Struct. Dyn.*, **2**, 143-160.

Chao, C.C. (1960) Dynamical response of an elastic half-space to tangential surface loadings, *Trans. ASME, J. Appl. Mech.*, 559-567.

Chapuis, J., Rebora, B. & Zimmermann, T. (1985) Numerical approach of crack propagation analysis in gravity dams during earthquakes, *Proc. 15th Int. Congr. Large Dams*, Lausanne, Switzerland, 451-473.

Charles, J.A., Abbis, C.P., Gosschalk, E.M. & Hinks, J.L. (1991) An engineering guide to seismic risk to dams in the United Kingdom, *BRE Report*, BRE, UK.

Chaudhary, A.B. & Bathe, K.-J. (1986) A solution method for static and dynamic analysis of three-dimensional contact problems with friction, *Comput. Struct.*, **24**, 855-873.

Chopra, A.K. (1967) Hydrodynamic pressures on dams during earthquakes, *J. Eng. Mech. Div ASCE*, **93**, 205-223.

Chopra, A.K. (1968) Earthquake behavior of reservoir-dam systems, *J. Eng. Mech. Div ASCE*, **94**, 1475-1500.

Chopra, A.K. (1970) Earthquake response of concrete gravity dams, *J. Eng. Mech. Div ASCE*, **96**, 443-454.

Chopra, A.K. & Chakrabarti, P. (1972) The earthquake experience at Koyna Dam and stresses in concrete gravity dams, *Earthquake Eng. Struct. Dyn.*, **1**, 151-164.

Chopra, A.K. (1978) Earthquake resistant design of concrete gravity dams, *J. Struct. Div ASCE*, **104**, 953-971.

Chopra, A.K. & Chakrabarti, P. (1981) Earthquake analysis of concrete gravity dams including dam-water-foundation rock interaction, *Earthquake Eng. Struct. Dyn.*, **9**, 363-383.

Chow, Y.K. (1985) Accuracy of consistent and lumped viscous dampers in wave propagation problems, *Int. J. Num. Meth. Eng.*, **21**, 723-732.

Clayton, R. & Engquist, B. (1977) Absorbing boundary conditions for acoustic and elastic wave equations, *Bull. Seism. Soc. Am.*, **67**, 1529-1540.

Clough, R.W. & Penzien, J. (1975) *Dynamics of Structures*, McGraw-Hill.

Clough, R.W. (1980) Nonlinear mechanisms in the seismic response of arch dams, *Proc. Int. Res. Conf. Earthquake Eng.*, Skopje, Yugoslavia, 669-684.

Clough, R.W. & Zienkiewicz, O.C. on behalf of the Committee on Analysis and Design of Dams of ICOLD (1987) Finite element methods in analysis and design of dams, *ICOLD Bulletin 30a*, Paris.

Cohen, M & Jennings, P.C. (1983) Silent boundary methods for transient analysis in *Computational Methods for Transient Analysis* edited by T.Belytschko and T.J.R. Hughes, Elsevier.

Cremonini, M.G., Christiano, P. & Bielak, J. (1988) Implementation of effective seismic input for soil-structure interaction systems, *Earthquake Eng. Struct. Dyn.*, **16**, 615-625.

Cruse, T.A. (1979) Two- and three-dimensional problems of fracture mechanics, Chapter 6 in *Developments in Boundary Element Methods - 1* edited by P.K. Banerjee & R. Butterfield, Applied Science Publishers Ltd.

Curbach, M. & Eibl, J. (1990) Crack velocity in concrete, *Eng. Fracture Mech.*, **35**, 321-326.

Dasgupta, G. & Chopra, A.K. (1979) Dynamic stiffness matrices for viscoelastic half planes, *J. Eng. Mech. Div. ASCE*, **105**, 729-745.

Desai, C.S., Zaman, M.M., Lightner, J.G. & Siriwardane, H.J. (1984) Thin-layer element for interfaces and joints, *Int. J. Num. Anal. Meth. Geomech.*, **8**, 19-43.

Droz, P. (1987) Modèle numérique du comportement non-linéaire d'ouvrages massifs en béton non armé, *Thesis No.682*, EPFL, Lausanne.

Eason, G., Fulton, J. & Sneddon, I.N. (1955/56) The generation of waves in an infinite elastic solid by variable body forces, *Phil. Trans. Royal Soc. London*, **A248**, 575-607.

El-Aidi, B. & Hall, J.F. (1989) Non-linear earthquake response of concrete gravity dams, Part 1: Modelling; Part 2: Behaviour, *Earthquake Eng. Struct. Dyn.*, **18**, 837-865.

Engquist, B. & Majda, A. (1977) Absorbing boundary conditions for the numerical simulation of waves, *Math. Comp.*, **31**, 629-651.

Eringen, A.C. & Suhubi, E.S. (1975) *Elastodynamics, Vol.II - Linear Theory,* Academic Press.

Ewing, W.M., Jardetzky, W.S. & Press, F. (1957) *Elastic Waves in Layered Media,* McGraw-Hill.

Fenves, G. & Chopra, A.K. (1984) EAGD-84, A computer program for earthquake analysis of concrete gravity dams, *Report No. UCB/EERC 84/11,* Earthquake Engineering Research Center, University of California, Berkeley.

Fenves, G. & Chopra, A.K. (1985a) Simplified earthquake analysis of concrete gravity dams: Separate hydrodynamic and foundation interaction effects, *J. Eng. Mech. ASCE,* **111**, 715-735.

Fenves, G. & Chopra, A.K. (1985b) Simplified earthquake analysis of concrete gravity dams: Combined hydrodynamic and foundation interaction effects, *J. Eng. Mech. ASCE,* **111**, 736-756.

Forrestal, M.J., Fugelso, L.E., Neidhardt, G.L. & Felder, R.A. (1966) Response of a half-space to transient loads, *Proc. Eng. Mech. Div. Specialty Conf. ASCE,* 719-751.

Garvin, W.W. (1956) Exact transient solution of the buried line source problem, *Proc. Royal Soc. London,* **A234**, 528-541.

Ghaboussi, J., Wilson, E.L. & Isenberg, J. (1973) Finite element for rock joints and interfaces, *J. Soil Mech. Founds. Div. ASCE,* **99**, 833-848.

Gioia, G., Bazant, Z.P. & Pohl, B.P. (1992) Is no-tension dam design always safe? - a numerical study', *Dam Eng.*, **III**, 23-34.

Goodman, R.E., Taylor, R.L. & Brekke, T.L. (1968) A model for the mechanics of jointed rock, *J. Soil Mech. Founds. Div. ASCE,* **94**, 637-659.

Goodman, R.E. (1976) *Methods of Geological Engineering in Discontinuos Rocks,* West Publishing Co..

Goodman, R.E. (1980) *Introduction to Rock Mechanics*, John Wiley & Sons.

Goudreau, G.L. & Taylor, R.L. (1972) Evaluation of numerical integration methods in elastodynamics, *Comp. Meth. Appl. Mech. Eng.*, **2**, 69-97.

Graff, K.F. (1975) *Wave Motion in Elastic Solids*, Clarendon Press.

Green, C.D. (1969) *Integral Equation Methods*, Thomas Nelson & Sons.

Greeves, E.J. (1991) The Modelling and Analysis of Linear and Nonlinear Fluid-Structure Systems with Particular Reference to Concrete Dams, *PhD thesis*, University of Bristol, Bristol.

Gutierrez, J.A. & Chopra, A.K. (1978) A substructure method for earthquake analysis of structures including structure-soil interaction, *Earthquake Eng. Struct. Dyn.*, **6**, 51-69.

Hadjian, A.H., Luco, J.E. & Tsai, N.C. (1974) Soil-structure interaction: continuum or finite elements, *Nucl. Eng. Des.*, **31**, 151-167.

Hall, J.F. & Chopra A.K. (1982) Two-dimensional dynamic analysis of concrete gravity and embankment dams including hydrodynamic effects, *Earthquake Eng. Struct. Dyn.*, **10**, 305-332.

Hall, J.F. (1986) Study of the earthquake response of Pine Flat dam, *Earthquake Eng. Struct. Dyn.*, **14**, 281-295.

Hallquist, J.O. (1991) LS - DYNA3D Theoretical Manual, *Livermore Software Technology Corporation Report 1018*, Livermore, USA.

Hilber, H.M., Hughes, T.J.R. & Taylor, R.L. (1977) Improved numerical dissipation for time integration algorithms in structural dynamics, *Earthquake Eng. Struct. Dyn.*, **5**, 283-292.

Hughes, T.J.R. & Liu, W.K. (1978a) Implicit-explicit finite elements in transient analysis: stability and theory', *Proc. ASME, J. Appl. Mech.*, **45**, 371-374.

Hughes, T.J.R. & Liu, W.K. (1978b) Implicit-explicit finite elements in transient analysis: implementation and numerical examples, *Proc. ASME, J. Appl. Mech.*, **45**, 375-378.

Hulbert, G.M. (1991) Limitations on linear multistep methods for structural dynamics, *Earthquake Eng. Struct. Dyn.*, **20**, 191-196.

Humar, J.L. & Jablonski, A.M. (1988) Boundary element reservoir model for seismic analysis of gravity dams, *Earthquake Eng. Struct. Dyn.*, **16**, 1129-1156.

Ibrahimbegovic, A. (1989) Dynamic analysis of large linear structure-foundation systems with local nonlinearities, *PhD Dissertation*, University of California, Berkeley, California.

Ibrahimbegovic, A. & Wilson, E.L. (1990) A methodology for dynamic analysis of linear structure-foundation systems with local nonlinearities, *Earthquake Eng. Struct. Dyn.*, **19**, 1197-1208.

Jaeger, C. (1979) *Rock Mechanics and Engineering*, Cambridge University Press.

Johnson, L.R. (1974) Green's function for Lamb's problem, *Geoph. J. Royal Astron. Soc.*, **37**, 99-131.

Kausel, E. & Tassoulas, J.L. (1981) Transmitting boundaries: a closed form comparison, *Bull. Seism. Soc. Am.*, **71**, 143-159.

Kausel, E. (1988) Local transmitting boundaries, *J. Eng. Mech. ASCE*, **114**, 1011-1027.

Kojic, S. & Trifunac, M. (1991) Earthquake stresses in arch dams - I: theory and antiplane excitation, *J. Eng. Mech. ASCE*, **117**, 532-552.

Kunar, R.R. & Rodriguez-Ovejero, L. (1980) A model with non-reflecting boundaries for use in explicit soil-structure interaction analyses, *Earthquake Eng. Struct. Dyn.*, **8**, 361-374.

Lamb, H. (1904) On the propagation of tremors over the surface of an elastic solid, *Phil. Trans. Royal Soc. London*, **A203**, 1-42.

Lane, R.G.T. on behalf of the Committee on Seismic Aspects of Dam Design of ICOLD (1983) Seismicity and dam design, *ICOLD Bulletin 46*, Paris.

Lang, H. (1961) Surface displacement in an elastic half-space, *Z. angew. Math. Mech.*, **41**, 141-153.

Lapwood, E.R. (1949/50) The disturbance due to a line source in a semi-infinite elastic medium, *Phil. Trans. Royal Soc. London*, **A242**, 63-100.

Laturelle, F.G. (1989) Finite element analysis of wave propagation in an elastic half-space under step loading, *Comput. Struct.*, **32**, 721-735.

Léger, P. & Boughoufalah, M. (1989) Earthquake input mechanisms for time-domain analysis of dam-foundation systems, *Eng. Struct.*, **11**, 37-46.

Léger, P. & Katsouli, M. (1989) Seismic stability of concrete gravity dams, *Earthquake Eng. Struct. Dyn.*, **18**, 889-902.

Léger, P., Sauvé, G. & Bhattacharjee, S.S. (1991) Dynamic substructure analysis of locally nonlinear dam-foundation-reservoir systems, *Dam Eng.*, **II**, 323-336.

Leliavsky, S. (1959/60) Uplift in gravity dams, *Water Power*, October 1959 - February 1960.

Liao, Z.P. & Wong, H.L. (1984) A transmitting boundary for the numerical simulation of elastic wave propagation, *Soil Dyn. Earth. Eng.*, **3**, 174-183.

Linsbauer, H.N. (1985) Fracture mechanics models for characterising crack behaviour in concrete gravity dams, *Proc. 15th Int. Congr. Large Dams*, Lausanne, Switzerland, 279-291.

Linsbauer, H.N. (1990) Application of the methods of fracture mechanics for the analysis of cracking in concrete dams, *Eng. Fracture Mech.*, **35**, 541-551.

Lotfi, V., Roesset, J.M. & Tassoulas, J.L. (1987) A technique for the analysis of the response od dams to earthquakes, *Earthquake Eng. Struct. Dyn.*, **15**, 463-490.

Lysmer, J. & Kuhlemeyer, R.L. (1969) Finite dynamic model for infinite media, *J. Eng. Mech. Div ASCE*, **95**, 859-877.

Lysmer, J. & Waas, G. (1972) Shear waves in plane infinite structures, *J. Eng. Mech. Div. ASCE*, **98**, 85-105.

Lysmer, J. (1978) Analytical procedures in soil dynamics, *Report No. UCB/EERC 78/29*, Earthquake Engineering Research Center, University of California, Berkeley, California.

Madabhushi, S.P.G. (1993) Numerical modelling of the semi-infinite extent of soil medium in dynamic soil-structure interaction problems, *Struct. Dyn. EURODYN '93*, 323-330.

Manolis, G.D. & Beskos, D.E. (1988) *Boundary Element Methods in Elastodynamics*, Unwin Hyman.

Meek, J.W. & Wolf, J.P. (1993) Cone models for nearly incompressible soil, *Earthquake Eng. Struct. Dyn.*, **22**, 649-663.

Miklowitz, J. (1978) *Elastic Waves and Waveguides*, North-Holland Publishing Co..

Miller, G.F. & Pursey, H. (1955) On the partition of energy between elastic waves in a semi-infinite solid, *Proc. R. Soc.* **A233**, 55-69.

Mir, R.A. (1994) An Experimental Investigation into the Seismic Induced Failure of Moderately High Concrete Gravity Dams, *PhD thesis*, University of Bristol, Bristol.

Mir, R.A. & Taylor, C.A. (1994) An experimental investigation into earthquake induced failure of medium to low-height concrete gravity dams, (accepted for publication) *Earthquake Eng. Struct. Dyn.*

Mlakar, P.F. (1987) Nonlinear response of concrete gravity dams to strong earthquake-induced ground motion, *Comput. Struct.*, **26**, 165-173.

Ngo, D. & Scordelis, A.H. (1967) Finite element analysis of reinforced concrete beams, *ACI J.*, 64, 152-163.

Norman, C.D. & Anderson, F.A. (1985) Reanalysis of cracking in large concrete dams in the US Army Corps of Engineers, *Proc. 15th Int. Congr. Large Dams*, Lausanne, Switzerland, 157-171.

Pal, N. (1976) Seismic cracking of concrete gravity dams, *J. Struct. Div. ASCE*, **102**, 1827-1844.

Pande, G.N., Beer, G. & Williams, J.R. (1990) *Numerical Methods in Rock Mechanics*, John Wiley & Sons.

Pekau, O.A., Chuhan, Z. & Lingmin, F. (1991) Seismic fracture analysis of concrete gravity dams, *Earthquake Eng. Struct. Dyn.*, **20**, 335-354.

Pekeris, C.L. (1955a) The seismic surface pulse, *Proc. Natn. Acad. Sci. USA*, **41**, 469-480.

Pekeris, C.L. (1955b) The seismic buried pulse, *Proc. Natn. Acad. Sci. USA*, **41**, 629-639.

Poulos, H.G. & Davis, E.H. (1974) *Elastic Solutions for Soil and Rock Mechanics*, John Wiley & Sons.

Prakash, S. (1981) *Soil Dynamics*, McGraw Hill.

Principia Mechanica Ltd. (1981) *Seismic Ground Motions for UK Design*, Report for BNFL and CEGB, UK.

Rescher, O.-J. (1990) Importance of cracking in concrete dams, *Eng. Fracture Mech.*, **35**, 503-524.

Robinson, A.R. (1977) The transmitting boundary - again, pp. 163-177 in *Structural and Geotechnical Mechanics* edited by J.W. Hall, Prentice-Hall.

Rots, J.G. (1991) Smeared and discrete representations of localized fracture, *Int. J. Fracture*, **51**, 45-59.

Saini, S.S., Krishna, J. & Chandrasekaran, A.R. (1972) Behavior of Koyna Dam - Dec. 11, 1967 earthquake, *J. Str. Div. ASCE*, **98**, 1395-1412.

Sandi, H. (1960) A theoretical investigation of the interaction between ground and structure during earthquakes, *Proc. 2nd Conf. Earthquake Eng., Japan*, **II**, 1327-1343.

Sauter, F. (1950) Der elastische Halbraum bei einer mechanischen Beeinflussung seiner Oberflache (Zweidimensionales Problem), *Z. angew. Math. Mech.*, **30**, 203-215.

Seed, H.B., Whitman, R.V. & Lysmer, J. (1977) Soil-structure interaction effects in the design of nuclear power plants in *Structural and Geotechnical Mechanics* edited by W.J.Hall, Prentice-Hall.

Sharan, S.K. (1992) Elastostatic analysis of infinite solids using finite elements, *Int. J. Num. Meth. Eng.*, **35**, 109-120.

Shipley, S.A., Leistner, H.G. & Jones, R.E. (1967) Elastic wave propagation - a comparison between finite element predictions and exact solutions, *Proc. Int. Symp. Wave Propagation and Dyn. Properties of Earth Materials*, 509-519, University of New Mexico Press.

Simic, M. & Taylor, C.A. (1992a) Transmitting Boundaries for Earthquake Response of Concrete Gravity Dams, *Report no. UBCE-EE-92-5*, Earthquake Engineering Research Centre, Department of Civil Engineering, University of Bristol, Bristol.

Simic, M. & Taylor, C.A. (1992b) Seismic Input for Earthquake Response of Concrete Gravity Dams, *Report no. UBCE-EE-92-6*, Earthquake Engineering Research Centre, Department of Civil Engineering, University of Bristol, Bristol.

Simic, M. (1993a) *EERC Technical Instruction TI42013.1*, Earthquake Engineering Research Centre, Department of Civil Engineering, University of Bristol, Bristol.

Simic, M. (1993b) *EERC Technical Note MS1091/TN/3B*, Earthquake Engineering Research Centre, Department of Civil Engineering, University of Bristol, Bristol.

Simic, M. (1993c) *EERC Technical Note MS1091/TN/4C*, Earthquake Engineering Research Centre, Department of Civil Engineering, University of Bristol, Bristol.

Simic, M. (1993d) *EERC Technical Note SWH493/TN5*, Earthquake Engineering Research Centre, Department of Civil Engineering, University of Bristol, Bristol.

Simic, M. (1993e) *EERC Technical Instruction TI42092*, Earthquake Engineering Research Centre, Department of Civil Engineering, University of Bristol, Bristol.

Simic, M. & Taylor, C.A. (1994) Concrete gravity dam-foundation discretisation as a function of radiation damping, submitted for review and possible publication in *Dam Eng.*.

Simic, M. (1994) *EERC Technical Note MS1091/TN/6B*, Earthquake Engineering Research Centre, Department of Civil Engineering, University of Bristol, Bristol.

Simons, H.A. & Randolph, M.F. (1986) Comparison of transmitting boundaries in dynamic finite element analyses using explicit time integration, *Int. J. Num. Anal. Meth. Geomech.*, **10**, 329-342.

Skrikerud, P.E. & Bachmann, H. (1986) Discrete crack modelling for dynamically loaded unreinforced concrete structures, *Earthquake Eng. Struct. Dyn.*, **14**, 297-315.

Smith, W.D. (1974) A nonreflecting plane boundary for wave propagation problems, *J. Computational Physics*, **15**, 492-503.

SOLVIA Engineering AB (1989/92) Users Manuals - *Reports SE 90-1, 90-2, 90-3, 90-4, 90-5* and *New Capabilities in Version 90.2*, SOLVIA Engineering AB, Sweden.

Tardieu, B. & Londe, P. (1992) Technical Note, *Dam Eng.*, **III**, 301.

Taylor, C.A., Daniell, W.E., Mir, R.A., Simic, M. & Hinks, J.L. (1994) The seismic behaviour of gravity dams in areas of low seismicity, *The British Dam Soc. Conf. on Reservoir Safety and the Environment*, Exeter, UK.

Toki, K., Sato, T. & Miura, F. (1981) Separation and sliding between soil and structure during strong ground motion, *Earthquake Eng. Struct. Dyn.*, **9**, 263-277.

Toki, K. & Miura, F. (1983) Non-linear seismic response analysis of soil-structure interaction systems, *Earthquake Eng. Struct. Dyn.*, **11**, 77-89.

Touhei, T. & Ohmachi, T. (1993) A FE-BE method for dynamic analysis of dam-foundation-reservoir systems in the time domain, *Earthquake Eng. Struct. Dyn.*, **22**, 195-209.

Triantafyllidis, T. (1991) 3-D time domain BEM using half-space Green's functions, *Eng. Anal. Boundary Elem.*, **8**, 115-124.

United States Bureau of Reclamation - USBR (1976) *Design of Gravity Dams*, USBR, Denver, Colorado, USA.

Vargas-Loli, L.M. & Fenves, G.L. (1989) Effects of concrete cracking on the earthquake response of gravity dams, *Earthquake Eng. Struct. Dyn.*, **18**, 575-592.

Venturini, W.S. (1983) *Boundary Element Method in Geomechanics*, Springer-Verlag.

Von Estorff, O. & Kausel, E. (1989) Coupling of boundary and finite elements for soil-structure interaction problems, *Earthquake Eng. Struct. Dyn.*, **18**, 1065-1075.

Von Estorff, O., Pais, A.L. & Kausel, E. (1990) Some observations on time domain and frequency domain boundary elements, *Int. J. Num. Meth. Eng.*, **29**, 785-800.

Von Estorff, O. & Prabucki, M.J. (1990) Dynamic response in the time domain by coupled boundary and finite elements, *Comp. Mech.*, **6**, 35-46.

Von Estorff, O. & Antes, H. (1991) On FEM-BEM coupling for fluid-structure interaction analyses in the time domain, *Int. J. Num. Meth. Eng.*, **31**, 1151-1168

Waggoner, F., Plizzari, G. & Saouma, V.E. (1993) Centrifuge tests of concrete gravity dams, *Dam Eng.*, **IV**, 144-171.

Wang, Y.C., Murti, V. & Valliappan, S. (1992) Assessment of the accuracy of the Newmark method in transient analysis of wave propagation problems, *Earthquake Eng. Struct. Dyn.*, **21**, 987-1004.

Weber, B., Hohberg, J.-M. & Bachmann, H. (1990) Earthquake analysis of arch dams including joint nonlinearity and fluid-structure interaction, *Dam Eng.*, **I**, 267-278.

Westergaard, H.M. (1933) Water pressures on dams during earthquakes, *Trans. Am. Soc. Civ. Eng.*, **98**, 418-433.

White, W., Valliappan, S. & Lee, I.K. (1977) Unified boundary for finite dynamic models, *J. Eng. Mech. Div ASCE*, **103**, 949-964.

Wolf, J.P. & Obernhuber, P. (1983) In-plane free-field response of actual sites, *Earthquake Eng. Struct. Dyn.*, **11**, 121-134.

Wolf, J.P. (1985) *Dynamic Soil-Structure Interaction*, Prentice-Hall.

Wolf, J.P. (1988) *Soil-Structure-Interaction Analysis in Time Domain*, Prentice-Hall.

Woods, R.D. (1968) Screening of surface waves in soils, *J. Soil Mech. Founds. Div. ASCE*, **94**, 951-979.

Yang, R., Tsai, C.S. & Lee, G.C. (1993) Explicit time-domain transmitting boundary for dam-reservoir interaction analysis, *Int. J. Num. Meth. Eng.*, **36**, 1789-1806.

Zienkiewicz, O.C., Valliappan, S. & King, I.P. (1968) Stress analysis of rock as a 'no tension' material, *Géotechnique*, **18**, 56-66.

Zienkiewicz, O.C. (1968) Continuum mechanics as an approach to rock mass problems, Chapter 8 in *Rock Mechanics in Engineering Practice* edited by K.G. Stagg & O.C. Zienkiewicz, John Wiley & Sons.

Zienkiewicz, O.C., Best, B., Dullage, C. & Stagg, K.G. (1970) Analysis of nonlinear problems in rock mechanics with particular reference to jointed rock systems, *Proc. 2nd Congr. Int. Soc. Rock Mech.*, Belgrade, Yugoslavia, 501-509.

Zienkiewicz, O.C., Hinton, E., Bicanic, N. & Fejzo, P. (1981) Computational models for the transient dynamic analysis of concrete dams, in *Dams and Earthquake*, Thomas Telford.

Zienkiewicz, O.C., Clough, R.W. & Seed, H.B. on behalf of the Committee on Analysis and Design of Dams of ICOLD (1986) Earthquake analysis procedures for dams, *ICOLD Bulletin 52*, Paris.

Zienkiewicz, O.C. & Taylor, R.L. (1991) *The Finite Element Method - Volume 2*, McGraw-Hill.